2023

The Role of Tau in Epidermal Stratification and Differentiation and its Implications in Skin Cancer

Illsley, Charlotte Sara

Copyright statement

UNIVERSITY OF PLYMOUTH

The Role of Tau in Epidermal Stratification and Differentiation and its Implications in Skin Cancer

By

Charlotte Sara Illsley

A thesis submitted to the University of Plymouth

in partial fulfilment for the degree of

DOCTOR OF PHILOSOPHY

Peninsula Dental School

Faculty of Health

January 2023

Dedication

There are so many people to thank for their encouragement, support and guidance over the last five years, without whom I would not have made it to this point. Although I would love to list everyone, I fear I would run out of space, and therefore I would like to acknowledge a few of those that have been instrumental throughout this pursuit of research.

This PhD has been an extremely rewarding, but challenging journey. I have acquired indispensable knowledge and experiences, alongside life-changing opportunities and friendships. This would not have been possible without the guidance of my supervisory team: Professor Bing Hu, Associate Professor Zoe Brookes and Professor Chris Tredwin. I am incredibly grateful for their patience and encouragement in developing my knowledge, skills and career.

To the members of the research group, Wai-Ling Kok, Yan Gao, Fan Yan, Chloe Walker, Portia Maddick, Donald Singer, Jemma Walker, Jonathan Davies, Yi Yang, thank you for all the techniques, laughter, tears, frustration and joy shared. It has been a pleasure to work with colleagues that all cared and helped each other when needed. A special thank you to “the girls”: Carly Bunston, Portia Maddick, Chloe Bolton, Jemma Walker, Sarah Ellwood and Gabriela Wojcik. I will treasure the memories we have made over the years and look forward to our continued friendship.

None of this would have been possible without the love, support and encouragement from my family. I would like to thank my dad Nick and brother Ben for being my voice of reason and for your unwavering faith that I could get to this stage. I have been incredibly lucky to have had parents who have supported my love of science from an early age and ultimately it was this love and encouragement which has enabled me to become the scientist I am today. For this, I will be forever grateful. Thank you to Nannie and Grandma Isabel, who patiently listened and reassured me when I needed it most. Thank you to my fiancé Chris, for his patience and support in everything I do.

Finally, to my mum, this is for you – who is sadly not with us anymore, but always believed I could one day become a doctor.

Acknowledgements

The author would like to thank the members of their supervisory team:

Professor Bing Hu (University of Plymouth),

Professor Christopher Tredwin (University of Plymouth),

Associate Professor Zoe Brookes (University of Plymouth).

Their research group:

Dr Wai-Ling Kok, Dr Chloe Walker, Dr Portia Grayson, Dr Donald Singer, Dr Jemma Walker, Dr Jonathan Davies, Yan Gao, Fan Yan

Other Academic Support:

Dr Emmanuella Guenova-Hötzenecker and Professor Wolfram Hötzenecker from the Dermatological Bio-bank University Hospital Zurich, Switzerland for the human skin samples used in this study. Dr Ansgar Poetsch and Dr Vikram Sharma for carrying out the analysis of the proteomic samples in this study. Dr Paolo Paganetti of the University of Lugano, Switzerland for providing the shRNA tau plasmids and Professor Alexander Zambon of the University of California for providing the Ki67 FUCCI viral reporter system.

This work has been supported by PUPSMD PhD studentship and the ERDF regional development fund to B.H.

Author's declaration

At no time during the registration for the degree of Doctor of Philosophy has the author been registered for any other University award without prior agreement of the Doctoral College Quality Sub-Committee.

Work submitted for this research degree at the University of Plymouth has not formed part of any other degree either at the University of Plymouth or at another establishment.

This study was financed with the aid of a studentship form the Peninsula Dental School, University of Plymouth. This work is supported by the ERDF regional development fund to Professor Bing Hu.

Publications:

- Walker, J.V., Zhuang, H., Singer, D., **Illsley, C.S.**, Kok, W.L., Sivaraj, K.K., Gao, Y., Bolton, C., Liu, Y., Zhao, M., Grayson, P.R.C., Wang, S., Karbanová, J., Lee, T., Ardu, S., Lai, Q., Liu, J., Kassem, M., Chen, S., Yang, K., Bai, Y., Tredwin, C., Zambon, A.C., Corbeil, D., Adams, R., Abdallah, B.M., Hu, B. (2019). Transit amplifying cells coordinate mouse incisor mesenchymal stem cell activation. ***Nature Communications,*** 10:3596. doi: 10.1038/s41467-019-11611-0.
- Denes, B.J., Bolton, C., **Illsley, C. S.**, Kok, W., Walker, J.V., Poetsch, A., Tredwin, C., Kiliaridis, S., Hu, B**.** (2019). Notch signalling coordinates periodontal ligament maturation through regulating Lamin A. ***Journal of Dental Research.*** doi:10.1177/0022034519871448.

Presentation at Conferences:

- Poster presentation at BSODR, Leeds 2019
- Oral presentation at University of Plymouth's Faculty of Medicine and Dentistry Annual Research Event, Plymouth 2018 (Best oral presentation prize winner)

Word count of main body of thesis: 77,959

Signed 

Date 10/05/2022

Abstract

The Role of Tau in Epidermal Stratification and Differentiation and its Implications in Skin Cancer

Charlotte Sara Illsley

Background:

Microtubule associated proteins are a group of proteins well characterised for their role in the stabilisation and polymerisation of microtubules, but they have been increasingly demonstrated to have a more diverse role within cells. Tau is a microtubule associated protein, well studied for its pathological role in Alzheimer's disease. Recent studies have provided evidence that tau is also expressed in the epidermal compartment of the skin. However, the precise roles of tau during epidermal stratification and differentiation are currently unknown.

Aims:

This study aims to investigate the role of tau in epidermal stratification and differentiation and its function in cutaneous squamous cell carcinoma (cSCC).

Methods:

Immunostaining was used to investigate tau expression in clinical samples, 2D cultures and 3D skin equivalents. To explore the functional significance of tau during keratinocyte differentiation and stratification, siRNA and shRNA were used to downregulate tau expression in keratinocytes and the cSCC cell line, A431. Gene and protein expression were assessed using RT q-PCR, Western blotting, and changes in cytoskeletal organisation were determined using immunofluorescence. The overexpression of tau was conducted through the generation of stable cell lines with a doxycycline inducible overexpression of tau.

The functional significance of tau overexpression was determined using a combination of RT q-PCR, Western blot and immunofluorescence analyses of 2D epidermal keratinocyte culture, MatTek© 3D epidermal models and cSCC cells *in vitro*. Co-Immunoprecipitation (CoIP) and subsequent proteomic analysis were performed to identify tau binding partners in growing and differentiated keratinocytes.

Results:

In healthy human skin, tau expression was upregulated in the differentiated population of suprabasal keratinocytes and displayed a distinct isoform specific expression throughout the epidermis. Overexpression of tau *in vitro* was found to initiate keratinocyte differentiation in 2D culture and 3D epidermal models. CoIP and subsequent proteomic analysis identified a discrete pattern of tau interactions in keratinocytes cultured under growing and differentiated conditions, with a specific subset of nuclear, cytoplasmic and membrane associated proteins identified to interact with tau through different stages of keratinocyte differentiation. Finally, in cSCC tau expression was linked to the differentiation status of the tumours. Furthermore, the downregulation and overexpression of tau was sufficient to induce changes to cytoskeletal organisation and cellular differentiation in cSCC *in vitro*.

Conclusions:

This study revealed that tau can orchestrate epidermal cell fate, differentiation and stratification in healthy human skin and cSCC. These findings are therefore anticipated to be a starting point for more functional research into the binding partners of tau during epidermal stratification, differentiation and their subsequent function in cancer.

Table of contents

List of figures

List of tables

Abbreviations

Abbreviation	Full name
0N	0 N-terminal
1N	1 N-terminal
2D	Two dimensional
2N	2 N-terminal
3D	Three dimensional
3R	3-repeat Tau
4R	4-repeat Tau
5 ALA	5-Aminolevulinic acid
5 FU	5 Fluorouracil
ABC	Ammoniumbicarbonate
AD	Alzheimer's Disease
AHNAK	Neuroblast differentiation-associated protein AHNAK
AJ	Adherens junction
AK	Actinic keratosis
ANXA2	Annexin A2
AP	Amyloid plaques
ARPC3	Actin-related protein 2/3 complex subunit 3
ATP6AP2	ATPase H+ transporting accessory protein 2
Aβ	β-amyloid protein
BCC	Basal cell carcinoma
Blast	Blasticidin
BM	Basement membrane
BSA	Bovine Serum Albumin
CAA	Chloroacetamide
$CaCl_2$	Calcium Chloride
CAFs	Cancer associated fibroblasts
CDK1	Cyclin-dependent protein kinase 1
CDK2	Cyclin-dependent protein kinase 2
CDK4	Cyclin-dependent protein kinase 4
CDK5	Cyclin-dependent protein kinase 5
CDKN2A	Cyclin dependent kinase inhibitor 2A
CDT1	Chromatin Licensing And DNA Replication Factor 1
CHCHD4	Coiled-Coil-Helix-Coiled-Coil-Helix Domain Containing 4
CLN5	Chloride voltage gated-channel 5
CSC	Cancer stem cell
cSCC	Cutaneous squamous cell carcinoma
CTSD	Cathepsin
DAPI	4'-6-diamidino-2-phenylindole
dH_2O	Distilled water
DLL1	Delta Like Canonical Notch Ligand 1
DMBA	7,12-dimethylbenz-[a]-anthracene
DMEM	Dulbecco Modified Eagle's Medium
DNA	Deoxyribonucleic acid

DOXY	Doxycycline
dsRNA	Double-stranded RNA
DSG2	Desmoglein 2
DSP	Desmoplakin
DTT	Dithiothreitol
E	Eluate
E. coli	*Escherichia coli*
ECM	Extracellular matrix
EEF1A1	Elongation factor 1-α 1
EEF2	Elongation factor 2
EGFR	epidermal growth factor receptors
EPU	Epidermal proliferative unit
esiRNA	Endoribonuclease-prepared small interfering RNA
FBS	Foetal Bovine Serum
FLNB	Isoform 2 of Filamin-B
FREIC	Faculty Research Ethics and Integrity Committee
FT	Flow-through
FTDP-17	Fronto-temporal dementia with Parkinson linked to chromosome 17
FUCCI	Fluorescent Ubiquitination-based Cell Cycle Indicator
GAGs	Glycosaminoglycans
GAPDH	Glyceraldehyde-3-Phosphate Dehydrogenase
Gem	Geminin
GRN	Granulin
GSK-3β	Glycogen-synthase kinase-3β
H&E	Haematoxylin and eosin
HBSS	Hank’s Balanced Salt Solution
HDF	Human dermal fibroblasts
HDFa	Human dermal fibroblasts adult
HEKn	Human Epidermal Keratinocytes (neonatal)
HIST1H4A	Histone 4A
HKGS	Human Keratinocyte Growth Serum
HPEKp	Human primary epidermal keratinocytes (pooled)
HPLC	High performance liquid chromatography
HPV	Human papillomavirus
HRP	Horseradish peroxidase
HSP90B1	Endoplasmin
HSPA5	Endoplasmic reticulum chaperone BiP
HSPA8	Heat shock cognate 71 kDa
HSPB1	Heat shock protein β1
HTA	Human Tissue Authority
IDP	Intrinsically disordered protein
IF	Intermediate filament
ITGA6	Integrin α6
ITGAV	Integrin αV
ITGB4	Integrin β4
K1	Keratin 1
K10	Keratin 10

K14	Keratin 14
K5	Keratin 5
KD	Knock down
KGF	Keratinocyte growth factor (FGF 7)
KO	Knock out
LAMA3	Laminin subunit α3
LAMA5	Laminin subunit alpha 5
LAMB3	Laminin subunit β3
LAMC2	Isoform Short of Laminin subunit gamma-2
LCM	Laser capture microdissection
LDS	Lithium Dodecyl Sulphate
LFQ	Label-free quantitation
LGALS1	Gakectin-1
Lrig1	Leucine Rich Repeats And Immunoglobulin Like Domains 1
MAP	Microtubule associated protein
MAPT	Microtubule Associated Protein Tau
MMP	Matrix metalloproteinases
mRNA	Messenger RNA
MT	Microtubules
MTBD	Microtubule binding domain
MTOC	Microtubule organising centre
MYH9	Myosin-9
MYL12A	Myosin regulatory light chain 12A
NCBP1	Nuclear cap-binding protein subunit 1
NCBP2	Nuclear cap-binding protein subunit 2
NFT	Neurofibrillary tangle
NMSC	Non-melanoma skin cancer
OCT	Optimum cutting temperature
PARK7	Parkinsonism Associated Deglycase
PBS	Phosphate buffered saline
PBST	1X PBS 0.1 % triton
PCR	Polymerase Chain Reaction
PFA	Paraformaldehyde
PKA	cAMP-dependent protein kinase
PKM	Isoform M1 of Pyruvate kinase PKM
PLEC	Plectin
PPT1	Palmitoyl-protein thioesterase 1
pRb	Retinoblastoma protein
PRD	Proline Rich Domain
PRDX2	Peroxiredoxin-2
PRDX3	Peroxiredoxin 3
q-PCR	Quantitative-Polymerase Chain Reaction
RAP1B	Ras-related protein Rap-1b
RLUC	*Renilla reformis* Luciferase
RNA	Ribonucleic acid
RNAi	RNA interference
rRNA	Ribosomal RNA
ROI	Region of interest

RPKM	Reads per kilobase of transcript per million mapped reads
RPS25	40S ribosomal protein S25
RT	Room temperature
rtTA	reverse tetracycline transactivator
S100A6	Protein S100
SB	Stratum basale
SC	Stratum corneum
SCC	Squamous cell carcinoma
SCs	Stem cells
SEM	Scanning electron microscope
SG	Stratum granulosum
shRNA	Short hairpin RNA
siRNA	Small interfering RNA
SNAPIN	SNARE-associated protein
SS	Stratum spinosum
TACs	Transit amplifying cells
TF	Serotransferrin
TFA	Trifluoroacetic acid
TJ	Tight junction
TME	Tumour micro-environment
TP53	Tumour protein 53
TPA	12-O-tetradecanoyl phorbol-13-acetate
TPM	Transcripts per million
TPM3	Tropomyosin α3 chain
TPM4	Tropomyosin α4 chain
TetO	Tet operator
TRE	Tetracycline-responsive promoter element
UV	Ultraviolet

1. Introduction and literature review

1.1. Healthy human skin

The skin is the largest organ in the human body, accounting for approximately 15% of an adult's body weight [1–4]. It plays an essential role in the protection of the body against a wide variety of environmental insults, such as ultraviolet (UV) radiation, viruses, pathogens and carcinogens. The skin also plays a role in the maintenance of homeostasis, ensuring that water is not lost from the skin surface and helping to maintain our body temperature [5]. Skin is a complex multi-layered structure, composed of three layers: the epidermis, dermis and hypodermis (Figure 1.1). Each component of human skin performs specialist functions, if any of these malfunction it usually results in an undesirable condition, anywhere from atopic dermatitis to cancer [2–4,6,7].

1.2. Structure and function of the epidermis

The epidermis is the outermost layer of the skin and functions as an impermeable barrier to the external environment; restricting pathogens, chemicals and radiation from entering the skin, whilst also preventing the loss of fluids to the external environment leading to dehydration [1–3]. The epidermis is organised into four hexagonally packed, stratified layers of specialised epithelial cells, known as keratinocytes [1,5]. Epidermal keratinocytes undergo a process of terminal differentiation, in which the innermost (basal) layer of stem cells (SCs) embark on a programme of differentiation [1,8–11]. These basal keratinocytes divide a small number of times as transit amplifying cells (TACs) before they cease to proliferate, delaminate, undergo morphological and transcriptional changes that culminates in the formation of dead, flattened, enucleated corneocytes that are eventually shed form the skins surface [3,10,12–15]. Upon commitment to terminally

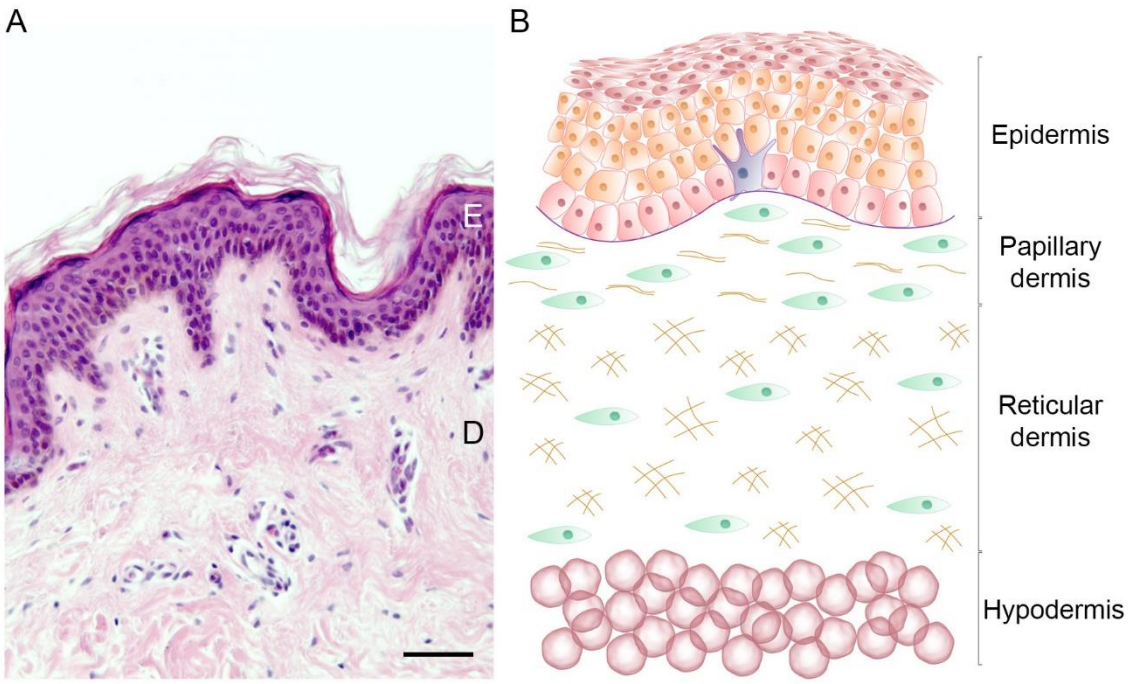

Figure 1.1.Structure of full thickness adult human skin.
A. Haematoxylin and eosin (H&E) staining of healthy human adult abdomen skin. E – epidermis, D – dermis. Scale bar 100 µm. **B.** Schematic depicting the organisation of full thickness human skin. Outermost layer, named the epidermis, primarily made up of keratinocytes. The dermis is separated from the epidermis by the basement membrane (BM). The dermis can be further classified into two layers, the papillary dermis (upper) and reticular dermis (lower), fibroblasts embedded in a rich ECM are the main cell type located here. The deepest layer of the skin is the hypodermis, made up of adipose tissue.

differentiate basal epidermal keratinocytes delaminate (detach) from the basement membrane (BM), move upwards and undergo three distinct differentiation stages: spinous, granular and corneal, in which major changes in transcription, function and morphology occur at each layer of transition [12] (Figure 1.2 and Figure 1.3). The self-renewing capacity of epidermal SCs *in vivo* is very high, with a basal cell committing to terminal differentiation and shed from the skins surface within a 4 week period [12,13]. It is this remarkable self-renewing capacity of skin SCs has led to its use as a model to further explore SC homeostasis and regeneration capabilities [2,12,16,17].

The epidermis must withstand mechanical insult and repair wounds throughout an individual's lifespan [18,19]. The epidermis utilises a robust network of keratin filaments and adhesion structures that help maintain both its structural, and functional integrity [10,11,20]. The cells cytoskeleton plays an integral role in this structural integrity through the maintenance of cell shape, polarity and cell differentiation [21–24].

1.2.1. From stem cells to differentiated cells

Epidermal keratinocytes undergo a specific tightly regulated programme of terminal differentiation controlled by various factors and integral to the epidermis role and structural integrity [1,25–27]. The SC niche of the epidermis resides in the innermost layer, known as the basal layer [2,3,28]. Although it is known that these epidermal SCs reside in the basal layer, there is still some debate whether all cells in the basal layer are SCs or if there is only a small number of SCs which exist in this layer [3,11,29].

In 1974, Christopher Potten structurally defined the epidermal proliferative unit (EPU) as a bed of 10 tightly associated basal cells that are able to yield an

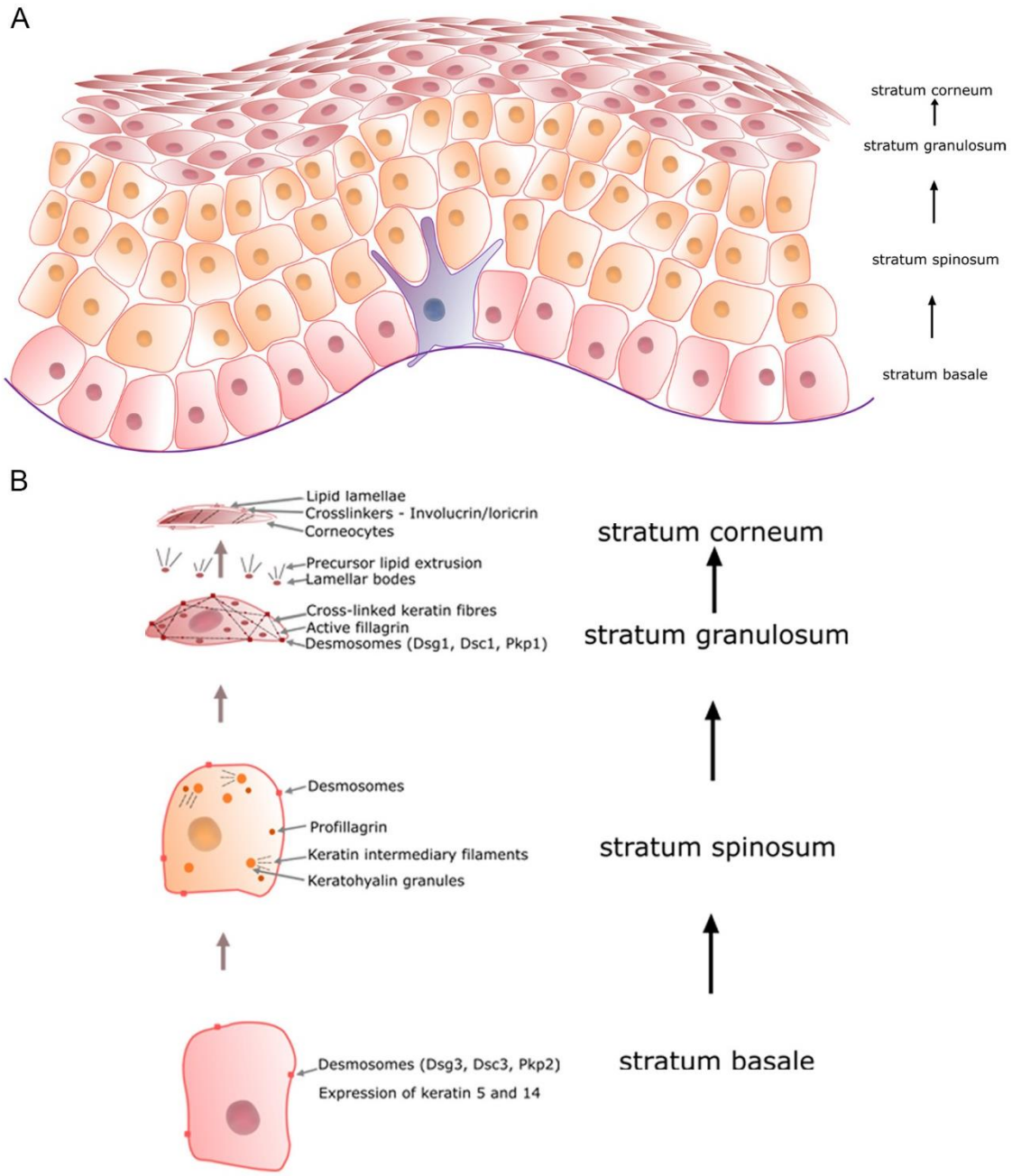

Figure 1.2. Structure of stratified epidermis in human skin.
A. The process of terminal differentiation of keratinocytes yields four distinct stratified layers in the human epidermis. The proliferative basal layer, lying on top of the basement membrane, produces three differentiated cell types; spinous cells, granular cells and eventually corneocytes in the stratum corneum. **B**. The programme of epidermal terminal differentiation is illustrated in the schematic. The SC niche of the epidermis is located in the basal layer, at the interface of the epidermis and dermis. When these cells commit to terminal differentiation they cease proliferating, move outwards and undergo many cellular changes and are eventually shed from the skin as flattened dead cells, enclosed in lipid lamellae.

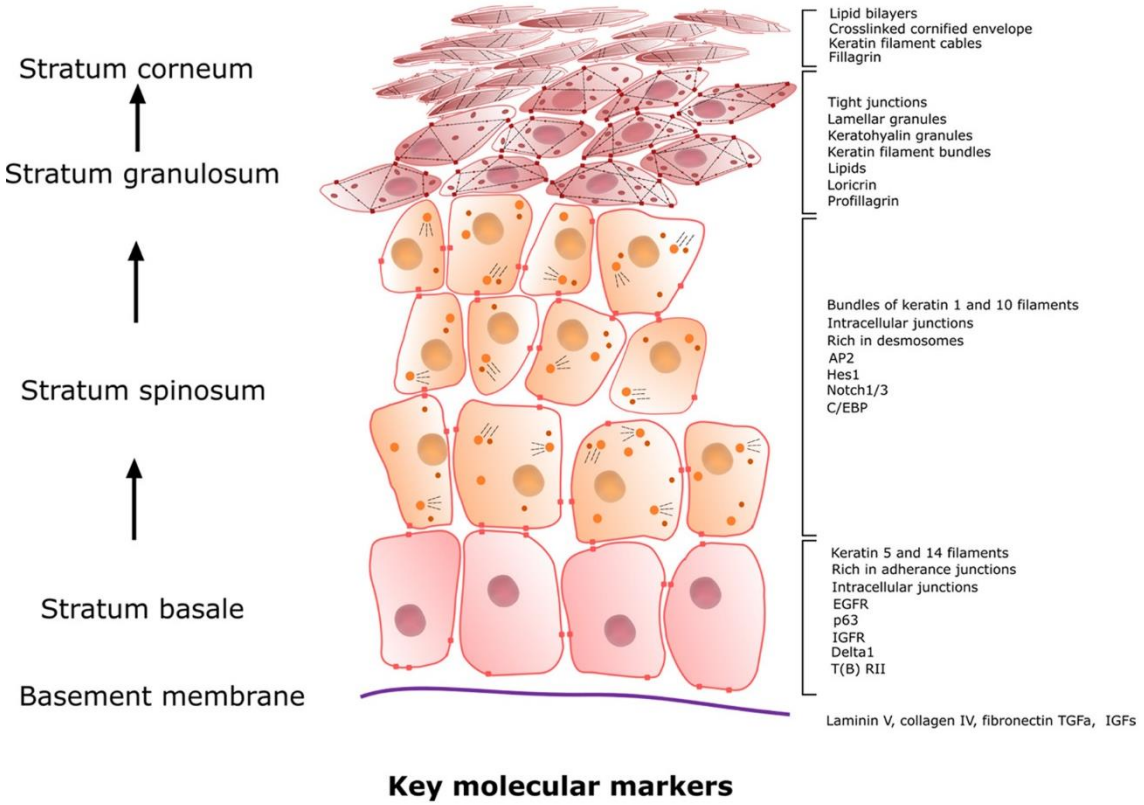

Figure 1.3. The key molecular markers expressed by each layer of the stratified epidermis is listed on the right.
In the early differentiation process, keratinocytes in the spinous layer switch their keratin synthesis from K5 and K14 to K1 and K10, these keratin intermediary filaments build up in the cells cytoplasm, filaggrin proteins bundle these into keratin filaments. In the granular layer the cells have a variety of lipids and enzymes enclosed in vesicles that form the lamellar bodies. At the same time, organelle and cellular degradation starts, resulting in the formation of flattened cells with a mixture of keratin cross-linked by involucrin and loricrin. The lipid covering surrounding the flattened corneocytes is esterified to involucrin, forming the water tight stratum corneum. Cell adhesion in the epidermis is through specialized cell–cell junctions: adherens junctions (AJ), desmosomes, and tight junctions.

increasing number of highly organised, larger, flattened superficial cells with a dispersed and even thickness of keratinised material [30]. The definition of the EPU led to the widely accepted hypothesis that there is one epidermal self-renewing SC per EPU and the other basal cells are TACs (committed cells that are capable of a limited number of divisions before exiting the basal layer and committing to terminal differentiation)[12,30]. In support of this idea it was found that cultured epidermal keratinocytes *in vitro* display three distinct phenotypic colonies; holoclones, paraclones and meroclones [29,31,32]. Holoclones were defined as highly proliferative colonies with a small, round, undifferentiated morphology that are able to be passaged long term. Paraclones are committed keratinocyte colonies with a large, flat, differentiated morphology, typical of terminally differentiated cells. Finally, meroclones are small heterogeneous colonies with a limited proliferative capacity and with a tendency to become senescent after a few passages [31,33]. Although the term holoclone refers to the proliferative capacity of the cells, Rochat *et al.* (1994) showed that the progeny of a single holoclone *in vitro* was able to reform a fully functional epidermis *in vivo* [34]. Therefore, a population of cells within these holoclone colonies must possess the fundamental characteristics of SCs. Meroclones on the other hand, have been linked to TACs [31].

An important factor in the EPU model is that each unit is autonomously maintained by asymmetrical cell division by a slow-cycling basal SC. However, more recent lineage tracing studies suggest that basal SCs do not adhere to the columnar boarders of the EPU model, but instead support an idea that a single SC population makes stochastic fate choices [22,35–38]. This model suggests that most (60-84%) rely on asymmetric divisions to generate one SC and one terminally differentiated cell [38–43]. For decades the accepted epithelial model of

homeostasis was that skin tissue was maintained by two separate population of progenitor cells. A population of self-renewing SCs were thought to give rise to TACs that in turn commit to terminal differentiation and form the distinct layers of the epidermis, in a process named symmetrical division [26,36,44]. However, more recent studies have suggested that this can be replaced with a model in which a single progenitor cell undergoes asymmetric division, replenishing epidermal cells that have been shed from the surface without a TAC [38] (Figure 1.4).

Additionally, it has been demonstrated that the spatial organisation of basal cells correlates with their SC status (Figure 1.5) [8,9,45,46]. Rete ridge structures have been shown to house the cycling cells of the epidermis, with TACs residing in the deep rete ridges, and SCs residing in suprapapillary plate (at the top of the folding that compliments the rete ridges) [8,45–47]. Using Ki67 and BrdU, to identify actively proliferating keratinocytes across different regions of the epidermis, early differentiating cells demonstrated a bias towards the rete ridges, while cells containing high β1 integrin levels were found located at the top of these ridges [45]. This high β1 integrin population were shown to be slow cycling and possess SC properties [46,48,49]. However, it has been shown that this pattern is location specific; in the breast, foreskin and scalp it is in the tip, but it is found to be the other way around in the foot and palm skin, where the SC population is thought to be located in the deep rete ridges in these locations [45]. Rete ridges increase the surface area of the epidermal-dermal junction, helping to provide mechanical stability to the skin [46]. This increased surface area allows for increase capillary-epidermal interface [46]. In skin capillaries protrude from the superficial vascular plexus to the papillary dermis with a close proximity to the epidermal-dermal interface; these are usually found to occur at the suprapapillary plate that occur between rete ridges, where it is thought the SC population resides [46,48,49]. These capillaries

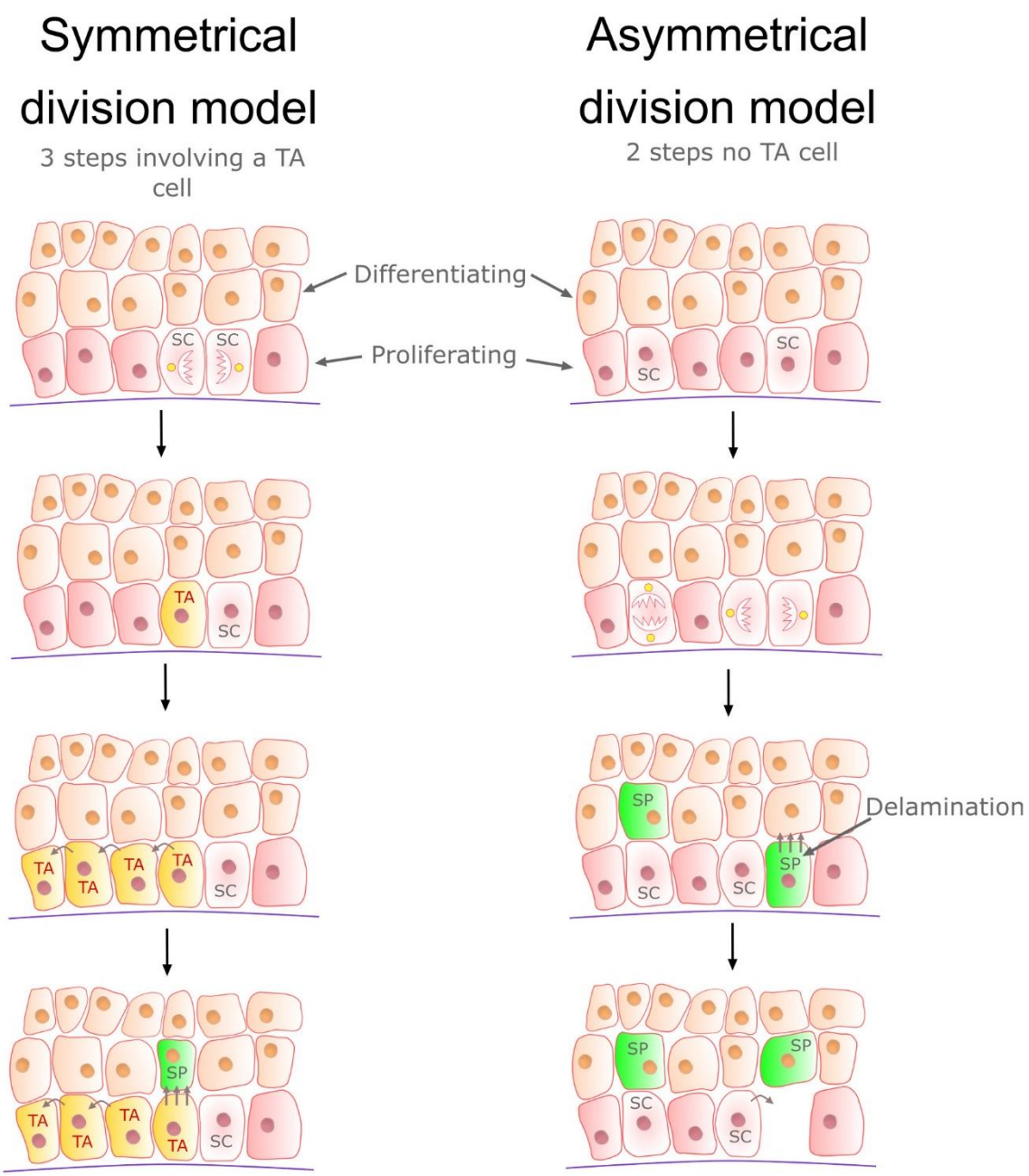

Figure 1.4. The two proposed cell division models for the maintenance of a stratified epithelium.
There are two main proposed models of epidermal division. The two models of epidermal division and subsequent homeostasis are outline in the schematics above. Symmetrical division involves 3 steps; dividing cells in the basal layer undergoing cell division with the spindle plane parallel to the basement membrane enabling the lateral expansion of the stem cells (SCs) generating a population of transit amplifying cells (TACs). Producing one daughter cell that inherits stem-like properties while the other embarks in terminal differentiation. These TACs are able to divide a small number of times before committing to terminal differentiation. Asymmetrical division on the other hand involves a single progenitor cell which undergoes asymmetrical division and replenishes epidermal cells that are shed from the surface without the need for a TAC.

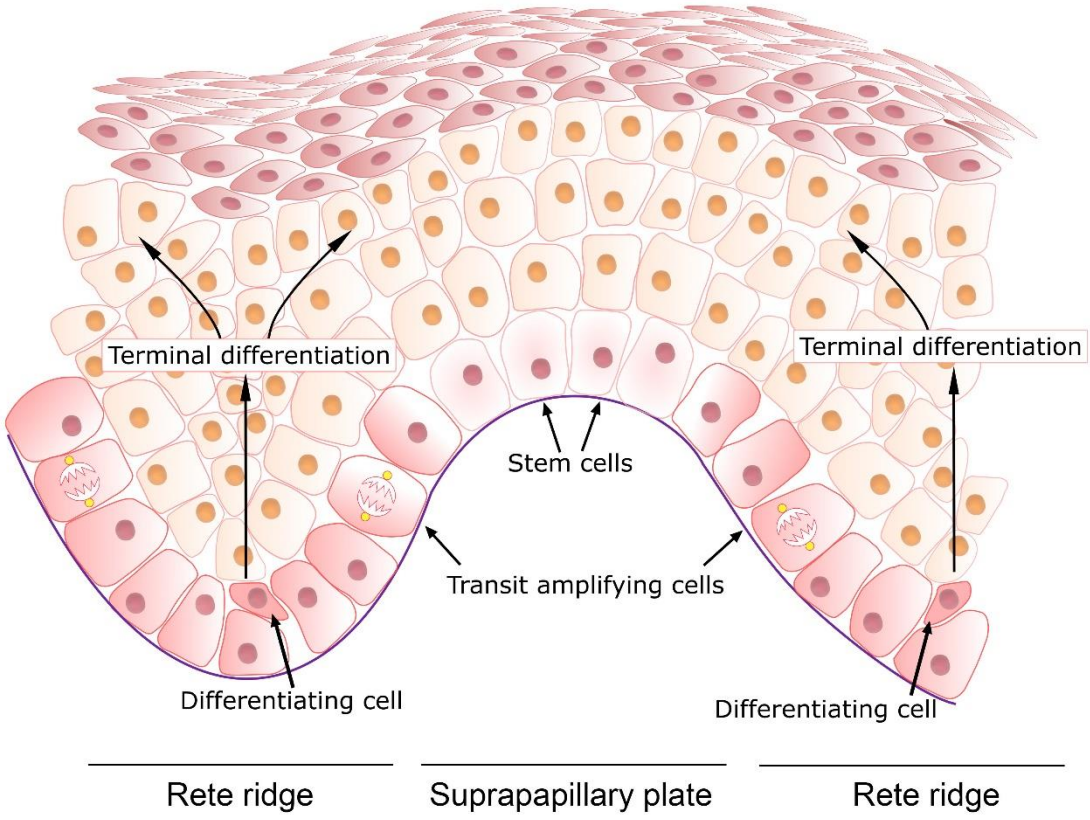

Figure 1.5. Distribution of stem cell and transit amplifying cells in the epidermis.
It is recognised that the spatial organisation of keratinocytes in the basal layer is linked to their stem cell (SC) status. Keratinocytes within rete ridges are transit amplifying cells (TACs) and the SC population are located in the suprapapillary plate (at the top of the folding that compliments the rete ridges) [50,51].

supply the epidermis with nutrients and oxygen and play a role in the temperature regulation through the modulation of blood flow (although most of this is controlled by the superficial plexus rather than the capillary loops) [46,48,49].

As cells commit to terminally differentiate they increase steadily in size, starting in the stratum spinosum, and switch from the expression of cytokeratin proteins K14 and K5 to K1 and K10 [10,15,22]. This switch remains the most reliable method of determining if a cell has committed to terminal differentiation. These suprabasal keratinocytes are known as spinous cells due to their bundles of K1/K10 forming their cytoskeleton that is tightly connected through cell-cell junctions known as desmosomes [52,53], providing a cohesive mechanical stability to the cells. Although these spinous cells have committed to terminal differentiation they are still biosynthetically active [10].

Keratins are the main structural proteins of the epidermis, changes of keratin expression takes place during the process of terminal differentiation, resulting largely through their changes in synthesis [10,11,33]. The transition between these networks is gradual rather than the complete reassembly of the proteins, this helps preserve the integrity of the tissue and the filament network through the differentiation process [20]. These spinous cells produce involucrin, a glutamine and lysine rich envelope protein, deposited into the inner surface of the plasma membrane of the cells [14,54].

As spinous cells differentiate into the granular layer they become permeable, stop synthesising keratin, envelope proteins and make their final proteins such as filaggrin; a histidine rich, basic protein involved in the bundling of thin filaments into macrofibrillar cables [3]. Loricrin is also synthesised at this late stage but becomes a major component of the cornified envelope that is deposited under

the plasma membrane of these granulated cells [11,33]. As a result of their increased permeability, an influx of calcium activates transglutaminase which in turn catalyses the production of y-glutamyl ε-lysine isopeptide bonds creating an indestructible biochemical crosslinks between the envelope proteins, creating the proteinacous sac to hold these keratin macrofibrils [11]. In this granular layer, cells are briefly anabolic but soon enter the destructive stage in which organelles in the cytoplasm are eliminated leaving the keratins as the primary cytoplasmic proteins encased in their cross-linked protein envelope [10]. Keratinocytes in the granular layer contain tight junctions, essential to keeping fluids within the body. Granular cells have a Kelvin's tetrakaidechahendron shape which is perfect to fill space, mechanical strength and maintenance of barrier function [22].

The final step of terminal differentiation involves the destruction of cellular organelles, including the nucleus, and the secretion of lipids, packed in lamellar granules to form the cornified envelope [10]. These dead, enucleated, stratum corneum cells provide an impermeable seal that allows the skin to become impermeable to the external environment [1,12]. Cornified cells are organised in a honeycomb architecture and are embedded in lipids that are not sensitive to UV light, unlike other lipids in the human body. Lipids in the stratum corneum are made up of 50% ceramides, 25% cholesterol and 15% free fatty acids. During epidermal stratification the transitions between layers coincides with lipid modifications. Activities of enzymes can be substantially reduced with changes to pH. Proteases in the stratum corneum function at neutral or slightly alkaline pH, whereas proteases such as phospholipases converting phospholipids into free fatty acids in the stratum basale and spinosum function at a pH of 5-5.5 [44,55].

This outer layer is continuously replenished as inner cells move outwards and are eventually shed from the skins surface [3,14].

1.2.2. Mechanisms controlling epidermal differentiation

1.2.2.1. Molecular control

Epidermal growth and differentiation must be carefully regulated, SCs must replace cells that have committed to terminal differentiation without hyper-proliferation occurring [8,56]. Too little proliferation leads to a thinning epidermal compartment and leads to a reduced structural integrity, however, too much proliferation leads to disorders such as psoriasis or cancer [2,57,58]. Therefore, epidermal homeostasis is essential to its function.

Basal cells receive proliferation cues, such as growth factors and mechanotransduction via cell surface receptors, from the underlying BM [59–61]. The BM is a highly specialised barrier between the dermis and epidermis composed of extracellular matrix (ECM) proteins and growth factors [6,9,36,62,63]. The BM enables the physical separation of the two skin compartments while conferring stability and acting as a dynamic interface between the two, allowing the diffusion of factors across the barrier [19,59]. The BM has been shown to play a major role in the regulation and homeostasis of the SC niche in human skin [47]. At all stages epidermal SCs remain in contact with this BM, rich in ECM proteins and growth factors that are thought to play a major role in the auto-regulatory circuit that guides epidermal SC maintenance and activity [13,47,62]. The BM thickness averages 0.05 μm and it's major components consist of collagen type IV, for strength and resilience enabling the BM to withstand mechanical stress, and laminin, allowing the passage of ions across this barrier, which together form non-covalent networks connected through mono/oligomeric nidogen and perclecan forming irregular polymers [19,64]; additional components of the BM are collagen V and fibrillin.

Through the process of epidermal differentiation, the distinct expression of specific cell-cell junctions can be found throughout basal, spinous and granular keratinocyte populations of the epidermis [65]. The distinct and specific expression of adherens junctions (AJs), tight junctions (TJs) and desmosomes have been identified as critical regulators of epithelial morphogenesis and have been shown to sense mechanical cues, signal to neighbouring cells and respond with short- or long-term cellular responses [18,24,65,66]. The short-term changes in cell-cell adhesion architecture can be translated by cells into long term responses through signalling pathways and transcriptional programmes; all of which play a role in regulating cell proliferation, differentiation and consequently epidermal organisation [18,23,24].

Basal keratinocytes attach to the BM through hemidesmosomes and focal adhesions [67]. Both adhesion complexes adhere to laminin, the main ECM ligand in the BM [60,65,67]. Hemidesmosomes have a transmembrane core of $\alpha_6\beta_4$ integrins, and they connect intracellularly to the keratin network in keratinocytes and extracellularly to the BM helping to provide mechanical strength in the epidermis [62,67,68]. Plectin is a major protein consistent of hemidesmosomes and desmosomes and is responsible for anchoring intermediate filaments (IFs) to the hemidesmosome complex [69,70].

Basal cells also bind to each other as well as the BM; they do this through desmosomes and adherens junctions [3,18,65,71]. In keratinocytes the IF bundles are anchored to and connected through cells junctions called desmosomes [72]. Desmosomes are specialised membrane domains that mediate the mechanics of cell adhesion and cytoskeleton organisation. Through this cohesive complex, this mechanical network allows the epidermis to have a high structural integrity allowing it to resist mechanical stress [52,72]. In the first few days after formation,

desmosomes are thought to be dependent on extracellular calcium levels for their maintenance at the plasma membrane [72]. Desmoplakin is the adaptor protein essential for the formation of desmosomes and like plectin, it belongs to the plakin family [69]. Mutations in desmosomal proteins lead to severe pathologies including epidermal blistering [66]. Although desmosomes are well characterised for anchoring the IF network, desmoplakin has also been shown to regulate microtubule reorganisation in the epidermis [73–77].

AJs are cadherin-based junctions that anchor the actin cytoskeleton to the plasma membrane [18,21,65,78]. Cadherins are a family of transmembrane proteins that mediate calcium dependent cell-cell adhesion; the calcium binding domains in cadherins are highly conserved [53]. E-cadherin is the most prominent transmembrane cadherin in the epidermis [79]. AJs form the physical linkages between cells through both lateral dimerisation on the same cell and adhesion dimerisation between E-cadherin molecules on adjacent cells [80]. There is a steep calcium gradient in the epidermis, with the highest levels of extracellular calcium found in the stratum granulosum [81,82]. This calcium gradient is known to play a role in epidermal differentiation *in vivo*, and changes in the concentration of calcium are well studied for initiating the establishment of cell-cell contacts. Not only does calcium trigger changes to cell-cell contacts but it also activates signalling complexes that change the distribution of cytoskeletal components and increase intracellular calcium concentration that in turn initiates the expression of genes containing response elements for calcium.

TJs, as the name would suggest form a complete seal between the cells, not allowing the movement of ions and solutes between cells (although this seal is not absolute) [21,80]. Calcium concentrations are also known to play a role in the formation and integrity of these cell junctions. The major transmembrane protein

in TJs are claudins which associate with intracellular proteins and anchor strands of the actin and microtubule cytoskeleton to the membrane. TJs are only present in the differentiated granular layer of the epidermis [37]. GAP junctions are another major cell-cell junction, they allow the passage of water and ions between cells, acting as a tunnel between cells [83,84].

1.2.2.2. Cytoskeletal changes

The cell cytoskeleton plays an integral role in the structural integrity of the epidermis through the maintenance of cell shape and polarity throughout the process of terminal differentiation [22,37,66,85,86]. The cell cytoskeleton is comprised of microtubules, actin, and IFs; all of which differ in size, protein composition and function [61].

Microtubules are the largest filaments in the cytoskeletal network, with a diameter of ~20-25 nm (Figure 1.6). Microtubules are composed of α- and β-tubulin heterodimers that assembled using energy from GTP to form cylindrical, hollow structures [87]. Microtubules are polarised structures with two distinct ends. The minus end, within the nucleating centres, are spatially organised and located near the nuclear membrane, while the plus end usually extends out into the periphery of the cell. Microtubules can switch between phases of rapid growth and shrinkage. These structures are very fluid and extremely dynamic, their dynamics are tightly, spatially and temporally regulated, named dynamic instability [87–90].

The microtubule cytoskeleton is responsible for controlling cell morphology, vehicle trafficking, cell polarity, motility, signalling and cell division [91]. Therefore, microtubule reorganisation during epidermal differentiation is essential for morphogenesis. Epidermal stratification relies on two mechanisms, delamination

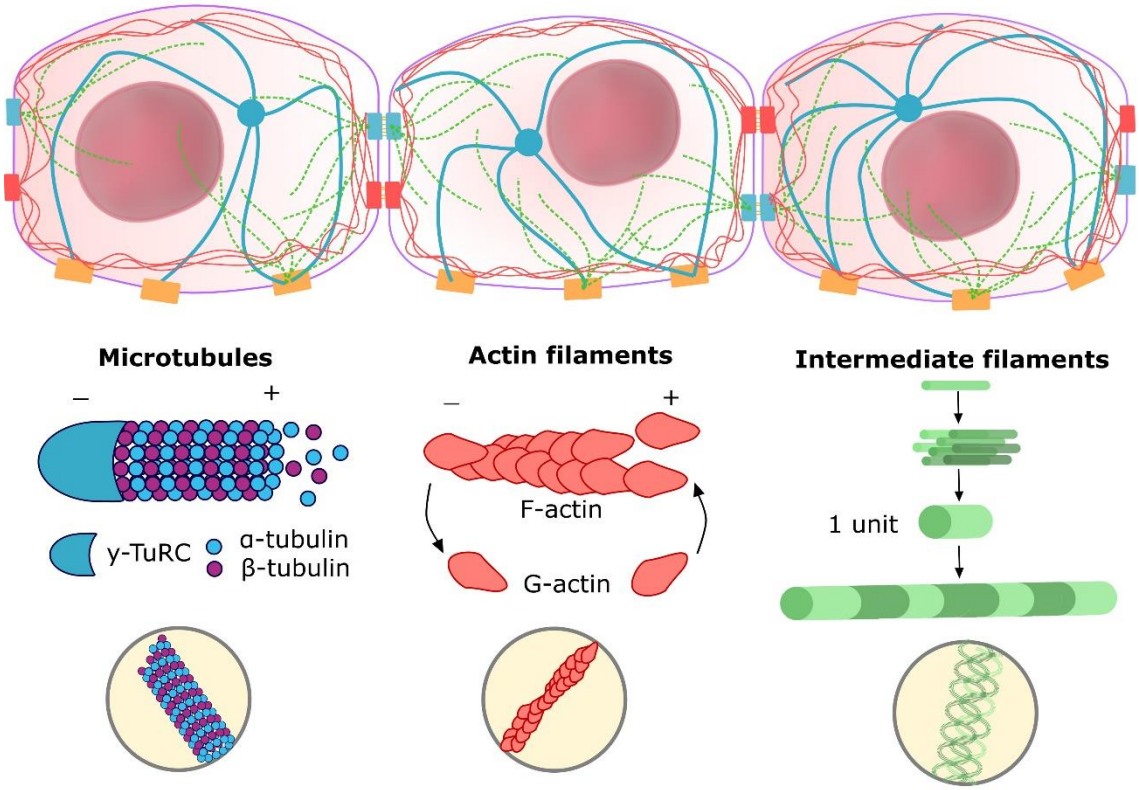

Figure 1.6. Components of the cytoskeleton.
Schematic representation of the three major components of the cytoskeletal network in eukaryotic cells which differ in size and protein composition. Microtubules are the largest filament in the cytoskeleton with a diameter of 25 nm. They are composed of α- and β-tubulin and are characterised by their dynamic instability. Actin filaments are the smallest filaments with a diameter of 7 nm. They are composed of globular actin (G-actin) molecules joined together to form filamentous actin (F-actin). Two F-actin join together to form a helical microfilament. Intermediate filaments (IFs) are as their name suggests mid-sized with a diameter of ~10 nm. Keratins are the major IF in epithelial cells and are strong and rope-like structures. IFs often work with microtubule networks providing support for the more delicate microtubule structures.

and spindle orientation [92–94]. In the stratified epidermis division in the parallel plane confines transiently dividing cells to the basal layer, named symmetric cell division. When cells commit to terminal differentiation cells must either delaminate, exit the basal layer and migrate to the skins surface or rotate their mitotic spindle 90° and divide asymmetrically. During interphase, microtubules initiate the formation of the centrosome, this network of microtubules is responsible for intracellular transport [95–98]. During the process of mitosis this network of microtubules is remodelled to form mitotic spindles allowing duplicate sets of chromosomes to line up and become divided between the two daughter cells. After mitosis, the spindle is dissembled and the microtubule network reassembles during interphase [92].

The process of terminal differentiation involves the assembly of strong intercellular desmosomal junctions and eventually results in the formation of the highly cross-linked, flattened, enucleated dead cells that are shed from the skin surface [9,14,99,100]. During this process of terminal differentiation, both the actin cytoskeleton and IF undergo dynamic reorganisation in their association with adherens junctions and desmosomes, respectively [54,70,86,101–103]. There is also a differentiation specific reorganisation of the microtubule cytoskeleton linked to the desmosomal linker protein desmoplakin [66,72,82,104].

In basal cells, microtubules form a cytoplasmic network stemming from an apical centrosome [66,97]. Whereas in suprabasal cells, microtubules are found to concentrate at the cortical edge with cell-cell junctions [66]. Cells in the basal layer have a cuboidal or short columnar morphology and when they undergo terminal differentiation they flatten and their cell packaging geometry differs between the layers. In mice, at embryonic day 14.5 (E14.5) the microtubule network of basal cells is found to be concentrated at the apical domain of the cells extending

downwards towards the base. In contrast, in stratified cells, the microtubules are concentrated at cell-cell borders and lack an obvious microtubule organising centre [66]. When calcium levels are raised *in vitro* to induce cell-cell adhesion and differentiation, re-organisation of the microtubule cytoskeleton can occur. For example, at early stages after calcium induced differentiation, microtubules concentrate at areas developing cell-cell contact, prominently in the apical domain [102,105]. By 72 h, cells are significantly differentiated, and microtubules concentrate at cell junctions and no longer display the radial association with the nucleus that is observed in keratinocytes maintain in low calcium conditions. The microtubule rearrangements *in vivo* and *in vitro* display a similar phenotype, with basal and differentiated keratinocytes both undergoing a stereotypical rearrangement of the microtubule cytoskeleton, involving a loss of the centrosomal/nuclear microtubule organising centre and accumulation of microtubules at intracellular junctions. The accumulation of microtubules at calcium stimulated cell junctions demonstrates a role for cadherin-mediated junctions in this process.

Desmoplakin connects desmosomal cadherin complexes with its head domain and to the IF cytoskeleton through its tail domain. α-catenin on the other hand, integrates E-cadherin-β-catenin complexes with actin dynamics, essential for the formation of adherens junctions. In transgenic epidermal specific loss of function mouse models, EMTB-3GFP, when compared with wild type (WT) both α-catenin and DP cKO resulted in a relatively normal epidermal microtubule organisation with the microtubule cytoskeleton concentrated at the junctions of the suprabasal cells [55]. In contrast however, the DP cKO models displayed a lack of polarised microtubules, instead displaying cytoplasmic aggregated microtubules [66]. Previously desmosomes and DP were not thought to play a role in microtubule

organisation [52]. When epidermal cells differentiate although the centrosome continues to nucleate microtubules its microtubule anchoring activity is lost. The microtubule anchoring protein ninein is released from the centrosome and relocated in a DP-dependent manner to develop desmosomal cell-cell junctions [66,96], allowing for a robust network of cortical microtubules in the differentiating layers.

Actin filaments are the smallest filaments within the cytoskeleton, with a diameter of 6-7 nm (Figure 1.6) [22,106,107]. They are made from globular actin monomers (G-actin) which polymerise to form a polymer of filamentous actin (F-actin) using the energy from ATP or GTP. Two actin filaments then combine to form a helical microfilament. In many types of cells, networks of actin filaments are found beneath the cell cortex, where they are anchored to the cell membrane through focal adhesions. Actin filaments are involved in cytokinesis and cell movement.

Actin filaments undergo a major reorganisation when cells enter mitosis in which they alter the cell shape through their reorganisation at the cell cortex [24,108]. Specifically, actin filaments at the cell cortex become thinner and promote a transition to a rounded shape; this shape being essential for mitotic spindle formation and function during mitosis. Both during the orientation of the spindle and when sister chromatids are pulled to opposite ends of the cell, the actomyosin cortex provides a rigid scaffold to counteract the forces exerted by the mitotic spindle [24]. Actin is also fundamental in final stages of mitosis in which the intracellular bridge is severed. During epidermal differentiation, the actin filaments become less abundant and their distribution changes. These changes are associated with the changes in AJs, focal adhesions and the loss of integrin receptors that occur during terminal differentiation [24,86].

IFs are, as their name suggests, a size in-between microtubules and actin, and can aggregate into bundles of 7-12 nm (Figure 1.6). Their role is primarily mechanical, in which they act as a scaffold for the cytoskeleton. Keratins are the main structural proteins of the epidermis and changes of keratin expression take place during the process of terminal differentiation, resulting largely through their changes in synthesis [10,11,33]. Keratins are exclusively expressed by epithelial cells and filaments are formed by pairs of type I and type II keratin assembled into filaments. Basal cells have an extensive intracellular cytoskeleton of dispersed network of keratin filaments, consisting of a 1:1 ratio of keratin proteins K5 (58 kDa) and K14 (50 kDa) [10,11]. This network of keratin filaments forms a branching network of attachments within the cells anchoring to the cell junctions, securing keratinocytes in different dimensions of the epidermis. It is this keratin-desmosome and keratin-hemidesmosome network that allows the epidermis to withstand significant mechanical force, enabling mechanical strain to be dissipated/distributed across the epidermis [52,53]. Spinous cells devote a lot of their energy to the synthesis of these new keratin proteins K1 (56.5 kDa) and K10 (67 kDa), forming cytoskeletal filaments that further aggregate into think bundles. [11]. Despite the switch in keratin synthesis, due to the long half-life of simple keratins, approximately 4 days, the presence of these keratins can persist alongside K1 and K10.

All three components of the cytoskeleton depend on each other for their function. Additionally, there have been reports in numerous cell types, of different interactions between the cytoskeletal components [70,109–114]. However, the full scope and complete mechanism of interactions between all the components remain unknown.

1.3. Cutaneous Squamous Cell Carcinoma

Epidermal tumours can be divided into two groups: melanoma and non-melanoma skin cancer (NMSC). Non-melanoma skin cancers are one of the most common forms of cancer in humans, accounting for 20% of malignancies in white populations [115] and originate most frequently in sun exposed areas of the skin.

Approximately 155,985 people each year develop non-melanoma skin cancer in the UK [116]. Basal cell carcinoma (BCC) is the most prevalent form, but although there are many subtypes, they do not often have significant clinical implications for the patient. In parallel to BCC, cutaneous squamous cell carcinomas (cSCCs) have a rich diversity of subtypes with varying clinical behaviours. Although SCC is usually cured through surgical excision, approximately 8% of patients relapse and 5% present with metastasis within 5 years. The prognosis is very poor in patients with metastatic SCC, with only a 10-20% survival rate over 10 years [117]. A better understanding of the early steps of SCC initiation, progression and metastasis is thus needed.

1.3.1. Epidemiology of squamous cell carcinoma

Data suggests that the European incidence rates of cSCC ranges between 9-96 per 100,000 males and 5-68 per 100,000 females [118], while UK incidence rates (2016-2018) were 320 per 100,000 males and 201 per 100,000 females [116]. Although SCC is thought to have a higher incidence in males, SCC originating on the legs has been found to be more common in females [115,119,120]. Systematic review of NMSC cases reveal a notably higher incidence in the South West of England, associated with the highest risk of UV radiation [121,122]. However, the incidence of SCC has been increasing worldwide at an alarming rate, this is thought to be due to changes in lifestyle, ageing population and increased organ

transplantation [118,120]; Incidence increases with age with an average age of mid-60s [123]. In the UK the incidence of NMSC has increased by 42% over the last decade [116].

Despite NMSC being one of the most common cancers in humans, the incidence rates are thought to be highly under-estimated. Policies for the recording of NMSC are varied across the cancer registries and often, although diagnosed cases are reported, registrations are excluded from figures for all cancers in many publications, and from national tumour registries. This is common practice in many cancer analyses and due to this unreliability in estimates variation in policies and practices for diagnosis and treatment have arisen. NMSCs also present in a rich number of subtypes, which makes histological confirmation and definitive diagnosis challenging and variable between practitioners. Registration of NMSC is not mandatory and in some countries the first case in a patient is registered, but any subsequent cases are not recorded [121,122]. Therefore, it is difficult to know the exact incidence rate and the subsequent mortality rates in different countries.

SCC usually develops in sun exposed areas, approximately 55% of cutaneous SCC develops on the head and neck, with 18% on the exterior surfaces of hand and forearms. Other common sites include legs (13%), back and shoulders (4%) and other regions (10%) [119,121,124]; SCC can however occur in any location, including the lips, anus and genitals. Solar radiation that reaches the earth's surface predominately consists of UV (280-380 nm) (UV radiation consists of UVB (280-315 nm) and UVA (315-380 nm)), visible (380-770 nm) and near infrared (770-1000 nm) spectra. UV light is the major risk factor for melanoma and other skin cancers [123]. UV activates a complex cascade of effects in human skin. Inflammation and ROS are key causes of photo-damage, they feed each

other and enhance the downstream cumulative effects. With time UV depletes cellular antioxidant levels and decreases the efficiency of these antioxidant systems which can lead to deoxyribonucleic acid (DNA) damage. The accumulation of thymine dimers as a result of DNA damage can consequently lead to the activation of the neuroendocrine system leading to the release of pro-inflammatory mediators. The inflammation caused and ROS cause oxidative damage to cellular proteins, lipids and carbohydrates leading to their accumulation in the epidermis and dermis, contributing to photo-ageing [125].

Factors that can increase the risk of SCC include Fitzpatrick skin types I and II (photosensitive skin types), sun exposure (outdoor occupations), age, immunosuppression and exposure to human papillomavirus (HPV) types 16, 18 and 31 [117]. Some inherited skin conditions are associated with an increased risk of SCC development. Exposure to UV radiation and sunlight, however, is the greatest risk factor of non-melanoma skin cancer.

1.3.2. Aetiology and pathogenesis of squamous cell carcinoma

1.3.2.1. Molecular phenotype of squamous cell carcinoma

All cancers are thought to share common pathologies and cancer development is based around 2 processes: the acquisition of mutations in genes or regulatory elements leading to a phenotypic consequence, and a Darwinian model of cancer evolution; enabling a selective advantage of mutated cells over cell populations without these heritable genetic variations. Genetic profiling studies have also shown that the skin is able to tolerate a high level of mutations commonly associated with cancer without displaying any signs of tumorigenesis [126]. Sun exposed skin cells are thought to carry thousands of point mutations and around 25-30% of these have an acquired point mutation [126,127]. The frequency of driver

mutations in human skin that remains phenotypically normal skin is remarkably high. It is estimated that 20% of normal skin cells in sun exposed areas carry driver mutations, some in levels that match SCC mutations [127], but do not acquire a transformation to a malignant potential.

In the early 2000s, Professors Hanahan and Weinberg proposed that when cells progress into a neoplastic state they acquire distinct characteristics, called the hallmarks of cancer (Figure 1.7). The hallmarks of cancer include evading cell death, enabling reproductive immortality, inducing angiogenesis, sustaining proliferative signalling, evading growth suppressors, activating invasion and metastasis, all underpinned by genome instability and mutation. This network provided a tool to help understand tumour pathogenesis [128]. In 2011, an updated paper was published to reflect some of the recent advances in the scientific community with additional hallmarks of cancer; avoiding immune detection, tumour promoting inflammation, genome instability and reprogramming of energy metabolism [129].

Under physiological conditions the epidermis is maintained through a tightly regulated, balanced process of differentiation and self-renewal, maintaining the structural and functional integrity of the tissue. Oncogenic lesions usually arise from the uncontrolled expansion of progenitor cells that are carrying driver mutations resulting in a change of cell fate and deviate from the steady state usually maintained within epidermal tissues [130,131]. In SCC the SC population is thought to rise from 1% in the healthy epidermis to 20% in SCC lesions [132,133].

Transcriptome analysis have revealed that thousands of protein encoding transcripts are altered in cSCCs [131,134–136]. cSCCs usually acquire more mutations than other common cancers, they contain over 4 times more mutations than

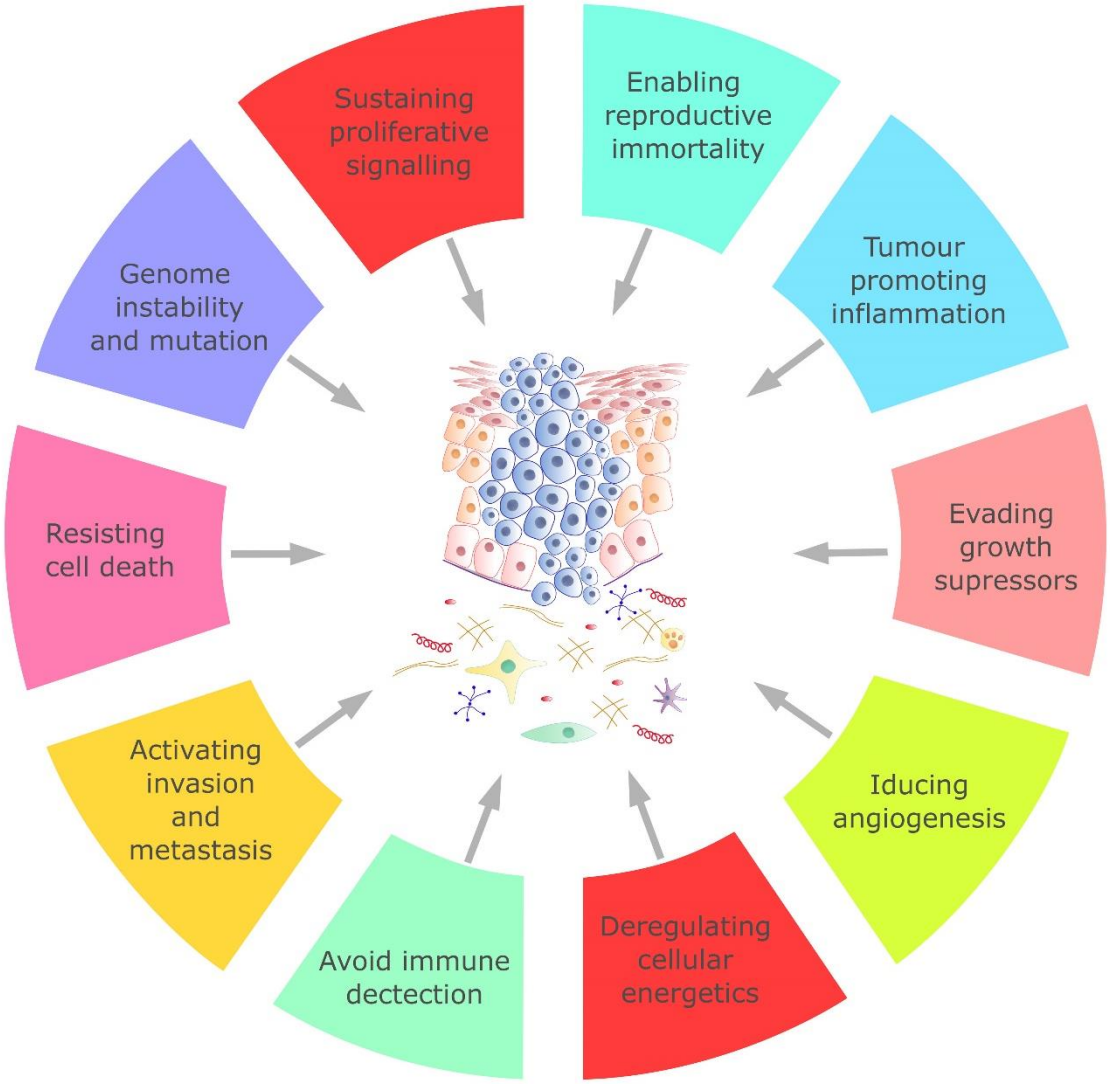

Figure 1.7. Hallmarks of cancer.
The hallmarks of cancer were introduced in the early 2000s by Professors Hanahan and Weinberg, which proposed that when cells progress into a neoplastic state they acquire distinct characteristics. Diagram adapted from [58,129].

melanoma and 5 times more mutation rates than in lung SCC [131,137,138]. Some of the driver mutations of cSCCs include tumour suppressor genes *TP53, CDKN2A, NOTCH 1 and NOTCH 2* and oncogenes *HRAS* and *KRAS* [131,139]*.* Most SCC tumours have a multitude of other genetic mutations that are sequentially acquired in addition to these key driver mutations [131,139]. Mutations in genes *TP53* and *Ras* have been found in sun damaged skin and AKs. These early events in SCC formation enable oncogenic transformation through their alteration of cell cycle dynamics, cytoskeletal changes and decreased apoptosis leading to uncontrolled keratinocyte proliferation. The consequential genomic alteration of other tumour suppressors, such as *TP63,* and oncogenes, such as *MYC* and *EGFR*, contribute to SCC progression.

Tumour protein 53 (*TP53*) is the most common mutated tumour suppressor gene in patients with SCC [57,118,134]. P53 plays a major role in regulating cellular responses to DNA damage and genomic instability. Activation of p53 leads to cell cycle arrest to enable DNA repair to take place, and initiates apoptosis if the DNA damage is irreparable [140]. Most *TP53* gene mutations arise from a single base mutation C → T at dipyrimidine sites, this p53 mutation allows tumour cells to evade apoptosis and clonally expand. UV radiation is well characterised for its enrichment of C → T transitions [135]. Cyclin dependent kinase inhibitor 2A (*CDKN2A*) gene is a protein coding gene responsible for several proteins. The most studied of which are the $p16^{INK4}$ and $p14^{ARF}$ proteins, both of which function as tumour suppressors and mutations have been found to be important in epithelial transformation [136,141]. $P16^{INK4}$ is responsible for specifically CDK4 from phosphorylating the retinoblastoma protein (pRb). $P14^{ARF}$ activates the p53 pathway in response to oncogenic signals by binding to the negative regulator of p53, MDM2, preventing p53 degradation, subsequently causing cell cycle arrest

and apoptosis [136,141]. The inactivation of *CDKN2A* is often found in SCCs through mutations, methylation of the gene promotor or chromosomal loss. Mutations or amplification of *Ras* genes are found in 10-20% of SCCs [141,142]. The overexpression of RAS downstream proteins (MAPK and cyclins) has also been reported in SCCs.

1.3.2.2. Clinical presentation of squamous cell carcinoma

The clinical presentation of SCC is extremely variable depending on the location and subtype. Although many classification schemes for SCC has been proposed, no definitive classification system has been widely accepted leading to the variation in diagnosis across laboratories and hospitals. The first histological grading of SCC was proposed by Broders in 1921 when he devised a four-tiered classification system with grade I, II, III and IV tumours accounting for >75, 50-75, 25-50 and <25% differentiated cells in each lesion compared to undifferentiated cells [143]. However, this system was neglected, and pathologists instead referred to tumours with a more simplistic system as well differentiated, moderately differentiated or poorly differentiated [124,144]. The most recently published guidelines were developed on behalf of the European Dermatology Forum in January 2017 [115,145].

Actinic keratosis (AK), also known as solar keratosis, are cutaneous lesions generally regarded as premalignant carcinomas [146,147]. AKs present in sun-damaged skin as scaly, pink or brown papules or plaques, often with erythematous base. They are often located on the face, scalp or back of the hands and arms. AKs usually arise from significant UV radiation damage in older and middle-aged Caucasians but can be found in younger individuals with chronic sun-damage. Histological analysis of AK lesions usually reveals a solar elastosis

in the dermis and can be used as an indicator of AK. AKs usually present with disorganised phenotype, loss of polarity, nuclear atypia and parakeratosis [146,147]. The atypical cells however do not reach full epidermal thickness, as atypia is usually localised to the basal layer of the epidermis. Abnormal cells in AK rarely extend down adnexal structures, such as sebaceous glands (SB) or hair follicles (HF). Parakeratosis and atypia usually stop in adnexal structures revealing a relatively normal corneal layer, this sparing feature is usually only found in AK.

Six subtypes of AK have been defined as atrophic, hypertrophic, pigmented, acantholytic, bowenoid and proliferative [144]. Atrophic AKs represent a sub-type displaying mild hyperkeratosis, atypical cells with large, hyperchromatic nuclei packed closely together resulting in a thinned epidermis. Hypertrophic AKs are usually thicker and clinically harder to diagnose due to more substrate to the lesion. They are usually located on the arm or back of the hand as these are the most sun exposed areas after the face and scalp. They usually present with evidence of solar elastosis and a thick, hyperkeratotic corneal layer. Pigmented AKs display an increased production of melanin pigmentation, usually restricted to the basal layer, but can also be found in dyskeratotic cells. Bowenoid AK resembles Bowen's disease in that keratinocyte atypia if found almost full thickness in the epidermis. However, it tends to have less disorder, crowding and nuclear hyperchromasia. Proliferative AK is a more recently characterised variant of AK and share similarities with other AKs but are often larger than 1 cm in size with a large spread of atypical keratinocytes in the base of the epidermis with some spread down HFs. They are usually resistant to standard topical treatments some epidermal buds are found infiltrating into the dermis. Because of its histological presentation and its aggressive nature some pathologists argue this is a superficial invasive, well differentiated form of SCC.

SCC *in situ*, traditionally referred to as Bowens Disease, involves atypical keratinocytes extending throughout and filling the full thickness of the epidermis [148]. SCC *in situ* classically displays hyperchromatic nuclei, hyper-cellular dense band of parakeratosis with large, packed, abnormal keratinocytes with full thickness atypia. SCC are associated with acanthosis (thickening of the skin), sometimes vacuole artefacts and the granular layer is usually lost and orthokeratin is replaced with parakeratin, but this is not always the case. When the granular layer is diminished and parakeratosis is observed it is usually when the epidermis is growing too quickly and there is not enough time for the normal process of differentiation to take place. In normal skin as the keratinocytes move from the basal layer to the corneum and undergo terminal differentiation, then developing a granular layer in which they break up their nucleus and the cellular components die. The keratin from the dead cells helps to produce the impermeable stratum corneum. However, when the cells are growing too quickly they do not have enough time to develop. In turn, the nuclei are retained and trapped in the corneal layer and pushed to the top, resulting in parakeratosis. This parakeratosis is therefore an indicator that the epidermis is not maturing normally and the cells are growing too fast or something is preventing the normal process of terminal differentiation. In AK or SCC lesions the adjacent normal epidermis usually presents with a thickened granular layer or licenification. This chronic reactive change is from repeated scratching or rubbing of the skin. In both AK and SCC people tend to pick or scratch their lesions, so this is often found adjacent to AK or SCC. SCCs *in situ* can also present with an eyeliner morphology, where the cells start to fill up the epidermis and spread out to the periphery, filling the epidermis, but leaving the normal uniform, monotonous keratinocytes of the basal layer intact. Pagetoid spread, where an individual cell

proliferation is found in the upper layers of the epidermis, is usually found in SCC and can be a distinguishing factor between AK and SCC *in situ*. These atypical cells are often found away from the main tumour and scattered and spread up into the adjacent epidermis.

The clinical appearance of SCC is largely defined by the level of differentiation of the lesion [118,119,148]. Well-differentiated lesions usually present as thick, scaly plaques, in contrast poorly differentiated SCC is often not scaly but instead presents as soft and ulcerated or as haemorrhagic [119]. The histological presentation of SCCs can also vary from dark blue to glassy pink. Keratinocytes can appear with an abundant glassy cytoplasmic phenotype in the epidermis of SCC lesions due to increased spinous layer containing K1 and K10. When an abundance of glassy keratinocytes is observed in patches of atypical cells moving down into the dermis often invasion is suspected. When the atypical cells break through the BM they tend to have paradoxical maturation and begin to shift their morphology from basal obtaining spinous cell characteristics. The contact with the collagen in the dermis causes the keratin expression to shift from K14 and K5 to K1 and K10.

It is estimated that up to 5% of SCC *in situ* become invasive, with approximately 20% developing metastasis [57,115,143,144,148,149]. However, it is not always a step like progression from AK, to *in situ* SCC to invasion. Invasive SCCs display full thickness atypia with invasion into the dermis. Necrosis is often observed in the centre of the nests and when the cells die, leaving large amounts of keratin which stains as bright pink patches in histological staining, helping to diagnose SCC, as other types of NMSC do not tend to display the same keratin phenotype. Sometimes invasive SCC can display a relatively normal epidermis with invasive nests below, for example SCC *in situ* can be found with nests only displaying

under the adjacent epidermis. Some lesions that are biopsied do not allow enough breath for diagnosis when the base is transected it is impossible to see what is happening below. This usually arises when there is a very thick hypertrophic, hyperkeratotic corneal layer which results in the regular depth of the excision not being sufficient to reach the base of the lesion. In these cases, the lesion is either biopsied again or carefully monitored. Sometimes tangential cutting can lead to misinterpretation of metastasis; islands can sometimes look like invasion when it is just hair follicles (HF) or sebaceous glands (SG) that the atypical cells have migrated down and the angle of the cut has resulted in a nest-like phenotype. In these samples. In these cases, the basal layer of the HF or SG should still look intact, whereas a budding nest of invasion will display an irregular keratinocyte morphology with tiny islands pushing out into the dermal collagen and solar elastosis [119,144]. Keratin pearls, a swirl of parakeratosis trapped within a nest of invasive carcinoma keratinocytes, are often characteristic of SCCs. Patients with invasive SCC usually present with a persistent ulcer or a non-healing wound.

1.3.3. Prognosis and current therapies of squamous cell carcinoma

Surgery is the main treatment for non-melanoma skin cancer [119,124,147,150]. It involves removing the cancerous tumour and some of the surrounding skin. Treatment is usually successful as, unlike most other types of cancer, there is a considerably lower risk that the cancer will spread to other parts of the body. However, although SCC is usually cured through surgical excision approximately 8% of patients relapse and 5% present with metastasis within 5 years. The prognosis is very poor in patients with metastatic SCC, with only a 10-20% survival rate over 10 years [115,117]. Metastasis is not only linked to tumour growth but can be controlled by other means such as epithelial-mesenchymal transition

(EMT), which allows cancer cells to dedifferentiate and acquire enhanced migratory and invasive properties. Well differentiated SCCs tend to possess a lower metastatic potential. Approaches to induce differentiation in early and or late stages of cancer therapies have been reported to be successful in SCCs [151,152]. Typically, SCCs are removed through surgical resection and a topical treatment of 5 FU is also used [150]. Interestingly, it has been reported that medications that target other skin cancers such as BCC or melanoma can lead to the formation of SCCs [153].

Although overall NMSC has a low mortality rate, it does still have an impact on patient quality of life and given its increasing incidence rates around the world it is emerging as a public health problem. An increased knowledge into the early alterations, biomarkers for metastatic potential and drivers for SCC will help develop new approaches for therapeutic interventions and management.

1.3.4. Cytoskeletal changes in squamous cell carcinoma

There are many changes that take place for each component of the cell cytoskeleton during cancer. Furthermore, the cytoskeleton can contribute to cancers by inducing ad supporting proliferation, activation of genes, invasion and metastasis [154–158].

Actin binding proteins, such as fascin, have been linked with the progression of cancer and resistance to some chemotherapies [154,155]. Fascin can organise F-actin into parallel bundles and are needed for the formation of cellular protrusions, thus playing an essential role in the migration and invasion of tumour cells. Alongside actin filaments, myosins can play role in cancer progression. Myosins convert chemical signals into mechanical force by moving along actin filaments through the hydrolysis of ATP. They also take part in cellular functions such as

migration, signal transduction, tumour suppression and adhesion. In SCCs, reduced myosin expression has been linked to tumour invasion and poor prognosis [158].

The epithelial-mesenchymal transition (EMT) is a complex process in which epithelial cancer cells acquire a mesenchymal phenotype, become more mobile and gain the ability to migrate away from the primary tumour site [159–163]. Subsequently large changes in cell polarity, cell junctions and the cytoskeleton take place. The actin cytoskeleton plays a major role in the process of EMT and the acquisition of a mesenchymal phenotype [164,165]. The formation of a leading edge in cancer cells requires the polymerisation of G-actin into F-actin, interaction with binding and contracting proteins all of which facilitate tumour cell migration and EMT [155,158].

The IF cytoskeleton in SCCs reflects the tumours differentiation status, and unlike healthy human skin, the switch in keratin synthesis is not as tightly regulated [136]. Due to acanthosis that usually occurs in SCC, a high number of cells have a K1:K10 IF network. Unlike in healthy human skin, parakeratosis is usually observed in the corneal layers as the IF network is not correctly broken down in the granular layer. IFs play a significant role in the EMT process in cancers, typically switching the expression of keratins to networks of vimentin [154,155]. E-cadherin is one of the cell adhesion molecules that has been shown to regulate EMT, and its reduced expression is regarded as an indicator of EMT [102,155]. Although a lot of research has taken place to investigate cytoskeletal changes and changes to cell adhesion in cancer, more in depth knowledge of the dynamic expression, re-arrangement and interactions of the cytoskeletal components during cancer initiation, invasion and migration is needed in order to develop more targeted therapies.

Microtubules are essential for many cellular processes including, but not limited to cytoskeletal assembly and function [158,166–168], and the regulation of the mitotic spindle during the process of mitosis [169]. The cytoskeletal rearrangements are essential in cancer, from their ability to migrate to their ability to metastasise. This importance of microtubules in cell division has made them an obvious and effective target for many cancer therapies [154,156,169–173]. Tubulin binding agents or microtubule inhibitors are important chemotherapeutic drugs as they can interfere with spindle dynamics, mitotic arrest and subsequent cell death in rapidly dividing cells [102,154,156,169–172,174]. These microtubule inhibitors can be divided into two groups; those that disrupt tubulin assembly and deplete microtubule levels (colcemid, colchine and vinca alkaloids) and those that promote assembly, increase tubulin density and cause stabilisation and bundling (taxanes and epothilones) [88,112].

Changes to the microtubule network occur in a wide variety of cancers, including tubulin isotype expression, posttranslational modifications, and changes to the expression of microtubule associated proteins (MAPs) [170,172]. The most well studied and characterised alteration in cancer is the tubulin isoform expression [172]. In humans there are 8 α-tubulin isotypes and 7 β-tubulin subtypes, tissue specific and developmental expression patterns [172]. Changes to the tubulin isoform expression in cancers have been linked to chemotherapeutic resistance and poor prognosis [172]. Specifically, βIII-tubulin is the most well characterised isotype across human cancers and elevated βIII-tubulin are associated with tumour development, aggressiveness and have been linked with poor prognosis in epithelial cancers [156,172,173]. High βIII-tubulin expression has also been shown to confer a decreased sensitivity to a broad spectrum of drugs not only tubulin targeting agents [172]. The microtubule network also exhibits a number of

posttranslational modifications, however very little is understood about the impact and regulation of these modifications [172].

A vast number of proteins are known to interact with tubulin, but the interaction of MAPs with tubulin have been shown to influence tubulin dynamics, chemotherapy efficacy and tumour behaviours in a wide variety of cancers [171,175]. However, the effect of MAPs in cancer cells is complex and further research to understand the functional consequences of these MAP proteins in various cancers is still required.

1.4. Microtubule associated protein tau

Since its discovery in 1975, microtubule associated protein tau (*MAPT*) has been a major subject of study, primarily in neurodegenerative research [176,177]. Tau was one of the first MAPs to be analysed, being discovered and characterised by Marc Kirschner and his team when trying to determine the associated factors involved in the self-assembly of tubulin sub-units into microtubules [176]. Tau research continued investigating its role in the stabilisation and regulation of microtubules dynamics in neurons and other cell types [178–181]. Research into the protein tau then gained momentum when it was found that tangled forms of this protein made up the paired helical filaments (PHFs) in the brain of Alzheimer's disease (AD) patients [177]. These PHFs, mainly composed of hyper-phosphorylated forms of tau, progressively disrupt the cytoskeleton of neurons leading to a lack of function, cell death and consequently neurodegenerative diseases, such as AD and frontotemporal Dementia.

Under physiological conditions tau's main, and most studied function is to promote micro-tubule assembly and stability. Tau plays a role in promoting tubulin polymerisation by binding to tubulin sub-units and stabilising microtubules, thus

supporting the cytoskeleton during cellular processes such as differentiation, polarisation and mitosis [182–185]. Tau has also been shown to play a role in axonal transport and neuronal polarity, morphogenesis and outgrowth [186]. Tau has two main ways to regulate microtubule stability; isoform expression and phosphorylation status [187,188].

1.4.1. *MAPT* gene and isoform expression

The tau protein is encoded by the microtubule-associated protein tau (*MAPT*) gene located on chromosome 17q21.31 [188]. The *MAPT* gene has 16 exons, with exons 0 and 14 transcribed but not translated and exons 2, 3, 4A, 6, 8, 10 and 14 alternatively spliced (Figure 1.8). There are 12 confirmed transcript variants of tau (Table **1**.**1**); alternative splicing of exon 2, 3 and 10 yields the 6 functional variant isoforms of tau found in the central nervous system (CNS), ranging from 352 to 441 amino acids in length and 60-74 kDa on SDS-PAGE (Table **1**.**1**) [187]. However, in the peripheral nervous system (PNS) and other tissues in the human body other transcript variants of *MAPT* messenger ribonucleic acid (mRNA) can be found, some of which

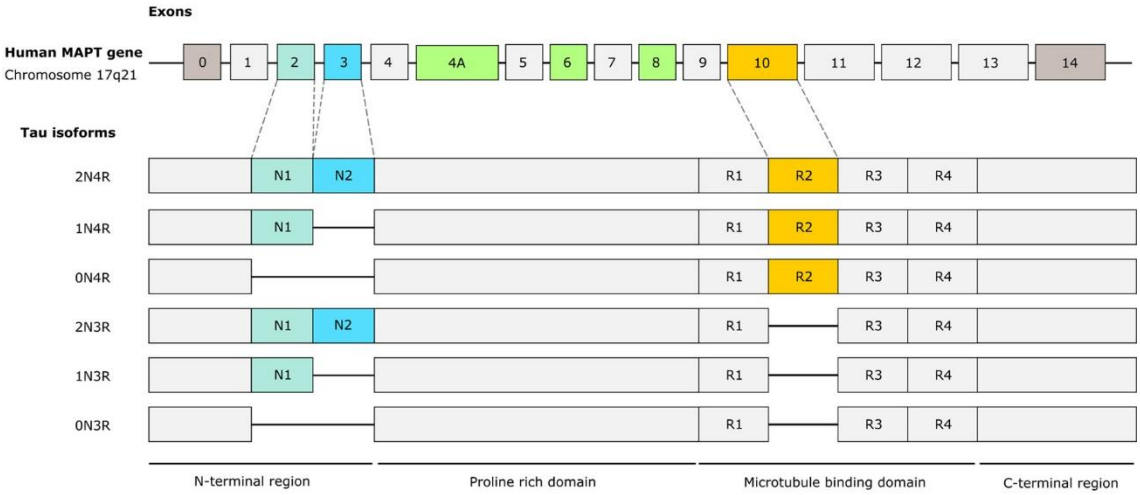

Figure 1.8. The *MAPT* gene, protein isoforms and structure.
The *MAPT* gene located on the long arm of chromosome 17 has 16 exons. Exon 0 forms part of the 5' untranslated region of the *MAPT* messenger ribonucleic acid (mRNA). Exon 4A, 6 and 8 (green) are rarely expressed in the brain but are transcribed in the mRNA of most peripheral tissues. Exon 14 forms part of the 3' untranslated region of the *MAPT* mRNA. Alternative splicing of exon 2 (cyan), 3 (blue) and 10 (yellow) generates the widely recognised six isoforms of tau. Structurally divided into four regions, and N-terminal acidic region, a proline rich domain (PRD), microtubule binding domain (MTBD) and the C-terminal region. Diagram adapted from [189].

Table 1.1**.Human microtubule associated protein tau (*MAPT*) recognised transcript variants.**

NCBI transcript variant	Accession number	Number of exons	Ensemble	Number of base pairs (bp)	Inserts/repeats	Number of amino acids (aa)	MW (kDa)	Apparent MW (kDa)
6	NM_001123066	15	*MAPT*-205	6644	2N4R	776	80	120
1	NM_016835	14	*MAPT*-212	6590	2N4R	758	77	110
2	NM_005910	12	*MAPT*-204	5639	2N4R	441	45.9	67
8	NM_001203252	11	*MAPT*-207	5546	2N3R	410	42.6	59
5	NM_001123067	11	*MAPT*-206	5552	1N4R	412	43.0	62
9	NM_001377265	13	*MAPT*-201	6815	1N4R	833	84	-
7	NM_001203251	10	*MAPT*-209	5459	1N3R	381	39.7	54
10	NM_001377266	11	*MAPT*-203	6524	1N3R	736	74	-
11	NM_001377267	9	-	4139	1N3R	280	28	-
3	NM_016834	10	*MAPT*-208	5465	0N4R	383	40.0	52
12	NM_001377268	10	-	5525	0N3R	352	36.7	48
4	NM_016841	9	*MAPT*-202	5372	0N3R	325	33	-

There are 12 recognised isoforms of tau and 8 predicted transcript variants. Transcript variants 2, 8, 5, 7, 3 and 12 are the six widely reported isoforms found in the CNS [178,190,191]. Additional information on the exact inclusion of exons in each transcript variant is displayed in Table 10.1.

include exon 4a within the proline rich domain of the transcript that results in a higher apparent molecular weight (Table 1.1 and Table 10.1.) [192–199].

Ribonucleic acid (RNA) splicing was initially discovered in the 1970s and involves the removal of certain sequences, often referred to as intervening sequences, or introns. The final mRNA construct therefore consists of the remaining sequences, called exons, which are connected to one another through this splicing process [200]. In 1977, it was also shown that, not only were introns excised but that alternative patterns of splicing within a single pre-mRNA molecule could yield different functional mRNAs, each containing different combinations of exons, a process which is now known as alternative splicing [200]. Alternative splicing enables mRNA to direct the synthesis of isoforms (protein variants) that may have different properties or cellular functions [201–204]. Alternative splicing of pre-mRNAs allows for an increase in phenotypic diversity without the corresponding increase in genome size [205–208]. The process of alternative splicing has been shown to play an important role in highly complex developmental pathways, such as the brain, heart, bone and skin [209,210].

The multiple isoforms of tau exist as a result of alternative splicing of the *MAPT* gene [193,211,212]. The cellular sub-localisation of tau isoforms has also been found to vary through different developmental stages within tissues, across different cell lines, tissues, brain regions, through differentiation status and intracellular compartments [188,212–217]. For example, in SH-SY5Y cell lines, both high and low molecular weight tau exist, localising to either the cytoplasm or the nucleus, depending on the differentiation status of the cells [218]. It is widely accepted that tau isoform expression in the brain depends on neuronal maturation and type; during normal brain development alternative splicing of tau results in a shift from short to long isoforms [212,213]. The smallest isoform, 0N3R, is predominantly found

in foetal brain, expressing three microtubule binding repeats on its C-terminal and zero N-terminal inserts, and it is usually referred to as foetal tau [191,219]. The other 5 well known isoforms of tau are larger and usually found in adult tissues, with three or four microtubule binding domains and the presence or absence of 1 or 2 N-terminal inserts [193,212–214]. Short tau isoforms, 3R, have a decreased affinity for microtubules due to reduced microtubule binding sites, suggesting their expression during development allows greater cell plasticity. Postnatal expression however, displays a shift to longer, mature, tau isoforms, indicating a role in stabilising micro-tubules in mature tissues. Although it is reported that tau exons 2, 3 and 10 show developmental changes, it was not clear if other paralogous microtubule associated proteins displayed a similar expression pattern [212]. For example, using multiple publicly available, de-identified transcriptomic datasets, Hefti *et al.* (2008) showed that exon 2 and 10 displayed marked changes in splicing not seen in any other gene or exon in the MAP family in humans [212]. Although tau exon 3 did not show any significant change, many papers have demonstrated a significant increase in 2N with age. Exon 10 expression has been shown to display the most significant transition in alternative splicing; increasing dramatically in the perinatal period, reaching a plateau that continued throughout childhood and adult life [212]. Exon 2 also displays a developmental transition reaching a plateau at 10 years old, whilst in the brain exon 3 may only show a small change in expression with age [212].

1.4.2. Structure and function of tau

1.4.2.1. The structural basis of tau binding

Tau can be structurally divided into four regions: an N-terminal acidic region, a proline rich domain (PRD), repeat domain region and a C-terminal region [220–222].

The precise epitopes across these regions may vary depending on alternative splicing and tau isoforms generated. The N-terminus of tau binds to plasma membrane components while the C-terminus binds to microtubules suggesting that tau can act as a linker protein between the two [221,223,224].

Tau has been characterised as a naively folded, intrinsically disordered protein (IDP), therefore lacking a well-defined three-dimensional structure, retaining a flexible conformation that is important to its role in cellular processes [221]. The hydrophilic nature of tau means it does not adopt the traditional folded structure displayed by many cytosolic proteins, rather various biophysical studies have shown that tau is instead natively folded and intrinsically disordered [178]. The polypeptide chain is highly flexible with a low content of secondary structures that are very transient therefore allowing high mobility of the protein (α-helix, β-strand and poly-proline II helix). Tau also has some secondary structure, but the precise folded structure of tau has been hard to characterise as most studies are performed in structure-inducing buffers [221,225]. Although recent studies have found ways to overcome some of these issues and using fluorescence resonance energy transfer and electron paramagnetic resonance have found that tau folds into a paperclip-like structure, whereby the two ends of the tau protein approach each other and the repeat domain [226] (Figure 1.9). The C- and N-terminal domain folded into the MTBD, with the N-terminal domain the outer arm of the paperclip. Although it is expected that this interaction and structure is specific, it is weak and fluctuating, as the stabilisation of this folded state could actually have pathological consequences removing tau's intrinsically disordered protein phenotype and abilities [226].

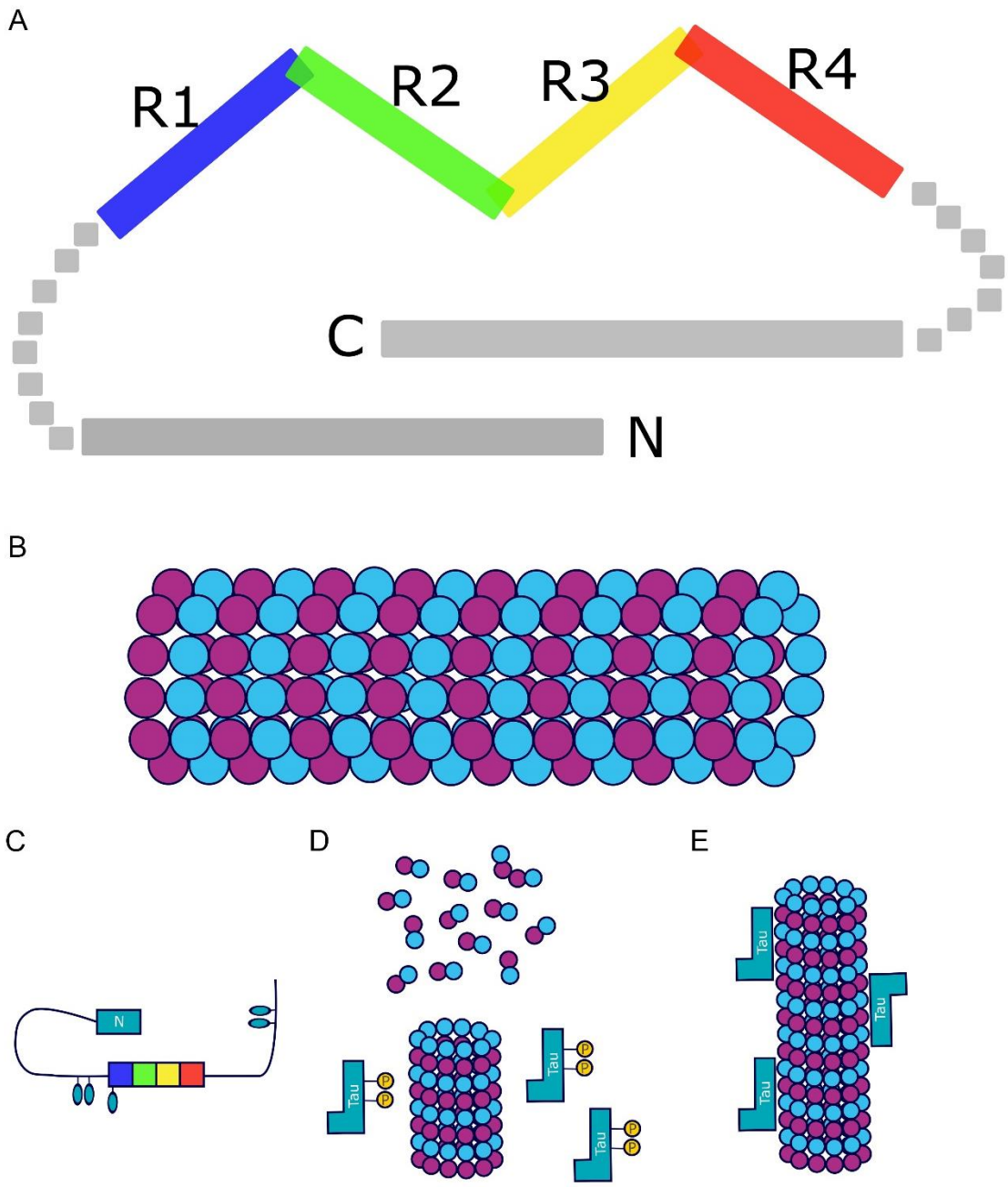

Figure 1.9. Tau protein structure and function.
A. Schematic demonstrating the structure of 2N4R tau under physiological conditions. The microtubule binding domain is displayed with different coloured repeats: R1 – blue, R2 – green, R3 – yellow and R4 - red. The N- and C-terminal domain repeats shown folding over this microtubule binding domain. The C-terminus domain has been shown to fold over the repeat domain, with the N-terminal domain folding over the C-terminus in a paperclip like structure. **B.** Example structure of microtubules, composed of α- and β-tubulin heterodimers displayed as blue and purple respectively in the figure. **C.** Schematic of tau demonstrating how phosphorylation can affect tau structure. **D&E.** Under physiological conditions the phosphorylation of tau can help regulate its binding affinity for microtubules, enabling its function in microtubule dynamics, transport and growth [226].

Tau is unusually highly soluble protein; it is around 27 times more soluble than an equivalent compact protein [178]. It is this high solubility that indicates that tau could be able to bind to many other proteins within the cell.

1.4.2.1.1. N-terminal domain

The N-terminal residue is mostly acidic and projects away from the microtubule surface. The remainder of protein has basic character, complementary to the acidic surface of microtubules [224,226]. The N-terminal domain has also been described as a polyelectrolyte polymer brush and may exert a repulsive force. It is thought that the N-terminal domain folds over the repeat domain, consistent with electrostatic interactions since the N-terminal domain and repeats have opposite net charges [226]. However, despite this hairpin folding, the mobility of the chain remains high throughout. It has been suggested that the N-terminal region of tau remains highly flexible and disordered even after binding to MTs [227].

Studies have shown that tau can act as an anchor for other cell components such as kinases, phosphatases, or plasma membrane proteins. The N-terminus has been primarily linked to it binding to these structures. The N-terminal domain of tau also binds to neural plasma membrane components, acting as a linker protein between plasma membrane and the microtubule network [216,223,224]. The N-terminal domain has further been linked to the regulation of microtubule spacing [199]. The knockout (KO) of the tau gene in mice has been shown to result in altered microtubule organisation in smaller axons [228]. Additionally, when tau constructs were used *in vitro,* transcript variants containing 0N4R, 2N4R and deltaNT (4R tau with its N-terminal domain deleted except for the part of the PRD which has been shown to be crucial for tau binding to MTs), deltaNT showed no detectable MT bundling, whilst 0N formed bundles, but to a lesser extent than 2N [229].

Highlighting that the N-terminal domain of tau does influence microtubule dynamics and the function of the tau protein, and how the expression of 0N in foetal life might enable greater microtubule plasticity.

1.4.2.1.2. Exon 4A, 6 and 8

Exons 4A, 6 and 8 are only expressed in peripheral tissues and not usually translated in the brain. Overall, very little attention has been directed into discovering the splicing regulation of these 3 exons in tau, as they are not key to the pathologies for which tau is widely researched. Instead, most of the attention has been directed to the alternative splicing of exon 2, 3 and particularly exon 10, all known to contribute to the pathology associated with tau. Despite this, some groups have worked to elucidate the function of exon 4A, 6 and 8.

The high molecular weight isoform of tau, ~110 kDa with the inclusion of exon 4A, was discovered in 1990s in the PNS, optic nerve and in cell lines derived from the neural crest [194,195,199]. The inclusion of exon 4A elongates the tau transcript and therefore protein and causes the N-terminal region to be further away from the microtubule binding domain, in turn increasing the spacing between MTs through its larger projection domain; spacing between microtubules in cells has been shown to range from 79–260 nm. Microtubule spacing allows the microtubule surface to be more accessible than their tightly packed counterparts, which is thought to help facilitate organelle and cargo transport [229,230]. It is hypothesised that the inclusion of exon 4A also improves axonal transport in peripheral tissues, protecting against the formation of pathological structures (aggregated tau in AD lack the inclusion of exon 4A). Interestingly, unlike the rest of the tau protein which has many sites of phosphorylation, the inserted region from exon 4A only has two phosphorylation sites [199].

Little attention has been directed to the expression of exon 6 and exon 8 in tau transcripts. Exon 6, originally thought to be a cassette, is found in both foetal and adult tissues, but is more highly expressed in adult tissues. However, very little is known about the expression and function of exon 6. Strangely, exon 8 is not usually found in human tissues and its function is not yet understood, but is widely expressed in bovine mRNA [193] (Table 10.1.).

1.4.2.1.3. Proline rich domain

MTBDs are needed for interaction with microtubules, but interestingly studies have shown that an isolated fragment containing only the MTBDs of tau is not as efficient in MT binding or tubulin polymerisation as full-length tau is. It was shown that the regions flanking the MTBD of tau, the PRD and C-terminal region, are important to enhance the binding of tau to MTs [227]. Some models suggest these regions enhance tau binding to MTs, albeit the exact mechanism is unknown. Other models include a “jaws” model, whereby the PRD, MTBD and C-terminal domains bind weakly to MTs, and binding is enhanced when two or more consecutive domains are associated with a single construct. Another model suggests that the initial binding of tau to microtubules is regulated by a MT-binding core within the MTBD and the flanking regions are regulatory [227]. It has been suggested that the PRD of tau, alongside the MTBD, plays a role in the proteins interactions with actin [231]. Although tau is an intrinsically disordered protein, it does have a tendency to form secondary structures, in particular β-strands in the MTBD and polyproline helices in the PRD [227].

1.4.2.1.4. Microtubule binding domain

Tau binds longitudinally along microtubules, spanning residues 242-367, covering the MTBD of tau. This direct interaction between the MTBD and

microtubules are thought to arise through the overall positive charge of the MTBD which interacts with the negatively charged residues of the tubulin monomers [179,181,225]. Studies have suggested that tau binding to microtubules is based around α-tubulin subunit with β-subunits detected on both sides. It is thought that R1 acts as the attachment point for tau binding to microtubules. However, most studies use taxol to study tau interactions with microtubules as taxol will stabilise microtubules and decrease the dynamics of the system. However, it has been shown that taxol displaces tau from microtubules due to competitive binding. This is thought to occur because the tau binding site to tubulin overlaps with the taxol binding site that is located ion β-tubulin on the inner surface of MTs [227]. This poses some limitations on the ability to study tau's structural formation using exogenous agents, such as taxol, but it is very difficult to study MTs in the absence of these stabilising agents due to MTs dynamic instability.

The 3-4 microtubule binding domains and the proline rich domain regulate growth rates and dynamics of microtubules. Prezel *et al.* (2017) used total internal reflection fluorescence to investigate how tau promotes microtubule assembly *in vitro*. This study demonstrated that 4R tau inhibits microtubule shrinkage and promotes growth, consistent with tau 4R microtubule stabilising activity [232]. Therefore, it is logical that shorter isoforms have decreased microtubule binding affinity and it has been reported that the inclusion of exon 10, and consequently the fourth microtubule binding domain, increases tau's affinity to bind to microtubules three-fold [222].

Consequently, it has been demonstrated that tau transcripts containing 4 MTBDs have an increased likelihood of aggregation. Furthermore, humans and mice with mutation in exon 10 show predominantly age-related neurodegenerative

phenotypes, not developmental phenotypes [192,212]; linked to the increased expression of 4R through an organisms lifetime.

1.4.2.1.5. C-terminal domain

Although the MTBD are thought to be the primary site directly binding to microtubules, some studies have provided evidence that tau can bind directly to microtubules with its N- and C-terminal domains. Studies have shown that the C-terminal domain can help regulate the interaction of tau with microtubules and with the plasma membrane [216,223,224].

1.4.2.2. The cellular localisation and function of tau

Tau is well known for its function in the promotion of assembly and stability of microtubules. However, in addition to its cytoskeletal localisation, tau has been detected on ribosomes of neuronal and glial cells, the plasma membrane of neuronal cell lines, and in the nucleus in many different cell lines [183,184,187,216,218,223,224,233–235]. Therefore, tau's function is thought to span from stabilisation of microtubules, axonal transport, cell plasticity and function, nucleic acid protection and to even cell signalling. This range of function has been linked to both the isoform expression and cellular sub-localisation of tau in different cell lines.

Tau was originally described as a microtubule associated protein with a cytoplasmic expression, linking microtubules in the cytoplasm to other binding partners such as cellular membranes or motor complexes [180,225]. All of which can be post-transcriptionally modulated through modifications such as phosphorylation, acetylation and glycosylation. In adult neurons, tau is mainly localised in axons where it can be found to interact with microtubules directly or by acting as a cross-bridge enabling microtubules to interconnect with other

cytoskeletal components (actin and neurofilaments). The main and most widely characterised role of tau is as a stabilising MAP, protecting against depolymerisation of MTs, decreasing the dissociation of tubulin at both ends of MTs, enabling an increased growth rate and decreased catastrophe events [227]. Isoforms with more repeat domains (2N4R) have been shown to bind more strongly to microtubules than those with shorter repeat domains (0N3R) [222]. Although this is the most studied function of tau, the tau:tubulin ratio is still not well characterised, but it is thought to range from 1:68 to 1:5 depending on the status of the cells [236].

Although tau is predominantly reported as a microtubule associated protein, tau also localises in the nuclear fraction of the cell and associate with DNA in many different cell types in humans [184]. The ability of tau to bind to DNA was originally suggested by Gorces *et al.* (1980) when the effect of DNA in microtubule assembly was studied [237]. The significance of nuclear tau localisation has since gained more attention, but its role is not yet completely understood. Tau has been found to be located in the nucleus both *in vivo* and *in vitro* in both neuronal and non-neuronal cells [183,184,233,234,238–241]. Tau has been shown to interact with DNA and RNA and has been shown to protect DNA from denaturation and free radicals [233]. This binding is to AT rich regions of DNA through the MTBD of tau. This binding is thought to possible confer chromosomal stability, play a role in epigenetic regulation of gene expression or participate in processing and/or silencing ribosomal RNA (rRNA) [182,184,215,234,239,241–243].

In addition to the cytoplasmic and nuclear localisation of tau, studies have also demonstrated that tau can interact with membrane associated proteins. It is the N-terminal domain of tau plays a role in the regulation of tau's association with

the plasma membrane. The association of tau with the plasma membrane has been shown to occur when tau is in its dephosphorylated state. Additionally, although tau is predominantly an intracellular protein there have been reports that tau can be secreted by cells [224,244]; although its function is yet unknown. However, due to the size of the protein there are also reports questioning this secretion and whether this protein could be taken up by cells.

1.4.2.3. Post-translational modifications of tau

Alongside alternative splicing, the degree of tau phosphorylation may also be developmentally regulated. More than 80 potential phosphorylation sites have been identified at serines, threonines and tyrosines. Around 20 sites have been linked to the function of the protein, but hyperphosphorylation at those or additional sites have been linked to development or pathologies. The phosphorylation of tau is carefully regulated through kinases and phosphatases (GSK-3β, CDK5, PKA and stress activated kinases).

The interaction of tau with tubulin can be regulated through post translational modifications (Figure 1.10). Phosphorylation can neutralise the positive charge of the MTBD that is required for the interaction of the MTBD, with the negatively charged residues of the tubulin monomers and alter the structural conformation of the protein [245]. Furthermore, the hyperphosphorylation of the tau protein significantly reduces its affinity for microtubules [246] (Figure 1.10).

1.4.3. Tauopathies

Taupathies are a collective group of pathological conditions associated with neurodegenerative disorders originating from the dysregulation and dysfunction of the tau protein. These disorders share common disease mechanisms and includes Alzheimer's Disease (AD), fronto-temporal dementia with Parkinson

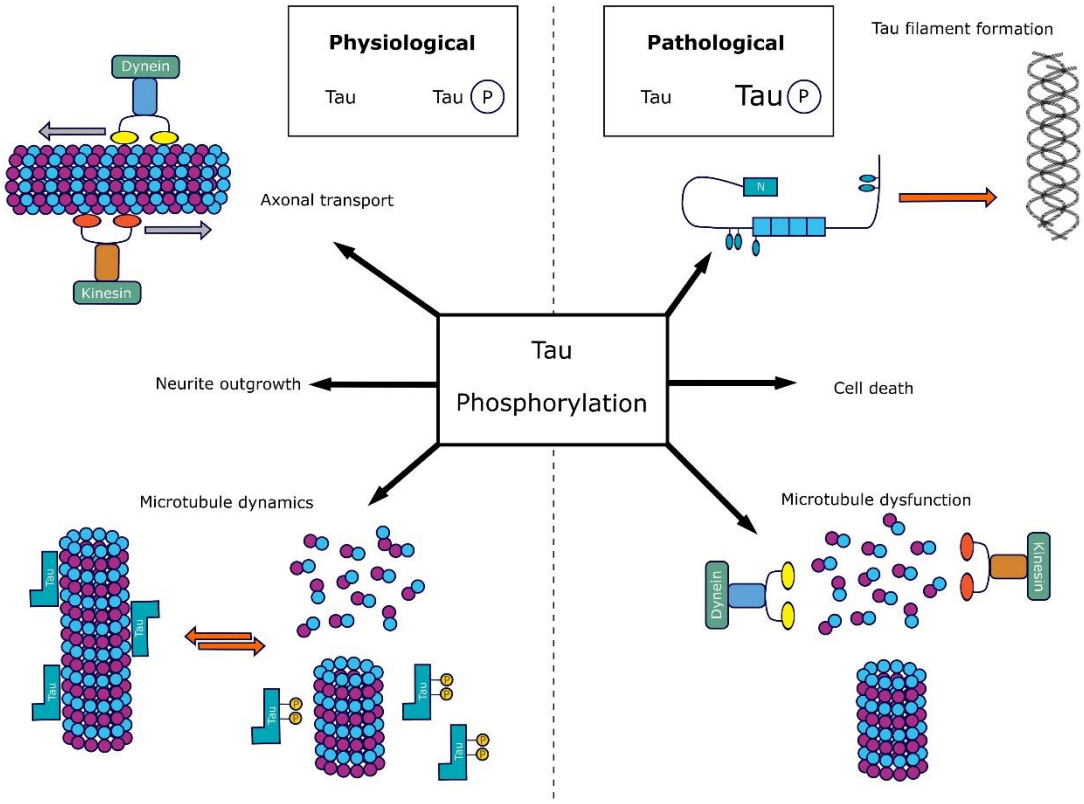

Figure 1.10. Tau phosphorylation under physiological and pathological conditions.
Tau currently has 80 reported phosphorylation sites, 20 of which have been linked to the proteins function. Under physiological conditions the phosphorylation of tau can help regulate its binding affinity for microtubules, enabling its function in microtubule dynamics, transport and growth. However, under pathological conditions where tau is hyper-phosphorylated, it can lead to a decreased binding affinity to microtubules leading to microtubule dysfunction, furthermore excessive unbound tau can result in the formation of tau protein aggregates, insoluble fibrils and consequently cell death. Microtubules, composed of α- and β-tubulin heterodimers displayed as blue and purple respectively in the figure. Diagram adapted from [247].

linked to chromosome 17 (FTDP-17), Picks disease, dementia pugilistica among many more [248–251]. Although they share common disease mechanisms, the tauopathies lead to diverse phenotypic manifestations, dysfunction and degeneration [250,252]. Tau is a highly soluble protein, but changes to the protein can cause it to misfold, become insoluble and form aggregates in cells [253]. These aggregates and loss of function can interfere with microtubule dynamics, resulting in the loss of transport of organelles and biochemicals causing cells to lose function eventually leading to neurodegeneration.

Tau mutations can be split into two categories, mutations that alter protein function and mutations that alter gene regulation [177,187,246,254]. Mutations G272V (exon 9), p301L, P301s, Δ280K (exon 10), V337M (exon 12) and R406W (exon 13) reduce the binding affinity of microtubules and or reduce the ability of tau to promote microtubule assembly compared to normal tau, therefore these mutations alter tau protein function. Exon 9, 12 and 13 are constitutively included in tau transcripts, therefore mutations to these exons affect all isoforms of tau, whereas mutations in exon 10, such as p301L, P301s, only affect 4R function.

Missense, silent and intronic tau mutations can lead to both the increased or decreased splicing of exon 10, by acting through different cis-acting regulatory elements [255]. These elements include an enhancer, which can be strengthened or destroyed, resulting in the inclusion or exclusion of exon 10 from tau transcripts. Exon 10 also contains a secondary regulatory element, exon splicing silencer, which when mutated results in the excess inclusion of exon 10. A third element, involved in inhibiting exon 10 silencing, is contained within the intronic sequence directly flanking the 5’ splice site of exon 10 and mutations in this element have also been found to increase the inclusion of exon 10 to tau transcripts[255]. Due to this multiple pathogenic mechanism of tau mutations the

phenotypic heterogeneity can be explained. N279K and S305N exon 10 mutations have been shown to affect the regulation of exon 10 but do not alter the binding affinity of tau to microtubules, splicing assays have revealed these mutations often result in the inclusion of exon 10 [255,256]. The exon 10 silent mutation, L284L, and intron 10 mutation immediately adjacent to the 3' end of exon 10 also leads to an increased inclusion of exon 10 [255,257].

1.4.3.1. Alzheimer's disease

Approximately 50 million people worldwide are currently living with dementia and this number is expected to rise to 152 million by 2050 [258]. AD is the most common cause of dementia and although it is a complex disorder one of the key neuropathological characteristics of AD is the presence of hyper-phosphorylated aggregated tau protein.

Post-translational modifications, hyperphosphorylation, acetylation and truncation result in the reduced binding affinity of tau to microtubules, allowing them to become self-aggregated, leading to instability of the cytoskeleton due to lack of bound proteins leading to neurodegeneration (Figure 1.10). Tau is found to accumulate in neurofibrillary tangles (NFTs) in the brain in AD [178]. In addition to hyperphosphorylation, cleavage and other conformational changes of tau have been shown to play a role in the pathogenesis of AD [194,246]. However, hyperphosphorylation has been shown to precede the conformation or cleavage of this protein. Mis-localised tau in neurons overexpressing tau also interacts with nucleoporins of the nuclear pore complex, disrupting the nuclear pore functions of nucleocytoplasmic transport and possibly contributing to tau related neurotoxicity [178,246,259].

1.5. A negative association of non-melanoma skin cancer and Alzheimer's disease

Ageing and cancer both represent complex biological pathways that have overlapping molecular mechanisms. Ageing is the persistent deterioration of the physiological function of an organism throughout its lifetime [260]. While cancer is the accumulation of damage to cells leading to the uncontrolled cell proliferation which results in a malignant growth within the body [58,129]. Ageing is widely accepted to be associated with a number of chronic and degenerative diseases, such as cognitive dysfunction and cardiovascular disease. Over the lifespan of an organism SCs accumulate DNA damage from a number of stressors (UV and ionising radiation, oxidants from normal metabolic processes). These SCs withdraw from the cell cycle and undergo a cell death mechanisms; such as apoptosis, autophagy or senescence. Resulting in a decreased pool of functional SCs and their progenitor cells which can contribute to impaired tissue homeostasis with ageing and age related degenerative pathologies. However, in cancer cells are able to evade these cell death pathways and instead accumulate further mutations that enable them to continue through the cell cycle and proliferate with their damaged DNA (*RAS*, *TP53*, *cMyc*, *CDKN2A*) [261,262].

Both ageing and cancer can result from the accumulation of damage to SC and progenitor cell populations over time. Although the incidence of diseases (such as cancer and neurodegenerative diseases) increases with age, there is epidemiological evidence that these two conditions actually exhibit an inverse comorbidity and opposing cellular behaviours have been reported between cancers and degenerative diseases [263–271]. Furthermore, a negative correlation between the incidence of NMSC formation and AD has been identified in a number of independent publications [263–266,268,271–273]. This inverse association

suggests that individuals diagnosed with AD have a reduced incidence of NMSC and concurrently, older patients with a history of NMSC are identified to be less likely to develop AD [263–266,268,271–274]. However, despite this observation, to the best of our knowledge, the exact mechanism behind this phenomenon is currently unknown. This is one of the fundamental observations on which the hypothesis to this thesis was developed.

1.5.1. Tau expression in healthy human skin

There is increasing evidence that proteins associated with neurological disorders, including AD, can be found in other tissues throughout the body [196–198,275]. Dermal fibroblasts are routinely used in neurological and AD research; reasons behind the use of this cell line are hard to find, but some sources have suggested it is because they are easy to access and culture *in vitro* while displaying similar expression profiles [276]. In addition, Kim *et al.* (2019) demonstrated how nerve fibres in the skin might act as a bio-marker for AD [198], and various other papers have alluded that although tau is not shown to be as highly expressed in skin as found in other tissues, these disease-related proteins can be found in the epidermal layer of the skin [104,197,277,278].

Microtubules are involved in the movement and positioning of vesicles and organelles, therefore they play essential roles in cellular polarisation and differentiation [279]. The functional diversity of microtubules can be achieved through many different mechanisms, one of which includes the binding of regulatory proteins some of which are microtubule associated proteins (MAPs) to soluble tubulin as well as to microtubule surfaces and ends [170]. The IF and cytoskeletal network undergo significant reorganisation during the programme of differentiation in the epidermis. Despite the major cytoskeletal changes in the skin

during terminal differentiation, there are a very limited number of publications demonstrating tau expression or function in human skin. Indeed, no publications that have characterised the function of tau in the epidermis. One publication investigating the cortical rearrangement of microtubules during cell differentiation demonstrated that in the epidermis MAPs can associate with desmosomal proteins such as desmoplakin [66]. Desmoplakin is a linker protein between the IF and desmosomal cadherin complexes and is essential to the formation of desmosomes and for the reorganisation of cortical microtubules. MAP2 and MAP4 were shown to be sufficient to induce microtubule stabilisation and cortical recruitment in keratinocytes, and were demonstrated to be up-regulated during terminal differentiation [75,278]. However, in desmoplakin-null cells, none of the MAPs were able to induce microtubule reorganisation, but they were able to bundle microtubules still. These studies suggest that MAPs interact with desmoplakin during keratinocyte differentiation to stabilise and reorganise microtubules to the cells cortex.

Most studies carried out to date have only confirmed tau expression as part of a different investigation, at no point did any study determine the isoform specific expression of tau in the epidermis. In the brain, the specific isoform expression of tau is thought to have a direct impact on its function. The alternative splicing of the N terminal region, through the exclusion or inclusion of exon 2 and 3, has a direct impact on its membrane binding affinity. Whilst the alternative splicing of exon 10 determines the number of microtubule binding domains the transcript encodes, and in turn the affinity of the tau protein to microtubules, it is reported that the inclusion of exon 10 results in a two times higher binding affinity of the other 3 microtubule binding domains together. Due to the important cytoskeletal changes that take place in the process of terminal differentiation the alternative

splicing of tau, and therefore the function of tau in keratinocytes could differ between the basal and suprabasal layers of the epidermis.

MAPT gene expression between 53 tissues was analysed and published in the Genotype-Tissue Expression (GTEx) portal, in which 8,555 samples from 570 donors was evaluated using RNA-seq. Unsurprisingly the highest median expression of tau was found in brain tissue at 50.30 RPKM in the cerebellum (Figure 10.1). Interestingly, it was shown that there was an increase in the expression of tau in sun-exposed skin samples compared to non-sun-exposed skin samples. Suprapubic skin samples, which are not often sun exposed areas, displayed 1.7 RPKM and 7.394 TPM, whereas sun-exposed skin from the lower leg was found to have 2.0 RPKM and 9.013 TPM (Figure 10.1). This was an interesting observation as most cSCC arise in sun-exposed areas, but nothing is currently known about tau expression in AKs or cSCCs. No significant difference was displayed in the expression of tau between male and females in non-sun-exposed or sun-exposed skin samples (Figure 10.1C). Microarray expression data also supports the expression pattern of tau between exposed and non-exposed skin samples (Figure 10.2).

1.5.2. Tau expression in the skin of patients with Alzheimer's disease

There is increasing evidence that proteins associated with neurodegenerative diseases are found in other tissues throughout the body [196,197,275,277,280,281]. The presence of misfolded proteins in the brain is a hallmark of AD and it is thought that protein aggregates could have a systemic expression pattern and might also be found in several tissues alongside the brain, including in the skin.

It is plausible that the skin and brain share similar molecular pathological alterations as they both share ectodermal origins[197,273,280,282,283]. Because of this,

some studies have looked at using the skin as a potential biomarker for living AD patients; identifying protein aggregates and different proteinopathies, removing the need for showing misfolded proteins in brain tissue (through biopsy or autopsy) or through genetic testing, the only current forms of definitive diagnosis [196–198,273,275,277,284]. Ildefonso *et al.* (2015) investigated the possibility of using skin biopsies from AD and non-degenerative dementia (NDD) patients as a potential diagnostic tool by using tau expression in the skin as a biomarker in living patients [277]. Comparing skin samples from AD, NDD and healthy skin samples (from similar demographics), it was shown that total tau and phosphorTau (AT8-phosphorylated at Ser202) were present in significantly higher levels in the epidermis of AD patients when compared to control patients and those with NDD. This supports the idea of using the epidermal compartment of skin samples for the clinical diagnosis of AD in living patients [197].

1.5.3. Tau expression in cancer

Tau expression and function in NMSC is currently unknown. Despite tau expression being identified in human skin, it is unclear what role this protein plays in terminal differentiation within the epidermis and how this protein might change or contribute to the initiation and progression of NMSC. MAPs have been shown to often become upregulated in cancers, and tau expression specifically has been shown to alter in a number of cancers, such as prostate, breast, low-grade gliomas, but nothing has been reported about the expression of tau in NMSC. The study of mechanisms that counteract, at tissue levels, the growth of aberrant cells during the early stages of cancer development are of high interest in the cancer field and are likely to have translational applications and/or implications.

Microtubules are extremely important to many cellular processes, including mitosis. This importance of microtubules to cell division has made them an important target for many cancer therapies. AD results in hyper-phosphorylated, un-functional tau protein in neuronal cells and therefore tau is no longer able to support the tubulin network leading to cell death and neurodegeneration. Tau has been linked to resistance to taxane-containing chemotherapies, as it binds to tubulin in the same location as paclitaxel in breast cancers [285,286]. Taxanes are widely used to treat ovarian, cervical, endometrial, breast, non-small cell lung cancer and gastric etc. Taxane interferes with spindle microtubule dynamics leading to cell-cycle arrest and consequently apoptosis, therefore when MAPs bind to the same binding site in β-tubulin as taxanes, they can interfere with their ability to work leading to resistance [287]. The abnormal expression of neuronal MAPs has been shown to take place in non-neuronal cancers [156,172]. Tau overexpression has been shown to correlate with poor outcomes in breast cancers and chemotherapy resistance and the hyper-methylation of CpG island in tau is associated with a poor prognosis in colorectal cancer patients [288]; this hyper methylation causes the exclusion of exon 10 from the RNA transcript of tau. However, in other cancers such as gastric, ovarian and low grade gliomas, tau expression has been linked to decreased proliferation, increased apoptosis and favourable responses to treatments.

Intriguingly, a positive association has been reported between AD and melanoma [289,290]; which is particularly interesting as there is a known negative association between melanoma and NMSC [122]. And it is well recognised that melanoma and NMSC have opposing mechanisms and often treatment for NMSC can result in an increased incidence of melanoma and vice versa. However, although there has been a large amount of research into the function of tau and its pathology in

the brain, little to nothing is known about its function or mechanism in the healthy epidermis or in SCC. The precise role of tau in the epidermis and the role of tau in NMSC initiation and progression this require exploration.

Thus, the hypothesis underpinning this thesis, is that tau is functionally significant in epidermal cell fate, stratification and differentiation, and that altered expression or function of tau occurs in cSCC. In turn, this mechanism may partly explain why AD patients, with abnormal tau expression, have a lower incidence of cSCC.

1.6. Aims and Objectives

This work therefore aims to investigate the molecular mechanisms underlying tau function in the epidermis, specifically to determine the role of tau and its isoforms in the process of epidermal stratification and differentiation. This work also aims to elucidate the function of tau in squamous cell carcinoma and investigate whether it has the potential to be utilised as a novel cancer therapy.

Aim: To investigate the expression and function of tau in healthy skin and squamous cell carcinoma.

Objectives:

1. Examine the total and isoform specific tau expression in healthy human skin samples at an RNA and protein level and identify the subcellular co-localisation of tau in each layer of the epidermis.
2. Evaluate the role of tau in epidermal keratinocytes through the manipulation of tau gene expression *in vitro* and examine the functional significance of tau in epidermal development and maintenance using three-dimensional *in vitro* epidermal models.

3. Identify potential binding partners of tau under basal and differentiated conditions using proteomic analysis.
4. Characterise tau expression in cutaneous squamous cell carcinoma, manipulate tau expression in an SCC cell line to investigate the functional role of tau and explore the translational potential of these findings for clinical applications.

2. Materials and methods

2.1. Cell Culture

2.1.1. Cells and maintenance

Human primary epidermal keratinocytes pooled (HPEKp) were purchased from CELLnTEC. HPEKp cells were cultured in complete CnT-Prime medium (CnT-PR, CELLnTEC) and 1% penicillin-streptomycin-antimycotic (11570486, Gibco).

Primary Human neonatal Epidermal Keratinocytes (HEKn) cells were purchased from Gibco (C0015C, Thermo Fisher Scientific). HEKn cells were cultured in complete EpiLife medium, containing EpiLife media (MEPI500CA, Gibco) with 1% Human Keratinocyte Growth Serum (containing 0.2% v/v Bovine pituitary extract, 1 µg/ml recombinant human insulin-like growth factor-I, 5 µg/ml bovine transferrin, 0.2 ng/ml human epidermal growth factor; HKGS; 10761364, Gibco) and 1% penicillin-streptomycin-antimycotic.

A431 cells (human SCC cell line) an EACC general cell line collection derived from an epidermal carcinoma of the vulva taken from an 85 year old female (85090402, Sigma). A431 cells were cultured in complete DMEM medium, containing Dulbecco Modified Eagle's Medium with 10% FBS, 2 mM Glutamine (25030149, Fisher Scientific) and 1% penicillin-streptomycin-antimycotic.

293FT cells (R70007, Invitrogen) were cultured in complete DMEM medium, containing Dulbecco Modified Eagle's Medium with 10% FBS and 1% penicillin-streptomycin-antimycotic.

All cells were incubated in a humidified incubator at 37°C and 5% CO_2.

2.1.2. Passaging of cells

Cells were passaged at 80 % confluency by first washing in Hank's Balanced Salt Solution (HBSS; 14175-053, Gibco), to remove any trypsin-inhibiting components typically found in cell culture media, followed by detachment using pre-warmed TrypLE Select® (12563-029, Gibco) and incubated until complete cell detachment was observed. The resulting cell suspension was neutralised in 5 ml fresh cell culture media and centrifuged at 1000 rcf for 5 min RT. The pellet was re-suspended in fresh complete medium and counted using a countless II Automate Cell Counter (AMQAX1000, Invitrogen). Cells were plated into cell culture dishes (15347026/10111351, Nunc) and cultured in a humidified incubator at 37°C and 5% CO_2.

2.1.3. Freezing and thawing of cells

Cells were dissociated and spun down as described in section 2.1.2. The resulting cell pellet was then suspended in chilled complete cell culture medium with 10 % dimethyl sulfoxide (DMSO; D2650, Sigma-Aldrich). Cells were slowly frozen in 1 ml aliquots at -80°C, before transfer the following day to liquid nitrogen tanks for long-term storage.

Vials of cells were thawed at 37°C and immediately diluted with complete cell culture medium. Cells were spun down at 1000 rcf and plated as described in section 2.1.2.

2.1.4. Plasmid preparation

2.1.4.1. Plasmids

Human HEKn, HPEKp and A431 cells were infected with lentiviral particles containing pINDUCER20-Tau [243] (AddGene ID: 92201) to overexpress 2N4R tau

and pINDUCER20 [291] (AddGene ID: 44012) as a plasmid control. Infected cells were selected with 800 µg/ml G418 (A1720, Sigma).

Human HEKn, HPEKp and A431 cells were infected with lentiviral particles containing Ki67p-FUCCI. Ki67p-FUCCI reporter lentiviral plasmids were kindly provided by Dr Alexander Zambon (Keck Graduate Institute, Claremont). Generation of lentiviral plasmids was carried out by Dr Donald Singer and achieved using open reading frames of mCherry-Cdt1(30/120)-pCSII-EF-MCS and mAG-hGeminin(1/110)-pCSII-EFMCS plasmids that were kindly provided by Dr Astsushi Miyawaki. These were subcloned into the pENTR-D-Topo vectors (K240020, Life Technologies). Subcloning using Gateway recombination of the 1.5 kb Ki67 proximal promoter (Ki67p) upstream of mAG and mCherry FUCCI reporters was performed into 2k7 lentiviral vectors allowing for blasticidin selection of cells at 7.5 µg/ml.

Human HEKn and HPEKp cells were infected with lentiviral particles containing shRNA pGreenPuro plasmids (SI505A-1, System Biosciences). Plasmids for the generation of lentiviral particles to generate stable keratinocyte tau KD cell lines in this study were kindly provided by Dr Paganetti [242]. Infected cells were selected with 1 µg/ml puromycin.

2.1.4.2. Bacterial culture

Plasmids received from AddGene were delivered as *Escherichia coli* (*E. coli*) bacterial stabs in agar. Bacteria were streaked onto a LB agar (12 g/L) plate containing 100 µg/ml ampicillin (A5354, Sigma) and incubated overnight at 37°C (14 h). Following overnight incubation, a single bacterial colony was selected and grown in 5 ml LB broth containing 100 µg/ml ampicillin to establish a starter culture and incubated at 37°C with vigorous shaking (~300 rpm) for 9 h. After 9

h, a 1:500 dilution of the starter culture was placed into 100 ml of fresh LB broth containing 100 µg/ml ampicillin in a 500 ml conical flask to allow for sufficient aeration. Bacterial culture was place at 37°C with vigorous shaking (~300 rpm) overnight (14 h).

2.1.4.3. Plasmid amplification and purification

Amplification and purification of plasmids was performed using QIAGEN® Plasmid Maxi Kit (1263, QIAGEN) according to the manufacturer's instructions. Overnight culture was harvested by centrifugation at 6000 rcf for 15 min at 4°C. The supernatant was removed ensuring the pellet was completely dry. 10 ml 4°C P1 buffer (containing 1:1000 LyseBlue and 100 µg/ml RNAse) was added to pellet and vigorously re-suspended. 10 ml P2 (lysis buffer) was added and inverted 6 times, until a homogenous blue colour change is observed, and incubated at RT for 5 min. 10 ml pre-chilled P3 was added to solution and carefully inverted 6 times, ensuring no breakage of genomic DNA and subsequent contamination occurs, or until the blue colour disappears and incubated on ice for 20 min. Following incubation on ice, sample is centrifuged at >20,000 rcf for 30 min at 4°C. Supernatant was removed and re-centrifuged at >20,000 rcf for 15 min at 4°C. QIAGEN® tip-500 was equilibrated with 10 ml QBT buffer and allowed to empty with gravity flow. Supernatant was then added to QIAGEN® tip and allowed to enter resin through gravity flow. QIAGEN® tip was washed twice with 30 ml QC buffer and allowed to move through by gravity flow. Following washes DNA was eluted using 15 ml QF buffer into a fresh 50 ml falcon tube. DNA was precipitated by adding 10.5 ml RT isopropanol (I9516, Sigma-Aldrich) to eluted DNA and inverted to mix. Samples were centrifuged at 15,000 rcf for 30 min at 4°C. Supernatant was carefully discarded and pellet washed with 70% ethanol in distilled water (dH_2O) and re-centrifuged at 15,000 rcf for 10 min and supernatant

carefully discarded. Pellet was air dried for 10 min before DNA was dissolved in 300 µl 10 mM TrisCl pH 8.0.

A NanoDrop 2000 UV-Vis Spectrophotometer (Thermo Fisher Scientific) was used to quantify the DNA and determine the purity of the sample.

2.1.4.4. Generation of lentiviral reporters and cell transfection

pINDUCER20 (44012, AddGene) and pINDUCER20 tau (92201, AddGene), are all 2nd generation vectors, as they have an intact 5' LTRs driving gene expression and therefore require Tat transactivation; whereas 3rd generation plasmids the 5' LTR will be truncated and fused with a heterologous promoter and therefore do not require Tat transactivation.

Two 10 cm dishes, per plasmid, were seeded with 2 x 10^6 293FT cells, a highly transfectable clonal isolate cell line derived from human embryonic kidney cells that have been transformed with the SV40 large T antigen. Dishes were incubated overnight until cells were 20-30% confluent. Per 10 cm dish 6.5 µg pax2 a gag/pol expression vector, 3.5 µg pmD2G a VSV-G expressing envelope and 10 µg of target vector were added to 250 µl 150 mM NaCl solution. 30 µl JetPEI® (101-40N, Polyplus) was added to 250 µl NaCl solution and gently mixed. The JetPEI® solution was added to the 250 µl DNA solution and incubated at RT for 30 min. During incubation 10 ml pre-heated fresh complete culture medium was added to each 10 cm dish to help stimulate growth and enhance lentiviral particles. Following 30 min incubation JetPEI®-DNA mixture was added drop wise to medium in dishes for co-transfection. The 293FT cells were left to incubate at 37°c and 5% CO2 for 48 or 72 h until collection. Following co-transfection high levels of viral RNA lentiviral particles were collected by removing media and filter

sterilised at 0.45 µM. viral RNA production can then be quantified using a NanoDrop before storage at -80°C until use.

Ki67-T2A-Fucci lentiviral particles for cell transduction were previously produced in our lab by Dr Donald Singer, by co-transfecting the Ki67-T2A-Fucci vectors with the MISSION® lentiviral packaging mix (SHP001, Sigma Aldrich) into 293FT cell line [292,293]. The viral supernatant was collected after 48h and filtered using 0.45 µm filter to remove cell debris.

2.1.5. Ki67p FUCCI viral infection

Cells were incubated with 1 ml of lentiviral supernatant containing the Ki67p FUCCI plasmid and 10 µg/ml Polybrene (TR-1003-G, EMD Millipore) for 2 h under normal culture conditions. After 2 h, the viral supernatant was replaced with complete culture medium. After 24 h the cells were washed with HBSS and fresh complete culture medium was added to cells. Infected cells were selected after 48 h using 7.5 µg/ml blasticidin (15205, Sigma-Aldrich).

2.1.6. Tau overexpression

There are many ways to control gene expression in mammalian cells, one way is to use tetracycline-responsive promotors to control the activity of a gene. The tetracycline system was developed for molecular biology in 1992 as a more efficient induction system than the *lac* system, commonly used at the time [294]. To test whether tau overexpression had on the differentiation status of keratinocytes, cells infected with a doxycycline-inducible vector for the overexpression of tau were generated. The pINDUCER20 vector is an inducible lenti-vector system, which carries both reverse tetracycline transactivator 3 (rtTA3) and neomycin-(G418) resistance genes under the UBC promoter as well as a cDNA of interest under the control of a tetracycline-responsive promoter [291]. The pINDUCER20

tau lenti-viral vector system allows for the tetracycline inducible overexpression of 441 aa (2N4R) tau with pINDUCER20 as plasmid control. Doxycycline was used to induce gene overexpression as it has a higher binding affinity to rtTA then tetracycline. Doxycycline also has a low cell toxicity and a known half-life of 24 h.

Cells were incubated with the lentiviral supernatant containing the pINDUCER20 or pINDUCER20 tau and 10 µg/ml Polybrene for 2 h under normal culture conditions. After 2 h, the cells were washed with HBSS and fresh complete culture medium was added to cells. Infected cells were selected after 48 h using 800 µg/ml G418 in A431 cells, and 250 µg/ml G418 in HEKn and HPEKp cells (A1720, Sigma-Aldrich).

Doxycycline hyclate (D9891, Sigma) was reconstituted in dH_2O at 1 mg/ml and filter sterilised at 0.45 µM. Cells infected with pINDUCER20 and pINDUCER20 tau were treated for 48 h with 100 ng/ml doxycycline in complete cell culture medium to overexpress Tau^{441} protein.

A431 cells previously infected with Ki67p-FUCCI were co-infected with pINDUCER20 tau to allow for cell cycle status to be tracked and analysed. Cells were selected with 7.5 µg/ml blasticidin and 800 µg/ml G418. Tau^{441} protein overexpression was driven by the addition of 100 ng/ml doxycycline for 48 h in complete DMEM media with 2 mM glutamine and selection antibiotics.

2.1.7. siRNA-mediated tau knockdown

One method of RNAi is through the use of small interfering RNA's (siRNA); double-stranded RNA (dsRNA), usually 20-27 nucleotides in length, which are complementary to mRNA of the target gene. Once siRNA has been transfected into cells, the dsRNA binds to an endonuclease protein, Dicer, which cuts dsRNA into short segments. The short dsRNA then bind to an Argonaute protein, a family

of proteins that play an important role in the regulation of gene expression, where one strand is selected and remains bound, as the guide strand, while the other is degraded. The combination of the guide strand, Argonaute and other proteins are collectively called the RNA induced silencing complex (RISC). The bound siRNAs direct RISC to bind to complementary target mRNAs. Once bound Argonaute catalyses the cleavage of the mRNA, which is then degraded, therefore silencing target gene expression [295]. Endoribonuclease-prepared siRNA (esiRNA) are generated from a gene specific cDNA template from the target mRNA. Reverse transcription into double stranded RNA is subsequently followed by the digestion, using *Escherichia coli* RNase III, generating a heterogeneous pool of siRNA that target the gene of interests mRNA [296]. This method allows for a specific knockdown of the protein of interest, resulting in lower levels of off-target effects than traditional, chemically synthesised siRNA with a single silencing trigger would enable.

Upon reaching 60% confluency cells were transfected with esiRNA using INTERFERin® (409-10, Polyplus) according to the manufacturer's instructions. Briefly, 20 nM of esiRNA and INTERFERin® was prepared in complete culture medium, vortexed and incubated for 20-30 min at room temperature (RT) to allow for transfection complex formation. During incubation 2 ml pre-heated fresh complete culture medium was added to each well of 6 well plate to help stimulate growth and enhance transfection. Following 20-30 min incubation esiRNA transfection mixture was added drop wise to medium in well. The transfected cells were left to incubate at 37°c and 5% CO2 for 48 or 72 h until collection. See appendix Table 10.8 for esiRNA sequences used in this study.

2.1.8. shRNA-mediated tau knockdown

Another widely used technique of RNAi is through short hairpin RNA (shRNA) to downregulating *MAPT* gene expression through the degradation of the associated mRNA. shRNAs are sequences of RNA around 80 bp in size that have a region of internal hybridisation that forms their hair pin like structure. When shRNAs are processed in a cell they form siRNA that knocks down gene expression [297]. Although the mechanism similar to esiRNA, shRNA-mediated knockdown can be incorporated into a plasmid, virally infected and incorporated into the genomic DNA; therefore a stable cell line can be generated allowing a constant knockdown, opposed to the transient knockdown using esiRNA. Therefore, enabling this study to overcome some of the nonspecific effects observed through the use of the transfection reagent in siRNA-mediated knockdown.

HEKn and HPEKp cells were infected with shRNA tau 1881, 2112 and control shRNA luciferase lentiviral particles. Cells were incubated with 1 ml lentiviral supernatant containing the shRNA tau or shRNA control pGreenPuro plasmids and 10 µg/ml Polybrene for 2 h under normal culture conditions. After 2 h, the cells were washed with HBSS and fresh complete culture medium was added to cells. Infected cells were selected after 48 h using 1 µg/ml Puromycin dihydrochloride hydrate (10781691, Fisher Scientific). See appendix Table 10.9 for shRNA sequences used in this study.

2.1.9. Stem cell attachment assay

Unfractionated low passage keratinocytes were detached as previously described and seeded onto BM coated dishes. Dishes were coated overnight at 4°C with BM proteins as described in Watt *et al.* (1993), containing 20 µg/ml

collagen type IV (C6745, Sigma), 20 µg/ml fibronectin (F0895, Sigma) and 6 µg/ml laminin (L4544, Sigma) in PBS. Following overnight incubation, dishes were washed with heat inactivated bovine serum albumin (BSA; A2153, Sigma) and incubated for 1 h at 37°C. Dishes were washed in media once before use.

Attached and floating fractions of cells were collected at 20, 40 and 60 min after seeding (Figure 2.1). Floating cells were collected in a 15 ml falcon tube and dishes washed once with HBSS to collect floating keratinocytes. Floating cell fractions were spun down at 1 rcf and the pellet and processed for RNA or protein extraction. RNA and protein from attached cells were collected directly from the dish and processed according to section 2.3 and 2.4 respectively.

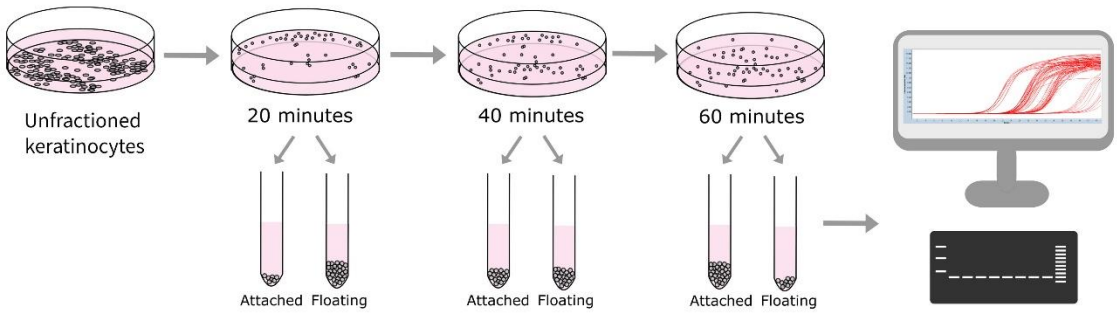

Figure 2.1. Schematic representation of the stem cell attachment assay.

2.1.10. Calcium differentiation

0.1 M Calcium Chloride (C7902, Sigma) stock was prepared in dH_2O and filter sterilised at 0.45 µM. Keratinocytes were differentiated with 1.7 mM Ca^{2+} in complete EpiLife medium. Keratinocytes were typically cultured for 24-96 h (depending on stage of differentiation) before analysis was carried out.

2.2. Human clinical samples

Human skin samples were kindly provided by Dr Emmanuella Guenova-Hötzenecker from the Dermatological Bio-bank (EK 647), Dermatological Clinic, University Hospital Zürich, Switzerland. Consent was taken from all patients and samples were collected in accordance with their Cantonal Ethics Commission Zürich. Samples were then transported in accordance with the appropriate University of Plymouth MTA protocols and governance. On arrival tissue samples were held under University of Plymouth Human Tissue Authority (HTA) licence and research was carried out under ethical approval from the University of Plymouth's Faculty Research Ethics and Integrity Committee (FREIC: 17/18-962), in accordance with the Human Tissue Act 2004.

Three cohorts of human samples were used in this study; healthy skin samples, with no diagnosed skin disorders, SCC samples and BCC samples, both with confirmed pathological diagnosis. The healthy skin biopsies were taken from older patients without an accompanying medical or clinical history. Any underlying disease could potentially alter cell function and the histological appearance of skin, hence this must be taken into consideration as one of the limitations of this study. Exclusion criteria for specific medical conditions and full skin sample characterisation would ideally be carried out for each patient to limit the possibility of this.

In total, 50 human skin samples were received for use in this study, including 12 healthy patient samples (7 frozen and 5 FFPE), 26 SCC patient samples (15 frozen and 11 FFPE) and 12 BCC patient samples (12 FFPE). Appendix Table 10.10 includes details of the age, gender, location and classification of all skin samples used in this study. Diagnosis was carried out by histopathologists at the University Hospital Zurich as part of standard diagnostic procedures. Frozen samples were stored at -80°C at our facility until processing, while paraffin

samples were stored at RT. Frozen and paraffin embedded tissue was processed onto slides as described below in section 2.5.1 and 2.5.2. Immunofluorescence and haematoxylin and eosin staining protocols were carried out as described below in section 2.5.3. When immunofluorescence and histological staining was performed matched patient slides were also stained; one SCC/BCC and the other from a healthy skin patient.

Following immunofluorescence analysis and image processing, sample staining was analysed and allocated a semi-quantitative score based on staining intensity, and percentage of positive cells within a region of the tissue [298]. Basal, spinous, granular and corneal layers of the epidermis alongside the dermis or stroma were assessed in healthy skin samples and SCC samples. Expression levels were categorised as: +, weak or scattered; ++, moderate expression; +++, strong expression. Blinding was not possible as each SCC or BCC sample presented with an obvious pathology, which was considered when imaging the tissue samples.

2.3. RNA Analysis

2.3.1. Laser capture microdissection of human skin samples for RNA extraction

Human skin samples were sectioned at 20 µm thickness on a Leica CM1850 cryostat. Sections were mounted onto PEN membrane glass slides (LCM0522, Applied Biosystems) and immediately stained with 1% Methyl Green (67060, Fuka Analytical) in 0.1% DEPC-treated water (D5758, Sigma; dH_20 treated with 0.1% DEPC and autoclaved to inactivate the DEPC) for 5 seconds, then washed four times in DEPC treated for 5 seconds and dried for 7 min. Laser capture microdissection (LCM) was performed on an ArcturusXT™ LCM instrument,

using CapSure® Macro LCM caps (LCM0211, Applied Biosystems) within 10 min of sectioning. The protocol was carried out as quickly as possible to maximise RNA yield and avoid RNA degradation. Samples were lysed using Tri-Reagent (93289, Sigma) for 20 min with frequent agitation, and then further processed for RNA extraction.

2.3.2. RNA extraction and quantification

RNA was extracted using the acid guanidinium thiocyanate-phenol-chloroform methodology [299]. Cell were washed briefly with HBSS before Tri-Reagent was added to extract the RNA. This was incubated at room temperature for 5 min and then collected into a 1.5 ml Eppendorf tube. Chloroform (C2432, Sigma) was added at a 5:1 ratio (lysate:chloroform). The samples were mixed by vortexing, and spun down at 18,000 rcf for 15 min at 4°C. The aqueous phase was collected and added to an equal ratio of isopropanol (34965, Sigma) and 1 µl GlycoBlue (AM9515, Ambion Applied Biosystems) so the pellet could be identified later. The sample was incubated overnight at -20°C, before spinning down at 18,000 rcf for 45 min at 4°C. The supernatant was discarded and 1 ml 70% ethanol (20821.321, VWR Chemicals; made up with DEPC-treated water) was added to the pellet and incubated at RT for 5 min, the samples were spun down at 12,000 rcf for 10 min at 4°C. The supernatant was removed and the pellet was re-suspended in 10-20 µl of 0.1% DEPC-treated water.

A NanoDrop 2000 UV-Vis Spectrophotometer (Thermo Fisher Scientific) was used to quantify the RNA and determine the purity of the sample. Quality control was assessed by analysis of the 260/280 and 260/230 ratios, which is an indicator for the presence of contaminants.

2.3.3. Reverse transcription

Reverse transcription of total RNA was performed using High Capacity cDNA Reverse Transcription kit (4368814, Applied Biosystems) in accordance with the manufacturer's instructions on a Veriti™ Thermal Cycler 96 well machine (Applied Biosystems). 1 µg of total RNA was reverse transcribed using the Multiscribe Reverse Transcriptase polymerase and random hexamer primers (see Table 10.4 for programme details). Following the completion of reverse transcription, cDNA samples were diluted in 180 µl of DEPC-treated water and stored at -20°C.

2.3.4. Primer design

Primers were designed against the CDS sequence for each gene, provided by NCBI gene (http://www.ncbi.nlm.nih.gov/gene/) using the Primer 3 website (http://biotools.umassmed.edu/bioapps/primer3_www.cgi) and validated using UCSC (http://genome.ucsc.edu/cgi-bin/hgPcr?command=start). Primers were designed to cross exons, in order to reduce the risk of DNA contamination being amplified. Primers were designed to give an amplicon length that reduces the risk of dimers and hairpins. Where possible primers were designed to bind towards the centre of the cDNA to ensure RNA degradation would not result in the removal of the primer's binding site. The details for the primers used are recorded in Table 10.6.

2.3.5. Real time q-PCR

Real Time (RT) quantitative-PCR (q-PCR) was performed in triplicate. Samples were combined with LightCycler® 480 SYBR Green I master kit (4887352001, Roche Life Science) (diluted 1:1 with the water provided in accordance with the manufacturer's instructions) and appropriate primers, made up in 10 mM Tris-Cl, listed in Table 10.6, in a ratio of 1:8:1 totalling 10 µl. This equates to a final primer

concentration of 1 µM. The samples were analysed with each primer in triplicate as a technical control.

The instrument used was a Roche LightCycler® 480 Instrument II 384-well block RT PCR machine, used according to the manufacturer's instructions. Programme details are explained in Table 10.5. Results were analysed using Comparative Ct methods. PCR 162 amplification was checked to ensure appropriate amplification curves and annealing temperature was obtained. GAPDH and 36B4 genes were used as housekeeping genes to normalise samples with the $2^{-\Delta\Delta C}$ method. All analyses were performed including the three replicates. All results were exported into Prism for statistical analysis (Version 9.3.0).

2.3.6. Semi-quantitative PCR

Products of RT q-PCRs and primers were validated using semi-quantitative PCR (sqPCR) analysis with agarose gels. Briefly, 1.5% agarose gel were made using 40 ml 1% TAE buffer (LSKMTAE50, Milipore) and 0.6 g agarose (BP160-100, Fisher Scientific) and microwaved until clear. When cooled 4 µl SYBR SAFE™ DNA gel stain (10,000X; S33102, Invitrogen) was added and mixed homogenously. Agarose gel mixture is then poured into small gel trap with comb inserted, avoiding air bubbles, and left to set for 30 min at RT or 10 min at 4°C. Once set, comb was carefully removed, gel trap was removed and agarose gel was submerged in TAE buffer. 10 µl of q-PCR cDNA product mixed with 2 µl loading dye and pipetted into each well of the gel, with 10 µl of 100 bp and 1 Kbp ladder at each end. Agarose gels were run at 100 V for 20-30 min at RT. Once run was complete and ladder separation had occurred, the gel was removed and scanned on a D-Digit® scanner using a blue light source and high-resolution CCD detectors (LiCor).

2.4. Protein Analysis

2.4.1. Total Protein extraction

Total protein content was extracted as follows. Culture medium was aspirated and washed with 1 ml HBSS. Cells were dislodged from the plate surface using a cell lifter (11577692, Fisher Scientific) in 1 ml HBSS and collected in a 1.5 ml Eppendorf tube and centrifuged at 14,000 rcf at 4°C. The supernatant was discarded and the pellet was re-suspended in 20-50 µl protein lysis buffer (Pierce™ RIPA buffer (89901, ThermoFisher Scientific) and 100X Halt protease and phosphatase inhibitor (78440, ThermoFisher Scientific)). Cell lysates were frequently agitated on ice for 30 min and then spun down at 14,000 rcf for 10 min at 4°C. The supernatant was collected and quantified and stored at -20°C until use.

2.4.2. Cytoplasmic and nuclear protein extraction

NE-PER Nuclear and Cytoplasmic Extraction Kit (Thermo Scientific; 78835, Lot MI0058) was used to extract nuclear and cytoplasmic protein fractions according to manufacturer's instructions. Briefly, approximately 1 x 10^6 cells were detached using pre-warmed TrypLE select and harvested by centrifugation at 500 rcf for 5 min. The pellet was then washed in PBS, transferred to a 1.5 ml Eppendorf tube and centrifuged at 500 rcf for 3 min, and the supernatant was completely removed from pellet. 100 µl ice cold CER I was added to pellet and vortexed vigorously for 15 seconds to fully-suspend the pellet. The fraction was incubated on ice for 10 min and 5.5 µl ice cold CER II added to solution which was then vortexed for 5 seconds and incubated on ice for 1 min. The sample was vortexed again before centrifugation at 16,000 rcf for 5 min at 4°C. Supernatant, containing cytoplasmic protein fraction, was immediately transferred to a clean pre-chilled Eppendorf

tube and stored at -80°C until processing. Insoluble fraction (pellet), containing the nuclear fraction, was re-suspended in 50 µl ice cold NER, incubated on ice and vortexed vigorously for 15 seconds every 10 min for 40 min. The sample was centrifuged at 16,000 rcf for 10 min at 4°C, after which the supernatant, containing the nuclear protein fraction, was immediately transferred to a clean pre-chilled Eppendorf tube and stored at -80°C until processing.

2.4.3. Co-Immunoprecipitation

Co-Immunoprecipitation (CoIP) was performed using µMACS™ isolation protocol (Miltenyi Biotec). Cells were lysed on ice for 30 min in lysis buffer containing 50 mM Tris-Cl (pH 7.5), 150 mM NaCl, 10% glycerol, 10 mM EDTA, 1% Triton (X-100, Sigma) and 1% complete protease and phosphatase inhibitor. Cell lysates were frequently agitated on ice for 30 min and then spun down at 16,000 rcf for 10 min at 4°C. The supernatant was collected in a pre-chilled tube and cell debris was pelleted and discarded.

Lysates were incubated with 5.2 µg monoclonal antibody or 5.2 µg rabbit IgG as a negative control overnight at 4°C on a rotator, followed by incubation the next day with 50 µl µMACS Protein G MicroBeads for 1 h on ice before processing to magnetic separation using µMACS columns. Lysate-MicroBead conjugates were loaded into µMACS columns and flow-through collected. Retained magnetic beads were washed four times with 200 µl of lysis buffer, followed by one wash in low salt containing buffer (Tris-Cl pH 8.0). Elution of labelled proteins was performed by adding 20 µl of preheated (95°C) loading buffer to the column for 5 min at RT. 50 µl loading buffer was applied to the column and the eluted immunoprecipitate was collected in a fresh collection tube. Samples were subsequently analysed by Western blot as described in section 2.4.5.

2.4.4. Protein quantification

BCA protein assay (23225, Pierce) was used to quantify total, cytoplasmic, membrane and nuclear protein fractions. Protein standards were prepared from a BSA standard (2 mg/ml) and serially diluted in PBS to yield 0, 25, 125, 250, 500, 750, 1000, 1500 and 2000 µg/ml. 25 µl of each protein standard was used to generate a standard curve of the assay. 2.5 µl of each protein sample was added to 22.5 µl of PBS, to both minimise the usage of the sample as well as mimic the standard diluent as closely as possible. BCA working reagent prepared as indicated by manufacturer's instructions and added to standards and samples. Absorbance was then measured at 562 nm using FLUOstar® Omega plate reader (Firmware version 1.43) and the Omega Software (5.11).

A standard curve was generated from set of nine protein standards and absorbance readouts were used to plot the linear regression line and associated equation. This equation was then used to calculate the protein concentration of each sample.

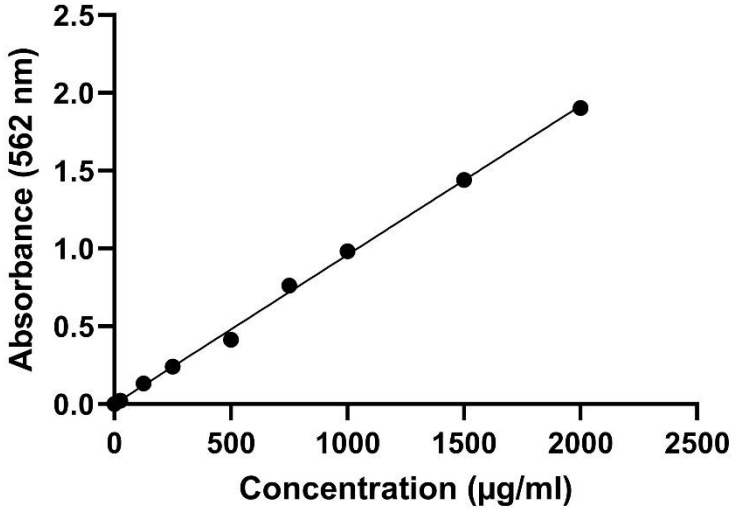

Figure 2.2. A typical standard curve from a BCA assay.
Representative standard curve of a BCA assay generated from a set of nine protein standards. Absorbance was measured at 562 nm using FLUOstar® Omega plate reader.

2.4.5. Western blotting (NuPAGE®)

Total, cytoplasmic, membrane and nuclear protein samples were processed as follows. All samples were normalised based on their concentration obtained according to 2.4.4.

Normalised protein samples were supplemented with 10x NuPAGE® Reducing agent (NP0004, Invitrogen) and 4x NuPAGE® Lithium Dodecyl Sulphate (LDS) sample buffer (NP0007, Invitrogen) to linearize and reduce the net charge of individual proteins within the samples. dH_2O was used to make the volume up to 20 or 25 µl depending on the well size of the gel. Samples were incubated at 37°C for 5 min and cooled on ice and spun down.

For proteins >200 to 14 kDa in size NuPAGE® MOPS running buffer (NP0001, Invitrogen) was prepared in accordance to manufacturer's instructions in dH_2O. 4-12% NuPAGE® Novex™ Bis-Tris gels (NP0335BOX and NP0336BOX, Invitrogen) were used in all western blotting experiments. XCell SureLock® Mini-Cell (EI0001, Invitrogen) was assembled with a 4-12% Bis-Tris gel and a dummy cassette to generate a closed circuit with an inner and outer chamber. NuPAGE® MOPS running buffer was added to the inner and outer chamber and wells were flushed out using running buffer. Protein ladders and samples were loaded into the wells and protein separation was carried out at 200V for ~55 min. PageRuler™ Pre-stained Protein Ladder (SM0671, Fermentas) indicated protein migration and transfer during the experiment, whilst protein size after development was determined using Novex™ MagicMark™ XP (LC5602, Invitrogen) protein ladder.

NuPAGE® transfer buffer (NP0006, Invitrogen) was prepared according to manufacturer's instructions in dH_2O and supplemented with 10% methanol

(322415, Sigma). Blotting pads were pre-soaked in transfer buffer at 4°C and Polyvinylidene fluoride (PVDF) membrane (0.45 µm; LC2005, Invitrogen) was activated through incubation in 100% methanol for 30 seconds before washing in dH_2O.

Upon completion of protein separation the gel was released from the cassette and the transfer apparatus was assembled in the following order from top to bottom in the cathode core; two pre-soaked blotting pads, filter paper, gel, methanol-activated PVDF membrane, filter paper and 3 pre-soaked blotting pads. Following assembly, the transfer apparatus was inserted into the XCell SureLock® Mini-Cell and filled with transfer buffer. The protein content was then transferred onto the PVDF membrane at 30V for 1 h 45 min. Following transfer the PVDF membrane was washed in dH_2O to remove any methanol residue.

Ponceau S (P7170, Sigma-Aldrich) is the sodium salt of a diazo dye which rapidly stains protein bands on PVDF membranes. A Ponceau stain is performed at this stage to determine if proteins have migrated uniformly, to check SDS-PAGE separation and to ensure the efficiency of the transfer. The membrane is briefly immersed in the Ponceau staining solution and then washed twice with dH_2O at RT. The membrane is imaged on a Fujitsu fi-60F flatbed scanner. The membrane is washed a further two times before detection of proteins is performed.

Detection of proteins was carried out using the iBind™ Flex Western device (SLF2000S, Invitrogen) with the iBind™ Flex solution (SLF2020, Invitrogen) as a washing buffer, blocking buffer and antibody diluent. The membrane was blocked for 5 min at RT in iBind™ Flex solution.

Antibodies were prepared in iBind™ Flex solution at the concentration listed in Table 10.7. Following blocking, the membrane was placed protein side down onto

the iBind™ card (SLF1010, Invitrogen). The mechanical force exerted by the lid allows for lateral sequential flow of the antibody and wash solutions over the protein side of the membrane. Upon completion, the membrane was washed three times in dH_2O to remove non-bound antibodies. Detection of Horseradish Peroxidase-conjugated (HRP) secondary antibodies was achieved with incubation of WesternSure™ Premium ECL substrate (926-95000, Li-Cor) for 5 min at RT. The membrane was digitally imaged on a C-DiGit® Chemiluminescent Western Blot Scanner (3600-00, Li-Cor) using the Image Studio™ software (version: 3.1; Li-Cor). See supplementary information section Table 10.7 for primary and secondary antibodies used in Western blotting in this study.

2.4.6. Proteomics

20 µg of protein samples were loaded into a NuPAGE 4-12% Bis-Tris protein gel (Invitrogen) and protein separation was carried out at 200V for ~50 min. BlueEye™ Pre-stained Protein Ladder (94964, Sigma) was used to indicate protein migration and to separate control and treated protein samples. Gel was rinsed with water before fixation using 40% (v/v) ethanol and 10% (v/v) acetic acid for 15 min with gentle agitation. The gel was washed twice in dH_2O and then stained overnight in QC colloidal Coomasie Blue G-250 (BioRad). The following day the gel was de-stained for 2 h with the water changed every 15 min until protein bands were clear and visible. Each sample lane was cut into four fractions and each fraction cut into 1 mm cubes in-gel tryptic digestion.

In-gel tryptic digestion was carried out to digest proteins into peptides. The gel pieces were washed three times with alternating ammoniumbicarbonate (ABC), 50% acetonitrile (ACN) and 100% ACN to shrink and swell the gel to remove contaminants and Coomasie Blue gel stain. Proteins were reduced with 10 mM

dithiothreitol (DTT) and subsequently alkylated with 50 mM 2-chloroacetamide in 50 mM ABC to block the sulfhydyryl groups of cysteine and prevent the formation of S-S bonds. Proteins were then digested overnight at 37°C with 12.5 ng/µl typsin in 50 mM ABC. After digestion, the peptides were extracted from the gel pieces and concentrated using a vacuum centrifuge at 30°C for 3-5 h.

After digestion the peptides were purified through a process of desalting and concentration before analysis with mass spectrometry. Purification was performed using homemade stop-and-go-extraction-tips (StageTips). StageTips were constructed using by stanched monolithic C18 material to fill a 100 µl pipette tip. Acidified peptides bind to the C18 material allowing the bound peptides to be washed before elution. Peptides were washed once with 0.5% acetic acid before elution in 40 µl organic solvent, containing 80% ACN and 0.5% acetic acid. After purification the peptides were analysed on a mass spectrometry system.

2.5. Histology

2.5.1. Cryosectioning

For histological and immunofluorescence analysis, samples were snap-frozen in optimum cutting temperature (OCT) compound (AGR1180, Agar Scientific) using liquid nitrogen. Frozen samples were cryosectioned in the sagittal plane at 20 µm thickness on a Leica CM1850 cryostat. Sections were mounted onto Polysine Microscope Adhesion Slides (10219280, Thermo Scientific) and allowed to air dry for 30 min before fixation for 30 min in freshly made 4% paraformaldehyde (PFA) solution in 10 mM phosphate buffered saline (PBS) and then washed twice in PBST (1X PBS with 0.1-0.3% triton) for 5 min per wash.

2.5.2. Microtome sectioning

Formalin fixed paraffin embedded (FFPE) samples were sectioned at 10 µm thickness on a microtome in the sagittal plane. Sections were floated onto tap water and then mounted onto Polysine Microscope Adhesion Slides and dried on a heat block at 42°C overnight (14 h). FFPE slides were deparaffinised by heating to 65°C for 20 min. The slides were then submerged in xylene twice for 5 min, followed by 5 min washes in 100%, 95% and 70% ethanol before briefly being submerged in tap water. The rehydration of the tissue ensured that antibodies can penetrate into the tissue, as both xylene and paraffin are hydrophobic and would have prevented this. Antigen retrieval was performed by placing the slides into preheated 0.01M citrate buffer solution (citric acid (Sigma Aldrich, C2404) in dH_2O and 0.05% Tween (Sigma Aldrich, P9416) pH 6.0) in a water bath at 98°C for 20 min. The slides were then washed in tap water twice before staining.

2.5.3. Haematoxylin and Eosin staining

Following fixation and washes with 10 mM PBS. Slides were covered in Harris Haematoxylin solution (HHS32, Sigma) for 2 min, until the nuclei appeared purple. Slides were washed twice in tap water to agitate the dye and remove excess particles. Samples were covered in acid alcohol solution (56694, Sigma) for 30 seconds to regress the haematoxylin solution. The slides were washed twice in water. Samples were then stained with Eosin solution (318906, Sigma-Aldrich) for two min, and washed twice in 70% ethanol, followed by two washes in 95% and 100% ethanol. Slides were cleared by placing in Xylene (534056, Honeywell Chemicals) for 2 min before finally being mounted using Eukitt quick hardening mounting medium (03989, Sigma-Aldrich).

2.5.4. Immunofluorescence

Slides were blocked for non-specific binding by incubation with PBST containing 5% Donkey Serum (D9663, Sigma), 0.25% cold water fish gelatine (G7765, Sigma) and 0.25% BSA. Primary antibodies were diluted in blocking buffer (for details see Table 10.2) and incubated overnight (14 h) at 4°C. Following overnight incubation slides were washed twice in PBST at room temperature before incubation with fluorochrome-conjugated secondary antibodies (for details see Table 10.3) for 2 h at RT. Cells were counterstained with 2 µg/ml 4'-6-diamidino-2-phenylindole in 10 mM PBS (1:10,000; DAPI; D9542, Sigma-Aldrich) for 5 min before mounting with DAKO fluorescence mounting medium (S3023, DAKO). See supplementary information Table 10.2 and Table 10.3 for list of primary and secondary antibodies used for immunofluorescence in this study. Every set of staining contained a negative control, with no primary antibody added and only a secondary antibody to exclude any unspecific staining from the secondary antibodies. An example of this is shown in Figure 10.3.

2.6. Imaging

2.6.1. Image acquisition

Cell culture images were captured using Leica DMIL LED Microscope with 10X or 20X objectives and a Leica DFC3000 G camera. The microscope was running Leica Application Suite Advanced Fluorescence (4.4). Histological images were captured using Leica DM1000 LED microscope with a Leica MC170 HD camera. The microscope was running Leica Application Suite software from Leica (4.4.0). Immunofluorescence images were captured using Leica DMI6000 confocal microscope using 10X, 20X, 40X (oil) or 63X (oil) objectives at a resolution of 2048 x 2048 with a Leica TCS SP8 attachment. The microscope ran LAS AF software from Leica (3.5.2.18963).

2.6.2. Image processing

Image processing was conducted using Adobe Photoshop CC (23.0.0). An image for each individual channel was exported from LasX software and opened in Photoshop. Layers were overlaid and adjustments could then be made to the exposure of each channel, any adjustments were carried out to all conditions and negative controls. To enable a better visualisation of the staining, a black and white image (of the merged 568, 488 and 405 nm images) was subtracted from the phase contrast image to allow a black background for the positive staining signal to be better visualised on a phase contrast layer. For this, layers were overlaid, duplicated and merged, this new layer as converted to black and white and subtracted from the phase contrast image.

2.6.3. Quantification

Quantification of total cell number and positive cell counts were measured in Photoshop using DAPI nuclear stain and or fluorescence as a positive cell indicator. A dot was placed on each nuclei or positive cell and counted using ImageJ (version 1.53f51) software. There were 2-3 repeats for each condition and there were 3-4 randomly selected images analysed for each sample. All cell counts were averaged and displayed mean ± SD.

Basal cell cross-sectional area was measured in ImageJ. Scale was set for each image used, then each cell was drawn around using a membrane associated immunofluorescence staining as a reference and the cross-sectional area was measured. Each condition had 2-3 repeats and for each sample there were 3-4 randomly selected images taken. The cross-sectional areas were averaged for each condition and displayed as mean ± SD.

Epidermal thickness was measured in LASX software (version 3.4.2). Measurements were taken at pre-selected defined points on every image to ensure no bias could take place; lines were drawn as layer over image denoting where the measurements would be taken. Total thickness was measured from the surface of the insert to the top of the corneum, while the cellular thickness (basal to granular) was measured from the surface of the insert to the top of the granular layer and the acellular thickness (corneal) was measured from the top of the granular layer to the surface of the corneal layer (Figure 10.18). Measurements were averaged and displayed as mean ± SD.

2.7. Statistics

All experimental data within this study was analysed using PRISM 9 software (Graph Pad). Each RT q-PCR was run in triplicate for experimental controls. $^{\Delta\Delta}$Ct method of analysis was performed, in which all experimental results are normalised first to internal housekeeping genes and then to control samples. This enabled background expression to be removed and expression levels could be compared relatively between experimental samples. For RT q-PCR analysis data was exported into Excel for comparative Ct analysis. Data was subsequently exported to PRISM for statistical analysis and presented as mean with the standard deviation. One-way or Two-way analysis of variance (ANOVA) followed by Bonferroni correction were used to compare replicate means by row and correct for multiple comparisons.

For multiple comparisons a One-way ANOVA was used to compare the means of three or more groups. This statistical test was used in conjunction with Tukey's multiple comparison post-hoc test, which compares every mean with every other mean, or Dunnett's post-hoc test which compares every mean with a control; both

tests enable for any unequal sample sizes and accounts for the scatter of the groups. A Two-way ANOVA was used to analyse data with two grouping variables, with Tukey's multiple comparison or Bonferroni post-hoc test to correct for multiple comparisons. Unpaired *t*-test was carried out to compare the means of two groups displaying a normal distribution. In all cases a confidence interval of 95% was used and a *p* value of <0.05 was regarded as statistically significant. Statistical significance was indicated by asterisks ($*p<0.05$, $**p<0.01$ and $***p<0.001$).

3. Tau expression in the epidermis is linked to the programme of terminal differentiation in keratinocytes

3.1. Introduction

To date, most research into tau has been conducted in neural tissues, with few reports of tau expression in peripheral tissues such as kidney, skeletal muscle, salivary glands and skin. Only a handful of studies have examined the total expression of tau in the epidermis [196,277,278], and to the best of our knowledge no investigation has been performed into the localised expression pattern or function of tau throughout the differentiated layers of the epidermis. Consequently, the role that tau plays in epidermal homeostasis and differentiation is still unknown.

The epidermis is a stratified squamous epithelium, where the innermost basal layer remains in contact with the BM and as cells move outwards, they enter a programme of differentiation, involving the formation of robust intracellular junctions, changes in gene expression and eventually destruction of cellular organelles. The skin undergoes major structural and expressional changes throughout the process of differentiation. The cytoskeletal network undergoes significant reorganisation during this programme of differentiation. Tau has been reported to play a role in the stabilisation of microtubules and IF networks in many cell types [179,184,245], but the role of tau in keratinocyte differentiation remains unclear. Understanding how tau interacts with the IF in keratinocyte differentiation might uncover strategies that could be used to inhibit the major cytoskeletal changes that take place during the initiation and progression of skin cancer.

3.2. Chapter aim and objectives

Chapter aim:

To investigate the expression of tau in the epidermis of healthy human skin.

Chapter objectives:

1. Characterise tau expression in the healthy epidermis at an RNA and protein level.
2. Investigate the specific isoform expression of tau throughout the stratified layers of the epidermis.
3. Explore the subcellular localisation of tau and identify any changes throughout keratinocyte differentiation.

3.3. Methods

The methods used in this chapter involve the use of human skin samples generously provided by Dr Emmanuella Guenova-Hötzenecker from the Dermatological Biobank (EK 647). Full details of donor consent, tissue collection, diagnosis and local ethical approval are outlined in methods Chapter 2.2 and individual patient tissue sample information is summarised in Table 10.10.

Diagnoses of patient biopsies were carried out by dermatologists at the University Hospital Zurich after initial collection as a standard procedure. Hematoxylin and Eosin (H&E) is a routine histological stain, used regularly by pathologists to analyse and generate clinical diagnoses of patient biopsies that can subsequently be used by physicians for treatment. Validation of a healthy phenotype of the human skin samples used in this study was performed at the start of the study using H&E (Methods 2.5.3), immunofluorescence analysis (Methods2.6) and q-PCR (Methods 2.3). One skin sample displaying an abnormal histology was

removed from the study before analysis of tau expression was performed. Blinding of samples was not possible as healthy, SCC and BCC samples present with obvious pathological lesions.

Tau expression in human skin samples was analysed at an mRNA and protein level. First, using isolated regions of interest (ROI) using LCM and subsequent RT q-PCR (Methods 2.3). All q-PCR data in this chapter was presented as the normalised mean ± standard deviation (SD) and analysed using GraphPad Prism (version 9.0.0). Each q-PCR was run in triplicate, producing experimental controls, and the $^{\Delta\Delta}$Ct method of analysis was performed, in which all experimental results are normalised first to internal housekeeping genes and then to control samples. This enabled the relative expression levels to be compared between experimental samples. Statistical significance of RT q-PCR data were determined by performing a One-way analysis of variance (ANOVA) or Two-way ANOVA followed by Bonferroni correction to compare replicate means by row and correct for multiple comparisons. This enabled the identification of how a response is affected by two factors: patient sample and epidermal population. Statistical significance was set at * $p < 0.05$, ** $p<0.01$ and *** $p<0.001$.

3.4. Results

3.4.1. Characterisation of healthy human skin samples used in this study

H&E staining indicated that the structural integrity of the tissue was preserved in all samples (Figure 3.1). No artefacts within the tissue were observed that would affect any staining performed and the tissue overall did not appear to be damaged or broken. H&E staining of the patient samples enabled the identification of the correct cellular compartments found in healthy human skin in all of the healthy biopsies received. A normal epidermis with an underlying dermis consisting of a

papillary and reticular dermis were identified in all healthy skin biopsies received. All healthy samples also displayed rete ridges and a pink dermis with fine collagen fibres in the papillary dermis and thicker bundles of collagen in the reticular dermis indicated from the pink eosin staining (Figure 3.1). No signs of solar elastosis were present; usually found in sun exposed skin samples where the collagen fibres are replaced with fragmented fibres of elastin, displaying a blue stain in the dermis, rather than a pink collagenous stain. High magnification of images revealed normal stratified, squamous epithelia in all the patient biopsies (Figure 3.1). Keratinocytes presented with a round or polygonal morphology with pink cytoplasm indicating a cytoplasm filled with cytokeratin. Cells in the basal layer were regularly spaced out and lined the BM in an organised layer. Keratinocyte nuclei were round indicating no obvious abnormalities. There was no obvious signs of mitosis occurring in the stratum spinousum, and eosin staining appeared darker in the granular layer; staining dark purple granuoles, indicating the presence of kerahanuole granules made up of loricrin, filaggrin and involucrin, as would be expected in healthy skin. The stratum corneum was present in all healthy skin samples used in this study, with no signs of parakeratosis, and there were no nuclei retained in the corneum. None of the healthy samples displayed a stratum lucium, confirming that the samples used were not obtained from skin located on the palm of the hands or sole of the feet. The lack of this layer also indicated that there were no signs of abnormalities in the skin from excess rubbing or scratching that can also generate a stratum lucium and thickening of the corneal layer of the epidermis.

Patient 2 and 3 (Figure 3.1A and B) samples displayed strong melanin staining in the basal layer and in suprabasal cells scattered throughout the epidermis. The melanin is located, as expected, on the superior surface of the cells.

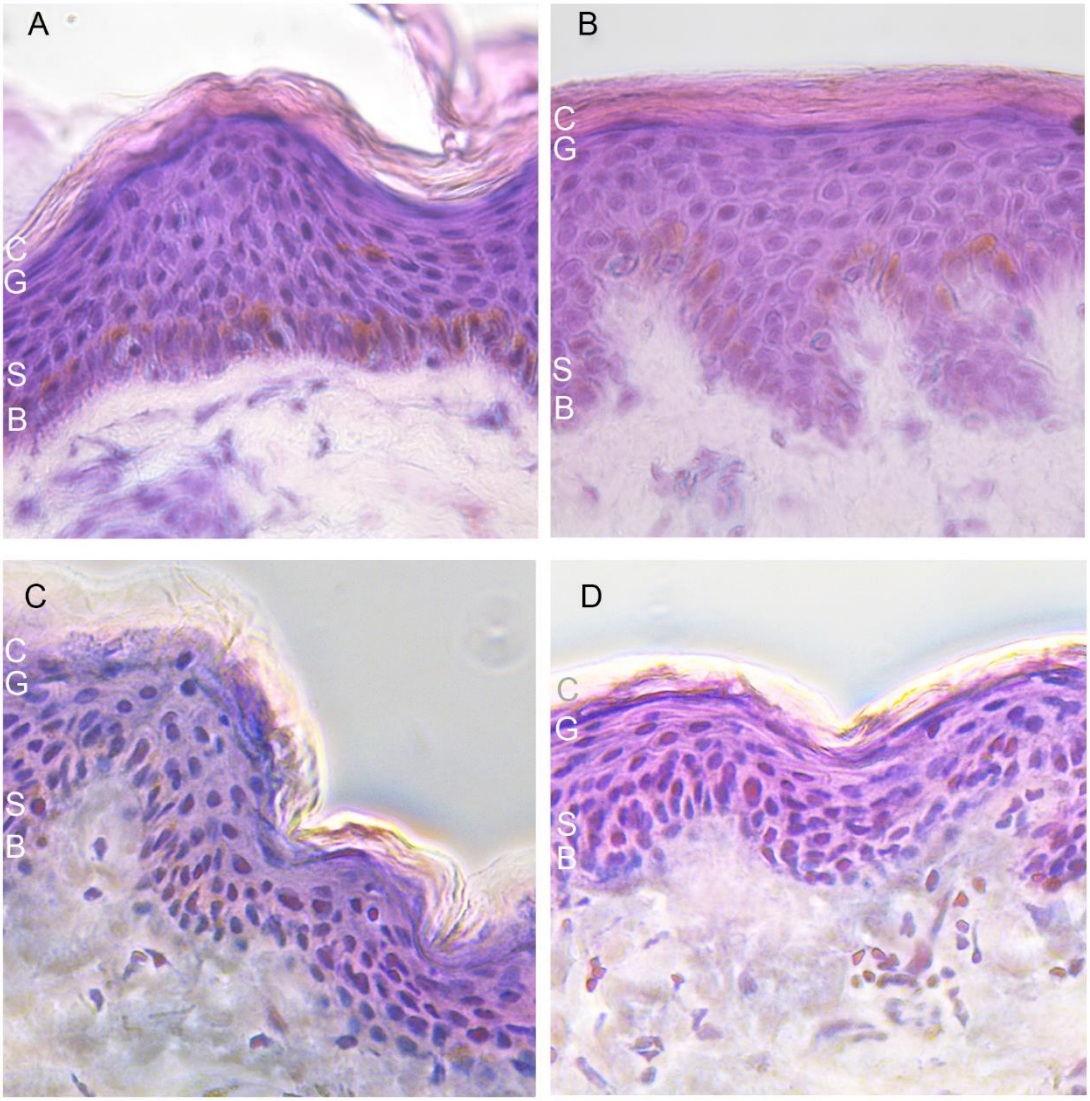

Figure 3.1. Haematoxylin and Eosin staining confirmed healthy phenotype in skin samples used in this study.
Representative haematoxylin and eosin staining of sagittal sections of healthy human skin samples used in this study. All samples displayed a healthy pink, collagenous dermis, with no signs of solar elastosis. A stratified, squamous epithelium was found in all samples, with clear separation from the dermis by a tightly packed, organised layer basal cells lining the basement membrane. The stratum corneum stained light pink with no nuclei present. **A.** Patient 2. **B.** Patient 3. **C.** Patient 6. **D.** Patient 7. Epidermal layers are indicated on each image in white text; B – Stratum basale, S – Stratum spinousum, G – Stratum granulosum, C – Stratum corneum.

Melanocytes can be observed scattered throughout the epidermis of some of the healthy skin samples, indicated by a slightly greyer appearance after H&E staining compared to epidermal keratinocytes. The cytoplasm of melanocytes can also be seen to leave a vacuole around the edge of the cells such as in Figure 3.1A. This artefact occurs due to the melanocytes lacking the strong cadherin and desmosomal links to keratin fibres that the keratinocytes possess. Therefore, after tissue processing a vacuole can be occasionally found in melanocytes around the membrane, whereas in keratinocytes this artefact would only be located around the nucleus of the cell.

Following the H&E staining, full characterisation of the healthy human skin samples was performed using immunostaining. Immunofluorescence of key stratification markers helped to confirm that the skin samples used in this study displayed the correct expression pattern expected in normal healthy human skin. One of the most widely used markers to identify keratinocytes in the stratum basale is cytokeratin-14 (K14). Immunofluorescence staining of healthy human skin confirmed K14 expression was restricted to the basal layer in nearly all samples, with low expression detected in the spinous layer of a few patients (Figure 3.2). In parallel, cytokeratin-1 (K1) is a widely used marker to identify suprabasal cells in healthy human skin samples. Therefore, immunofluorescence staining was performed to ensure that healthy human skin samples displayed a clear and correctly differentiated stratum spinosum. Basal keratinocytes were negative for the expression of K1, with only the immediately adjacent spinous and suprabasal cells expressing this cytokeratin within the epidermis as would be expected in a healthy epidermis (Figure 3.3).

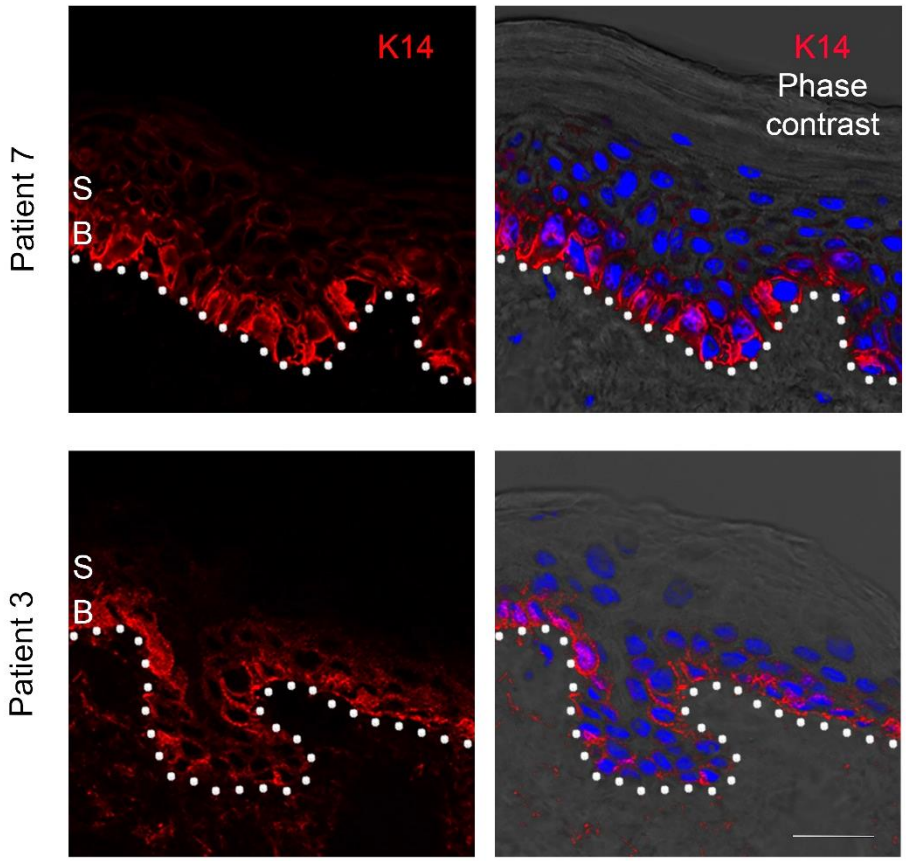

Figure 3.2. Keratin-14 expression is restricted to the basal layer in healthy human skin samples.
Representative immunofluorescence staining of cytokeratin-14 (K14) from healthy human skin samples (n=6). Strong K14 (red) expression was restricted to the basal layer in the epidermis as expected in healthy skin samples. B – Stratum basale, S – Stratum spinosum. White dotted lines represent the epidermal-dermal boundaries. Nuclei counterstained with DAPI (blue) and displayed with the phase contrast image to allow epidermal morphology to be visualised. Scale bar 25 µm.

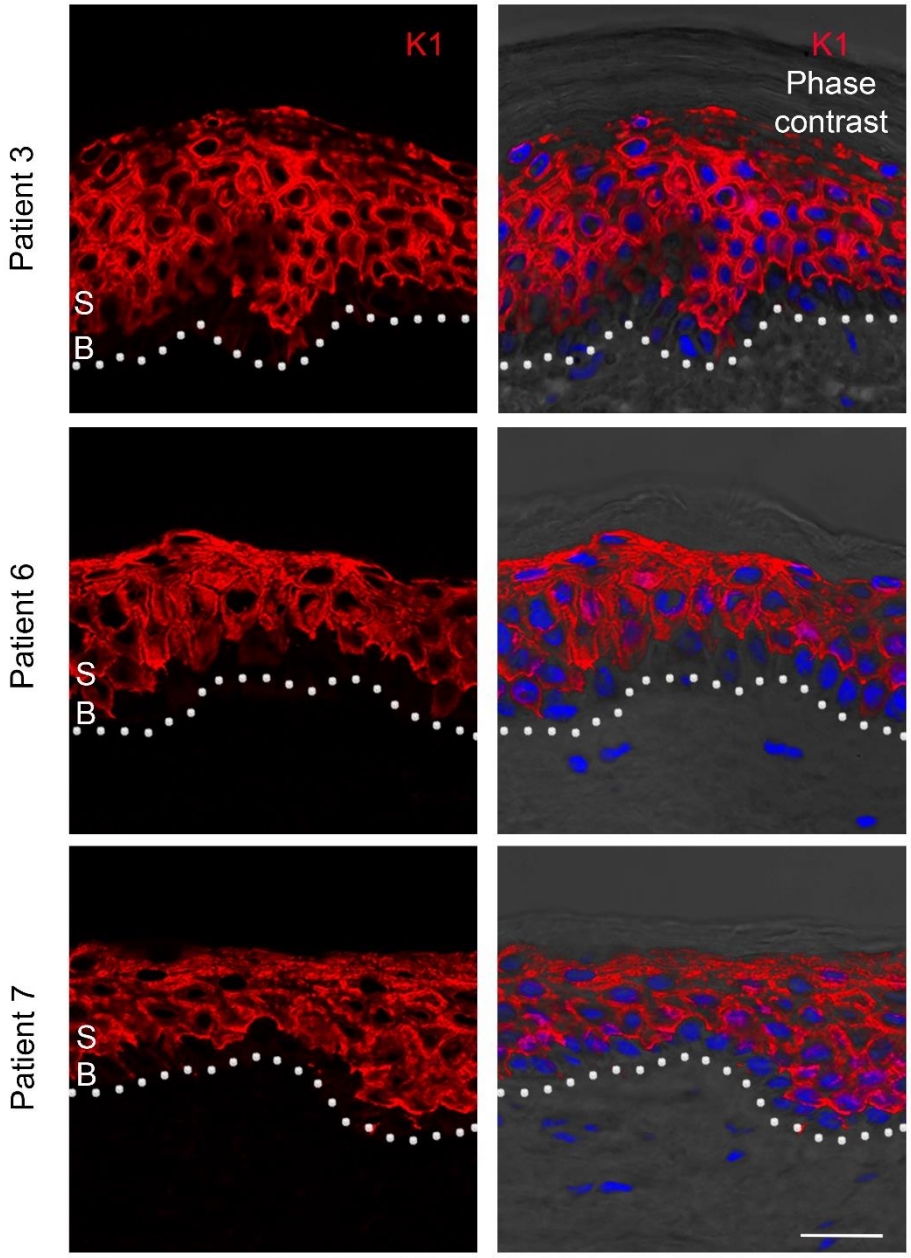

Figure 3.3. Keratin-1 expression is restricted to the suprabasal keratinocyte population in healthy skin samples.
Representative immunofluorescence staining of cytokeratin-1 (K1) in healthy human skin samples used in this study (n=6). K1 (red) expression is absent in basal keratinocytes and restricted to the spinous and granular layer of the epidermis. B – Stratum basale, S – Stratum spinosum. White dotted lines represent the basement membrane. Nuclei counterstained with DAPI (blue) and displayed with phase contrast images of the epidermis for accurate visualisation of sample morphology. Scale bar 25 µm.

The SC niche of the epidermis is located in the innermost, basal layer of the epidermis [28]. Ki67, a marker of cell proliferation, is expressed in cells in active phase of the cell cycle, but it is not expressed in quiescent cells in G_0. Immunofluorescence staining of healthy skin biopsies confirmed in all samples used in this study Ki67 positive cells were scattered throughout the basal layer (Figure 3.4). Some sections showed Ki67 positive cells in the basal and suprabasal layer, suggesting cell divisions perpendicular to the BM were taking place rather than the delamination of keratinocytes (Figure 3.4). Loricrin is a major protein in the cornified envelope, and it is expressed by terminally differentiated epidermal keratinocytes in the granular layer. All healthy biopsies used in this study correctly showed strong loricrin expression in the granular layer as expected in healthy human skin (Figure 3.5) with no or little staining in basal and spinous cells.

The expression profile of proteins in the healthy epidermis is summarised in Table 3.1, highlighting how different layers and cell types in the epidermis can be identified through the expression of differentiation markers. This table will aid in the identification of differentiation specific tau expression and co-localisation in the epidermis in section 3.4.2.2.

3.4.2. Tau expression in healthy human skin

Following the full characterisation of the healthy human skin samples, tau expression throughout the epidermis was investigated at an RNA and protein level. The characterisation of tau expression under physiological conditions was performed to further investigate the role of tau in epidermal differentiation. Immunofluorescence staining was initially performed to confirm and identify tau protein expression patterns in the healthy epidermis.

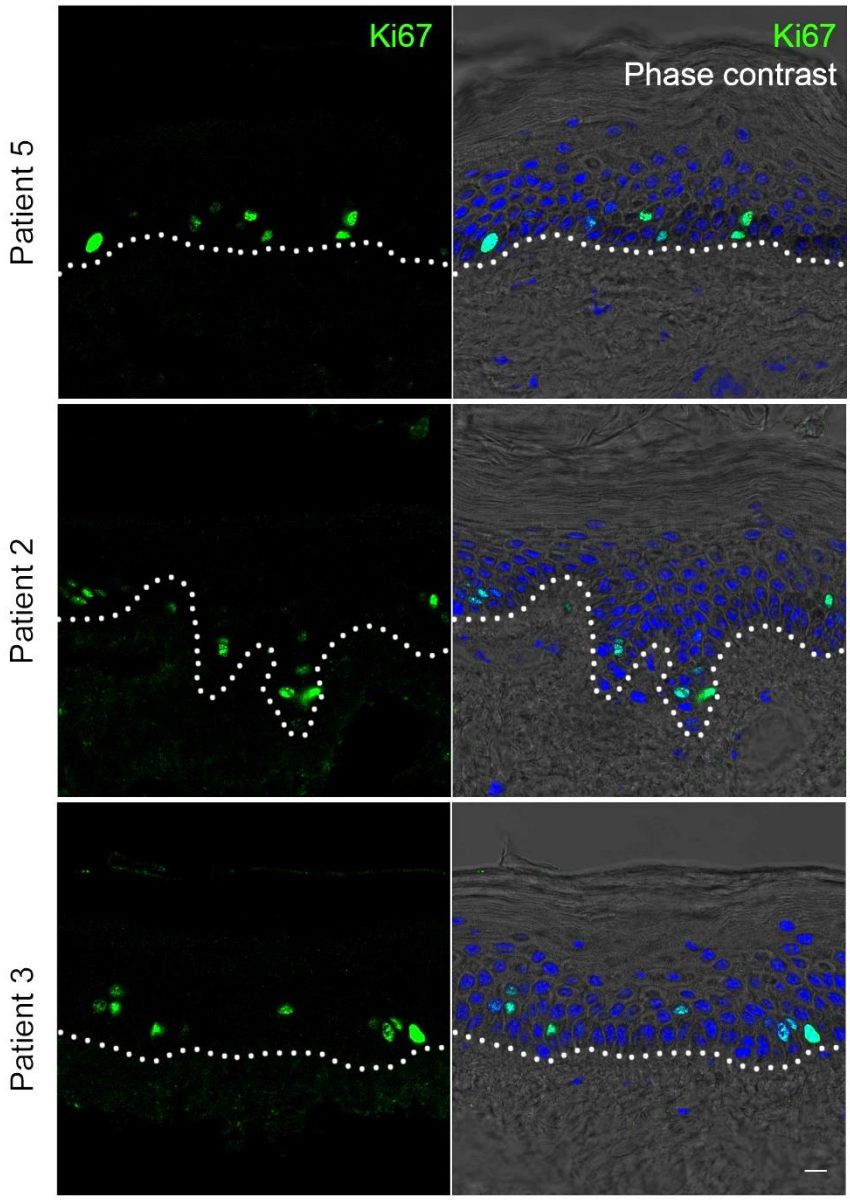

Figure 3.4. Proliferating cells in the basal layer of the healthy epidermis. Representative images of immunofluorescence staining of the healthy human skin biopsies (n=6). Ki67 (green) was mostly restricted to the basal layer of the epidermis. White dotted lines represent the epidermal-dermal boundaries. Nuclei counterstained with DAPI (blue) and displayed with phase contrast images for visualisation of sample morphology. Scale bar 10 µm.

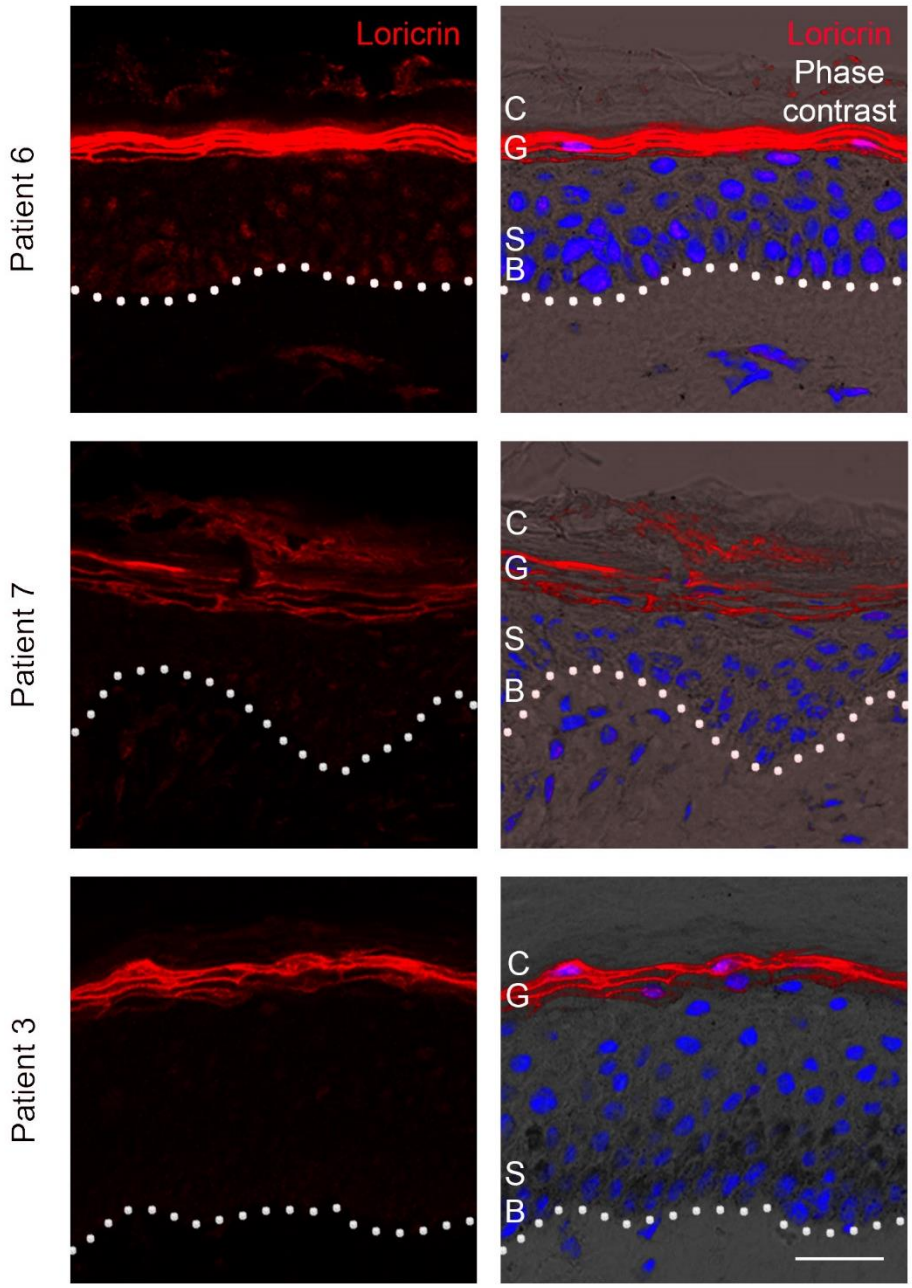

Figure 3.5. Loricrin expression is restricted to the granular layer of the epidermis in healthy skin samples.
Representative immunofluorescence staining of terminal differentiation protein loricrin (red) in healthy human skin samples (n=6). Loricrin expression was restricted to the granular layer of the epidermis, with no or little expression in the basal or spinous layers. B – Stratum basale, S – Stratum spinousum, G – Stratum granulosum, C – Stratum corneum. White dotted lines represent the epidermal-dermal boundaries. Nuclei counterstained with DAPI (blue) and displayed with phase contrast images. Scale bar 25 µm.

Table 3.1. An overview of immunofluorescence staining presented in healthy human skin biopsies.

Marker	Healthy human skin tissue				
	Epithelial				Mesenchymal
	Stratum Basale	Stratum Spinosum	Stratum Granulosum	Stratum Corneum	Dermis
Keratin 14	+++	+			
Integrin-α6	+++				
Ki67	++	+			+
Keratin 1		+++	+++		
Loricrin		+	+++		
Filaggrin		+	+++		
Vimentin	+*				+++

Staining profiles demonstrate the expression patterns observed in the skin tissue, enabling identification of specific populations in tissue samples, and aid in the identification of individual cell populations later in cell culture conditions.
* Scattered vimentin staining can be found in other cell types in the epidermis, such as dendritic cells. Expression levels are categorised as: +, weak or scattered; ++, moderate expression; +++, strong expression.

3.4.2.1. Tau displays distinct expression patterning in basal and suprabasal keratinocytes

Analysis of tau expression in healthy skin samples was performed with three commercially generated monoclonal antibodies with epitopes corresponding to different regions of the tau protein (Table 10.11). Tau [E178] is a recombinant rabbit monoclonal antibody commercially generated using a synthetic peptide within human tau 705-719. The immunogen corresponds to a fragment within the C-terminal region of the protein that is present in all isoforms with or without post-translational modifications [300]. The tau5 is a mouse monoclonal antibody commercially generated using purified bovine microtubule associated proteins as the immunogen and then screened for monoclonal antibodies that recognised tau specifically. This antibody is specific for an epitope that lies between amino acids Ser210-Arg230 of human tau, which corresponds to a fragment within the proline rich domain (PRD) that is present in all isoforms with or without post-translational modifications [301]. The tau clone AT8 mouse monoclonal antibody recognises a phosphatase sensitive epitope on PHF-tau [302,303]. It is reported that there is no cross-reactivity to non-phosphorylated tau. The epitope recognises the phosphorylated Ser202 residue. Although Ser202/Thr205 is the primary phosphor-epitope recognised by the AT8 antibody, but there are reports of it also recognising Ser199/ser202 and Thr205/Ser208. This phosphor site is located within the proline rich domain (PRD) that is present in all isoforms but will only bind to those with phosphorylation as a post-translational modification at the specific epitope region.

Immunofluorescence staining with tau [E178] revealed that tau is broadly expressed in all keratinocytes within the epidermis with significantly increased expression in the suprabasal populations (Figure 3.6 and Figure 3.7). However,

the cellular localisation of tau expression can be observed to change through the differentiated layers of the epidermis. Tau [E178] expression in basal cell populations was mainly restricted to the nucleus with low levels of tau protein detected in the cytoplasm and asymmetrically distributed tau expression at the basal membrane of basal cells (Figure 3.6B and Figure 3.7B). Although tau was identified in the nucleus of all basal cells, the expression density of tau in this basal population varied amongst neighbouring cells. Additionally, although tau expression was mainly identified in the nucleus, cells within the folding of the rete ridges also showed tau expression. This was asymmetrically distributed to the basal surface of the cells where they attached to the BM (Figure 3.6B). These rete ridge structures are important to the structural integrity of the epidermis, are known to house the SC population (Figure 1.5) and within these folding's, known as the suprapapillary plate, keratinocytes display special cytoskeletal arrangements [50,51,104]. In contrast, throughout the suprabasal keratinocytes tau [E178] was found to be expressed in both membrane, cytoplasmic and nuclear compartments of the cell (Figure 3.6C and Figure 3.7C). Strikingly, the highest levels of protein expression were found in cells of the granular layer of the epidermis. Although tau [E178] showed expression was confined mostly to the nucleus in the basal layer of the epidermis, the majority of this population were negative for phosphorylated tau (Figure 3.6B and Figure 3.7B). However, immediately adjacent to the basal population, the suprabasal population containing differentiated keratinocytes, stained positively for phosphorylated tau (AT8) (Figure 3.6 and Figure 3.7). No tau protein was detected in the

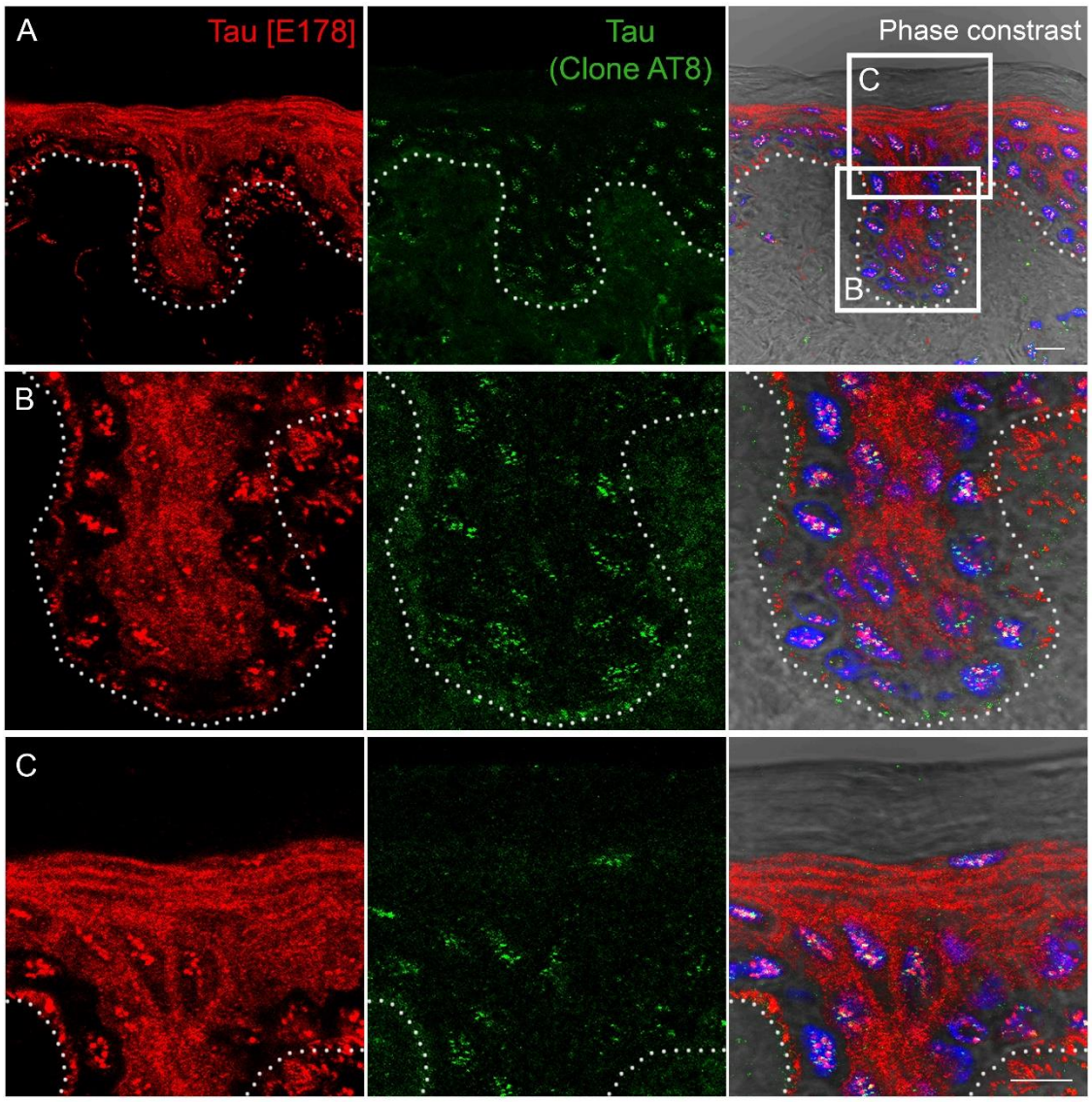

Figure 3.6. Tau expression throughout the healthy epidermis.
Tau expression was detected with rabbit monoclonal antibody Tau [E178] (red) and mouse monoclonal phosphorylated tau antibody clone AT8 (green), specific to phosphorylated tau at Ser202/Thr205 in sagittal sections of healthy human skin by immunofluorescence. **A**. Representative immunofluorescence staining of cryo-frozen patient 6 healthy skin sample with acetone fixation (n=6). Tau expression was upregulated in suprabasal populations with the highest expression in the granular cells. All skin samples used in this study demonstrate the same expression pattern of tau. **B**. Tau expression can be seen to be largely restricted to the nuclear fraction in basal keratinocytes. However, the basal cells located in the suprapapillary plate (the upper folding of the rete ridges) were found to have strong staining in the basal surface that is attached to the basement membrane. **C**. Suprabasal cells are found to express tau in both the cytoplasm and nucleus unlike basal cells. Although tau expression is found throughout the epidermis highest tau protein expression is found in the granular layer of the epidermis. White dotted lines represent the epidermal-dermal boundaries. Nuclei were counterstained with DAPI (blue) and all channels are displayed with the phase contrast image in the right panel to allow accurate visualisation of sample morphology. Scale bar 10 µm.

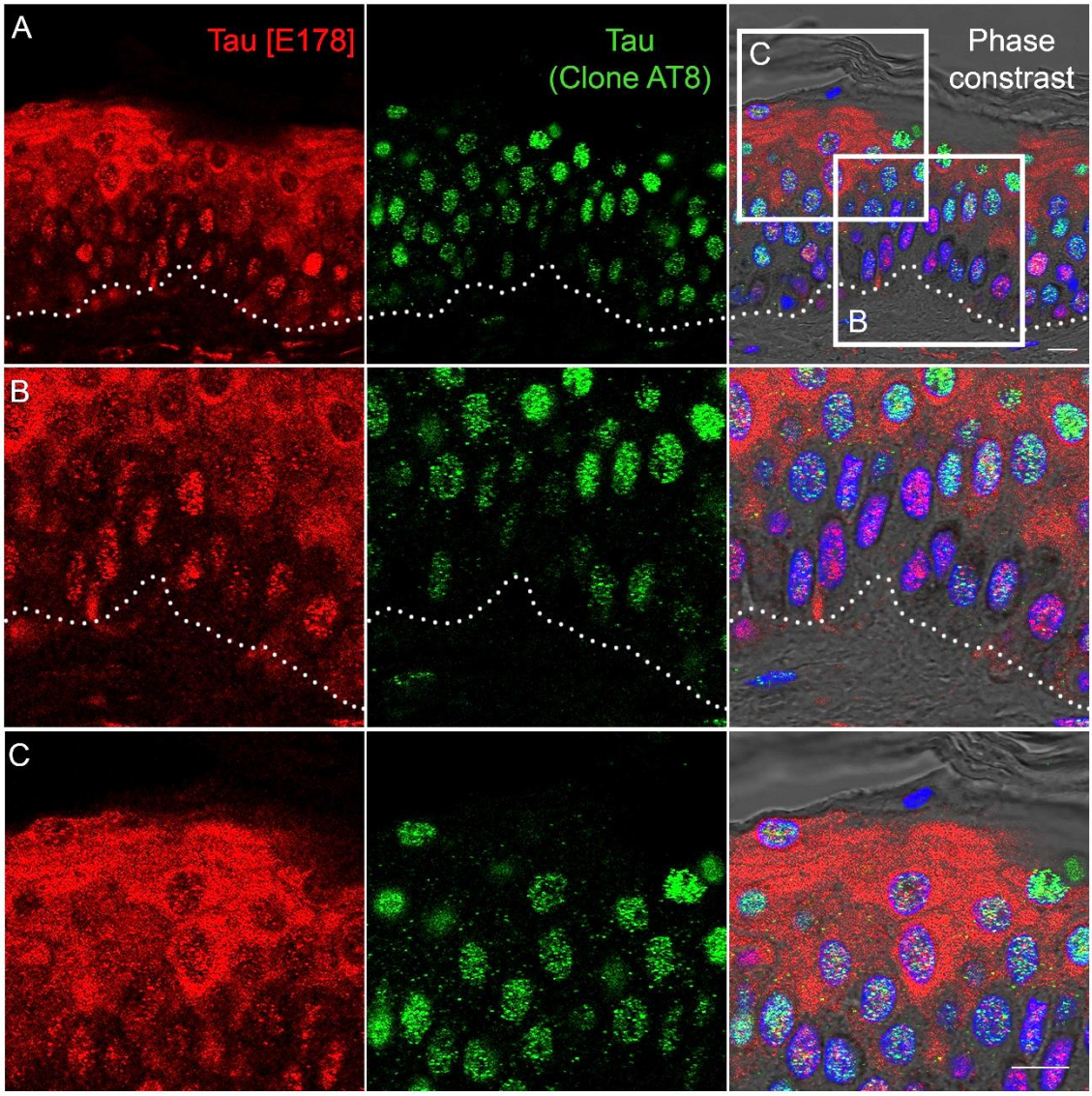

Figure 3.7. Tau expression is up regulated in suprabasal differentiated cells of the epidermis.
A. Representative immunofluorescence staining of tau [E178] (red) and mouse monocolonal phosphorylated tau antibody clone AT8 (green), specific to phosphorylated tau at Ser202/Thr205 in an FFPE sagittal section of patient 9 healthy skin sample (n=5). Tau expression is significantly increased in the suprabasal cells of the epidermis. **B.** Tau [E178] is absent in the cytoplasm of the basal keratinocytes and is restricted to the nucleus of this population. Phosphorylated tau (clone AT8) is mostly absent in basal keratinocytes with increased phosphorylated expression in the suprabasal cells. **C.** In contrast to basal cells, suprabasal cell populations display tau [E178] expression in both the nuclear and cytoplasmic fractions of the cells. Phosphorylated tau (clone AT8) expression is strikingly higher in the suprabasal population of differentiated keratinocytes. White dotted lines represent the basement membrane. Nuclei were counterstained with DAPI (blue) and all channels are displayed with the phase contrast image in the right panel to allow accurate visualisation of sample morphology. Scale bar 10 µm.

outermost layer of the epidermis, the stratum corneum (Figure 3.6C and Figure 3.7C). The sudden disappearance of tau in the corneal layer of the epidermis suggests that tau does not play a role in the barrier function, nor does the protein maintain its integrity in the final stages of differentiation.

To further investigate the molecular expression pattern of tau, identify any changes to tau isoforms throughout the epidermis and ascertain how this might be influenced by the cells differentiation status, regions of tissue were selected and removed through LCM. Due to the distinct patterning of tau expression observed in the epidermis through immunofluorescence it would have been inaccurate to extract and analyse RNA from the whole epidermal tissue. Therefore, LCM was performed to extract total RNA from two regions of interest (ROI) in the epidermis; the basal and suprabasal populations (Figure 3.8). The basal layer of the epidermis is well recognised to contain the SC and TAC population, whereas the directly adjacent suprabasal keratinocytes contain differentiated, stratified epidermal keratinocytes.

To confirm the two ROI had been successfully captured, specific markers associated with epidermal differentiation were first analysed by q-PCR. RNA expression of specific markers associated with basal, and suprabasal keratinocytes confirmed that the two populations were correctly captured in all skin samples (Figure 3.9). All samples displayed a decreased K14 and K5 expression in the suprabasal population relative to the basal population (Figure 3.9 and Figure 10.4). In all skin samples the relative expression of K1 and K10 in the captured suprabasal tissue was at least 3 times higher than the

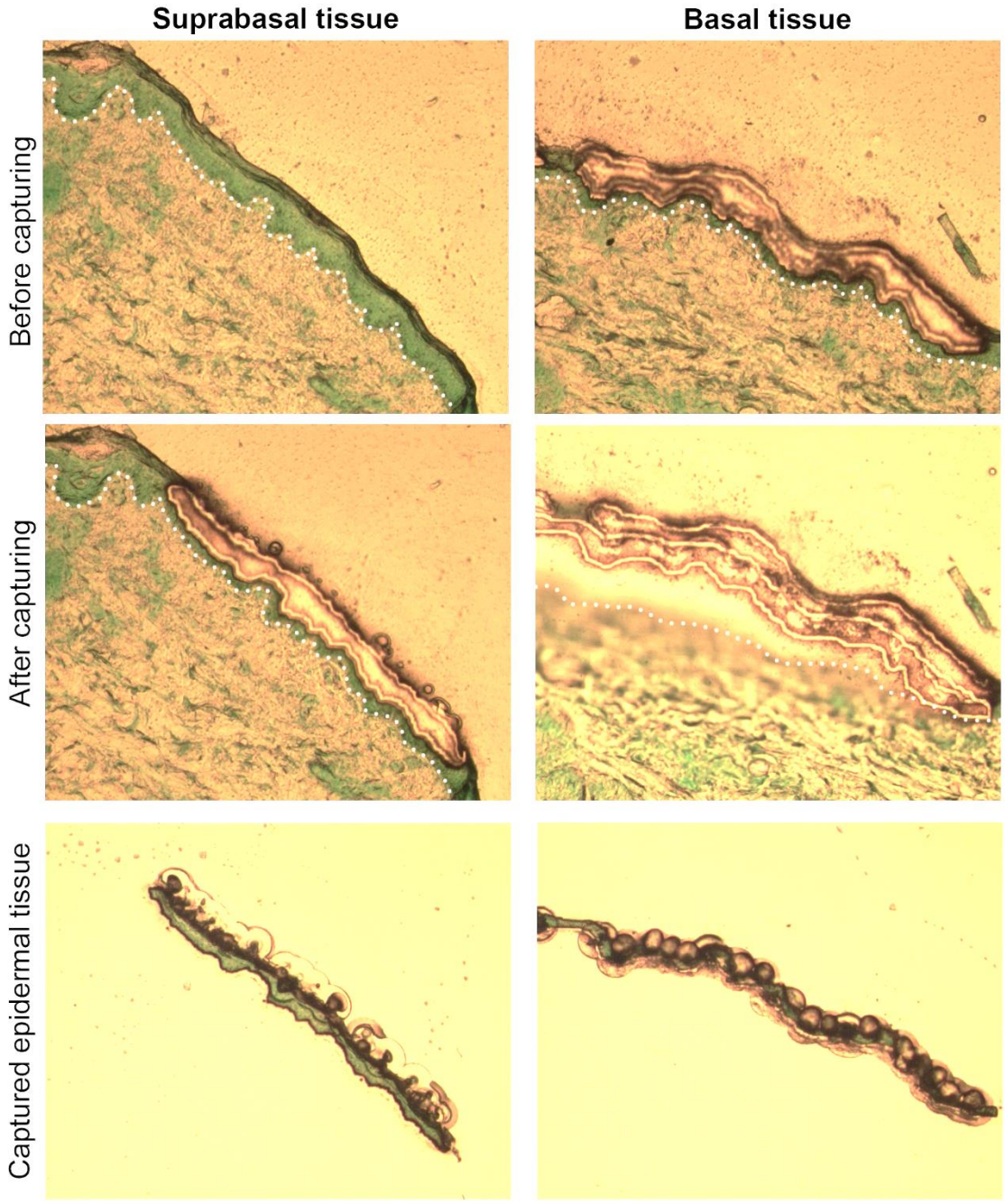

Figure 3.8. Isolation of basal and suprabasal epidermal tissue using Laser Capture Microdissection.
Representative images of LCM-captured epidermal basal and suprabasal regions of interest (ROI). **Top**: Methyl green stained sagittal section of the human epidermis prior to cutting with ultraviolet (UV) laser and LCM extraction. The dotted line represents the boundary of the human epidermis. **Middle**: Representation of suprabasal and basal ROI removed from original tissue after cutting with UV laser and melting tissue onto cap with InfaRed (IR). Middle left: suprabasal tissue removed from tissue sample. Middle right: basal tissue removed from tissue sample. **Bottom**: ROI tissue cut on CapSure® Macro LCM caps. Black circles are IR-melted film.

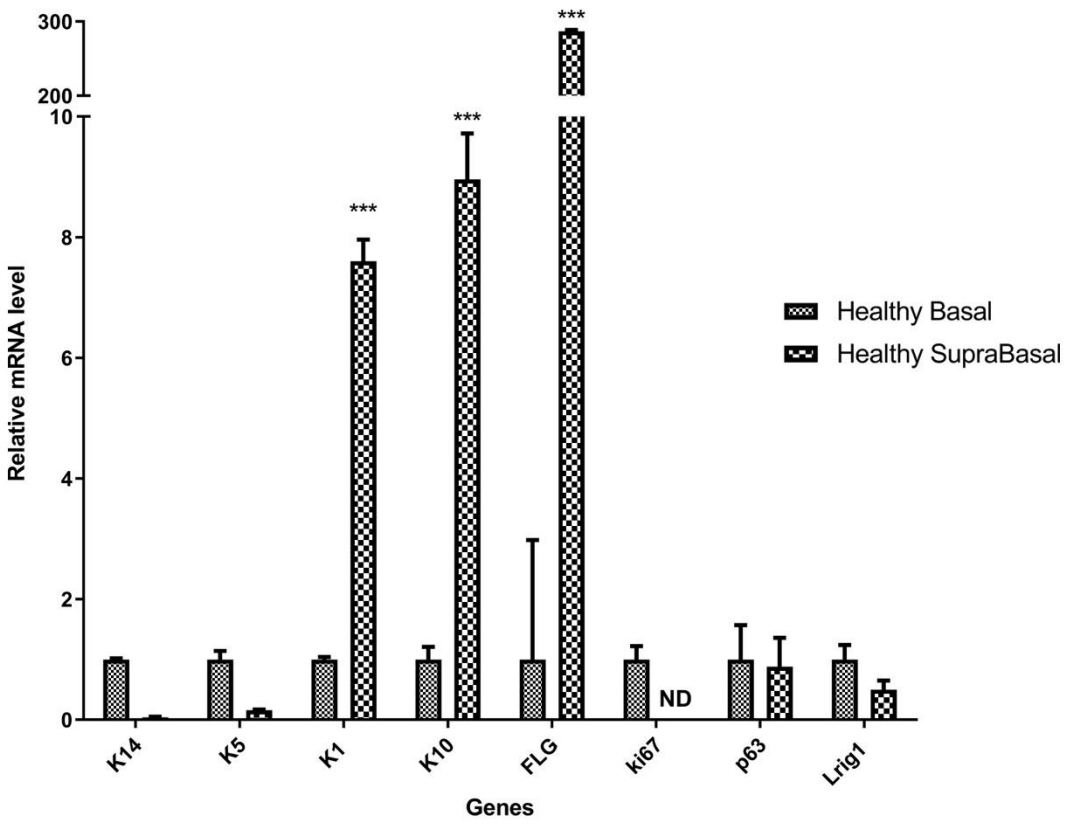

Figure 3.9. RT q-PCR analysis of the two epidermal regions of interest isolated from healthy human skin using Laser Capture Microdissection.
Representative RT q-PCR analysis of basal and suprabasal regions of interests using LCM (n=5). Representative expression patterns from patient 3 captured regions of interest (ROI) are displayed showing the two distinct populations were successfully isolated, with Glyceraldehyde-3-Phosphate Dehydrogenase (GAPDH) as a reference gene. Basal ROI showed high relative expression of K14, K5, Ki67 and Lrig1 compared to the suprabasal population. Suprabasal ROI showed a significantly increased relative expression of differentiation markers; K1, K10 and filaggrin. Ki67 expression was not detected in the suprabasal population. All 5 human skin samples isolated demonstrate the same expression patterns. FLG – filaggrin; ND – not detected. Ct values normalised to GAPDH and $2^{-\Delta\Delta Ct}$ method of analysis used. Relative expression levels are displayed as mean ± SD. Two-way ANOVA with Bonferroni correction was used to test significance; *** $p<0.001$.

expression detected in the captured basal population, with patient 7 and 3 displaying a 7-9 fold change in K1 and K10 expression (Figure 3.9 and Figure 10.4). All samples showed a significant increase in filaggrin expression in the suprabasal ROI (Figure 3.9 and Figure 10.4). Patient 3 and 7 samples demonstrated a dramatic relative expression increase in filaggrin, with a fold change of 286 and 335 respectively (Figure 3.9). Terminal differentiation proteins such as, filaggrin and involucrin, would not normally be expected to be expressed by cells in the basal layer, and expression should only be limited to spinous cells as either immature proteins as pro-fillagrin or mature proteins such as involucrin and filaggrin. Ki67 expression, as expected, decreased in the suprabasal population across samples, with non-detectable levels in most of the suprabasal populations (Figure 3.9). In the healthy epidermis, suprabasal cells should have committed to terminal differentiation and should not have been active in the cell cycle. P63 was also recognised as a marker for proliferation and displayed a decreased expression profile in the captured suprabasal region across human samples. Additionally, Lrig1, a recognised SC marker in the epidermis, is decreased in captured suprabasal tissue (Figure 3.9). sq-PCR results allowed validation of the RT q-PCR results and validation of primers for LCM work. Agarose gel images also allowed the identification of whether primers were effective at amplifying the gene of interest (Figure 10.4).

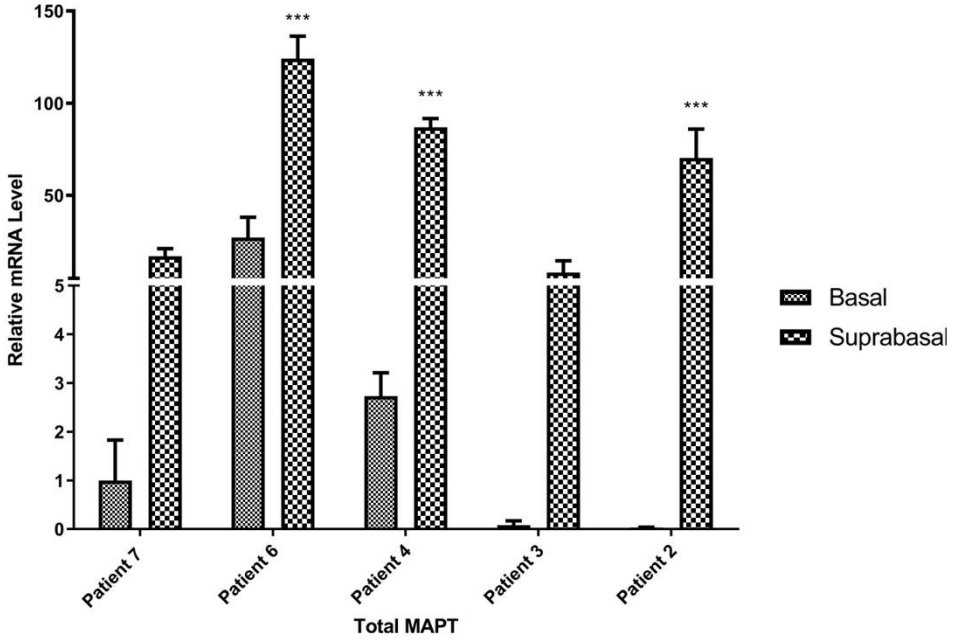

Figure 3.10. RT qPCR analysis of *MAPT* mRNA expression levels in the healthy human epidermis.

A. Representative RT q-PCR analysis of *MAPT* mRNA expression in basal and suprabasal cell populations in the healthy human epidermis (n=3). *MAPT* expression is increased in all suprabasal populations of patient samples analysed in this study. Relative expression of target gene, *MAPT*, was calculated by normalisation to patient 7 basal tissue using Glyceraldehyde-3-Phosphate Dehydrogenase (GAPDH) as a reference gene with $2^{-\Delta\Delta Ct}$ method of analysis used. Relative expression levels are displayed as mean ± SD. Two-way ANOVA with Bonferroni correction was used to test significance; *** $p<0.001$.

Once the populations were confirmed to have been correctly isolated, tau expression between the two layers was assessed. Primer pairs were designed to target different regions of the tau RNA transcript and to target isoform specific regions of RNA. *MAPT* primer pairs were designed to target all isoforms of tau at the C-terminal and microtubule binding domains respectively. The results indicated that in all patient biopsies total tau expression was higher in the captured suprabasal cell population compared to the captured basal cells (Figure 3.10A). Although these results confirmed that total tau expression was higher in suprabasal cell populations, as also observed through immunofluorescence analysis, the specific tau isoform expression have not yet been reported. So far in this study, all primers and antibodies have been used to detect all isoforms of tau, therefore is it unclear if any changes in isoform expression take place during epidermal differentiation. To investigate this, the LCM captured RNA from the basal and suprabasal ROI was used to explore the relative expression of tau isoforms between the two populations.

Isoform specific primers were used to detect alternative splicing of exon 2, 3 and 10 in tau transcripts between the basal and suprabasal ROI captured by LCM. Each primer was designed to span the exon junction and detect only their transcript of interest. For example, the 0N primer pair spanned the exon junction between 1 and 4; this probe detects an exon junction that is present only in 0N tau variant with the exclusion of transcripts containing exon 2 or 3 (Figure 3.11A). Figure 3.11 and Figure 3.12 demonstrate where each isoform specific primer pair binds on the tau RNA transcript and which exons each primer flanked, to exclude other transcript variants. These primer pairs can therefore detect 0N, 1N, 2N, 3R and 4R transcript variants of tau. RT q-PCR revealed that, as expected, tau isoform expression was different between the basal and suprabasal keratinocyte

populations. This suggested that alternative splicing in the epidermis leads to a transition in expression of tau isoforms during the process of epidermal differentiation. RT q-PCR data demonstrated that 0N isoform expression is higher in the basal layer in almost all samples, as it could be seen to decrease significantly the suprabasal population in all but one of the human samples analysed in this study (Figure 3.11B). 1N expression showed increased relative expression in suprabasal populations in two of the skin samples analysed (Figure 3.11D). Both patient 2 and 4 were found to have a smaller increase in differentiation markers between the captured basal and suprabasal populations compared to other samples. 2N transcript variants was upregulated in all samples and demonstrated a significant increase in expression in patient 6, 4 and 2 (Figure 3.11F).

Alternative splicing of the microtubule binding domain in the epidermis revealed a relative increase in both isoforms in the suprabasal populations, consistent with the increase in total tau expression found in this population. 3R transcript variants showed a much smaller, insignificant increase in expression compared to 4R transcript variants (and Figure 3.12B and D), and patient biopsy 7 showed decreased 3R expression. Interestingly, 4R isoform expression showed a consistent significant increase in the suprabasal population of all samples analysed in this study compared to the basal cell populations (Figure 3.12D).

To help validate the results from the q-PCR and confirm that the PCR had correctly amplified the gene of interest from the LCM captured ROI a semi quantitative PCR was conducted. RT q-PCR products were run on an agarose gel to allow visualisation of the amplified product to ensure a single band was detected. All products displayed a single band and no primer dimers were detected and bands displayed the correct amplicon size (Figure 10.6). 2N product

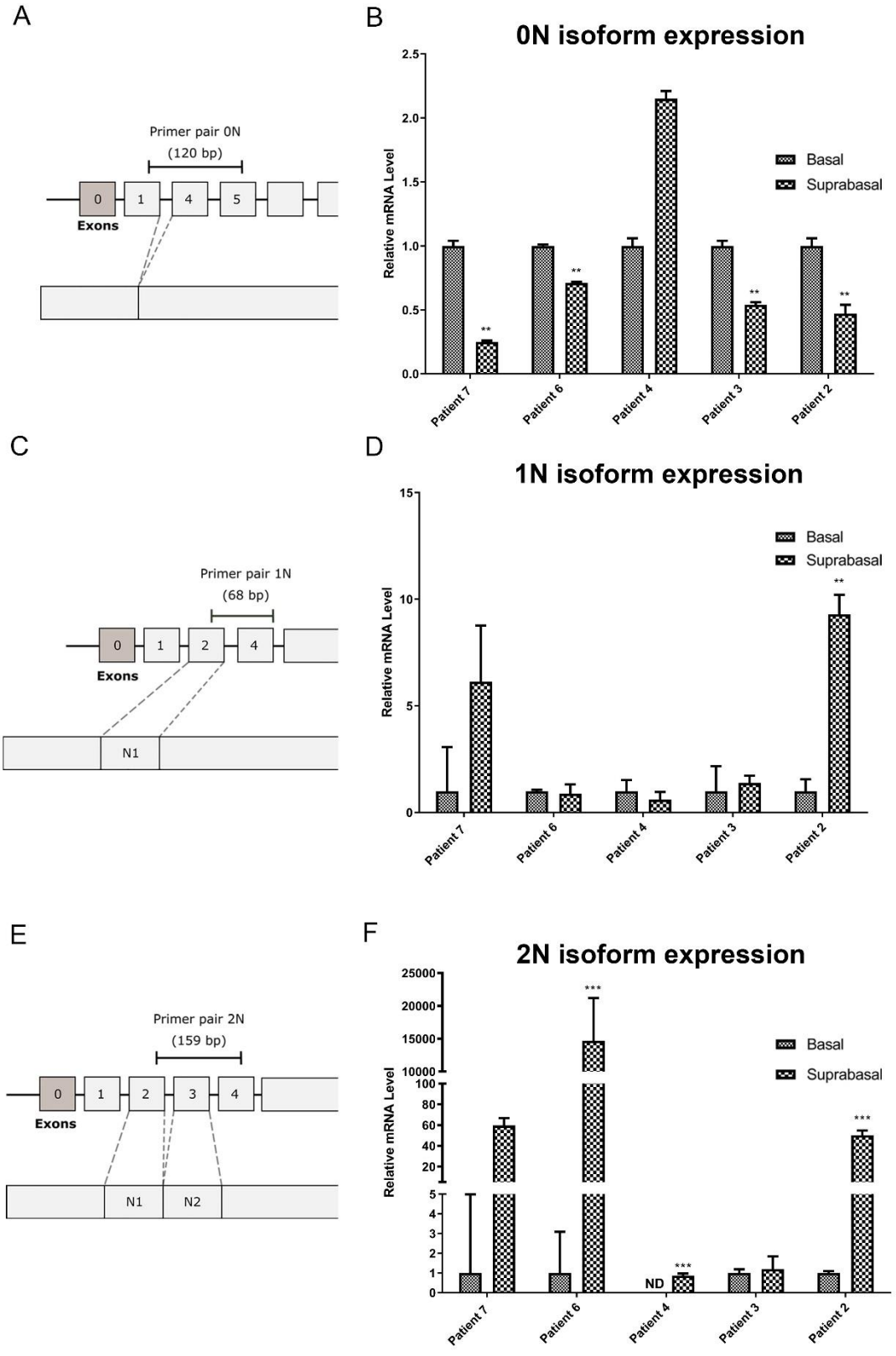

Figure 3.11. N-terminal tau expression in the healthy human epidermis. RT q-PCR analysis of 0N, 1N and 2N tau isoform expression from basal and suprabasal tissue captured by LCM in healthy human patient biopsies. Alternative splicing between the basal and suprabasal populations of the epidermis generate different expression patterns of tau transcript 0N, 1N and 2N being detected between the two cell populations. **A.** Schematic indicating where *MAPT* isoform specific 0N primer pair flank exon 1-5 to exclude transcripts containing exon 2 or 3 to detect only 0N isoforms. Exon 0 and 14 transcribed but not translated. **B.** 0N

isoform expression is downregulated in suprabasal cell populations in all human samples analysed in this study. **C.** 1N specific isoform primer pairs bind to exon 2 and 4 excluding tau transcripts with the inclusion of exon 3 (2N isoforms) or 0N isoforms that do not contain exon 2. **D.** 1N isoform expression is increased in the suprabasal population in most human biopsies used in this study. **E.** Schematic showing where 2N isoform specific primer pair bind to on 2N tau transcript variant. Primer pairs flank exon 2, 3 and 4 amplifying only variants that contain exon 2 and 3, therefore excluding any other isoforms. **F.** 2N isoform expression is significantly increased in the suprabasal population of most patient biopsies. All relative RNA expression between the basal and suprabasal tissue populations normalised to Glyceraldehyde-3-Phosphate Dehydrogenase (GAPDH) as reference gene and $2^{-\Delta\Delta Ct}$ method of analysis used method of analysis used (n=2). Relative expression levels are displayed as mean ± SD. Two-way ANOVA with Bonferroni correction was used to test significance; **p<0.01, *** p<0.001.

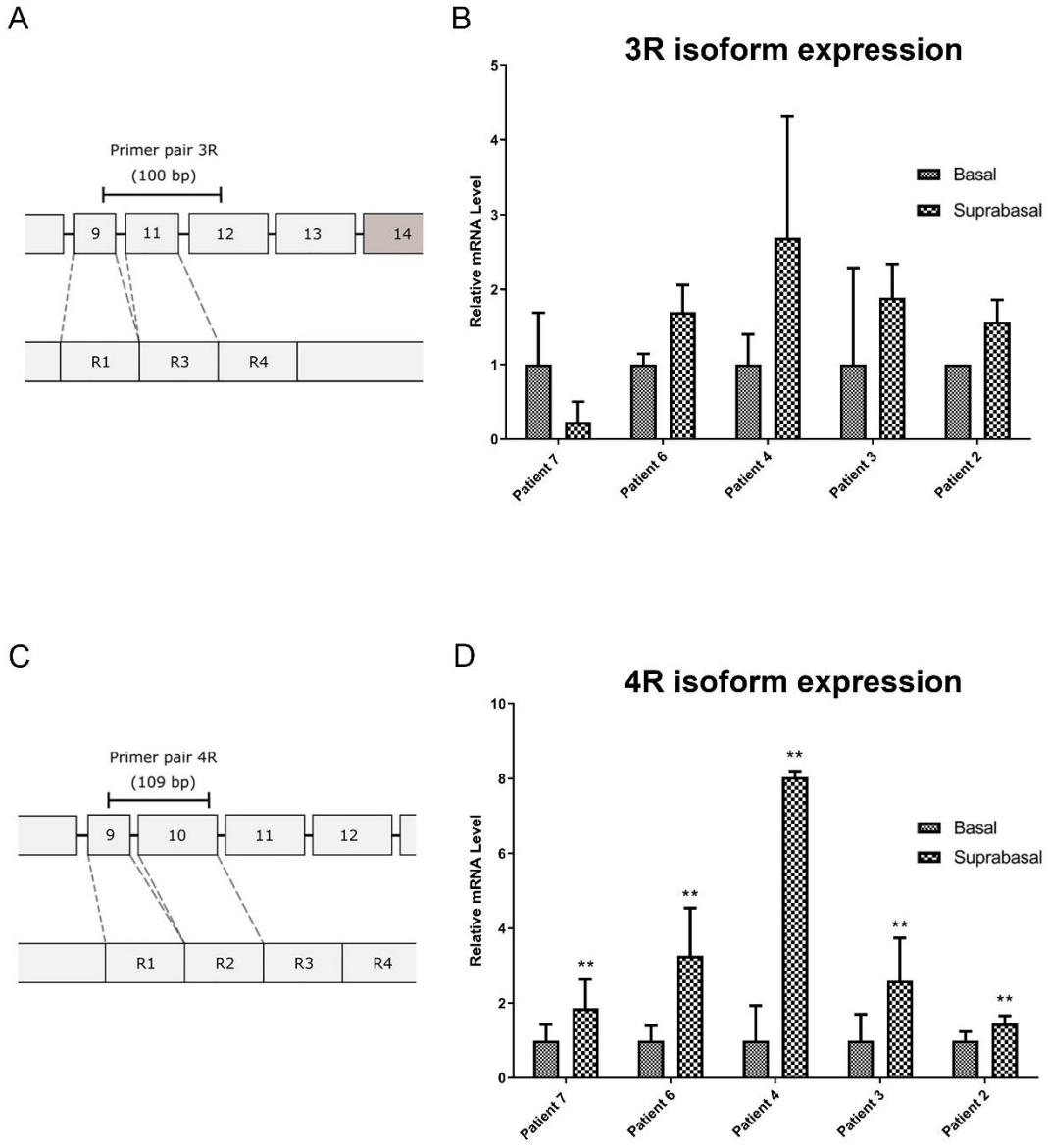

Figure 3.12. Alternative splicing of the microtubule binding domain of tau is increased in suprabasal cells in the epidermis.
RT q-PCR analysis of 3R and 4R tau isoform expression from basal and suprabasal tissue captured by LCM in healthy human patient biopsies. Both 3R and 4R transcript variants are increased in suprabasal cells, consistent with increase in total tau expression by suprabasal cells. **A.** Schematic demonstrating where the 3R isoform specific primer pairs bind to the 3R tau transcript. Primer pairs flank exon 9-12, excluding any transcripts that contain exon 10. **B.** 3R tau expression is generally increased in suprabasal cells, with the exception of patient 7, but does not reach the threshold for statistical significance. **C.** Schematic indicating where 4R isoform specific primer pairs bind to the tau transcript. 4R primer pair flanks exon 9 and 10, excluding any 3R transcripts due to the lack of exon 10 in these isoforms. **D** 4R isoform expression is significantly increased in all suprabasal tissue across all patient biopsies. Relative RNA expression between the basal and suprabasal tissue populations normalised to Glyceraldehyde-3-Phosphate Dehydrogenase (GAPDH) as reference gene. $2^{-\Delta\Delta Ct}$ method of analysis used method of analysis used (n=2). Relative expression levels are displayed as mean ± SD. Two-way ANOVA with Bonferroni correction was used to test significance; ** $p<0.01$.

Table 3.2. Summary of total tau and isoform specific expression obtained through q-PCR analysis of the basal and suprabasal keratinocyte populations from laser capture microdissection.

Tau expression	Basal	Suprabasal
Total tau	++	+++
Isoform 0N	+++	++
Isoform 1N	+	++
Isoform 2N	+	++
Isoform 3R	++	+++
Isoform 4R	+	+++

Total tau expression is increased in the suprabasal epidermis. 0N isoform expression is decreased in differentiated cells. 1N and 2N expression is increased in the suprabasal population. 3R and 4R isoforms see an overall increase in expression consistent with the overall tau expression increase that is observed between the two populations. 4R isoform shows a consistent increase in differentiated cells across all patient samples. Expression levels are denoted as: +: low expression; ++: medium expression; +++ high expression.

size was correct in the suprabasal sample, but basal sample showed the wrong amplicon size, but did not display a Ct value in q-PCR but instead was not detectable. 1N primer pair displayed a slightly higher product size when run on a gel, but a single band was detected and when primer BLAST was run for the primers only 1N isoforms were detected as the target sequence with no other potential binding partners (Figure 10.6). Table 3.2 displays a summary of total and isoform specific expression of tau as detected from LCM captured basal and suprabasal tissue of patient biopsies in this study.

3.4.2.2. Subcellular localisation of tau in the healthy epidermis and its potential binding partners

Following the confirmation and characterisation of tau expression throughout the epidermis in healthy samples and establishing the optimum sample preparation techniques in 3.4.2.1, it was important to next confirm tau protein subcellular localisation throughout the epidermis. This enables a better understanding of the role of tau within the epidermis when performing later functional investigations. Here, tau was co-stained with some well-recognised markers of differentiation and specific markers for cellular structures to determine the localisation of tau expression in basal and suprabasal keratinocytes.

Tau has been reported to be a linker protein between the cytoskeleton and the cell membrane. To investigate if it's expression in the suprabasal cells was restricted to the cytoplasm, or if membrane staining could also be observed, samples were co-stained with tau [E178] and E-cadherin; a transmembrane cell-adhesion protein in the cadherin superfamily that is widely expressed in epithelial tissues. Immunofluorescence staining showed that, as expected, E-cadherin was expressed strongly in the cell membrane of keratinocytes throughout the

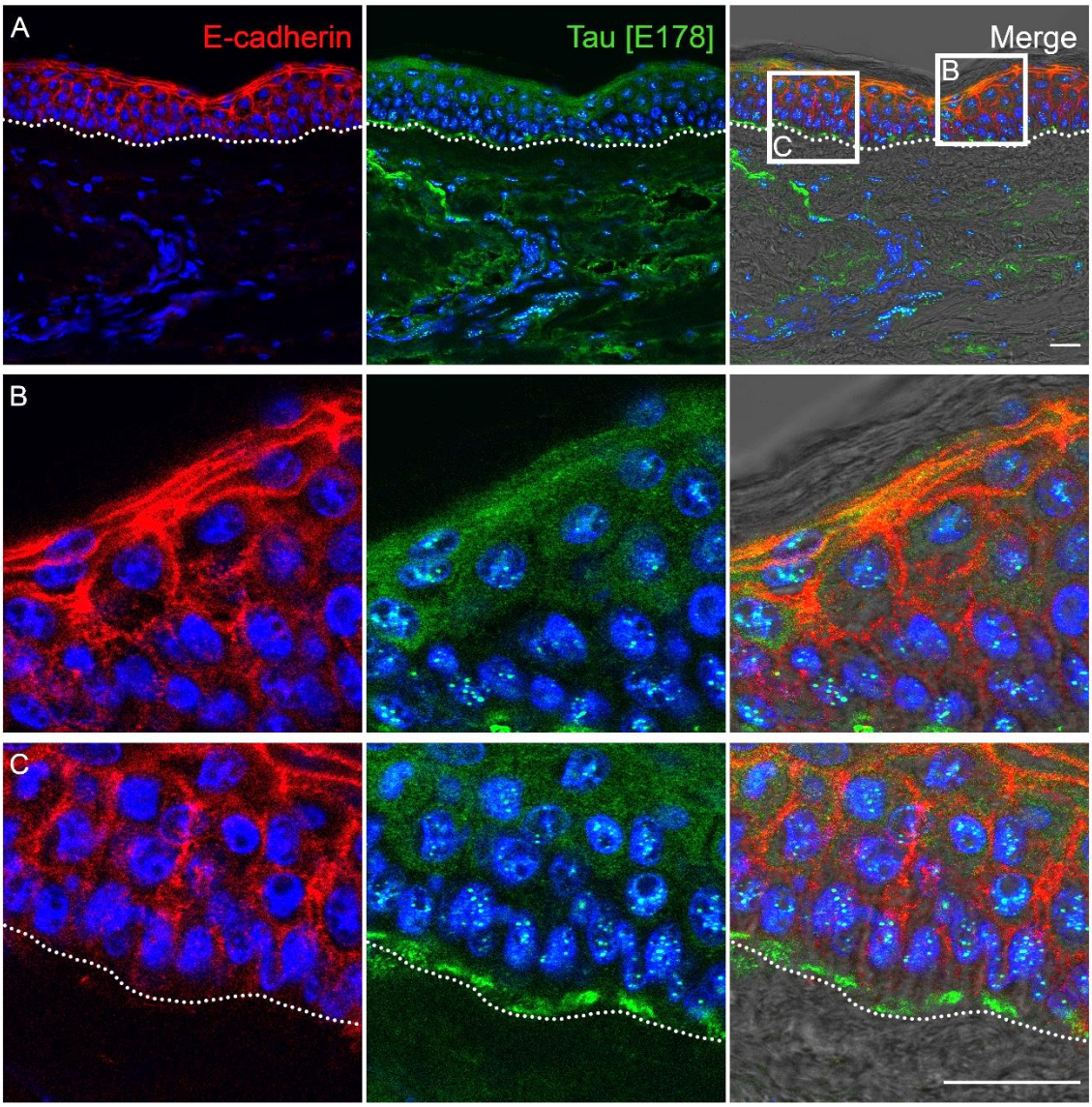

Figure 3.13. Immunofluorescence analysis of tau and E-cadherin expression in healthy human skin samples.
A. Representative immunofluorescence staining of tau [E178] (green) and E-cadherin (red) in the healthy epidermis of patient 6 (n=6). **B.** E-cadherin staining was very strong in the granular layer of the epidermis. It is in this granular layer that tau can be observed to co-localise with the membrane. **C.** Tau expression in the basal layer is largely restricted to the nucleus, with the exception of rete ridge regions of the basement membrane where tau is observed to be polarised to the basal surface of these cells. White dotted line denotes the basement membrane. Nuclei are counterstained with DAPI (blue) and all channels are displayed with the phase contrast image in the right panel to allow accurate visualisation of sample morphology. Scale bar 25 µm.

epidermis (Figure 3.13). E-cadherin staining was particularly strong in the granular layer of the epidermis (Figure 3.13B). Tau expression was mostly restricted to the nuclear fraction of basal cells, with the exception of asymmetrically distributed tau expression on the basal membrane within rete ridges (Figure 3.13C). Correlating with cells moving up through the epidermis, into the spinous layer, tau expression could also be observed in the cytoplasm as well as the nucleus, with little co-localisation with E-cadherin. However, in the granular layer tau [E178] expression appeared to co-localise with E-cadherin at the cell membrane (Figure 3.13B).

To help investigate the tau expression in the basal layer, patient samples were co-stained with tau [E178] and Ki67; enabling the identification of cells active in the cell cycle. Ki67 positive cells were scattered throughout the basal layer, with no positive cells found in the upper differentiated layers (Figure 3.14A and C). Figure 3.14B shows some Ki67 positive cells parallel to the BM have reduced tau staining compared to surrounding cells. Cells located in the suprapapillary plate of the epidermis, where tau is observed on the basal surface of keratinocytes in contact with the BM, overall showed reduced Ki67 expression compared to other regions of the epidermis (Figure 3.14D).

Keratinocytes in the basal layer of the epidermis displayed lower levels of phosphorylated tau (clone AT8), compared to their suprabasal counterparts (Figure 3.7). To confirm this population exhibited a lower level of phosphorylation status of tau, and that phosphorylated tau was confined to the nucleus populations, immunofluorescence staining was carried out with E-cadherin and Integrin-α^6; an integrin restricted to undifferentiated cells in the basal layer. As previously detected, tau (clone AT8) was mostly absent in the basal cells and no

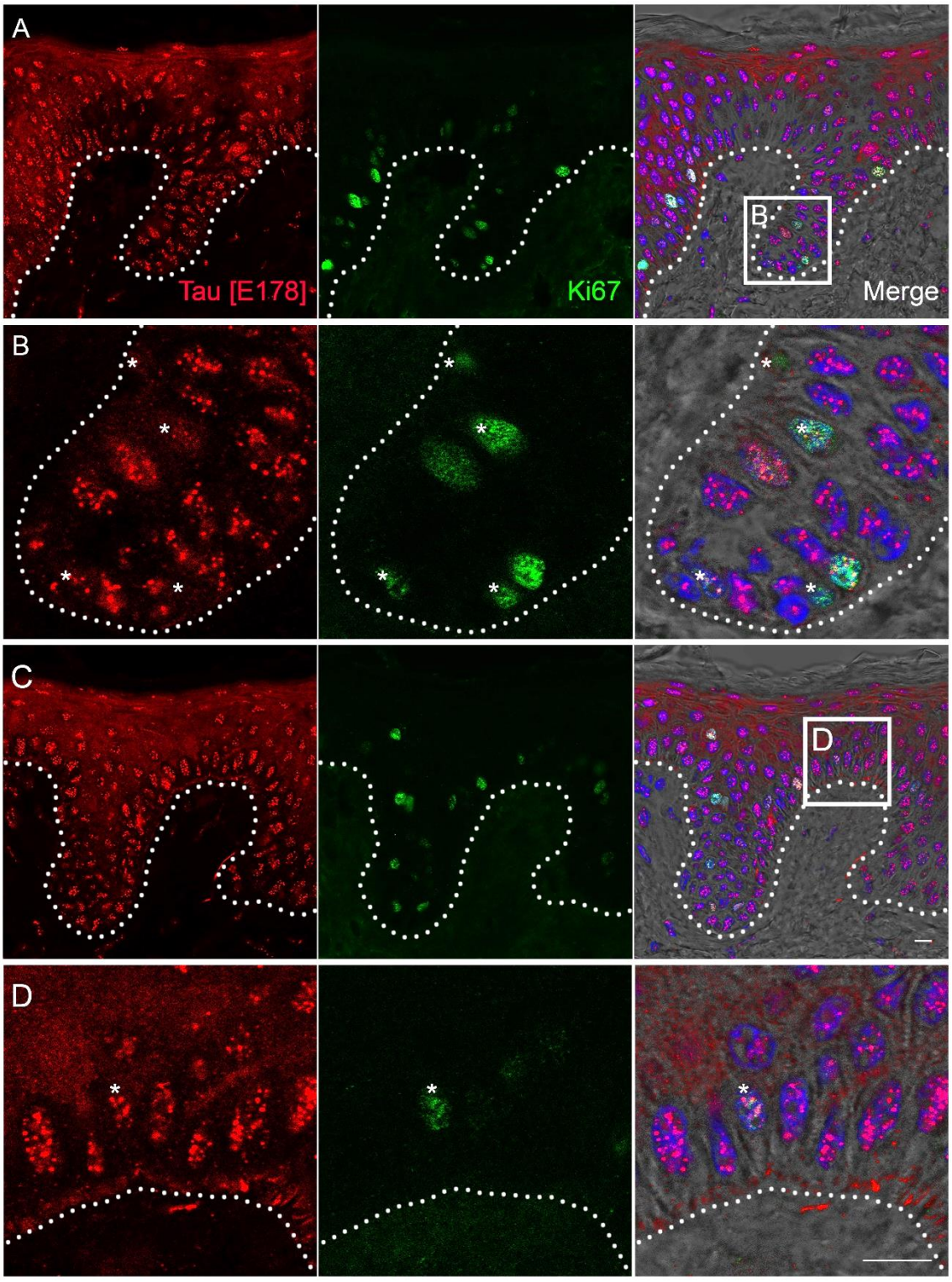

Figure 3.14. Immunoflurescence analysis of tau and ki67 expression in the epidermis.

A&C. Representative immunofluorescence staining of tau [E178] (red) and Ki67 (green) of patient 7 healthy skin biopsy (n=6). Ki67 positive cells are scattered throughout the basal layer of the epidermis, with no proliferation observed in the terminally differentiated layers of the epidermis. **B.** High magnification images of the basal layer within a rete ridge structure show Ki67 positive cells parallel to the basement membrane. Some of these cells have reduced tau expression in the nucleus; indicated by stars. **D.** High magnification image of a suprapapillary plate region of the epidermis, between rete ridges, where tau expression can be

observed polarised to the basal surface of the cells. Most cells in these regions showed reduced Ki67 staining. Nuclei counter stained with DAPI (blue) and all channels are displayed with the phase contrast image in the right panel to allow accurate visualisation of sample morphology. White dotted line indicates the basement membrane. Scale bar 10 µm.

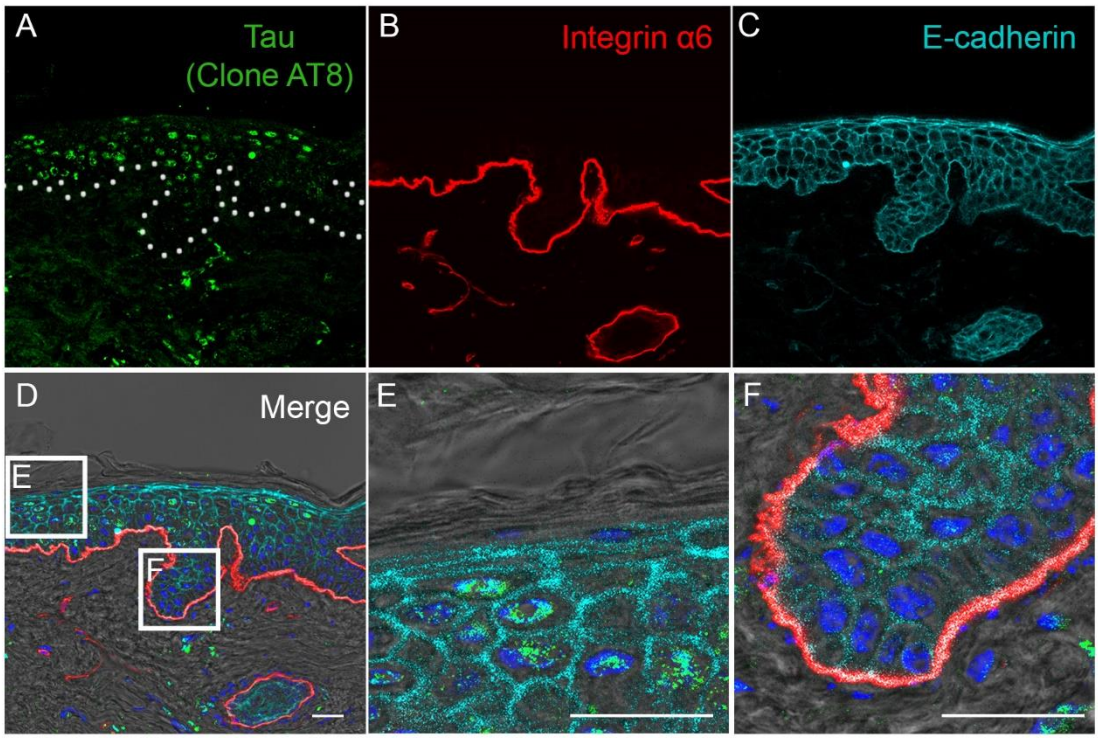

Figure 3.15. Immunofluorescence analysis of phosphorylated tau in the epidermis.
A-D. Using a tau antibody (clone AT8) (green), which binds exclusively to phosphorylated tau (Ser202/Thy205) with no cross reactivity to normal tau, patient samples were co-stained with integrin-α^6 (red) and E-cadherin (cyan) (n=6). **E.** Phosphorylated tau (clone AT8) is absent in most basal keratinocytes. Using integrin-α^6 to label basal cells attached to the basement membrane, and E-cadherin to mark the cell membrane, it can be seen that the majority this population of cells are negative for phosphorylated tau (clone AT8). **F.** Phosphorylated tau expression in the suprabasal cells is restricted to the nucleus with no cytoplasmic, or membrane staining observed. Nuclei counter stained with DAPI (blue) and all channels are displayed with the phase contrast image in **D-F** to allow accurate visualisation of sample morphology. White dotted line denotes the epidermal-dermal junction. Scale bar 25 µm.

co-localisation was observed between tau (clone AT8) and E-cadherin in the suprabasal population (Figure 3.15).

Due to the relatively un-reported and un-characterised expression of tau in skin, another widely used antibody against tau was used to confirm the expression pattern observed. Tau5 binds to the proline rich domain in the centre of the protein, whereas tau [E178] binds to the C-terminal domain of the protein. Assessment of tau protein expression within the healthy human epidermis using tau5, revealed a distinctly different expression pattern to that revealed by tau [E178]. Immunostaining of healthy human skin demonstrated that expression of the tau5 epitope was mostly restricted to the upper granular layers of the epidermis, with weaker scattered staining throughout the lower layers of the epidermis. Co-staining with terminal differentiation proteins confirmed the granular localisation, with expression restricted to the same layer of the epidermis as loricrin (Figure 3.16). In parallel to tau [E178], no nuclear staining was observed with tau5 antibody.

Although co-staining with loricrin in this study allowed the identification of tau expression in the granular layer of the epidermis, it is not clear whether this was membrane or cytoplasmic staining. Therefore, staining was carried out with E-cadherin to allow for any co-localisation with the cells plasma membrane to be identified. Immunofluorescence revealed that E-cadherin and tau5 do co-localise throughout the epidermis, but stronger co-localisation was observed in the granular layer where tau5 staining tended to be strongest (Figure 3.17). Tau5 expression was shown to be primarily membrane, with scattered cytoplasmic staining but no nuclear localisation observed (Figure 3.17C).

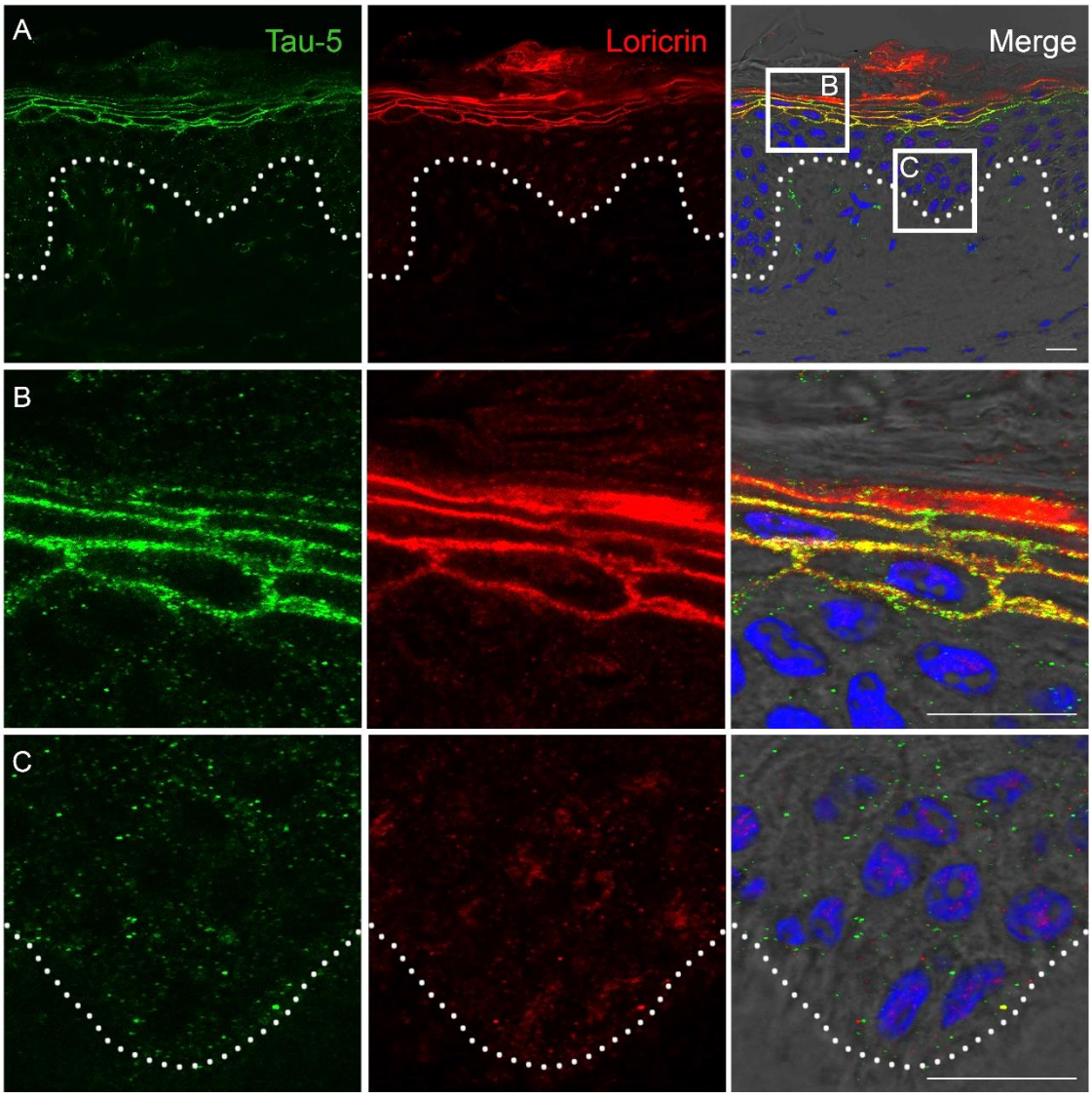

Figure 3.16. Immunofluorescence analysis of tau 5 and loricrin expression in the granular layer of the epidermis.
A. Representative immunofluorescence of loricrin (red) and tau5 (green) staining of patient 7 skin sample (n=6). **B.** High magnification images of the granular show that tau5 expression is almost exclusively found in the granular layer of the epidermis co-localising with loricrin. **C.** Very little or no loricrin and tau5 expression is detected in the lower layers of the epidermis. White dotted line marks the epidermal-dermal junction. Nuclei counter stained with DAPI (blue) and all three channels are displayed with the phase contrast image in the right panel to allow accurate visualisation of sample morphology. Scale bar 25 µm.

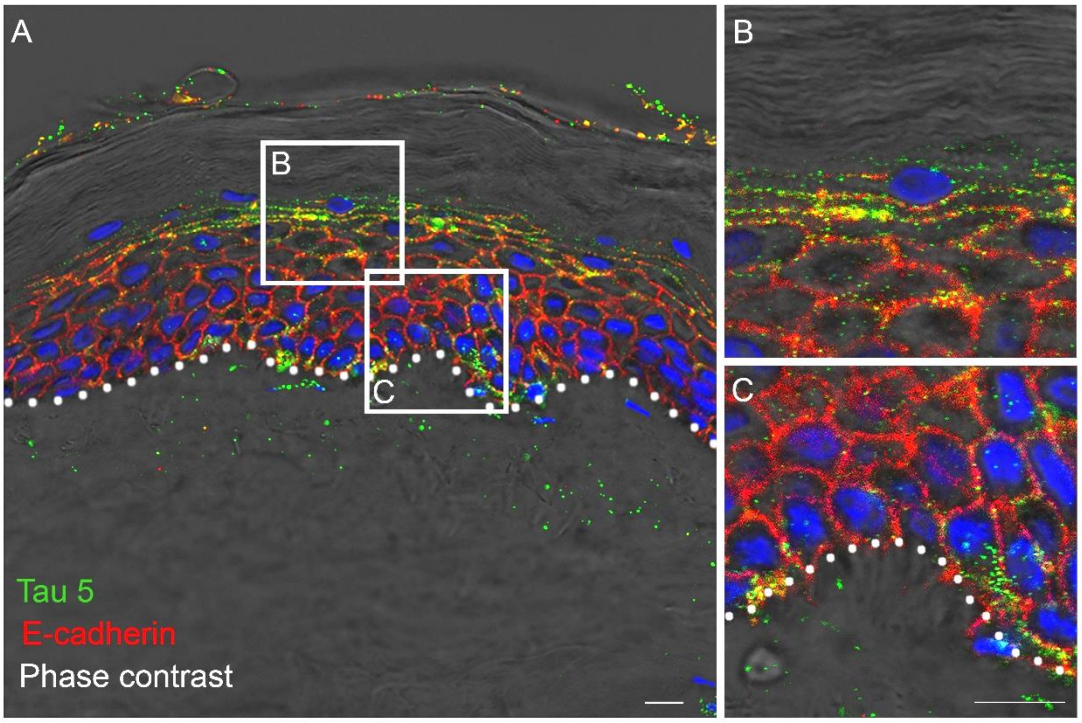

Figure 3.17. Immunofluorescence analysis of the co-expression of tau5 and E-cadherin in the epidermis.
A. Representative immunofluorescence staining of patient sample 2 with tau5 (green) and E-cadherin (red) displayed with the phase contrast image to allow accurate visualisation of sample morphology (n=6). **B.** Tau5 and E-cadherin can be seen to co-localise in the suprabasal of the epidermis. **C.** Although E-cadherin is found throughout the epidermis, only scattered tau5 staining can be observed in basal and spinous cells. White dotted line indicates the basement membrane. Nuclei counterstained with DAPI (blue) and all channels are displayed with the phase contrast image in the right panel to allow accurate visualisation of sample morphology. Scale bar 10 µm.

Tubulin expression was restricted to the cytoplasmic fraction of keratinocytes with no nuclear or membrane staining observed (Figure 3.18). Keratinocytes in the lower spinous and particularly the basal layer showed stronger tubulin staining, when compared to those in the suprabasal layers (Figure 3.18B and C). Tau [E178] expression was asymmetrically distributed to the basal surface of the cells in the rete ridge regions of the basal keratinocytes is located underneath the tubulin staining in the basal cells in these locations suggesting a possible role in cell adhesion to the BM (Figure 3.18C). Although there was stronger tubulin staining in the cytoplasm of basal cells, this population of cells had little cytoplasmic expression of tau [E178]. In the suprabasal cell populations tau [E178] expression is stronger in the cytoplasm co-localising with tubulin. Neither tubulin, nor tau were detected in the corneal layer (Figure 3.18B).

The overall staining profile of tau in the epidermis is summarised in Table 3.3 and Figure 3.19, indicating the layer of the epidermis each tau antibody was identified in and the specific epithelial markers that are expressed in each layer. The composition of this table enabled the identification of keratinocyte tau expression and differentiation status in the epidermis, this will also aid in the validation of keratinocyte population expression later *in vitro* in cell culture conditions in Chapter 4.

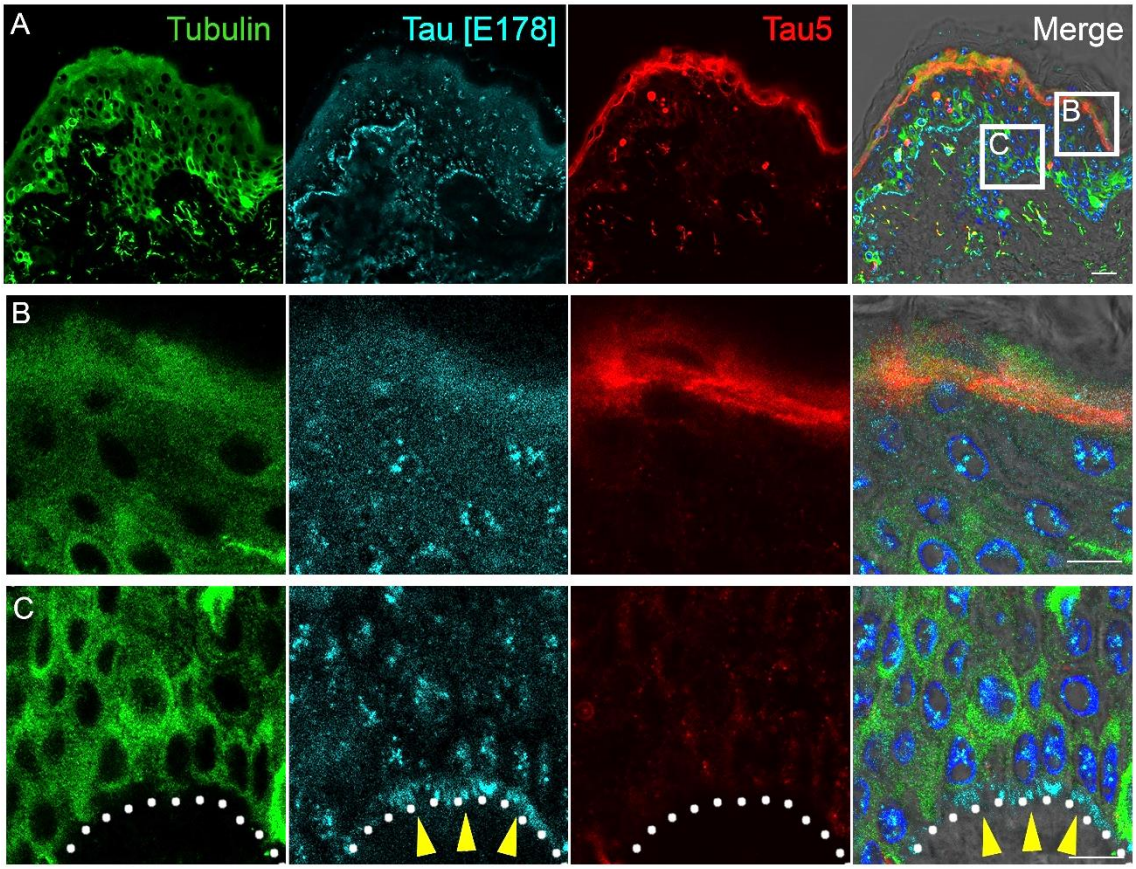

Figure 3.18. Tubulin and tau expression in the healthy human epidermis. **A.** Representative immunofluorescence staining of α-tubulin (green), tau [E178] (cyan) and tau5 (red) (n=11). Scale bar 20 µm. **B.** High magnification images of the suprabasal region of the epidermis Scale bar 10 µm. **C.** High magnification image of the lower epidermis, highlighting the basal population of keratinocytes in contact with the BM. Scale bar 10 µm. White dotted line represents the basement membrane. Yellow arrows indicate the localisation of tau to the basal membrane of basal cells in contact with the BM located within rete ridges of the epidermis. Nuclei were counter stained with DAPI (blue) and all channels are displayed with the phase contrast image in the right panel to allow accurate visualisation of sample morphology.

Table 3.3. An overview of Tau immunofluorescence staining presented in healthy human skin biopsies.

Antibody	Healthy human tissue				
	Epithelial				Mesenchymal
	SB	SS	SG	SC	Dermis
Tau [E178]	++	+++	+++		++
Tau 5	+	+	+++		++
PhosphorTau	+	++	+++		+
Keratin 14	+++	+			
Integrin-α^6	+++				
Ki67	++	+			+
Keratin 1		+++	+++		
Loricrin		+	+++		
Filaggrin		+	+++		
Tubulin	+++	++	++		++
E-Cadherin	+++	+++	+++		
Vimentin	+*				++

Staining profiles demonstrate the discrete staining patterns of Tau observed in the skin tissue, enabling identification of specific populations in tissue samples, and identifying individual cell populations later in cell culture conditions. Tau expression was detected throughout the epidermis, but different antibodies demonstrated distinct staining profiles. Tau [E178] was identified throughout the epidermis but increased in suprabasal populations. Tau 5 expression was significantly upregulated in granular populations of keratinocytes. Phosphor tau was also identified to increase in the suprabasal populations of keratinocytes. SB – Stratum basal, SS – Stratum spinosum, SG – Stratum granulosum, SC – Stratum corneum. Weak or scattered expression levels are labelled as: +, moderate expression as ++ and strong expression as +++. * Staining likely from other cell types found in the epidermis.

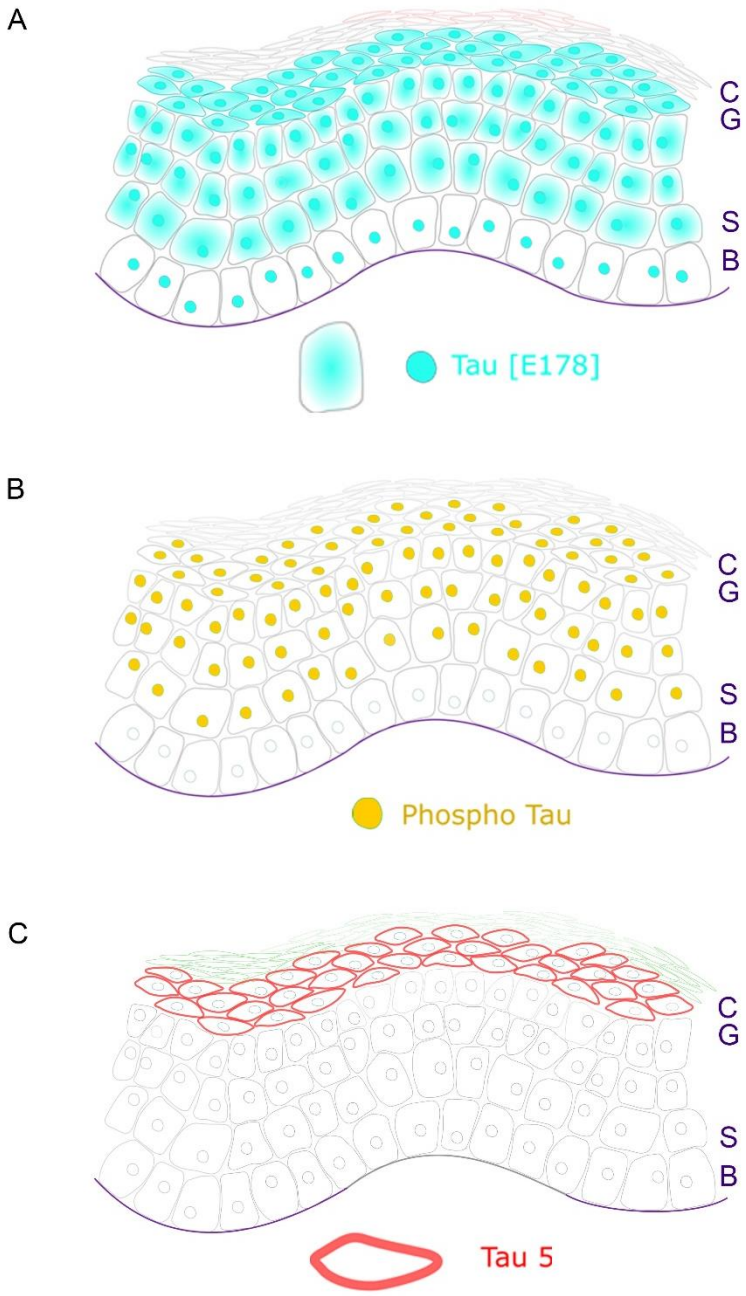

Figure 3.19. Summary of tau expression staining in healthy human skin from tau antibodies used in this study.
Schematics representing the expression profiles observed in healthy human skin using the three commercial tau antibodies throughout this study. The epitope of each antibody corresponded to different regions of the tau protein and displayed distinct expression patterns in the epidermis. **A.** Expression profile of recombinant rabbit monoclonal tau [E178] antibody targeting the C-terminal region of the tau protein that is present in all isoforms. Tau [E178] displayed a broad expression throughout the epidermis, but its localisation shifted throughout the stratified, differentiated layers of the epidermis. In basal keratinocytes tau staining was punctate and highest in the nucleus and the basal membrane of basal keratinocytes within rete ridges. In spinous cells, nuclear tau could still be detected, but expression was also found in the cytoplasm. In the granular layer tau [E178] was found in the nucleus, cytoplasm and membrane expression was also identified. No tau expression was detected in the corneal layers suggesting

that tau does not have a major role in barrier function, or that the tau protein does not maintain its integrity through the final stages of keratinocyte terminal differentiation. **B.** Expression profile of Phosphorylated tau (Ser202/Thy205) (clone AT8) antibody targeting a phosphatase sensitive epitope on PHF-tau. Phosphor tau was exclusively observed in the nucleus in all keratinocytes in the epidermis. Although scattered staining was observed in the basal cells, phosphor tau expression was highest in the suprabasal regions of the epidermis. **C.** Expression profile of mouse monoclonal tau5 antibody targeting Ser210-Arg230 which lies within the proline rich domain of the tau protein that is present in all isoforms. Tau5 expression was primarily observed in the granular layer of the epidermis, in which it co-localised with terminal differentiation proteins and membrane associated proteins. Epidermal layers denoted in purple text as: B – Stratum basal, S – Stratum spinosum, G – Stratum granulosum, C – Stratum corneum.

3.5. Discussion

Overall, this chapter has successfully demonstrated that tau is expressed in human skin and its location and expression is linked to the differentiation status of epidermal keratinocytes. Additionally, using LCM, the previously unknown expression of tau isoforms throughout the epidermal layers was characterised. Using immunofluorescence to highlight markers of differentiation and cellular structures, this chapter has also successfully established the localisation of tau throughout the differentiated epidermis.

The first aim of this study was to confirm tau expression in the epidermis and identify any changes to expression throughout the layers. Although a few studies had identified that tau was expressed in the epidermis, there have been no previous studies investigating any regional changes to tau expression throughout the differentiating epidermis. Like many proteins, it seems likely that tau expression changes are linked to epidermal differentiation; tau expression was higher in the suprabasal populations, with the highest expression found in the granular keratinocytes, which is consistent with other findings [75,196,197,275,277,278]. As previously described, keratinocytes undergo major changes during terminal differentiation; keratinocytes cease proliferating, delaminate and undergo transcriptional and morphological changes that culminate in the formation of dead, fattened, enucleated corneocytes that create the impermeable stratum corneum in the epidermis. In this study, tau was not detected in the corneal layer, suggesting that either, it does not have a major role in barrier function, or the protein does not maintain its integrity throughout the final stages of keratinocyte differentiation; this is logical, as tau is an extremely soluble protein, and would not be expected to survive the breakdown and packaging of proteins in the final stages of terminal differentiation.

Although tau is primarily reported as a cytoplasmic protein, tau displays a diverse cellular distribution. In this study, tau was observed in the nuclear compartment of all keratinocytes in the epidermis, consistent with many reports linking tau to a role in the nuclear compartment of cells in neuronal and non-neuronal cells [183,241,243,304]. Although nuclear tau has been characterised in many cell types, including dermal fibroblasts, it has not been characterised before now in keratinocytes. Studies have shown that when other cell lines are exposed to oxidative stress, tau expression can be upregulated to help protect DNA from free radical induced damage [241,305]. These studies have relevant implications on understanding the localisation of tau expression in keratinocytes, as sun exposed skin experiences oxidative stress though exposure to UVA and UVB radiation. Whether tau confers some DNA protection against this exposure in keratinocytes requires further investigation *in vitro*.

Although tau expression was found in the nucleus of all basal keratinocytes, the expression density varied amongst neighbouring cells and across different locations in the epidermis. It is recognised that the spatial organisation of basal cells correlates with their SC status. Rete ridge structures have been suggested to house the cycling cells of the epidermis, with TACs residing in the deep rete ridges, and SCs residing in suprapapillary plate, at the top of the folding that compliments the rete ridges, consistent with the observations in this study [45,50,51]. However, tau expression on the basal surface of slow cycling basal keratinocytes located in the suprapaillary plate has not previously been reported and its role in the structural integrity of these cells remains unknown. The role of tau in the suprapapillary plate and its possible interactions with cell-matrix adhesion proteins in the SC and TAC populations therefore warrants further investigation,

to gain understanding of tau expression and function in SC, TACs and differentiated keratinocyte populations.

The ability of a cell to maintain and adapt its cytoskeletal system to environmental changes is crucial for cell survival. The cells microtubule cytoskeleton is responsible for vital cellular processes such as, cellular division, migration and morphogenesis, and the assembly-disassembly of the tubulin system is closely linked with SC lineage and differentiation [22]. While actin is relatively more stable, microtubules are more dynamic. It is established that in basal keratinocytes the microtubule network is organised in a centrosomal array, while differentiation leads to the loss of the centrosomal microtubule organising centre and eventually microtubule organisation into cortical arrays [66,92,95,306]. Although the tubulin dynamics have been increasingly investigated in the epidermis, the MAPs responsible for the observed changes during epidermal differentiation have not been. The unique organisation of the microtubule networks is dependent on a variety of MAPs that help control microtubule assembly, bundling and binding to organelles. Tau performs this role through multiple interaction sites on the protein, driving stabilisation and inhibiting shrinkage of microtubules. 4R isoforms were identified to be upregulated in suprabasal cells, suggesting that the alternative splicing of tau is dependent on the keratinocyte differentiation status and that this isoform may play a role in the accompanying tubulin dynamics. The inclusion of exon 10, and consequently the fourth microtubule binding domain, increases tau's affinity to bind to microtubules three-fold [222].

Studies have shown that when basal cells differentiate into spinous cells there is an increase in microtubule catastrophe events, in which growth of the microtubule network suddenly switches to rapid disassembly [90,92]. In other cell types, MAPs are known to stabilise and rescue microtubules after catastrophe events [180,307],

whereby normal growth is resumed. This is consistent with the increase in tau expression found in suprabasal cells in this study [308]. Raising the possibility that MAPs may underlie the tubulin dynamics that are observed at specific stages of keratinocyte differentiation. This is in line with the findings of this study, where tau expression patterns are linked to the differentiation status of the keratinocytes with the highest expression levels of tau observed in granular cells. Unfortunately, distinct staining of tubulin structures is very difficult *in vivo*, therefore tubulin dynamics alongside tau expression require further investigation *in vitro* using 2D and 3D systems.

During terminal differentiation, major changes occur to the expression of many different proteins, with a rearrangement of the cells cytoskeletal and IF network, linked to the changes in keratinocyte function. Tau is best known for its role as a microtubule stabilising protein; thus, it is logical that with increasing cytoskeletal and IF changes microtubule associated protein expression, it would be upregulated to help stabilise these changes. This increased expression of MAPs observed in keratinocytes during differentiation in this study, have also been reported in other cell types [175,279,309,310].

Upon cell differentiation the microtubule network reorganises and accumulates at the cell cortex [66]. The microtubule rearrangement requires the reorganisation of associations with desmosomes and other cell adhesion junctions that are prominent in the suprabasal layers of the epidermis. It is this association of the cortical microtubules with these cell adhesion junctions that are responsible for the strong barrier function of the skin [66,75]. MAP2, MAP4 and tau have all been shown to promote this accumulation of cortical microtubules in culture [75], but studies have shown that in the absence of the desmosomal protein, desmoplakin, the formation of cortical microtubules was inhibited, and MAPs were not sufficient

to promote cortical microtubule organisation, although tau could still bundle microtubules [75]. The upregulation of tau in the suprabasal epidermis found in this study is consistent with the observations in the literature [75,196,197,275,277,278]. Further investigation is needed to determine if tau interacts directly with desmoplakin in the formation of strong adhesions with desmosomal proteins in the differentiated layers of the epidermis, or if it supports the stabilisation of microtubules. The implication that pathological forms of these proteins might have on the differentiation of these cells in AD and skin cancer also warrants further investigation.

The membrane localisation of tau has also been shown to link the cells plasma membrane to cytoskeletal networks in a non-desmosomal dependent manner using neuronal cell lines. Interactions of tau with the cell membrane are thought to be dependent on the proteins N-terminal projection domain [216,224]. In this study tau was found to localise with the cell membrane in terminally differentiated granular keratinocytes. In these suprabasal cells there was an increase in the 1N and 2N transcript variants of tau, consistent with findings that the N-terminal region is dependent for interactions with the plasma membrane. The association of tau with the plasma membrane is reported to also depend on its phosphorylation status in many cell types, specifically the AT8 epitope is not found to associate with the plasma membrane in neuronal cells [224], supporting the absence of phosphorylated tau in the plasma membrane found in this study. Interestingly, the targeting of tau to the plasma membrane has been shown to play a role in the development of neuronal polarity [235]; polarity in the epidermis is fundamental for its development and stratification [37].

As keratinocytes transition from the spinous layer to the granular layer they start to become flattened. Little has been reported about this change in cell shape in

the granular layer, but using a strategy to disrupt microtubules by the overexpression of spastin in the epidermis under the control of doxycycline, Muroyama *et al.* (2017) showed that in the absence of microtubules differentiating keratinocytes were not capable of flattening [92]. Spastin is a microtubule severing protein which is able to dramatically disturb the microtubule organisation in cells and when spastin was overexpressed in keratinocytes cell shape defects were observed. It was shown that microtubules are required for the initial flattening during the spinous to granular transition but are not essential for the maintenance of shape thereafter. These patterns of microtubule dynamics during epidermal differentiation in agreement with the observations of tau expression in this study.

One of the methods employed by this chapter to investigate the aims, was to characterise the regional changes in molecular expression patterns between basal and differentiated keratinocytes, particularly as this has never been reported in the skin. To achieve this, LCM technology was used to capture basal and suprabasal populations in the epidermis to analyse the relative RNA tau isoform expression. Interestingly, it was observed that, despite variation in the relative expression between samples, in suprabasal populations there was a consistent decrease in shorter transcript variants of tau and an increase in 4R transcript variants with four microtubule binding domains. This indicates that 4R isoform of tau is alternatively spiced in suprabasal keratinocytes to accompany the major changes in tubulin dynamics within these cell populations. In the brain, it is well recognised that shorter isoforms of tau are only found in foetal brain tissue as the reduced microtubule binding affinity allows for higher plasticity of the cells [212]. On the other hand, mature or differentiated neurons are found to possess longer isoforms of tau, with a higher binding affinity for microtubules and cell membranes and therefore a much higher ability to support and stabilise cells

than their shorter counterparts. In the epidermis the shortest isoforms of tau were observed in basal populations, and immunofluorescence revealed that tau expression was restricted to the nucleus in basal keratinocytes. These findings are consistent with the literature, as in neuronal and non-neuronal cell types, although the exact transcript variant is unidentified, it is reported that nuclear tau is usually shorter transcript variants of tau [187].

It would be interesting to collate the relative isoform expression with patient information, such as the age and site-specific location of the human skin samples. Previous studies have shown that isoform expression can change between young and mature tissues. However, this has never been identified in the skin. Skin displays a large heterogeneity depending on sample location and age; expression patterns might not be representative of the whole tissue. This vast diversity of human skin is likely to be part of the reason that variation was observed between samples in relative expression data. Although there was some variation in isoform specific expression between the patient samples, every skin sample in this study had consistently higher tau expression in suprabasal cells. Some of the reasons that transcript variant data could have variation between samples is age, anatomical location, sun exposure, other cell types. Variation between patient samples could arise from biopsies being taken from different anatomical locations. Because tau expression is uncharacterised in human skin, it is unknown whether tau expression is different in different anatomical locations. Anatomical location can also dictate sun exposure of skin and this sun exposure could have a role in expression pattern observed. For example, there could be mutations, such as Patched or p53 mutation; not enough of an accumulation to cause cancer, but enough to create a slightly altered phenotype. Genetic profiling studies have shown that the skin is able to tolerate a high level of mutations

associated with cancer without displaying any signs of tumorigenesis [126,311]. The epidermis could contain mutations that have no selective advantage to the cells, therefore not displaying any phenotypic consequence of biological advantage. Sun exposed skin cells are thought to carry thousands of point mutations and around 25-30% of these have an acquired point mutation [126,127]. The frequency of driver mutations in human skin remaining phenotypically normal skin is remarkably high. It is estimated that 20% of normal skin cells in sun exposed areas carry driver mutations, some in levels that match SCC mutations [127], but this still does not transform into malignant potential.

Immunofluorescence staining was heavily used in this study to initially analyse tau expression in human skin samples. Interestingly, using antibodies targeting different epitopes of tau revealed different protein expression patterns. The entire epidermis is positive for the tau [E178] epitope with the highest expression found in suprabasal cells. Whereas the tau5 epitope was mostly restricted to the granular layer of the epidermis. The tau5 epitope is located in the proline rich domain (PRD) of the protein, a region which should be present in all isoforms of tau and therefore should result in the same expression pattern as tau [E178]. However, tau is well characterised for its dynamic instability and the binding of tau dramatically effects its 3D conformation. When tau is not bound the C- and N-terminal regions are located over the PRD, whereas when tau is bound to microtubules or membrane compartments tau opens and the PRD is exposed [216,231]. This conformational change to the tertiary structure of tau could explain why different expression patterns are observed with antibodies that are designed to target different epitopes of tau [312]. Therefore, the tau5 antibody may not work when tau is in its native 3D conformation. However, when this antibody was used for Western blot, the antibody demonstrated the same bands as tau [E178]

throughout keratinocyte populations. This suggests that the tau5 antibody is able to bind to the protein of interest when run on an SDS-PAGE gel after protein denaturisation.

Studies have indicated that, as well as expression levels, careful regulation of post translational modifications of MAPs are needed in cells during cell differentiation [185,218,219,313]. The phosphorylation status of tau has been shown to modulate its function. To detect phosphorylated tau in the epidermis, an antibody that recognised a phosphatase-sensitive epitope, without cross-reactivity to normal tau, was used. Generally phosphorylated tau was absent in basal layer. Interestingly, studies have shown that only un-phosphorylated tau binds to and protects neuronal DNA following stress [239]. Phosphorylated tau has been reported to be absent in cells during mitosis [182], which could explain why cells located in the basal layer of the epidermis may be negative for phosphorylated tau. The basal layer comprises both SC and TACs, and different cell types located within in epidermis also have to be taken into consideration. Further investigation into the positive and negative phosphorylated tau populations in the basal layer are needed. The presence or absence of phosphorylated tau in the epidermis could also be linked to calcium levels. The modulation of tau phosphorylation has been reported to be associated with calcium levels in neurons [247]. Calcium levels in the epidermis change throughout the differentiated layers of the epidermis, so the phosphorylation status of the cells could be linked to calcium levels in the epidermis.

One of the major limitations of this study was the number of healthy clinical samples used. In total 12 healthy patient biopsies were used: 7 frozen and 5 FFPE samples. Should it be repeated, an increased cohort of heathy biopsies, might have enabled a higher significance level of some of the findings and

therefore, a clearer understanding of the expression patterns of tau. However, healthy human skin samples are hard to obtain due to limited availability and ethical limitations. Most healthy skin samples are obtained from excess skin removed during cosmetic surgery or post-mortem; excess skin is often from abdominal or breast whilst post-mortem skin is often from an older donor. Other healthy skin biopsies are hard to obtain due to ethical reasons as healthy skin is not routinely removed without a medical reason. Unfortunately, there was no medical history supplied with the biopsies used in this study. Some of the healthy human skin samples used in this study were from older patients, and due to the lack of medical history, in future studies possible medications and underlying health conditions need to be considered alongside interpretation of findings. However, most healthy skin biopsies were from males so menopause associated changes in oestrogen levels would be significant. To help overcome some of these limitations, the expression patterns of differentiation markers were assessed in skin samples, such that any samples presenting as normal skin but expressing abnormal differentiations markers, could be excluded from the study to improve validity and reduce variation of the data.

Another limitation of this study was the sample preparation. Despite 12 healthy patient biopsies being received, only 7 biopsies were frozen in OCT, the rest were FFPE sampled sectioned onto poly-lysine slides. Although these FFPE samples were analysed with immunofluorescence, LCM could not be carried out. This was due to the fact samples would need to be sectioned onto special PEN membrane glass slides. Therefore, LCM of ROI could only be performed on samples embedded in OCT. However, in the future, *in situ* hybridisation using BaseScope probes could allow us to overcome some of these limitations, using both fresh frozen and FFPE sample slides. BaseScope probes targeting each of the six

major functional variants of tau were designed by the author in collaboration with the probe design team of BioTechne (Figure 10.8) and preliminary BaseScope investigation has commenced. However due to time limitations alongside major troubleshooting of permeabilisation and probe hybridisation protocols, BaseScope was not completed within the time frame of this project, remaining an area of continuing investigation.

Returning to the current findings, although it is generally assumed that mRNA translated into protein, mRNA levels do not always mirror protein expression [314,315]. Several reports have shown that there is a weak correlation between mRNA and protein levels. Posttranscriptional modifications, protein half-lives and experimental variance can all have an effect on the differences between mRNA and protein levels in a tissue of interest that might reduce the ability to get a clear expression profile [314]. Therefore, although immunofluorescence analysis confirmed protein expression, to further analyse tau expression in the epidermis, it would have been preferable to quantitatively assess protein expressing using a Western blot. However, due to the small amount of each patient sample available this has not yet been possible so far in this project. If more samples could be sourced total protein from the epidermis could be extracted through the dissociation of the epidermis, using dispase or heat, or through protein extraction from ROI using LCM, allowing for protein expression to be quantitatively confirmed in clinical samples.

To try and overcome some of these limitations, in subsequent chapters, all sample analysis will be further validated *in vitro*, using healthy epidermal keratinocytes under strict culture control conditions. This will also enable analysis of specific changes to isoform expression during cell differentiation. Another technique being utilised in subsequent chapters, is the formation of *in vitro* 3D

epidermal models. Although the gold standard for the study of integrated physiological systems are animal models, there are many limitations that come alongside their use, including: cost, high throughput and increasing ethical concerns. Thus, human healthy keratinocytes and 3D epidermal models will be developed within this thesis henceforth. In addition, EpiDerm™ models, a well-established 3D highly differentiated reconstructed epidermal model from MatTek©, will be used. These models are intended to represent healthy, young epidermis, and validate tau expression patterns in skin, without confounding factors such as sun exposure, human disease or medications. Once established, *in vitro* models can then also be carefully manipulated to look for tau expression changes or differentiation changes upon different treatments and conditions.

3.6. Conclusion

In conclusion, this chapter has demonstrated a clear correlation between epidermal differentiation and tau expression in healthy human skin. Both isoform expression and sub-cellular localisation of tau displayed a distinct expression pattern in each population of keratinocytes alluding for changes in its function throughout the process of keratinocyte differentiation. Considering the limitations of the current study, these findings also provide the basis for further experiments *in vitro* to establish the functional role tau plays in the process of differentiation and stratification in epidermal keratinocytes. Determining the function of tau in epidermal differentiation and stratification could potentially enable a novel approach to skin therapies for differentiation deficient skin abnormalities, from psoriasis to cancer.

4. Tau promotes keratinocyte differentiation and stratification

4.1. Introduction

In the previous chapter clinical samples indicated the subcellular localisation and expression of tau was linked to the differentiation status of the epidermal keratinocytes. A significant difference in tau expression between the basal cell populations and their suprabasal counterparts was observed, alongside a change in the splice variants between these populations. To validate these findings and investigate the functional significance of tau in the epidermis, *in vitro* analysis was conducted using primary epidermal cells. Tau expression levels were investigated throughout varying stages of differentiation and manipulated to help establish the function of tau in epidermal differentiation. The overall aim of this chapter therefore, was to establish the molecular function of tau in epidermal stratification and differentiation, with the models for achieving this presented henceforth. **Epidermal keratinocytes *in vitro***

Cultured cells *in vitro* are often comprised of a mixed population of cells with varying proliferative capabilities. Most keratinocyte culture medium promotes SC and TAC populations, which discourages terminal differentiation of cultured keratinocytes. However, although primary keratinocytes can be cultured in SC promoting medium, it is thought that 30-50% of these cells still display a differentiated phenotype [29,31,32], with an increased cell size and expression of some proteins associated with differentiation. Despite the progression of epidermal research since the 1980s, there remains a lack of specific epidermal SC markers, unlike other fields, such as haematopoietic cells [316,317]. Therefore, when keratinocytes are maintained in basal media to promote “stemness”, it is

difficult to distinguish the SC and TAC populations. TACs have a lower capacity for self-renewal compared to SCs and have a higher probability of undergoing terminal differentiation. A traditional method, developed by Jones and Watt in 1993, enabled the isolation the SC and TACs populations of keratinocytes *in vitro* based on their expression of β1-integrins [29,45,49]. The SC attachment assay was based on the high surface expression of β1-integrins in epidermal SC populations and their subsequent rapid adhesion to BM proteins [49]. Whereas their TAC counterparts have a lower binding affinity, allowing the separation of the two populations. Upon cell seeding, cells that attached readily to the coating were shown to have a high colony forming ability (SC population), whereas the floating population were found to undertake terminal differentiation after 1-5 rounds of division (TAC population).

4.1.2. Three-dimensional skin models

Although tissues and organs are three-dimensional (3D), the study of many organs to understand their formation, function and pathology is often conducted in two-dimensional (2D) systems or in animal studies. Whilst 2D systems have allowed for important conceptual advances, they lack the ability to mimic cellular micro-structures and micro-environments required in native human skin tissue. 3D manufactured tissue models are thus allowing an approach to bridge the gap between traditional 2D cultures and animal studies. *In vitro* epidermal models can be generated by seeding epidermal keratinocytes onto a feeder layer, devitalised dermis or cell culture insert until a confluent layer of cells forms, after which an air-liquid interface is established to mimic the natural environment of the skin. This air liquid interface, alongside an extracellular increase in calcium, induces keratinocyte commitment to terminal differentiation and stratification.

The use of 3D models of epidermal morphogenesis allows identification of genes/proteins involved in the process of epidermal stratification, a process cannot easily be simulated in 2D. Although the terms stratification and differentiation are sometimes used interchangeably in the epidermis they have very distinct definitions. Keratinocyte differentiation is the process in which a cell changes from one cell type to another, this is usually to become more specialised. Stratification on the other hand, refers to squamous epithelial cells which are arranged in layers upon a BM structure. This places only basal cells in contact with the BM, whilst other layers adhere to each other to maintain their structural integrity. Although there has been a large number of studies into the mechanisms underpinning epidermal stratification, there remains many molecules and pathways involved in the process of stratification and epidermal barrier formation that remain unknown. Chapter 3 suggested that tau expression in the epidermis was linked to keratinocyte differentiation and stratification status, however the role tau plays in the epidermis remains unknown.

4.2. Chapter aim and objectives

Chapter aim: To establish the molecular function of tau in epidermal stratification and differentiation.

Chapter objectives:

1. Investigate the expression of tau and establish its molecular function throughout stages of keratinocyte growth and differentiation.
2. Explore the functional significance of tau in keratinocyte cell fate, stratification and differentiation.

4.3. Methods

4.3.1. Cell culture

The methods used in this chapter involve the cell culture of two healthy human epidermal cell lines; neonatal human epidermal keratinocytes (HEKn) and adult human pooled primary epidermal keratinocytes (HPEKp).

To induce keratinocyte differentiation *in vitro* keratinocytes were treated with 1.7 mM Ca^{2+} in complete cell culture medium. Keratinocytes were typically cultured for 24-96 h before RNA or protein was collected and subsequent analysis was carried out.

4.3.2. Tau Knockdown

The HEKn and HPEKp cells were subjected to endoribonuclease-prepared small interfering RNA (esiRNA) knockdown of *MAPT* as described in Methods 2.1.7. Validation of tau knockdown was performed using RT q-PCR, Western blotting and immunofluorescence analysis. The knockdown cells were used to assess the cells differentiation status and differentiation potential when exposed to high calcium levels (1.7 mM). Keratinocytes were also subjected to short hairpin RNA (shRNA) mediated tau knockdown to generate a stable cell line for tau knockdown (methods 2.1.8). Briefly, cells were infected with lentiviral particles containing shRNA tau 2112, 1881 or luciferase control shRNA (Table 10.9).

4.3.3. Tau overexpression

The HEKn cells were infected with pINDUCER20 and pINDUCER20 tau using lentiviral particles as described in methods 2.1.4.4. Validation of tau^{441} (2N4R isoform) overexpression was confirmed by RT q-PCR, immunofluorescence and Western blotting.

4.3.4. Three-dimensional epidermal models

3D epidermal models used in this study were purchased from MatTek©. EpiDerm™ models were shipped at 4°C for 48-72 h. EpiDerm™ were received 3 days after initial culture still submerged in culture medium. Upon receipt, models were cultured submerged in 1.8 ml EPI-100-1S medium in a 24 well plate for 24 h. EpiDerm™ models were then subjected to subsequent treatments as indicated below. For each treatment, control cells cultured as indicated by MatTek© protocol were cultured in parallel.

4.3.4.1. Tau overexpression in EpiDerm™ models

To overexpress tau in EpiDerm™ models, following 24 h of submerged culture in EPI-100-1S, models were incubated with pINDUCER20 and pINDUCER20 tau lentiviral particles for 6 h at 37°C. After 6 h, the viral supernatant was removed and replaced with EPI-100-1S medium, with or without 10 ng/ml doxycycline added to culture medium of pINDUCER20 tau to overexpress 2N4R tau in the 3D skin models.

4.3.4.2. Culture and maintenance of EpiDerm™ models

The air-liquid interface was established by lifting the EpiDerm™ models using a 12 well plate designed by MatTek©. Culture medium was removed from inside the insert and 5 ml EPI-100-3S medium was added to the surrounding well. Inserts were cultured for 48 h. Media was changed to EPI-100-3S2A Incubated for a further 48 h. Finally, for completion of culture, EpiDerm™ models were cultured in EPI-100-3S4A/5A medium for 48-72 h. Maintenance medium (PI-100-NMM-3) was used to culture inserts between days 7 to 10.

EpiDerm™ models were cultured for 4, 7 or 10 days after the air liquid interface was established. After the culture period, models were removed from culture and fixed in ice cold 4% PFA overnight at 4°C. Following fixation, models were

washed three times in PBS before undergoing sucrose dilutions (10, 20 and 30%) prior to embedding in OCT. EpiDerm™ model filters were cut out of plastic insert and placed in OCT and frozen using LN. Embedded samples were kept at -80°C until sectioning. Samples were sectioned in a cryostat at 20 µm onto poly-lysine slides.

4.4. Results

4.4.1. Tau expression correlates with keratinocyte cell status

To investigate whether there was a correlation between epidermal SC status and tau expression, keratinocytes displaying SC properties were separated from their committed progeny. A SC attachment assay was performed to examine whether, as suggested from the *in vivo* data, rapidly adhering SCs had a lower expression pattern of tau than their floating TAC counterparts. Attached and floating fractions of cells were collected at 20, 40 and 60 min after seeding for RNA and protein analysis (Figure 10.10). To ensure the correct isolation of the two keratinocyte populations, the expression of key SC and differentiation markers was analysed. The population of keratinocytes that adhered most readily to collagen type IV, fibronectin and laminin, had very low expression levels of differentiation markers, such as K1, K10, filaggrin and involucrin (Figure 4.1). In contrast, the floating cell population displayed significantly higher expression levels of these differentiation markers at all of the time points analysed (Figure 4.1). As time increased the relative expression of differentiation markers within the floating population

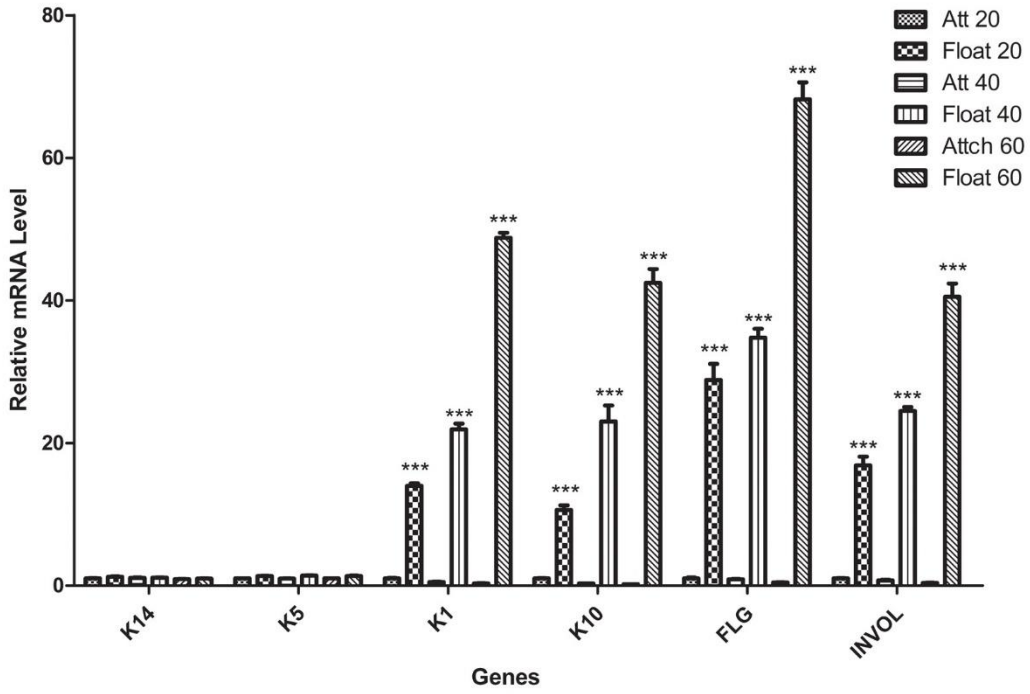

Figure 4.1. RT q-PCR analysis of stem cell and transit amplifying keratinocyte cell populations isolated *in* vitro through their affinity bind to basement membrane protein coatings.

Cell culture dishes were coated with basement membrane proteins, laminin, collagen IV and fibronectin. Un-fractioned HEKn P2 cells were detached and seeded onto coated dishes. Attached and floating cell populations were collected at 20, 40 and 60 min after seeding for RNA extracted. Following cDNA synthesis RT q-PCR was carried out to look for any changes in the transcription of differentiation associated proteins. RT q-PCR data revealed the correct expression of markers of differentiation between attached and floating cell populations collected from the assay (n=3). FLG – filaggrin; Invol – involucrin. Ct values normalised to 36B4 and $2^{-\Delta\Delta Ct}$ method of analysis used. Relative expression levels are displayed as mean ± SD. Two-way ANOVA with Bonferroni correction was used to test significance; *** $p<0.001$.

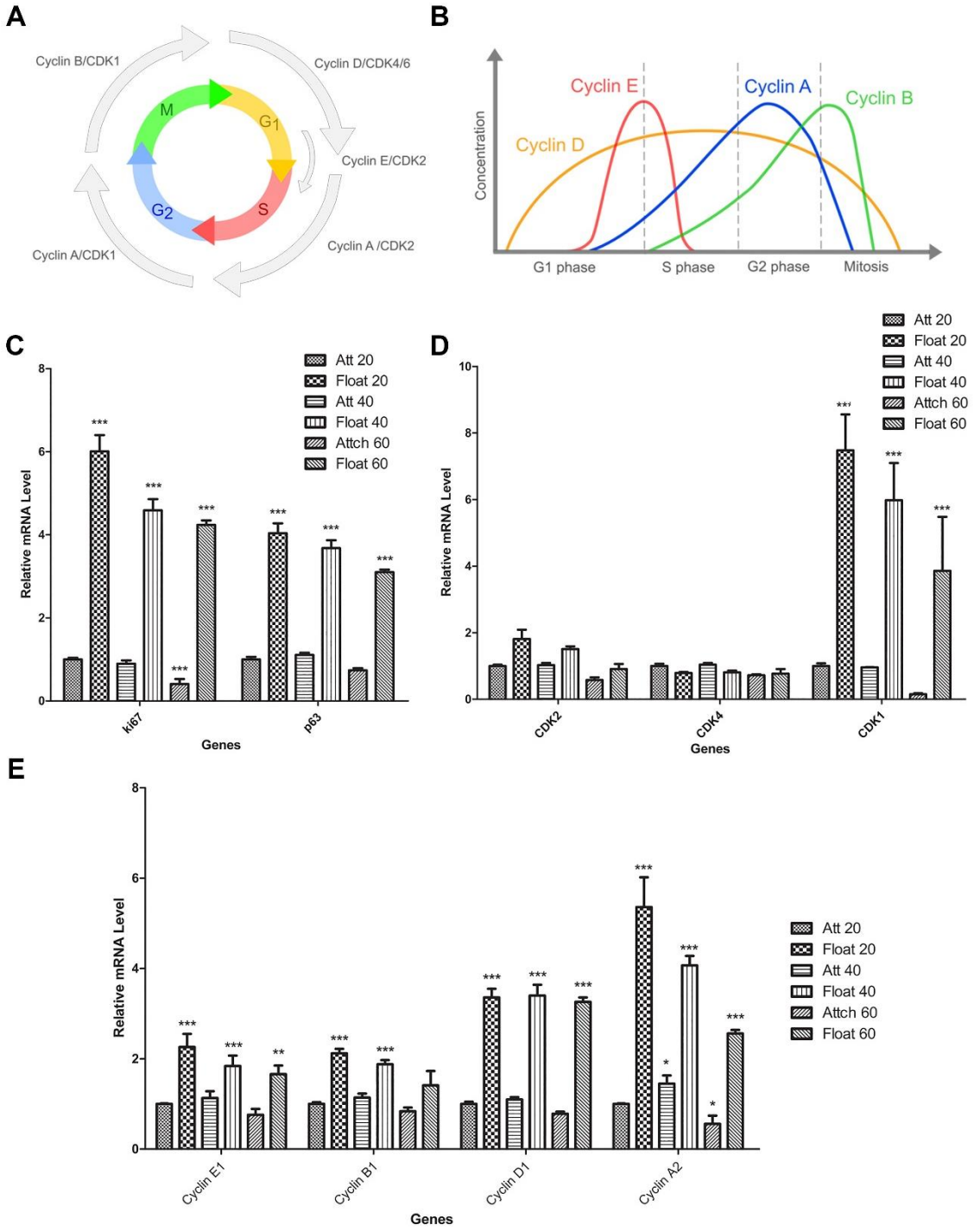

Figure 4.2. Cell cycle status of attached and floating populations of keratinocytes from stem cell attachment assay.
A&B. Schematic demonstrating the stages of the cell cycle with the associated expression of cyclin and CDKs at each phase in a ubiquitination dependent manner. **C-E.** Representative RT q-PCR analysis of genes associated with cell proliferation in attached and floating populations of keratinocytes. Ct values normalised to 36B4 and $2^{-\Delta\Delta Ct}$ method of analysis used. Two-way ANOVA with Bonferroni correction was used to test significance; *p<0.05, ** p<0.01, *** p<0.001.

increased, confirming that the cells isolated at 60 min had more of a differentiated phenotype than those collected in the floating fraction at 20 and 40 min.

To further confirm the correct isolation of keratinocyte populations, a panel of proliferation markers were screened using a q-PCR. Figure 4.2 shows, as expected, the floating population of keratinocytes display a much higher relative expression of all proliferation and cyclin markers than the attached populations. The floating fraction of cells displayed significantly higher expression levels of proliferation markers, Ki67 and p63, compared to the keratinocytes that attached readily to the BM coating (Figure 4.2C). A higher relative expression of CDK1 and Cyclin A2 was also observed in the floating population (Figure 4.2D and E), suggesting that the majority of this population of cells were in G_2 phase of the cell cycle (Figure 4.2A and B); a phase of cell growth and preparation for mitosis.

Following the confirmation that the attachment assay successfully isolated the keratinocyte populations, these cell fractions were used to investigate the relative expression levels of tau between keratinocyte SC and TAC populations. RT q-PCR analysis revealed that total tau expression was significantly higher in the floating cell populations, compared to the attached fraction at all collection time points (Figure 4.3). To investigate which isoforms of tau were expressed in the different cell fractions, tau isoform specific primers were used, targeting the alternatively spliced N- and C-terminal regions (Figure 4.4 and Figure 4.5). The relative expression of 0N variants remained largely unchanged between the two captured populations (Figure 4.4A). 3R showed insignificant fluctuations in relative expression levels (Figure 4.5B). In contrast, 2N and 4R transcript variants were increased in floating cell populations across all time points compared to the attached populations (Figure 4.4D and Figure 4.5D).

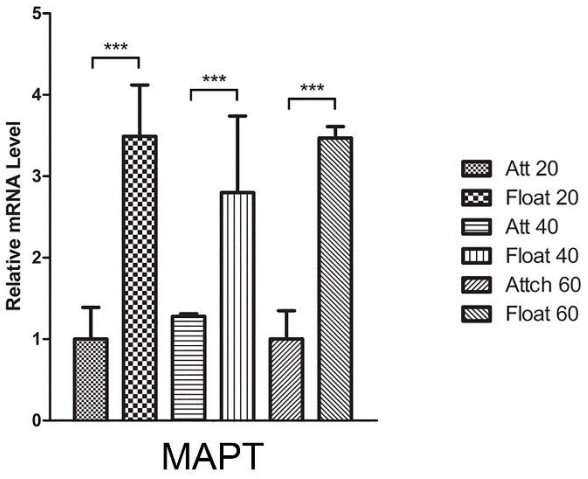

Figure 4.3. Total tau expression in attached and floating populations of keratinocytes isolated from stem cell attachment assay.
RT q-PCR analysis of attached and floating keratinocyte populations isolated using a stem cell attachment assay using a primer pair that bind to all isoforms of tau (n=3). Ct values normalised to 36B4 as a housekeeping gene and $2^{-\Delta\Delta Ct}$ method of analysis used. The relative expression levels are displayed as mean ± SD. Significance was tested with a One-way ANOVA with Bonferroni correction. *** $p<0.001$.

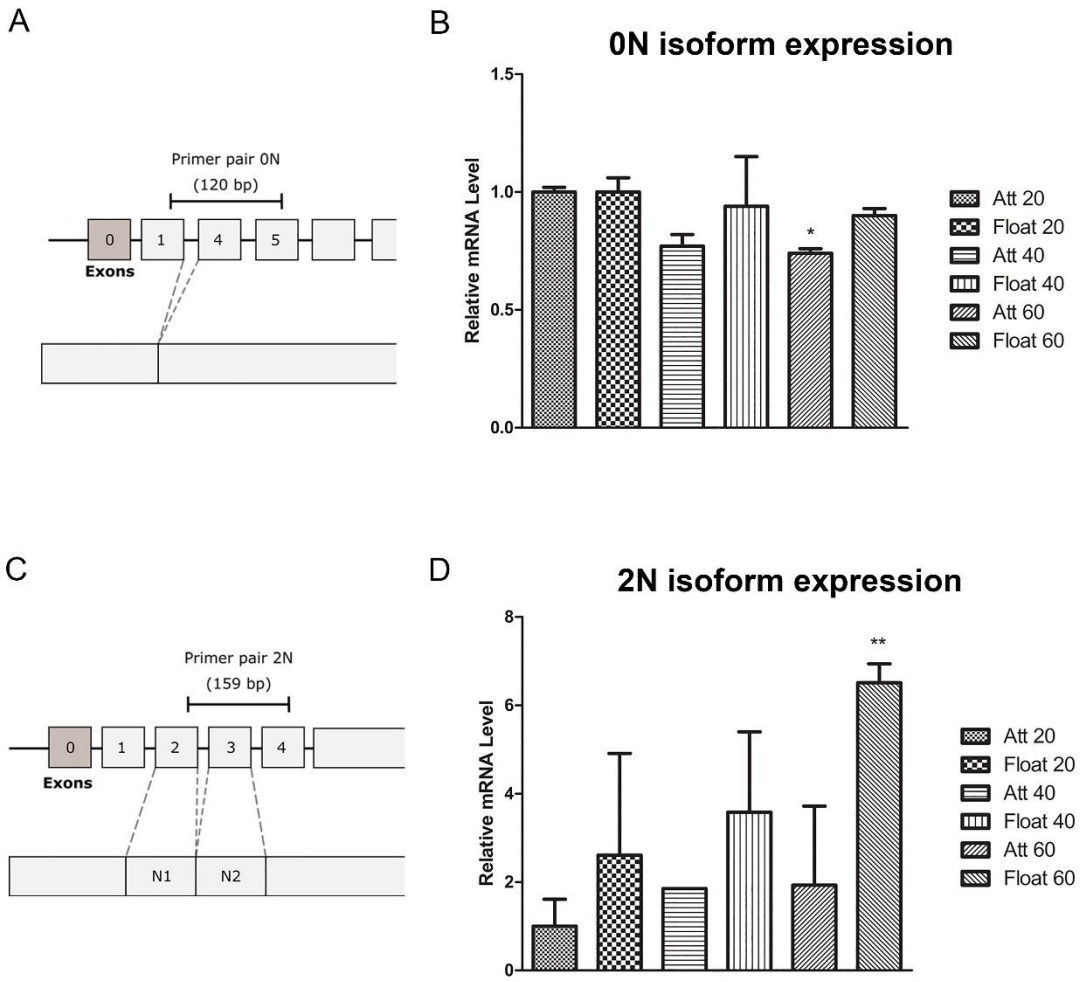

Figure 4.4. Alternative splicing of the N-terminal region of *MAPT* in attached and floating populations of keratinocytes isolated from stem cell attachment assay.

Using the SC attachment assay, isoform specific expression of tau transcripts between SC and TAC populations were compared. **A.** Schematic demonstrating that the 0N isoform primer pairs binds to the tau transcript lacking exons 2 and 3. Flanking exon 1, 4 and 5 this primer pair excluded all other transcript variants containing additional exons. **B.** RT q-PCR analysis of the relative expression of 0N tau transcripts between attached and floating keratinocyte populations. **C.** Schematic indicating how 2N isoform primer pairs bind to the tau transcript, binding to exon 2 and 4 allowing the inclusion of exon 3, detecting transcripts containing both N terminal domains. **F.** RT q-PCR analysis of the relative expression of 2N transcript variants of tau. Ct values normalised to 36B4 and $2^{-\Delta\Delta Ct}$ method of analysis used. Relative expression levels are displayed as mean ± SD. One-way ANOVA with Bonferroni correction was used to test significance; *p<0.05, ** p<0.01.

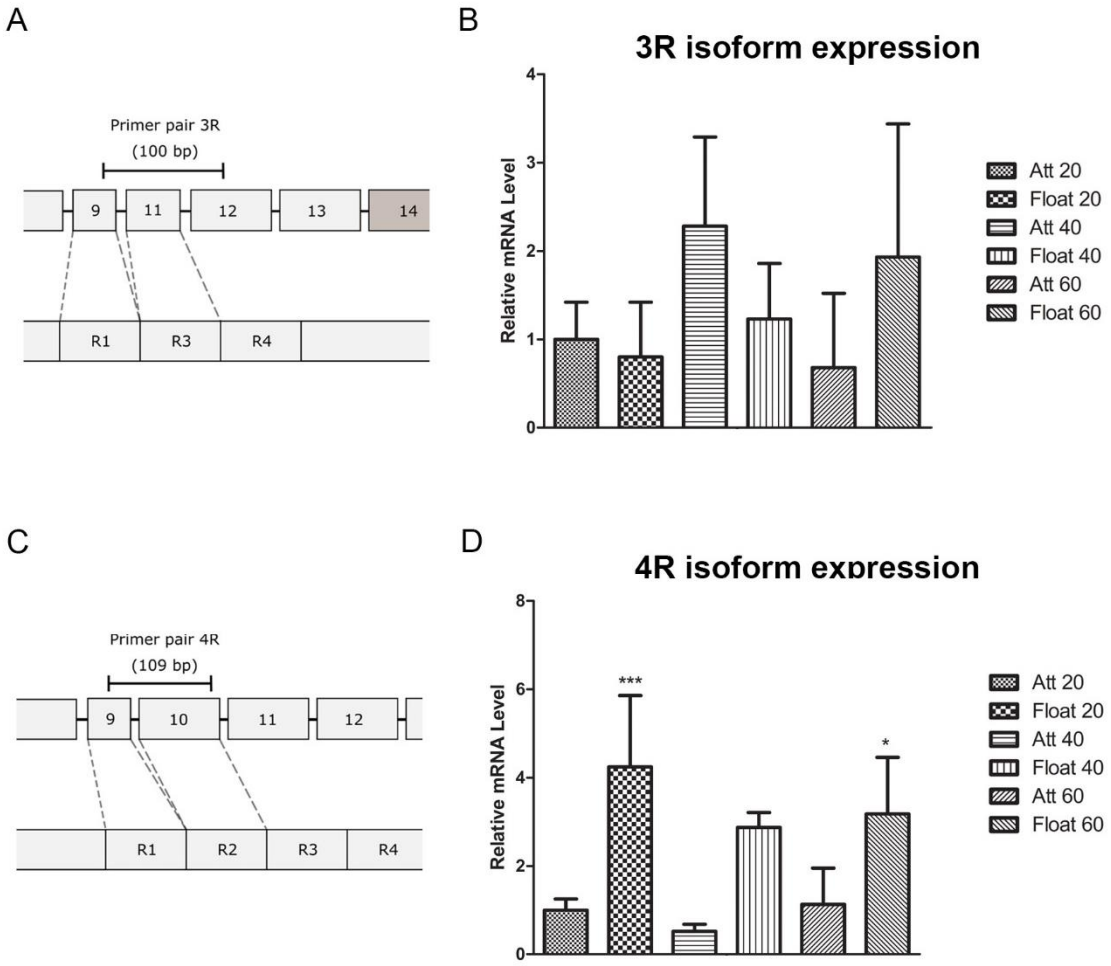

Figure 4.5. Alternative splicing of the C-terminal domain of *MAPT* in attached and floating populations of keratinocytes isolated from stem cell attachment assay.

Using the SC attachment assay to isolate the SC and TACs, the alternative splicing of the microtubule binding domain in these populations was investigated. **A.** Schematic indicating where 3R isoform primer pairs bind on the tau transcript. The 3R primer pair flanks exon 9-11, excluding any 4R transcripts containing exon 10. **B.** RT q-PCR analysis of the relative expression of 3R transcript variants between the floating and attached populations. **C.** Schematic demonstrating where 4R isoform primer pairs bind on the tau transcript. 4R primers flank exons 9-10, only amplifying transcripts containing exon 10. **D.** RT q-PCR analysis of the relative expression of 4R isoforms of tau. Ct values normalised to 36B4 and $2^{-\Delta\Delta Ct}$ method of analysis used. Relative expression levels are displayed as mean ± SD. One-way ANOVA with Bonferroni correction was used to test significance; *p<0.05, *** p<0.001.

4.4.2. Tau is dynamically expressed throughout the cell cycle

The SC attachment assay identified that tau expression was consistently higher in the proliferative, TAC population of keratinocytes compared to the less proliferative SC population. The transition of cells from a state of quiescence into proliferation is a key step in tissue homeostasis. However, it is often it is difficult to distinguish quiescent cells and those that are active in the cell cycle. Therefore, to further investigate tau expression in quiescent SCs and throughout stages of the cell cycle, keratinocytes were infected with a fluorescent-based reporter has been established to enable the visualisation of the spatio-temporal dynamics of a cells progression through the cell cycle [318,319]. Using the cells Ki67 promotor to drive the expression of the Fluorescent Ubiquination-based Cell Cycle Indicator (FUCCI), cells in G1, S, G2/mitosis (M) could be identified and the indirect detection of quiescent (G_0) cells also enabled (Figure 4.6).

The FUCCI system is based around the careful regulation of Geminin and Chromatin licensing and DNA replication factor 1 (Cdt1) within the cell, to ensure cell cycle replication only occurs once. Geminin and Cdt1 are direct substrates of the APC^{Cdh1} and SCF^{Skp2} complexes; E3 ligase activities that mark a variety of proteins with Ub in a cell cycle dependent manner, as the cell cycle is controlled by ubiquitin (Ub)-mediated proteolysis. SCF^{Skp2} is a direct substrate of APC^{Cdh1} and also functions as a feedback inhibitor of APC^{Cdh1}, meaning that these two ligase activities oscillate reciprocally/inversely during the cell cycle. The APC^{Cdh1} complex is active in the late M and G_1 phase and therefore Cdt1 accumulates in these stages of the cell cycle whilst geminin is degraded. Whereas the SCF^{Skp2} complex is active in the S, G_2 and M phases, and therefore Geminin accumulates within these stages and Cdt1 is degraded. The FUCCI construct uses this oscillating expression of Geminin and Cdt1 which are conjugated to monomeric

Azami-Green (mAG) protein or mCherry fluorophores respectively, therefore allowing different phases of the cell cycle to be detected via fluorescence (Figure 4.6B). During the transition between G_1 to S phase of the cell cycle cdt1 levels are decreasing whilst geminin levels are increasing and both proteins are present, therefore both mCherry and mAg are also expressed leading to the nuclei appearing yellow in the S phase of the cell cycle.

Keratinocytes were successfully infected with Ki67p FUCCI lentiviral particles (Figure 4.6C). Most cells were identified in G_1 phase of the cell cycle (70.96%) and %), G_2/M (20.64%) with a small proportion of cells in S phase (3.25%) and G_0 (5.15%) (Figure 10.11). This is a normal observation as G_1 is the longest phase of the cell cycle, with cells typically in this phase for 11 h, whereas S typically lasts 8 h, G_2 lasts 4 h and mitosis 1 h [320]. In a mixed population of cells it is expected that 1% of cells are quiescent, but the keratinocytes in this condition are cultured in SC promoting medium, so 5% in G_0 is unsurprising.

Chapter 3 revelaved that in healthy human skin the expression density of tau was different between neighbouring cells in the basal layer and so far this chapter has demonstrated that tau expression levels are lowest in SCs compared to their TAC and differentiated counterparts. To explore this further the FUCCI system was used to identify tau expression throughout different stages of the cell cycle. FUCCI cells were co-stained using a tau antibody with a secondary antibody in the far red spectrum so that all fluorescence could be visualised in paralell. Interestingly, consistent with findings in this study, colourless (G_0) cells (indicated with yellow arrow in Figure 4.7) appeared to have a lower tau expression compared to those in G_1, S and G_2 phases of the cell cycle (Figure 4.7). Cells in G_0 and G_1 phases of the cell cycle displayed punctate nuclear expression of tau. Cells in G_2 phases of the cell cycle disaplyed a significantly higher expression of

tau than all other phases of the cell cycle, indicating that tau is upregulated during cell division and consistent with what we have observed so far. Therefore, as the expression of tau was observed to be upregulated during cell proliferation, immunolfuorescece anaysis was performed to further invesigate tau expession in keratinocytes throughout different stages of mitosis.

Immunofluorescence staining, using tubulin to identify spindle formation and progression of mitosis alongside tau, of a mixed population of keratinocytes revealed tau displays a disctinct expression pattern throughout mitosis (Figure 4.8). During interphase, tau is observed in the nucleus in punctate stainning, but absent in the nucleolus, with low levels of tau expression in the cytoplasm (Figure 4.8A). Following the G_2/M checkpoint cells undertake prometaphase and metaphase stages of mitosis; metaphase occurs when the nuclear membrane has been broken down, after which the mitotic spindle is established and chromosome have align at the metaphase plate. During metaphase tau was observed highly expressed throughout the cell, surrounding the mitotic spindle and surrounding the chromosomes at the metaphase plate (Figure 4.8B); tau was not observed to co-localise directly with the chromsomes, tau was absent where the nuclear material was located and instead tau was only found to surround the DNA. During anaphase centromeres dissemble and sister chromatids move towards opposite ends of the cell. Tau was found expressed throughout the cell during this phase as the sister chromatids were moved to opposite ends of the cell (Figure 4.8C). During later stages of anaphase and the first stages of telophase in which actin filaments form a contractile ring, forming an ingressign furrow to enable cytokinesis to take place, tau could be observed to co-localise with the ingressing furrow in the cells (Figure 4.8C). Strong expression of tau can

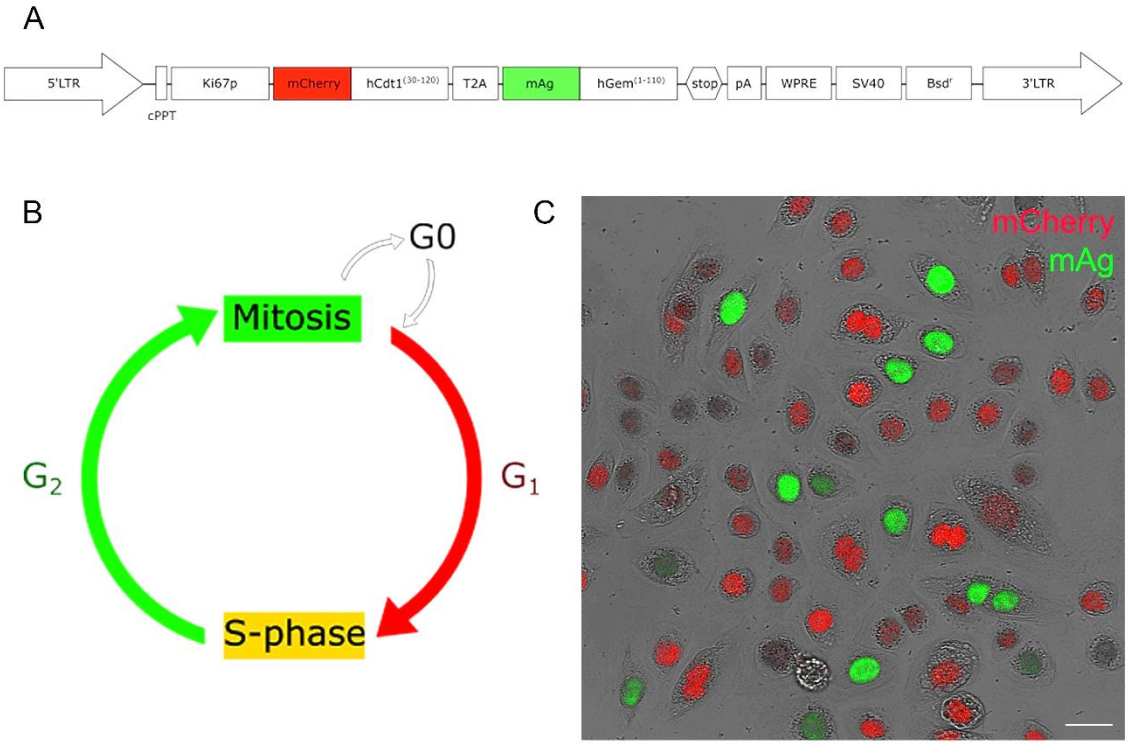

Figure 4.6. Ki67p fluorescent ubiquitination based cell cycle indicator (FUCCI) in epidermal keratinocytes.
The cell cycle is dependent on the careful regulation and periodic degradation of Geminin (Gem) and Chromatin licensing and DNA replication factor 1 (Cdt1) within the cell, to ensure cell cycle replication only occurs once. In FUCCI cells the expression of Geminin and Cdt1 are linked to the expression of green and red fluorophores respectively, allowing different stages of the cell cycle to be visualised via fluorescence **A.** Schematic demonstrating the Ki67p-FUCCI lentiviral reporter plasmid used to create lentiviral particles for infection of epidermal keratinocytes. Ki67p FUCCI lentiviral reporter incorporates a Ki67 promoter that restricts the expression of the fluorophore complexes to actively cycling, allowing the identification of quiescent cells in G_0 phase of the cell cycle. Blasticidin resistance gene allows for selection of cells in culture to ensure colourless cells are infected but not active in the cell cycle. mCherry (red) and mAG (green) fluorophores are regulated by the expression of hCdt1 and hGem (geminin) respectively, all of which are under the Ki67 promoter. **B.** Schematic demonstrating m-Cherry and mAG expression throughout the stages of the cell cycle. G_1 (red), S-phase (yellow) and G_2 and mitosis (green). As Cdt1 is expressed in both G_0 and G_1 phases of the cell cycle, the incorporation of the Ki67 promoter enables the discrimination of quiescent cells (G_0) as Ki67 expression only occurs throughout the cell cycle and is absent in G_0, therefore these cells appear colourless. **C.** Representative cell culture image of HPEKp cells infected with Ki67p FUCCI under selection using blasticidin. Cells can be observed in G_1 (red), G_2 (green) and G_0 (colourless). Scale bar 25 µm.

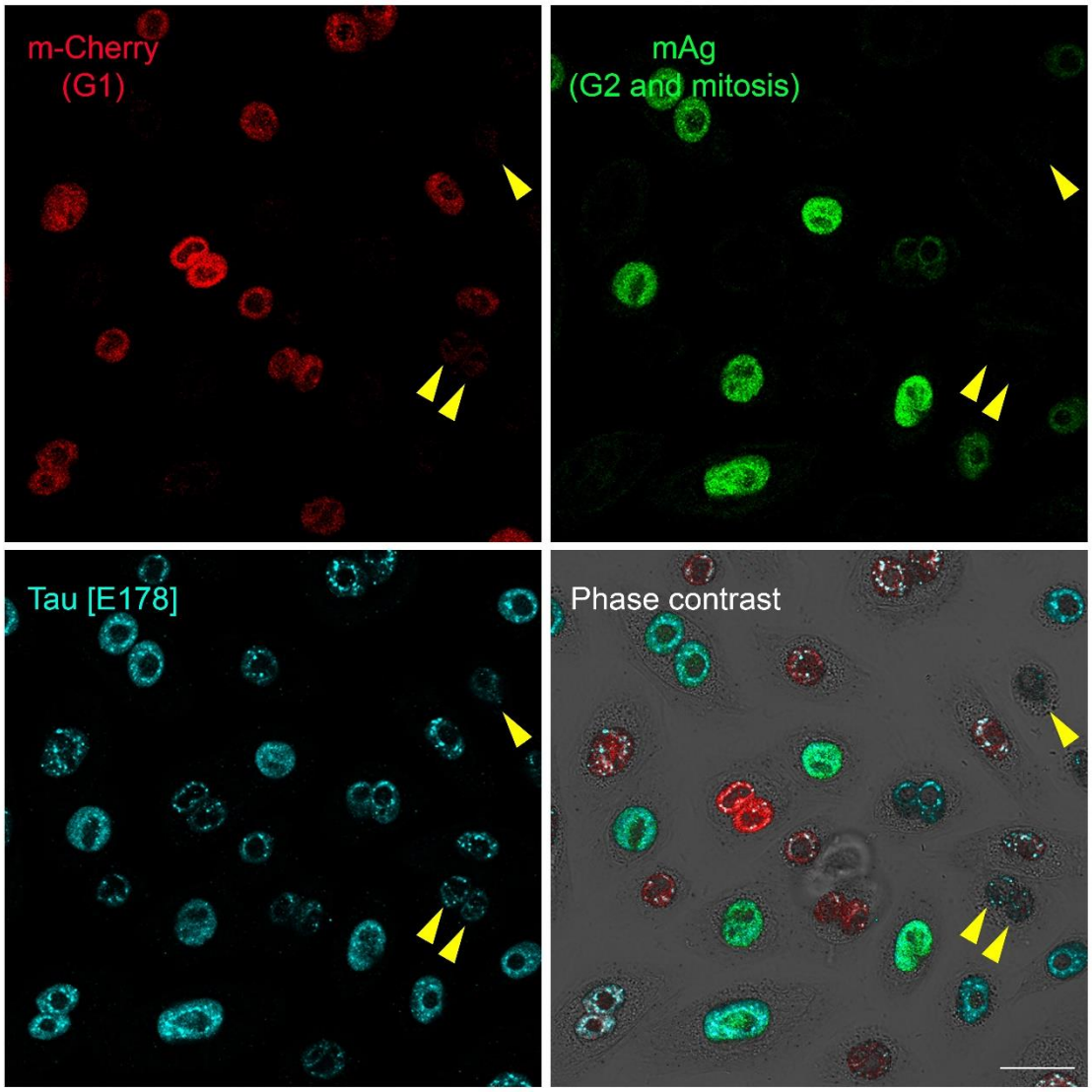

Figure 4.7. Tau expression during cell cycle dynamics in epidermal keratinocytes.
To investigate tau expression in epidermal keratinocytes throughout different stages of the cell cycle, Ki67p FUCCI infected HPEKp were co-stained with tau [E178] (cyan). FUCCI infected cells indirectly allow the detection of quiescent cells, as the construct used the Ki67 promotor to drive the expression of florophores, therefore quiescent cells (G_0) appear colourless. mCherry (red) expression with hCdt1 allows the visualisation of G_1, mCherry/mAg (yellow) indicates S phase and mAg (green) expression with hGem indicates G_2 and mitosis. Yellow arrow indicates colourless (G_0) cells. Interestingly, consistent with findings in this study, colourless (G_0) cells appear to have lower tau expression compared to those in G_1 (red), S (yellow), G_2 and M (Green) phases of the cell cycle. All channels are overlaid and displayed with the phase contrast image in the bottom right panel to allow visualisation of cellular staining. Scale bar 25 µm.

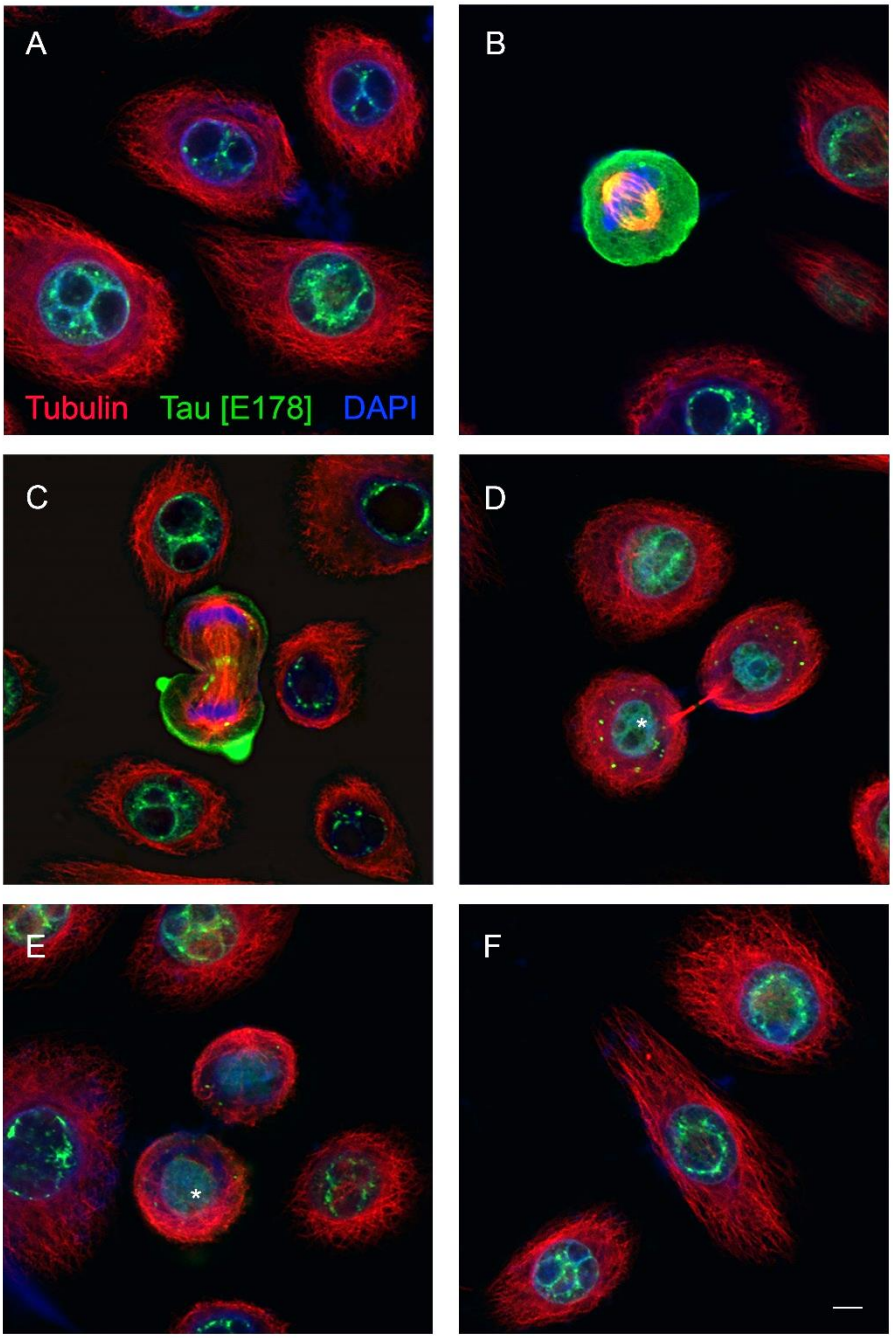

Figure 4.8. Immunofluorescence analysis of tau expression throughout stages of mitosis in keratinocytes.
Representative immunofluorescence staining of tau [E178] (green) and tubulin (red) in HEKn cells during stages of mitosis. Nuclei counter-stained with DAPI (blue). **A.** Interphase; tau is found displaying punctate staining in the nucleus, absent however in the nucleolus. Tau expression is detected at low levels in the cytoplasm. **B.** Metaphase; the mitotic spindle has been established and chromosomes have aligned at the metaphase plate**.** Tau expression can be observed strongly throughout the cell surrounding the mitotic spindle and chromosomes. **C.** Anaphase/telophase; centromeres disassemble and sister chromatids mode to opposite ends of the cell. Actin filaments form a contractile ring to form an ingressing furrow to enable cytokinesis. Tau was detected around daughter nuclei in anaphase/telophase and surrounding the mitotic spindle

throughout this phase. **D.** Cytokinesis; following telophase and the ingression of the membrane the abscission phase of the cell cycle commences. The nuclear membrane is reformed and the membrane is severed within the intracellular bridge. Tau is detected throughout the nucleus again by cytokinesis. Interestingly, one daughter cell appears to have slightly higher tau expression in the nucleus. Asterisk indicates daughter cell that has increased tau levels in nucleus. Punctate staining can be observed surrounding the nucleus at the posterior end of the cell. **E.** Independent daughter cells. The membrane has been completely severed and the cells enter G1 phase of the cell cycle. Again, one daughter cell can be observed to have higher tau expression in the nucleus, an asterisk indicates the daughter cell that has increased tau levels in nucleus. **F.** Interphase; punctate tau staining in nucleus, with low levels of cytoplasmic tau expression detectable in keratinocytes cultured in basal medium. Scale bar 5 μm.

also be identified remianing at the cell membrane of keratinocytes, while the cytoplasmic expression of tau decreases compared to its expression during metaphase (Figure 4.8C). In the later stages of telephase, during the abcission phase of cytokinesis, the nuclear membrane reforms, chromosomes decondense and the membrane is served within the intracellular bridge. Interestingly, at this stage of mitosis tau expression is mostly restricted to the nucleus again with little membrane or cytoplasmic tau identified (Figure 4.8D). Dispite this, during this phase of mitosis tau was consistently identified surronding the newly formed nucleus, displaying punctate expression at regular intervals throughout the cytoplasm, a phenomenon never reported before (Figure 4.8D). During the abcission phase of cytokinesis, tau was no longer observed at the intracellular bridge (Figure 4.8D). Finally, once the intracelluar bridge has been severed two independent daugher cells are formed (Figure 4.8E). Tau expression is detected in the nucleus once the independent daughter cells have been formed (Figure 4.8E). Interestingly, one daughter cell often inherited higher expression levels of tau when observed in culture (Figure 4.8D and E); however the significance of this has not yet been determined.

4.4.3. Keratinocyte differentiation modulates tau isoform expression in the epidermis

In this study, *in vivo* data indicated that the isoform expression of tau correlates to the differentiation status of keratinocytes. The routine cell culture of keratinocytes is performed with media promote a growing phenotype in which cells continue to clonally expand and discourage differentiation to allow for longer term viability of cells in culture. Therefore, to compare tau expression in growing and differentiated keratinocytes, cell differentiation was induced. A well-recognised method of partially replicating epidermal differentiation *in vitro* is the

extracellular increase in calcium concentration. To test if an increase extracellular calcium from 60 µM to 1.7 mM was sufficient to induce keratinocyte differentiation *in vitro*, cells were treated with high calcium medium for 48 and 72 h before RNA and protein were collected for analysis. Control cells were cultured in complete culture medium containing 60 µM calcium to maintain a stem-like state. Early passage cells were used in all experiments to help ensure a growing phenotype was maintained in the cell population and help reduce any experimental variation observed. Figure 4.9 demonstrates that 1.7 mM extracellular calcium levels were sufficient to induce a differentiated phenotype in keratinocyte cells compared to their control, further confirmed using proteomic analysis (Figure 10.19 and Figure 10.20).

Keratinocyte morphology changed, displaying an adhesive network of cells with increased size in the calcium treated population, compared to the small, round or polygonal morphology observed in the control cell population (Figure 4.9A and B). Keratin expression was found to switch from K14/K5 in the control cells to K1/K10 expression in calcium treated cells by 48 h (Figure 4.9C). Filaggrin and involucrin, terminal differentiation markers expressed in granular cells, showed an increased expression by 48 h, but a higher relative expression was observed by 72 h (Figure 4.9D).

Immunofluorescence and q-PCR analysis of healthy human skin in Chapter 3 showed a change in both total tau and tau isoform expression between the basal and suprabasal tissue populations. Therefore, using a high concentration of calcium to effectively induce keratinocyte differentiation *in vitro*, tau expression patterns were compared between growing and differentiated keratinocyte populations at 48 and 72 h. There was a small increase in tau expression at 48 h, but by 72 h tau expression could be observed to significantly increase

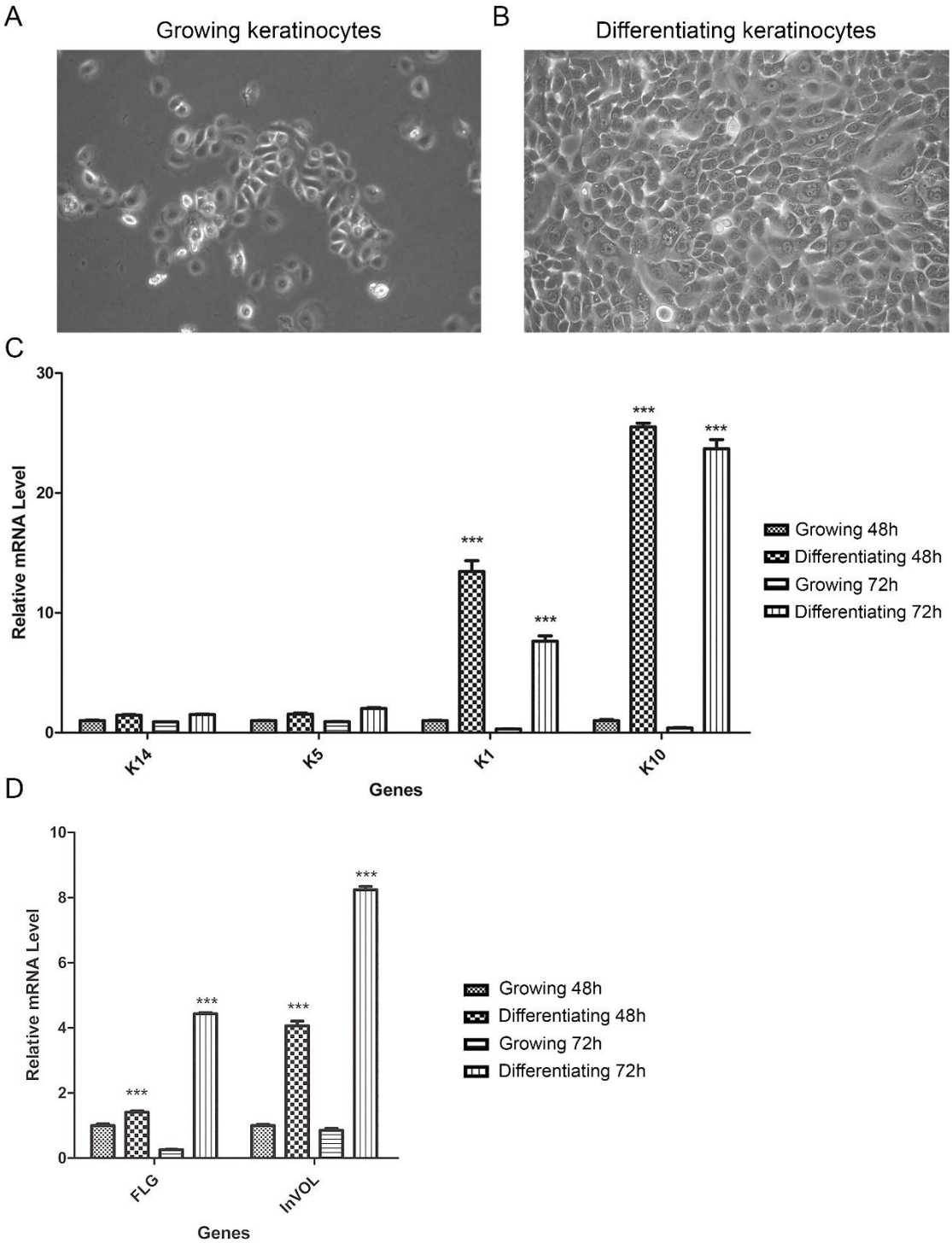

Figure 4.9. Keratinocyte differentiation is induced by increased extracellular calcium levels

HEKn cells were cultured for 48 and 72 hours in culture medium containing extracellular calcium levels from 60 µM (promoting keratinocyte growth) or 1.7 mM (promoting keratinocyte differentiation). **A.** Cell culture images of HEKn cells cultured in growing conditions at 72 h. **B.** Cell culture images of HEKn cells cultured in differentiating conditions at 72 h. **C.** Representative RT q-PCR analysis of differentiation markers between control and calcium treated keratinocytes. **D.** RT-q-PCR analysis of terminal differentiation markers. FLG – filaggrin; Invol – involucrin. Ct values normalised to 36B4 and $2^{-\Delta\Delta Ct}$ method of analysis used. Relative expression levels are displayed as mean ± SD. Two-way ANOVA with Bonferroni correction was used to test significance; *** $p<0.001$.

compared to the control (Figure 4.10A). This progressive increase is consistent with the expression of terminal differentiation proteins filaggrin and involucrin in Figure 4.9D, and the immunofluorescence staining in Chapter 3; the degree of tau expression is correlated to the degree of epidermal differentiation.

The alternative splicing of tau in calcium induced differentiated keratinocytes was assessed using RT q-PCR with isoform specific primer pairs. There was little change in the relative expression levels of 0N variants of tau between control and differentiated keratinocytes, and 1N isoforms were not detected (Figure 4.10B). On the other hand, as expected, 2N isoform expression was increased at each time point in the calcium treated cells. 3R isoform expression remained constant until 72 h, where an increased expression level was observed in the calcium treated cells, consistent with the overall, significant increase in tau expression at 72 h calcium treatment (Figure 4.10B). The expression of tau 4R transcript variant, however, was significantly increased after 72 h of calcium treatment in keratinocyte cells compared to the control (Figure 4.10B).

Analysis of tau protein expression between the control and differentiated keratinocytes was performed using Western blot and immunofluorescence. Western blotting of total, cytoplasmic and nuclear protein fractions revealed an overall increase in tau in calcium treated keratinocytes (Figure 4.11). Calcium differentiated keratinocytes demonstrated a decrease in total tau expression in the nuclear protein fraction, with an accompanying decrease in phosphorylated tau protein levels. Phosphorylated tau protein was mostly restricted to the total and nuclear protein fraction, with little or no cytoplasmic phosphorylated tau detected (Figure 4.11).

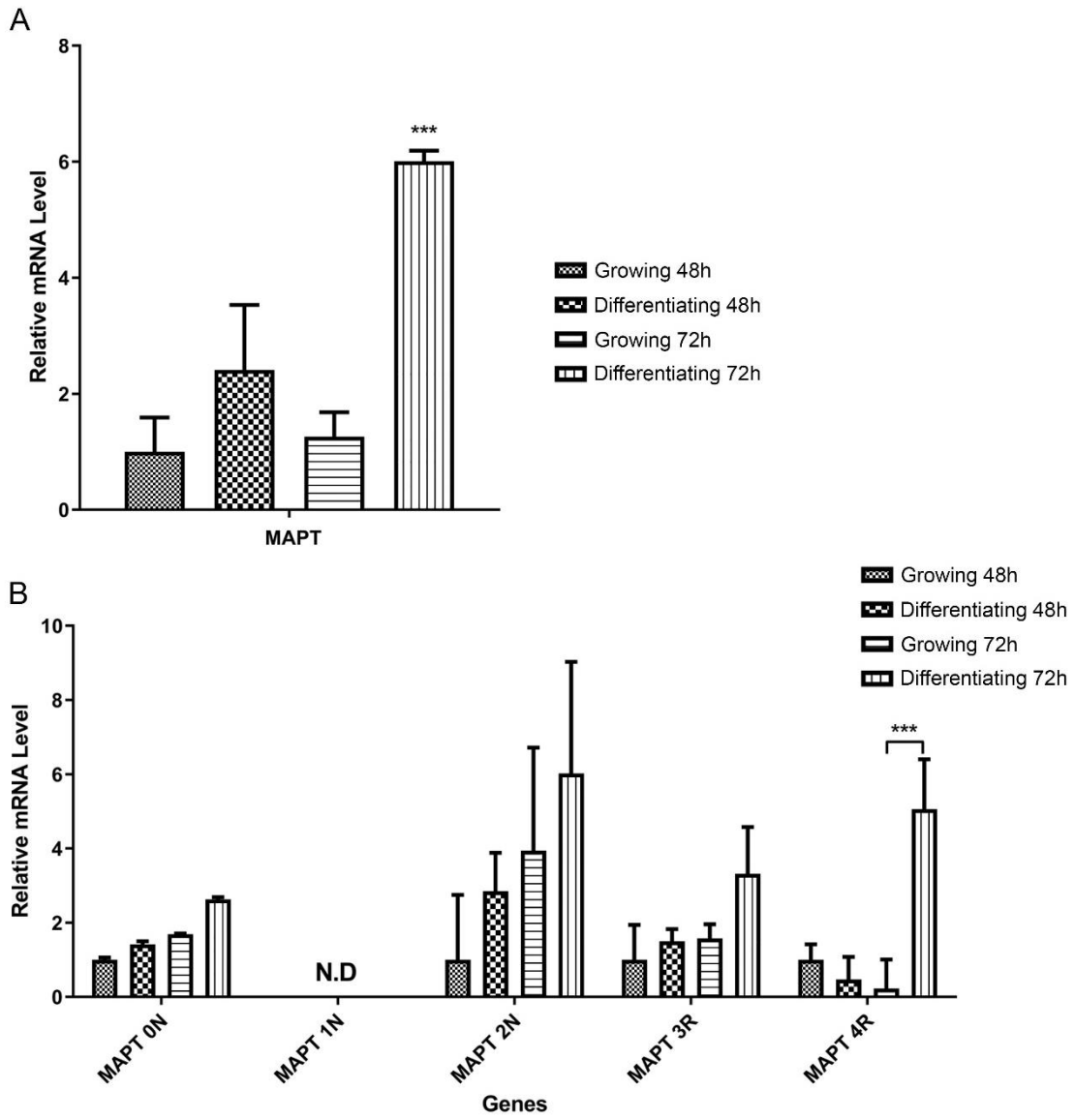

Figure 4.10. Tau expression in epidermal keratinocytes following calcium induced cell differentiation.

A. Representative RT q-PCR analysis of the relative expression of tau in control and calcium differentiated HEKn cells 48 and 72 h after treatment. One Way ANOVA with Bonferroni correction was used to test significance. **B.** Relative RT q-PCR analysis of the relative expression of tau isoforms in control and differentiated keratinocyte populations. Ct values normalised to 36B4 and $2^{-\Delta\Delta Ct}$ method of analysis used. Relative expression levels are displayed as mean ± SD. One or Two-way ANOVA with Bonferroni correction was used to test significance. *** $p<0.001$. N.D – not detected.

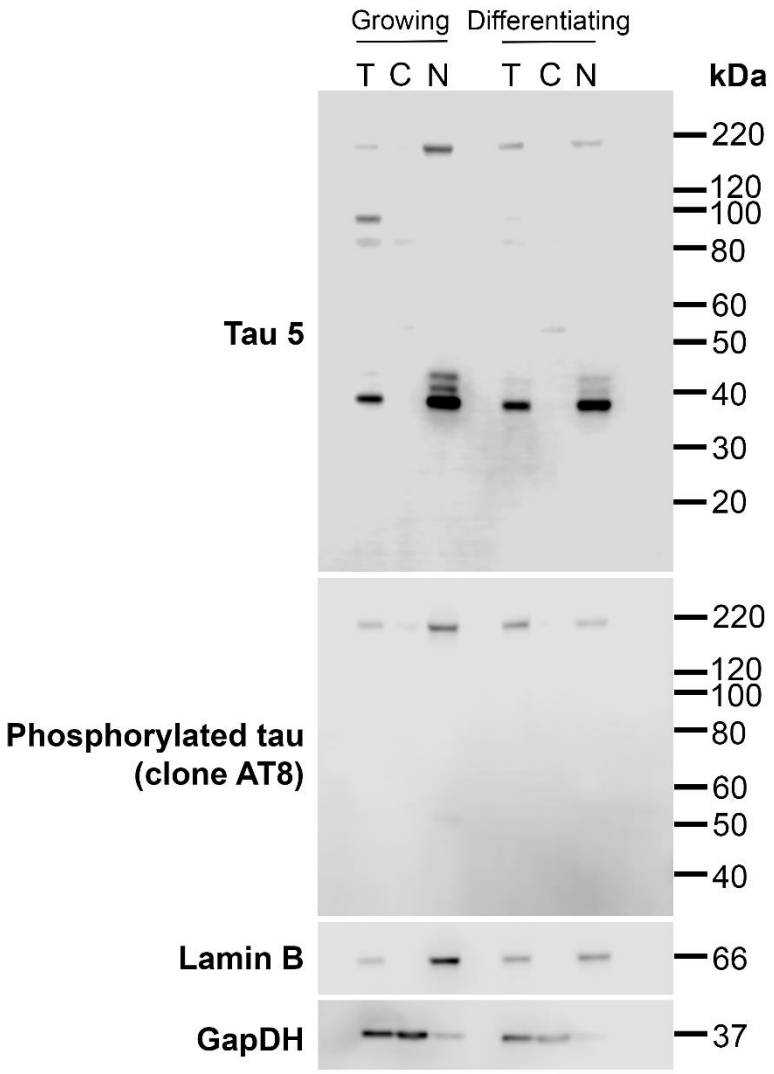

Figure 4.11. Analysis of tau protein expression and localisation in growing and differentiated epidermal keratinocytes.
Representative Western Blot analysis of total, cytoplasmic and nuclear protein in keratinocyte cells 72 h after calcium induced differentiation and a control keratinocyte population cultured under cell culture conditions promoting cell growth. Total, cytoplasmic and nuclear protein fractions were extracted from cells 72 h after calcium treatment. Lamin B1 and Glyceraldehyde-3-Phosphate Dehydrogenase (GAPDH) were used to demonstrate purity of the nuclear and cytoplasmic fraction respectively. T – Total, C – Cytoplasmic, N – Nuclear.

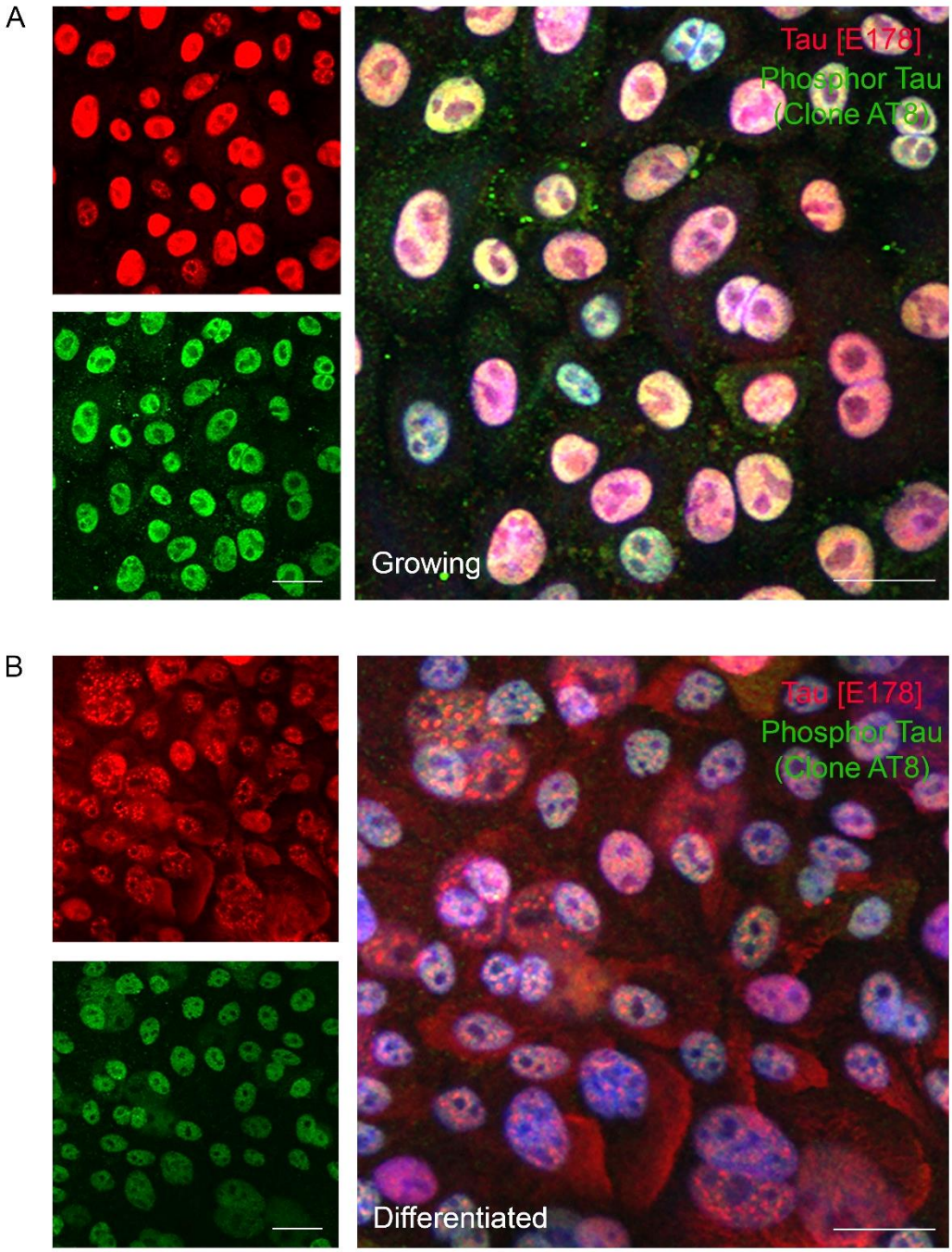

Figure 4.12. Immunofluorescence analysis of tau expression in keratinocyte cells.
Representative immunofluorescence analysis of tau [E178] (red) and phosphorylated tau (green) expression in HEKn cells with and without calcium induced differentiation (n=3). Nuclei counterstained with DAPI (blue) and all channels overlaid in the panel on the right. **A.** In keratinocyte cells cultured under basal promoting culture conditions total and phosphorylated tau expression was highest in the nucleus. Tau was absent in the nucleolus in both growing and differentiating keratinocytes. **B.** Calcium treated keratinocytes 48 h after increase in extracellular calcium increase displayed tau expression in the nuclear and cytoplasmic fraction of the cells. Tau was also identified to be polarised at the cortical edge of the cells. Phosphorylated tau was observed to decrease following calcium induced keratinocyte differentiation. Scale bar 25 µm.

Immunofluorescence analysis of tau protein expression upon cell differentiation was consistent with Western Blot findings (Figure 4.12). In control keratinocytes tau expression was highest in the nucleus, with low levels of cytoplasmic expression identified (Figure 4.12A). Whereas strikingly, in the differentiated population of keratinocytes tau showed an overall increase, with cytoplasmic expression also identified (Figure 4.12B). Tau was identified polarised at the cortical edge of the cells following calcium induced differentiation (Figure 4.12B). Phosphorylated tau was found to decrease in the nucleus of the differentiated population, consistent with western blot findings (Figure 4.12B). Total and phosphorylated tau appear to be mostly absent in the nucleolus, instead only co-localising with the DAPI staining in the nucleus (Figure 4.12). Tau presented with speckled staining in the nucleus, more prominent in differentiated population of cells (Figure 4.12B).

Microtubules in keratinocytes cultured in growing conditions were correctly identified growing from the centre of the cell out to the cell periphery, in agreement with other studies labelling the centrosome as the primary MTOC (Figure 10.12A). However, in calcium treated cells this organisation was lost and instead a cortical array of microtubules was observed (Figure 10.12B). To assess the cytoplasmic expression of tau in keratinocytes, immunofluorescence analysis of tau [E178] with tubulin was carried out (Figure 4.13). Tau is expressed at low levels throughout the cytoplasm but can be observed asymmetrically distributed to the membrane nearest the MTOC in growing keratinocytes (Figure 4.13A). In differentiated keratinocytes, along with the cortical arrangement of microtubules, tau was asymmetrically distributed and co-localised with tubulin at the cortical edge of differentiating cells (Figure 4.13B).

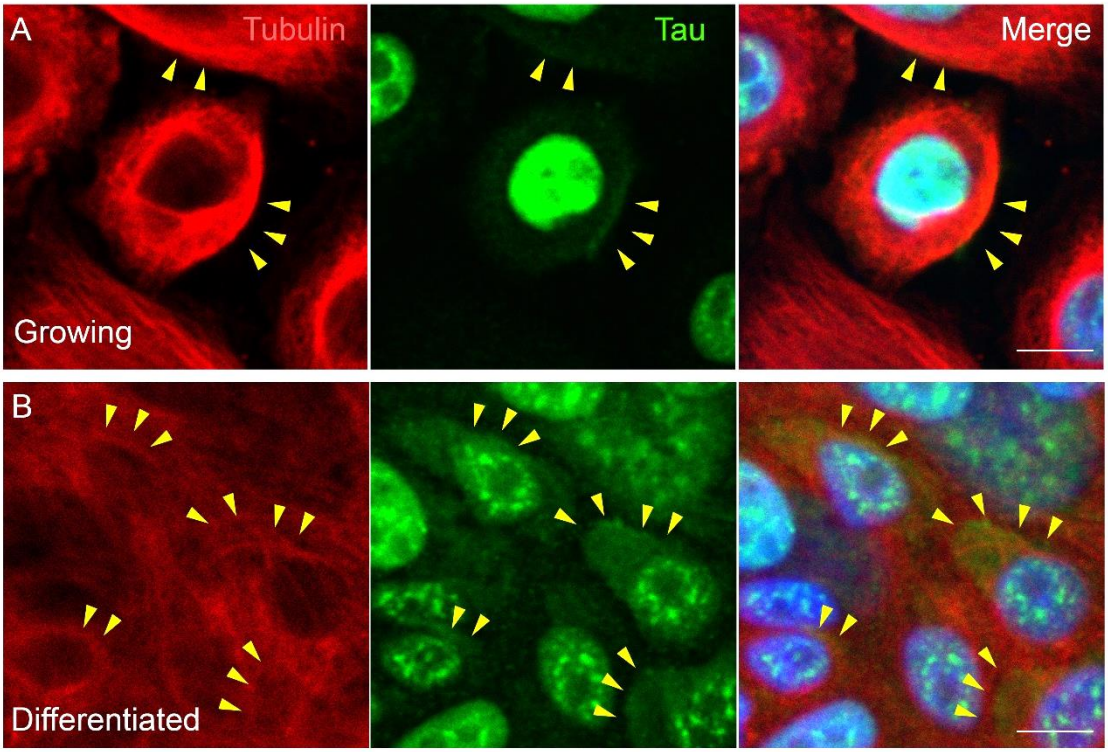

Figure 4.13. Immmunoflurescence analysis of tau localisation with tubulin in growing and differentiating keratinocytes.
Representative immunofluorescence analysis of tubulin (red) and tau (green) in HEKn cells under growing and differentiating cell culture conditions (n=3). **A.** Keratinocytes cultured in growing cell culture conditions displayed a microtubule network that grew from the MTOC to the periphery of the cell. Tau was identified to be polarised to the edge of the cell closest to the MTOC in growing keratinocytes. **B.** 1.7 mM calcium was supplemented medium to induce keratinocyte differentiation for 48 h. Extracellular increase in calcium levels leads to the formation of cortical array of microtubules and co-localisation of tubulin and tau expression in the cytoplasm. Nuclei counter-stained with DAPI (blue) and all channels are merged in the right panel to allow accurate visualisation of cellular morphology. Scale bar 10 µm.

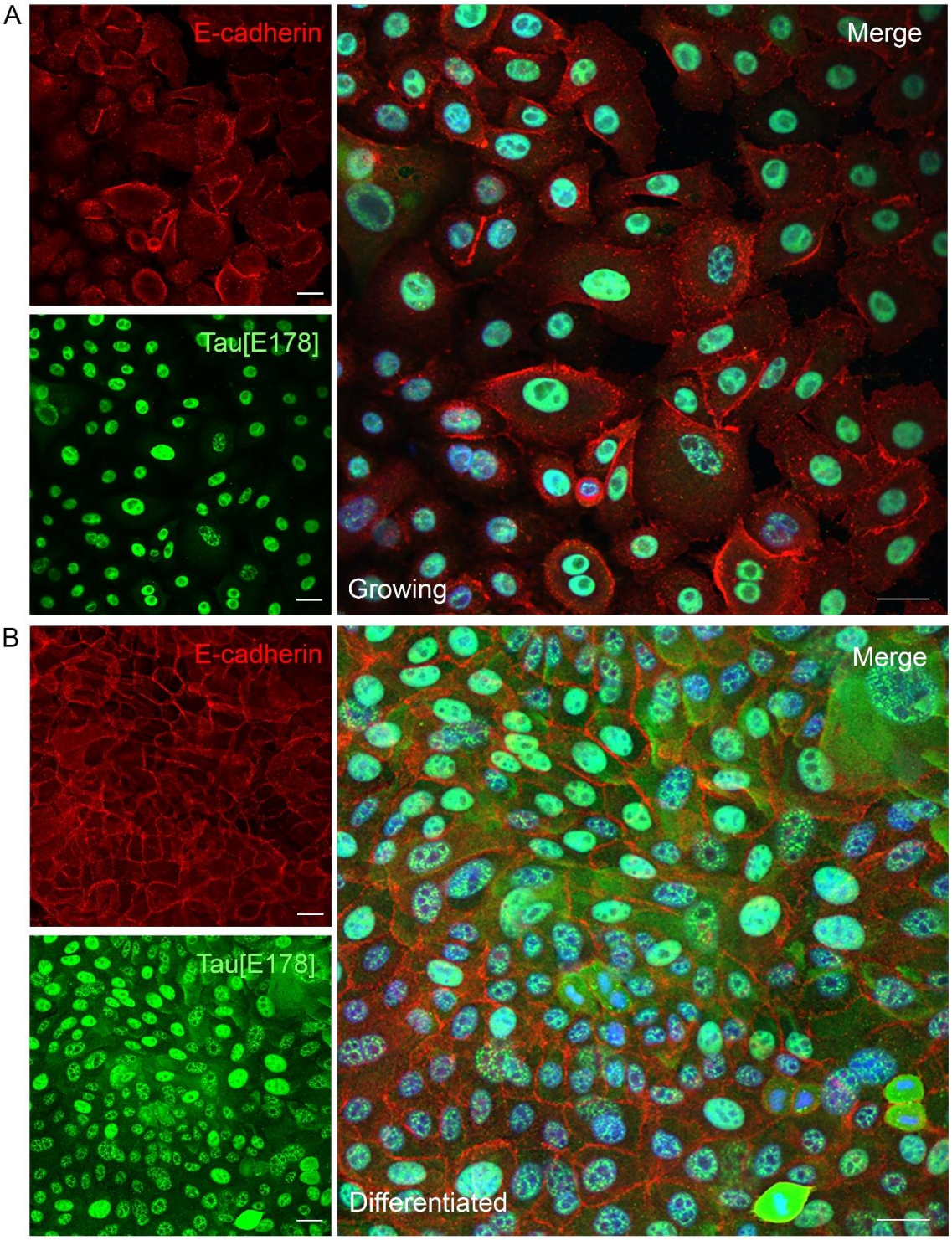

Figure 4.14. Tau co-localisation with the plasma membrane in differentiated keratinocytes.
Representative immunofluorescence analysis of E-cadherin (red) and tau [E178] (green) expression in keratinocyte cells with and without calcium induced cell differentiation (n=3). **A.** Keratinocyte cells cultured under growing conditions. **B.** Differentiated keratinocyte cells 48 h after extracellular calcium levels were increased. Nuclei counter stained with DAPI (blue) and all channels are merged in the right panel to allow accurate visualisation of cellular morphology. Scale bar 25 µm.

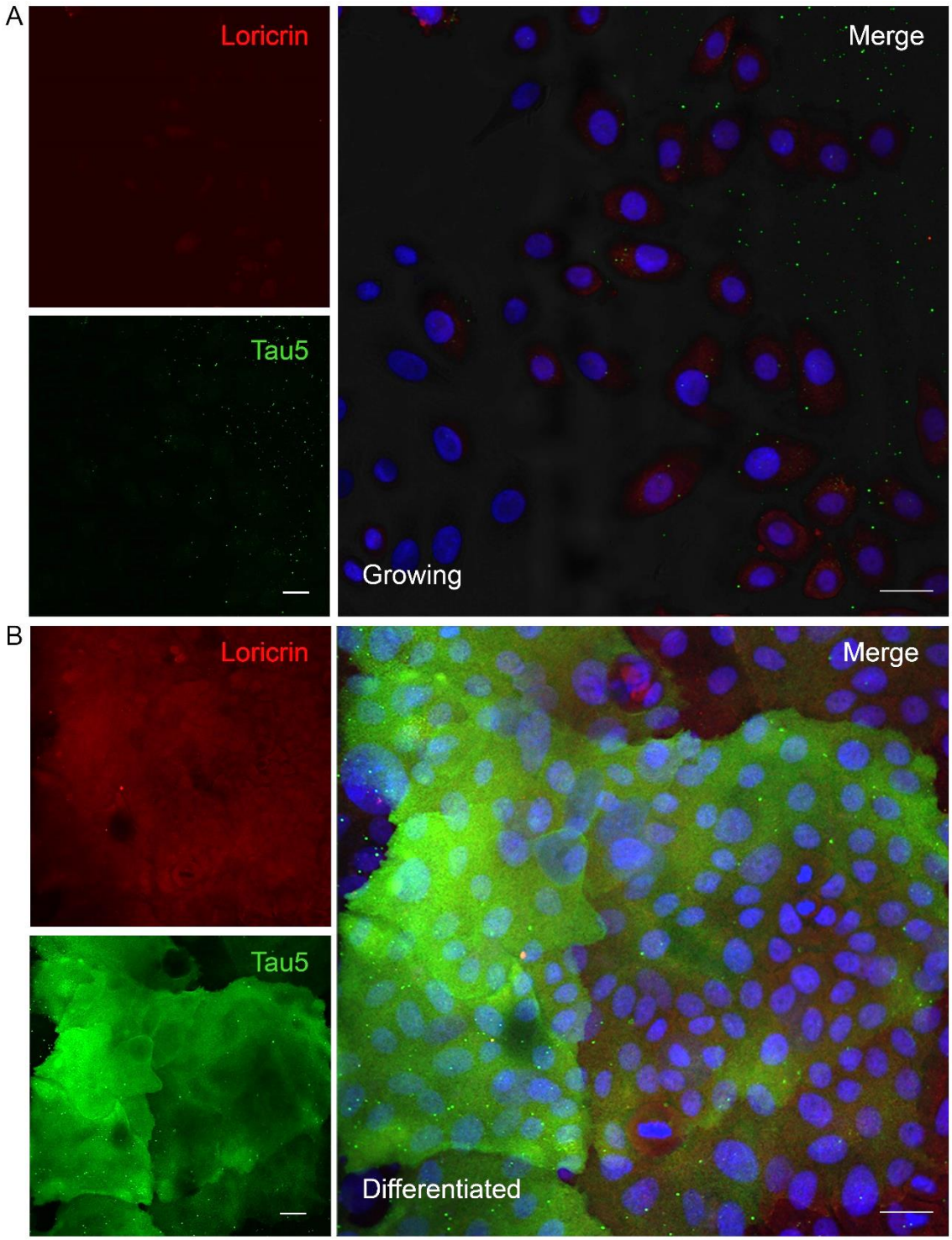

Figure 4.15. Tau5 is co-expressed with loricrin in differentiated epidermal keratinocytes.
To characterise the expression of tau5 in keratinocytes *in vitro,* HEKn cells were analysed using immunofluorescence with tau5 (green) expression alongside terminal differentiation marker loricrin (red). **A.** Immunofluorescence analysis of tau5 and loricrin expression in growing keratinocyte cells showed little or no expression of either protein. **B.** Immunofluorescence analysis of HEKn cells cultured in differentiation medium, containing high concentration of calcium showed that loricrin expression was induced following differentiation and tau5 positive cells could be detected. Nuclei counterstained with DAPI (blue) and all channels are merged in the right panel to allow accurate visualisation of cellular morphology. Scale bar 25 µm.

The subset of cellular proteins that are associated with plasma membranes is of high biological importance. The plasma membrane delineates the cell and provides a physical boundary between the cell and its environment. Plasma membrane proteins play important roles in cell–cell interactions, material transport, and signal transduction. The N-terminal and MTBD of tau have been shown to associate with the plasma membrane in different cell types. Following keratinocyte differentiation tight junctions and desmosomes are formed, therefore the association of tau with the membrane following keratinocyte differentiation is particularly interesting. Therefore, to further investigate the localisation and association of tau with membrane associated proteins, immunofluorescence analysis was carried out with tau and E-cadherin. Immunofluorescence revealed that the cortical localisation of tau does co-localise with E-cadherin at the plasma membrane following calcium induced cell differentiation (Figure 4.14). Further investigation is needed to determine the exact protein interactions that take place at the cell membrane in differentiated keratinocytes. Immunofluorescence analysis showed tau5 expression *in vivo* was restricted to the granular layer of the epidermis, alongside loricrin expression. Immunofluorescence analysis of keratinocyte cells *in vitro* using the tau5 antibody, also presented with positive tau5 staining exclusively in the differentiated population of epidermal keratinocytes alongside loricrin expression (Figure 4.15).

4.4.4. Knockdown of tau interrupts the programme of differentiation in keratinocytes.

4.4.4.1. siRNA-mediated tau knockdown

A widely used technique to manipulate gene expression is through the use of RNA interference (RNAi), silencing or downregulating gene expression through

the degradation of the associated mRNA. esiRNA was used to knockdown (KD) tau expression in keratinocyte cells, with esiRNA targeting *Renilla reformis* Luciferase (*RLUC*) as a negative control. Assessment of tau mRNA levels revealed that esiRNA-mediated downregulation leads to a 70% reduction tau mRNA expression after 48 h (Figure 4.16). Interestingly, *MAPT* KD induced a significant increase in the relative expression of genes associated with differentiation in keratinocytes (Figure 4.17A). Western Blot analysis of K1 expression showed that K1 was significantly upregulated following *MAPT* KD compared to control (Figure 4.17B and C). KD of *MAPT* induced a significant reduction in Ki67 expression and caused a reduction in the expression of cyclins and CDKs involved in S, G2 and M phases of the cell cycle (Figure 4.18).

The effects demonstrated so far are only from keratinocytes cultured under basal promoting, growing culture conditions, however earlier in this chapter, using immunofluorescence analysis, it was demonstrated that tau expression in basal populations was restricted to the nucleus, with little or no cytoplasmic expression observed. Conversely, it was shown that following calcium induced cell differentiation, expression of tau was found to be upregulated in the cytoplasmic and nuclear fragments of the cells. Therefore, to further investigate the role tau may play in keratinocyte differentiation, tau was knocked down in differentiated populations of keratinocytes. This determined whether the knockdown of tau had a different effect in differentiated keratinocytes and possibly on cellular differentiation. Keratinocytes were differentiated with calcium, as demonstrated earlier in 4.4.3, and treatment with esiRNA *MAPT* and *RLUC* was performed at the same time as extracellular calcium levels were increased. Thereby, enabling the identification of any changes to the differentiation process as a result of the KD of tau. RT q-PCR data revealed that tau was effectively knocked down in

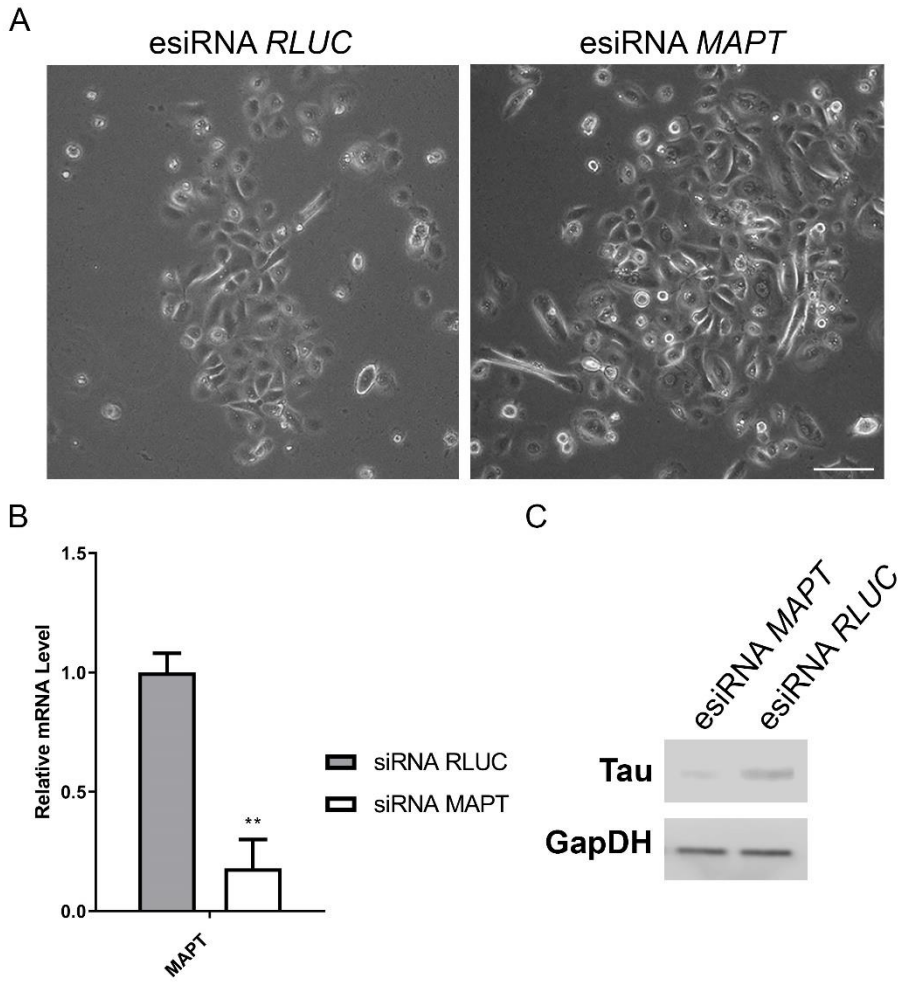

Figure 4.16. Tau is successfully knocked down in growing epidermal keratinocytes using esiRNA.
Knockdown of *MAPT* in human epidermal keratinocytes (HEKn) using transfection reagent INTERFERin®. RNA and total protein was collected 48 h after transfection. **A.** Representative cell culture images of siRNA *RLUC* and *MAPT* cells respectively. Scale bar 75 µm. **B.** Representative RT q-PCR analysis of *MAPT* knockdown after 48 h of treatment with esiRNA *MAPT* (n=3). Ct values normalised to 36B4 and $2^{-\Delta\Delta Ct}$ method of analysis used. Relative expression levels are displayed as mean ± SD. An unpaired *t*-test was used to test significance; ** $p<0.01$. **C.** Western Blot validation of tau protein 48 h after tau knockdown with esiRNA *MAPT*. Glyceraldehyde-3-Phosphate Dehydrogenase (GAPDH) was used as housekeeping gene.

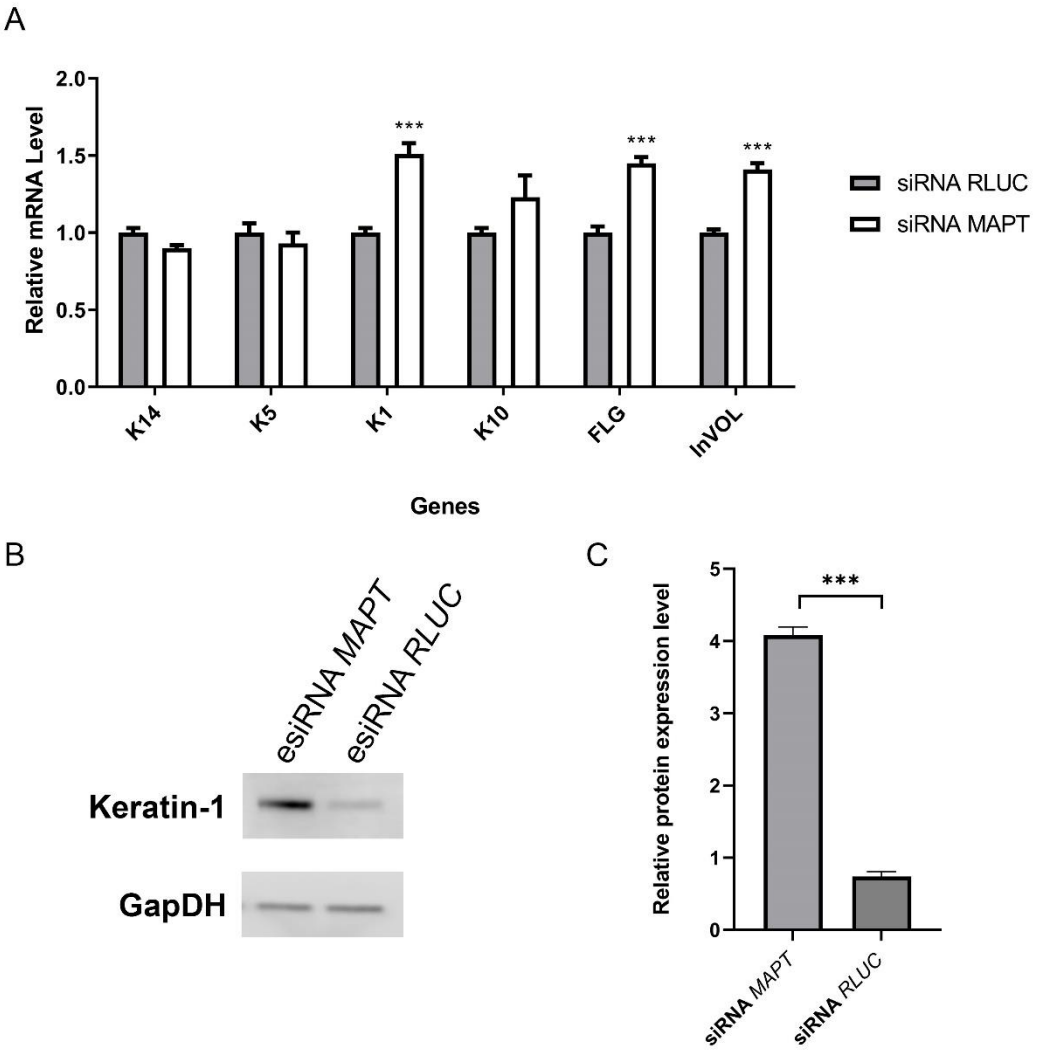

Figure 4.17. Characterisation of keratinocyte differentiation as a result of siRNA-mediated *MAPT* knockdown.

A. Representative RT q-PCR analysis of HEKn cells 48 h after treatment with esiRNA *MAPT* with esiRNA *RLUC* as a negative control (n=3). K14 – keratin 14; K5 – keratin 5; K1 – keratin 1; K10 – keratin 10; FLG – filaggrin; Invol – involucrin. Ct values normalised to 36B4 and $2^{-\Delta\Delta Ct}$ method of analysis used. Relative expression levels are displayed as mean ± SD. Two-Way ANOVA with Bonferroni correction was used to test significance; *** $p<0.001$. **B.** Western blot analysis of keratin-1 48 h after *MAPT* knockdown with esiRNA. Glyceraldehyde-3-Phosphate Dehydrogenase (GAPDH) was used as a housekeeping gene. **C.** Quantification of the relative expression of keratin-1 protein following tau knockdown. An unpaired *t*-test was used to test significance; *** $p<0.001$.

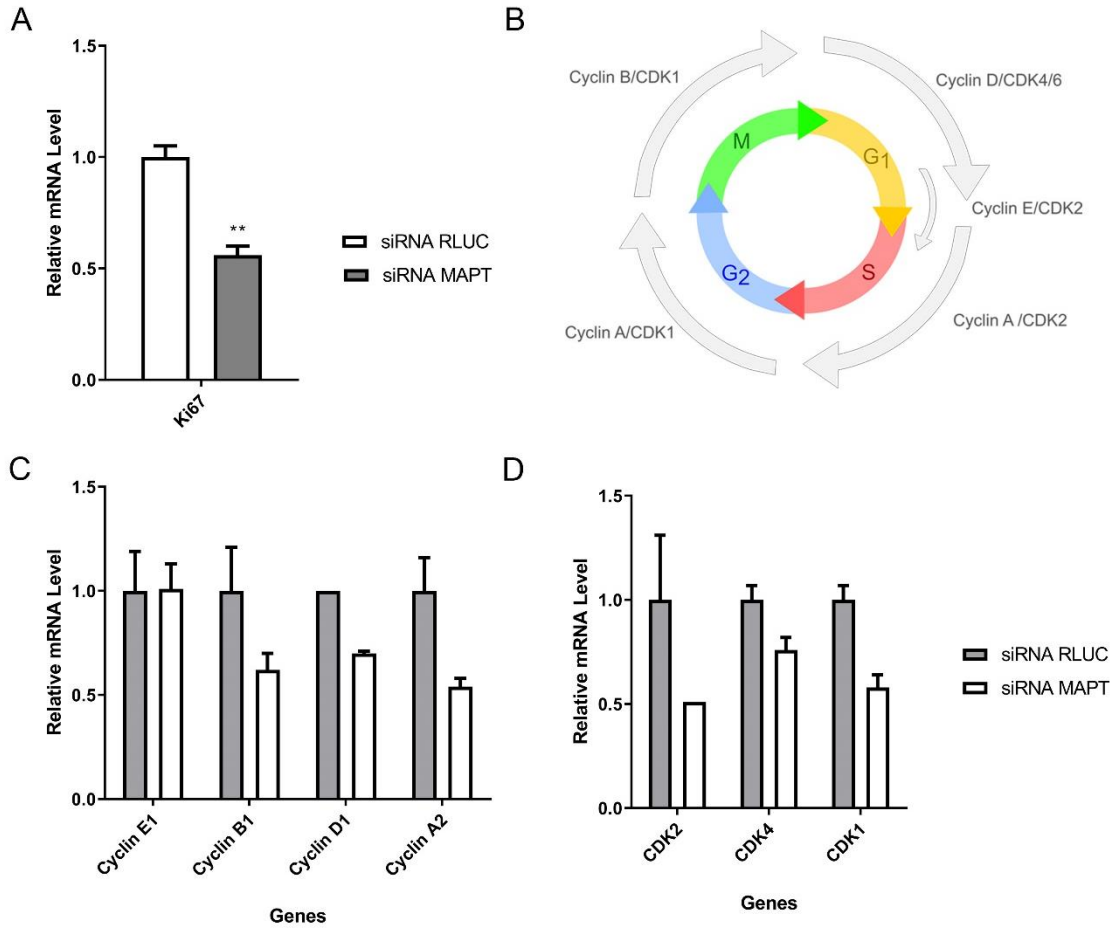

Figure 4.18. Cell cycle status of growing keratinocytes following siRNA-mediated knockdown of tau.
Representative RT q-PCR analysis of the relative expression of proliferation markers in HEKn cells after 48 h of treatment with esiRNA *MAPT*. esiRNA *RLUC* was used as a negative control (n=3). **A.** RT q-PCR analysis of proliferation marker, Ki67. Ki67 expression was significantly reduced in esiRNA *MAPT.* One Way ANOVA with Bonferroni correction was used to test significance. **B.** Schematic demonstrating the stages of the cell cycle with the associated expression of cyclins and CDKs at each phase. **C.** RT q-PCR analysis of CDK expression following knockdown of *MAPT.* **D.** RT q-PCR analysis of cyclin expression in keratinocytes following *MAPT* knockdown. Ct values normalised to 36B4 and $2^{-\Delta\Delta Ct}$ method of analysis used. Relative expression levels are displayed as mean ± SD. Two-way ANOVA with Bonferroni correction was used to test significance; ** $p<0.01$.

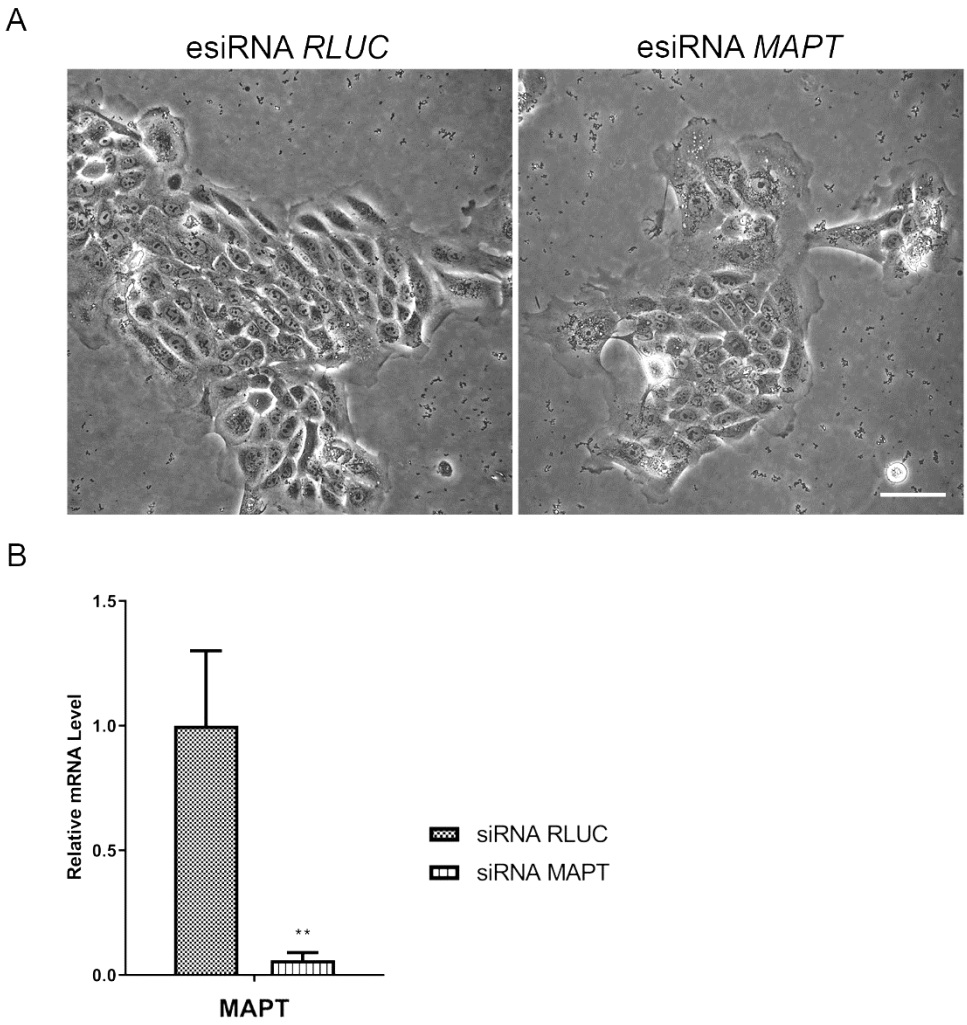

Figure 4.19. siRNA-mediated knockdown of *MAPT* in differentiating epidermal keratinocytes.
To test the effect of tau knockdown in differentiating populations of epidermal keratinocytes, cells were treated with esiRNA *MAPT* at the same time as the extracellular calcium levels were increased from 60 µM to 1.7 mM (n=2). **A.** Representative cell culture images of epidermal keratinocytes cultured under differentiation culture conditions with treatment with esiRNA *RLUC* and with esiRNA *MAPT*. Scale bar 75 µm. **B.** 72 h after treatment with calcium and esiRNA. RT q-PCR analysis showed the successful knockdown of tau with esiRNA *MAPT,* compared to esiRNA *RLUC.* Ct values were normalised to 36B4 and $2^{-\Delta\Delta Ct}$ method of analysis used. Relative expression levels are displayed as mean ± SD. An unpaired *t*-test was used to test significance; ** $p<0.01$.

esiRNA *MAPT* treated cells compared to all controls (Figure 4.19). Changes to keratinocyte morphology were visible following tau KD (Figure 4.19A). In control conditions, the formation of a tightly packed adhesive network of cells could be observed and cells maintained an organised morphology (Figure 4.19A). However, after treatment with siRNA *MAPT* significant changes to the cells morphology could be observed; cells presented with an enlarged size, speckled and granular cytoplasm, and abnormal nucleus, significantly more extensive than those created by the addition of transfection reagent (Figure 4.19A).

As expected, all keratinocytes treated with calcium displayed a significant increase in differentiation associated gene expression, compared to keratinocytes cultured in basal promoting culture medium (data not shown). However, tau KD caused a significant decrease in the expression of differentiation gene expression compared to siRNA *RLUC* (Figure 4.20). This suggested that tau KD in keratinocyte differentiation might disturb the differentiation process. RT q-PCR revealed that Ki67 decreased following esiRNA *MAPT* treatment compared to the control (Figure 4.21A). This was consistent with decreased Ki67 expression, and the relative expression of all cyclins and CDKs were decreased after tau knockdown (Figure 4.21C and D).

4.4.4.2. shRNA-mediated tau knockdown

Using two tau shRNA plasmids, stable tau KD keratinocyte cell lines were generated with shRNA luciferase as a control (Figure 4.22 and Figure 4.23). The efficiency of the tau knockdown varied across the two cell lines, with 1881 displaying a 40-50% KD while 2112 cells had 79-80% tau KD (Figure 4.22, Figure 4.23 and Figure 4.24). This difference in efficiency of the tau KD was evident in the phenotypic presentation of the two cell lines; 2112 cells presented with a

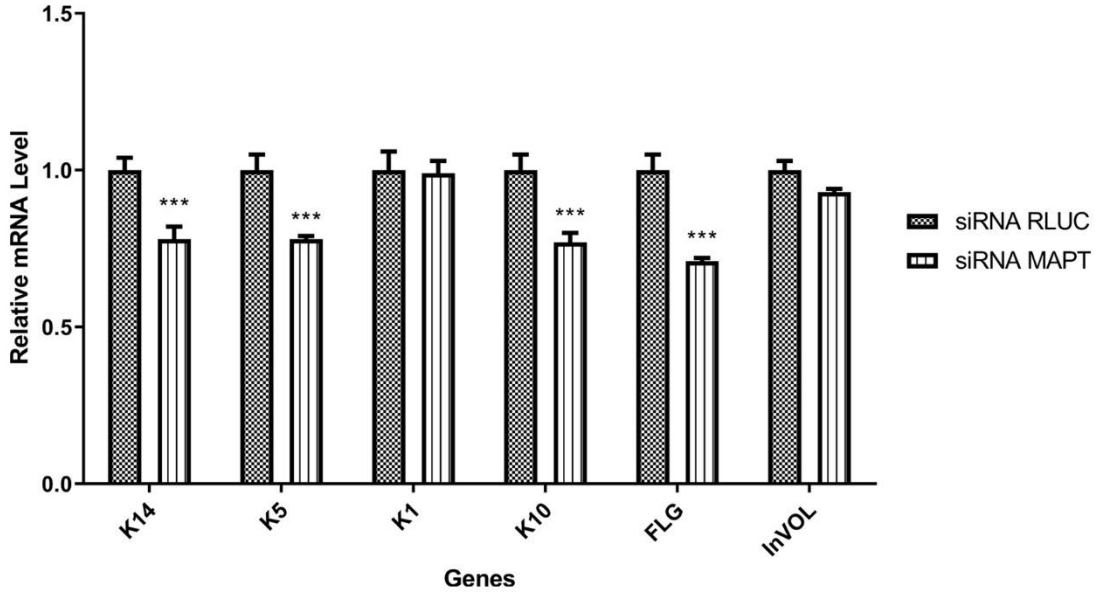

Figure 4.20. Keratinocyte differentiation is reduced following siRNA-mediated *MAPT* knockdown.
To investigate whether the knockdown of tau had an effect on the progression of keratinocyte differentiation, HEKn cells were treated with esiRNA *MAPT* at the same time that extracellular calcium was increased to 1.7 mM; esiRNA *RLUC* was used as a negative control (n=2). **A.** Representative RT q-PCR analysis of genes associated with differentiation in keratinocytes 48 h after treatment with esiRNA *MAPT.* K14 – keratin 14; K5 – keratin 5; K1 – keratin 1; K10 – keratin 10; FLG – filaggrin; INVOL – involucrin. Ct values were normalised to 36B4 and $2^{-\Delta\Delta Ct}$ method of analysis used. Relative expression levels are displayed as mean ± SD. Two-way ANOVA with Bonferroni correction was used to test significance; *** $p<0.001$.

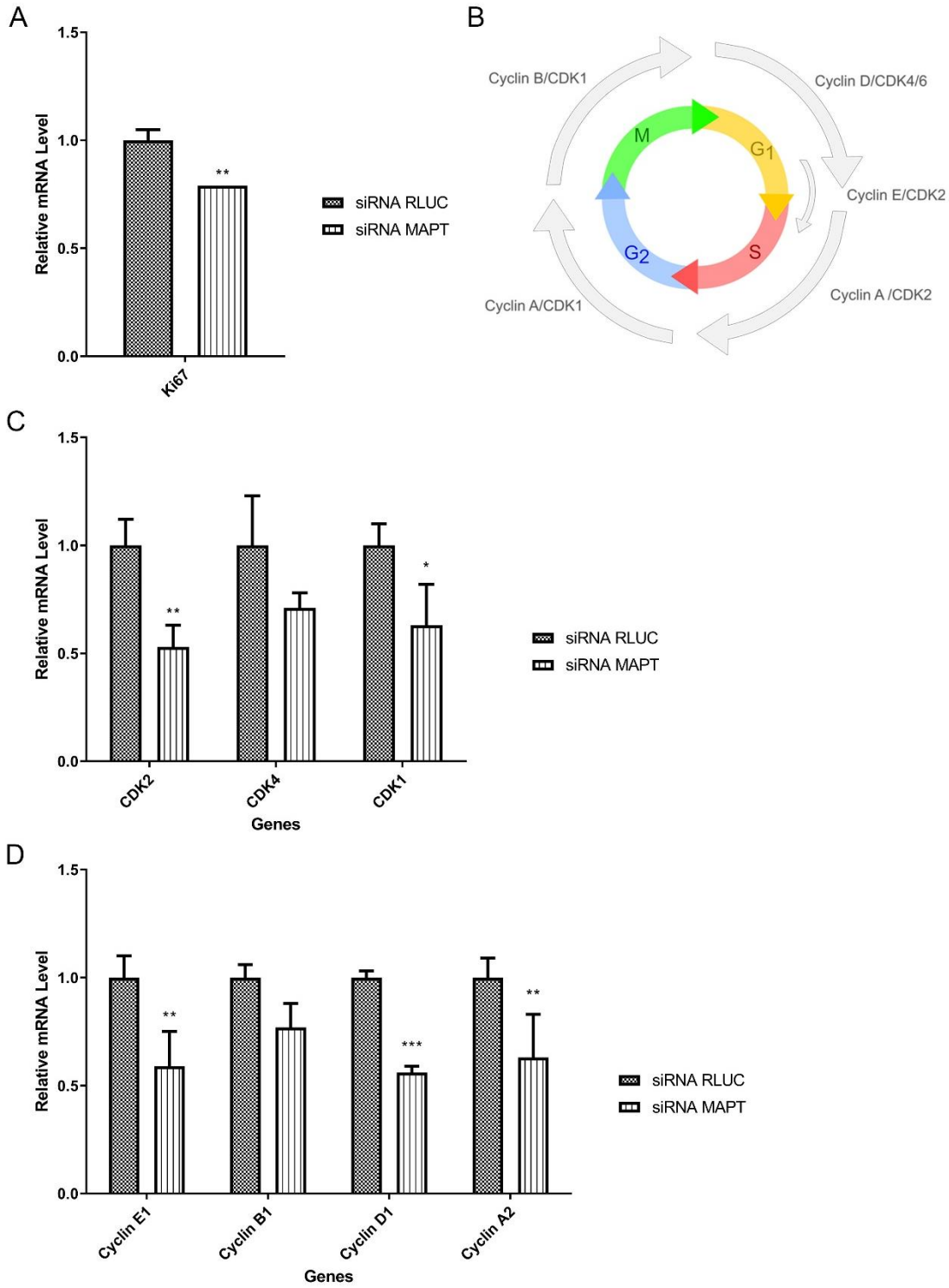

Figure 4.21. Cell cycle status following the siRNA-mediated knockdown of tau in differentiating keratinocytes.

A. Representative RT q-PCR analysis of the relative gene expression of ki67 and p63 in differentiated keratinocytes following tau knockdown. **B.** Schematic demonstrating the stages of the cell cycle with the associated expression of cyclins and CDKs. **C.** Representative RT q-PCR analysis of the relative gene expression of CDKs following tau knockdown in differentiated keratinocytes. **D.** Representative RT q-PCR analysis of the relative gene expression of cyclins following tau knockdown in differentiated keratinocytes. Ct values normalised to 36B4 and $2^{-\Delta\Delta Ct}$ method of analysis used. Relative expression levels are displayed as mean ± SD (n=2). Two-way ANOVA with Bonferroni correction was used to test significance; * $p<0.05$, **$p<0.01$, *** $p<0.001$.

much larger cell size compared to the control and 1881 cells (Figure 4.22B). Additionally, differentiating 2112 cells displayed a disorganised phenotype that were unable to correctly form cell-cell adhesions that are characteristic of differentiating keratinocytes (Figure 4.23B).

RT q-PCR analysis of the differentiation status of keratinocytes following tau KD in growing keratinocytes revealed a significant increase in the relative expression of keratin 10 in shRNA tau 1881 and 2112 cells compared to their control (Figure 4.25A); immunofluorescence analysis revealed an increase in the expression of keratin1 following tau KD in keratinocytes (Figure 10.13). Interestingly, despite the increase in the expression of proteins associated with the early stages of keratinocyte differentiation, no increase in the expression of terminal differentiation proteins was identified (Figure 4.25A). RT q-PCR analysis of differentiating keratinocytes showed that, consistent with the observations with siRNA, shRNA tau KD significantly inhibited differentiation of keratinocyte cells in both cell lines (Figure 4.25B and Figure 10.13). Correlating with the efficiency of the tau KD in the two cell lines, shRNA tau 2112 cells displayed a greater decrease in the expression of genes associated with keratinocyte differentiation compared to 1881 cells (Figure 4.25B and Figure 10.13).

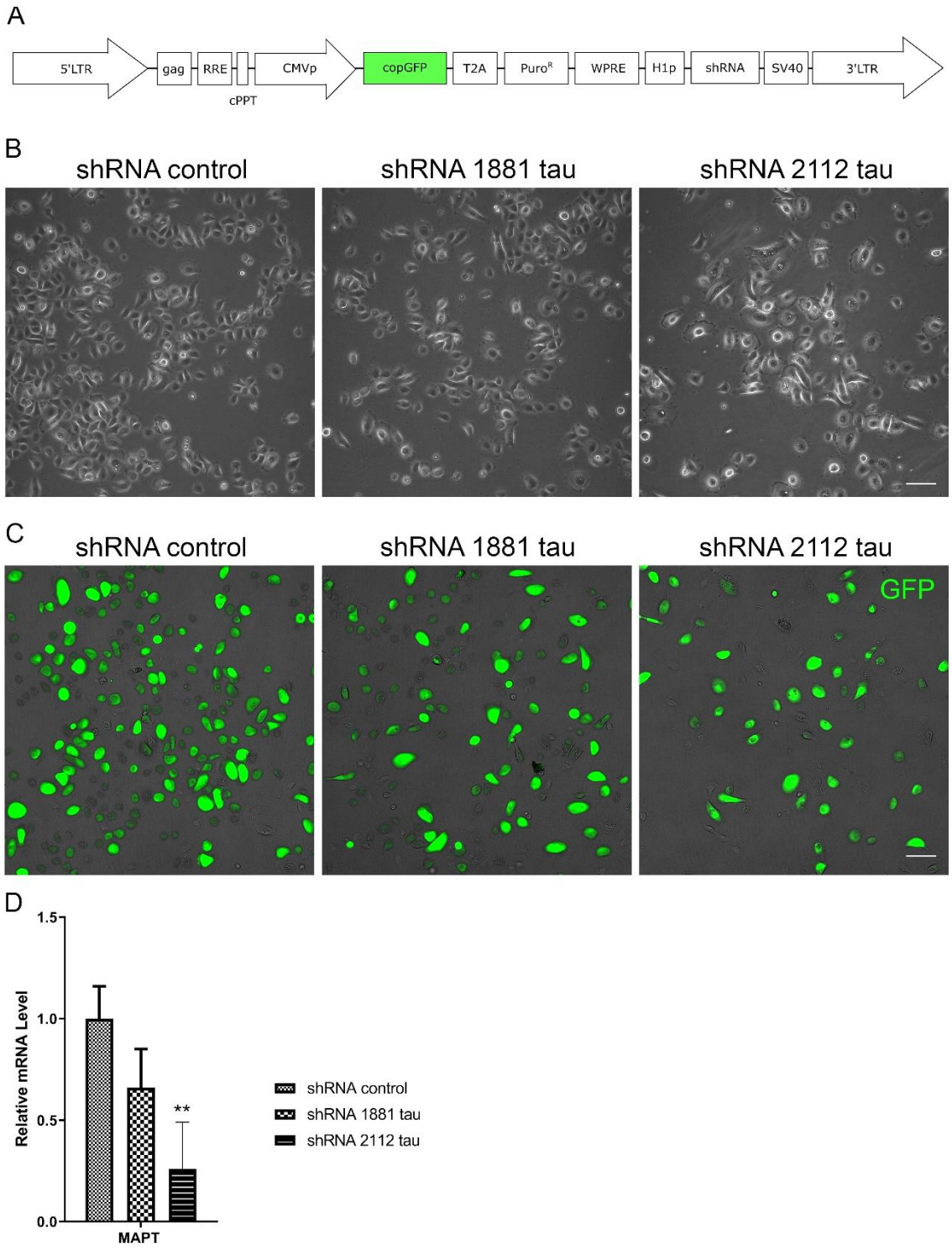

Figure 4.22. shRNA-mediated knockdown of tau in growing keratinocytes. **A.** Schematic representation of the plasmid backbone that was used in this study to generate stable shRNA tau cell lines. **B.** Representative cell culture images of shRNA control, shRNA 1881 and 2112 tau generated stable cell lines (n=3). Scale bar 100 µm. **C.** Representative GFP expression carried within the plasmid to show successful infection and selection in HPEKp cells. Scale bar 100 µm. **D.** Representative RT q-PCR analysis of tau KD in shRNA 1881 and 2112 tau cells compared to the shRNA control. Ct values normalised to 36B4 and $2^{-\Delta\Delta Ct}$ method of analysis used. Relative expression levels are displayed as mean ± SD. One-way ANOVA with Bonferroni correction was used to test significance; * p<0.05, **<0.01, *** p<0.001.

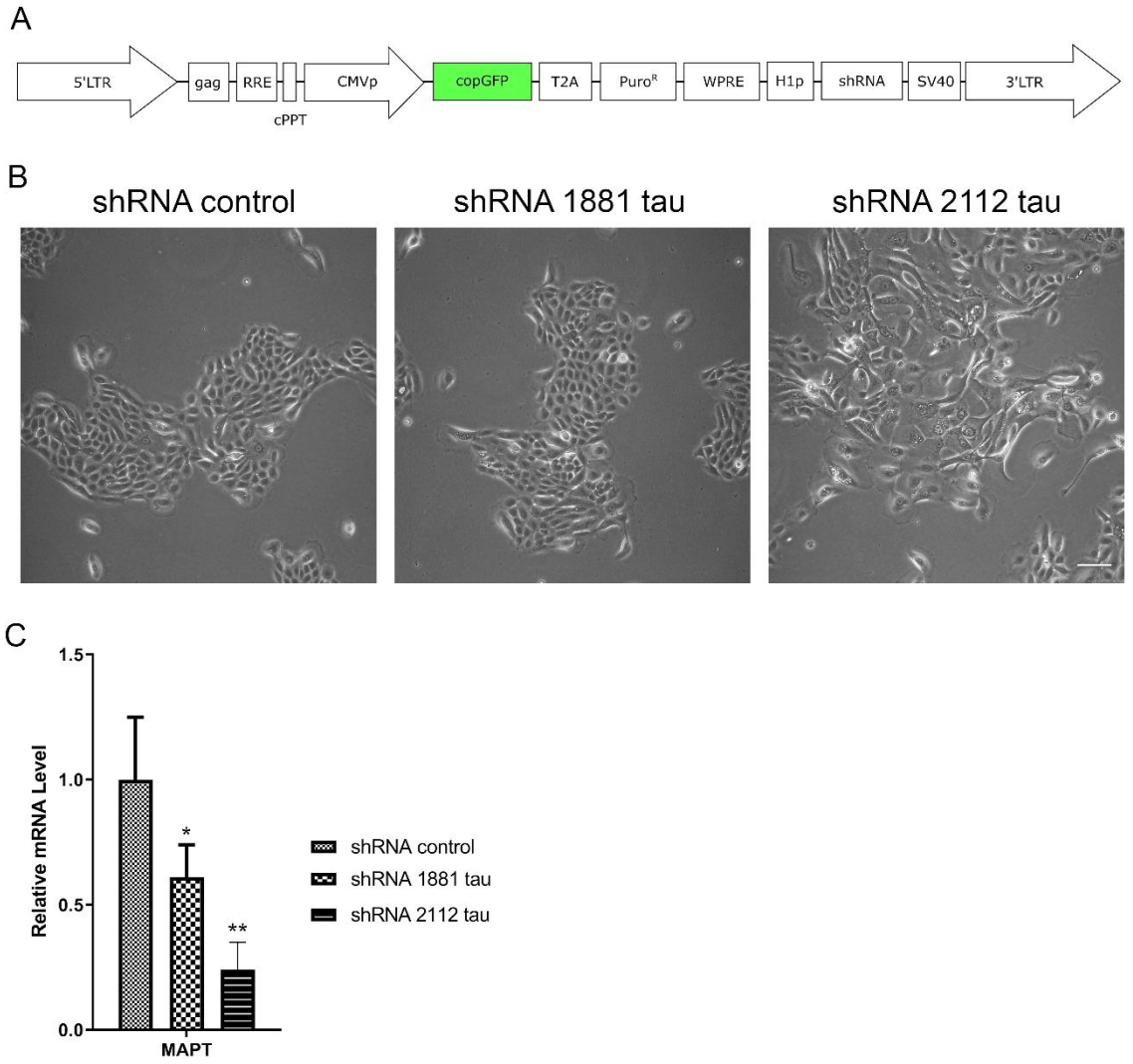

Figure 4.23. shRNA-mediated knockdown of tau in differentiating keratinocytes.

A. Schematic representation of the plasmid backbone that was used in this study to generate stable shRNA tau cell lines. **B.** Representative cell culture images of shRNA control, shRNA 1881 and 2112 tau stable cell lines following 48 h of high concentration calcium treatment (1.7 mM [Ca^{2+}]) to induce cell differentiation (n=3). Scale bar 100 µm. **C.** Representative RT q-PCR analysis of tau KD in shRNA 1881 and 2112 tau compared to the shRNA control cells under differentiation promoting culture conditions. Ct values normalised to 36B4 and $2^{-\Delta\Delta Ct}$ method of analysis used. Relative expression levels are displayed as mean ± SD. One-way ANOVA with Bonferroni correction was used to test significance; * p<0.05, **<0.01, *** p<0.001.

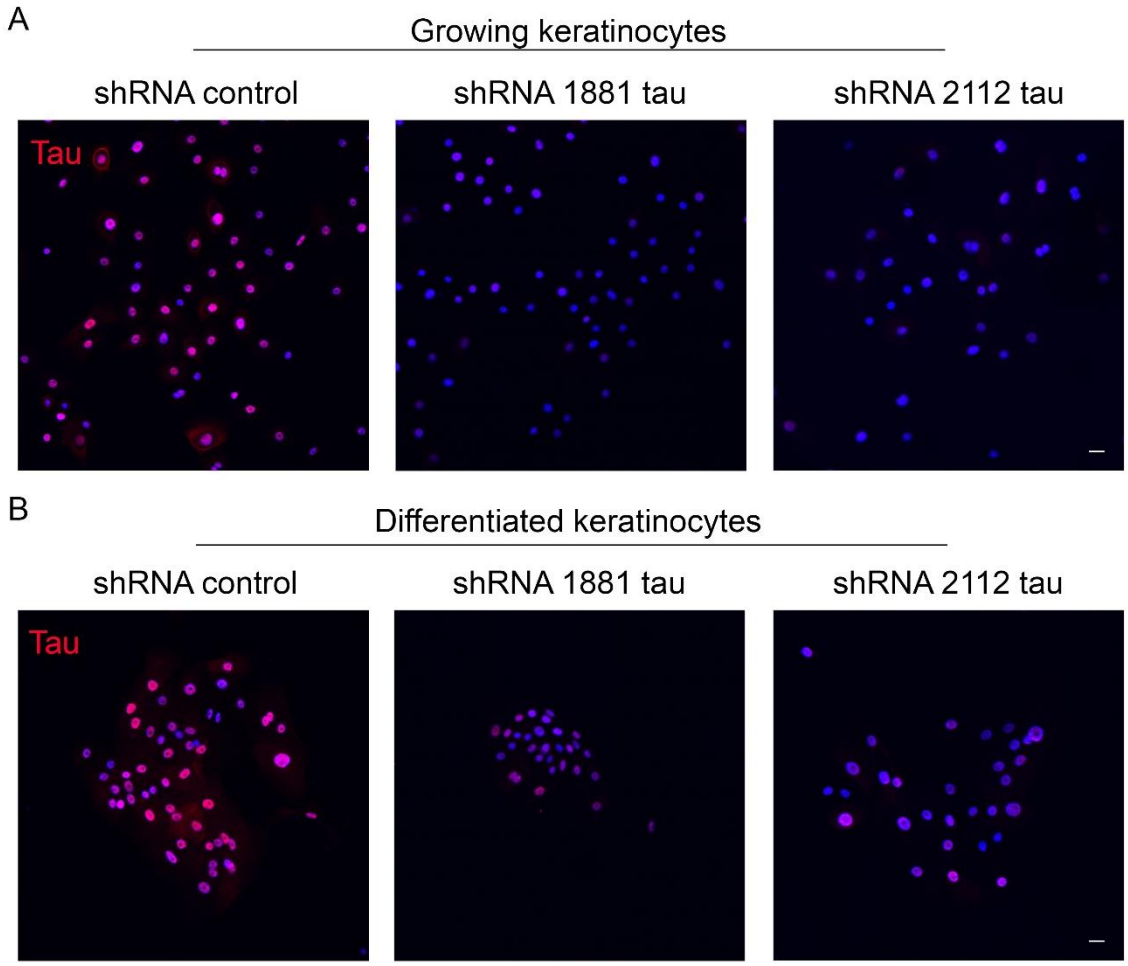

Figure 4.24. Tau knockdown in growing and differentiating epidermal keratinocytes.
Representative immunofluorescence analysis of tau expression (red) in tau knockdown stable cell lines. Keratinocytes were infected with lentiviral particles containing shRNA tau 1881 and 2112 plasmids. Control plasmids with shRNA luciferase were used as a negative control. **A.** Keratinocytes cultured under growing culture conditions. **B.** Keratinocytes gown in high calcium cell culture medium (1.7 mM [Ca^{2+}]) for 48 h to induce keratinocyte differentiation. Nuclei counterstained with DAPI (blue). Scale bar 25 µm.

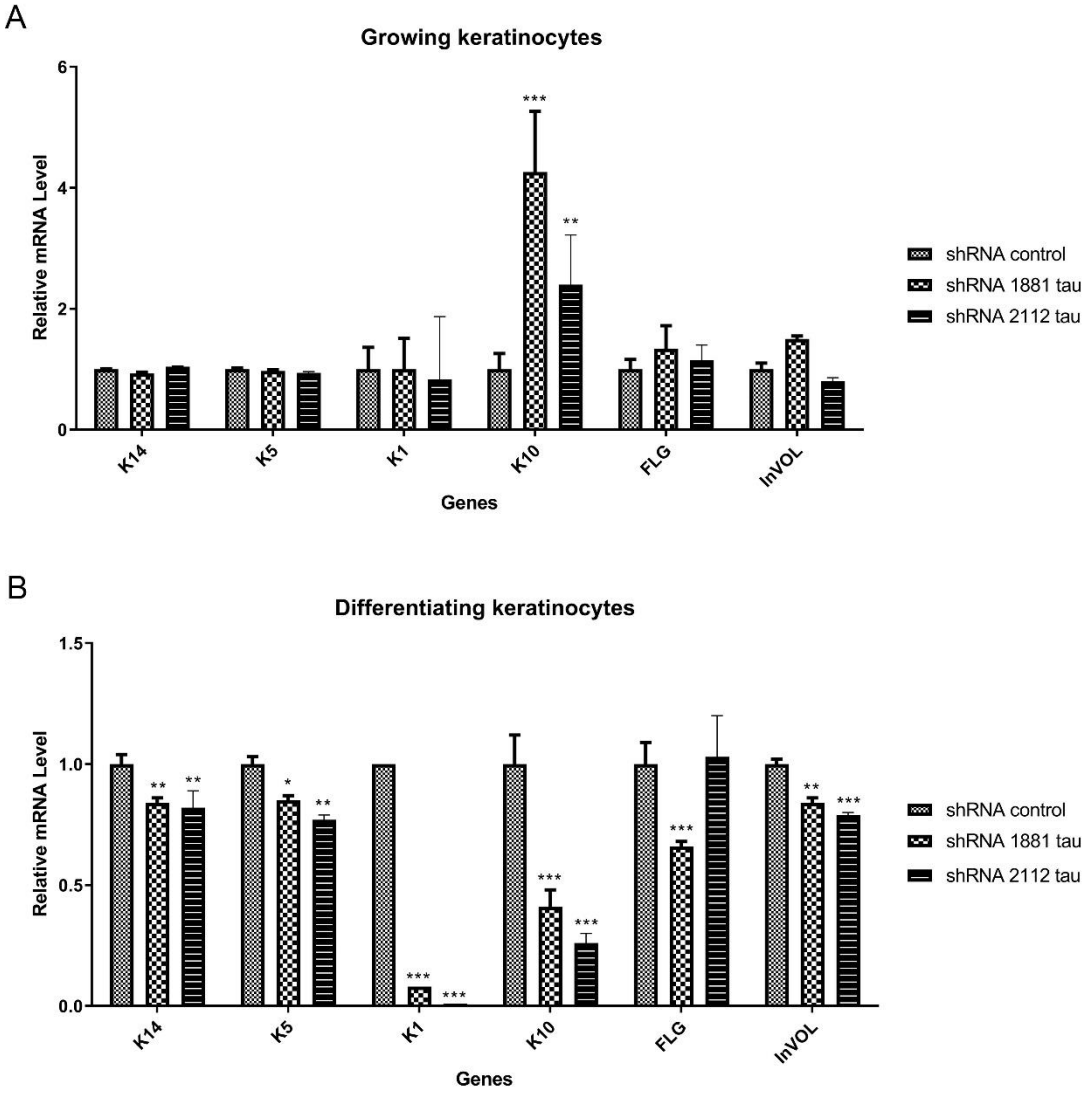

Figure 4.25. RT q-PCR analysis of the differentiation status of keratinocytes following shRNA-mediated knockdown in growing and differentiated keratinocytes.

A. Representative RT q-PCR analysis of genes associated with a growing or differentiated phenotype in growing keratinocytes following shRNA mediated stable knockdown of tau. **B.** Representative RT q-PCR analysis of genes associated with a growing or differentiated phenotype in keratinocytes cultured in culture conditions promoting cell differentiation (1.7 mM [Ca^{2+}]) following shRNA mediated stable knockdown of tau. RT q-PCR performed in triplicate, Ct values normalised to 36B4 and $2^{-\Delta\Delta Ct}$ method of analysis used. Relative expression levels are displayed as mean ± SD. Two-way ANOVA with Bonferroni correction was used to test significance; * $p<0.05$, **<0.01, *** $p<0.001$.

In growing keratinocytes, K14 filaments were organised in loose bundles throughout the cytoplasm that run alongside the nucleus (Figure 4.26A). However, following tau KD K14 filaments became less organised, less evenly distributed throughout the cytoplasm and appeared fragmented (Figure 4.26B and C). Following keratinocyte differentiation, as expected, in control cells K14 expression was reduced (Figure 4.26D), however when tau was KD in differentiating keratinocytes K14 reduction did not occur, but instead appeared as thick, disorganised bundles throughout the cytoplasm (Figure 4.26E and F).

Immunofluorescence analysis of the microtubule network also revealed some changes following shRNA tau KD (Figure 4.27). In growing conditions, control cells displayed a well distributed tubulin network surrounding the nucleus, with a slight polarisation to one side of the cell (Figure 4.27A). However, shRNA tau 1881 and 2112 shRNA tau keratinocytes the normal distribution of tubulin was disturbed; shRNA tau 1881 cells had a smaller morphology with a fragmented tubulin network that lost some of the networks polarity (Figure 4.27B). shRNA tau 2112 keratinocytes were significantly larger with a loss of tubulin polarity and their microtubule network did not show an even distribution throughout the cell and appeared to have lost their MTOC (Figure 4.27C). Under differentiated conditions tubulin correctly reorganised to the cortex in shRNA control keratinocytes (Figure 4.27D). However, tau KD caused disturbance to the tubulin network and 1881 cells show a slight cortex rearrangement of the tubulin network (Figure 4.27E). Whereas shRNA tau 2112 displayed long filamentous network of microtubules with little to no cortex rearrangement (Figure 4.27F). Tubulin staining also highlighted the lack of cell-cell adhesion in shRNA tau 2112 cells, compared to shRNA control and shRNA tau 1881 cells (Figure 4.27F). Analysis of the actin

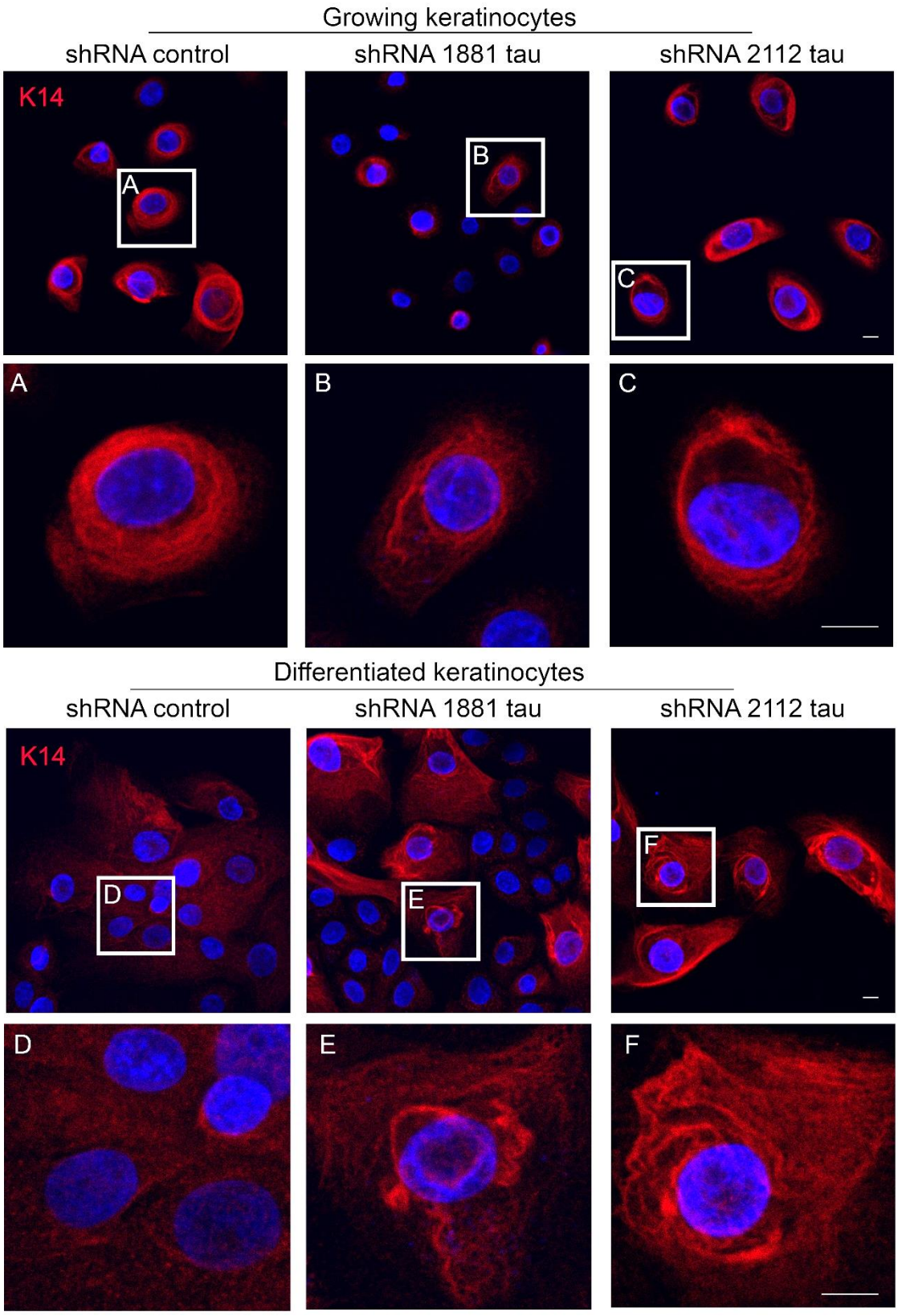

Figure 4.26. Disturbance of the keratin-14 intermediate filament network following tau knockdown in keratinocytes.
Representative immunofluorescence analysis of K14 (red) expression following shRNA-mediated tau knockdown. **A-C.** Growing epidermal keratinocyte cells. **D-F.** Keratinocytes gown in high calcium cell culture medium (1.7 mM [Ca^{2+}]) for 48 h to induce keratinocyte differentiation. Nuclei counterstained with DAPI (blue). Scale bar 10 µm.

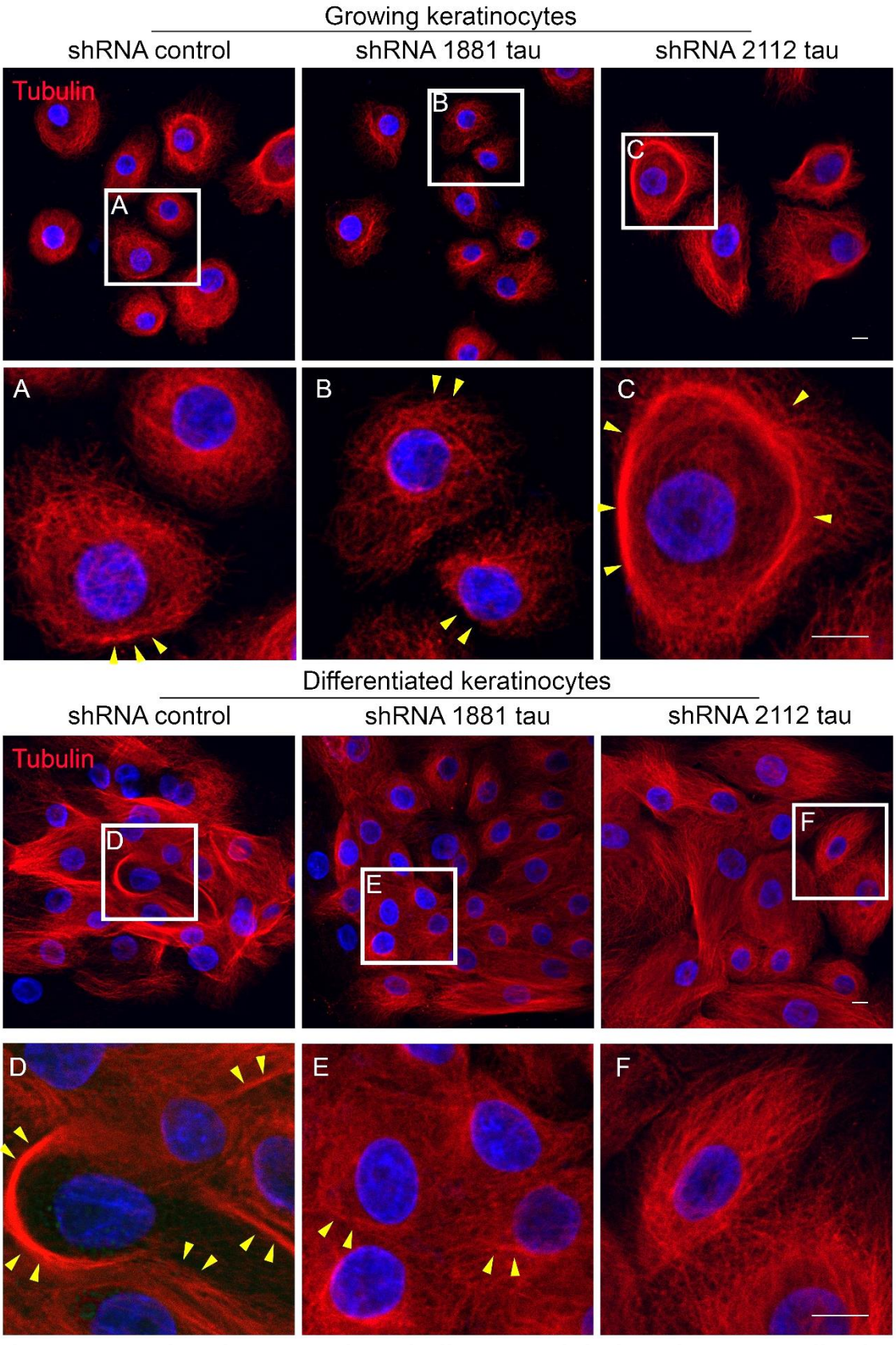

Figure 4.27. Disturbance to the tubulin network in keratinocytes following tau knockdown.

Representative immunofluorescence analysis of tubulin (red) following tau knockdown in keratinocytes. **A-C.** Keratinocytes cultured under growing cell culture conditions. **D-F.** Keratinocytes gown in high calcium cell culture medium (1.7 mM [Ca^{2+}]) for 48 h to induce keratinocyte differentiation. Yellow arrows

indicate the polarisation of the tubulin network in growing keratinocytes and the cortex rearrangement of microtubules in differentiating keratinocytes. Nuclei counterstained with DAPI (blue). Scale bar 10 µm.

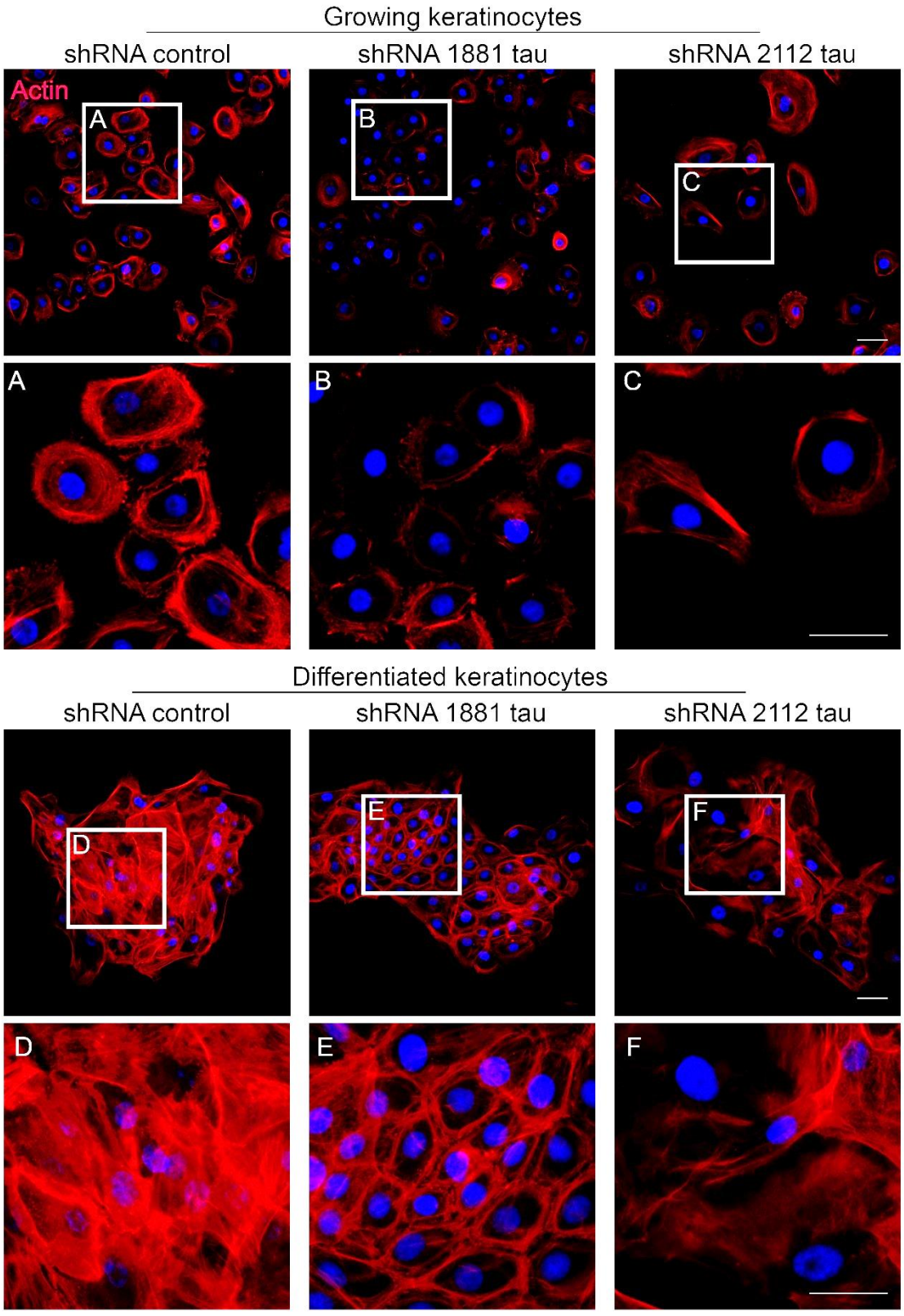

Figure 4.28. Actin expression is reduced following shRNA-mediated tau knockdown.

Representative immunofluorescence analysis of tubulin (red) following tau knockdown in keratinocytes. **A-C.** Keratinocytes cultured under growing cell culture conditions. **D-F.** Keratinocytes gown in high calcium cell culture medium (1.7 mM [Ca^{2+}]) for 48 h to induce keratinocyte differentiation. Nuclei counterstained with DAPI (blue). Scale bar 50 µm.

filament network revealed that overall actin was reduced in both growing and differentiated keratinocyte populations following tau KD (Figure 4.28).

4.4.5. Overexpression of tau in keratinocytes promotes keratinocyte differentiation.

Keratinocytes were infected with lentiviral particles containing pINDUCER20 tau plasmid to generate a doxycycline inducible tau overexpression stable cell line (Figure 4.29). To confirm the lentiviral infection, selection and subsequent overexpression of 2N4R (441 aa) tau following doxycycline treatment in keratinocytes, RNA and protein was extracted from keratinocytes for analysis. RT q-PCR analysis confirmed that after 48 h tau was significantly overexpressed in doxycycline treated pINDUCER20 tau infected keratinocytes (Figure 4.30A and Figure 10.15). Using tau isoform specific primer pairs, q-PCR analysis also confirmed that doxycycline treatment induced the overexpression of 2N 4R transcript variants of tau (Figure 4.30B and Figure 10.15). Western blot analysis of total protein demonstrated a strong clear band in the infected cells treated with doxycycline at 67 kDa (Figure 4.31A). Furthermore, immunofluorescence analysis showed that upon treatment with doxycycline, tau was clearly overexpressed in keratinocyte cells, displaying a cytoplasmic expression only usually detected in differentiated keratinocyte populations (Figure 4.31B). Interestingly, tau was also observed in the nucleolus following overexpression, which is not observed in control keratinocyte cells (Figure 4.31B).

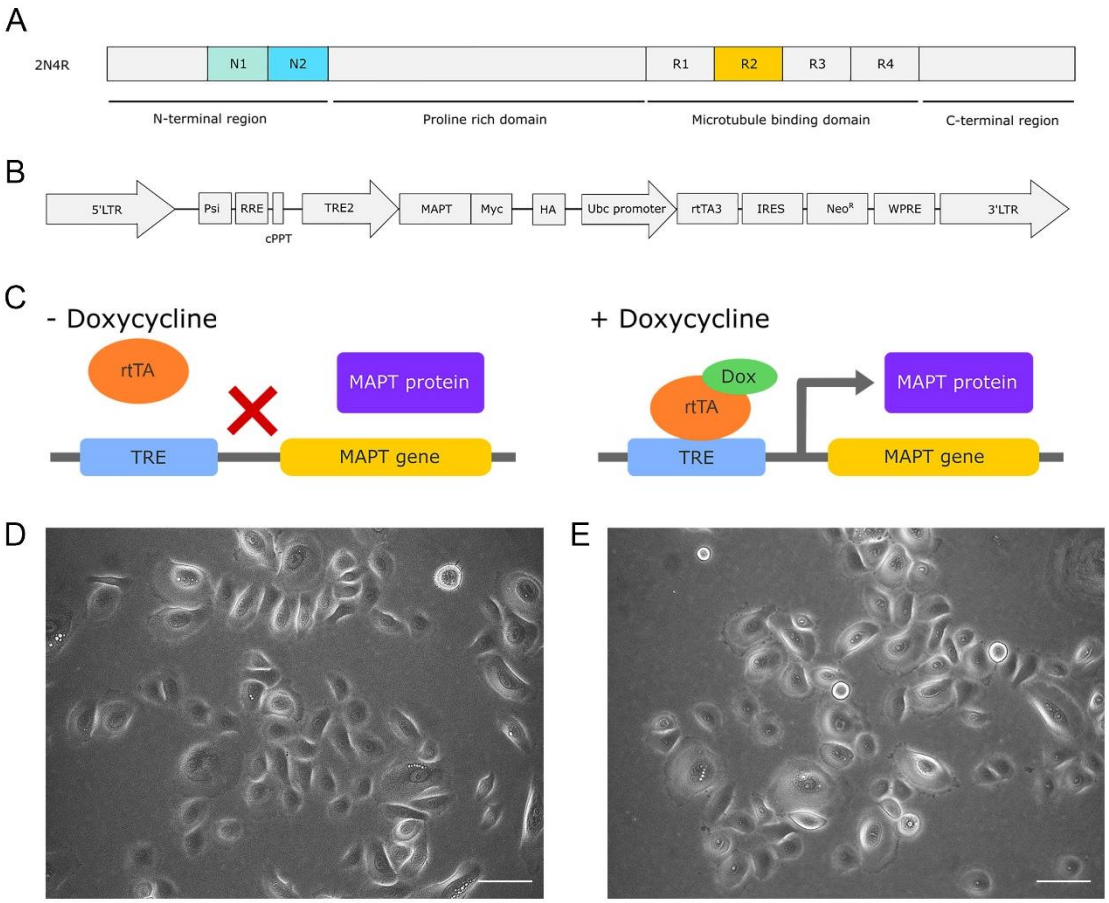

Figure 4.29. Tetracycline inducible overexpression of 2N4R (441 aa) tau in epidermal keratinocytes.
A. 2N4R (441 tau) transcript variant of tau. **B.** pINDUCER20 tau plasmid construct used to create lentiviral particles for infection of epidermal keratinocytes. rtTA3 and neomycin (G418)-resistance genes under the UBC promoter as well as a cDNA of interest under the control of a tetracycline-responsive promoter. **C.** Schematic displaying how the tetracycline inducible tau overexpression system works, and how gene expression is regulated by the presence and absence of tetracycline. When no doxycycline is present, the rtTA transcription factor cannot bind to the promoter and gene expression is not induced. When doxycycline is present, doxycycline binds to the rtTA transcription factor and allows it to bind to the DNA at the *Tet*-op promoter, subsequently driving gene expression of 441aa tau. rtTA – reverse tetracycline transactivator. TRE – tetracycline-responsive promoter element. tetO – Tet operator. **D.** HEKn cells infected with pINDUCER20 tau without doxycycline in the culture medium. Cells were kept under antibiotic selection using 800 µg/ml G418. **E.** HEKn cells infected with pINDUCER20 tau treated with 10 µg/ml doxycycline. Cells kept under antibiotic selection using 800 µg/ml G418. Scale bar 75 µm.

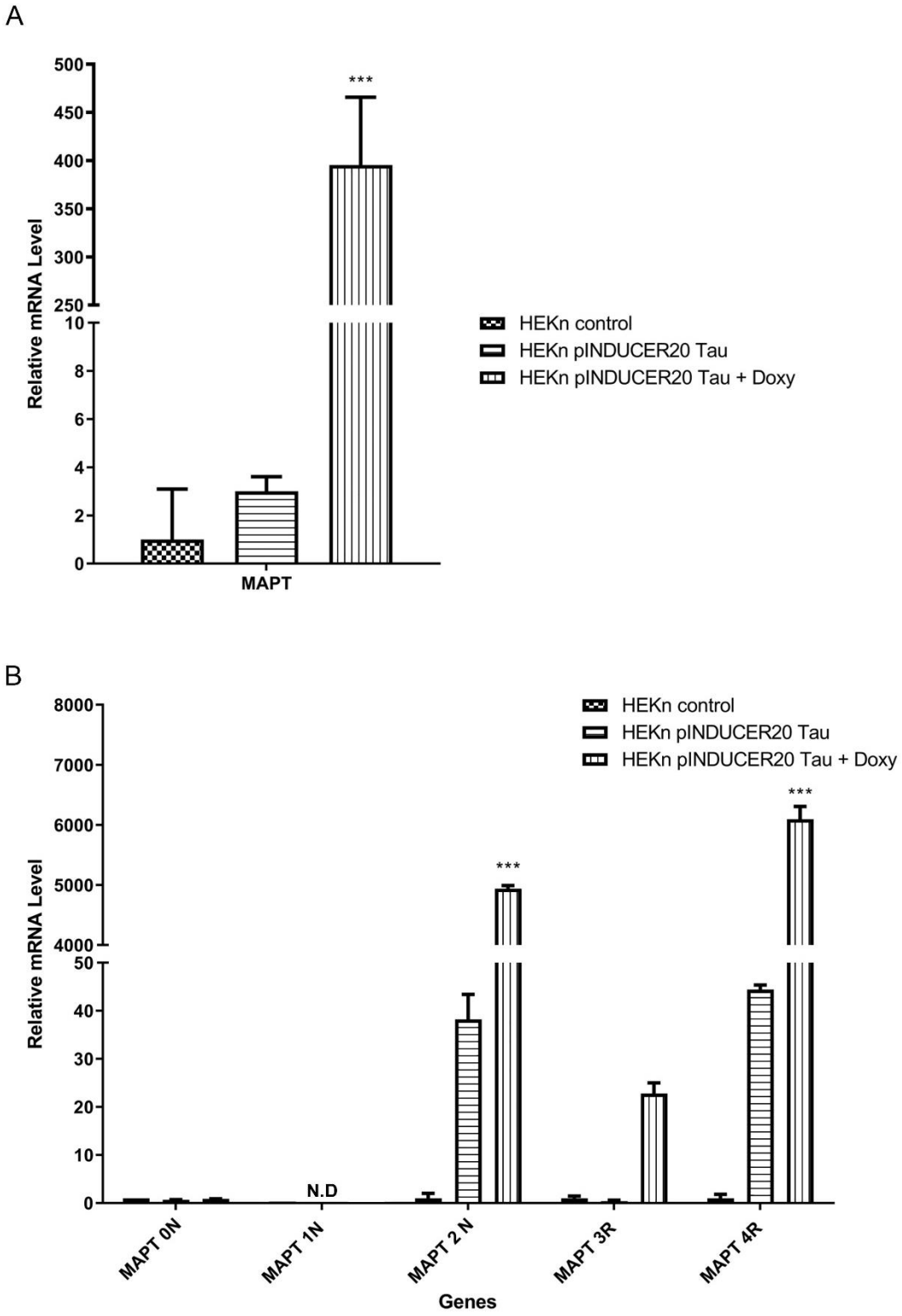

Figure 4.30. Tau is significantly overexpressed in pINDUCER20 tau keratinocytes when induced with doxycycline.

A. RT q-PCR analysis of relative total tau RNA expression in pINDUCER20 tau HEKn cells with and without doxycycline (doxy) compared to HEKn control. **B.** The relative expression of tau isoforms in pINDUCER20 tau with and without doxycycline compared to HEKn control cells. Ct values normalised to 36B4 and $2^{-\Delta\Delta Ct}$ method of analysis used. Relative expression levels are displayed as mean ± SD. Two-way ANOVA with Bonferroni correction was used to test significance; * p<0.05, **<0.01, *** p<0.001.

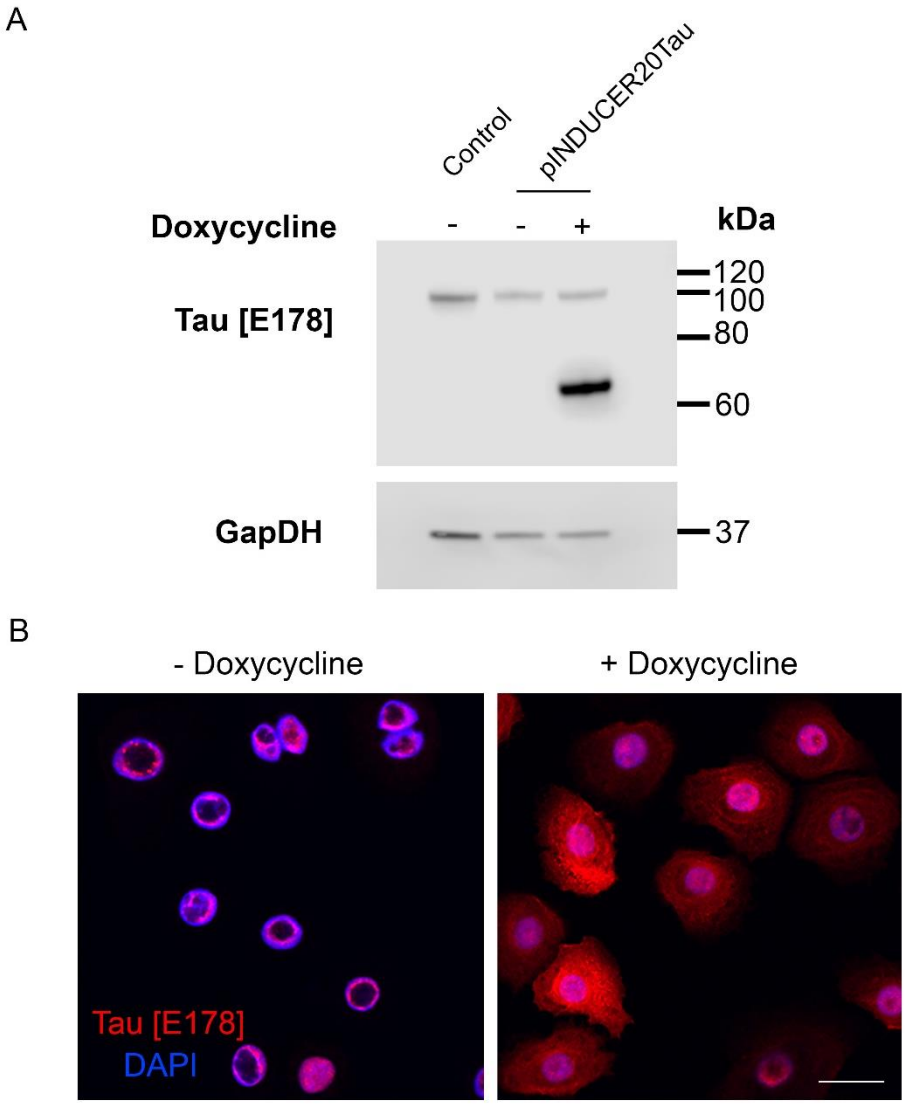

Figure 4.31. Tetracycline inducible overexpression of 2N4R tau in epidermal keratinocytes.
2N4R (441 aa) tau is overexpressed in growing pINDUCER20 tau HEKn cells after 48 h treatment with doxycycline. **A.** Total protein from pINDUCER20 tau HEKn P6 cells with and without the addition of doxycycline. Normal HEKn P6 as a control. Strong band at 67 kDa can be observed in the doxycycline treated HEKn cells. Glyceraldehyde-3-Phosphate Dehydrogenase (GAPDH) was used as housekeeping gene. **B.** Immunofluorescence analysis of tau [E178] (red) in pINDUCER20 tau HEKn cells with and without doxycycline. Nuclei were counterstained with DAPI (blue). Scale bar 25 µm.

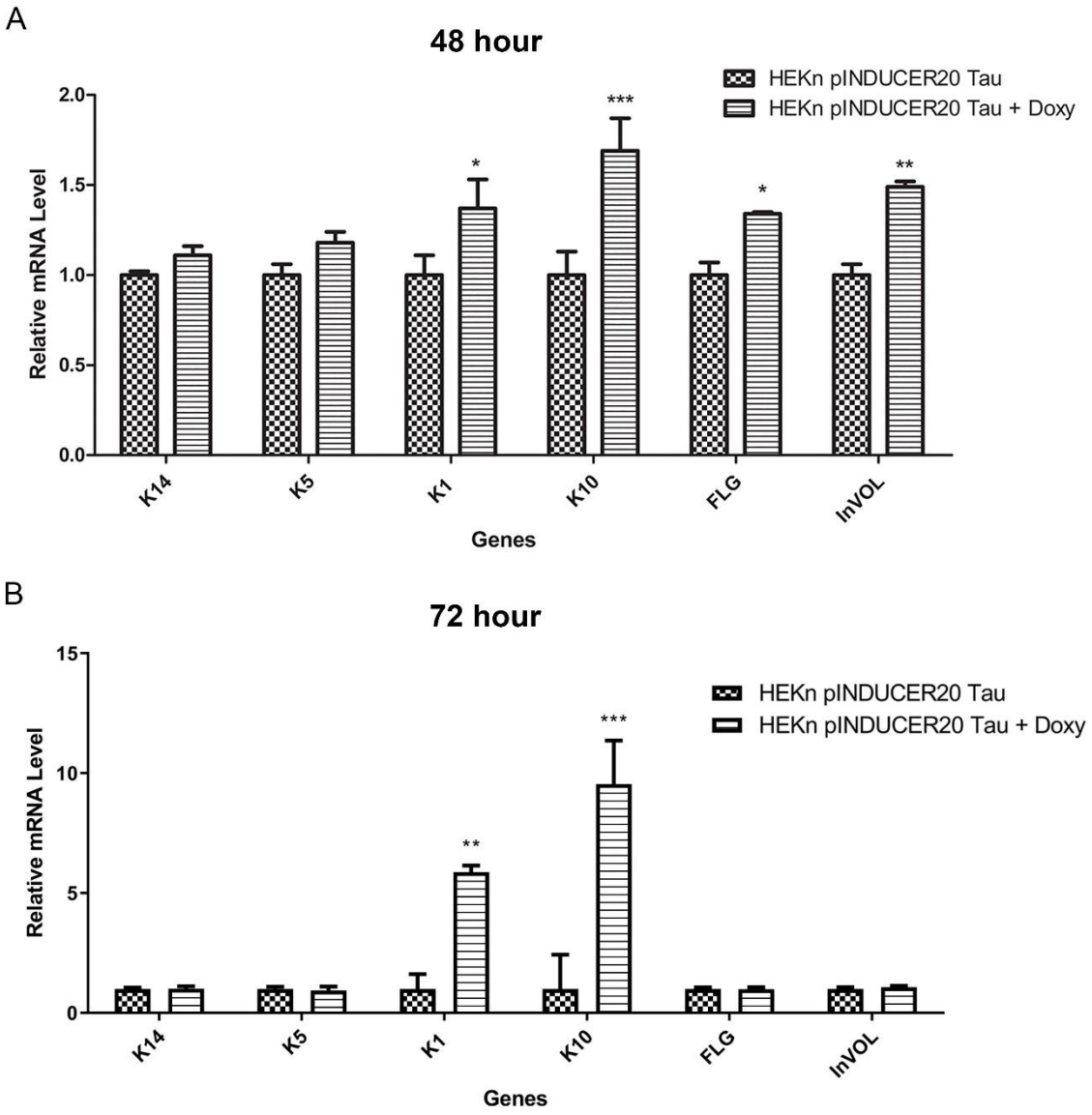

Figure 4.32. Tau overexpression in epidermal keratinocytes induces differentiation.
HEKn cells infected with pINDUCER20 tau under growing culture conditions were treated with doxycycline (doxy) to drive the overexpression of 2N4R (441 aa) tau. **A.** RT q-PCR analysis from total RNA collected 48 h after doxycycline treatment. **B.** RT q-PCR analysis from total RNA collected 72 h after doxycycline treatment. K14 – keratin 14; K5 – keratin 5; K1 – keratin 1; K10 – keratin 10; FLG – filaggrin; INVOL – involucrin. Ct values normalised to 36B4 and $2^{-\Delta\Delta Ct}$ method of analysis used. Relative expression levels are displayed as mean ± SD. Two-way ANOVA with Bonferroni correction was used to test significance; * $p<0.05$, **<0.01, *** $p<0.001$.

To determine whether the overexpression of 2N4R tau had an effect on keratinocyte differentiation, RT q-PCR analysis was first used to assess a panel of differentiation markers in pINDUCER20 tau keratinocyte cells with and without doxycycline. 48 and 72 h time points were chosen to check for expression of genes associated with keratinocyte differentiation, consistent with the time points used for calcium induced differentiation earlier in this chapter.

RT q-PCR analysis revealed that 48 h after the doxycycline induced tau overexpression, differentiation associated gene expression of K1, K10, filaggrin and loricirn were significantly upregulated (Figure 4.32A). Strikingly, following 72 h of tau overexpression, the relative expression of K1 and K10 were significantly increased, 5.9 and 9.5 fold respectively, compared to their control (Figure 4.32B). Interestingly, the expression of filaggrin and loricrin did not follow the same pattern, and were not significantly increased by 72 h (Figure 4.32B). However, a longer time point may have allowed the identification of increased expression of these terminal differentiation genes following tau overexpression. The time dependent increase in the expression of differentiation markers seen here is similar to previous observations with calcium induced differentiation (Figure 4.9); in which the longer the treatment the higher the expression of differentiation associated proteins. To ensure the effects observed were not due to the treatment with doxycycline control cells with and without doxycycline treatment were analysed and it was found that doxycycline treatment had little or no effect on the differentiation of keratinocyte cells (Figure 10.16).

Following the observations from q-PCR analysis, to further confirm the upregulated expression of differentiation associated proteins following 2N4R tau overexpression, Western Blot and immunofluorescence analysis of differentiation associated proteins were carried out. Western Blot analysis confirmed a

significant increase in K1 expression following tau overexpression compared to controls (Figure 4.33A and B). Immunofluorescence analysis also confirmed there was an increase in keratin-1 and loricrin expression in cells 72 h after tau had been overexpressed compared to their control (Figure 4.33C). Although q-PCR analysis suggested that by 72 h there was not a significant increase in the expression of terminal differentiation marker loricrin, immunofluorescence analysis did show a significant increase in the expression of loricrin, especially in the larger keratinocyte cells (Figure 4.33B). Overall an increased cell size was also observed in keratinocytes following tau overexpression, another phenotype associated with keratinocyte differentiation (Figure 10.17 and Figure 4.33 - Figure 4.35).

As tau is a tubulin associated protein and well characterised in other tissues for its role in tubulin stabilisation, immunofluorescence analysis was performed to assess the morphology of the tubulin network in tau overexpressing keratinocytes. Strikingly, a major change in the tubulin network could be observed following tau overexpression. Control cells displayed a well-defined, dense and organised tubulin network, with tubulin fibres spread from the nucleus to the entire body of the cell (Figure 4.34A). However, the doxycycline induced overexpression of 2N4R tau induced a vastly different organisation of the tubulin network (Figure 4.34C and Figure 4.35B). The overall tubulin network resembled differentiated keratinocytes, with tubulin localising at the cortex of the cell, although no cell adhesion or cell-junctions were not observed between neighbouring cells. Immunofluorescence analysis revealed that although tubulin was distributed throughout the cytoplasm, the defined organisation of the tubulin fibres was lost at 48 h (Figure 4.34) and by 72 h clear bundles of tubulin were observed reorganised to the cell cortex (Figure 4.35). In the cytoskeletal system,

although microtubules are characterised by their dynamic instability, actin filaments are relatively stable. There are a small number of publications providing evidence that tau is able to bind and interact with actin filaments [181,324]. To investigate actin organisation and identify any changes following tau overexpression in keratinocytes, phalloidin was used to stain actin filaments in the cells in control and tau overexpressing conditions (Figure 4.35). Actin expression was increased around the periphery of the cell following tau overexpression compared to its controls (Figure 4.35B).

Interestingly, during immunofluorescence analysis fewer cells were observed in the mitotic stage of the cell cycle after tau overexpression, compared to the controls. Therefore, to further investigate this observation, RT q-PCR analysis was performed to assess the gene expression of a panel of proteins associated with proliferation and cell cycle progression. Analysis revealed a decreased expression of some genes associated with proliferation and cell cycle progression (Figure 4.36). The relative expression of Ki67 was found to decrease, with a specific decrease in cyclin B1 and CDK1, both of which are involved in the M phase of the cell cycle (Figure 4.36).

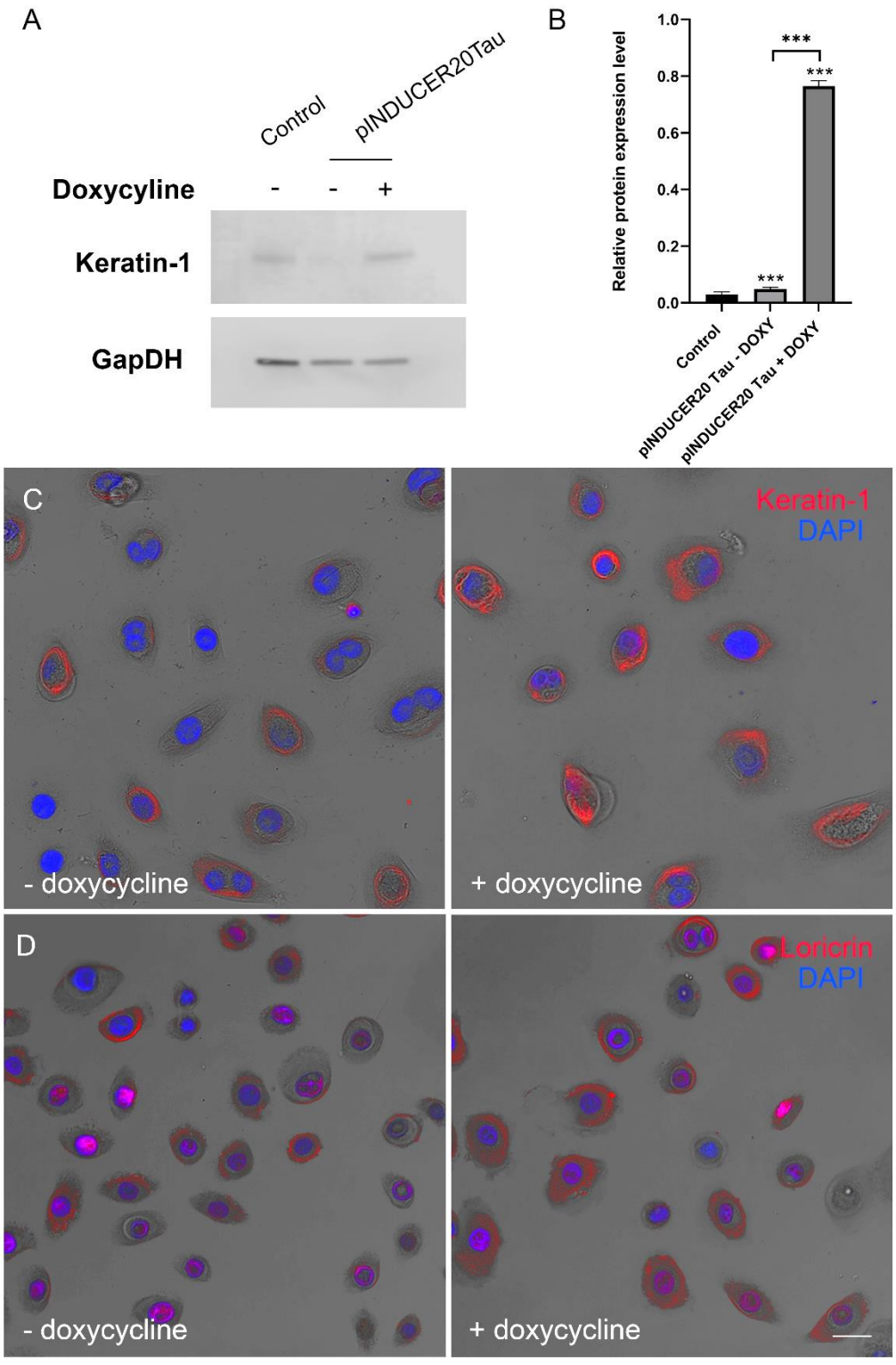

Figure 4.33. The expression of differentiation associated proteins, keratin-1 and loricrin, are increased in epidermal keratinocytes when tau is overexpressed.

A. Western blot analysis of K1 expression following tau overexpression in HEKn cells. Glyceraldehyde-3-Phosphate Dehydrogenase (GAPDH) was used as a housekeeping gene. **B**. Quantification of the relative expression of K1 protein following tau overexpression. **C&D.** Immunofluorescence analysis of K1 (red) and loricrin (red) expression was performed 72 h after tau expression was induced in HEKn cells. Nuclei counterstained with DAPI (blue). Scale bar 25 µm.

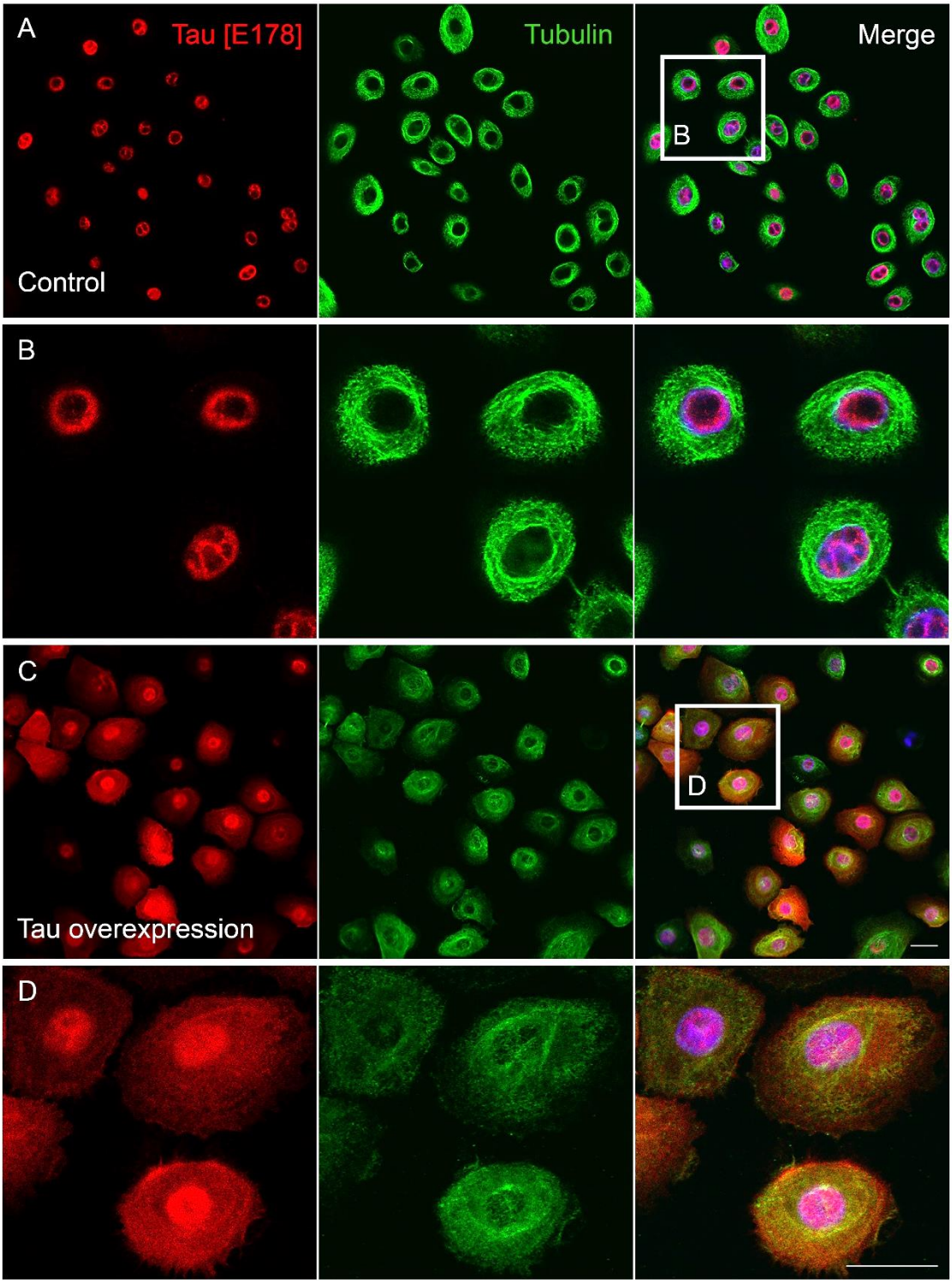

Figure 4.34. Tau overexpression in epidermal keratinocytes induces reorganisation of the tubulin network.
Immunofluorescence analysis of tau [E178] (red) and tubulin (green) expression in pINDUCER20 tau HEKn cells after 48 h with and without doxycycline (n=3). **A&B.** pINDUCER20 tau HEKn cells cultured without doxycycline display a dense and organised tubulin network spreading from the nucleus to the entire body of the cell. **C&D.** Immunofluorescence analysis of pINDUCER20 tau HEKn cells cultured with doxycycline for 48 h lost their tubulin organisation. Tubulin appeared to be localising towards the cells cortex. Nuclei counterstained with DAPI (blue) and all channels are merged in the right panel to allow accurate visualisation of cellular morphology. Scale bar 25 µm.

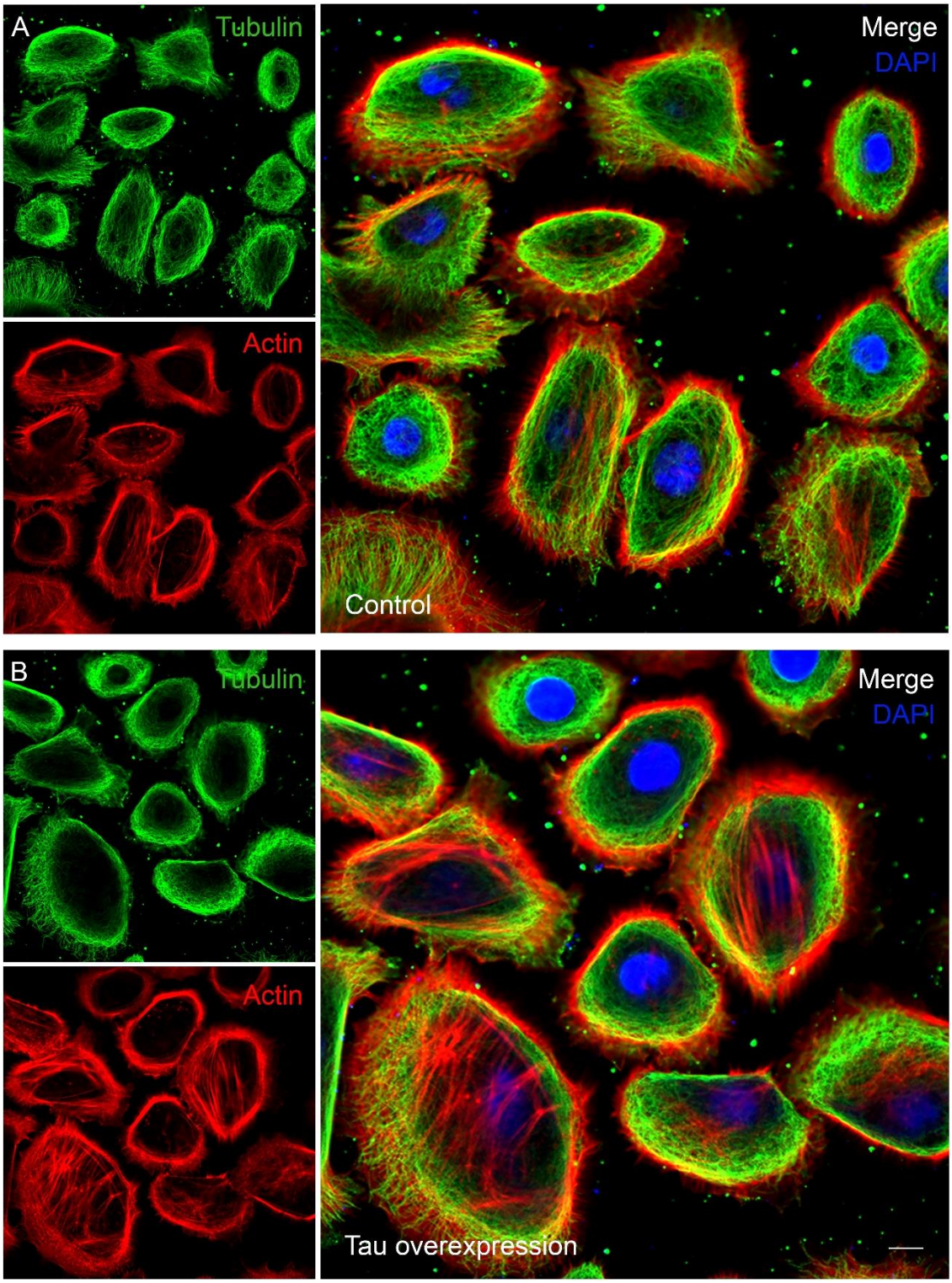

Figure 4.35. The rearrangement of the microtubule network to the cells cortex and increase in actin expression following tau overexpression in keratinocytes.

Representative immunofluorescence analysis of tubulin (green) and actin filaments (red) in growing keratinocytes 72 h after tau overexpression. **A.** pINDUCER20 tau HEKn without doxycycline displayed a well-defined, dense and organised tubulin network, with tubulin fibres spread from the nucleus to the entire body of the cell. Actin was identified around the periphery of the cell. **B.** pINDUCER20 tau HEKn with doxycycline displayed clear bundled tubulin

localising to the cortex of the cell. Nuclei counterstained with DAPI (blue) and all channels are merged in the right panel to allow accurate visualisation of cellular morphology. Scale bar 10 µm.

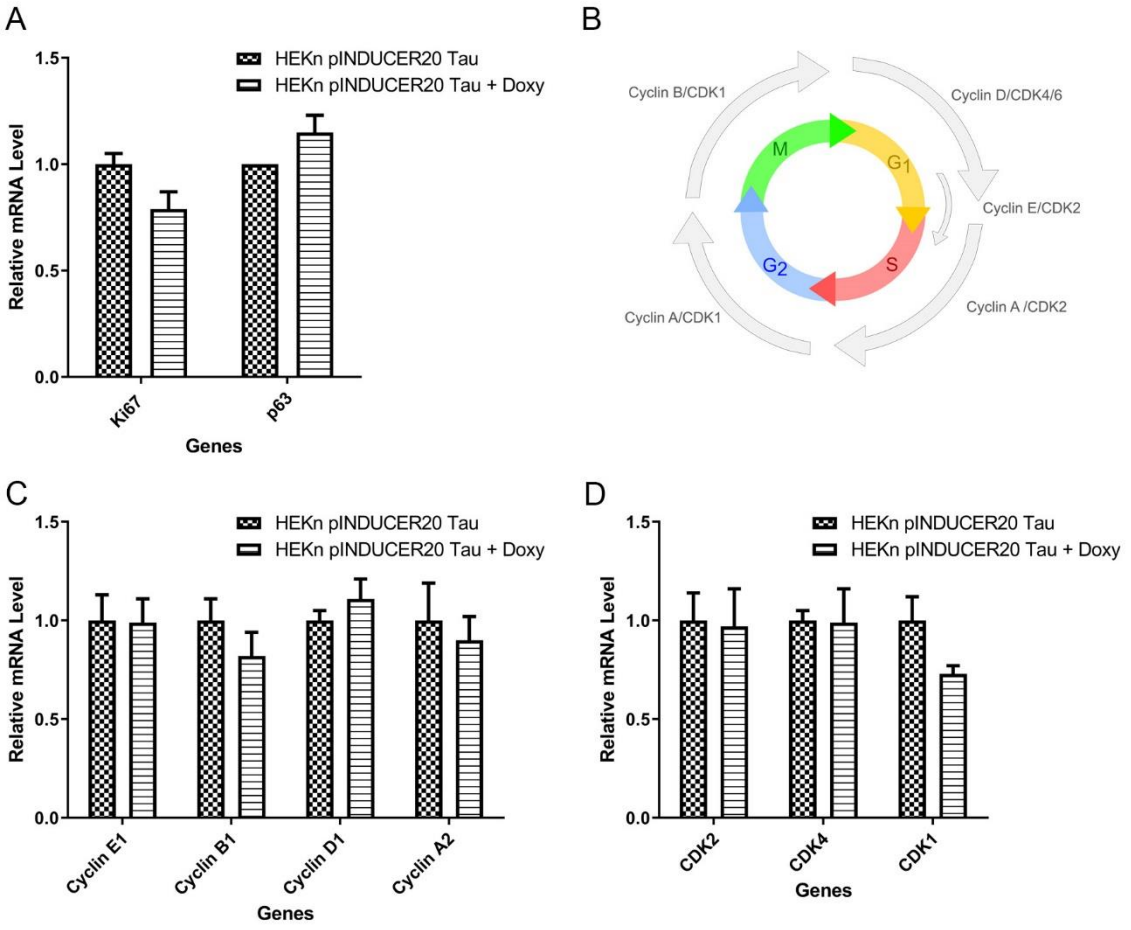

Figure 4.36. Tau overexpression reduces keratinocyte proliferation and progression through the cell cycle in epidermal keratinocyte cells.
A. Representative RT q-PCR analysis of Ki67 and p63 expression following tau overexpression. **B.** Schematic demonstrating cyclin and CDK expression throughout the distinct stages of the cell cycle. **C&D.** Representative RT q-PCR analysis of cyclin and CDK expression when 2N4R tau is overexpressed in HEKn cells. Ct values were normalised to 36B4 and $2^{-\Delta\Delta Ct}$ method of analysis used. Relative expression levels are displayed as mean ± SD. Two-way ANOVA with Bonferroni correction was used to test significance.

4.4.5.1. Functional analysis reveals tau overexpression alters the programme of stratification and differentiation in three-dimensional epidermal model.

So far, this chapter has demonstrated that tau regulates keratinocyte entry into differentiation. However, although tau overexpression has been shown to induce differentiation in cultured epidermal keratinocytes, to confirm its functional significance in the epidermis, the effect of tau on epidermal stratification and differentiation was validated in a 3-dimentional (3D) epidermal model. Epidermal models used in this study were purchased from MatTek©. EpiDerm™ models were shipped 3 days after generation and were still submerged in culture medium. Models were exposed to air-liquid interface 24 h after receipt and cultured for a further 7 or 10 days before fixation and subsequent analysis (Figure 4.37).

4.4.5.1.1. Characterisation of skin equivalent system as a model of epidermal stratification and differentiation

Before Epiderm™ models could be used to functionally assess the role of tau in epidermal differentiation, it was essential to first confirm that EpiDerm™ were a good model for healthy human skin. Therefore, immunofluorescence analysis was carried out in EpiDerm™ models to assess the expression of key epidermal proteins. Expression profiles of key proteins were then compared against healthy human skin to ensure EpiDerm™ was an appropriate model to use in this study to mimic healthy human skin (Figure 4.38; Figure 4.39; Figure 4.40).

EpiDerm™ models displayed a normal, stratified epithelium containing 4 distinct layers. Overall, the EpiDerm™ was slightly thicker than healthy human skin (Figure 4.38). However, the majority of this height was due to the increased

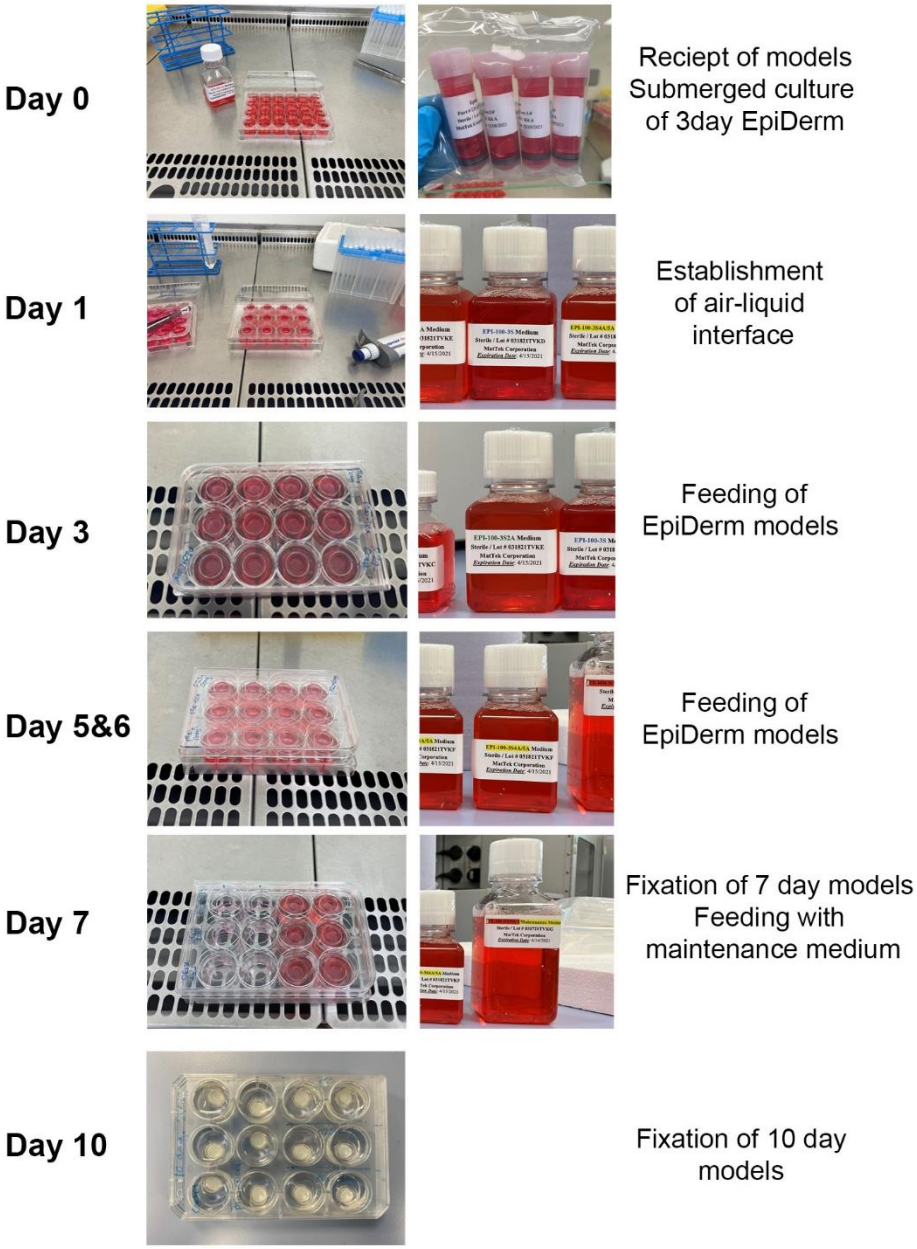

Figure 4.37. Timeline of EpiDerm™ culture.
In this study 3D epidermal models (EpiDerm™) were purchased from MatTek©. EpiDerm™ models were received submerged in culture medium 3 days after initial culture. Upon receipt, models were cultured submerged in medium for 24 h. Air-liquid interface was established the following day in a 12 well plate designed by MatTek© to allow sufficient culture medium to be added to the outer well. Inserts were fed every 24 - 48 h until completion at 7 days, where half of the EpiDerm™ models were fixed and embedded in OCT for analysis. The remaining inserts were cultured for a further 72 h with maintenance medium before fixation at 10 days for subsequent analysis.

thickness of the stratum corneum in EpiDerm™. In healthy skin under physiological conditions, everyday abbrasion leads to cells being shed from the skins surface, but *in vitro* there is nothing to cause shedding of the top layer of the stratum corneum, thus thickening of this layer can occur. Keratinocytes within EpiDerm™ models appear slightly larger than those found in healthy skin, which could also be responsible for the increased thickness observed (Figure 4.38).

Keratinocytes in the basal layer of EpiDerm™ models presented with a round or polygonal morphology, were neatly organised along the bottom of the insert and has round nuceli with no obvious abnormlities. K14 expression was correctly expressed in the basal population of cells and integrin-α6 staining was identified throughout the basal population in MatTek© models (Figure 4.38). K14 expression was observed at lower levels throughout the suprabasal cells, probably due to the long half-life of keratin to help maintain the structural integrity of the epidermis, when keratin expression switches in differentiation. Because EpiDerm™ models are mature 7 days after air liquid interface, it is likely that K14 is retained for structural integrity during this differentiation programme that in healthy human skin takes four weeks.

Ki67 is resticted to mostly the basal layer, with occassional scattered spinous cells just above the basal layer positive for the proliferation marker (Figure 4.38). Ki67 expression was significantly higher in EpiDerm™ models at 7 days compared to healthy human skin (Figure 4.38). However, the basal cells in healthy human skin are replenishing differentiating cells in a homeostatic mechniasm, whereas EpiDerm™ basal cells developed a full thickness epithelium in just over 7 days/ Thus, it is unsurprising that at 7 days there are a large number of proliferaing cells; one of the limitations of the model. EpiDerm™ are cultured in proliferating promoting medium up to day 7, then after the

epithelium has fully matured are cultured in maintenance medium. Subsequently, at the later time point of 10 days, significantly less Ki67 positive basal cells could be obeserved due to the maintenance medium, with the epithelium being mainated rather than being established.

Spinous cells in EpiDerm™ models correctly expressed keratin-1 and had a slightly larger morphology compared to the basal cells (Figure 4.39). Terminal differentiation protein, loricrin, was found in the granular layer of EpiDerm™ models, but this layer was much thicker than the granular layer in healthy human skin samples (Figure 4.39). As briefly described, the corneal layer was thicker than that found in the majority of human skin samples, but was very similar to the corneum in patient three's biopsy (Figure 4.39). Due to the lack of abrasion and exposure to external environmental insults in culture there is nothing to clear cells from the corneal layer. Some nuclei could be observed in some of the EpiDerm™ samples, along with small amounts of K14 and K1. This could be due to the quick development of the skin samples leading to retention of some nuclei and imcomplete differentiation during the intial formation of the epithelium, another limitation of the 3D system.

Before manipulating tau expression levels in epidermal models, tau expression levels and its localisaton within the EpiDerm™ models were assessed. Immunofluorescence analysis with tau [E178] showed that similar to healthy human skin, tau was found in the nucleus of basal cells, with cytoplasmic expression found in the upper layers of the epidermis (Figure 4.40). However, in human biopsies the cytoplasmic expression of tau was more pronounced than in the EpiDerm™ model. Interestingly, tau5 expression was observed in a larger population of keratinocytes. Tau5 was found to be expressed in the granular layer in healthy human skin, and although the overall staining profile was increased in

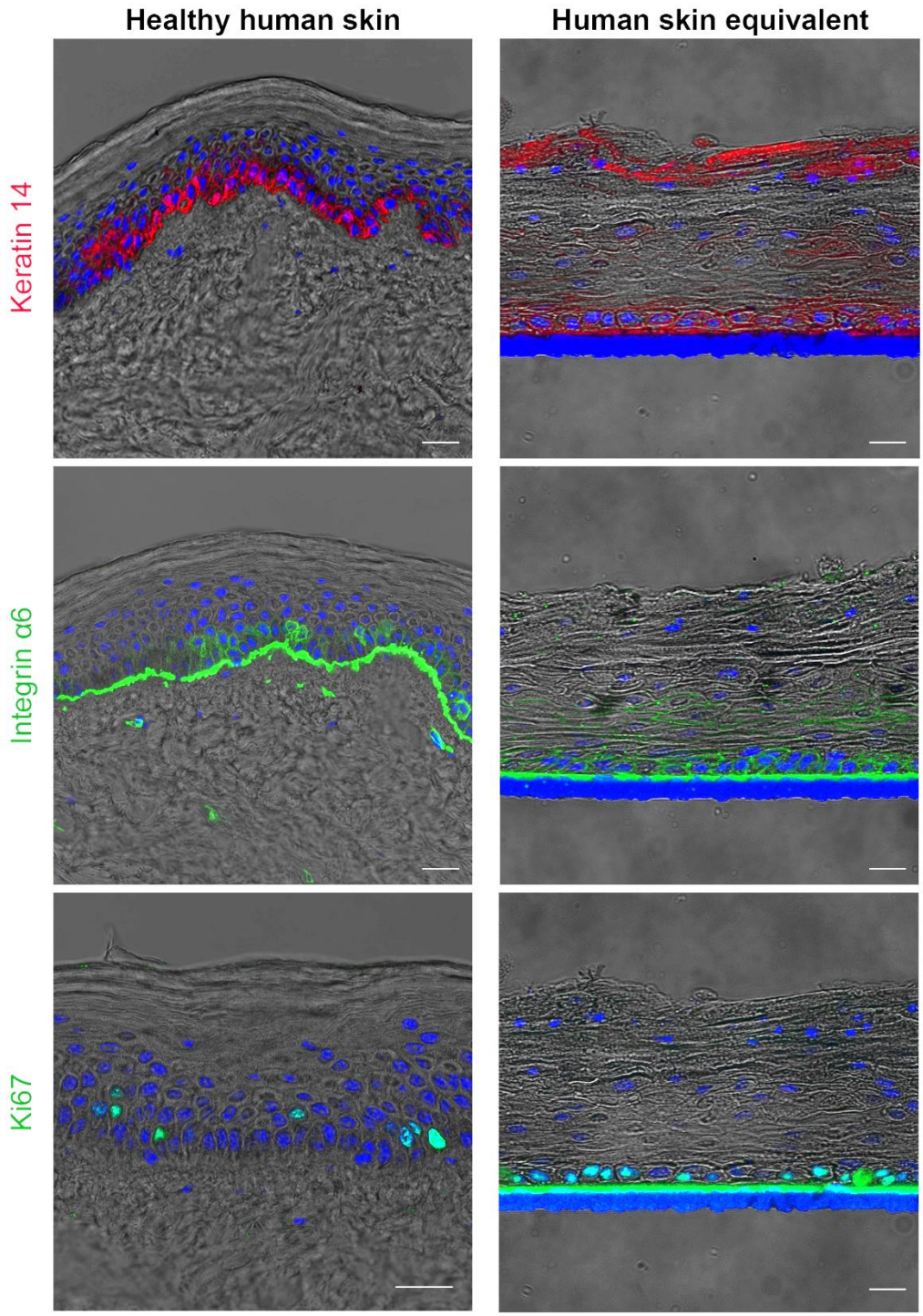

Figure 4.38. Immunofluorescence analysis of markers in healthy human skin compared to the human skin equivalent system used in this study. Immunofluorescence analysis of EpiDerm™ model at 7 days compared to healthy human skin. Keratin-14 expression (top) was mainly restricted to the basal layer of keratinocytes. Integrin-α6 expression (middle) was observed in all cells in contact with the insert, in the epidermis all cells in contact with the basement membrane are positive for integrin-α6. Ki67 expression (bottom) was found throughout the basal layer in epidermal models and the epidermis. Representative immunofluorescence images of healthy human skin in this figure are from patient 3 biopsy. Nuclei counterstained with DAPI (blue) and displayed with phase contrast for sample visualisation. Scale bar 25 µm.

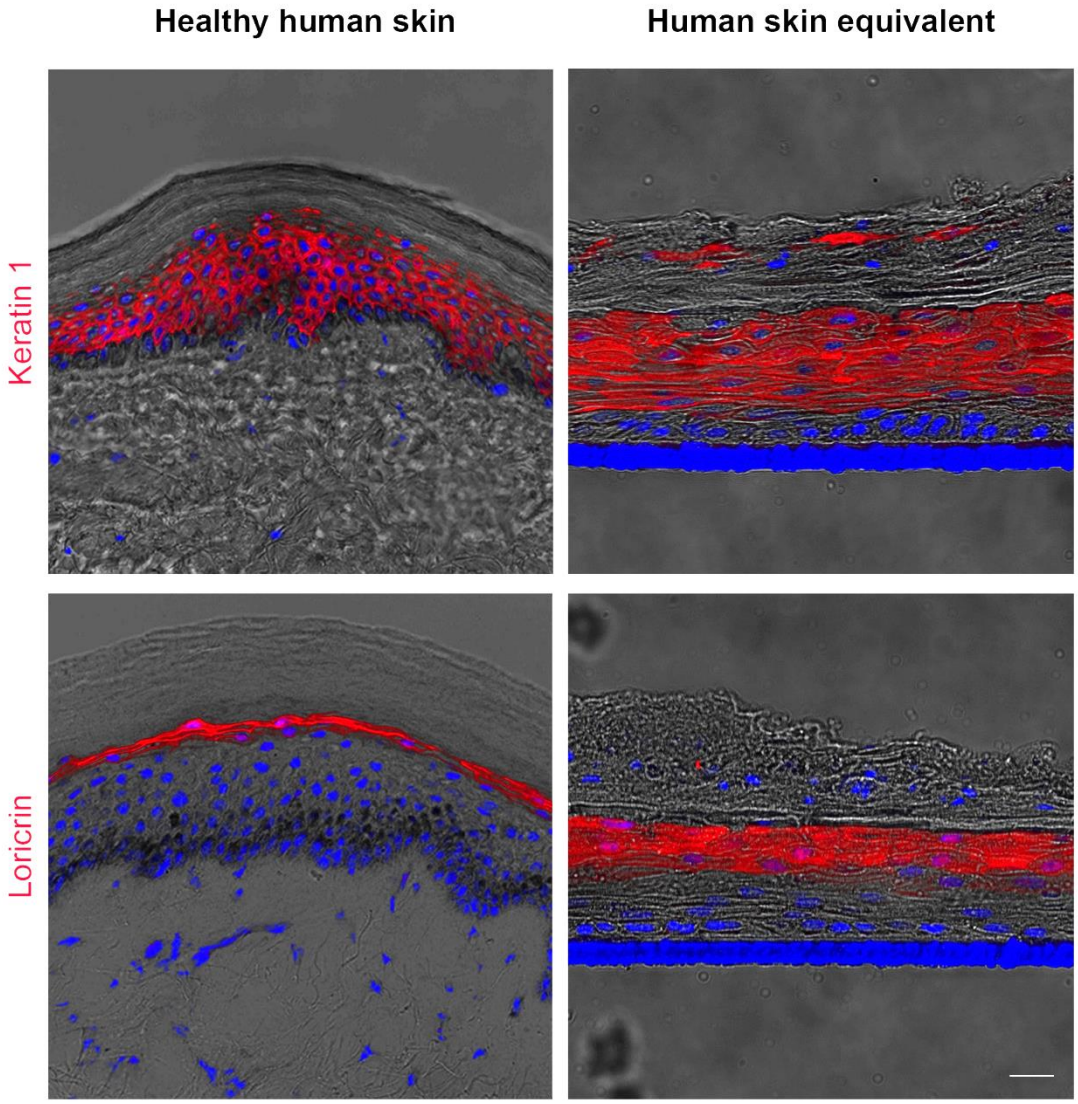

Figure 4.39. Immunofluorescence analysis of differentiation markers in healthy human skin compared to the human skin equivalent system used in this study.
Representative immunofluorescence analysis of terminal differentiation proteins keratin-1 and loricrin in EpiDerm™ models at 7 days compared to clinical samples. Keratin-1 (top) was observed to be exclusively expressed by suprabasal keratinocytes in the EpiDerm™ model at 7 days, similar to the expression pattern found in the native epidermis. Terminal differentiation protein (bottom) was expressed in the uppermost, elongated, flattened cells in the EpiDerm™ model. Although the location of loricrin expression was similar to native human skin samples, the population of cells expressing this protein was increased in the EpiDerm™ model. Representative immunofluorescence images of healthy human skin in this figure are from patient 3 biopsy. Nuclei counterstained with DAPI (blue) and displayed with phase contrast images for sample visualisation. Scale bar 25 µm.

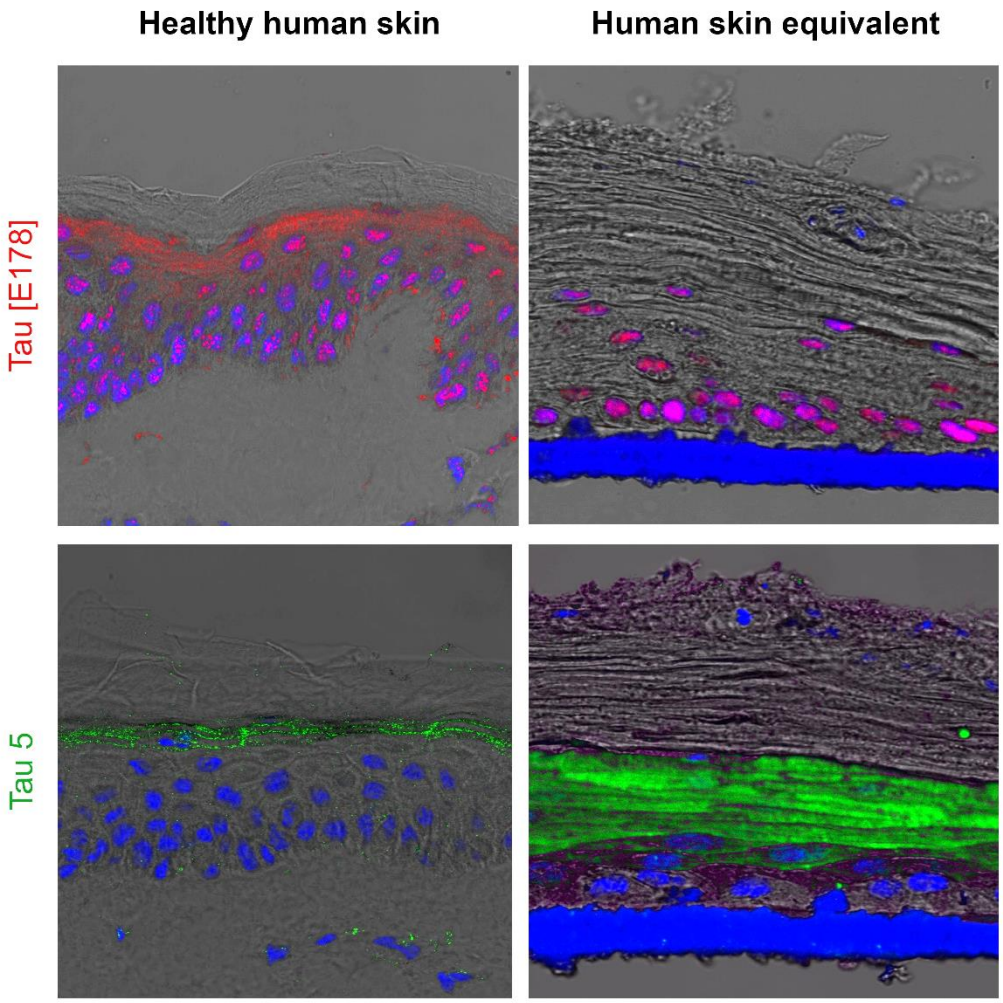

Figure 4.40. Tau expression in EpiDerm™ models compared to patient biopsies.
Representative immunofluorescence analysis of tau expression in EpiDerm™ skin model morphology under normal culture conditions compared to healthy human skin samples. Tau 5 (green) and tau [E178] (red) staining is displayed with representative images of healthy human skin samples (left) and EpiDerm™ models (right). Nuclei counterstained with DAPI (blue) and displayed with phase contrast images for visualisation of morphology. Scale bar 25 µm.

EpiDerm™ models, this larger proportion of positive cells was consistent with the increased cell layer expressing loricrin that was also observed cmpared to human skin samples (Figure 4.40).

Overall the EpiDerm™ epidermal equivalent acurately resemled human skin, with each of the four layers expressing the revelent markers to allow its use in this study for the functional analysis of tau in epidermal stratification and differentitation.

4.4.5.1.2. Tau overexpression induces changes to the differentiation and stratification programme in three-dimensional epidermal model

Following the full characterisation and confirmation that EpiDerm™ was an appropriate representative healthy 3D skin model for in this study, tau expression levels were artificially manipulated to address the significance of tau in epidermal stratification and differentiation.

To address the functional significance of 2N4R tau in the process of epidermal stratification and differentiation, 3-day submerged EpiDerm™ models were infected with lentiviral particles to drive the overexpression of 2N4R tau in a doxycycline dependent mechanism. Doxycycline was added or omitted from the culture medium during the course of EpiDerm™ culture. EpiDerm™ models were collected at 7 and 10 days after air-liquid interface was established. MatTek© protocols suggest a fully mature epidermis occurs after 7 days, but a later time point was also chosen to assess epidermal formation after 10 days following a longer time period of tau overexpression. Therefore, EpiDerm™ models were cultured with maintenance medium between 7 and 10 days. Doxycycline known to have some effects on cells, therefore, EpiDerm™ models were infected with the empty vector pINDUCER20 and these infected inserts were treated with

doxycycline, to ensure that doxycycline itself is not responsible for any observed changes to epidermal stratification and differentiation. The empty vector pINDUCER20 will also be used to confirm that the process of lentiviral particle infection and the presence of the pINDUCER20 plasmid does not have a significant effect on EpiDerm™ morphology. These controls also allowed any unintentional induction of tau overexpression to be identified, as some cell culture mediums contain some tetracycline from serum. Although the unintentional activation of the system was ruled out earlier in the chapter, the medium provided by MatTek© was proprietary, so the controls would have enabled the identification of any unintentional activation of the system from the new culture medium.

To verify the successful overexpression of tau following infection with pINDUCER20 tau and induction of overexpression using doxycycline, immunofluorescence analysis was performed. The expression of tau in overexpression models was observed to be upregulated. Immunofluorescence analysis confirmed that tau expression was upregulated in the nuclear and cytoplasmic fraction of epidermal cells, in by contrast in control EpiDerm™ models tau expression was restricted to the nuclear fraction of basal and most suprabasal cells, with a cytoplasmic expression of tau observed in granular populations of keratinocytes (Figure 4.41).

The epidermal histology and layer specific morphology in EpiDerm™ models following the overexpression of tau were analysed next looking at the effect of tau overexpression on the stratification and differentiation of the epidermis. For the purpose of the next section of analysis, stratification was defined as the arrangement of adherent, layers of squamous epithelial cells upon the basement

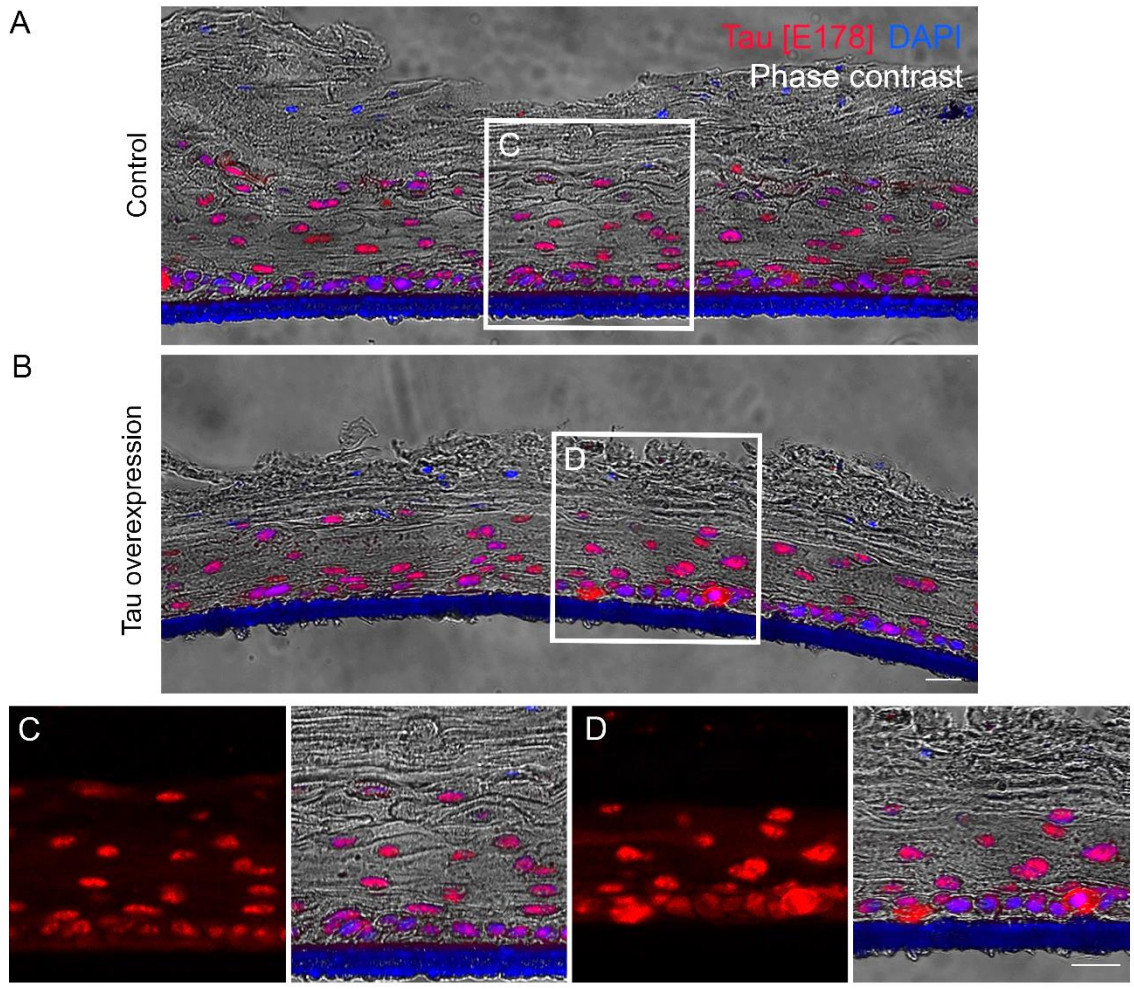

Figure 4.41. Tau can be sucessfully overexpressed in EpiDerm™ models. EpiDerm™ inserts were received from MatTek© as immature epidermal models submerged in culture medium, 3 days after initial cell seeding. Immature epidermal inserts, still submerged in culture medium, were infected with pINDUCER20 and pINDUCER20 tau for 6 h before air-liquid interface was established. EpiDerm™ models were subsequently treated with or without doxycycline in the cell culture medium to drive the tetracycline dependent overexpression of 2N4R (441 aa) tau. **A.** Representative immunofluorescence analysis of tau [E178] (red) expression in control EpiDerm™ model 7 days after air-liquid interface was established. **B.** Representative Immunofluorescence analysis of EpiDerm™ model infected with pINDUCER20 tau lentiviral particles and treated with doxycycline to induce tau overexpression in keratinocyte cells. **C.** High magnification image of tau [E178] expression in control EpiDerm™ models. Tau expression was observed mostly restricted to the nucleus with cytoplasmic expression restricted to cells in the granular layer. **D.** High magnification image of EpiDerm™ models following 7 days of tau overexpression. Tau [E178] expression can be observed in the nucleus and cytoplasm of many cells. Expression level of tau was found to be much higher than in the control, indicating that successful infection and subsequent overexpression of tau following treatment with doxycycline was achieved. Nuclei counterstained with DAPI (blue) and displayed with phase contrast images to allow epidermal morphology to be visualised. Scale bar 25 µm.

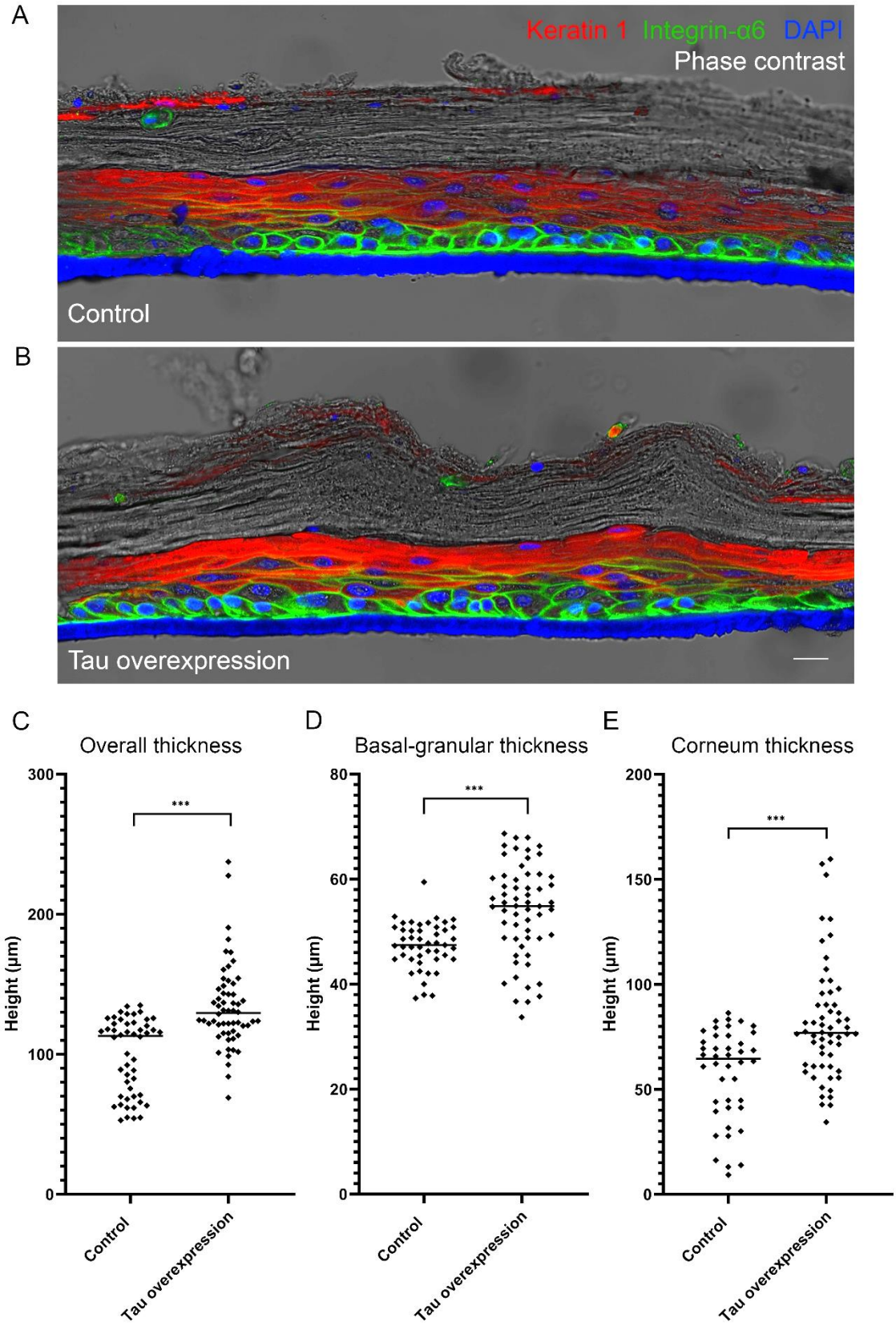

Figure 4.42. Overexpression of 2N4R tau induces a significant increase in epidermal thickness.
EpiDerm™ thickness changes upon tau overexpression 10 days after air-liquid interface. **A&B.** Representative immunofluorescence analysis of integrin-α6 (green) and keratin-1 (red) in control (A) and tau overexpression (B) EpiDerm™ models following 10 days of air-liquid interface culture. Nuclei counterstained with

DAPI (blue) and displayed with phase contrast images for visualisation of epidermal stricture. Scale bar 25 µm. **C.** Overall EpiDerm™ thickness was observed to significantly increase compared to the control. A significant difference was also observed compared to pINDUCER20 tau without doxycycline treatment. **D.** Basal-granular thickness in EpiDerm™ models was reduced compared to the control although not reaching the threshold for statistical significance. **E.** Corneal thickness in EpiDerm™ models was significantly increased following tau overexpression compared to all control conditions. 6-12 images were measured for each condition, 5 measurements were taken on every image at defined intervals to reduce bias. An unpaired *t*-test was used to test significance; *** $p<0.001$.

membrane, while differentiation was defined as the process in which a cell changes from basal to spinous, granular and corneal through terminal differentiation. To first assess the overall effect tau overexpression had on epidermal models, total epidermal thickness was quantified. This was further broken down into height of the basal-granular epidermal layers (living layers) and the thickness of the corneal layer (dead, enucleated layer) across all EpiDerm™ samples at 10 days. Overall, tau overexpression in EpiDerm™ models resulted in a significant increase in overall thickness compared to the control, despite the large variation in epidermal thickness to be observed (Figure 4.42C). To further investigate the changes to EpiDerm™ thickness, both living layer and corneal layer thickness was quantified next to determine where the increased thickness was arising from. Tau overexpression in EpiDerm™ models resulted in a significant increase in living layers (Figure 4.42D). Additionally, most strikingly, following the quantification of stratum corneum thickness, there was a significant increase exclusively in the corneal thickness of tau overexpression EpiDerm™ compared to all control conditions (Figure 4.42E).

To continue the investigation into the changes in epidermal thickness following tau overexpression, the overall keratinocyte cell number, basal cell number and proliferation status was assessed to identify any possible causes for the changes in epidermal thickness observed when tau is overexpressed.

There was a significantly increased thickness of the living layer of the EpiDerm™ models following tau overexpression. Therefore, total cell number counts were conducted by quantifying nuclei within living layers and compared across conditions; nuclei retention in the corneal layer were not counted. Strikingly, a significantly decreased overall cell number was observed in tau overexpressing EpiDerm™ models compared to control conditions (Figure 4.43C). Basal cells in

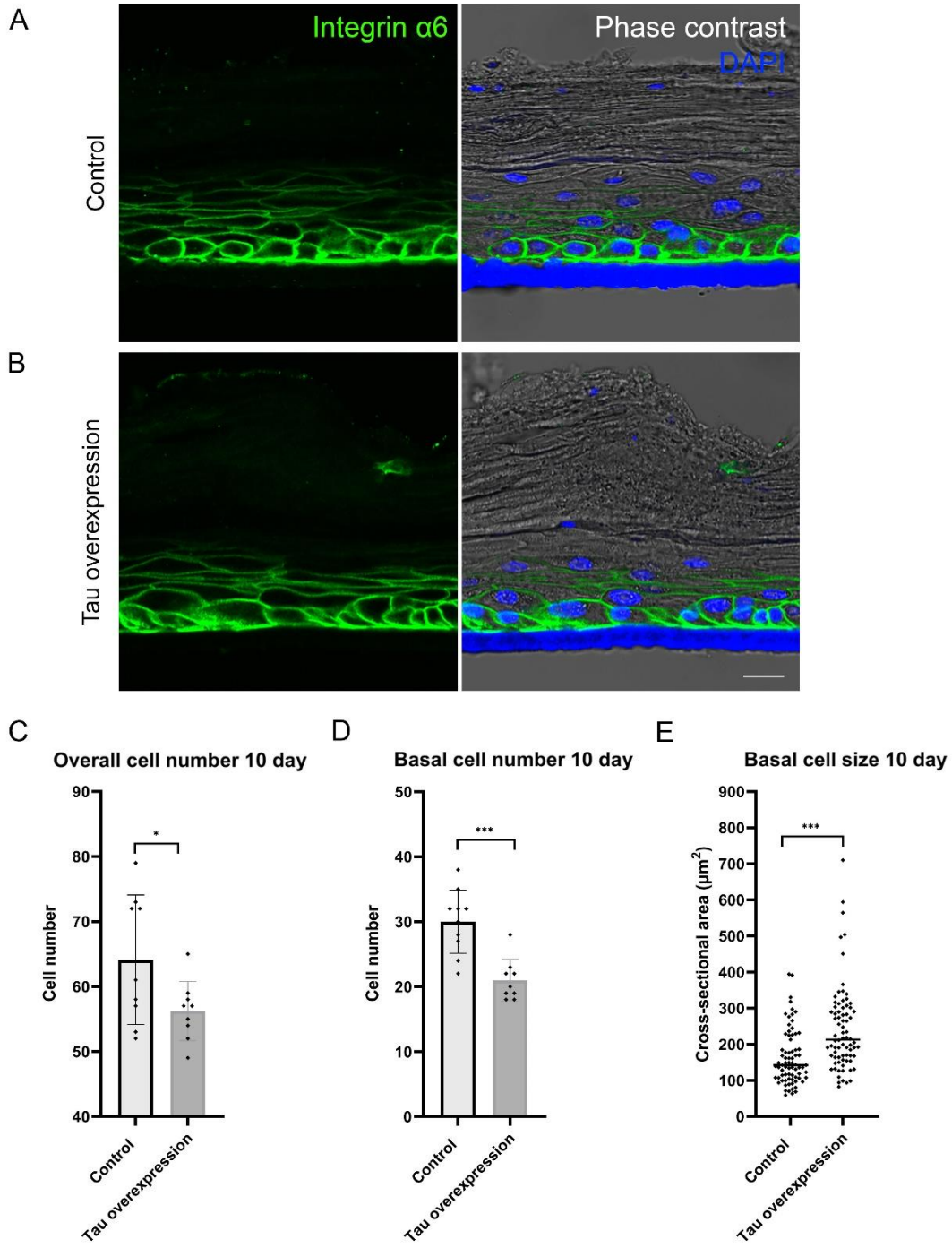

Figure 4.43. Investigation into basal cell size following tau overexpression in epidermal models.
A. Representative immunofluorescence analysis of integrin-α6 (green) in control EpiDerm™ models cultured according to MatTek© standard protocol. Basal cells can be identified with a small round, neatly organised morphology along the bottom of the insert. **B.** Representative immunofluorescence analysis of integrin-α6 (green) in tau overexpression EpiDerm™ model. Basal cells displayed a larger, less organised phenotype along the membrane. Nuclei counterstained with DAPI (blue). Scale bar 25 μm. **C.** Quantification of overall cell number revealed that following tau overexpression a significantly decreased cell number occurred. **D.** A significant decrease in basal cell number was observed when tau was overexpressed in EpiDerm™ models. **E.** Analysis of the cross-sectional area

of basal keratinocytes revealed that when tau is overexpressed the average basal cell size is significantly increased compared to control conditions. 6-12 images were measured for each condition. Every basal cell in contact with the basement membrane (insert) was measured in each image using integrin-α6 to outline the cell surface. An unpaired *t*-test was used to test significance; * $p<0.05$, **<0.01, *** $p<0.001$.

contact with insert were also quantified and compared across conditions. Consistent with observations, quantification revealed a significant reduction in basal cell number following tau overexpression compared to other conditions (Figure 4.43D). Immunofluorescence analysis with integrin-α6 also revealed that following tau overexpression basal cells were visibly larger compared to controls (Figure 4.43A and B). Therefore, to quantify basal cell size across experimental conditions, the cross-sectional area of basal cells were measured and analysed. Quantification revealed that tau overexpression resulted in a significantly larger basal cell size compared to all control conditions (Figure 4.43E).

Following the confirmation that tau overexpression led to an increased keratinocyte cell size and decreased basal cell number along the BM, changes in cell behaviour was next investigated. To further examine the status of the basal cells following tau overexpression, immunofluorescence analyses using markers associated with the proliferation and differentiation status of keratinocytes in the epidermis were carried out. Analysis and quantification of basal keratinocytes using proliferation marker, Ki67, revealed that Ki67 positive basal cells could be observed in clusters scattered exclusively throughout the basal layer (Figure 4.44A). There was no significant increase in the overall number of positive Ki67 cells after tau overexpression compared to controls. However, when the percentage of Ki67 positive cells was calculated, due to the decreased basal cell number after tau overexpression, an increased percentage of Ki67 positive basal cells could be observed when tau was overexpressed, compared to all control conditions. However, this difference did not reach the threshold for statistical significance (Figure 4.44B).

The expression of p63 was also examined due to its role in the regulation of epidermal differentiation and stratification. A distinct immunostaining profile was

observed following tau overexpression relative to its controls. A striking decrease in the total number of p63 positive cells were observed after tau overexpression (Figure 4.45). The expression of p63 in basal keratinocytes after tau overexpression also dramatically decreased. The relative distance of p63 positive cells from the BM was decreased in tau overexpression conditions, whereas in control insert models p63 staining was observed to extend higher into the suprabasal population of keratinocytes (Figure 4.45A). However, to ensure these findings were not due to the decreased basal cell and overall cell number resulting from tau overexpression, quantification of the percentage of positive p63 cells was carried out. Upon quantification it was confirmed that there was a significant decrease in the percentage of p63 positive keratinocytes in the total, basal and suprabasal populations after tau overexpression (Figure 4.45B).

Next, the distribution of keratins and terminal differentiation proteins in EpiDerm™ models were assessed to allow the identification of basal, early and late stages of keratinocyte differentiation to be assessed. Immunofluorescence analysis with K14 highlighted the differences in basal organisation along the basal layer in control and tau overexpression EpiDerm™ models (Figure 4.46). In all control inserts keratinocytes can be observed as small round or polygonal cells that were neatly organised along the insert surface with each cell in contact with the bottom of the insert (Figure 4.46A and C). Whereas cells in tau overexpression models showed a less organised, elongated phenotype consistent with the changes observed so far in this study. In basal keratinocytes keratin IFs are usually bundles near the nucleus, whereas in differentiated cells, keratin IFs usually originate from the perinuclear region and are instead distributed towards periphery of the cell. K14 was found throughout the epidermal layers in all EpiDerm™ models. Analysis of K14 expression also revealed a

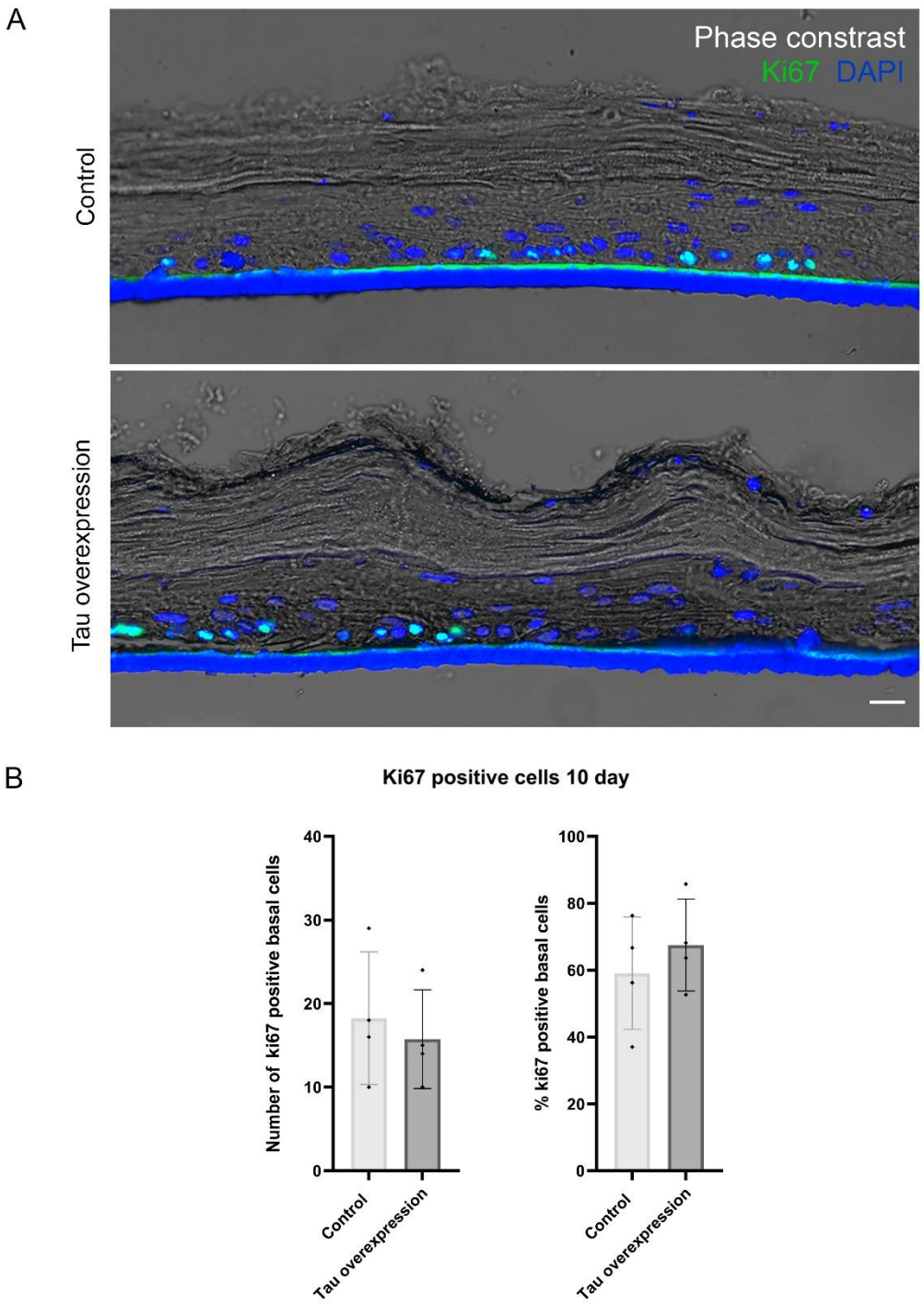

Figure 4.44. Tau overexpression induces an increased population of proliferating basal cells in EpiDerm™ models.
A. Representative immunofluorescence analysis of proliferation marker, Ki67 (green), in control and tau overexpression EpiDerm™ models 10 days after air-liquid interface was established. Nuclei counterstained with DAPI (blue). Scale bar 25 µm. **B.** Quantification of Ki67 positive cells in EpiDerm™ models. Findings are displayed as Ki67 positive cell count, and also as the percentage of Ki67 positive cells. Due to the differences identified in the basal cell number across different conditions percentage positive Ki67 basal cells allows for a more representative indication of basal cell behaviour. An unpaired *t*-test was used to test significance.

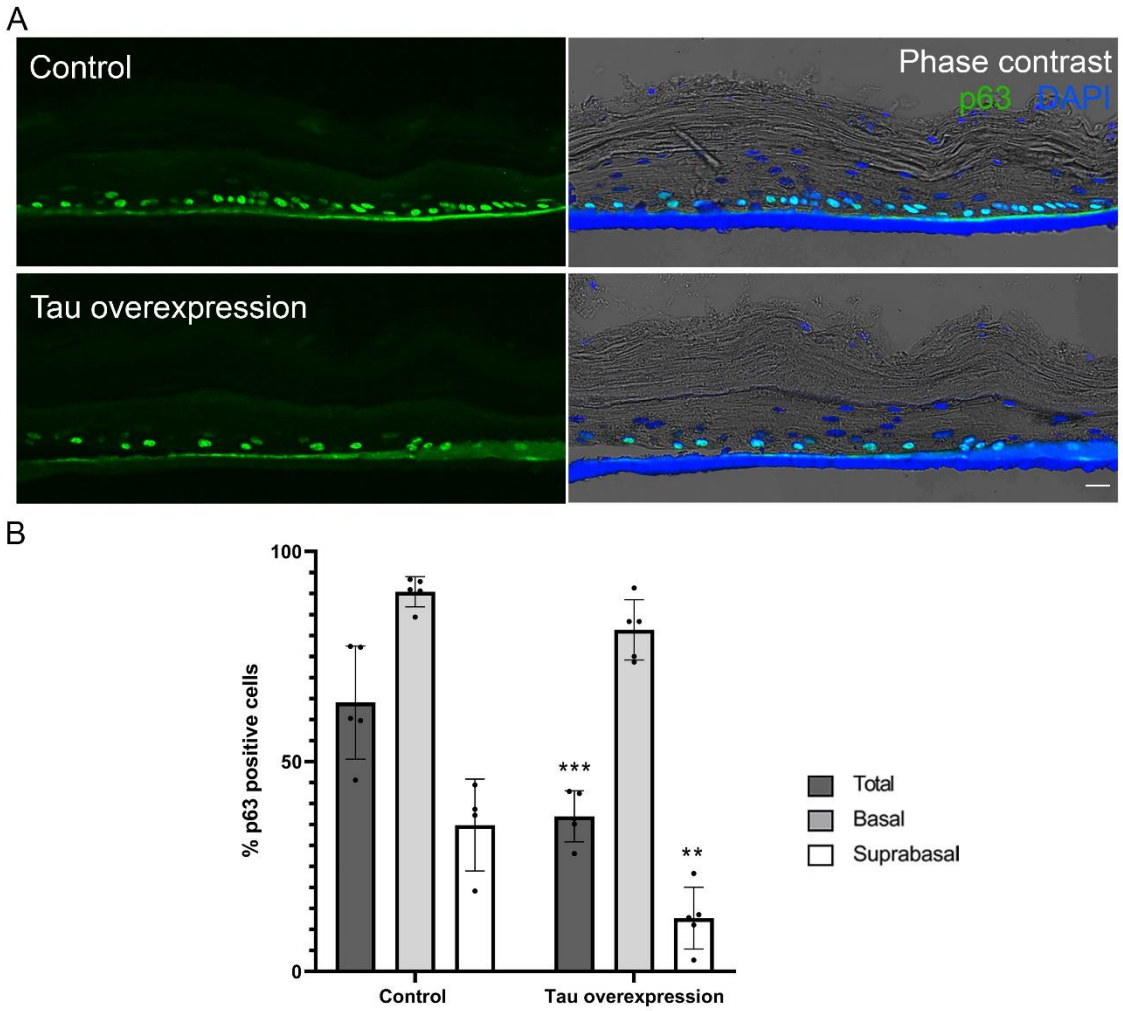

Figure 4.45. Tau overexpression decreases populations of p63 positive epidermal keratinocytes

A. Representative immunofluorescence analysis of p63 (green) in control and tau overexpression EpiDerm™ models after 10 days of air-liquid interface culture. There was a significant reduction in the overall number of p63 positive cells that could be observed in the epidermis. The total number of basal cells expressing p63 was decreased, however the overall reduction in basal cell number was also evident. The number of positive suprabasal cells was also decreased alongside the suprabasal cell number decreased that is observed. Nuclei counterstained with DAPI (blue) and displayed alongside phase contrast images for visualisation of sample morphology. Scale bar 25 μm. **B.** Quantification of percentage of total, basal and suprabasal p63 positive cells in the EpiDerm™ models following 10 days of culture. Analysis of revealed that following tau overexpression there was a significant reduction of the percentage of total and suprabasal epidermal cells that expressed p63. Two-way ANOVA with Bonferroni correction was used to test significance; **<0.01, *** p<0.001.

distinct phenotype in the suprabasal cells following tau overexpression (Figure 4.46). Cells were highly compacted with an elongated, flattened phenotype indicating a change in stratification of the epidermal compartment compared to controls (Figure 4.46D). Further investigation with differentiation associated proteins exclusively expressed in this suprabasal population will allow for a deeper insight into some of the changes that might be taking place.

Stratification of epithelial tissue is an important process in epidermal homeostasis and function. The changes to suprabasal morphology were further investigated and immunofluorescence analysis with K1 confirmed these initial observations identifying not only changes to epidermal differentiation, but also stratification (Figure 4.47). Initial observations revealed a striking increase in K1 expression in tau overexpressing models compared to all control conditions, indicating an increased differentiation status as shown in 2D cell cultures earlier in this chapter (Figure 4.47). Interestingly, K1 was also observed branching down into the basal layer at points along the insert, a finding not identified in control conditions. The changes to the spinous and granular cell morphology were emphasised by the K1 staining; the K1 staining almost presented as a smear, and the cells seem to be elongated in granular layer (Figure 4.47). Consistent with the increased expression of K1 following tau overexpression, immunofluorescence analysis with terminal differentiation protein, loricrin, revealed a significant increase in granular cells after tau overexpression compared to all control conditions (Figure 4.48). The decreased nuclei within the granular layer was also highlighted, with granular cells appearing as stretched with significantly less nuclei identified in this layer compared to the controls, highlighting the effect of tau overexpression to the stratification of the keratinocytes (Figure 4.48).

Markers of adherens junctions were also investigated between tau overexpression models and its controls (Figure 4.49). It is well established that epidermal differentiation entails a tightly coordinated rearrangement of intracellular junctions. Immunofluorescence analysis with E-Cadherin emphasised the reduced living layers observed when tau is overexpressed compared to the control and the changes to the suprabasal layers demonstrated through staining with keratin-1 and loricrin. E-Cadherin also highlighted the disorganised and flattened phenotype of epidermal cells following tau overexpression (Figure 4.49). There was not much E-Cadherin expression observed between BM and cells, but instead between the neighbouring cells throughout the layers of epidermis (Figure 4.49). When tau was overexpressed it was found that E-Cadherin expression was reduced compared to its controls (Figure 4.49). Interestingly, in the granular layer of the epidermis there was a significant reduction of E-cadherin compared to controls (Figure 4.49D).

Finally, changes to the stratum corneum were analysed. Quantification of corneal thickness earlier in this chapter demonstrated a significant thickening following tau overexpression compared to all other conditions, but additional changes to the stratum corneum were also observed. Interestingly, there were less nuclei detected in the corneal layers of EpiDerm™ models overexpressing tau than the controls. The stratum corneum displayed a highly compact phenotype following tau overexpression, with more K14 and loricrin retained at surface of corneum compared to its controls (Figure 4.46 and Figure 4.48). In tau overexpression models ridges were formed in the stratum corneum, a finding not observed in any of the controls (Figure 4.42). Taken together, these results confirm the findings of this study so far and prove that tau has a functional significance in promoting epidermal stratification and commitment to terminal differentiation.

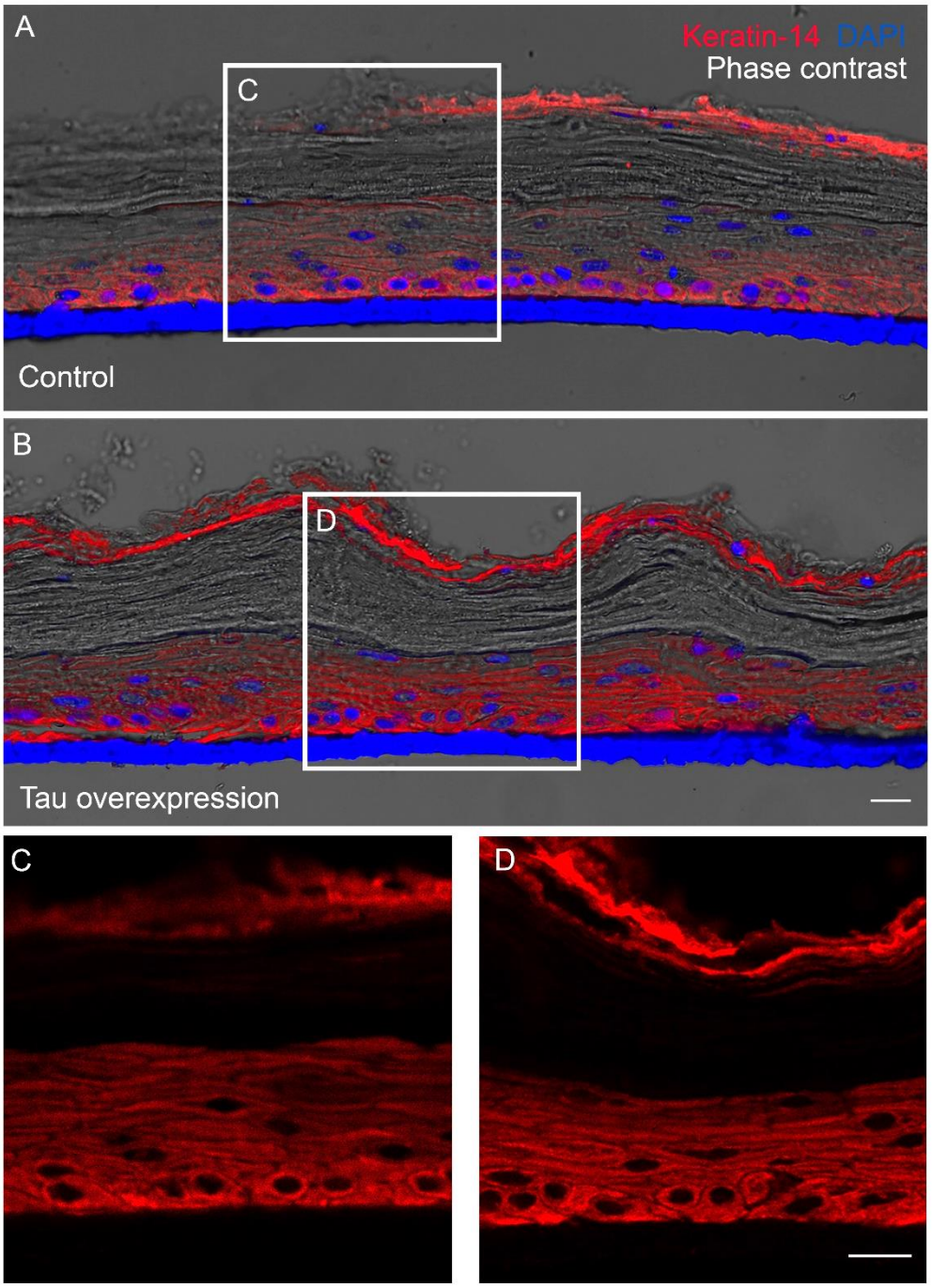

Figure 4.46. Keratin-14 organisation in EpiDerm™ models following tau overexpression.

Representative immunofluorescence analysis of keratin-14 (red) expression when tau is overexpressed in EpiDerm™ models compared to its control 10 days after air-liquid interface was established. **A.** Control EpiDerm™ insert model 10 days after air liquid interface was established. **B.** 2N4R tau overexpression in EpiDerm™ insert 10 days after air liquid interface was established. **C.** High magnification images of control EpiDerm™ models revealed small round or polygonal, organised basal keratinocytes in contact with the basement membrane. **D.** High magnification images of EpiDerm™ with tau overexpression revealed a less organised, elongated phenotype consistent with changes observed throughout this study. Nuclei counterstained with DAPI (blue) and displayed with phase contrast images to allow visualisation of sample morphology. Scale bar 25 µm.

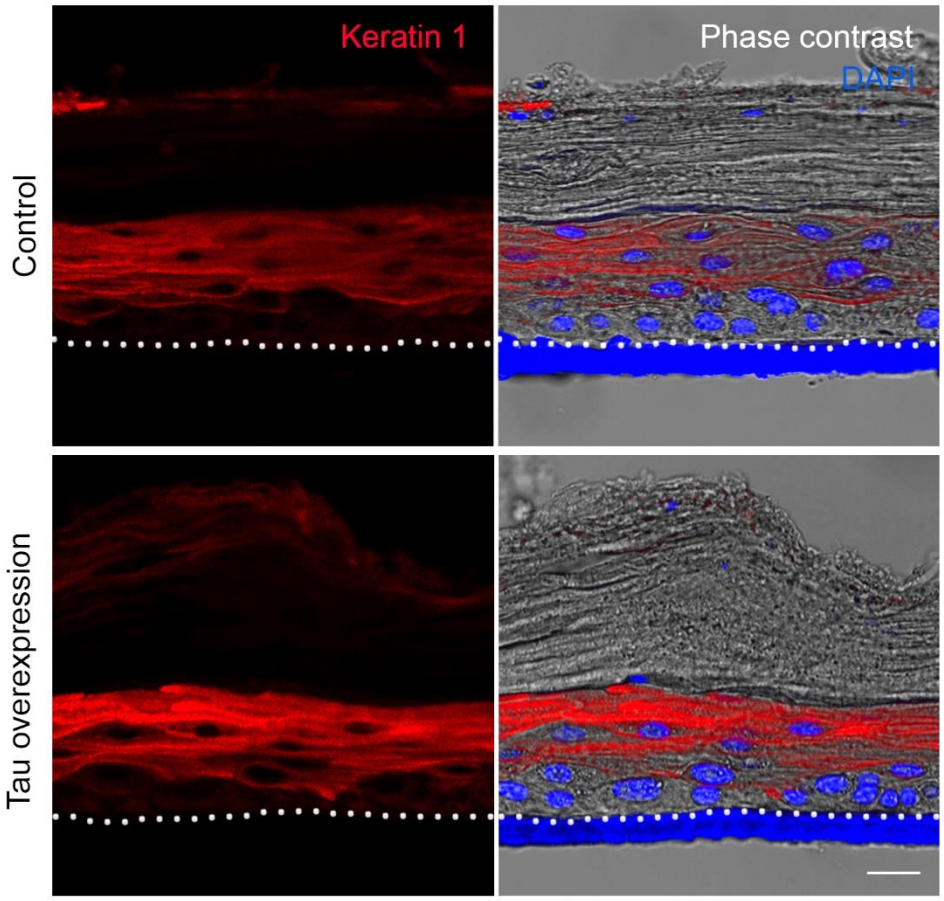

Figure 4.47. Differentiation marker, keratin-1, expression is increased in the epidermis when tau is overexpressed.
Representative immunofluorescence analysis of keratin-1 (red) when tau is overexpressed compared to its controls. Tau overexpression in EpiDerm™ insert models results in a significant increased expression of keratin-1. Keratin-1 was also observed branching into the basal layer at points throughout EpiDerm™ models, an observation not identified in any of the control conditions. Keratin-1 staining also highlighted differences to the morphology of suprabasal cells after tau overexpression. Spinous and granular cells displayed an elongated morphology compared to controls and keratin-1 staining appeared almost as a smear in this population. These observations indicate that tau overexpression leads to a change in not only the differentiation but also the stratification programme of epidermal keratinocytes, an observation that would not be possible in 2D cell culture. Nuclei counter stained with DAPI (blue) and displayed with phase contrast images to allow morphology visualisation. White dotted line depicts the surface of the insert in which basal cells are attached. Scale bar 25 µm.

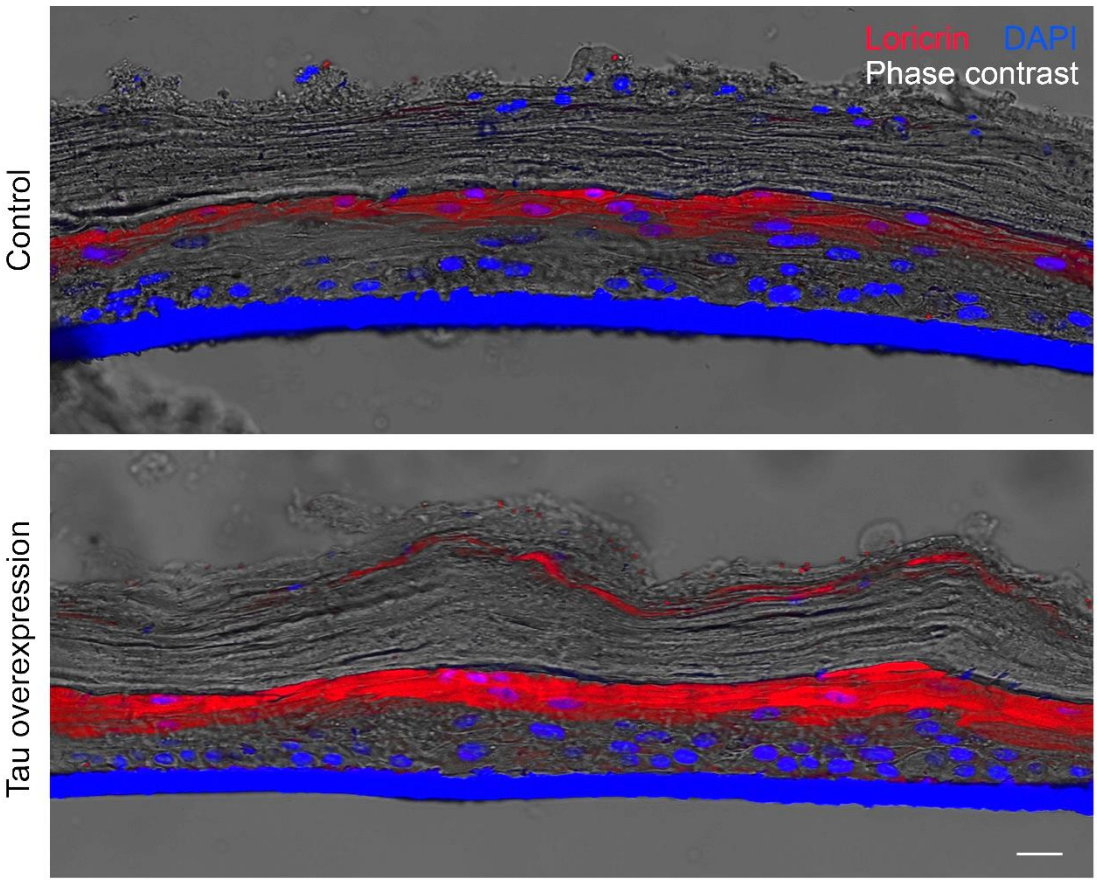

Figure 4.48. Granular cell morphology chnages following tau overexpression.
Immunofluorescence analysis of loricrin, a protein expressed in terminally differentiated proteins in the granular layer of the epidermis, in EpiDerm™ models following tau overexpression. 10 days of tau overexpression led to a significant increase in loricrin compared to the controls. Granular cells had an elongated phenotype and a decreased in the number of nuclei within this layer could be observed with tau overexpression. Nuclei counter stained with DAPI (blue) and displayed with phase contrast images to allow morphology visualisation. Scale bar 25 µm.

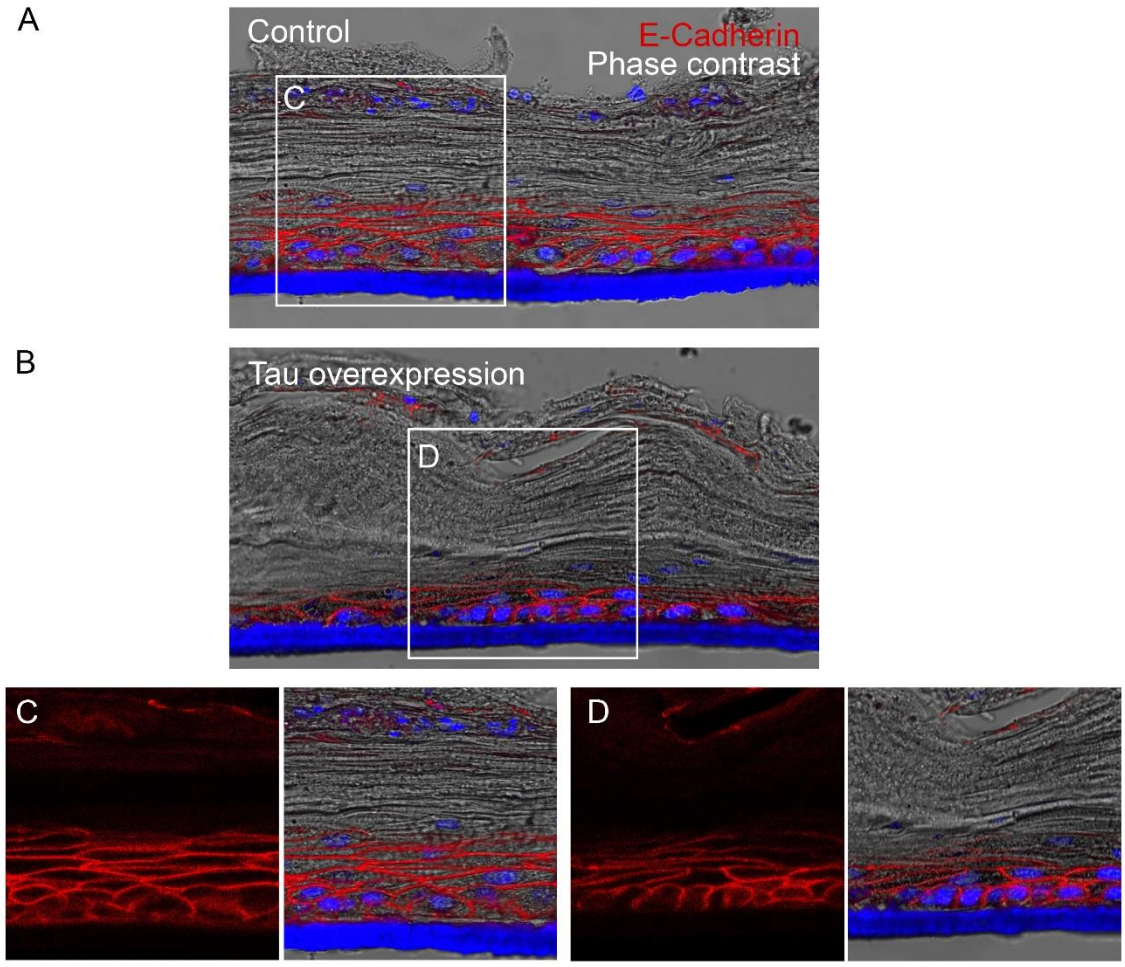

Figure 4.49. Adherens junctions following 10 days of tau overexpression in EpiDerm™ inserts.
Representative immunofluorescence analysis of E-Cadherin (red) expression in EpiDerm™ insert models 10 days after air liquid interface was established. **A&C.** Control EpiDerm™ model displayed E-cadherin expression throughout the living layers of the epidermis. Keratinocytes had an organised stratified phenotype with small rounded cells in contact with the insert at the basal surface, with larger cells in the spinous layer, and finally flattened cells in the granular layer. E-cadherin was absent in the stratum corneum. **B&D.** Tau overexpression in EpiDerm™ inserts displayed a flattened stratified epidermis compared to controls and exhibited reduced E-cadherin throughout the epidermis. E-cadherin highlighted the changes in cell morphology compared to the controls. E-cadherin expression was significantly reduced in the granular layer compared to controls. Nuclei counter stained with DAPI (blue) and displayed with phase contrast images to allow morphology visualisation. Scale bar 25 µm.

4.5. Discussion

In summary, using *in vitro* methods this chapter has successfully demonstrated that tau plays a role in differentiation and stratification of the healthy human epidermis, a previously unknown finding. Using epidermal keratinocytes, the expression patterns of tau that were discovered *in vivo* in Chapter 3 were confirmed, and the functional role of tau in the differentiation and stratification of the epidermis was established. Although a primarily a microtubule associated protein, this study has shown that tau can be found in cytoplasmic, nuclear and membrane fractions of epidermal keratinocytes. The overexpression and downregulation of tau in keratinocytes showed that tau can orchestrate epidermal stratification and keratinocyte commitment to terminal differentiation *in vitro*.

Cultured keratinocytes *in vitro* consist of a mixed population of cells with differing proliferation capabilities. All keratinocytes in this study, unless otherwise stated, were cultured in cell culture medium to help promote “stem like” growing cell populations. However, as keratinocytes behaviour and phenotype vary depending on their differentiation status it was important to also find a method of distinguishing the SC and TAC population of keratinocyte to establish a correct evaluation of tau expression between these populations. In chapter 3, evaluation of the tau expression in the epidermis of clinical samples revealed that amongst the basal layer of cells the tau expression differed between neighbouring keratinocytes. A SC attachment assay, first developed by Jones and Watt in 1993 [49], was performed and determined that rapidly adhering cells had lower expression of tau than their TAC counterparts, supporting the observations *in vivo.* Additionally, as anticipated 2N and 4R tau transcript variants were significantly increased in TAC cell populations; consistent with the findings from the LCM captured ROI from healthy skin biopsies in Chapter 3. The expression

of 2N 4R variants of tau arises from the inclusion of exon 3 and 10 in the tau transcript, resulting in a longer isoform of tau which appears to be upregulated in differentiated epidermal keratinocytes. Although this finding is previously unreported in keratinocytes, it is consistent with publications from other cell types [185,213,219,238,309,325,326]. Interestingly, 1N isoforms of tau were not detected in keratinocytes *in vitro,* however the significance of this finding and differences to keratinocytes *in vivo* are not currently understood and require further investigation. It is possible that the discrepancies could come from other cell types likely to be located in the epidermis of the clinical samples, of which it was not possible to remove prior to analysis with LCM.

This study has successfully demonstrated that tau is dynamically expressed throughout the cell cycle in keratinocytes. In all keratinocyte cells *in vivo* and *in vitro*, tau could be located in the nuclear compartment of the cell and within this study cells in G_2 and M phases of the cell cycle showed highest levels of nuclear tau. During the process of mitosis the microtubule network is remodelled to form the mitotic spindles that allow chromosomes to line up and become divided between the two daughter cells [182–184]. The process of mitosis as tightly regulated and the stabilisation of this mitotic spindle is essential; however, very little is known about the role of tau during mitosis, and no studies have previously investigated this in keratinocytes. This study demonstrated a stabilising role for tau during the process of mitosis, in which tau expression was upregulated and found to support the mitotic spindle during metaphase, anaphase, telophase and cytokinesis. Additionally, it was observed that following mitosis one daughter cell inherited higher tau levels than the other. This could possibly be linked to their cell status, with TACs expressing higher levels of tau than SCs as demonstrated

in this chapter. Studies have provided evidence that epidermal cell fate can be influenced by the inheritance of certain proteins or transcription proteins [38].

This study has shown that tau isoforms have a distinct expression profile throughout the stages of keratinocyte differentiation. Consistent with observations *in vivo,* tau expression shifts from short isoforms to longer isoforms following keratinocyte differentiation and was found to correlate to its function within each population of keratinocytes.

DAPI staining allowed the identification of the nucleous, as the nuceolus appeared darker, almost as a black cavity in the nucleus, due to the three-fold lower concentration of DNA in the nucleous compared to the surrounding nucleoplasm (exclusing centromeres) [327]. Tau was located in the nucleus of all keratinocytes, displaying a distribution throughout the nucleus with the exception of the nucleolus. Contrasting to reports in neuronal cels that tau can play a role in nucleoulus organisation [183,215,238,304]. Indicating that in epidermal keratinocytes tau displays more of an association with DNA than nucleoular organisation. Nuclear tau has been reoprted in many cell lines, and has been linked to DNA protection, chromosome stablitly and regulation of gene expression [182,184,215,234,239,241–243]. Although keratinocytes often incur exposure to UV radiation, there are no reports to date which have linked tau in keratinocytes to a DNA protective role. This is an area that deserves further investigation to determine the mechanism by which tau might confer a protective mechanism to DNA from some of the stressors keratinocytes experience and its implications in cancer. Although tau was identified highly expressed in the nucleus of growing cells, it could be observed asymmetrically distributed to the plasma membrane nearest the MTOC; similar to the distribution of tau to the basal surface in contact with the BM of basal keratinocytes in clinical samples from Chapter 3. It is well

recognised that the MTOC is positioned between the leading edge and nucelus in migrating cells creating a polarised morphology [328], so it is of particular interest that *in vitro* tau was found to be asymmetrically distributed to the leading edge of keratinocyte cells. In gliblastoma cells tau has been shown to regulate cell migration through the remodelling of the microtubule and actin network [329].

In this chapter, when keratinocytes were differentiated tau expression was upregulated consistent with *in vivo* findings from Chapter 3. Following calcium induced differentiation tau expression remained asymmetrically distributed to the cortical edge of the keratinocyte cells co-localising with the cortical microtubule network; the funcitonal significance of this will be investigaited with the proteomic analsysis of binding partners in Chapter 5. The subset of cellular proteins that is associated with plasma membranes is of high biological importance; the plasma membrane delineates the cell and provides a physical boundary between the cell and its environment and plasma membrane proteins play important roles in cell–cell interactions, material transport, and signal transduction [24,67,72,82]. In many cell lines tau has been reported to play an important role in microtubule stability and part of this role is through stabilisation to the plasma membrane [216,223,224]. The N-terminus and MTBD have been shown to bind to the plasma membrane or membrane associated proteins with longer tau isoforms displaying a higher affinity for plasma membrane binding [216]; which is consistent with the changes in tau isoform expression between basal and differentiated keratinocytes that has been identified within this study.

Although tau could be identified in the cytoplasm and membrane fraction of keratinocyte cells, at this stage it was not understood what tau's binding partners were. However, changes were identified to all components of the cytoskeleton following tau KD and overexpression in keratinocytes. The most widely published

role of tau is in its microtubule stabilising, therefore it would be interesting to investigate microtubule dynamics and tau interactions throughout keratinocyte differentiation in more detail. In most studies *in vitro* into tubulin dynamics are traditionally assessed with the aid of taxol. Although taxol is a very effective microtubule stabilising agent, studies have provided evidence that to stabilise microtubules taxol displaces tau from tubulin [179]; this is thought to occur due to the tau binding site on microtubules overlaps with the taxol binding site that is located on β-tubulin on the inner surface of MTs [227]. Therefore, future experiments could continue to explore MT dynamics and the functional role of tau in the cytoskeletal network of keratinocytes using a scanning electron microscope (SEM) to analyse cytoskeletal structure and immunogold to label tau and investigate its interactions with the cytoskeletal network and organelles in differentiated cells.

Western blotting revealed an interesting finding within this study. Due to the previously uncharacterised expression of tau in the epidermis, it was unknown which isoforms of tau could be identified, but Western blot analysis revealed big tau (110 kDa), alongside other isoforms of tau, expressed in keratinocytes in all stages of growth and differentiation. Big tau arises from the inclusion of exon 4a within the tau transcript and there are many publications demonstrating that peripheral tissues express big tau isoforms [194–196,330,331]. Very little research has been conducted into the function of big tau, but publications in other cell lines have linked its expression and function to the spacing of microtubules, allowing for the efficient movement of cargo around cells and causing the microtubule surface to be more accessible [194,195,330]. Further investigation is needed to determine the functional significance of big tau in epidermal keratinocytes.

Another interesting observation in this study, was the finding using the tau5 antibody in western blotting. *In vivo* and *in vitro* immunofluorescence staining revealed that the tau5 antibody only displayed a positive signal in terminally differentiated or granular cells, however, western blotting with tau5 revealed bands in both growing and differentiated keratinocytes in total, nuclear and cytoplasmic fractions; mirroring the results from the tau [E178] antibody. A possible explanation for these findings could be the tertiary structure of the protein and the epitope of this particular antibody that lies within the PRD. The process of Western blotting involves the denaturisation and linearisation of the protein prior to running on an SDS-PAGE gel. Therefore, it is likely that in its native conformation the tau5 antibody cannot bind to the tau protein, but after denaturisation tau5 is able to display a positive signal on the Western blot. This is also consistent with the immunofluorescence analysis in which tau5 is normally located in the cytoplasm or at the surface of the plasma membrane, in which publications have indicated that when bound to microtubules or membrane associated proteins the conformational structure is changed and exposes the region of the protein in which the tau5 epitope is designed to bind and subsequently visualised with immunofluorescence.

There are many methods to induce keratinocyte differentiation, such as serum, incubation temperature, growth factors and inhibitors, the best method within this study were found to be serum free medium with an increased calcium concentration to induce a differentiated phenotype [84,322,332]. Although an increase in the extracellular calcium concentration is a powerful technique to mimic the phenotype of differentiated keratinocytes, keratinocytes *in vivo* receive multifactorial external cues which are not all able to be replicated *in vitro*. 2D systems are not capable of providing cues for keratinocytes to flatten and

enucleate as is observed in the granular and corneal layer of the epidermis. Therefore, this limitation needed to be taken into account when interpreting *in vitro* findings.

Within this study it was found that KD of tau interrupts the programme of differentiation in keratinocytes. Consistent with our observations, some studies have shown that when microtubule dynamics are inhibited, improper differentiation can occur [310,333]. Using *C.elegans* Lacroix *et al.* (2014) demonstrated that the suppression of microtubule dynamics impaired the differentiation of their egg laying apparatus [310]. While Hsu *et al.* (2018) showed that microtubule dynamics are essential for the formation of the epidermis and that the destabilisation of the cytoskeleton interfered with the barrier formation in the epidermis [333].

The switch between keratin expression remains the most widely accepted indicator of keratinocyte commitment to terminal differentiation, so it was particularly interesting that tau KD in growing cells induced a significant increase in the expression of early differentiation markers. However, despite the increased expression of early differentiation markers, genes associated with terminal differentiation were not upregulated. Consistent with the findings in this study that differentiating keratinocytes, in which the final stages of terminal differentiation are inhibited with depleted tau levels. Strikingly, tau KD in differentiating keratinocytes generated very distinct morphological and biological alterations. *In vitro* tau KD provided evidence that tau is required for terminal differentiation of keratinocytes, as when tau was KD in keratinocytes treated with high calcium levels differentiation was inhibited. Morphological changes that were observed in tau differentiating keratinocytes support the hypothesis that tau is required for epidermal stratification, in which major changes in cell shape take place. The

findings are in line with the literature demonstrating that when dynamic alterations are not supported in the epidermis terminal differentiation and therefore barrier formation is inhibited [310,333].

Within this study two methods of RNAi were performed, esiRNA and shRNA mediated tau KD, and tau KD was assessed after at least 48 h due to half-life of tau of 28.1 h [243]. However, the method of RNAi using esiRNA did pose a problem for keratinocyte viability and resulted in an increase in keratinocyte differentiation in both tau KD and negative control, placing a limitation on the conclusions that could be drawn using this method alone. The process of transfection delivers exogenous nucleic acids, such as esiRNA, into cells, this delivery can be achieved through physical methods such as electroporation, micro-injection or sonoporation, all of which are often toxic to cells. However, usually the use of chemical compounds enables transfection with a higher cell viability and INTERFERin® is a highly efficient transfection agent allowing lower levels of esiRNA to be used than other agents. However, all transfection protocols need to transport encapsulated genetic material into cells, which usually makes membranes more porous and cells more sensitive to extracellular calcium levels in the media; this is likely to be why increased differentiation of cells is be observed in esiRNA *RLUC* treated cells when compared to the control. shRNA mediated knockdown allowed for the viral infection with shRNA plasmid enabled the generation of a stable cell line of keratinocytes removing some of the limitations of chemical mediated transient knockdown with siRNA. Unlike siRNA-mediated KD, the shRNA control cell line did not display any undesirable characteristics and the effects of tau KD were able to bet better identified without the drawbacks of the transfection protocol.

To investigate the functional significance of tau KD, the effect of tau on epidermal stratification and differentiation was validated in a 3D epidermal model. However, the continuous treatment of epidermal models with esiRNA for 7-10 days led to a poor morphology in both tau knockdown and the negative control and did not allow for the accurate investigation into the functional significance of tau in the epidermis (data not shown). Therefore, to help overcome this, stable keratinocyte cell lines infected shRNA tau to KD tau expression were generated. However, due to time limitations, extensive work with the generated stable tau KD cell lines has not yet been possible and only preliminary findings are reported within this chapter. Future work with these stable cell lines will include the generation of epidermal insert models to investigate further in 3D systems the differentiation and stratification of keratinocytes with tau knocked down, proteomic analysis following tau knockdown and further investigation into the functional significance of tau knockdown on cellular structures using EM. Within the time frame of this study it was not possible to generate a 3D model with tau effectively knocked down. Various methods of tau KD in 3D epidermal systems were tested within this study, but siRNA mediated knockdown posed challenges to the viability of cells due to the transfection reagent. Drugs that interfered with tau proteins, such as LMTX and CongoRed, were also used in 3D models, but again the effects of the drugs on the cells could not be linked directly to tau levels and it is likely they also had other interacting proteins (data not shown). In addition to further work with the shRNA tau generated stable cell lines, future work would include tau knockout (KO) using a Crisper-Cas9 system; methods using RNAi are only able to KD protein levels by approximately 70%, whereas, gene KO would allow for a more complete understanding of a cells morphology and behaviour without tau expression.

One of the limitations of knocking down tau expression is the possibility of a redundancy of function with other MAPs expressed in the epidermis [75,278,279,334,335]. Although other MAPs, such as MAP2, MAP4, MAP7 and E-MAP-115 are expressed in the epidermis, they are normally involved in the recruitment and polymerisation of microtubules rather than in the stabilisation of microtubules. However, some studies have shown that in other systems when tau or other MAPs are KD, remaining MAPs are able to redistribute and can sometimes rescue or reduce the phenotype of tau knockdown in a small way [87,95].

As demonstrated in this study, a shift in tau expression is observed in differentiated keratinocytes, with a significant increase in the expression of 2N4R isoforms of tau. However, it remained unclear whether the upregulation of tau was due to cytoskeletal changes induced by keratinocyte differentiation, or if the upregulation of tau following the initiation of differentiation had a direct effect on the organisation of the cytoskeletal and cell adhesion network. Therefore, to help investigate what role 2N4R tau had in keratinocyte differentiation and if 2N4R tau alone was able to induce keratinocyte differentiation, a stable tetracycline inducible 2N4R tau overexpression cell line was generated. Throughout this study, doxycycline was used instead of tetracycline; doxycycline is a second-generation tetracycline antibiotic that has a safer pharmacological profile [336]. A limitation of this study was that a stable cell line infected with the empty plasmid vector was not able to be generated in a keratinocyte cell line. Various techniques to infect keratinocyte cell lines with pINDUCER20 were used, but lentiviral infection was not successful and cells never survived antibiotic selection. To overcome this limitation normal cultured keratinocytes, alongside pINDUCER20 tau infected cell lines were used with and without doxycycline treatment to reduce

any unspecific effects, arising from the infection protocol or doxycycline treatment, from being incorrectly correlated.

This study has demonstrated that the overexpression of 2N4R tau promotes terminal differentiation in both 2D and 3D epidermal keratinocytes. In the literature there are vast differences in the effect the overexpression of tau has on cells in other body systems. For example, the overexpression of 2N4R human tau in *Drosophila* a neurodegenerative phenotype is observed [243], 4R tau overexpression in SY5Y cell line can result in a greater susceptibility for cell death [337] and 4R tau expression may be sufficient to induce mitotic delay of cells in larval eyes and brains [214]. The differences between these observations are likely to arise from different cell types being used, with tau playing different roles within each cell line and specific cellular sub-localisation. Although the effects of tau overexpression have not been widely investigated in epidermal keratinocytes, the results of this study are consistent with studies in which microtubules are stabilised inducing accumulation of cell junctions, microtubule distribution to the cortex and the later stages of terminal differentiation are enhanced; promoting epidermal barrier formation [333].

Of course *in vitro* experiments always hold their limitations; not only the lack of three-dimensional phenotypical morphology of the tissue, but also the method of culturing epidermal keratinocytes *in vitro* [316]. The importance of spatial and temporal bio-chemical micro-environmental cues on a tissues ability to function and regenerate is widely recognised, although the mechanisms remain poorly understood [338]. Tissue engineering is a multidisciplinary field that combines the principles of engineering with molecular biology to develop reconstructed biological substitutes *in vitro* to allow for the real time study of tissues and organs [339–343]. Artificial micro-environments are rapidly being developed to help study

these microenvironments *in vitro* in a near physiological fashion. Allowing for an increased understanding of tissue pathologies and enhanced treatment options. Tissue engineering holds great potential to enable insights and advance the study of healthy and malfunctioning tissue development and enhance clinical based approaches to therapies. Most of the healthy skin samples used in Chapter 4 of this study were from older donors, contributing to the necessity to develop and use an *in vitro* skin model generated from younger healthy keratinocyte cells to confirm the tau expression patterning throughout differentiation and stratification. MatTek© is a well-established company that has been developing *in vitro* 3D tissue models for 25 years. MatTek's EpiDerm™ is a patented 3D tissue epidermal model made from human neonatal epidermal keratinocytes cultured in top of tissue culture inserts which has been validated and used in over 374 publications [344–346]. The overexpression of tau within these models displayed a clear and definitive phenotype in which both stratification and differentiation processes were altered, confirming the 2D findings of this study.

Microtubules are defined by their dynamic instability, and many cellular processes depend on this property for their function. When 2N4R tau was overexpressed in keratinocytes, microtubules were observed to reorganise to the cortex, resembling their distribution during keratinocyte differentiation. These are consistent with studies demonstrating that the four MTBDs have a high affinity for microtubules in which polymerisation of microtubules is enhanced, causing the microtubules to become stable structures and their flexibility to be diminished [179,245]. Further investigations into tau:MT interactions will reveal if it is the excessive binding of tau to microtubules that is inducing differentiation in epidermal keratinocytes through MT stabilisation, or alternatively which organelles and pathways tau is interacting with to induce epidermal

differentiation. Previous studies have demonstrated that stabilisation of microtubules is sufficient to prevent the cells from undergoing mitosis by preventing the mitotic spindle from being assembled resulting in cell cycle arrest in phase G1/G2 , consistent with the findings of this current study [179,245,308,333].

This study has also demonstrated that 2N4R tau overexpression significantly increases keratinocyte cell size in both 2D and 3D systems. An increased cell size is consistent with the keratinocyte differentiation that is also induced after tau overexpression in keratinocytes. At this point it is difficult to conclude if the increased cell size was a direct result of this induced cell differentiation or if it is due to the regulation of cell size through actin and microtubule dynamics, but instead required further investigation.

Tau overexpression resulted in changes to the stratification and differentiation profile of epidermal models. Manipulation of tau expression in stratified epitheliums is not widely researched so the results of this study were previously unreported. Increased cellular differentiation in epidermal structures resulted in the increased thickness of the stratum corneum and decrease of living layers. Rete ridges were observed in EpiDerm™ models overexpressing tau, it is likely this is as a result of the increased differentiation of regions of the EpiDerm™ model. The infection and overexpression in this system is not perfect model so could be that some patches have more cells overexpressing tau than others, therefore leading to the formation of these corneal ridges in regions where tau overexpression is highest. The cells within the living layers displayed an altered phenotype, with a tightly packed, elongated shape expressing higher levels of terminal differentiation proteins. Successful stratification requires basal cell proliferation to provide the cells required to form the multi-layered tissue [26,37,347]. In this study, tau overexpression models exhibited high levels of basal cell

proliferation, suggesting that high levels of TACs and possibly the reduction of SC population. Not only could this explain why AD patients have dry and itchy skin [348], but also have important implications in cSCC. It would be interesting to also examine markers of adherens junctions, hemidesmosomes, desmosomes and tight junctions as epidermal differentiation entails a tightly coordinated rearrangement of intracellular junctions to accompany the major changes that take place to the cytoskeletal network of the cells.

The use of 3D epidermal models here, allowed us to overcome some of the limitations associated with the clinical samples from Chapter 4; such as skin from older donors, sun exposure, medications and underlying medical conditions as healthy young keratinocytes used in the generation of the 3D epidermal model. However, 3D *in vitro* skin models also have limitations of their own; the epidermis is actually comprised of a mixed population of cells and interactions with the BM and underlying dermis play a major role in keratinocyte cell fate. Additionally, although the EpiDerm™ model was supplemented with culture medium containing growth factors, the medium used was proprietary so we do not know what growth factors and supplements are contained within the medium. Finally, although the model was a useful tool to establish the functional significance of tau in epidermal stratification and differentiation, the EpiDerm™ model represents epidermal development and formation, not necessarily at the effect of tau overexpression under physiological conditions. It would be interesting in the future to investigate the effect of tau overexpression after the epidermis has been established; as would occur in AD. Another aspect of this work for future studies would be to investigate the effect of an overexpression of other isoforms of tau. 2N4R tau was overexpressed in this study due to it being the primary isoform that is detected in differentiated keratinocytes and we were investigating the effect

that this isoform of tau had on differentiation and why it is upregulated. However, in future studies it would be interesting to overexpress 0N3R transcript variants and other short isoforms to determine if this promoted a SC phenotype and did not induce differentiation in keratinocytes. Finally, although the lentiviral particles carrying the pINDUCER20 tau plasmid were only introduced into models at 3 days submerged, tau overexpression can be observed in the majority of the cells in the EpiDerm™ model. However, it is likely that the plasmid had not been successfully taken up by all epidermal cells within the EpiDerm™ model; one of the limitations of this system. Nevertheless, this could explain why corneal ruffling could be exclusively observed in tau overexpression models resulting from patches of tau overexpressing keratinocytes.

As demonstrated earlier in this chapter a shift in tubulin dynamics is known to accompany keratinocyte differentiation. However, it is still unclear how tau induces keratinocyte differentiation and what its downstream targets are. Proteomic analysis in Chapter 6 will help to identify binding partners and help to define the mechanism in which 2N4R tau overexpression induces keratinocyte differentiation.

4.6. Conclusion

In conclusion, this Chapter has confirmed that that tau displays a distinct expression profile in SC, TACs and differentiated keratinocytes. This chapter has also demonstrated that through alternative splicing and sub-cellular localisation, tau can influence epidermal cell fate and orchestrate keratinocyte differentiation and stratification. Tau is required for the process of terminal differentiation in keratinocytes and overexpression of 2N4R isoforms can stimulate keratinocyte differentiation and stratification in 2D and 3D systems. Taken together, these

results provide an interesting area for further investigation into the mechanisms underpinning tau’s involvement in keratinocyte differentiation and stratification.

5. Identifying binding partners and targets in human epidermal keratinocytes using proteomic analysis

5.1. Introduction

So far, this study has successfully demonstrated the specific expression patterns of tau throughout the epidermis and how these are linked with epidermal differentiation. It has also established how silencing and overexpression of tau can affect the differentiation and stratification programme in keratinocytes. But to date, the exact binding partners of tau have not yet been confirmed. Immunofluorescence staining has shown tau expression and localisation changes between basal and differentiated cells, but the exact protein interactions and binding partners of tau have not yet been confirmed. Protein interactions of tau are of interest because although the expression pattern and functional role of tau in epidermal stratification and differentiation has been established the exact mechanism underlying these changes remains unknown. Determining the proteins that tau interacts with in different phases of cell differentiation, will enable a greater understanding of how and why changes might occur in pathological conditions such as AD or cancer and how this could be mitigated by future therapies.

Chapter 4 demonstrated that in epidermal keratinocytes 2N4R tau overexpression could induce keratinocyte differentiation and changes to the stratification of keratinocytes. However, the mechanisms underpinning this induction of differentiation are not yet completely understood. It is not clear if tau induces differentiation through direct interactions with proteins, or if it has an indirect effect by controlling gene expression of key proteins.

5.2. Chapter aim and objectives

Chapter aim:

To identify tau binding partners and targets in human epidermal keratinocytes.

Chapter objectives:

1. Establish the binding partners of tau in growing and differentiated keratinocyte populations using proteomic analysis.
2. Understand some of the downstream targets of tau following tau overexpression in keratinocytes.

5.3. Methods

5.3.1. Cell culture

The methods used in this chapter involved the use of the cell culture with the HPEKp cell line. HPEKp cells were grown in SC and TAC promoting CnT Prime media or high calcium (1.7 mM) CnT Prime medium, to promote keratinocyte differentiation.

5.3.2. Co-immunoprecipitation

72 h prior to protein extraction HPEKp cells were differentiated using 1.7 mM extracellular calcium. HPEKp were also cultured in CnT prime without calcium as the control population. Following 72 h of differentiation, cells were lysed and CoIP was carried out as described in Methods 2.4.3 using 5.2 µg tau [E178] monoclonal antibody or 5.2 µg rabbit IgG. Samples were collected and subsequently analysed by Western blot and proteomic analysis.

5.3.3. Tau overexpression

To identify up and downregulation of proteins following tau overexpression pINDUCER20 tau, HPEKp cells were cultured in the presence or absence of 100 ng/ml doxycycline to drive 2N4R tau. Total protein was extracted from cells as described in Chapter 2.1.6 and proteomic preparation and analysis was performed.

5.3.4. Proteomic analysis

Proteomic analysis was carried out for both sets of experiments as described in Chapter 2.4.6. Samples were kindly analysed on a mass spectrometry system by Dr Ansgar Poetsch (tau overexpression samples) and Dr Vikram Sharma (CoIP samples).

STRING analysis was carried out to identify potential protein interactions and display a description of a local interactome [349]. The STRING database v11 uses known and predicted protein interactions from a range of sources to identify potential and known direct and indirect associations of a group of proteins. Proteins identified through proteomics were input into the programme and the full interaction network along with the functional enrichment of the network was exported. All interaction sources were used (textmining, neighbourhood, experiments, databases, gene fusion and co-occurance). The edges indicate both functional and physical protein interactions.

5.4. Results

5.4.1. Tau binding partners in growing and differentiated keratinocytes

To identify potential pathways regulated by tau during epidermal differentiation and stratification, co-immunoprecipitation (CoIP) was performed followed by proteomic analysis in protein extracts prepared from cells cultured under growing

(SC/TAC promoting) conditions and differentiation conditions (in which keratinocytes were treated with 1.7 mM Ca^{2+}). Total protein was extracted from cells from the two cell populations and CoIP was carried out using tau [E178] and rabbit IgG as a control. Proteomic sample preparation was subsequently performed and quantitative mass spectrometry allowed the identification of tau binding partners in basal and differentiated conditions.

To first confirm the successful immunoprecipitation of tau, protein analysis of eluate and flow-through fractions were analysed with Western Blot (Figure 5.1). Ponceau S staining of the membrane following the successful transfer of each protein fraction, demonstrated that the eluted fractions had much less protein compared to total and flow-through fractions, but protein could still be visualised within these lanes (Figure 5.1A). Ponceau S stain showed numerous, although faint, bands in eluate; indicating that CoIP successfully retained proteins bound to tau throughout the protocol. The membrane was probed with a tau [E178] antibody and clear strong bands in the tau eluted protein sample in both control and differentiated conditions could be identified (Figure 5.1B). No band was detected in either of the tau flow through fractions, suggesting that the IP of tau was highly efficient. The IgG flow through and eluate had detectable bands comparable to the total lysate protein samples that were loaded as a control. Therefore, to help establish the binding partners and protein interactions of tau in growing and differentiated keratinocyte populations, proteomics analysis of each protein fraction was performed.

Proteomic analysis of the protein fractions from CoIP identified 23 proteins in the IP tau eluate fraction in growing keratinocytes (Figure 5.2 and Figure 10.21), and 11 proteins in the IP tau eluate fraction in differentiated keratinocytes (Figure 5.3

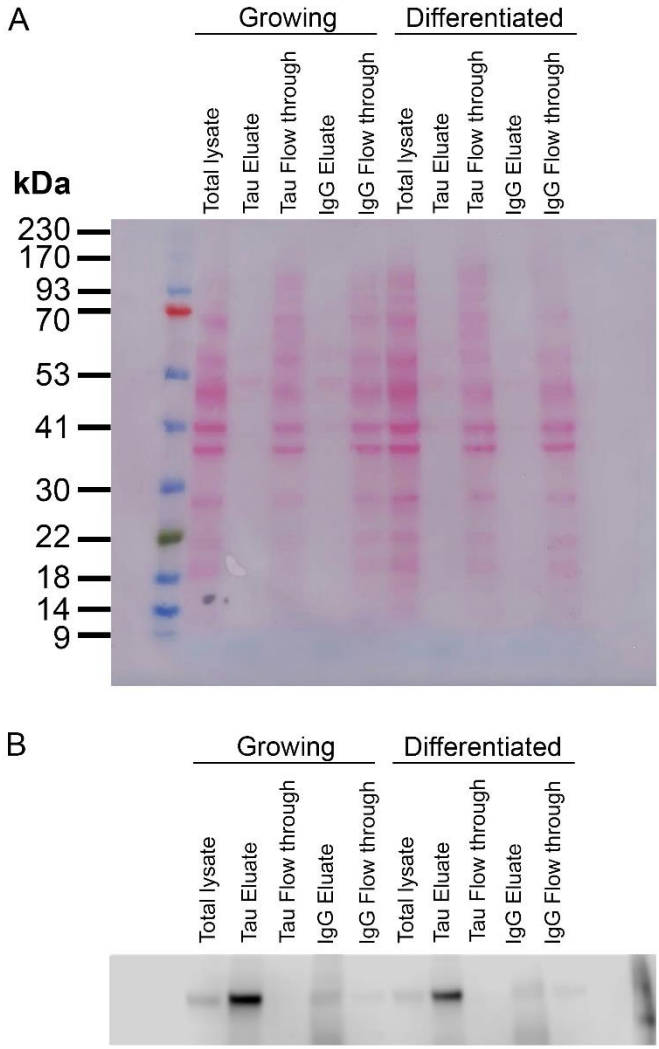

Figure 5.1. Western Blot analysis of control and calcium induced differentiation fragments following co-immunoprecipitation.
A. Representative Ponceau staining of Western Blot membrane of co-immunoprecipitation (CoIP) fractions. Tau [E178] was used to elute tau and rabbit IgG as used as a control in basal and differentiated keratinocyte populations. **B.** Representative western blot analysis of tau in each fraction obtained through CoIP (n=2). Strong, clear bands in the tau eluted fraction were identified in both growing and differentiated conditions, no bands were detected in the flow through fraction. Whereas IgG flow-through and eluate showed low insignificant levels of tau in both fractions.

and Figure 10.22). The binding proteins identified under growing conditions had a diverse subcellular distribution and range of function, however STRING analysis revealed 50 edges compared to the expected number of 17 edges; significantly more interactions than expected for a random set of proteins of a similar size. Hemidesmosome assembly, cytoskeleton organisation and cell adhesion were some of the biological processes and molecular functions highlighted in the binding partners of growing keratinocytes (Figure 10.21). Interestingly, most binding proteins identified in differentiated keratinocytes were localised with the membrane. STRING analysis revealed 19 edges compared to the 1 expected edge, meaning that the network had significantly more interactions than expected for a random set of proteins of a similar size. Hemidesmosome assembly, cytoskeleton organisation and cell adhesion were some of the biological processes and molecular functions that were identified in the binding partners of differentiated keratinocytes (Figure 10.22).

Three proteins were found to consistently bind to tau in both growing and differentiated keratinocytes: plectin, laminin subunit-α3 and laminin subunit-β3 (Figure 5.2 and Figure 5.3). Immunofluorescence analysis of plectin expression in keratinocytes showed that in control cells plectin was asymmetrically distributed to the cells cortex (Figure 5.4A). However, following tau KD plectin polarisation is lost and instead plectin is expressed throughout the cell cortex (Figure 5.4B and C). Further investigation is needed to determine how tau KD prevents asymmetrical plectin distribution and its wider impacts on cell polarity, migration and consequently epidermal stratification.

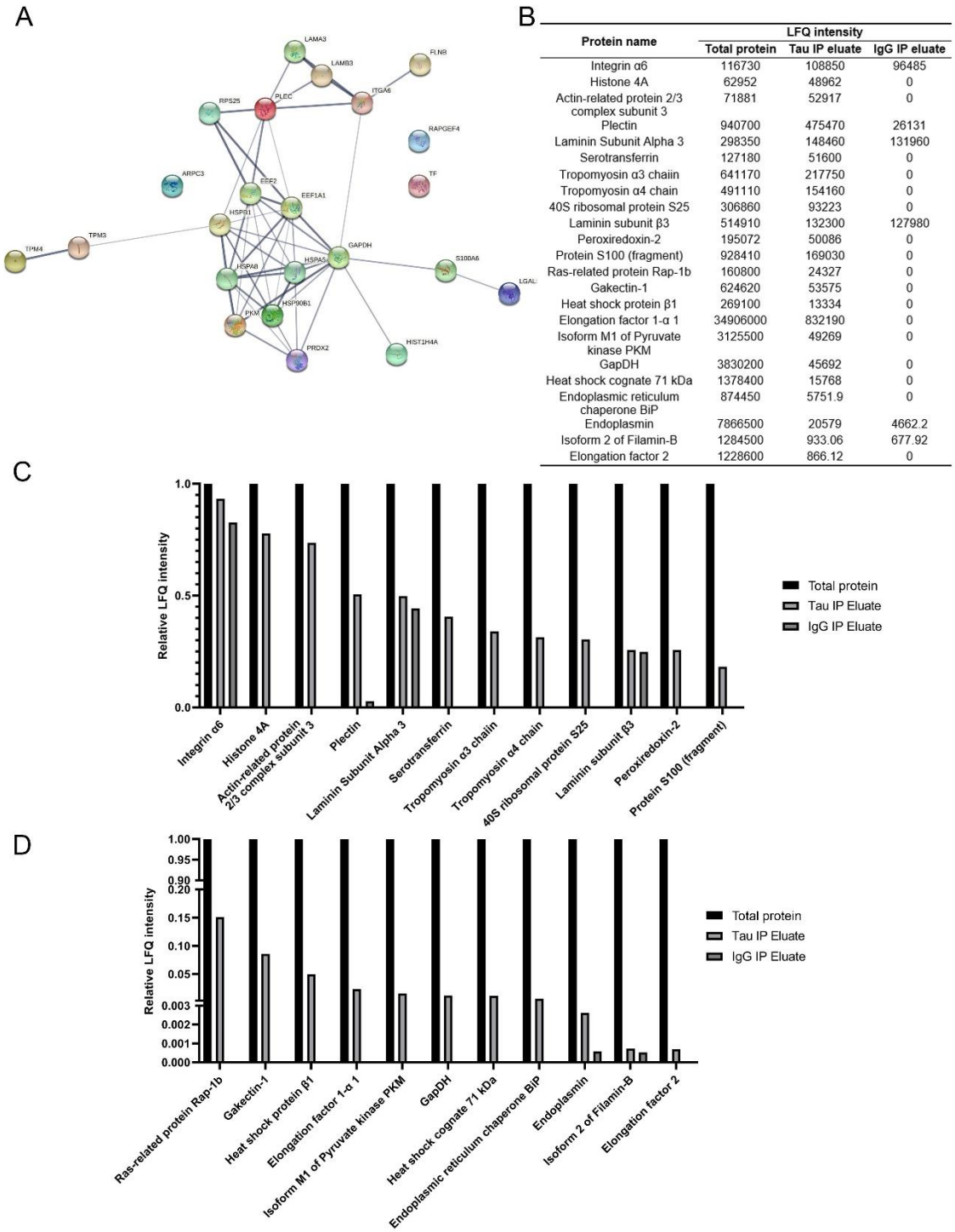

B

Protein name	LFQ intensity		
	Total protein	Tau IP eluate	IgG IP eluate
Integrin α6	116730	108850	96485
Histone 4A	62952	48962	0
Actin-related protein 2/3 complex subunit 3	71881	52917	0
Plectin	940700	475470	26131
Laminin Subunit Alpha 3	298350	148460	131960
Serotransferrin	127180	51600	0
Tropomyosin α3 chaiin	641170	217750	0
Tropomyosin α4 chain	491110	154160	0
40S ribosomal protein S25	306860	93223	0
Laminin subunit β3	514910	132300	127980
Peroxiredoxin-2	195072	50086	0
Protein S100 (fragment)	928410	169030	0
Ras-related protein Rap-1b	160800	24327	0
Gakectin-1	624620	53575	0
Heat shock protein β1	269100	13334	0
Elongation factor 1-α 1	34906000	832190	0
Isoform M1 of Pyruvate kinase PKM	3125500	49269	0
GapDH	3830200	45692	0
Heat shock cognate 71 kDa	1378400	15768	0
Endoplasmic reticulum chaperone BiP	874450	5751.9	0
Endoplasmin	7866500	20579	4662.2
Isoform 2 of Filamin-B	1284500	933.06	677.92
Elongation factor 2	1228600	866.12	0

Figure 5.2. Tau interacting proteins in growing keratinocytes.
Proteomic analysis of eluted tau IP fraction of HPEKp cells identified 23 binding partners of tau in keratinocytes cultured under growing culture conditions. Culture medium was used to promote SC and TAC keratinocyte populations and all results were normalised to eluted fraction of rabbit IgG control (n=1). **A.** STRING analysis of tau binding proteins under growing conditions. The network edges are shown through the thickness of the line between nodes which indicates the strength of the supporting data. **B.** Table of raw label-free quantitation (LFQ) intensity values from proteomic analysis in the total protein, tau eluate and IgG eluate protein fractions. **C&D.** Relative LFQ intensity of tau binding proteins compared to total protein fraction and IgG IP eluate.

A

Protein name	LFQ intensity		
	Total protein	Tau IP eluate	IgG IP eluate
Cathepsin	132250	89091	0
Plectin	1404900	888670	0
Myosin-9	1740200	1023700	770590
Myosin regulatory light chain 12A	297560	139990	0
Isoform Short of Laminin Subunit-γ2	436330	52652	0
Integrin β4	331020	15312	0
Laminin subunit-α3	387300	15886	0
Desmoplakin	723630	26878	0
Laminin subunit-β3	475050	17219	0
Neuroblast differentiation-associated protein	2737000	3083.5	0
Annexin A2	6298824	993.1	0

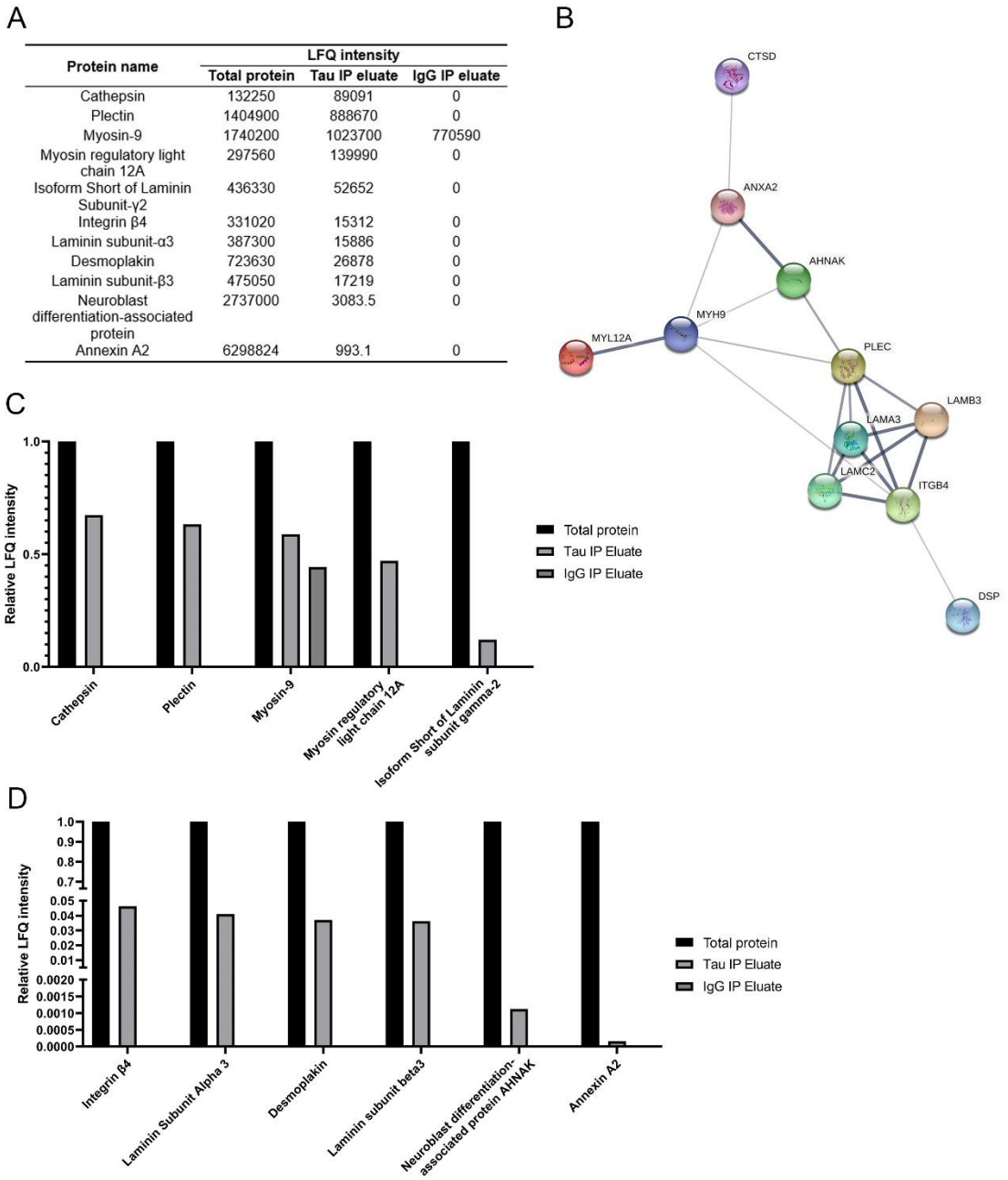

Figure 5.3. Tau interacting proteins in differentiating keratinocytes.
Proteomic analysis of eluted tau IP fraction of HPEKp cells identified 11 binding partners of tau in differentiated keratinocytes cultured in high calcium culture conditions. Culture medium was used to differentiate keratinocyte populations for 72 h and all results were normalised to eluted fraction of rabbit IgG control (n=1). **A.** STRING analysis of tau binding proteins under differentiating cell culture conditions. The network edges are shown through the thickness of the line between nodes which indicates the strength of the supporting data. **B.** Table of raw label-free quantitation (LFQ) intensity values from proteomic analysis in the total protein, tau eluate and IgG eluate protein fractions. **C&D.** Relative LFQ intensity of tau binding proteins compared to total protein fraction and IgG IP eluate.

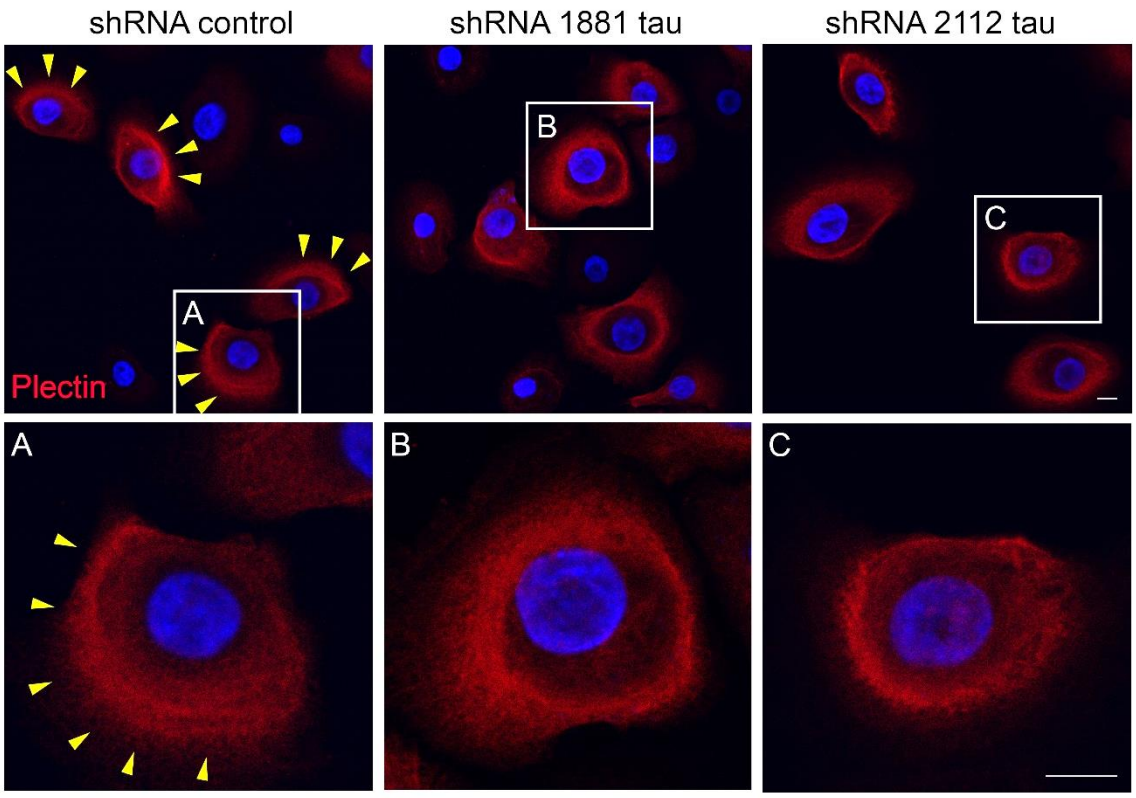

Figure 5.4. Disturbance of plectin distribution following tau knockdown in epidermal keratinocytes.
Representative immunofluorescence analysis of plectin (red) in epidermal keratinocytes following tau knockdown (n=3). **A.** shRNA control cells cultured under growing conditions display an asymmetrical distribution of plectin to the cells cortex. **B.** shRNA tau 1881 under growing conditions the asymmetrical plectin distribution is lost. **C.** shRNA tau 2112 under growing cell culture conditions plectin asymmetrical distribution is lost and is instead found throughout the cell cortex. Yellow arrows indicate the asymmetrical distribution of plectin. Nuclei counterstained with DAPI (blue). Scale bar 10 µm.

5.4.2. Proteomic analysis of epidermal keratinocytes following tau overexpression

Chapter 5 demonstrated that an overexpression of the 2N4R isoform of tau could promote differentiation and stratification in epidermal keratinocytes, however the exact mechanism was not determined. Therefore, one of the aims of this chapter was to discover if tau indirectly affects the transcription of proteins associated with the phenotype observed from tau overexpression or whether tau interacts directly with its downstream targets. Consequently, proteomic analysis of the cells proteome following tau overexpression was carried out. 2N4R tau overexpression was induced in epidermal keratinocytes, using the pINDUCER20 tau infected HPEKp cells, and overexpression was induced through addition of doxycycline to cell culture medium for 72 h. Total protein was extracted from cells, proteomic sample preparation was carried out and quantitative mass spectrometry allowed the identification of proteins up and downregulated following tau overexpression.

343 proteins were identified to be significantly upregulated following tau overexpression and 535 significantly downregulated proteins. STRING analysis of the downregulated protein list revealed 3778 edges in comparison to the expected number of 2162 edges, which meant the network had significantly more interactions than expected for a random set of proteins of a similar size. STRING analysis identified a significant decrease in proteins involved in peptidyl-cysteine oxidisation, mitochondrial translational and translational termination biological processes following tau overexpression in keratinocytes (Figure 5.5 and Figure 5.6). Biological process peptidyl-cysteine oxidation was identified as significant as 3 out of 4 proteins in network were downregulated (Figure 5.6); Coiled-Coil-Helix-Coiled-Coil-Helix Domain Containing 4 (CHCHD4), Peroxiredoxin 3 (PRDX3) and Parkinsonism Associated Deglycase (PARK7).

A

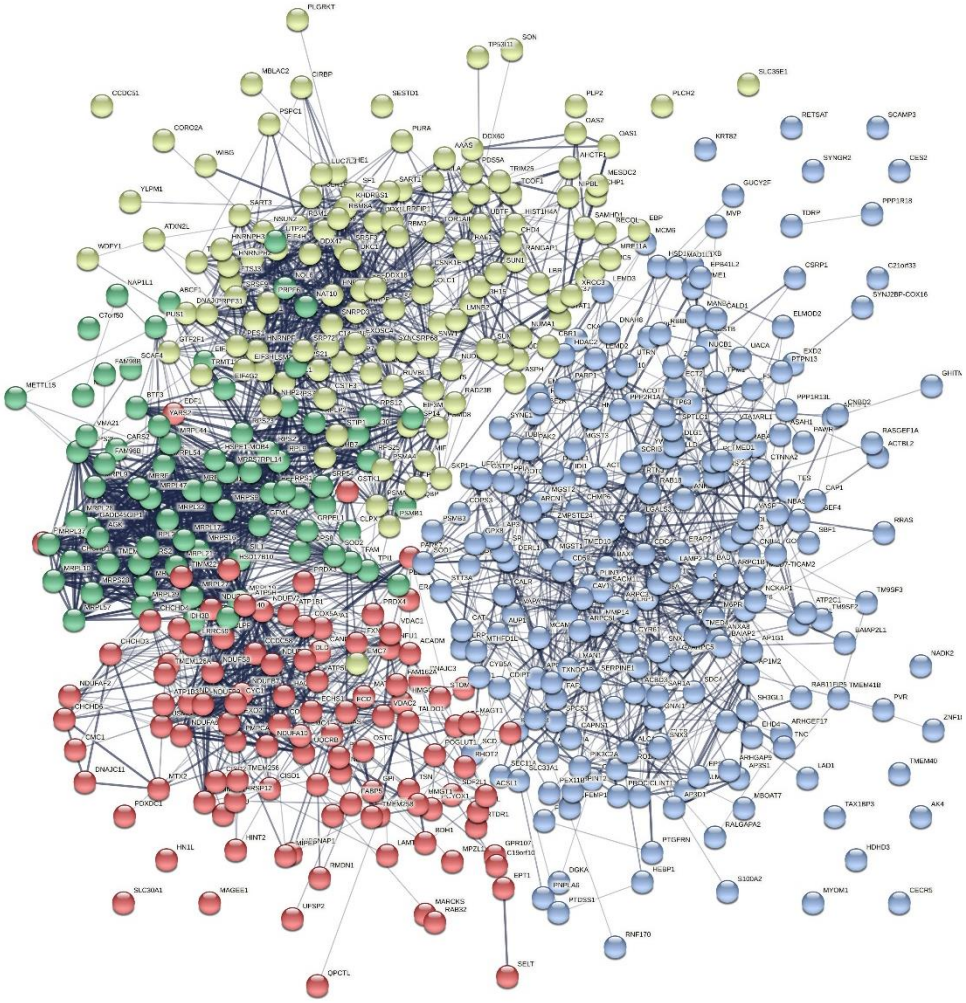

B

Biological Process (Gene Ontology)

GO-term	description	count in network	strength	false discovery rate
GO:0018171	peptidyl-cysteine oxidation	3 of 4	1.44	0.0436
GO:0070125	mitochondrial translational elongation	26 of 90	1.02	2.21e-14
GO:0070126	mitochondrial translational termination	26 of 91	1.02	2.52e-14
GO:0006415	translational termination	27 of 99	1.0	1.92e-14
GO:0032543	mitochondrial translation	29 of 114	0.97	7.52e-15

Molecular Function (Gene Ontology)

GO-term	description	count in network	strength	false discovery rate
GO:0032050	clathrin heavy chain binding	4 of 8	1.26	0.0373
GO:0004602	glutathione peroxidase activity	6 of 20	1.04	0.0102
GO:0016684	oxidoreductase activity, acting on peroxide as acceptor	10 of 45	0.91	0.00061
GO:0004601	peroxidase activity	9 of 41	0.9	0.0019
GO:0003735	structural constituent of ribosome	31 of 159	0.85	8.78e-13

Cellular Component (Gene Ontology)

GO-term	description	count in network	strength	false discovery rate
GO:0031429	box H/ACA snoRNP complex	3 of 5	1.34	0.0186
GO:0005786	signal recognition particle, endoplasmic reticulum targeting	3 of 6	1.26	0.0258
GO:0005885	Arp2/3 protein complex	4 of 11	1.12	0.0115
GO:0005762	mitochondrial large ribosomal subunit	18 of 56	1.07	4.22e-11
GO:0001401	SAM complex	4 of 13	1.05	0.0180

Figure 5.5. STRING analysis of protein downregulation following tau overexpression

A. Diagram of the protein interactions between 535 differentially expressed proteins retrieved from STRING analysis. The colour of the nodes represents the 4 clusters the dotted line represents the edges between clusters. Disconnected nodes or proteins with no known interactions around the edge. The network edges are shown through the thickness of the line between nodes which indicates the strength of the supporting data. STRING analysis of the downregulated protein list revealed 3778 edges in comparison to the expected number of 2162 edges, which meant the network had significantly more interactions than

expected for a random set of proteins of a similar size. **B.** Biological processes, molecular function and cellular compartments identified by STRING analysis to be upregulated following tau overexpression in epidermal keratinocytes. Peptidyl-cysteine oxidation biological process with 3 out of 4 proteins in network downregulated.

STRING analysis of the upregulated protein list revealed 1669 edges in comparison to the expected number of 1000 edges, which meant the network had significantly more interactions than expected for a random set of proteins of a similar size (Figure 5.7). STRING analysis identified five out of nine proteins associated with lysosomal lumen acidification were upregulated following tau overexpression (Figure 5.8); ATPase H+ transporting accessory protein 2 (ATP6AP2), progranulin (GRN), SNARE-associated protein (SNAPIN), palmitoyl-protein thioesterase 1 (PPT1) and chloride voltage gated-channel 5 (CLN5). 22 proteins associated with cadherin binding and 33 proteins associated with cell adhesion binding were also identified to be upregulated following tau overexpression (Figure 5.9); laminin Subunit Alpha 5 (LAMA5), desmoglein 2 (DSG2) and integrin-αV (ITGAV) were a few of the upregulated proteins.

Upregulation of cell adhesion proteins was consistent with the differentiated phenotype observed in this study following tau expression. Proteins associated with nuclear cap binding complex were also identified through from proteomics (Figure 5.7); nuclear cap-binding protein subunit 1 (NCBP1) and nuclear cap-binding protein subunit 2 (NCBP2). Validation of a sample of the proteins highlighted via proteomic analysis, demonstrated that there was a general increase in the relative expression of most proteins identified through proteomics. Interestingly however, there was no significant change in transcription of the proteins snapin and granulin following tau overexpression (Figure 5.10); suggesting that tau is having direct effect on protein rather than an indirect effect on the proteins via transcriptional regulation. Therefore, validation at a protein level was carried out. Using Western blotting it was confirmed that granulin protein levels were increased following tau overexpression in keratinocytes compared to control conditions (Figure 5.11).

A

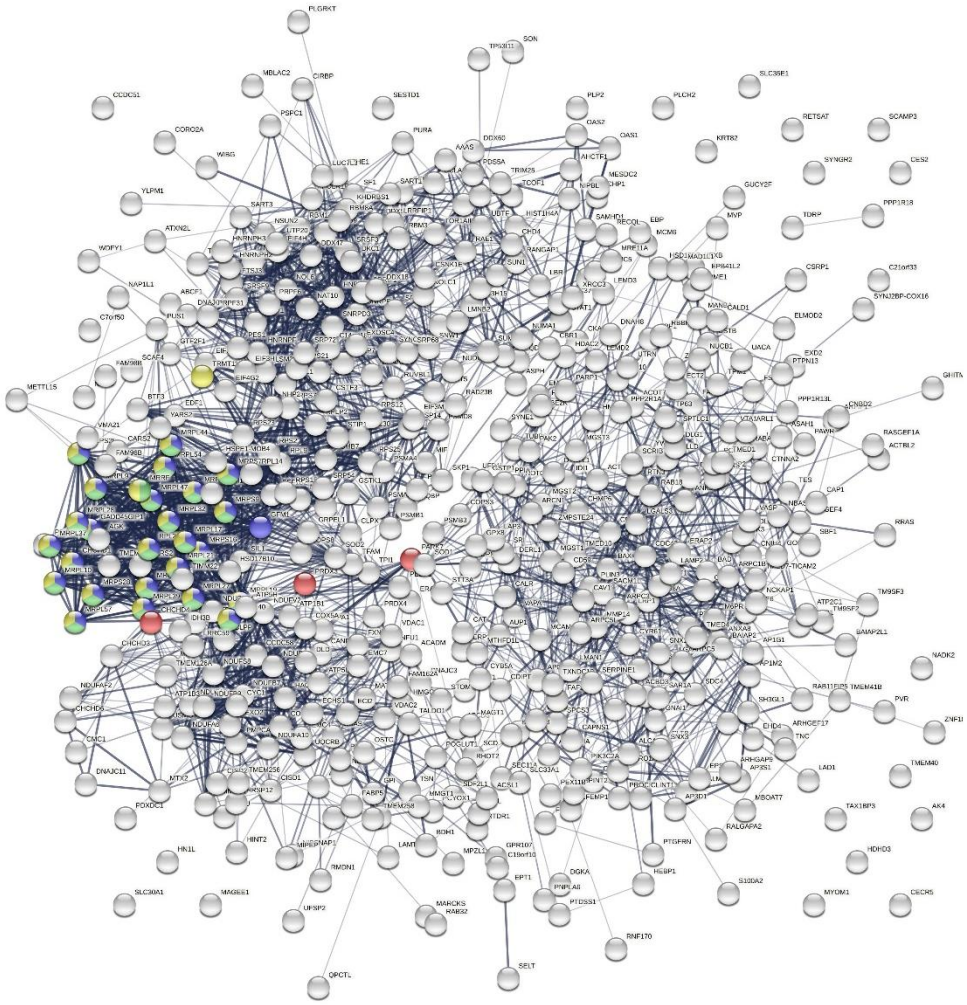

B

Biological Process (Gene Ontology)				
GO-term	*description*	*count in network*	*strength*	*false discovery rate*
GO:0018171	peptidyl-cysteine oxidation	3 of 4	1.44	0.0436
GO:0070125	mitochondrial translational elongation	26 of 90	1.02	2.21e-14
GO:0070126	mitochondrial translational termination	26 of 91	1.02	2.52e-14
GO:0006415	translational termination	27 of 99	1.0	1.92e-14
GO:0032543	mitochondrial translation	29 of 114	0.97	7.52e-15

Figure 5.6. STRING analysis of protein downregulation identifying proteins involved in peptidyl-cysteine oxidisation, mitochondrial translational and translational termination biological processes.
Peptidyl-cysteine oxidation biological process with 3 out of 4 proteins in network down (red); Coiled-Coil-Helix-Coiled-Coil-Helix Domain Containing 4 (CHCHD4), Peroxiredoxin 3 (PRDX3) and Parkinsonism Associated Deglycase (PARK7). Mitochondrial translational elongation (blue), mitochondrial translational termination (green) and translational termination (yellow) were some of the other biological processes highlighted by STRING analysis.

To investigate the expression of granulin and snapin in the epidermis under physiological conditions, RT q-PCR and immunofluorescence analysis was carried out. There was a significant increase in most genes associated with lysosomal lumen acidification in differentiated keratinocytes (Figure 10.23). Little change to nuclear cap binding complex genes was identified, but a significant decrease in genes associated with peptidyl-cysteine oxidation was observed (Figure 10.23). Immunofluorescence analysis of granulin and snapin in healthy human skin showed that granulin is broadly expressed throughout the epidermis (data not shown). Snapin expression was strongest in the granular layer of the epidermis where it was localised primarily to the nuclear and perinuclear regions, but low levels of snapin could be identified in the cytoplasm of basal and suprabasal cells in the epidermis.

A

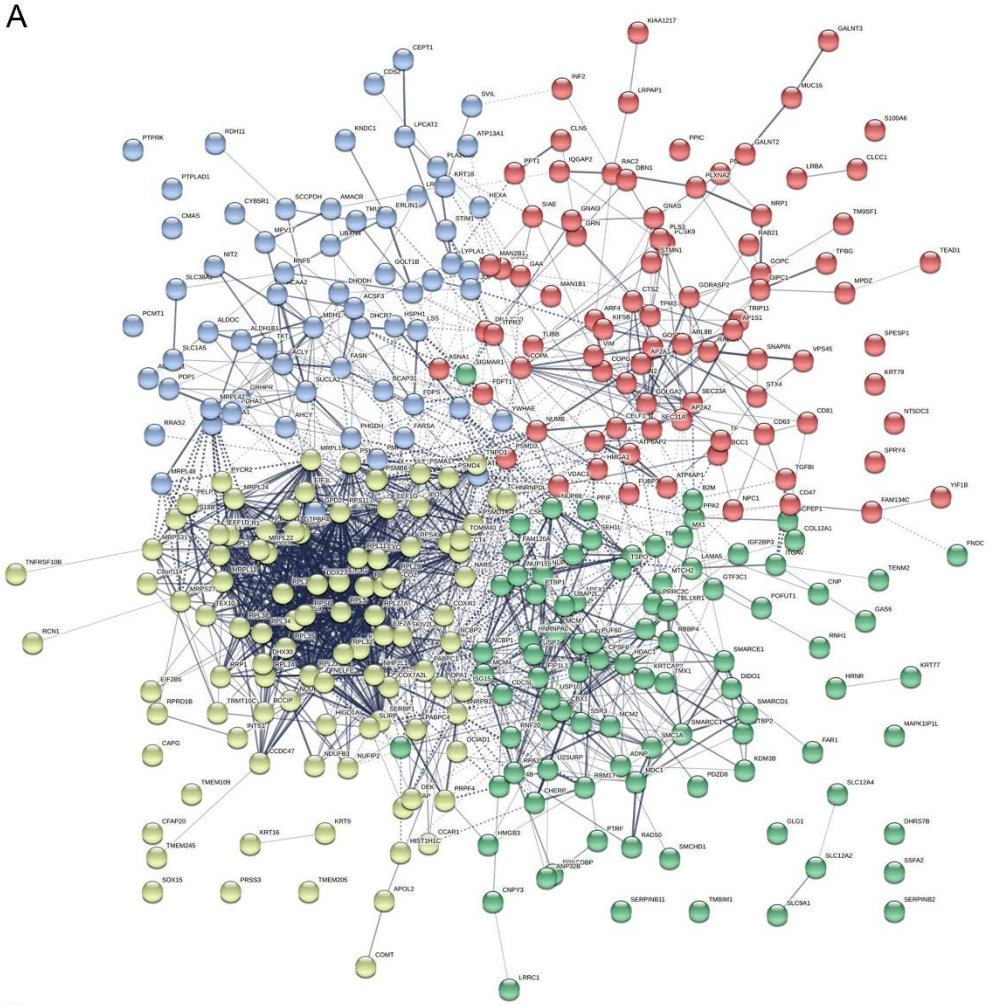

B

Biological Process (Gene Ontology)

GO-term	description	count in network	strength	false discovery rate
GO:0007042	lysosomal lumen acidification	5 of 9	1.5	0.00043
GO:0006267	pre-replicative complex assembly involved in nuclear cell cy...	3 of 7	1.39	0.0399
GO:0008611	ether lipid biosynthetic process	4 of 12	1.28	0.0127
GO:0098789	pre-mRNA cleavage required for polyadenylation	4 of 13	1.24	0.0157
GO:0006268	DNA unwinding involved in DNA replication	4 of 15	1.18	0.0220

Molecular Function (Gene Ontology)

GO-term	description	count in network	strength	false discovery rate
GO:0003735	structural constituent of ribosome	24 of 159	0.94	3.04e-11
GO:0003723	RNA binding	107 of 1649	0.57	6.72e-29
GO:0005198	structural molecule activity	41 of 635	0.57	4.51e-09
GO:0045296	cadherin binding	22 of 334	0.57	0.00016
GO:0003729	mRNA binding	17 of 289	0.53	0.0131

Cellular Component (Gene Ontology)

GO-term	description	count in network	strength	false discovery rate
GO:0042555	MCM complex	3 of 9	1.28	0.0271
GO:0031080	nuclear pore outer ring	3 of 9	1.28	0.0271
GO:0071564	npBAF complex	3 of 12	1.15	0.0481
GO:0005838	proteasome regulatory particle	4 of 20	1.06	0.0200
GO:0022625	cytosolic large ribosomal subunit	11 of 56	1.05	1.33e-06

Figure 5.7. STRING analysis of protein upregulation following tau overexpression.

A. Diagram of the protein interactions between 343 differentially expressed proteins retrieved from STRING analysis. The colour of the nodes represents the 4 clusters the dotted line represents the edges between clusters. Disconnected nodes or proteins with no known interactions around the edge. The network edges are shown through the thickness of the line between nodes which indicates the strength of the supporting data. STRING analysis of the upregulated protein list revealed 1669 edges in comparison to the expected number of 1000 edges,

which meant the network had significantly more interactions than expected for a random set of proteins of a similar size. **B.** Biological processes, molecular function and cellular compartments identified by STRING analysis to be upregulated following tau overexpression in epidermal keratinocytes. 5 out of 9 proteins associated with lysosomal lumen acidification were found upregulated following tau overexpression. Proteins associated with cadherin binding and cell adhesion binding were upregulated following tau overexpression. 22 of 334 cadherin binding proteins upregulated. Cadherin upregulation is consistent with differentiated phenotype that has been observed in keratinocytes throughout as desmosomal and cadherin proteins are increased following keratinocyte differentiation.

A

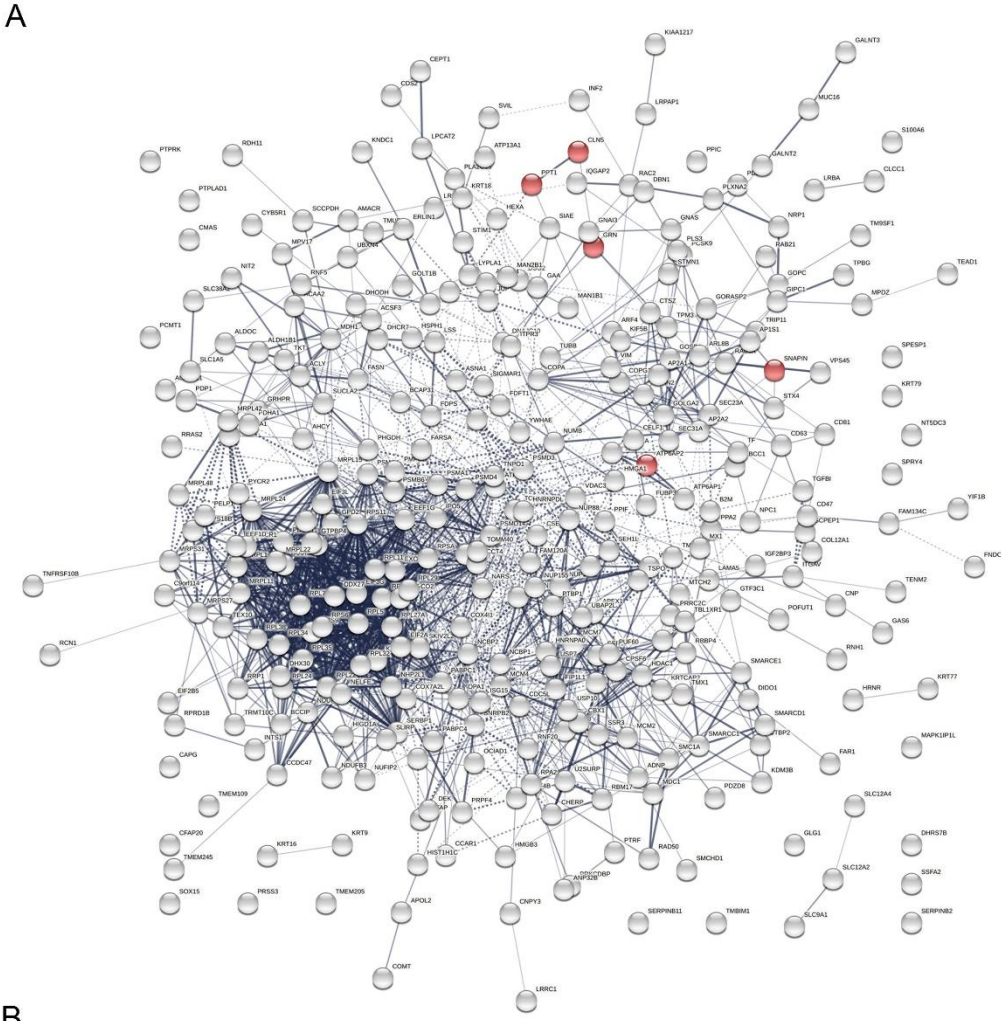

B

Biological Process (Gene Ontology)

GO-term	description	count in network	strength	false discovery rate
GO:0007042	lysosomal lumen acidification	5 of 9	1.5	0.00043
GO:0006267	pre-replicative complex assembly involved in nuclear cell cy...	3 of 7	1.39	0.0399
GO:0008611	ether lipid biosynthetic process	4 of 12	1.28	0.0127
GO:0098789	pre-mRNA cleavage required for polyadenylation	4 of 13	1.24	0.0157
GO:0006268	DNA unwinding involved in DNA replication	4 of 15	1.18	0.0220

Figure 5.8. STRING analysis of the upregulation of lysosomal lumen acidification proteins upregulated following tau overexpression.
5 out of 9 proteins associated with lysosomal lumen acidification were found upregulated following tau overexpression; ATPase H+ transporting accessory protein 2 (ATP6AP2), Progranulin (GRN), SNARE-associated protein (SNAPIN), palmitoyl-protein thioesterase 1 (PPT1) and chloride voltage gated-channel 5 (CLN5).

A

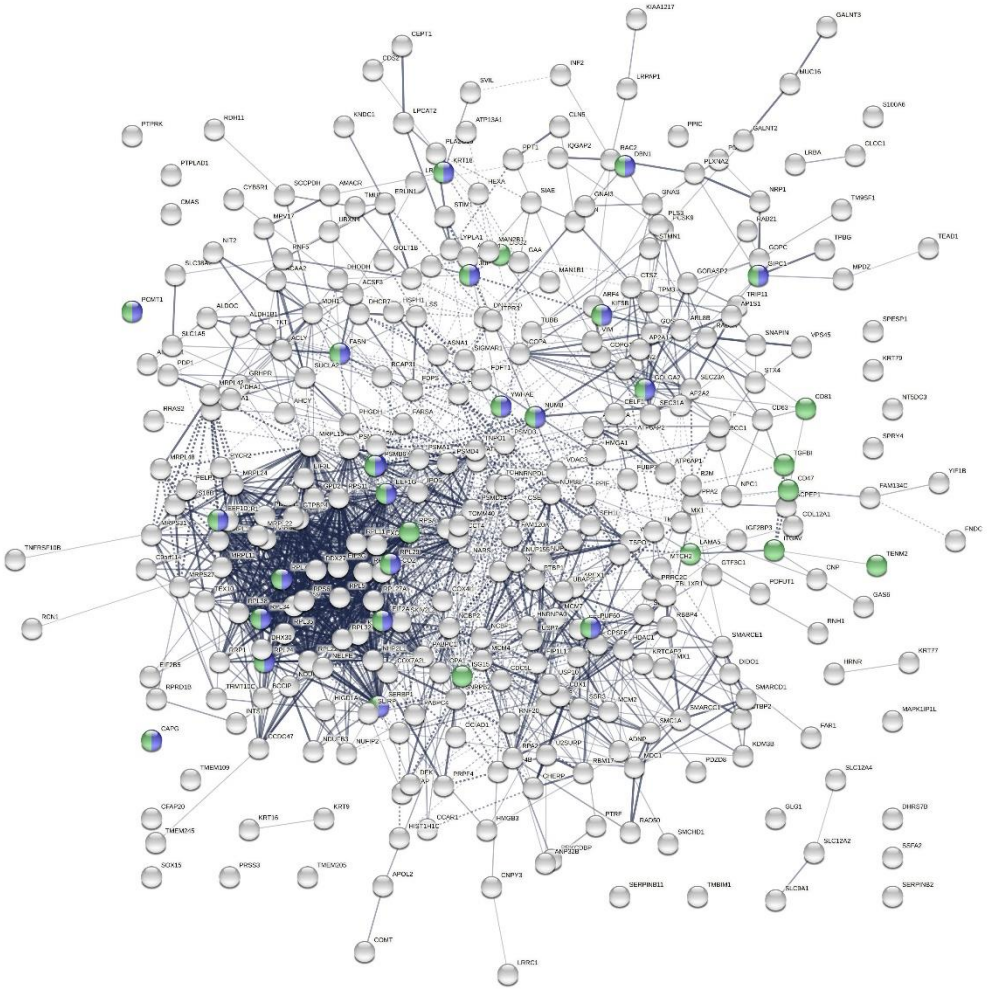

B

Molecular Function (Gene Ontology)

GO-term	description	count in network	strength	false discovery rate
GO:0003735	structural constituent of ribosome	24 of 159	0.94	3.04e-11
GO:0003723	RNA binding	107 of 1649	0.57	6.72e-29
GO:0005198	structural molecule activity	41 of 635	0.57	4.51e-09
GO:0045296	cadherin binding	22 of 334	0.57	0.00016
GO:0003729	mRNA binding	17 of 289	0.53	0.0131
GO:0050839	cell adhesion molecule binding	31 of 538	0.52	1.32e-05
GO:0003676	nucleic acid binding	123 of 3947	0.25	2.00e-08
GO:0097159	organic cyclic compound binding	165 of 5916	0.2	6.55e-09
GO:1901363	heterocyclic compound binding	160 of 5831	0.19	5.13e-08
GO:0005488	binding	265 of 12516	0.08	6.35e-05

Figure 5.9. STRING analysis of the upregulation of cadherin and cell adhesion binding proteins following tau overexpression.
Proteins associated with cadherin binding and cell adhesion binding were upregulated following tau overexpression. Cadherin upregulation is consistent with differentiated phenotype that has been observed in keratinocytes throughout as desmosomal and cadherin proteins are increased following keratinocyte differentiation; laminin subunit α5 (LAMA5), desmoglein 2 (DSG2) and integrin-αV (ITGAV).

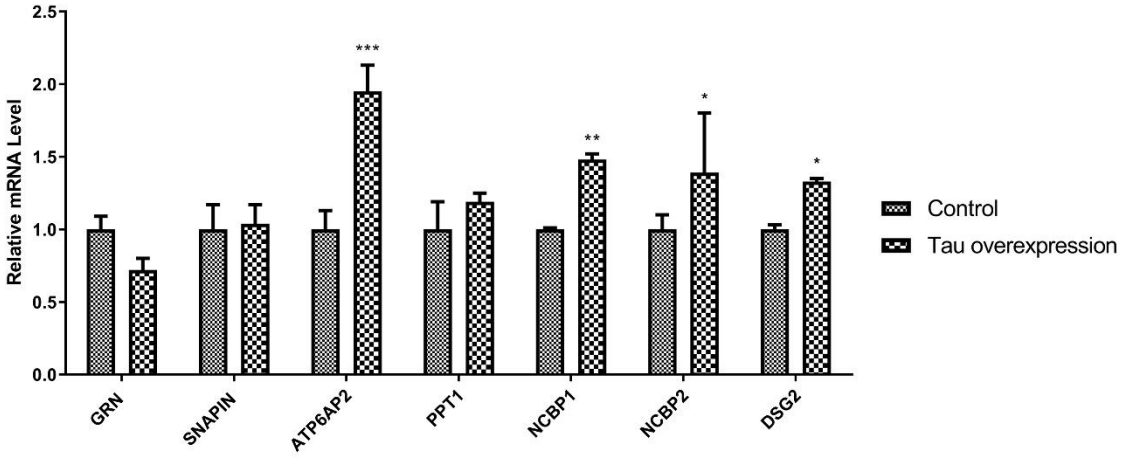

Figure 5.10. Gene expression of lysosomal acidification, nuclear cap-binding and cadherin binding proteins identified through proteomics to be upregulated following tau overexpression in keratinocytes.
Representative RT q-PCR analysis of the relative gene expression of proteins identified upregulated during proteomic analysis. Ct values normalised to 36B4 and $2^{-\Delta\Delta Ct}$ method of analysis used. Relative expression levels are displayed as mean ± SD (n=3). Two-way ANOVA with Bonferroni correction was used to test significance; *p<0.05, ** p<0.01, *** p<0.001.

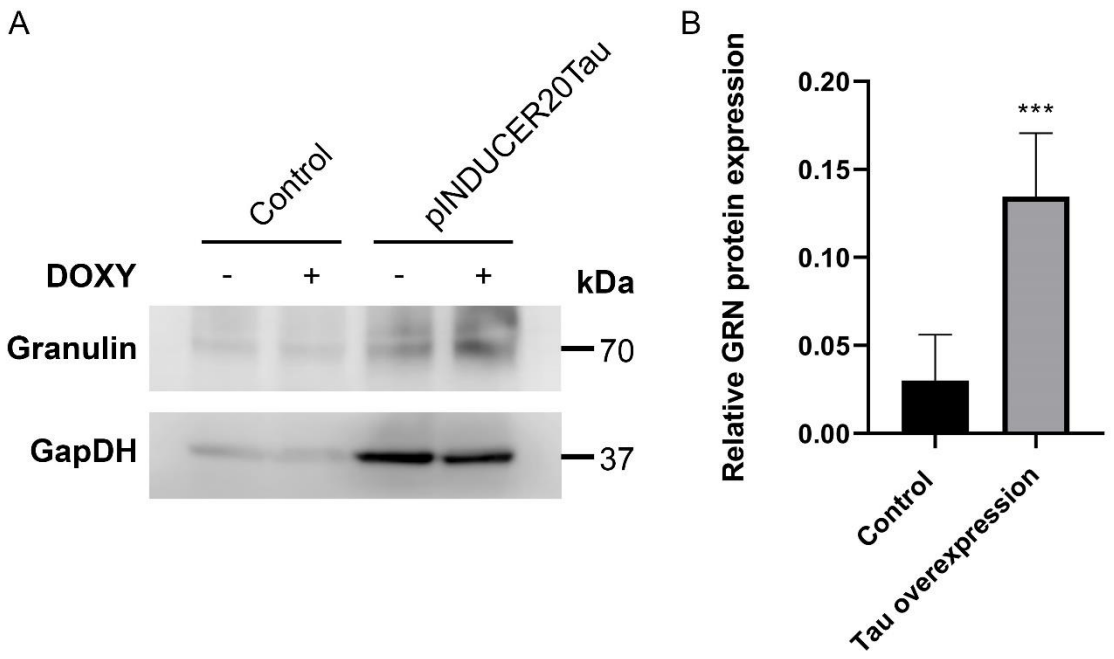

Figure 5.11. Keratinocytes present with increased lysosomal lumen acidification protein, granulin, following tau overexpression.
Proteomic analysis identified lysosomal lumen acidification proteins to be upregulated following tau overexpression in keratinocytes. RT q-PCR analysis did not identify any of the expression of the proteins to be upregulated, however following Western blot analysis granulin (GRN) was identified to be higher in the keratinocytes overexpressing tau to the controls. Indicating that tau is likely to interact directly with granulin rather than an indirect transcriptional control of the protein. **A.** Western blot analysis of granulin expression following tau overexpression in HEKn cells. **B.** Quantification of the relative expression of granulin protein following tau overexpression. Each condition was normalised to its control to reduce any variation observed through infection and doxycycline treatment.

5.5. Discussion

This chapter has successfully demonstrated that tau interacts with a number of proteins involved in cytoskeletal organisation and cell adhesion. Additionally, it has proven that the binding partners of tau shift following keratinocyte differentiation. Finally, proteomic analysis of keratinocytes following tau overexpression identified several downstream targets of tau, some of which may be linked to the final stages of autophagy; lysosomal lumen acidification.

Proteomic analysis allowed the identification of a discrete pattern of tau interactions under growing and differentiation conditions. Under growing conditions, a number of tau binding partners with a nuclear, cytoplasmic and membrane localisation were identified, whilst under differentiated conditions tau interacting proteins were mostly found to associate with the plasma membrane. Although there were a number of interactions that were transient, some were consistent throughout both growing and differentiated keratinocyte populations. Tau interactions with 3 hemidesmosome and desmosome associated proteins were consistent through both keratinocyte cell populations; laminin-α3, laminin-β4 and plectin.

Epidermal cell fate entails a tightly coordinated process involving the rearrangement of intracellular junctions and cytoskeletal changes [22,23,61]. Plectin is a linker protein which is crucial for anchoring the IF network to hemidesmosomes and desmosomes [67,69,70,82,350]; plectin deficiency in the epidermis leads to skin blistering diseases [69]. Plectin has also been shown to play a role in the crosstalk with the actin and microtubule network [69,351–353] and act not only as a linker, but can also be involved in regulating the dynamics of the filamentous networks; however, the exact mechanisms of this regulation remain

unknown. A few studies have reported some interaction of MAPs and plectin [351,354], but no study had previously linked plectin and tau interactions within hemidesmosome and desmosome architecture and homeostasis of the epidermis. The binding of tau to hemidesmosome structures is consistent with the observations in chapter 4, in which tau was found to be localised to the basal surface of basal cells in contact with the BM in the suprapapillary plate. Furthermore, the involvement of tau in cell attachment explains why tau KD cells were so difficult to culture and often displayed an altered morphology. Tau interacting directly with hemidesmosome and desmosome associated proteins is consistent with the decreased cortex rearrangement of MT and IF networks in chapter 5 when tau is KD in epidermal keratinocytes; providing more evidence that tau helps to regulate cell adhesion and epidermal cell fate through its interaction with hemidesmosome and desmosomal proteins. Investigation into plectin expression found that under growing conditions plectin is symmetrically polarised to the membrane, however, tau KD cells lost their plectin polarisation, suggesting that tau directly influences not only interactions between cytoskeletal components and hemidesmosome/desmosomal structures but also the formation of hemidesmosome/desmosomal complexes at the membrane. Strikingly, in chapter 5 it was demonstrated that in growing keratinocytes tau expression is also asymmetrically polarised with the MTOC. However more research is needed to determine how tau KD prevents plectin polarisation and the functional significance of this finding. Further investigation will enable us to determine if this loss of polarity is due to a lack of microtubule and keratin filament recruitment to cell junctions at the cell cortex by tau and the implications this might have on epidermal migration, stratification and wound healing [328].

Laminin-α3, laminin-β4 are both components of laminin 332 which is secreted by epidermal keratinocytes and is a critical component of the BM and forms a major part of hemidesmosomes in cell adhesion [67,350,355]. In addition to cell adhesion, laminins have also been shown to influence cell migration and cell differentiation [63]. The identification of laminin proteins in the eluted fraction could be as a consequence of the strong interactions the hemidesmosome complexes; they might not be directly bound to the tau protein but eluted in the eluate fraction through their string bonds to the hemidesmosome complex. Additionally, although normally in physiological conditions keratinocytes would lose hemidesmosome adhesions following differentiation, the interaction laminin in both growing and differentiated keratinocytes *in vitro* might be that because cells are adhered to a surface as even differentiated keratinocytes still express hemidesmosome markers. Whereas, under physiological conditions, differentiated keratinocytes would have detached from the BM and migrated upwards through the layers of the epidermis towards the surface of the skin.

In the growing population of keratinocytes 23 proteins were identified to bind to tau. The proteins had a varied sub-localisation consistent with where tau has been identified in keratinocytes; nuclear (histone proteins, heat shock proteins), cytoplasmic (actin binding proteins, filamin B, ribosomal proteins, RAS RAP-1B, elongation factors, GAPDH) and membrane (integrin-α6, plectin, laminins, galectin-1, RAS related protein Rap-1b).

There are previous publications showing tau interactions with histone proteins [356] and heat shock proteins [357,358]. The binding of tau to histone proteins is consistent with the observed localisation of tau in the nucleus of keratinocytes. An unexpected binding partner of tau that was identified in growing keratinocytes was GAPDH. GAPDH is an important enzyme within energy metabolism and is

required for ATP synthesis through anaerobic glycolysis in the cytoplasm [359,360]. Although there are not many reports demonstrating that tau interacts directly with GAPDH, there are some reports suggesting some interaction between the two proteins in other systems within the body [359,360], but very little detail of the mechanism or function of these interactions have been identified. It has been demonstrated that within the hippocampus of patients with AD GAPDH co-localises with tau in NFTs and immunoprecipitated with PHF-tau [360]. Studies have suggested that in its native conformation tau might act as a chaperone or anti-chaperone and influence the denaturisation and reactivation of GAPDH *in vitro* [359]. However, to the best of our knowledge this is the first study showing tau might interact with GAPDH in epidermal keratinocytes and further investigation will be needed to elucidate the functional significance of this interaction.

The identification of actin as a binding partner of tau in growing keratinocytes is consistent with reports in the literature. The reports of tau interactions with actin are shown to occur through its PRD [181,231,324]. Actin is a key player in cell migration and polarisation [111]; consistent with the asymmetrical distribution of tau to the leading edge of the cells cortex with the MTOC that was observed in Chapter 4. In line with the identification of actin as a binding partner of tau in growing keratinocytes Filamin B was also identified. Filamin B is a cytoplasmic protein involved in cellular communication through the crosslinking of actin and linking the cytoskeleton to the cell membrane [78,86,109,361] and has been shown to play an important role in development [361]. Additionally, RAS related protein Rap-1b is known to regulate multiple cellular processes within cells, this protein localises to the cell membrane and is involved in integrin mediated signalling [362]. Although there are no supporting publications demonstrating a direct interaction between

tau and filamin B or Rap-1b, their cellular functions are consistent with other reported tau binding partners and other proteins identified within this study.

One of the limitations of this experiment is that the binding partners of tau have been identified in a mixed population of growing keratinocytes; this mixed population will consist of SC, TACs and some cells which are likely to have committed to terminal differentiation. However, because both CoIP methods and proteomic analysis require a high starting protein concentration to ensure proteins present will be detected, CoIP of tau on fractioned keratinocyte populations (SCs, TACs) has not yet been possible. Rather it will be a future avenue for investigation. It will also be interesting to investigate if the binding partners of tau change within sub-populations of growing keratinocytes and how this might be linked to the cells function and to the maintenance of epidermal homeostasis.

Both populations had interactions with integrins, but interestingly, in the growing keratinocyte conditions integrin-α6 was identified as binding partner, whilst in differentiated conditions integrin-β4 was identified as a binding partner of tau. This is intriguing as integrins are heterodimers and integrin-α6 and integrinβ4 interact with each other to become critical components of hemidesmosomes; it appears that they were independently identified as binding partners in growing and differentiated keratinocyte populations. The functional significance of this shift in tau binding requires further investigation.

In differentiating keratinocyte populations, consistent with the findings in Chapters 3 and 4 of this study, a different localisation profile of tau binding partners was observed, with most binding proteins associated with the plasma membrane and cytoplasmic fraction of the cells. The identification of myosin-9

and -10 are consistent with the findings in the previous Chapters, in which tau expression was found to be upregulated during cell division and cytokinesis and play a role in determining cell shape. Additionally, neuroblast differentiation-associated protein is a component of desmosomes, consistent with the identification of desmoplakin as a binding partner of tau in differentiating keratinocytes and tau's role in cell-cell adhesion. Interesting, in the differentiated population cathepsin was identified as a binding partner of tau. Cathepsins are acid proteases involved in protein degradation within lysosomes [363], consistent with the downstream lysosomal lumen acidification target proteins of tau identified in this chapter. Taken together, analysis of the tau interactome under growing and differentiated conditions, suggests that tau can regulate keratinocyte entry into differentiation and the balance between keratinocyte proliferation and differentiation through regulation of cell adhesion networks. The findings also suggest tau has a functional significance in influencing epidermal cell fate.

Interestingly, tubulin was not identified in the eluted fraction of CoIP in growing or differentiating keratinocytes. The microtubule network is the largest constituent of the cytoskeleton and the lack of tubulin in the IP fraction could be as a result of the size of the tubulin network preventing tubulin from staying bound throughout the protocol. Additionally, some tau interactions may be too transient, or not as tightly bound, in turn not detected with this method. In the literature, most tubulin:tau interactions are conducted using tubulin for IP and identifying tau in the eluted fraction. For the purposes of this study and considering the limited time frame, this experiment would not have enabled the identification of all of the binding partners of tau. However, future work will include the use of tubulin for CoIP and other methods to investigate tau:tubulin interactions in keratinocytes; such as proximity ligation assays and SEM with immunogold to stain tau to

identify subcellular localisation and organelle interactions in more detail. Another consideration of this study to be aware of are the limitations of calcium differentiation. Although high extracellular calcium levels are a good method to mimic and induce a terminal differentiation phenotype *in vitro* [84,322,332], an increased calcium level only, is not sufficient to completely mimic terminal differentiation in keratinocytes; as in 2D systems stratification cannot occur.

This chapter successfully identified several downstream targets of tau linked to lysosomal lumen acidification, cadherin binding and cell adhesion binding, nuclear cap binding complex. Most of the proteins identified in these biological pathways were also shown to increase in transcriptional level, suggesting that tau had an indirect effect on the proteins through their transcriptional control. The expression of cell adhesion and cadherin binding proteins, laminin's, desmoglein and integrin's, were significantly upregulated following tau overexpression, consistent with binding partners. Plectin was also identified in proteomic analysis to be upregulated following tau overexpression, but just below the threshold applied to detect significant upregulation of proteins. The transcription of lysosomal lumen acidification proteins on the other hand were not upregulated in keratinocytes following tau overexpression, suggesting that tau might be interacting directly with lysosomal lumen acidification proteins. Preliminary validation supported this hypothesis, as granulin protein levels were significantly increased following tau overexpression.

Autophagy is Greek for *self* (auto) *eating* (phagy), and is a highly conserved mechanism used by cells as a response to cellular stress. It is a catabolic process that allows the cell to recycle organelle and protein components through encapsulation and subsequent lysosomal degradation [364]. Lysosomal lumen acidification is a stage in the final phases of autophagy in which the lysosomal

cargo gets degraded [365]. Autophagy is well characterised as an integral pathway in the formation of the granular layer of the epidermis [332,366–368]. Although in differentiated keratinocytes an increase in the transcription of lysosomal lumen acidification proteins was shown, in tau overexpressing keratinocytes, this early increase in the levels of granulin protein without an increase in the transcription, indicated that tau is likely to have a direct effect on the protein. Consistent with the findings of this study, recent publications have suggested that lysosomal lumen acidification is more dynamic than previously thought and that lysosomal pH might actually be dynamically regulated in some cell types [365].

Granulin and snapin were two of the proteins identified to be increased through direct interactions between tau and granulin and snapin, rather than indirect effects through transcriptional regulation. Granulin is a large glycoprotein encoded by *PGRN* gene located on 17q21 that encodes a 68.5 kDa protein which has been linked to various cellular processes [369]. Granulin is highly expressed in epithelial cells and studies have suggested a role for granulin in regulating protein homeostasis via the lysosomal pathway in epithelial proliferation, wound healing and cancer [370]. Additionally, granulin and snapin expression are increased in many neurodegenerative diseases, including AD [369,371]. Although granulin and snapin were not identified as binding partners of tau with CoIP, cathepsins were identified in the differentiated tau IP elate, consistent with protein binding partners involved in lysosomal lumen acidification during keratinocyte differentiation. In line with the findings of this chapter, in which is it suggested that tau might play a role in lysosomal regulation, studies have demonstrated that tau is an unusually stable protein at extremely acidic solutions [372]. Additionally, microtubules are well characterised to act as scaffolds and control the localisation of lysosomes within a cell [172]; which correlates with the identification of big tau within keratinocytes in

this study, known to increase microtubule spacing in cells to enable more efficient transport of cargo along microtubules [330].

Taken together, the results suggest that tau might play a stabilising role for a selection of proteins associated with lysosomal lumen acidification during stages of terminal differentiation. Future work could include proteomic analysis of tau overexpression with CoIP to identify the binding partners following tau overexpression, comparing to both growing and differentiated keratinocytes. Additionally, further investigations into the exact mechanisms of interaction are still required, as are the mechanisms underpinning tau's regulation of lysosomal acidification during keratinocyte differentiation and its implications in disease.

5.6. Conclusions

In conclusion this chapter uncovers a specific subset of tau binding partners in keratinocytes, which are linked to their cell status and provides evidence for downstream targets of tau in epidermal differentiation and stratification. Biochemically, plectin and other cell adhesion proteins were shown to interact directly with immunoprecipitated tau *in vitro.* Future research into tau's intracellular interactome, including how tau contributes to hemidesmosome and desmosome structure and function, and subsequently its significance in epidermal cell fate, is an exciting avenue for further exploration.

6. Exploring tau expression and function in cutaneous squamous cell carcinoma

6.1. Introduction

This study has demonstrated that tau is involved in the differentiation of the epidermis under physiological conditions, however cancer is known to be a disease lacking cell differentiation and tau expression and function in cSCC is so far unknown. Studying the mechanisms that counteract, at tissue levels, the growth of aberrant cells during the early stages of cancer are of high interest in the cancer field and are likely to have translational implications. Therefore, one of the objectives of this chapter was to manipulate tau expression patterns in SCC cell line and analyse if the overexpression of tau is sufficient to induce the differentiation of SCC cells, therefore suggesting a translational application of tau in the treatment of cSCC.

6.1.1. A431 cells

The A431 cell line was developed in 1973 as part of a series of cell lines in established from solid tumours by D. J. Giard *et al.* [373]; the A431 cell line was derived from an epidermoid carcinoma of the vulva taken from an 85 year old female. The cell line is reported as hypertriploid, with a modal chromosome number of 74 and 1% of cells possessing higher ploidies. Sequencing showed that A431 cells have 1,405 deletions, 27% of the is genome amplified and only 2% lost [315]. The cell line is negative for HPV [374], has high numbers of epidermal growth factor receptors (EGFR) and displays incomplete differentiation [375]. The cell line is often used to investigate proliferation and apoptosis and to date there are 4,566 publications of studies using this cell line.

Tumour protein 53 (*TP53*) is the most common mutated tumour suppressor gene in patients with cSCC and most *TP53* mutations arise from a single base mutation C → T at dipyrimidine sites [57,118,134]. A431 cells have a missense mutation in exon 8 of the p53 gene codon 273, whereby the pathogenic variant substitutes 818G>A (CGT>CAT) resulting in a change of an arginine to a histidine, Arg273His (R273H), at the protein level [376].

6.1.2. Cancer Stem Cells

In the early growth of skin tumours, cancer cells form a neoplastic lesion embedded in the epithelium, usually separated from the surrounding tissue by the BM; this is called carcinoma *in situ* [377]. Tumours consist of a heterogeneous population of cancer cells with distinct phenotypic states and differing functional attributes. Within this heterogeneity, there is a population of cancer stem cells (CSCs). CSCs are tumour cells that possess the principle properties of self-renewal, tumour initiation capacity and long-term population potential [13,159,342,378]. They have the ability to transition between SC and non-SC states and are able to evade cell death and metastasise through their ability to stay dormant for long periods of time [16,159,342,379]. CSCs reside in niches and respond to cues from its tumour microenvironment (TME), which includes the stroma and surrounding epithelium [159,380,381]. Generally, CSCs are resistant to conventional therapies, as they are usually designed to target hyper-proliferating cells in which CSCs evade through their quiescence [382].

One of the limitations in skin research is that there is no reliable SC marker for both healthy human skin and SCC. However, recently CD80 has been shown to be a promising marker of CSCs in cSCC. Miao *et al.* (2019) showed a population of tSCs could be characterised through their expression of integrin-α^{6+}, $TGFb^{+}$,

SOX2^{+}, SOX9^{+} and CD80^{+} [383]; introducing the idea that CD80 could be used in cSCC to identify tSCs.

6.1.3. Cancer and cell adhesion

The interaction between tumour cells and their ECM and basement are key in understanding tumorigenesis, as most tumours show an increased cell-matrix adhesion. Adhesion to the BM plays an integral role in tumour invasion and subsequently metastasis. Cell adhesion molecules, such as E-cadherin and its associated proteins are involved in cancer pathology. In healthy cells catenin proteins bind to E-cadherin on the cell surface membrane to anchor the cells cytoskeleton forming adhesion junctions [81,100]. However, in SCC and other cancers there is a reduction in the expression of E-cadherin and its associated proteins, leading to loss of cell-cell junctions therefore enabling increased cell motility, often associated with increased proliferation, migration and consequently invasion and metastasis [162]. Chapter 4 and 5 identified that tau played a role in cell-ECM and cell-cell adhesion in keratinocytes, however, the expression and function of tau in cSCCs is currently unknown.

6.2. Chapter aim and objectives

Chapter aim:

Characterise tau expression and function in cutaneous squamous cell carcinoma.

Chapter objectives:

1. Explore the subcellular location of tau and identify any changes throughout regions of cSCC.
2. Investigate the functional significance of tau in cSCC.
3. Evaluate the translational potential of finings for clinical applications.

6.3. Methods

6.3.1. Clinical samples

The methods used in this chapter involve the use of human SCC and BCC samples generously provided by Dr Emmanuella Guenova-Hötzenecker from the Dermatological Bio-bank (EK 647). Full details of donor consent, tissue collection, diagnosis and local ethical approval are outlined in Chapter 2.2. Diagnosis of patient biopsies was carried out by dermatologists at the University Hospital Zurich after initial collection as a standard procedure. Staining of SCC samples allowed the characterisation of tumour sample morphology and sample integrity following tissue processing to be analysed; two samples displaying poor tissue integrity were identified and excluded from the study. NMSC samples were taken from both male and female patients, from a range of anatomical locations (Table 10.10). However, many of the biopsies are from common sites of SCC formation; usually in sun exposed locations such as the lower leg or head. The age of patients used in this study ranged between 42 - 97 years old. No information on Fitzpatrick skin type, or medical background was provided with any of the samples used in this study.

Tau expression in clinical samples was analysed at an RNA and protein level. First, using *in situ* hybridisation with isolation of regions of interest using LCM and subsequent RT q-PCR (Methods 2.3).

6.3.2. Cell culture

The methods used in this chapter involve the cell culture of the A431 cell line. The A431 cells were subjected to esiRNA knockdown of *MAPT,* as described in methods 2.1.7. Validation of successful tau knockdown was performed via RT q-

PCR, Western blotting and immunofluorescence. A431 cells were infected with pINDUCER20 and pINDUCER20 tau, as described in methods 2.1.6 to overexpress 2N4R isoform of tau. Cells were selected using 800 µg/ml G418. 2N4R tau overexpression was induced through doxycycline treatment in cell culture medium for at least 48 h of pINDUCER20 tau infected A431 cells. Validation of 2N4R tau overexpression was confirmed by RT q-PCR, immunofluorescence and Western blotting. A431 cells were infected with the lentiviral particles containing the Ki67p FUCCI plasmid as described in methods 2.1.5. Infected cells were selected after 48 h using 7.5 µg/ml blasticidin. FUCCI infection was confirmed by visualising cells under a Leica SP8 confocal microscope and confirming expression of mCherry (red) and mAg (green).

6.4. Results

6.4.1. Clinical sample analysis reveals different expression profile of tau in squamous cell carcinoma

6.4.1.1. Characterisation of squamous cell carcinoma clinical samples

H&E staining of SCC patient biopsies highlighted, as expected, the vast differences in SCC presentation between patient samples. However, all SCC samples used in this study presented with full-thickness, atypical keratinocytes (Figure 6.1). High magnification images revealed large, packed abnormal keratinocytes with hyperchromatic nuclei extending throughout the epidermis (Figure 6.1B and E). All samples displayed acanthosis (a thickening of the epithelium) with large, disorganised dysplastic keratinocytes and some evidence of mitosis taking place in the suprabasal layers (Figure 6.1B); immunofluorescence staining of proliferation markers shown later in this chapter enabled the confirmation of this. Most biopsies presented with a hyper-cellular

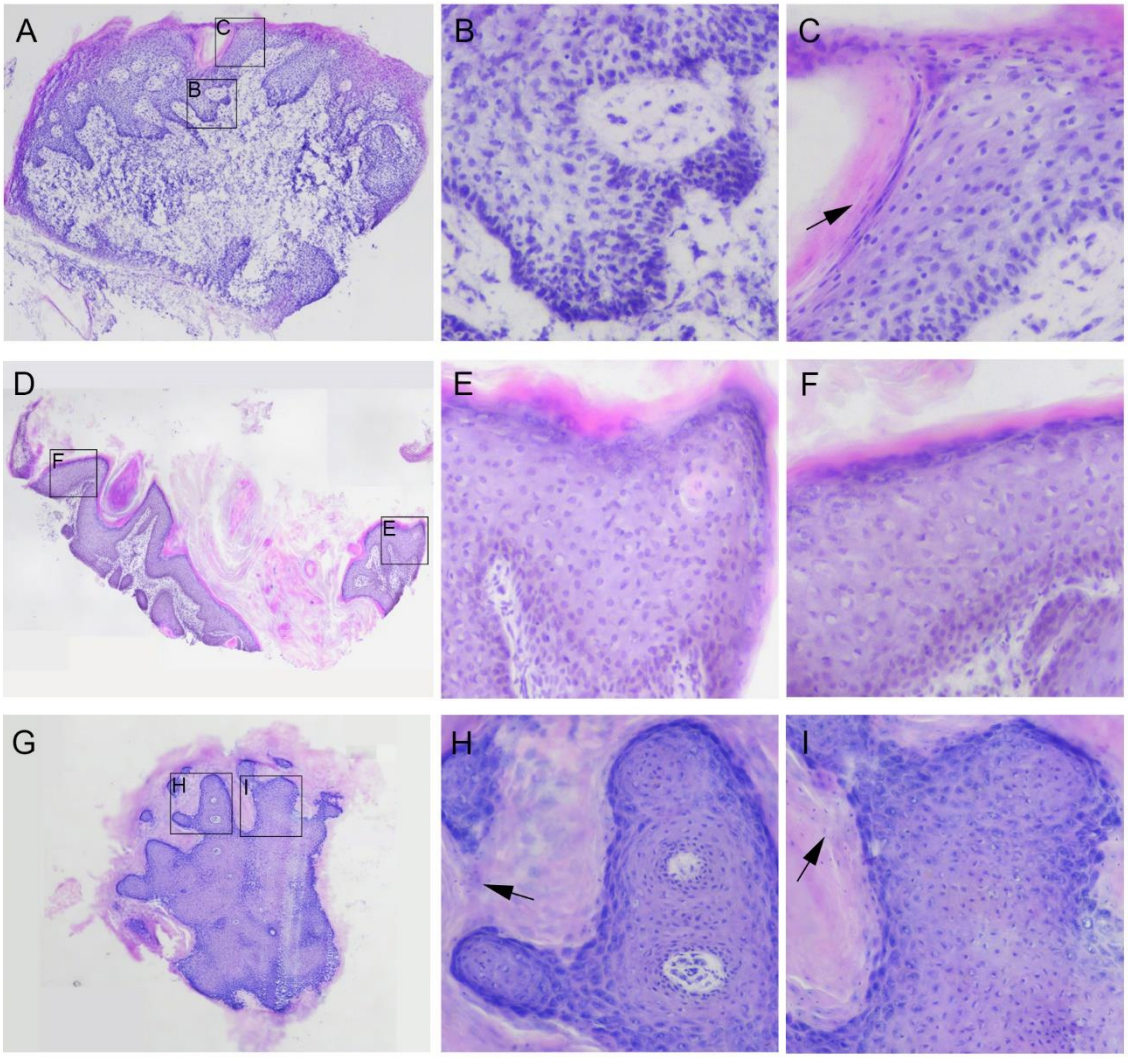

Figure 6.1.Haematoxylin and Eosin staining of squamous cell carcinoma samples used in this study.
Representative H&E staining of cryofrozen SCC samples used in this study (n=5). All samples displayed acanthosis and full thickness dysplasia, with large abnormal nuclei. Nuclei were retained in the corneal layer in nearly all SCC samples. Parakeratosis and pagetoid spread were common features of SCC samples. **A.** Patient 19 SCC biopsy from male forehead, a common sun-exposed location for SCC presentation. **B.** High magnification image of Patient 19 biopsy reveals a highly packed, disorganised cluster of cells in the basal layer. **C.** High magnification images of the suprabasal region of patient 19 biopsy revealed retained nuclei in the stratum corneum (as indicated by arrows) and lack of a granular layer. **D.** Patient 18 SCC biopsy from female head, a common sun-exposed location for SCC formation. **E&F.** High magnification images of patient 18 biopsy revealed highly packed and disorganised basal cells with mitosis occurring in the suprabasal region of the tumour. Patient 18 showed pagetoid spread, where abnormal keratinocytes could be located in the epithelium away from the main body of the tumour. **G.** Patient 17 SCC biopsy from female lower leg, one of the most common locations of SCC formation in females. **H&I.** High magnification images of patient 17 biopsy revealed retained nuclei in the corneal layer. Small pockets of stroma can be identified scattered throughout the biopsy.

dense band of parakeratosis (Figure 6.1D and G), and all biopsies lacked an obvious granular layer. Pagetoid spread could be observed in some biopsies, with abnormal cells found away from the main tumour and found scattered and spread up into the adjacent epidermis (Figure 6.1F). This was not observed in all biopsies, as some samples were only from the lesion and lacked much of a surrounding stroma or adjacent epithelium (Figure 6.1G). The histological presentation of SCCs varied from dark blue to glassy pink depending on the lesion, as demonstrated in Figure 6.1. Keratinocytes appeared with a glassy phenotype, due to the larger, proliferative spinous layer found in SCCs containing K1/K10; immunofluorescence staining, and experiments later in this chapter helped to confirm this.

Some tissue processing artefacts could be observed in some samples whereby gaps formed around the nucleus of some keratinocytes (Figure 6.1C and F). These gaps sometimes formed after processing due to the strong cadherin and desmosomal links to the IFs in keratinocytes. Therefore a vacuole formed between the cytoplasm and the nucleus in keratinocytes, a phenomenon that is not observed in other cells in the epidermis (melanocytes or Langerhans cells). Interestingly, all SCC samples used in this study showed a significant decrease in melanin throughout the epidermis, compared to the melanin expression that was observed in healthy samples in Chapter 3.

All samples used in this study were SCC *in situ,* however it is often difficult to diagnose invasive SCC and the diagnosis tends to be SCC *in situ* at least, as tangential cutting can sometimes make it look like invasion; depending on how the sample has been sectioned, islands of keratinocytes might be observed in the dermis, but these can sometimes be associated with sebaceous glands or with hair follicles and it is just the way the section is cut that makes it look like invasive

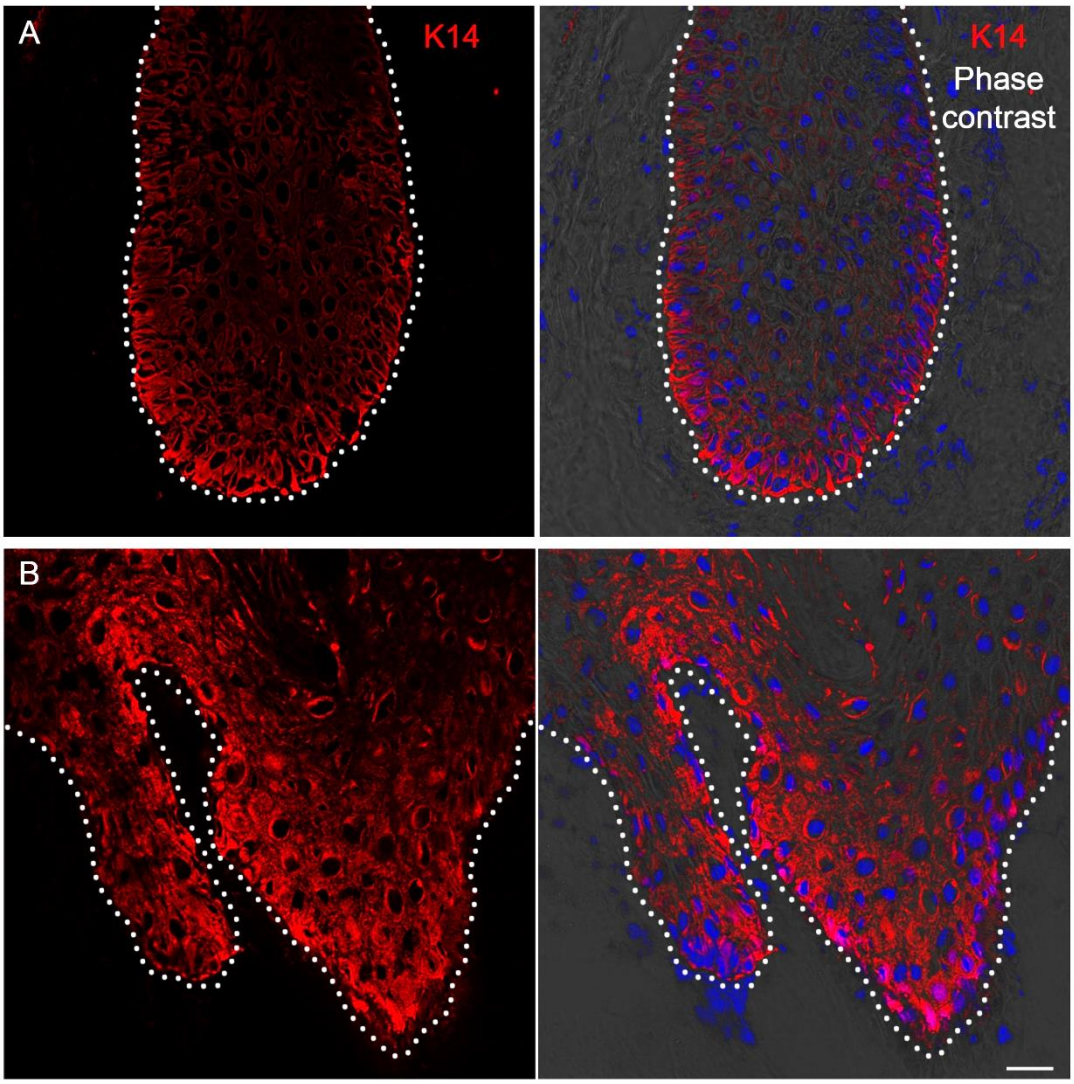

Figure 6.2. Immunoflurescence analysis of keratin-14 expression in cutaneous squamous cell carcinoma samples.
Representative immunofluorescence staining of cytokeratin-14 (K14) (red) in SCC samples (n= 5). K14 was abundant throughout the basal layer and highlights the tightly packed, disorganised phenotype of the basal keratinocytes in SCC samples. K14 was also retained throughout the suprabasal keratinocytes, although staining was strongest in the basal cells. This can be associated with the long half-life of keratins or is sometimes observed when incomplete differentiation takes place in keratinocytes **A.** Representative staining taken from patient 19 biopsy. **B.** Representative staining taken from patient 18 SCC biopsy. Dotted line represents the epithelial-stromal boundary. Nuclei counterstained with DAPI (blue) and displayed with the phase contrast image to allow the sample morphology to be visualised. Scale bar 25 µm.

SCC (Figure 6.1D). The dermis of SCC samples used in this study appear blue (Figure 6.1), a phenomenon that usually indicates solar elastosis in skin samples, arising from chronic sun exposure and resulting in elastic fibre fragmentation and loss of collagenous fibres in the dermis. The resulting skin sample does not stain in a strong pink colour following H&E staining compared to healthy human skin. Higher magnification images revealed that in most SCC biopsies used in this study the underlying stroma consisted of cancer associated fibroblasts and densely packed inflammatory cells (Figure 6.1); this sea of plasma cells underneath is a reactive phenomenon that is observed in SCC and BCC samples.

Following H&E staining, immunofluorescence analysis was used to identify key differentiation markers throughout the SCC samples. K14 expression was abundant throughout the basal layer (Figure 6.2) and highlighted the tightly packed, disorganised phenotype of the basal cells. Although K14 expression was highest in the basal population, K14 was observed retained throughout suprabasal cells of SCC samples. Immediately adjacent to the basal layer, the spinous layer was highly positive for K1. The extent of the acanthosis throughout SCC samples was highlighted with K1 staining, K1 was widely expressed throughout the disorganised population of suprabasal cells in SCCs and some staining in the basal population (Figure 6.3). The proliferation marker, Ki67, as expected was also identified in clusters in both basal and suprabasal regions of the SCC lesions (Figure 6.4). Expression of terminal differentiation protein, loricrin, was significantly lower than the expression found in healthy human skin samples, with most regions not expressing loricrin within the biopsies. However, although the granular layer was often absent in SCCs due to incomplete differentiation, some samples showed positive staining for loricrin (Figure 6.5A). Nevertheless, although loricrin could be identified in the suprabasal layers of

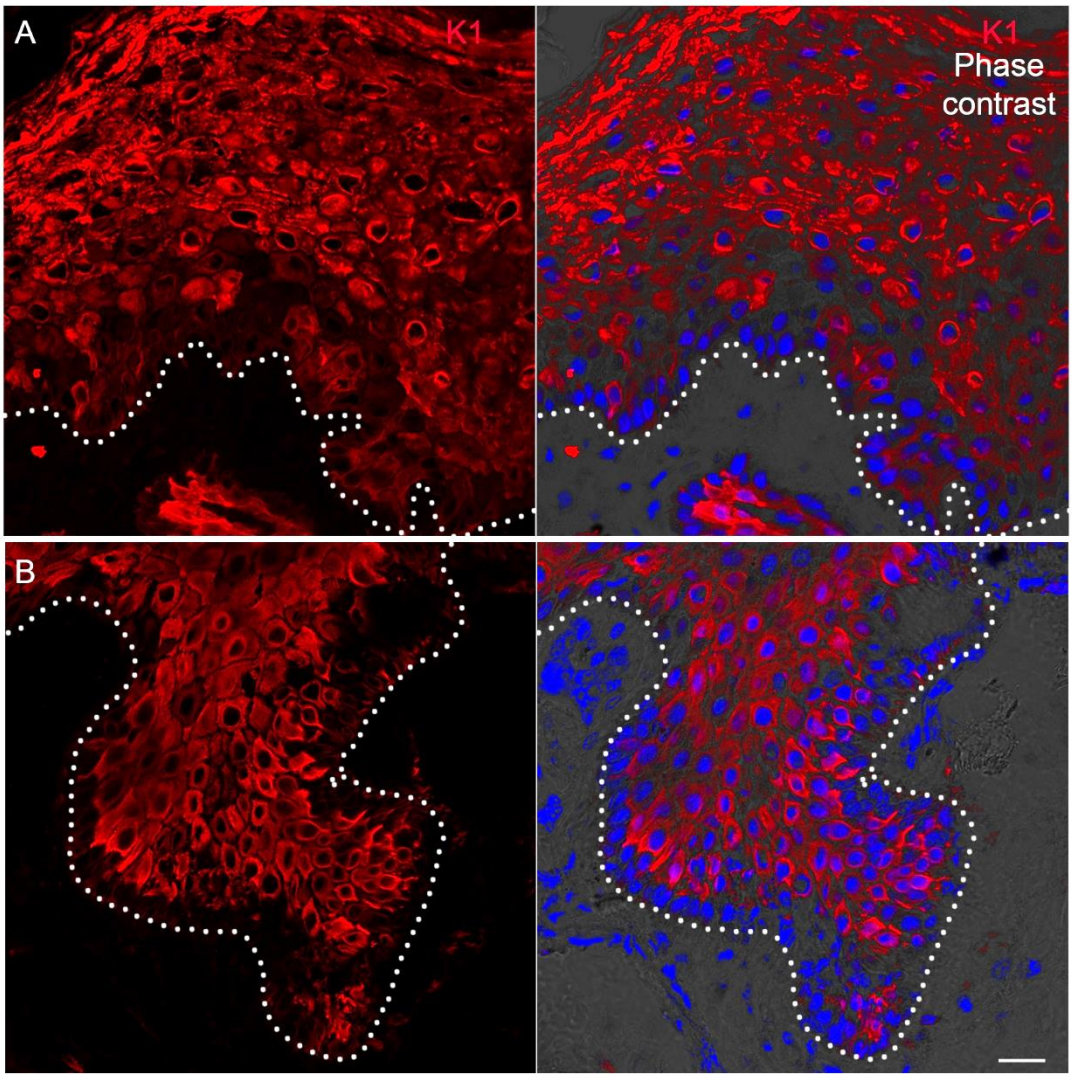

Figure 6.3. Immunofluorescence analysis of keratin-1 expression in squamous cell carcinoma samples.
Representative immunofluorescence staining of cytokeratin-1 (K1) in SCC skin samples used in this study (n=5). K1 (red) expression was mostly absent in the basal population of cells and is almost exclusively expressed in the suprabasal population of cells. **A.** Representative staining from patient 18 biopsy. **B.** Representative staining taken from patient 19 SCC biopsy. Nuclei counterstained with DAPI (blue) and displayed with phase contrast images for visualisation of sample morphology. White dotted lines represent the epidermal-stromal boundary. Scale bar 25 µm.

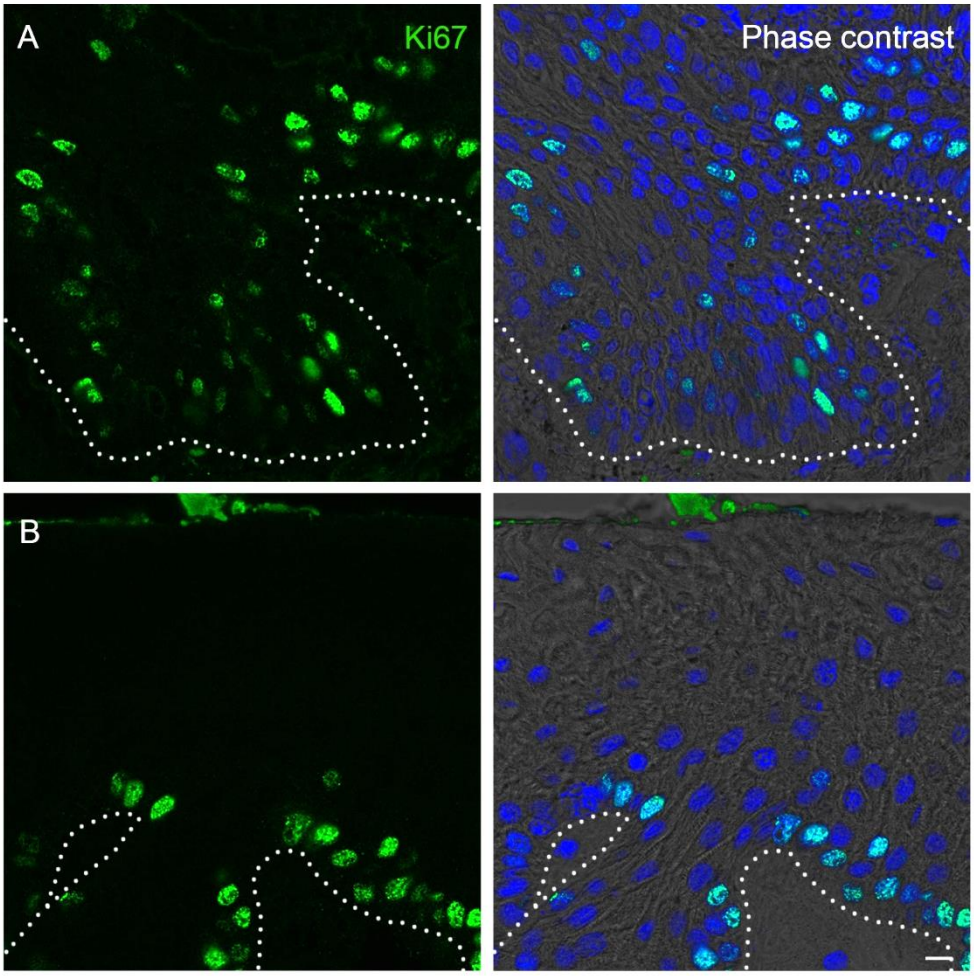

Figure 6.4. Immunofluorescence analysis of cell proliferation in squamous cell carcinoma samples.
Representative immunofluorescence staining of proliferation marker, Ki67, in SCC samples (n=5). Ki67 (green) was found scattered throughout the basal and suprabasal regions of SCC biopsies. **A.** Patient 19 displayed a significantly high number of proliferating cells in the epidermal compartment in both basal and suprabasal tissue. **B.** Patient 18 showed a significantly high number of proliferating cells within the lesion as expected in a SCC biopsy. Images are displayed with alongside phase contrast images for visualisation of sample morphology. White dotted lines indicate epithelial-stromal boundary. Nuclei counter stained with DAPI (blue). Scale bar 10 µm.

some limited regions within SCC biopsies, it was often absent within most other regions within the same patient biopsies (Figure 6.5C).

SCCs are often found to acquire more mutations than other common cancers and the most common mutation identified in SCCs is a mutation in *TP53*. Immunofluorescence analysis with an antibody that recognises a mutant form of p53 highlights the vast number of cells carrying p53 mutation within SCC samples compared to healthy human skin samples (Figure 6.6). Although low levels of p53 mutations are expected in healthy human skin, due to frequent exposure of the skin to UV, these usually result in senescence and are usually cleared. However, when these are not cleared and instead accumulate usually result in undesirable effect such as SCC as demonstrated by the significant p53 staining within SCC tumours in Figure 6.6. Healthy human skin samples showed no or little p53 mutations within the epidermis, and scattered staining in the dermis, whereas SCC samples displayed extensive widespread p53 mutations within the lesions (Figure 6.6).

There are often stromal changes that are also associated with SCC formation, as demonstrated through the blueish appearance following H&E staining in Figure 6.1. These stromal changes were additionally confirmed using immunofluorescence to investigate tenascin C and periostin expression, indicating an activated stroma. Tenascin C was absent in the dermis of healthy human skin, but its expression was present in the activated stroma of SCC samples (Figure 6.7).

CD80 expression was not present in healthy human skin (data not shown) only background staining could be observed, with no specific staining for either bmi1 or CD80 in healthy samples. However, in SCC samples bmi1 co-localised with

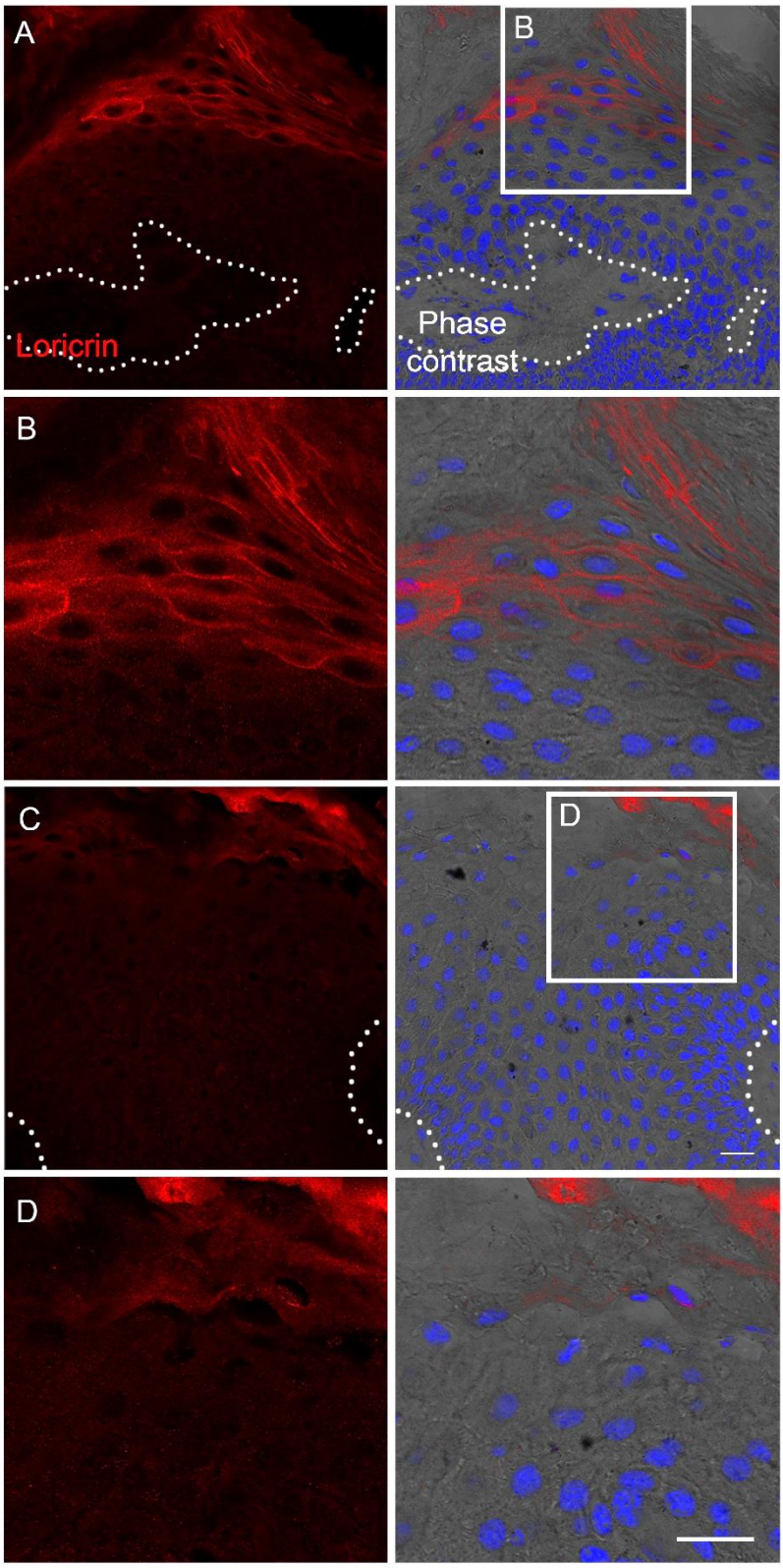

Figure 6.5. Loricrin expression in squamous cell carcinoma samples. Representative immunofluorescence analysis of loricrin expression in SCC samples. Loricrin expression was mostly absent in SCC samples, however, some differentiated regions within tumour samples expressed loricrin in the uppermost layers. **A.** Representative immunofluorescence analysis of loricrin (red) from patient 19 (n=5). Although the granular layer is often absent in SCCs, some regions displayed loricrin expression within regions that showed a more differentiated phenotype. **B.** Higher magnification images highlight the loricrin

expression found in the uppermost layers of the tumour. **C.** However, most regions within the tumour loricrin is mostly absent, consistent with the absence of the granular layer in most SCCs. **D.** High magnification images highlight the absence of loricrin in the suprabasal layers of SCC samples. White dotted lines indicate epithelial-stromal boundary. Nuclei counter stained with DAPI (blue) and images displayed with alongside phase contrast images for visualisation of sample morphology. Scale bar 25 µm.

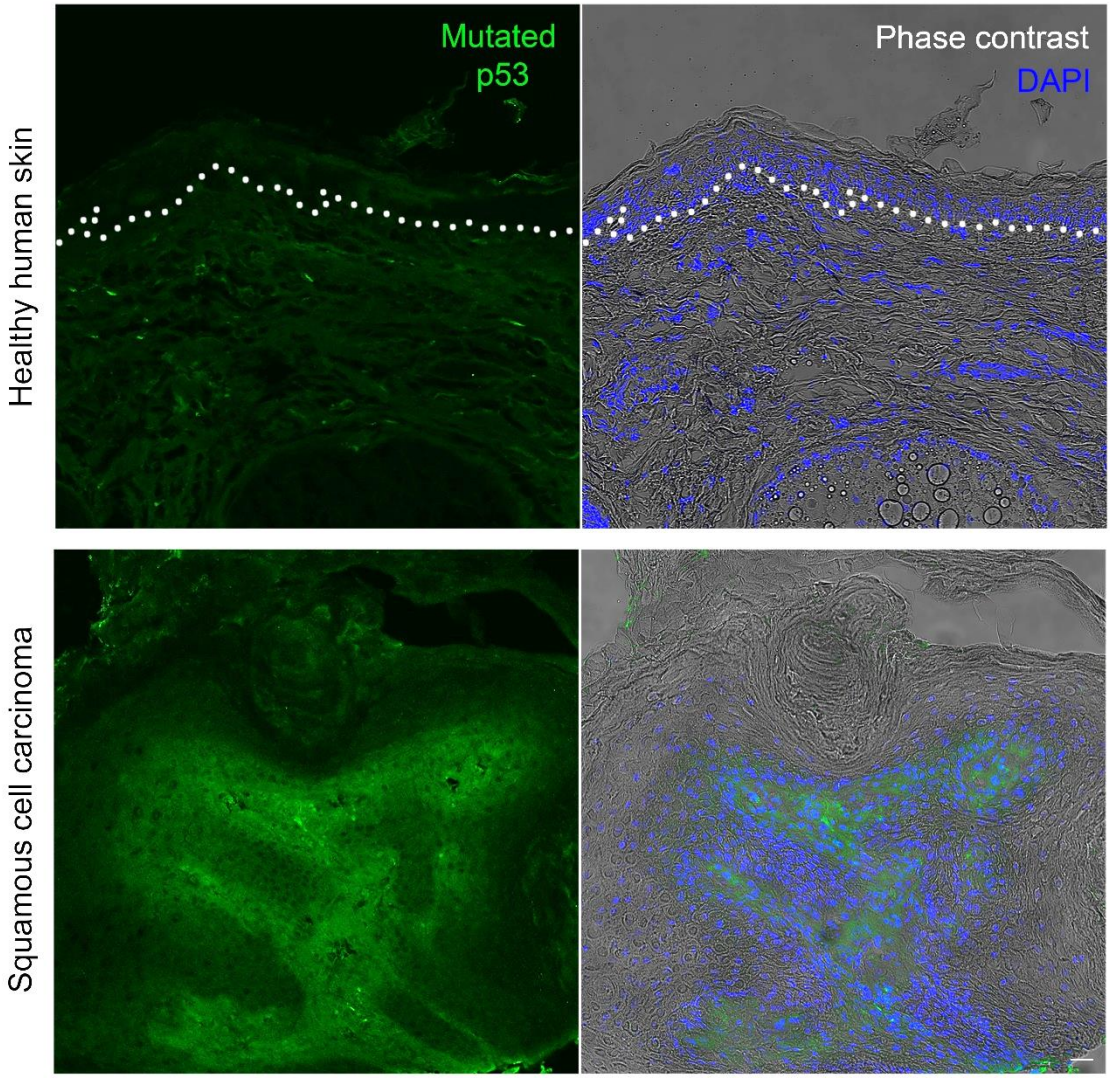

Figure 6.6. Immunofluorescence analysis of P53 mutations in squamous cell carcinoma tumours compared to healthy human skin samples.
Representative immunofluorescence analysis of mutant p53 (green) in healthy skin samples and SCC biopsies. Healthy human skin samples show no or little p53 mutations within the epidermis, and only scattered staining in the dermis. SCC samples express high levels of mutated p53, with extensive widespread p53 mutations within the lesions. White dotted lines represent the epidermis-dermis boundary. Nuclei counterstained with DAPI (blue) and displayed alongside phase contrast images for visualisation of sample morphology. Scale bar 25 µm.

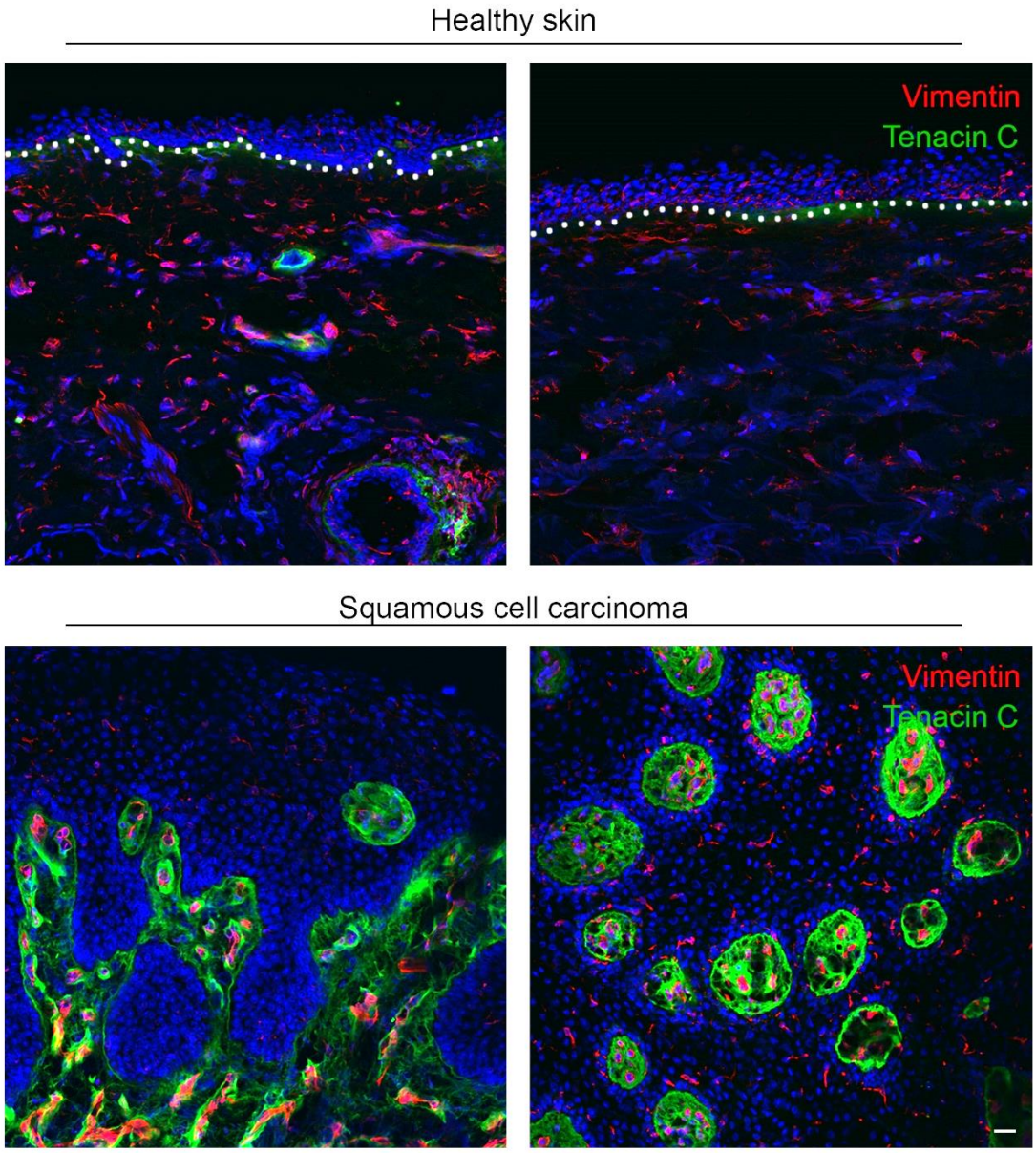

Figure 6.7. Tenascin C expression in the stroma of squamous cell carcinoma tumours compared to healthy human skin.
Representative immunofluorescence analysis of tenascin C (green) and vimentin (red) expression in healthy and SCC skin samples (n=6). Tenascin C was mostly absent in the dermis of healthy patients, but the expression was upregulated and strongly expressed in the activated stroma of SCC samples. Top left: Patient 7. Top right: Patient 6. Bottom left: Patient 19. Bottom right: Patient 17. Nuclei counterstained with DAPI (blue) for visualisation of sample morphology. White dotted lines represent the epidermal-dermal boundary in healthy human skin samples. Scale bar 25 µm.

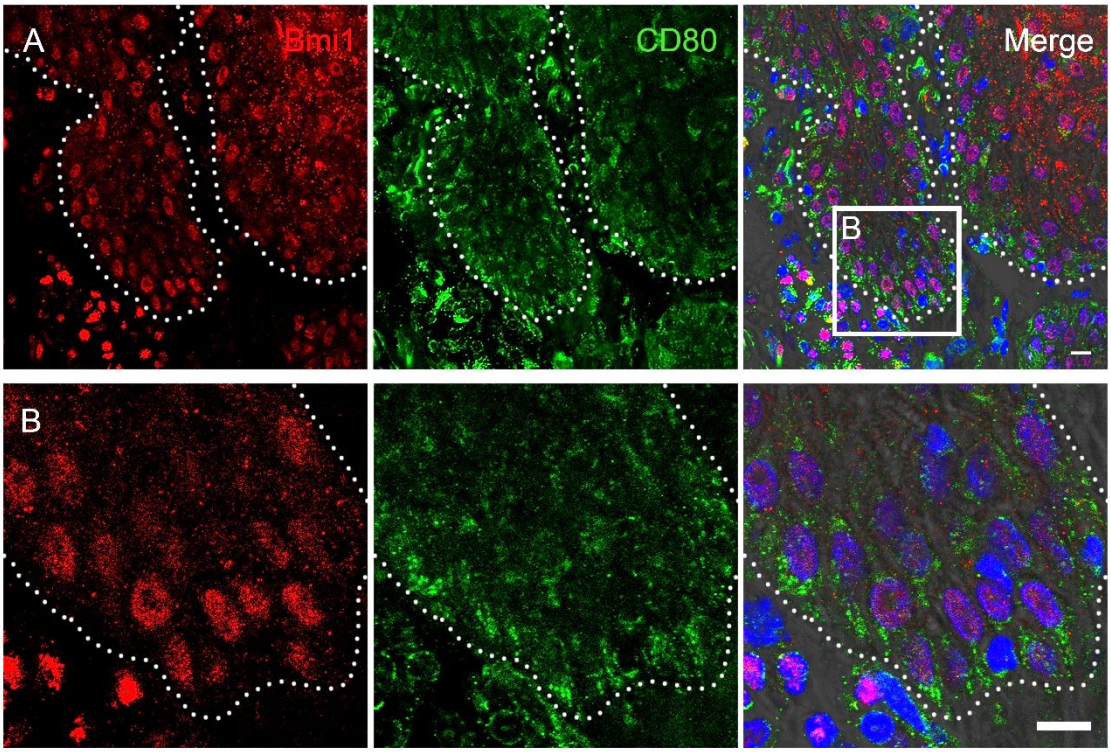

Figure 6.8. Immunofluorescence analysis of CD80 and bmi1 expression in squamous cell carcinoma.
Representative immunofluorescence analysis of bmi1 (red) and CD80 (green) in SCC biopsies (n=5). **A.** SCC biopsy reveals a population of basal cells positive for both CD80 and bmi1. Representative image taken from patient 18 biopsy. **B.** High magnification images reveal a distinct population of basal cells that express higher levels of CD80 alongside strong bmi1 expression. Nuclei counterstained with DAPI (blue) and displayed with phase contrast images for visualisation of sample morphology. White dotted lines represent the epidermal-stromal boundary. Scale bar 10 µm.

Table 6.1. An overview of immunofluorescence staining profile of squamous cell carcinoma biopsies.

Marker	Squamous cell carcinoma				
	Epithelial				Mesenchymal
	Stratum Basale	Stratum Spinosum	Stratum Granulosum*	Stratum Corneum**	Stroma
Keratin 14	+++	+			
Integrin α6	+++				
CD80	++				
Bmi1	++	+			
Ki67	++	++			+
Keratin 1		+++	+++		
E-Cadherin	+	+	++		
Loricrin			+/++		
Vimentin	+***				+++
Tenascin C					+++

Staining profiles demonstrate the discrete staining patterns observed in the SCC biopsies, which enabled the identification of specific populations in tissue samples, and individual cell populations later in the Chapter. Expression levels were categorised as: +, weak or scattered; ++, moderate expression; +++, strong expression. *The granular layer is often absent in SCCs but can depend on the differentiation status of the lesion. **The stratum corneum is often not the same in SCC, due to incomplete programme of differentiation, incomplete packaging of proteins and retention of nuclei within this layer. ***Staining might have been from other cell types found in the epidermis or EMT of the SCC cells.

CD80 positive basal cells (Figure 6.8). CD80 positive cells were found along the epidermal-stromal boundary, alongside bmi1 positive cells. The proportion of bmi1 positive cells were higher than expected, whereas CD80 identified a more distinct population of SCC basal cells.

The expression profile of proteins in SCC samples is summarised in Table 6.1, highlighting how different layers and cell types in the tumour can be identified through the expression of differentiation markers.

6.4.1.2. Tau expression and cellular localisation changes in squamous cell carcinoma

Following the full characterisation of the SCC samples used in this study, the tau expression throughout SCC biopsies at an RNA and protein level was analysed. The characterisation of tau expression under pathological conditions will allow for identification of differences in expression compared to the expression pattern identified under physiological conditions in Chapter 3and 4. Changes in tau isoform expression in SCC compared to healthy human skin is currently unknown and identifying any changes can help to elucidate the function of tau in SCC and identify possible novel cancer treatments.

To characterise and identify tau protein expression patterns throughout SCC biopsies, immunofluorescence analysis was initially performed. Three commercially generated antibodies were used that targeted different regions of the tau protein, which were also used in Chapter 3 to investigate tau expression throughout the healthy epidermis, therefore allowing direct comparisons between healthy and SCC to be performed. Immunofluorescence analysis with tau [E178] revealed that tau was broadly expressed throughout the SCC biopsies, with expression restricted to the nucleus in the basal and most of the suprabasal cell

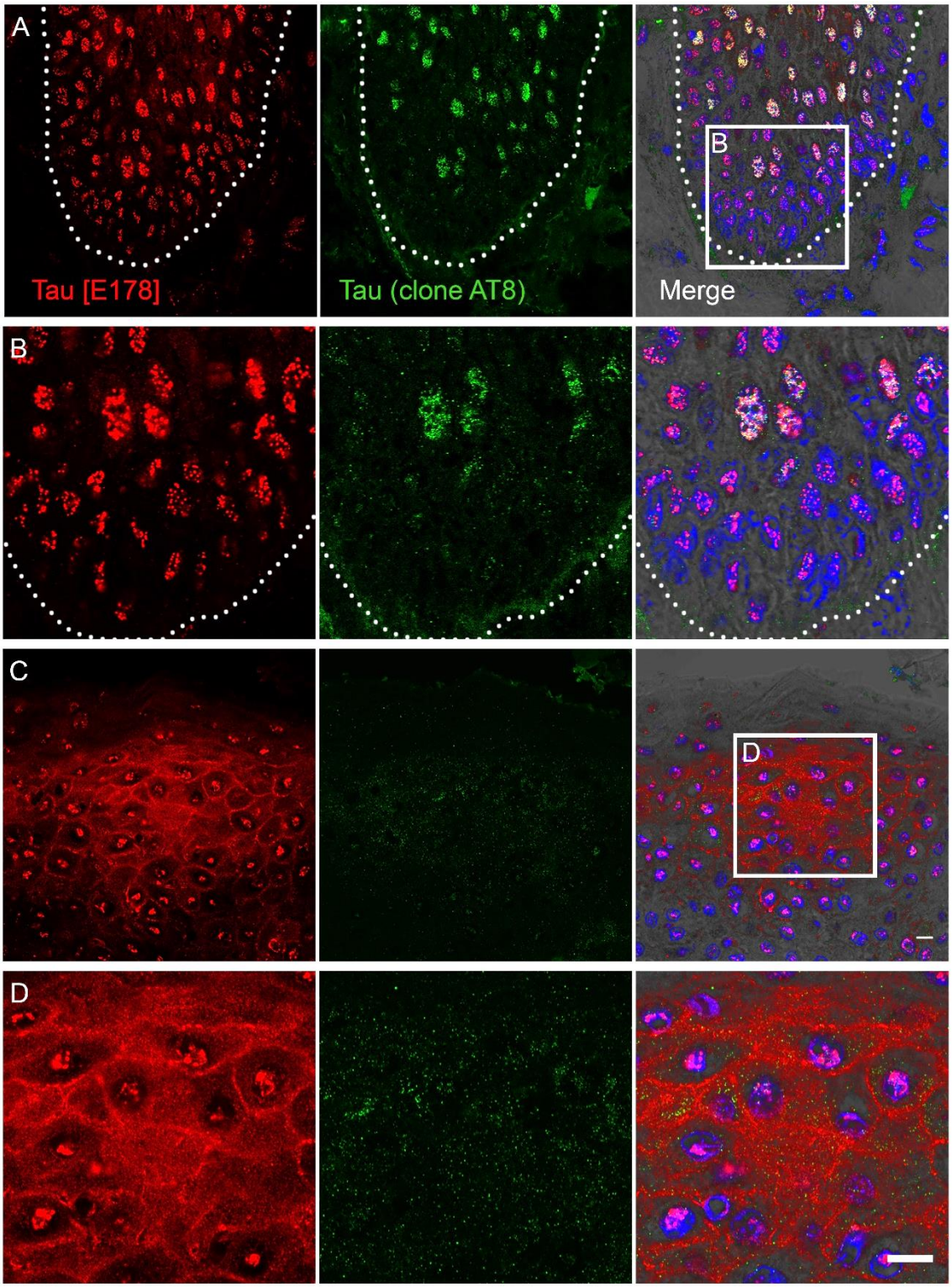

Figure 6.9. Immunoflurescence analysis of tau expression in squamous cell carcinoma samples.

Representative immunofluorescence analysis of tau [E178] (red) and phosphorylated tau (clone AT8) (green) in in sagittal sections of SCC tumour biopsies (n=5). **A.** Tau is broadly expressed within SCC tumours and is mostly restricted to the nuclear fraction of cells. Although total tau was found throughout the epidermal compartment, phosphorylated tau was absent in the basal and immediately adjacent suprabasal cells. **B.** High magnification images of the basal region of the tumour show that although tau is almost exclusively restricted to the nuclear fraction of the epidermal cells, not all basal cells displayed the same

expression level of tau. **C.** Total tau expression was identified in the nucleus, cytoplasm and membrane fractions of some islands of SCC cells located near the surface of the tumour. **D.** High magnification images demonstrate that tau expression can clearly be observed along cell junctions of this population of suprabasal tumour cells. Nuclei counterstained with DAPI (blue) and all channels are displayed with the phase contrast image in the right panel to allow accurate visualisation of sample morphology. White dotted lines represent the epidermal-stromal boundary. Scale bar 10 µm.

population (Figure 6.9 and Figure 6.10). Tau expression in the cytoplasm of keratinocytes was only identified in suprabasal cells near the surface of the tumour (Figure 6.9D and Figure 6.10B). These regions were often the populations that stained most strongly for differentiation markers compared to the rest of the tumour. Interestingly, the strong tau expression within the basal surface of cells attached to the BM identified in healthy human skin, was lost in the majority of regions within SCC samples (Figure 6.9 and Figure 6.10).

Although there was strong expression of tau identified in the nucleus of basal and suprabasal cells, not all cells demonstrated the same expression level (Figure 6.9B and Figure 6.10C). Similar to healthy skin samples, some cells had significantly lower levels of tau in the nucleus compared to most of the surrounding cells within the epidermal compartment. Whilst mitotic cells within the tumour also had significantly higher tau expression compared to its neighbouring cells (Figure 6.9C), immunofluorescence staining also confirmed that tau was absent in the nucleolus of all cells. Although basal and suprabasal cells in SCC biopsies expressed total tau, phosphorylated tau was absent in basal and suprabasal cells lying directly adjacent to the basal layer (Figure 6.9B and Figure 6.10C). Phosphorylated tau was restricted to the upper regions of suprabasal cells within all SCC tumours and its expression was exclusively in the nuclear fraction of the cells (Figure 6.9 and Figure 6.10). Unlike healthy human skin, the cytoplasmic expression was found at the superficial surface of the suprabasal population in SCC samples. Although SCC samples displayed acanthosis, this was not a sufficient explanation for the differences observed here. The lack of cellular differentiation in SCCs was a possible explanation for the lack of cytoplasmic expression in SCC lesions. Another striking observation

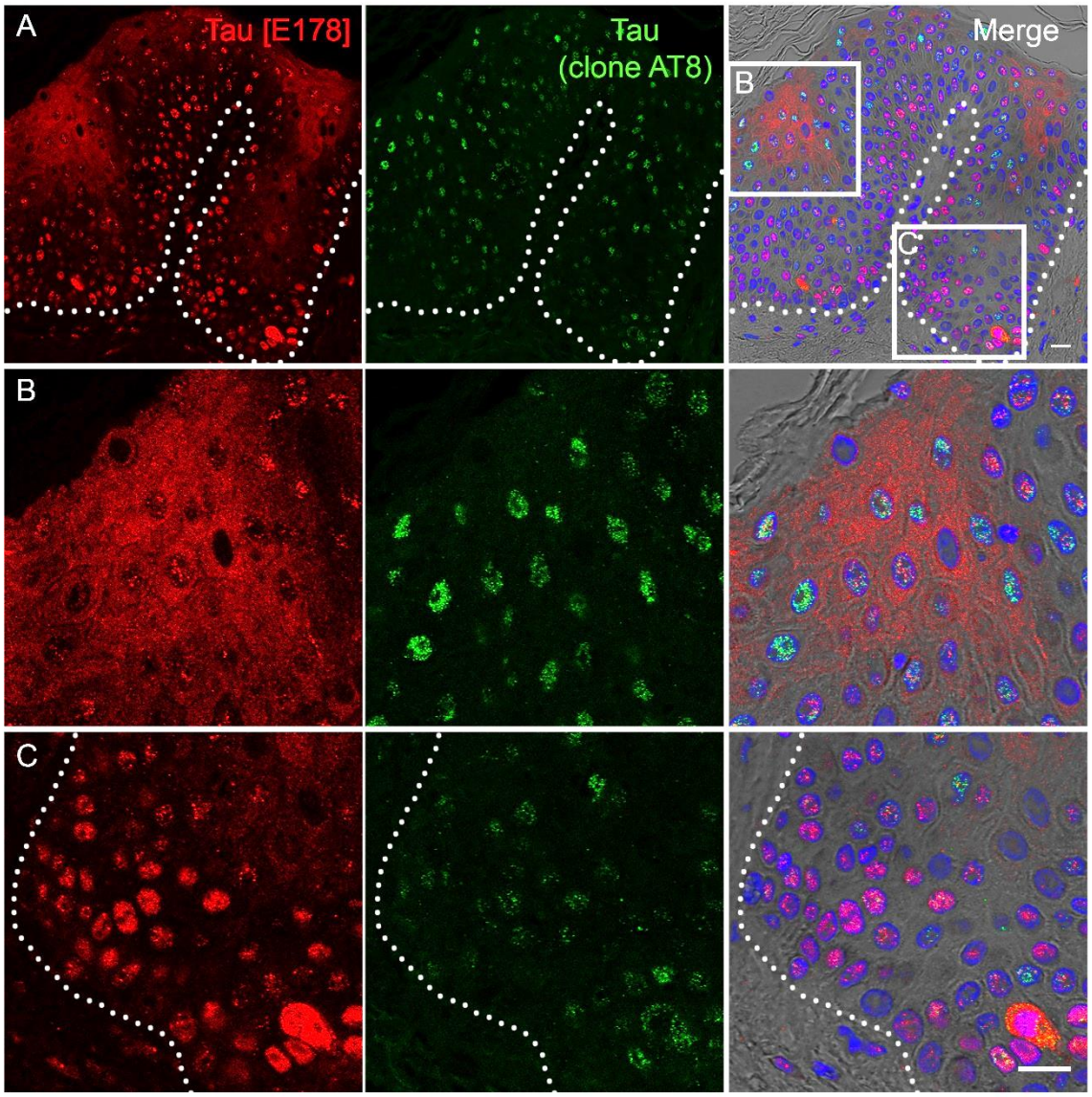

Figure 6.10. Tau expression in squamous cell carcinoma samples. Representative immunofluorescence analysis of tau in FFPE SCC biopsies (n=6). **A.** Tau [E178] (red) was identified throughout the tumour with expression switching from nuclear, to nuclear, cytoplasmic and membrane. Phosphorylated tau (clone AT8) (green) was restricted to the suprabasal population of cells. **B.** High magnification images of islands of SCC cells reveal clear tau expression in the nuclear, cytoplasmic and membrane fractions of cells. Phosphorylated tau was much higher in the suprabasal population of cells compared to the basal cells within the tumour. **C.** High magnification of the basal region of the tumour show that tau is almost exclusively expressed within the nucleus of basal SCC cells. Despite basal cells only displaying nuclear expression of tau, not all cells had the same expression level, and some cells had significantly lower nuclear tau expression compared to their neighbouring cells. Mitotic cells on the other hand had significantly higher expression levels of total tau compared to its neighbouring cells. Phosphorylated tau was mostly absent in the basal cells within SCC tumours. Nuclei counterstained with DAPI (blue) and all channels are displayed with the phase contrast image in the right panel to allow accurate visualisation of sample morphology. White dotted lines represent the epidermal-stromal boundary. Scale bar 10 µm.

was the strong tau expression along cell junctions of suprabasal cells (Figure 6.9C and D).

Although this study was primarily investigating tau expression in SCC, tau expression in basal cell carcinoma (BCC) was also evaluated (Figure 10.24). Immunofluorescence analysis of tau expression in BCC samples revealed that tau was highly expressed throughout each lesion. Nearly all of the cells in each nest demonstrated a nuclear localisation of tau throughout the patient biopsies (Figure 10.24). Interestingly, there was less cytoplasmic tau observed in the suprabasal and granular layers of the BCC biopsies, despite BCCs being traditionally characterised as not interfering with the differentiation of the uppermost layers of the epidermis; marking a difference to the suprabasal cells in healthy human skin samples. This suggests that although suprabasal cells within BCC lesions might morphologically resemble granular cells, there is likely to be some molecular differences in these cell populations. Interestingly, in this study, BCC samples also revealed a significant increase in both the number of positive cells and the expression density of phosphorylated tau throughout BCC lesions compared to SCC and healthy human skin biopsies (Figure 10.24). In healthy human skin and SCC, phosphorylated tau was lowest and almost absent in the basal layers. However, in the BCC samples the majority of crowded, palisading basal cells showed a high level of phosphorylated tau in the nucleus (Figure 10.24).

To further investigate tau expression in SCC, the molecular expression pattern of tau isoforms in SCC biopsied regions of tissue were isolated and removed using LCM. LCM was performed to extract total RNA from two ROI in each SCC lesion; the basal SC population, where it is thought most CSCs reside [383], and the suprabasal population. The morphology of the SCC samples was very different

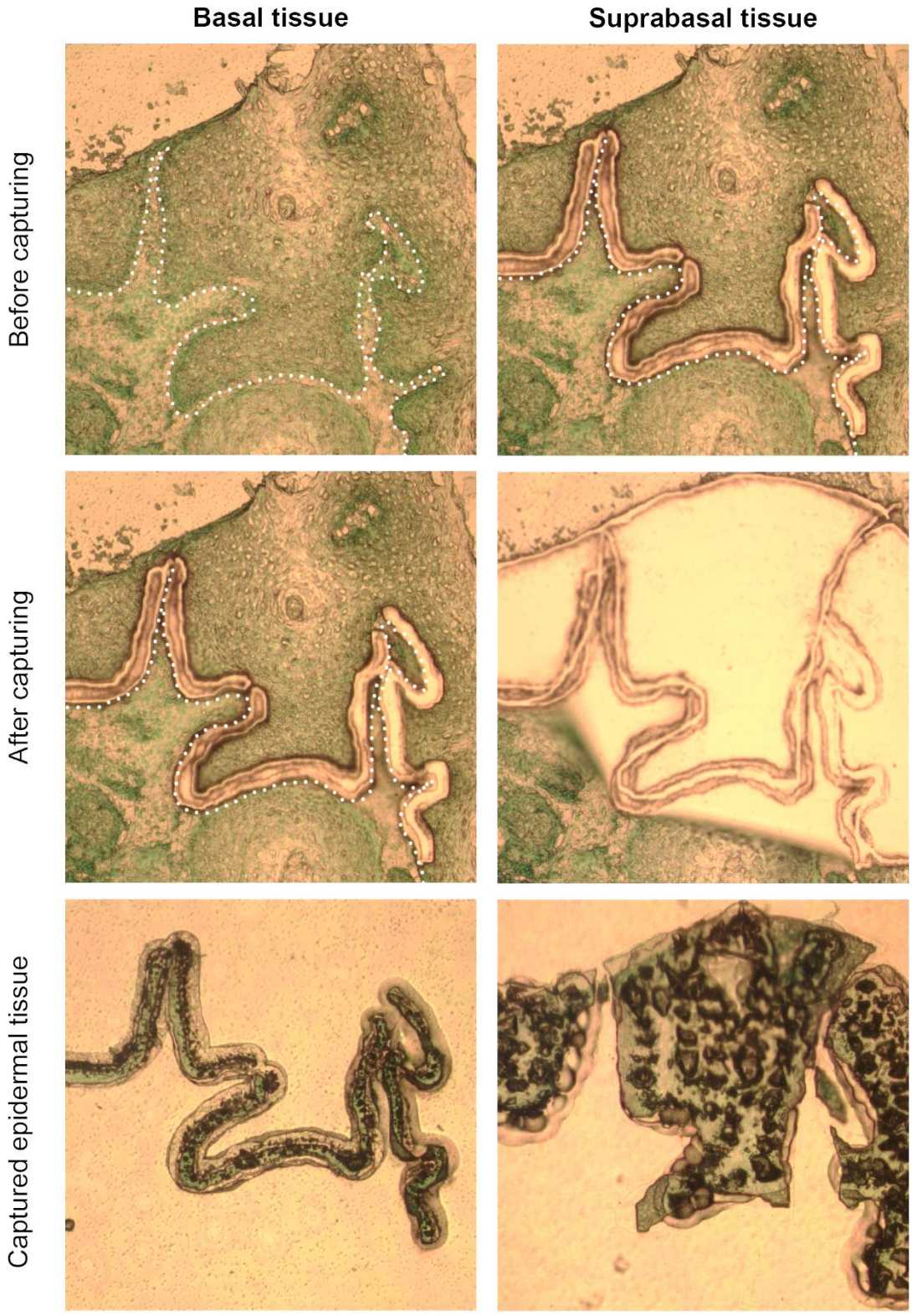

Figure 6.11. Isolation of basal and suprabasal tissue from squamous cell carcinoma samples using Laser Capture Microdissection.
Representative images of LCM-captured basal and suprabasal regions of interest (ROI) from patient 18 SCC sample. **Top:** Methyl green stained sagittal section of SCC sample prior to cutting with ultraviolet (UV) laser and LCM extraction. The dotted line represents the epidermal-stromal boundary. **Middle:** Representation of suprabasal and basal ROI removed from tissue after cutting with UV laser and melting tissue onto cap with an IR laser. **Bottom**: ROI tissue on CapSure® Macro LCM caps. Black circles are IR-melted film.

to healthy human skin and between patient biopsies, so although there was much variation in the suprabasal population, it could not be further divided into separate regions. Rather one suprabasal ROI was taken, this needed to be taken into account when the histological results were analysed. In SCC samples both basal and suprabasal cells contained proliferating cells, although CSCs are thought to lie adjacent to the BM [383].

To confirm the two ROI had been successfully isolated by LCM, RT q-PCR analysis was carried out using primers assess the expression of genes associated with a basal or SC phenotype, alongside gene expression found in differentiated populations. RT q-PCR analysis confirmed that the gene expression associated with a basal phenotype was highest in the basal population, with a significant decrease in the relative expression of K14, K5, Ki67, p63, DLL1 and integrin-α6 (Figure 6.12A and Figure 10.25). Although there was a significant decrease in the expression of these genes, the difference was not as large as in the healthy human skin samples, which is consistent with the immunofluorescence analysis performed in this Chapter. Ki67 expression was decreased in the suprabasal population however, consistent with immunofluorescence, Ki67 was still detected in this suprabasal population of SCC cells (Figure 6.12A, Figure 10.25 and Figure 6.4). Consistent with these findings, the relative gene expression of differentiation associated proteins was significantly increased in the captured suprabasal ROI (Figure 6.12B and Figure 10.25). Filaggrin and involucrin expression was significantly upregulated in the suprabasal ROI, with barely detectable levels in the basal population (Figure 6.12B and Figure 10.25).

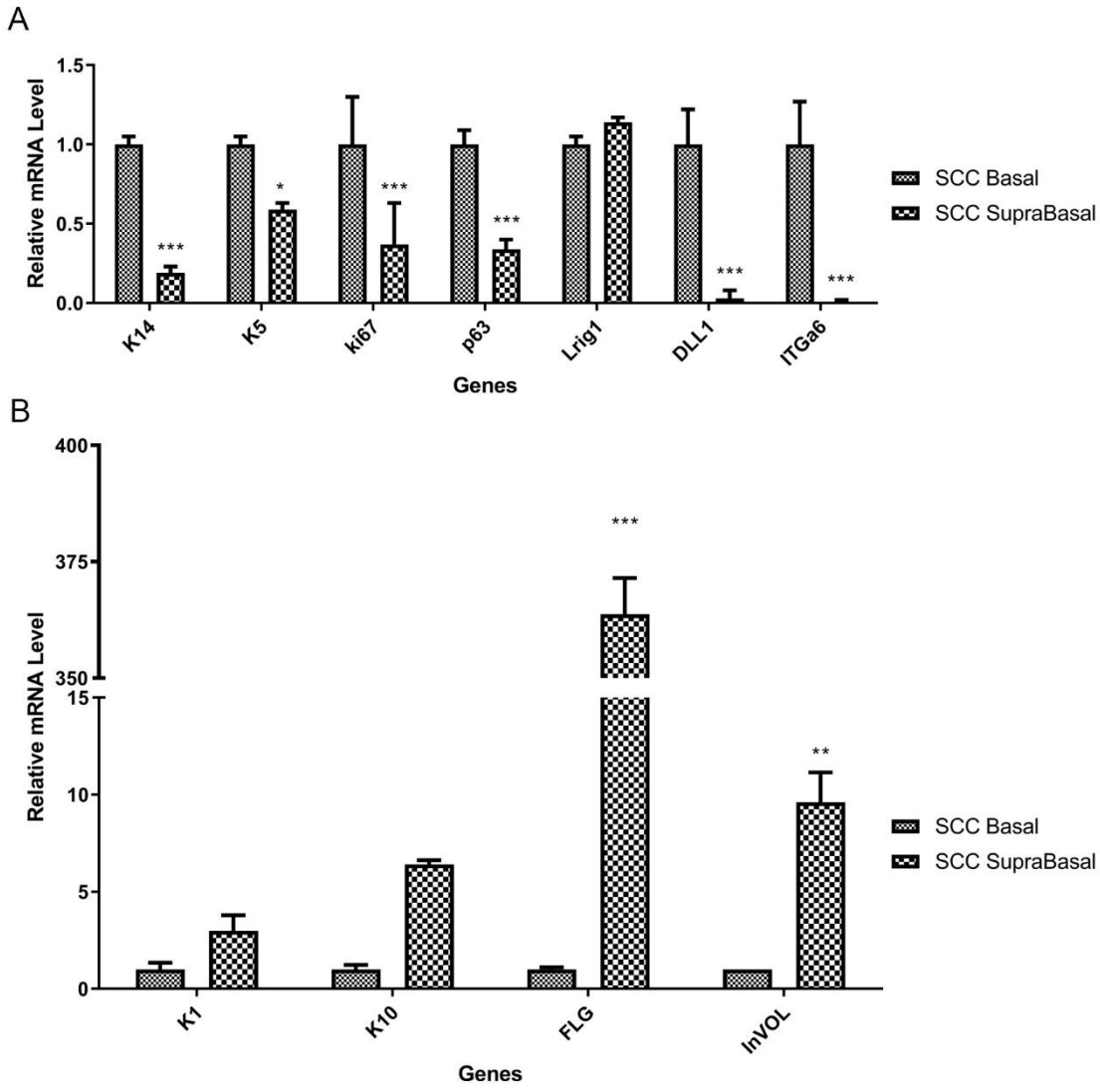

Figure 6.12. RT q-PCR analysis of isolated regions of interest in squamous cell carcinoma samples using Laser Capture Microdissection.
Representative RT q-PCR analysis of gene expression in LCM captured basal and suprabasal ROI from patient 19 SCC sample. **A.** Relative gene expression of genes associated with a basal phenotype were downregulated in the captured suprabasal tissue. Ki67 was still detected in the suprabasal region as expected in SCC samples, although it was downregulated. **B.** Relative gene expression of genes associated with differentiation were upregulated in suprabasal ROI compared to basal populations. There was a very significant increase in filaggrin (FLG) and involucrin (INVOL) expression in all SCC biopsies analysed as so little was detected in the basal populations. Ct values normalised to Glyceraldehyde-3-Phosphate Dehydrogenase (GAPDH) and $2^{-\Delta\Delta Ct}$ method of analysis used. Relative expression levels are displayed as mean ± SD. Two-way ANOVA with Bonferroni correction was used to test significance; *p<0.05, ** p<0.01, *** p<0.001.

Once the successful isolation of the ROI was confirmed, the molecular changes in expression of tau between the ROIs was investigated. RT q-PCR analysis of total tau expression revealed a significant increase in tau expression in the suprabasal ROI compared to the basal ROI (Figure 6.13). Further investigation into the isoform specific expression within each captured population revealed that 1N was not detected in SCC samples using isoform specific primer pairs and overall 0N expression showed a patient specific pattern; similar to the pattern observed in healthy human skin samples (Figure 6.14B). On the other hand, 2N isoform expression was significantly increased in the suprabasal ROI of SCC samples compared to the basal ROI (Figure 6.14D).

Alternative splicing of the microtubule binding domain of tau was also investigated in the suprabasal population of cells in SCC biopsies (Figure 6.15). Expression of 3R was shown to fluctuate between patient samples, as also observed in healthy skin samples (Figure 6.15B). Expression of 4R tau variants were increased in the suprabasal ROI of all sample analysed, but the relative increase only reached the threshold for statistical significance in the patient 18 biopsy (Figure 6.15D). Overall, 2N 4R isoforms were repeatedly increased in the suprabasal cell populations, consistent with the findings in healthy skin.

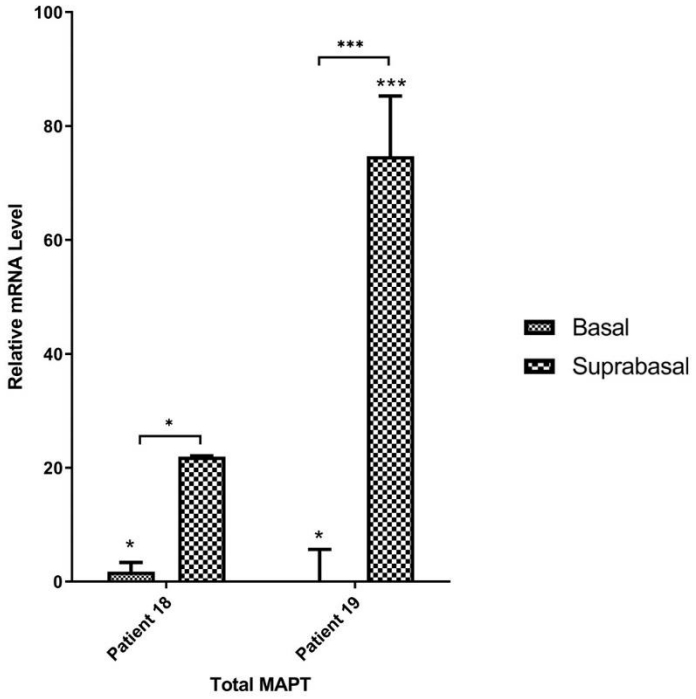

Figure 6.13. Tau expression is highest in the suprabasal cells in squamous cell carcinoma samples.
Representative RT q-PCR analysis of total tau expression in in basal and suprabasal cell populations in SCC samples. *MAPT* expression is increased in all suprabasal populations of patient SCC samples analysed in this study. Ct values normalised to basal ROI using Glyceraldehyde-3-Phosphate Dehydrogenase (GAPDH) as a house keeping gene and $2^{-\Delta\Delta Ct}$ method of analysis used. Relative expression levels are displayed as mean ± SD. Two-way ANOVA with Bonferroni correction was used to test significance; *p<0.05, ** p<0.01, *** p<0.001.

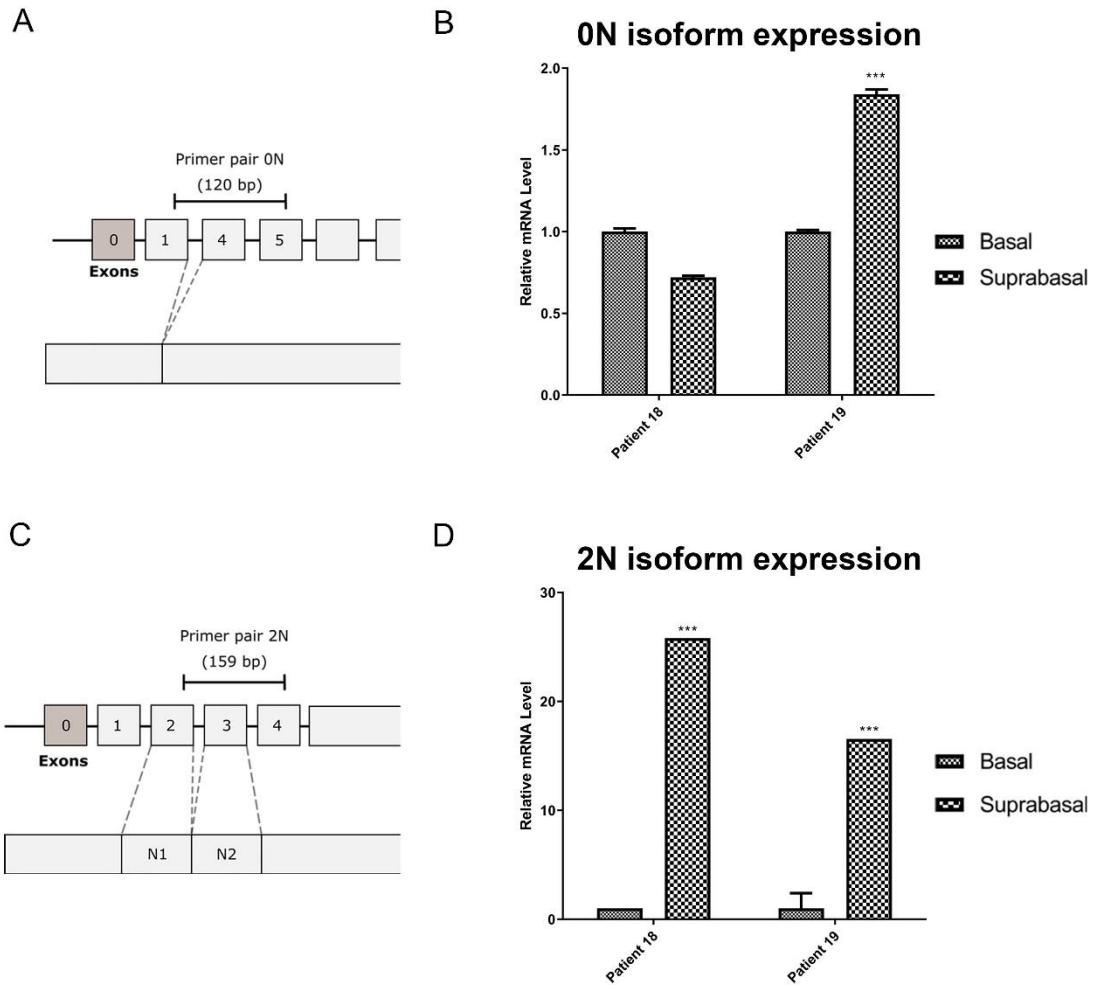

Figure 6.14. Alternative splicing of N-terminal region of tau in squamous cell carcinoma

RT q-PCR analysis of 0N and 2N tau isoform expression from basal and suprabasal tissue captured by LCM in SCC patient biopsies. Alternative splicing between the basal and suprabasal populations generate different expression patterns of tau between the two cell populations. **A.** Schematic indicating where *MAPT* isoform specific 0N primer pair flank exon 1-5 to exclude transcripts containing exon 2 or 3 to detect only 0N isoforms. Exon 0 and 14 transcribed but not translated. **B.** 0N isoform expression showed a patient specific expression pattern with inconsistent increase or decrease depending on the patient. **C.** Schematic showing where 2N isoform specific primer pair bind to on 2N tau transcript variant. Primer pairs flank exon 2 3 and 4 amplifying only variants that contain exon 2 and 3, therefore excluding any other isoforms. **D.** 2N isoform expression was significantly increased in the suprabasal population showing a clear transition to tau isoforms containing a longer N-terminal domain. Ct values normalised to basal ROI using Glyceraldehyde-3-Phosphate Dehydrogenase (GAPDH) as a house keeping gene and $2^{-\Delta\Delta Ct}$ method of analysis used. Relative expression levels are displayed as mean ± SD. Two-way ANOVA with Bonferroni correction was used to test significance; *** $p<0.001$.

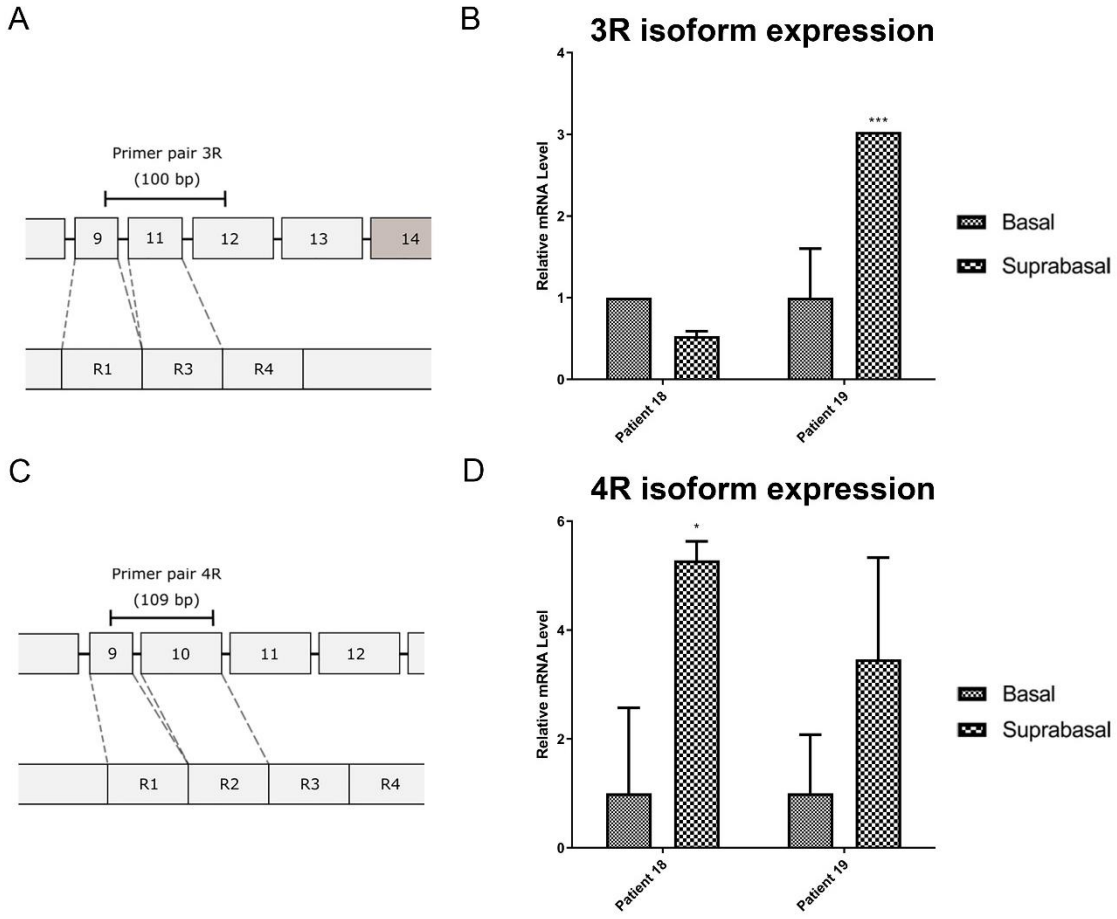

Figure 6.15. Alternative splicing of microtubule binding domain of tau in squamous cell carcinoma.
RT q-PCR analysis of 3R and 4R tau isoform expression from basal and suprabasal tissue captured by LCM in SCC patient biopsies. Alternative splicing between the basal and suprabasal populations generate different expression patterns of tau between the two cell populations. **A.** Schematic demonstrating where the 3R isoform specific primer pairs bind to on the 3R tau transcript. Primer pairs flank exon 9-12, excluding any transcripts that contain exon 10. **B.** 3R tau expression was observed to be patient specific and did not show a consistent pattern of up or downregulation in suprabasal populations. **C.** Schematic indicating where 4R isoform specific primer pairs bind to on the tau transcript. 4R primer pair flanks exon 9 and 10, excluding any 3R transcripts due to the lack of exon 10 in these isoforms. **D.** 4R isoform expression was increased in the suprabasal population all samples, but only reached the threshold for statistical significance in patient 18 biopsy. Ct values normalised to basal ROI using Glyceraldehyde-3-Phosphate Dehydrogenase (GAPDH) as a house keeping gene and $2^{-\Delta\Delta Ct}$ method of analysis used. Relative expression levels are displayed as mean ± SD. Two-way ANOVA with Bonferroni correction was used to test significance; *p<0.05, *** p<0.001.

Table 6.2. Summary of total and isoform specific RNA expression from RT q-PCR analysis of basal and suprabasal regions of interest populations captured by laser capture microdissection of squamous cell carcinoma samples.

Tau expression	Basal	Suprabasal
Total tau	++	+++
Isoform 0N	++	++
Isoform 1N	N.D	N.D
Isoform 2N	+	+++
Isoform 3R	++	++
Isoform 4R	+	+++

Total tau expression was increased in the suprabasal epidermis. 0N isoform expression did not show a significant change between cell populations. 1N was not detected (N.D) and 2N expression was significantly increased in the suprabasal population, with very low expression in the basal cells. 3R and 4R isoforms were also found to be alternatively spliced, consistent with the overall tau expression increase that is observed between the two populations. 4R isoform demonstrated a consistent increased expression in differentiated cells across all patient samples. Expression levels were denoted as: +: low expression; ++: medium expression; +++ high expression.

6.4.1.3. The subcellular localisation of tau in squamous cell carcinoma samples reflects the lack of differentiation

Following the characterisation of tau expression in SCC samples at an RNA and protein level, identifying tau localisation throughout each lesion, the next aim of this chapter was to characterise the role of tau in cSCC. Therefore, to enable a better understanding of what role tau plays in SCC, it was important to determine subcellular localisation of tau and identify possible interacting proteins of tau. This chapter has so far demonstrated that tau expression is upregulated in SCC lesions compared to healthy skin samples, and the expression pattern of tau differs compared to the expression observed in healthy skin samples. Therefore, further experiments with immunofluorescence analysis using well recognised markers of differentiation and cellular structures enabled the investigation of whether the expression pattern of tau in SCC was also linked to the cells differentiation status.

Using CD80 as an indicator of CSCs, SCC samples were co-stained for CD80 and tau to determine any changes of tau expression between CSCs and neighbouring basal cells. In healthy keratinocytes tau expression was lowest in the quiescent SC population and was upregulated in TAC cells. $CD80^+$ SCC cells were located along the BM and consistent with our hypothesis, tau expression in these $CD80^+$ cell population was lower than neighbouring $CD80^-$ cells (Figure 6.16B).

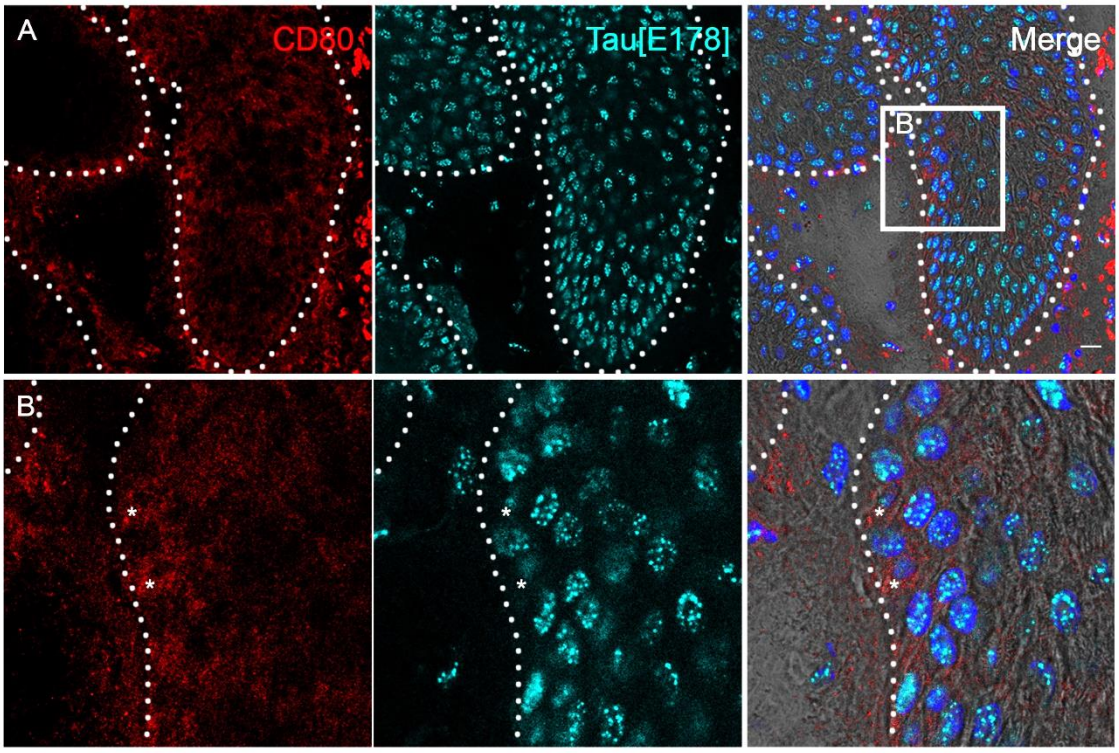

Figure 6.16. Tau expression is lower in CD80 positive basal cells compared to neighbouring cells.
Immunofluorescence analysis of CD80 (red) and tau [E178] (cyan) in SCC biopsies revealed that CD80 positive basal cells had lower levels of tau expression compared to their neighbouring basal and suprabasal cells (n=5). CD80 has been shown to be a marker of cancer SCs in SCC samples. Located in the basal layer these CD80 positive cells are indicated with an asterisk. **A.** Representative immunofluorescence analysis of a SCC biopsy from patient 18. **B.** CD80 positive basal cells display lower tau [E178] staining compared to their neighbouring counterparts. Stars mark CD80 positive cells which can also be observed to have less tau staining. Nuclei counterstained with DAPI (blue) all channels are displayed with the phase contrast image in the right panel to allow accurate visualisation of sample morphology. Scale bar 10 µm.

Proliferating cells were restricted to the basal layer in healthy human skin, however in SCCs proliferating cells were not restricted to the basal layer, but instead found throughout the epidermis in both basal and spinous layers (Figure 6.17). SCs have a higher proliferative capability compared to their TAC counterparts; it is predicted that in normal tissue SCs comprise 1% of the epidermal cell population, rising to 20% of the population in SCCs. Immunofluorescence analysis of Ki67 and tau expression in SCC samples revealed a proportion of Ki67 positive cells that had lower levels of tau staining. However, more investigation is needed *in vitro* to determine whether these are SCs or TACs, as Ki67 only labels proliferating cells and cannot distinguish between SCs and TACs or the stage of cell proliferation. As Ki67 is broadly expressed throughout cell proliferation, it would be interesting to investigate which stage of proliferation these cells are in and if tau expression is linked directly to each phase as indicated in keratinocytes in Chapter 4.

Although total tau was broadly expressed in the nucleus of cells throughout the lesion, phopho tau was observed to be absent in the basal fraction of SCCs. Indeed, using integrin-α6 to mark basal cells, Figure 6.18 demonstrates that integrin-α6 positive basal cells lack phosphorylated tau. Phosphorylated tau was observed only in suprabasal cells, where it's expression was restricted to the nucleus, with no localisation in the cytoplasm or membrane observed in any SCC samples (Figure 6.18).

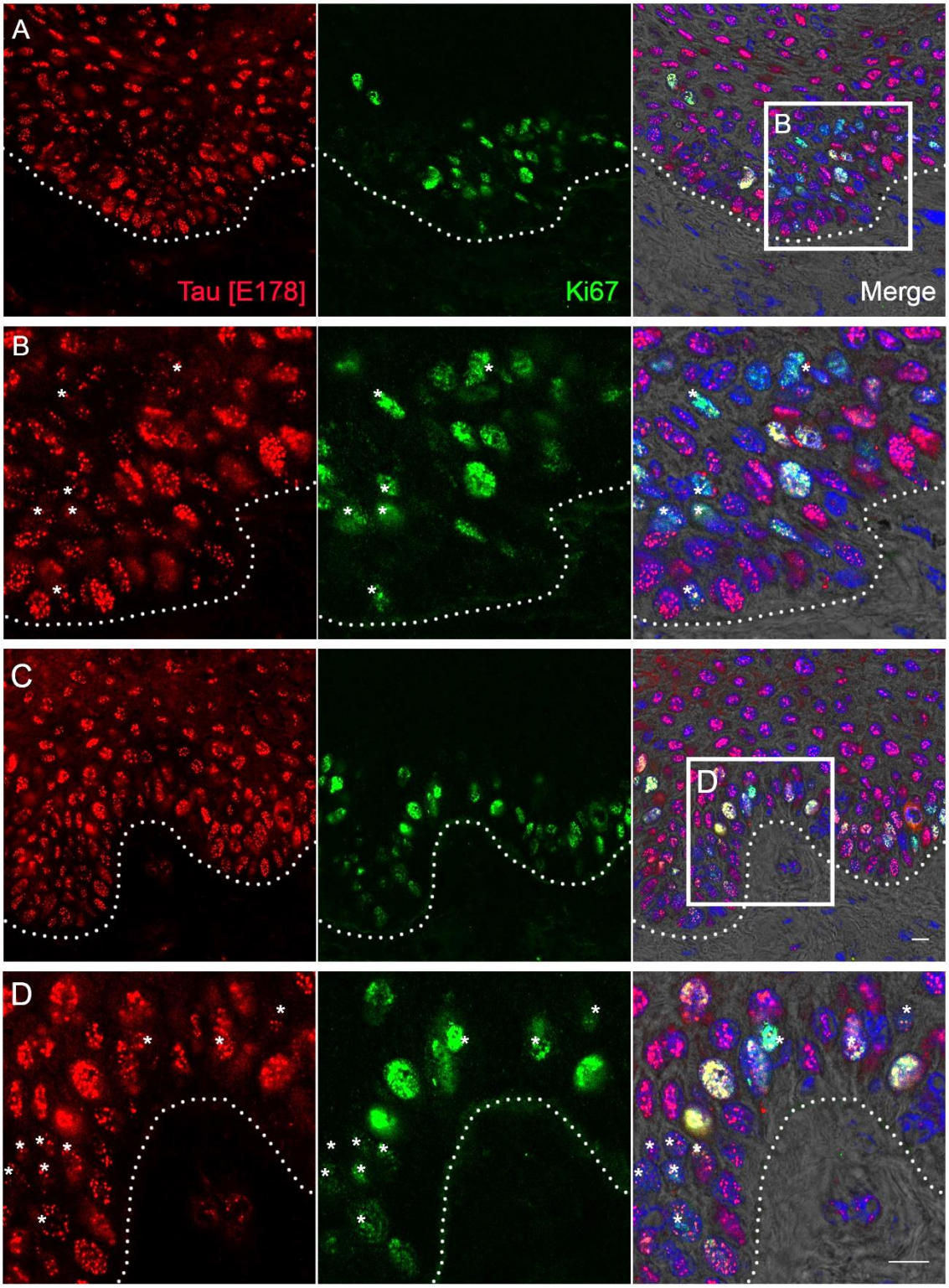

Figure 6.17. Tau expression in proliferating cells in squamous cell carcinoma.

Representative immunofluorescence analysis of proliferation marker, Ki67 (green) and tau (red) in SCC patient 19 biopsy (n=5). In SCC proliferating cells are not restricted to the basal layer and instead can be found in basal and suprabasal populations. SCs have a higher proliferative capability compared to their TAC counterparts; it is predicted that in normal tissue SCs comprise 1% of the epidermal cell population, rising to 20% of the population in SCC. **A&C.** Immunofluorescence analysis revealed that Ki67 positive cells can be found scattered throughout the basal and suprabasal populations of the tumour and tau

expression is restricted to the nucleus, but some cells display higher nuclear expression than others. **B&D.** High magnification images reveal that a proportion of Ki67 positive cells had lower tau levels in the nucleus then their neighbouring cells; indicated by stars. Nuclei counterstained with DAPI (blue) and all channels are displayed with the phase contrast image in the right panel to allow accurate visualisation of sample morphology. White dotted lines represent the epidermal-stromal boundary. Scale bar 10 µm.

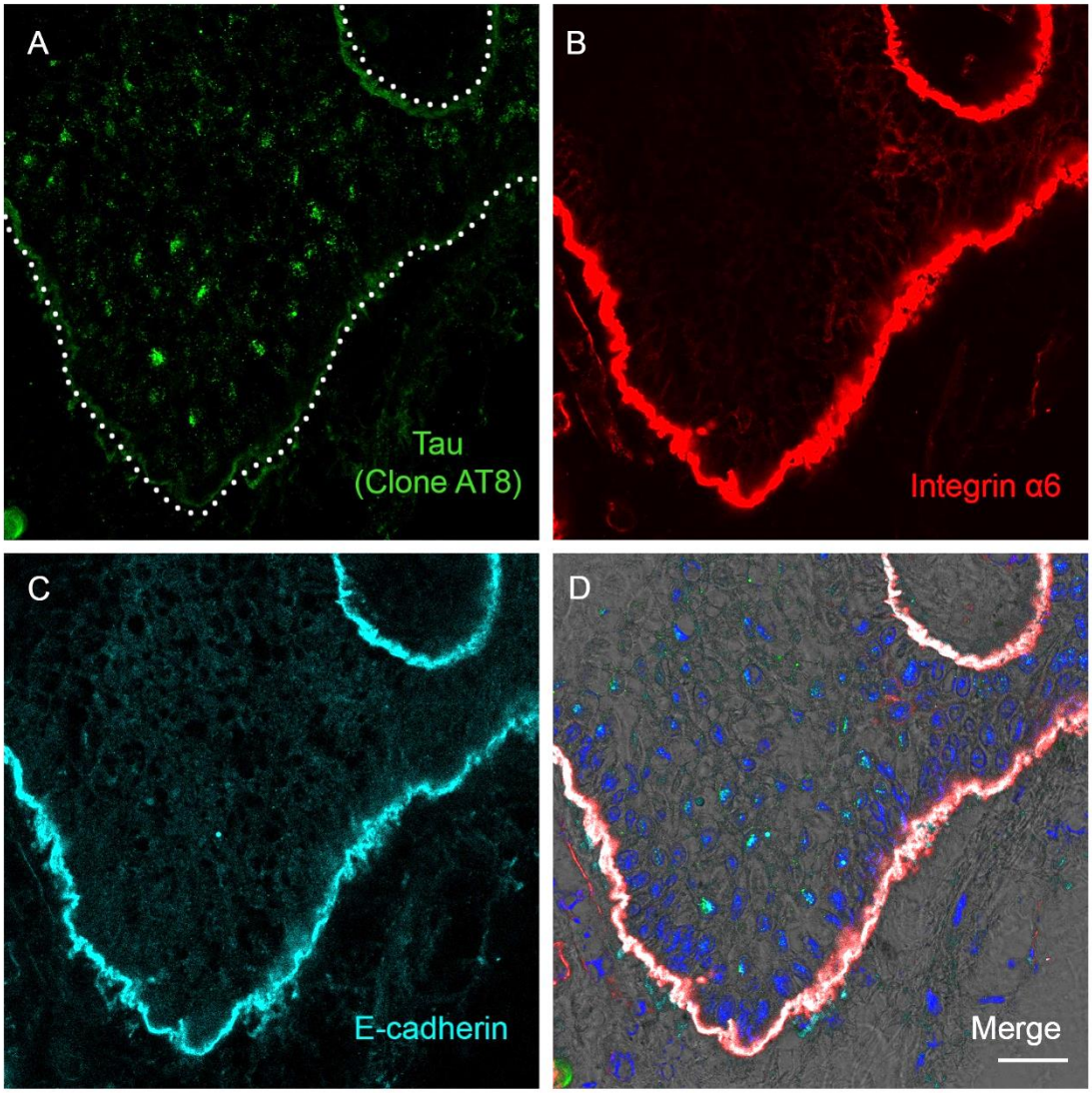

Figure 6.18. Phosphorylated tau is mostly restricted to the suprabasal population of cells in squamous cell carcinoma.
Immunofluorescence analysis of phosphorylated tau (green), Integrin-α6 (red) and E-cadherin (cyan) (n=5). **A.** Phosphorylated tau was absent in the basal keratinocyte populations, staining was only observed in the suprabasal population where its expression can only be detected in the nucleus. **B.** Intergin-a^6 labelled basal cells along the stromal boundary. **C.** E-cadherin labelled the cell membrane of the tumour cells. E-cadherin staining is significantly decreased in SCC epithelium compared to the healthy epidermis. **D.** Tau, Integrin-α^6 and E-cadherin staining merged and displayed alongside phase contrast image for visualisation of sample morphology. Dotted line represents the epidermal-stromal boundary and nuclei counterstained with DAPI (blue). Scale bar 25 µm.

In this study, SCC samples displayed high levels of integrin-α6 expression, whilst a reduced expression of E-cadherin was observed in all SCC samples (Figure 6.18). Although E-cadherin expression is reduced in SCC samples, slightly higher E-cadherin expression levels was found in the suprabasal regions of the biopsies. It was in these regions that tau [E178] expression co-localised with the cell membrane (Figure 6.19B). Tau expression was mostly restricted to the nuclear fraction of basal cells, however tau expression in the basal surface of cells connected to the BM occurred in some regions of the tumours, but was lost in most regions of SCCs (Figure 6.19D).

In Chapter 3 it was revealed that tau5 expression in healthy skin was mostly restricted to the cell membrane in granular layer of the epidermis, along with terminal differentiation markers such as loricrin. However, in SCCs the granular layer is often absent and initial characterisation of SCC samples used in this study confirmed the expression of terminal differentiation proteins, such as loricrin, varied within tumour samples and across patient biopsies (Figure 6.5). Therefore, the population of tau5 positive cells in SCC biopsies was expected to dramatically decrease, as tau5 was hypothesised to be associated with differentiated keratinocytes in healthy human skin. Immunofluorescence analysis of tau5 with E-cadherin and loricrin in SCC samples was carried out and strikingly, tau5 expression was not restricted to the uppermost layers of the epidermis in SCC samples and its expression was actually increased compared to healthy human skin (Figure 6.20; Figure 6.21). Tau5 did not co-localise with loricrin in SCC samples, but instead was found to be branching down into the tumour; the basal and immediately adjacent suprabasal cells remained absent for tau5 staining (Figure 6.20). Unlike the healthy epidermis, tau5 could be identified within the corneal layers of SCC samples, probably due to the incomplete differentiation.

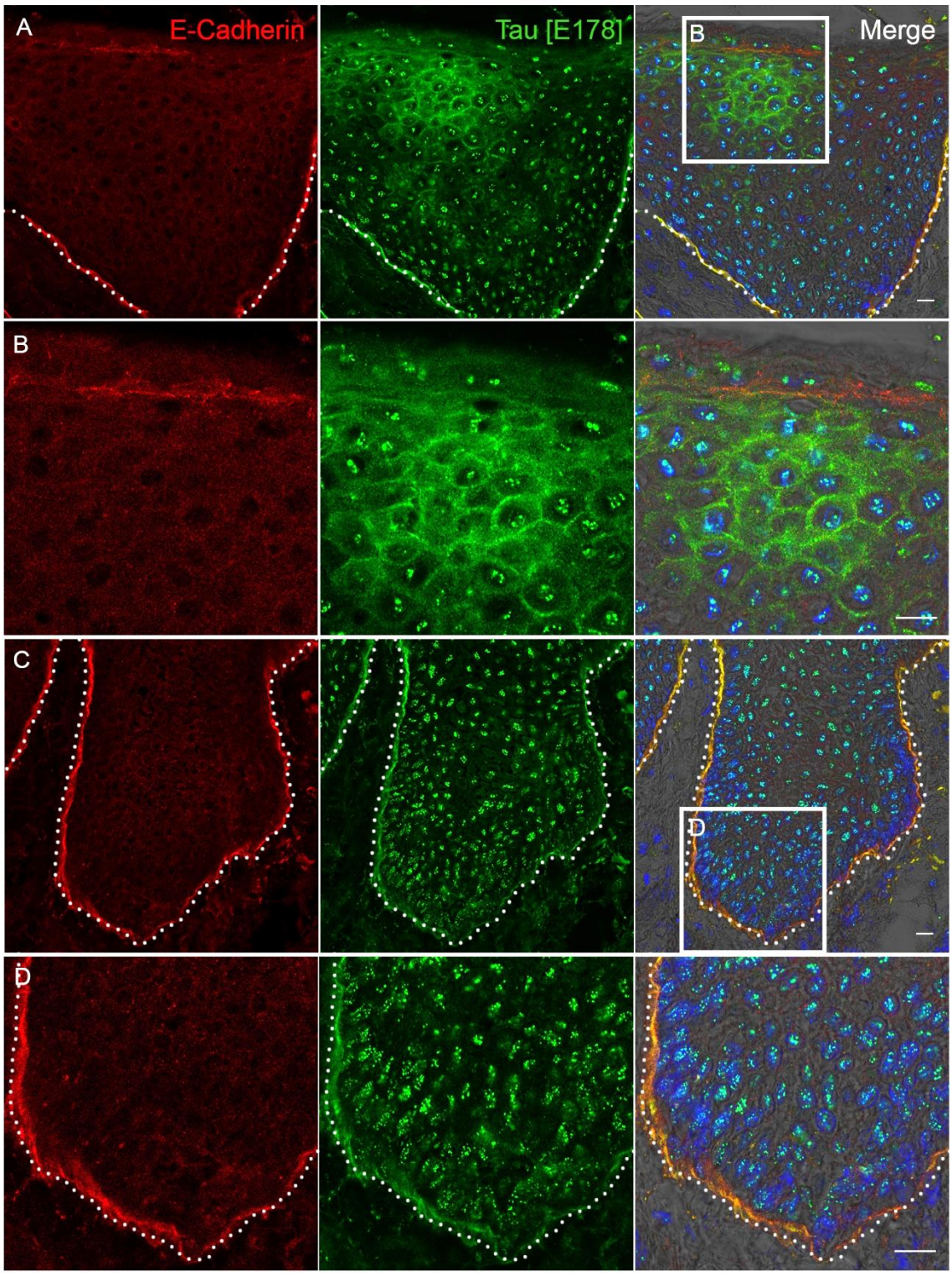

Figure 6.19. E-cadherin and tau expression in squamous cell carcinoma. Representative immunofluorescence analysis of E-cadherin (red) and tau [E178] (green) in SCC samples (n=5). **A&B.** Representative immunofluorescence analysis of suprabasal cells. Scale bar 10 µm. **C&D.** Representative immunofluorescence analysis of basal cells. Nuclei counterstained with DAPI (blue) and all channels are displayed with the phase contrast image in the right panel to allow accurate visualisation of sample morphology. White dotted lines represent the epidermal-stromal boundary. Scale bar 10 µm.

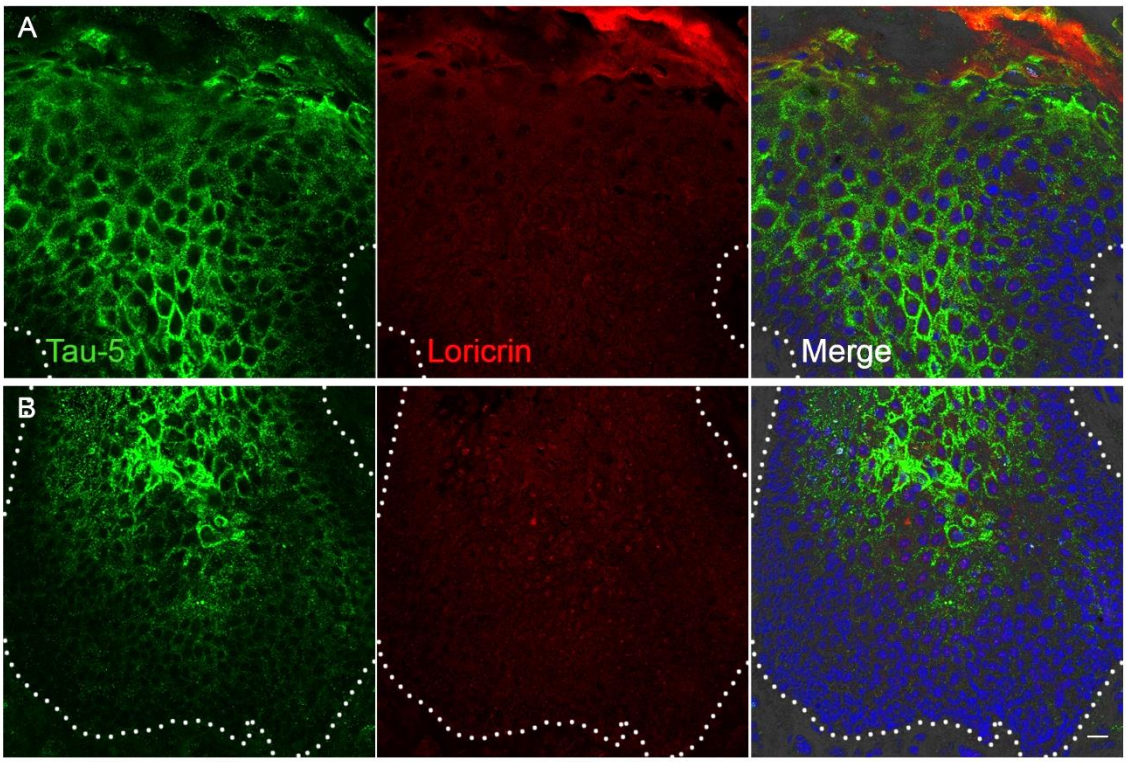

Figure 6.20. Tau5 and loricrin expression in squamous cell carcinoma. Representative immunofluorescence analysis of tau5 (green) and loricrin (red) in SCC. Interestingly, in the healthy epidermis tau5 was restricted to the granular layer where it co-localise with terminal differentiation protein loricrin, however, SCC usually lacks a granular layer due to incomplete differentiation of tumour cells. Therefore, it was assumed tau5 would be absent in SCC samples, however strikingly tau5 was actually increased compared to healthy skin samples and tau5 was extended down through the tumour. **A.** Tau5 displayed staining that appeared to be localised to the cell membrane with some possible cytoplasmic expression detected in the cells closest to the surface. Loricrin is mostly absent within SCCs, so co-localisation with tau5 is minimal. Tau5 could be identified within the corneal layers of SCC, probably due to the incomplete differentiation. **B.** Tau5 staining was absent in the basal and suprabasal cells directly adjacent to the basement membrane. Nuclei counterstained with DAPI (blue) and all channels are displayed with the phase contrast image in the right panel to allow accurate visualisation of sample morphology. White dotted lines represent the epidermal-stromal boundary. Scale bar 10 µm.

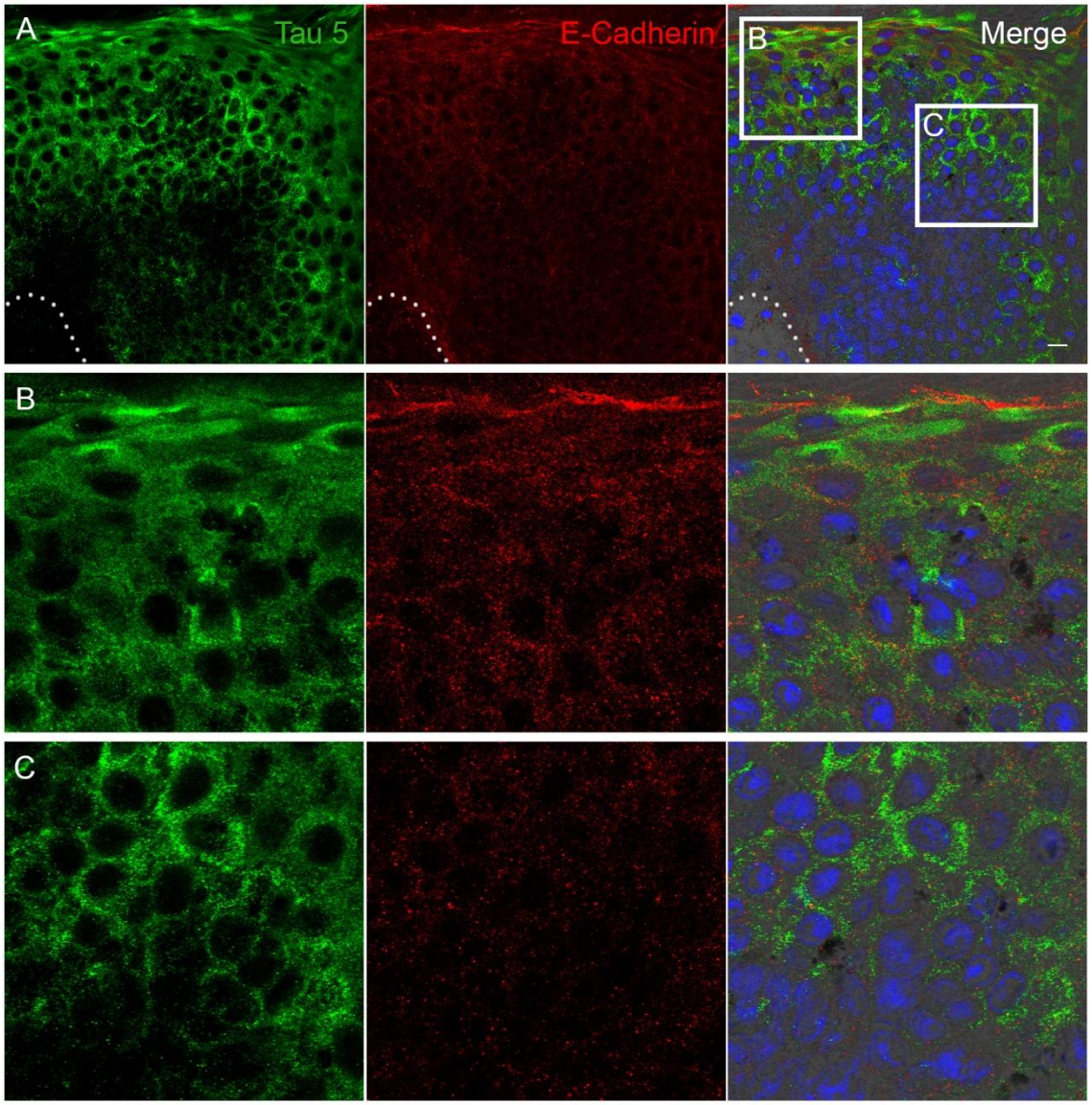

Figure 6.21. Tau5 and E-Cadherin expression in squamous cell carcinoma. **A.** Representative immunofluorescence analysis of tau 5 (green) and E-cadherin (red) in SCC samples (n=5). **B.** High magnification images of tau5 in the upper region of the tumour where tau5 was identified in the membrane fraction of the cells, co-localising with E-cadherin. Tau5 in the cells at the surface displayed a cytoplasmic expression of tau5 and evidence of tau5 retention within the stratum corneum. **C.** High magnification images show that tau5 staining decreased alongside the decreased E-cadherin within the tumour. Nuclei counterstained with DAPI (blue) and all channels are displayed with the phase contrast image in the right panel to allow accurate visualisation of sample morphology. White dotted lines represent the epidermal-stromal boundary. Scale bar 10 µm.

However, like healthy skin tau5 did co-localise with the E-cadherin staining in SCC samples (Figure 6.21B), and cells near the surface appeared to show cytoplasmic tau5 staining (Figure 6.21B). Interestingly, tau5 staining was observed in cell populations that retained more E-cadherin, while the populations that expressed little E-cadherin did not stain positive with tau5 antibody (Figure 6.21).

To further investigate whether tau 5 could also be detected in the cytoplasm, or if it was just resticted to the membrane fraction, Tau5 and tubulin staining was carried out (Figure 6.22). Unlike in healthy human skin, where mitosis is refined mostly to the basal layer, mitosis is often found in the spinous cells of SCC, this is reflected in the tubulin staining (Figure 6.22B). Mitosis can be seen occurring in the spinous cells and this mitosis is highlighted by the tubulin staining in the nucleus, showing the start of the mitotic spindle developing. Tau [E178] staining was also co-localised to the tubulin staining in the nucleus of the dividing cells (Figure 6.22).

The tau5 staining in Figure 6.22 highly resembles the spines that are associated with spinous cells, and suggests that tau might associate with the desmosomal and cell adhesion proteins in spinous cells. Although Figure 6.20 and Figure 6.21 indicated that tau5 displayed a membrane localisation, immunofluorescence analysis with tubulin showed a slight overlap with tau5 in the cytoplasm (Figure 6.22). Other studies have shown that tau can act as a linker protein between membrane associated proteins and the cytoskeletal network. However, further investigation would be needed to determine whether tau co-localises with desmosomal associated proteins in epithelial cells and acts as a linker to the cytoskeletal network.

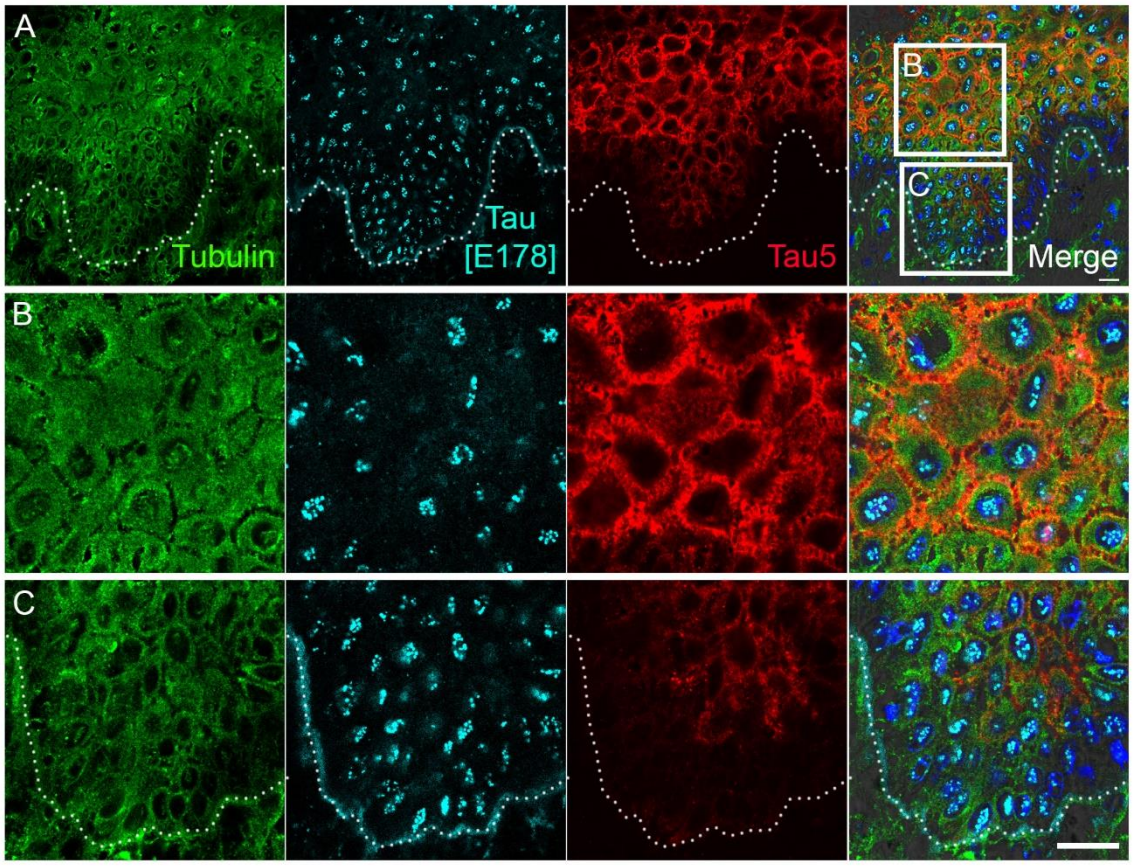

Figure 6.22. Tubulin and tau expression in squamous cell carcinoma.
A. Representative immunofluorescence analysis of tubulin (green), tau [E178] (cyan) and tau 5 (red) in SCC samples (n=5). **B.** High magnification of suprabasal cells shows a clear localisation of tau5 with the plasma membrane. Spinous cells within the epidermis get their name from the strong cell-cell connections through desmosomes, due to the 'spines' that connect the cells that can sometimes be observed after tissue processing. The tau5 staining highly resembles these spines, suggesting that tau might associate with desmosomal proteins in suprabasal SCC cells. **C.** High magnification of basal cells along the epithelial-stromal boundary shows an absence of tau5 staining in the basal and immediately adjacent suprabasal cells. Nuclei counterstained with DAPI (blue) and all channels are displayed with the phase contrast image in the right panel to allow accurate visualisation of sample morphology. White dotted lines represent the epidermal-stromal boundary. Scale bar 10 µm.

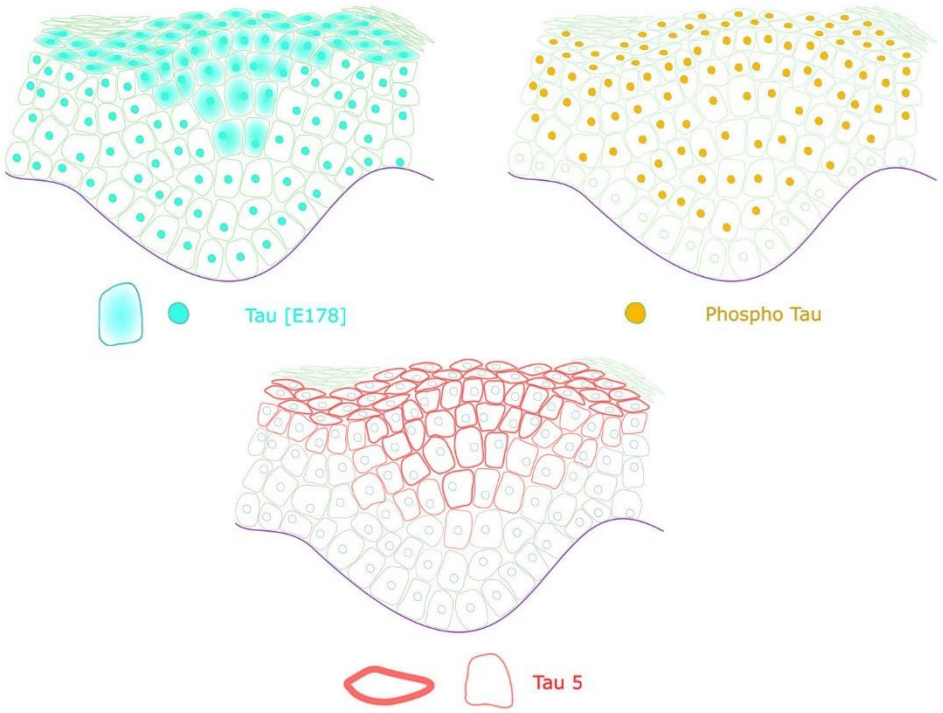

Figure 6.23. Schematic summary of tau antibody expression in SCC lesions.
Schematic representations of the tau expression profiles observed in SCC samples using the three commercial tau antibodies throughout this study. The epitope of each antibody corresponded to different regions of the tau protein and displayed distinct expression patterns in the epidermis. **A.** Expression profile of recombinant rabbit monoclonal Tau [E178] antibody targeting the C-terminal region of the tau protein that is present in all isoforms. Tau [E178] displayed a broad expression throughout the epidermis, but not all cells displayed the same level of tau expression. Some cells within the tumour had significantly lower tau expression within the nucleus compared to the surrounding cells. While cells undergoing mitosis has significantly higher levels of tau. Consistent with the acanthosis and lack of differentiation within SCC samples, tau [E178] staining was mostly restricted to the nucleus, with membranous and cytoplasmic expression in some cells in contact with the BM and detected in islands of cells which displayed some level of differentiation. Small levels of tau could also be detected within the corneal layers in SCC samples, an observation not found in healthy human skin when correct terminal differentiation takes place. **B.** Expression profile of Phosphorylated tau (Ser202/Thy205) (clone AT8) antibody targeting a phosphatase sensitive epitope, reported to have no cross reactivity to unphosphorylated tau. The antibody recognises phosphorylated Ser202/Thr205, Ser199/Ser202 and Thr205/Ser208 sites which are located in the PRD of the protein and is present in all isoforms. Phosphor tau was exclusively found in the nucleus of SCC cells, but almost no phosphorylated tau was observed in basal cells within SCC biopsies and instead was restricted to the suprabasal populations. **C.** Expression profile of mouse monoclonal Tau5 antibody targeting Ser210-Arg230 which lies within the PRD of the tau protein that is present in all isoforms. Tau5 expression was observed co-localised with mainly membrane associated proteins, with some evidence of cytoplasmic expression in the uppermost cells. Tau5 was not restricted to the uppermost cells, instead was

found branching down into the tumour, however basal and suprabasal cells immediately adjacent to the basal cells did not stain positively for tau5. It is hypothesised that the expression patterns of tau5 reflect the 3D structural conformation of the protein, as tau5 should be able to detect all isoforms of tau, but immunofluorescence staining only detects membranous tau, which in its bound form is predicted to expose its proline rich domain, which could explain the absence of tau5 staining in the lower epidermis in which membrane staining was not observed.

Table 6.3. An overview of Tau immunofluorescence staining presented in healthy and SCC human skin biopsies.

Antibody	Healthy human tissue					SCC				
	Epithelial				Mesenchymal	Epithelial				Mesenchymal
	SB	SS	SG	SC	Dermis	SB	SS	SG*	SC**	Stroma
Tau [E178]	++	+++	+++		++	++	+++	+++	+	++
Tau 5	+	+	+++		++		++	+++	+	++
PhosphorTau (clone AT8)	+	++	+++		+		++	+++		+
Keratin-14	+++	+				+++	+			
Integrin-α6	+++					+++				
CD80						++				
Bmi1						++	+			
Ki67	++	+			+	++	++			+
Keratin-1		+++	+++				+++	+++		
E-Cadherin	+++	+++	+++			+	+	++		
Loricrin		+	+++					+/++		
Tubulin	+++	++	++		++	+	++	++		++
Vimentin	+***				++	+***				+++
Tenascin C										+++
Periostin										+++

Staining profiles demonstrate the discrete staining patterns of tau observed in cSCC compared to healthy human skin. SB – Stratum basal, SS – Stratum spinosum, SG – Stratum granulosum, SC – Stratum corneum. Expression levels are categorised as: +, weak or scattered; ++, moderate expression; +++, strong expression. *The granular layer is often absent in SCCs, but can depend on the differentiation status of the lesion. **The SC is often not the same in SCC, due to incomplete programme of differentiation, incomplete packaging of proteins and retention of nuclei within this layer. ***Staining could be from other cell types found in the epidermis or EMT of the SCC cells.

6.4.2. Investigating tau function using squamous cell carcinoma cell line

The second objective of this chapter was to investigate the functional significance of tau in cSCC. This was achieved by different methods *in vitro* to analyse tau expression in SCC cells followed by manipulation of tau expression *in vitro*, to investigate the functional role of tau in SCC in the differentiation of SCC cells.

In this study, experiments *in vitro* were performed using a SCC cell line, A431. It appeared that tau expression was higher in SCC clinical samples than in the healthy epidermis. To quantitatively assess the observation, total RNA was extracted from A431 cells and compared to total RNA extracted from HEKn and HPEKp cells. RT q-PCR analysis confirmed that the relative expression of total tau was significantly higher in the SCC cell line A431, compared to both healthy keratinocyte cell lines (Figure 6.24A). Almost all isoforms of tau were also increased in A431 cells, with the exception of 1N transcript variants (Figure 6.24A). 4R transcript variants displayed the most significant relative increase in expression, but 4R transcript variants expression was low in basal keratinocytes, possibly explaining why such a large difference was observed. Therefore, RT q-PCR data was also analysed alongside calcium differentiated keratinocytes, to compare the expression of tau levels in differentiated keratinocytes and SCC cells. Interestingly, tau expression in A431 cells was still higher than in the calcium differentiated HEKn cells (Figure 6.24B). Immunofluorescence analysis with the three antibodies used throughout this study demonstrated that in A431 cells tau [E178] was found almost exclusively in the nucleus, consistent with staining in clinical samples (Figure 6.25A and B). Tau [E178] staining also showed varying tau expression levels between neighbouring cells, some cells have higher nuclear expression than others. Very little tau5 was detected in A431 cells cultured under normal cell culture conditions. When tau5 staining was

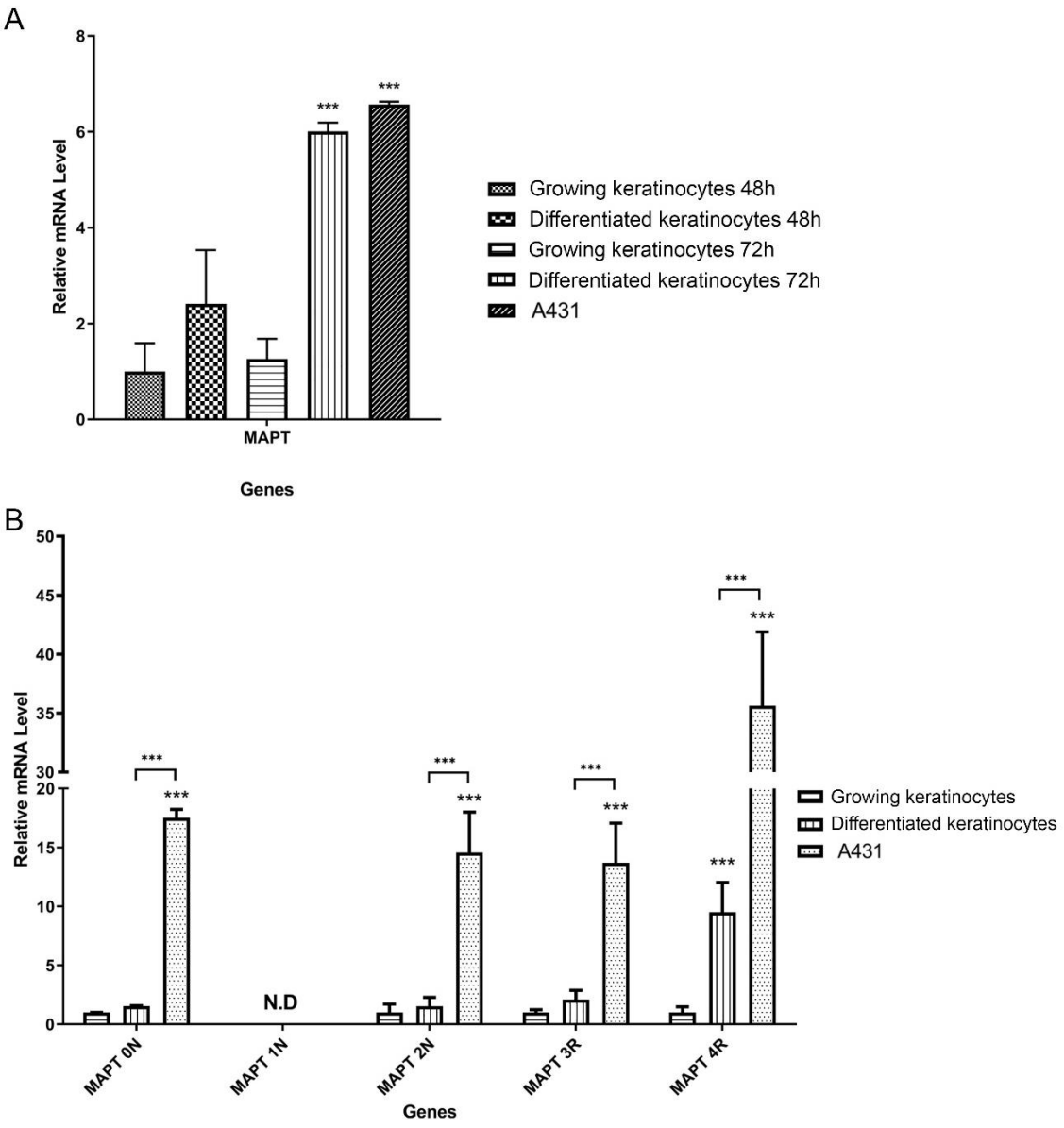

Figure 6.24. Tau expression in A431 cells compared to healthy keratinocytes.

A. Representative RT q-PCR analysis of total tau expression in A431 cells compared to healthy growing and differentiated at 48 and 72 h (Ca^{2+}) keratinocytes (n=3). **B.** RT q-PCR analysis of tau isoform expression in A431 cells compared to growing and differentiated keratinocytes at 72 h (n=3). Ct values normalised to 36B4 and $2^{-\Delta\Delta Ct}$ method of analysis used. Relative expression levels are displayed as mean ± SD. Two-way ANOVA with Bonferroni correction was used to test significance; *** $p<0.001$.

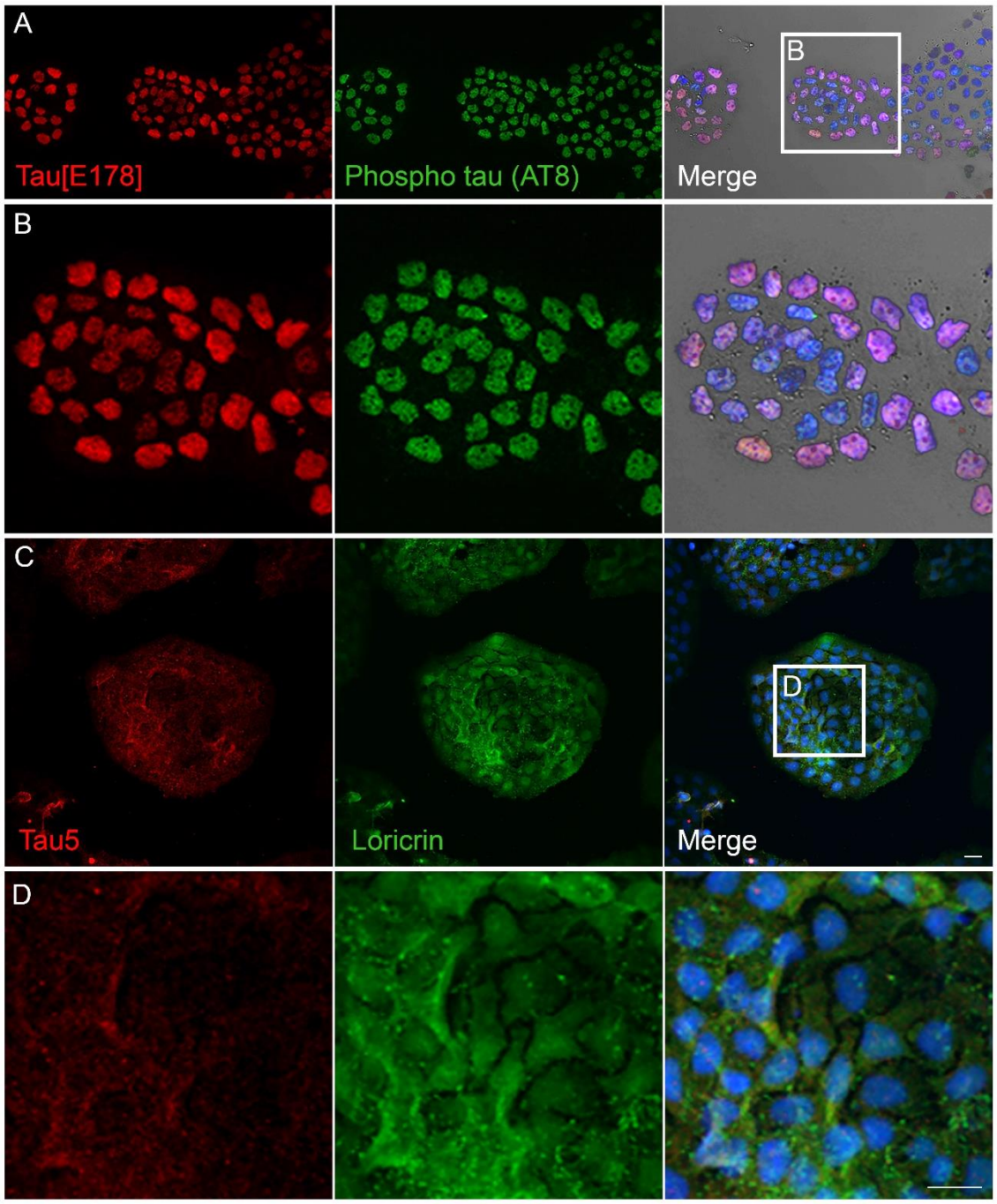

Figure 6.25. Immunoflurescence analysis of tau expression in A431 cells using three commercially generated antibodies used throughout this study. Immunofluorescence analysis of tau expression in A431 cells using the three tau antibodies used in this study (n=3). **A.** Representative immunofluorescence analysis of tau [E178] (red) and phosphorylated tau (green) in A431 cells. **B.** High magnification images show tau is restricted to the nucleus in A431 cells, with little or no cytoplasmic or membrane expression detected under normal cell culture conditions. **C.** Representative immunofluorescence analysis of tau5 (red) and loricrin (green) expression in A431 cells. **D.** High magnification images show little tau5 can be detected in A431 cells cultured under normal cell culture conditions. If tau5 staining was detected it was often associated with A431 cells displaying a more differentiated phenotype, as can be seen with the co-localisation of loricrin and tau5 expression. Nuclei counterstained with DAPI (blue) and all channels are displayed with the phase contrast image in the right panel to allow accurate visualisation of cell morphology. Scale bar 25 µm.

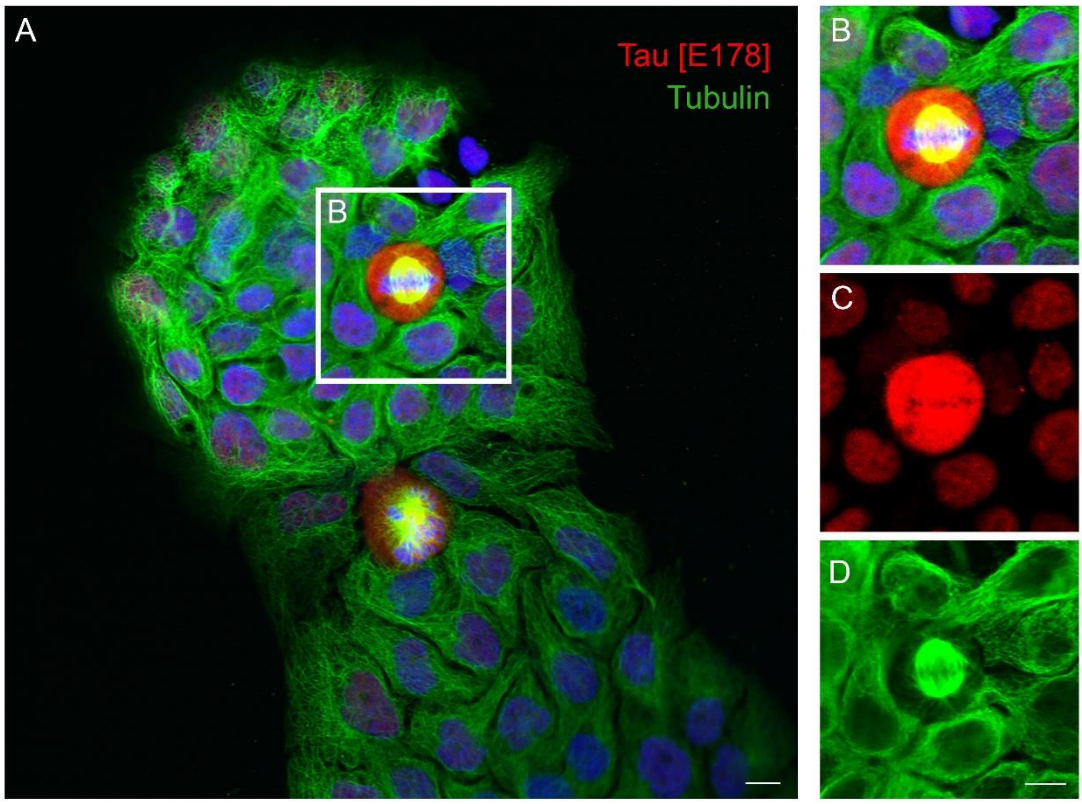

Figure 6.26. Immunoflurescence analysis of tau and tubulin expression in mitotic cutaneous squamous cell carcinoma cells.
A. Representative immunofluorescence analysis of tubulin (green) and tau [E178] (red) in A431 cells (n=3). Tau is restricted to the nuclear fraction of growing A431 cells. However, when mitosis takes place in A431 cells, tau can be observed throughout the cell surrounding the microtubules and chromosomes. **B-D.** High magnification image of an A431 cells during metaphase in which the mitotic spindle has been established and the chromosomes can be observed aligned along the metaphase plate. Tau can clearly be observed highly expressed throughout the cell and surrounding the chromosomes. Nuclei counterstained with DAPI (blue). Scale bar 10 µm.

detected it was often associated with A431 cells displaying a more differentiated phenotype, as can be seen with the co-localisation of loricrin and tau5 expression; consistent with observations in this study so far. As observed *in vivo*, A431 cells display increased tau [E178] staining co-localised with the mitotic spindle supporting the nuclear material during mitosis; this suggests tau may have a potential role in the stabilisation of mitosis in SCC cells.

6.4.2.1. Distinct tau expression profile can be found in A431 cell subpopulations

The SC attachment assay is a well-recognised method of separating healthy epidermal SCs from their TAC counterparts [49] however, it has not previously been reported as a method of separating SC and TAC populations of cancer cells. CSCs cells possess some of the same properties and characteristics as healthy keratinocyte SC populations, but the proportion of CSCs is expected to be much larger than the SC population in healthy epidermal keratinocytes. In healthy epidermal keratinocytes Chapter 4 identified that tau expression levels in SCs were much lower than their TAC counterparts. To test whether this also occurs in CSCs, the SC attachment experiment was conducted using un-fractioned A431 cells. As previously described, plates were coated with BM proteins to encourage SC attachment due to the increased integrin expression in SC populations. Attached and floating cell populations were collected at 20, 40 and 60 min after cell seeding (Figure 10.26). There was a strikingly large population of cells attached 20 min after cell seeding, and cells started regaining their cell shape after just 40 min with an almost normal polygonal physiology by 60 min (Figure 10.26); a significantly higher proportion of A431 cells attached compared to HEKn or HPEKp cells.

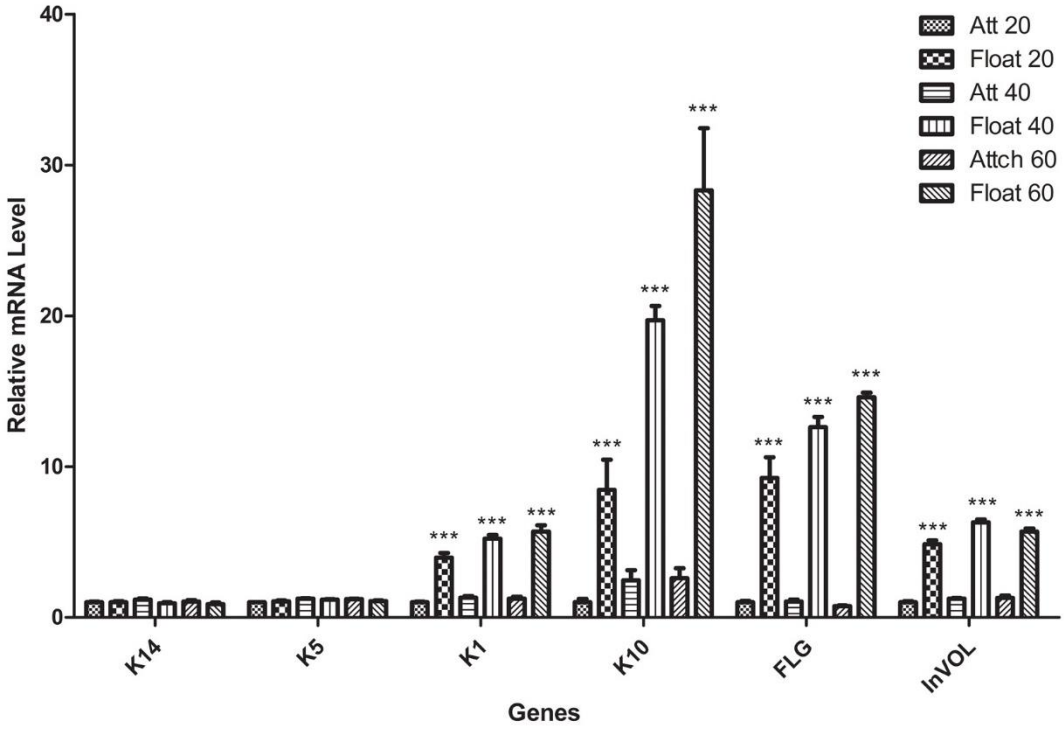

Figure 6.27. Gene expression of attached and floating A431 cell populations from a stem cell attachment assay.
Representative RT q-PCR analysis of attached and floating population of A431 cells. Floating populations displayed significant upregulation of keratin 1 (K1) and 10 (K10) alongside filaggrin (FLG) and involucrin (Invol). Ct values normalised to 36B4 and $2^{-\Delta\Delta Ct}$ method of analysis used. Relative expression levels are displayed as mean ± SD. Two-way ANOVA with Bonferroni correction was used to test significance; *** $p<0.001$.

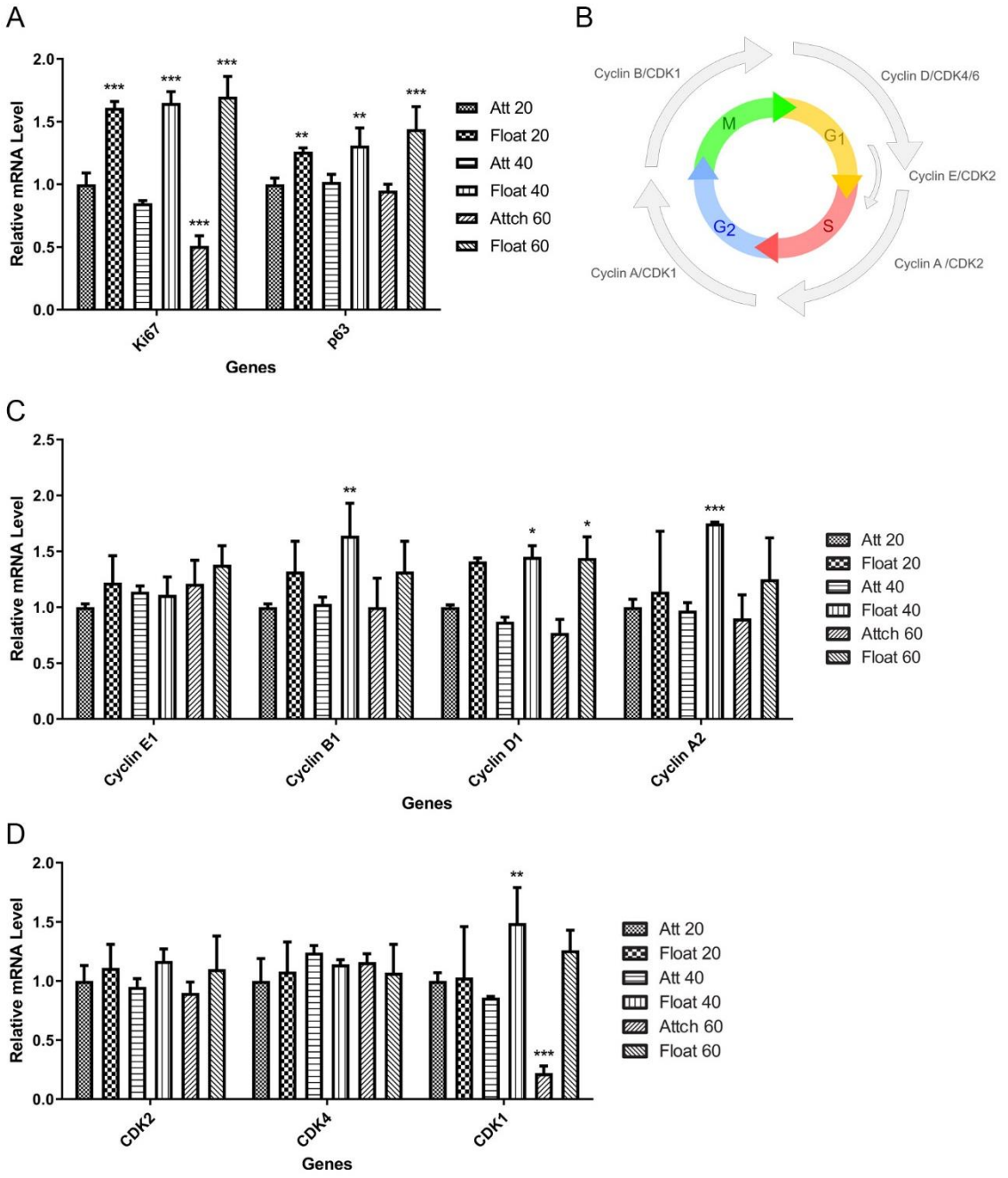

Figure 6.28. Cell cycle status of attached and floating A431 cell populations. **A.** Ki67 and p63 are significantly upregulated in the floating population compared to the attached population at every time point analysed. **B.** Schematic demonstrating the various stages of the cell cycle and the associated cyclins and CDKs at each stage. **C-D.** Representative RT q-PCR analysis of cyclin and CDK expression between attached and floating A431 cell fractions.. Ct values normalised to 36B4 and $2^{-\Delta\Delta Ct}$ method of analysis used. Relative expression levels are displayed as mean ± SD. Two-way ANOVA with Bonferroni correction was used to test significance; *p<0.05, ** p<0.01, *** p<0.001.

To assess whether this experiment had isolated populations of cells possessing SC and TAC properties, RT q-PCR analysis was used to evaluate gene expression of a panel of differentiation associated markers. Data revealed that the SC attachment assay effectively separate populations of A431 cells based on their differentiation status (Figure 6.27). Attached A431 populations were shown to express much lower levels of differentiation markers compared to their floating counterparts. K1 and K10 expression was found to be increased up to 5.7 and 28.3 fold compared to the attached cell populations respectively, whilst terminal differentiation markers filaggrin and involucrin were 14.5 and 6.3 fold higher in the floating population of cells respectively (Figure 6.27).

To further characterise this population, RT q-PCR analysis was performed on genes associated with cell proliferation and cell cycle progression. The floating population of A431 cells had significantly higher expression levels of Ki67 and p63 (Figure 6.28A). This active status in the cell cycle of the floating population was further supported by the increased relative expression of cyclins and CDKs in the floating cells compared with the attached population (Figure 6.28C and D).

Total and isoform specific tau expression was then analysed between these two populations of cells. Interestingly, despite the significant differences in differentiation and proliferation status between these two populations, analysis with q-PCR revealed that relative total tau expression remained fairly constant (Figure 6.29A). A significant increase in total tau expression was only observed between the attached and floating population at 40 min, but other time points remained relatively unchanged. Further investigation into isoform specific expression revealed some significant changes to the isoform expression of tau in attached and floating populations of A431 cells (Figure 6.29B-E).

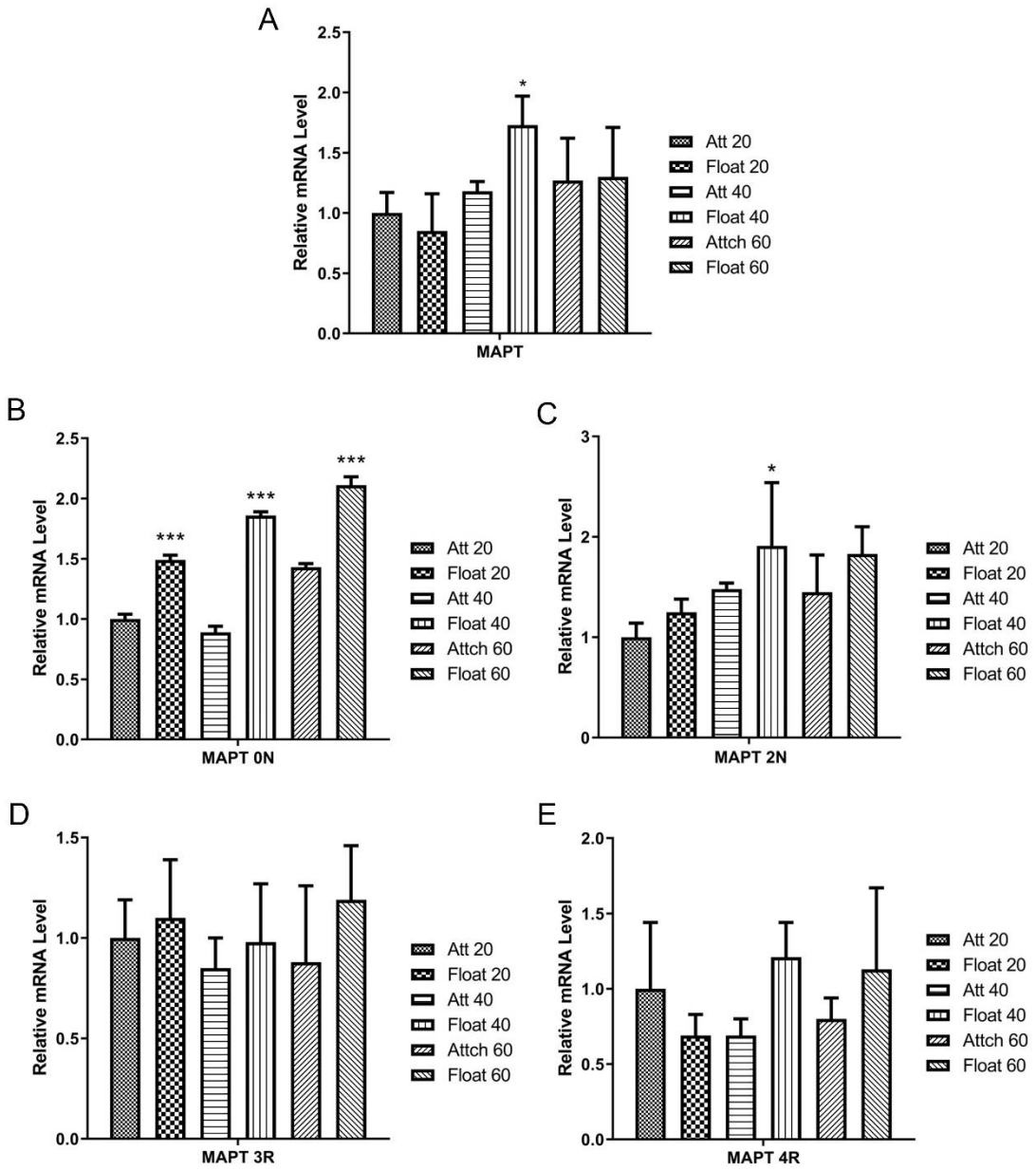

Figure 6.29. Total and isoform specific tau expression in attached and floating A431 cell populations isolated through a stem cell attachment assay.

A. Representative RT q-PCR analysis of total tau expression revealed that tau was fairly consistent in attached and floating populations, with a significant increase only observed in the floating population at 40 min. **B.** 0N expression was increased in floating populations. **C.** 2N isoform expression was increased in the floating population at each time point analysed. **D.** 3R expression was slightly increased in the floating population at each time point, but not enough to reach statistical significance. **E.** 4R isoform expression showed an increase in the floating population at 40 and 60 min but not enough to reach statistical significance. Ct values normalised to 36B4 and $2^{-\Delta\Delta Ct}$ method of analysis used. Relative expression levels are displayed as mean ± SD. One-way and Two-way ANOVA with Bonferroni correction were used to test significance; *p<0.05, ** p<0.01, *** p<0.001.

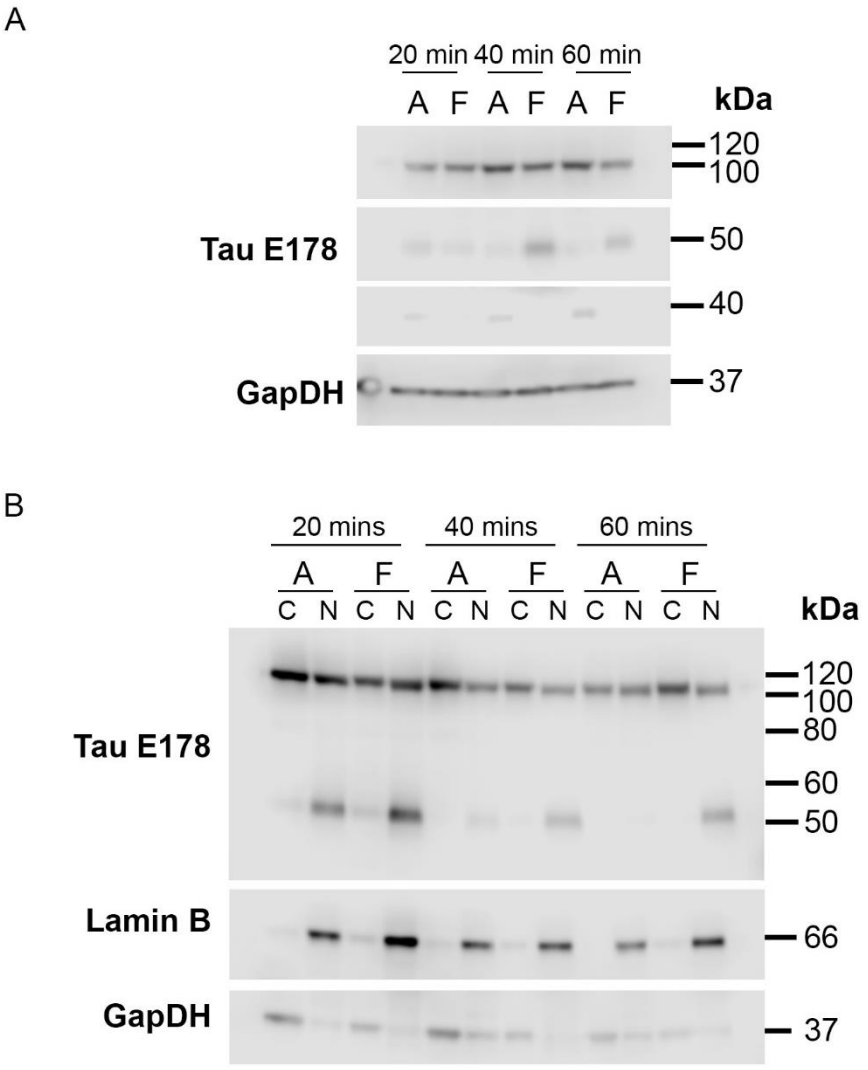

Figure 6.30. Western blot analysis of total protein expression and localisation in attached and floating A431 cells from stem cell attachment assay

A. Total protein was extracted from floating and attached A431 cell populations 20, 40 and 60 min after cell seeding. Western Blot analysis was performed to assess the tau expression between the SC populations and their TAC counterparts. Western blotting revealed that attached populations at 20, 40 and 60 min displayed a band at 40 kDa. Floating populations displayed a higher band at 50 kDa at 40 and 60 min. The band at 110 kDa was also identified throughout each sample indicating big tau expression. **B.** Cytoplasmic and nuclear protein was extracted and fractioned from attached and floating cell populations at 20, 40 and 60 min after seeding onto basement membrane coated dishes. Western blot analysis demonstrates that shorter isoforms of tau, 55 kDa, were highest in the nuclear fraction of cells compared to the cytoplasmic fraction. Big tau was detected in both nuclear and cytoplasmic fractions of cells. 55 kDa tau expression was consistently higher in the nuclear fraction of the floating cells (TAC) fraction compared to the attached (SC) population. Lamin B1 and Glyceraldehyde-3-Phosphate Dehydrogenase (GAPDH) were used to demonstrate purity of the nuclear and cytoplasmic fraction respectively. A - Attached; F - Floating; C – Cytoplasmic; N – Nuclear.

Analysis revealed that in the floating population, 0N transcript variants of tau were significantly higher in the floating population at each time point analysed (Figure 6.29B). Analysis of 2N expression however, revealed increased expression in the floating population at all time points, but this change was only significant at 40 min; consistent with the observations of total tau expression (Figure 6.29C). RT q-PCR analysis of alternative splicing of the microtubule binding domain in attached and floating populations revealed a slight increase in both 3R and 4R isoform expression in floating populations, although not quite reaching the threshold for statistical significance (Figure 6.29D and E).

To further confirm these changes observed at a transcriptional level, protein expression was analysed whereby total, nuclear and cytoplasmic protein were extracted from the attached and floating A431 cell populations at 20, 40 and 60 min. Western blot analysis was then performed to assess the tau expression and localisation between the SC populations and their TAC counterparts (Figure 6.30). The difference in transcriptional variants highlighted by q-PCR analysis was confirmed with Western blotting. Western blotting revealed that attached populations of A431 cells at 20, 40 and 60 min displayed a band at 40 kDa, indicating shorter isoforms of tau. Floating populations displayed an increased band at 50 kDa at 40 and 60 min, consistent with the increased tau expression identified with q-PCR in the floating population at 40 and 60 min. The usual band at 110 kDa was identified throughout each sample indicating the inclusion of exon4A in some tau transcripts in both SC and TAC cells. Additionally, Western blot analysis of cytoplasmic and nuclear fractions of each cell population further confirmed that smaller isoforms (55 kDa) of tau were detectable in the nuclear fraction of A431 cells, while big tau was identified in both the cytoplasmic and nuclear fraction of A431 cells. 55 kDa tau was consistently higher in the nuclear

fraction of the floating cells compared to the attached population. This is consistent with observations throughout this study that tau expression is higher in TACs and differentiated cell populations compared to SC populations.

6.4.2.2. Investigating tau function in A431 cell line

Gene expression of tau was manipulated using esiRNA to knockdown tau expression and a tetracycline inducible overexpression plasmid, which overexpressed 2N4R isoform of tau in A431 cells and allowed the functional significance of tau in A431 cells to be evaluated.

6.4.2.2.1. Knockdown of tau interrupts cytoskeletal dynamics in A431 cells and induces cellular differentiation

To investigate the role tau plays in SCC cells, tau expression levels were manipulated *in vitro*. With the use of RNAi mediated downregulation of tau gene expression, the effect on A431 cell differentiation, cell cycle progression and cytoskeletal organisation was investigated. Using esiRNA to knockdown *MAPT* expression with esiRNA targeting *RLUC* as a negative control (Figure 6.31), RT q-PCR revealed that treatment with esiRNA *MAPT,* tau was successfully downregulated, with a 90% reduction in mRNA (Figure 6.31B). This knockdown was further confirmed at a protein level using Western blot and Immunofluorescence analysis (Figure 6.31C-D). Interestingly, knockdown of *MAPT* induced a significant increase in genes associated with differentiation in A431 cells compared to the control (Figure 6.32). The increase in keratin-1 expression in A431 cells following siRNA-mediated knockdown of tau was confirmed using Western blotting (Figure 6.32B and C). An increased cell size and alterations to cell shape was also identified when tau was KD in A431 cells (Figure 6.31A, Figure 6.33 and Figure 6.34).

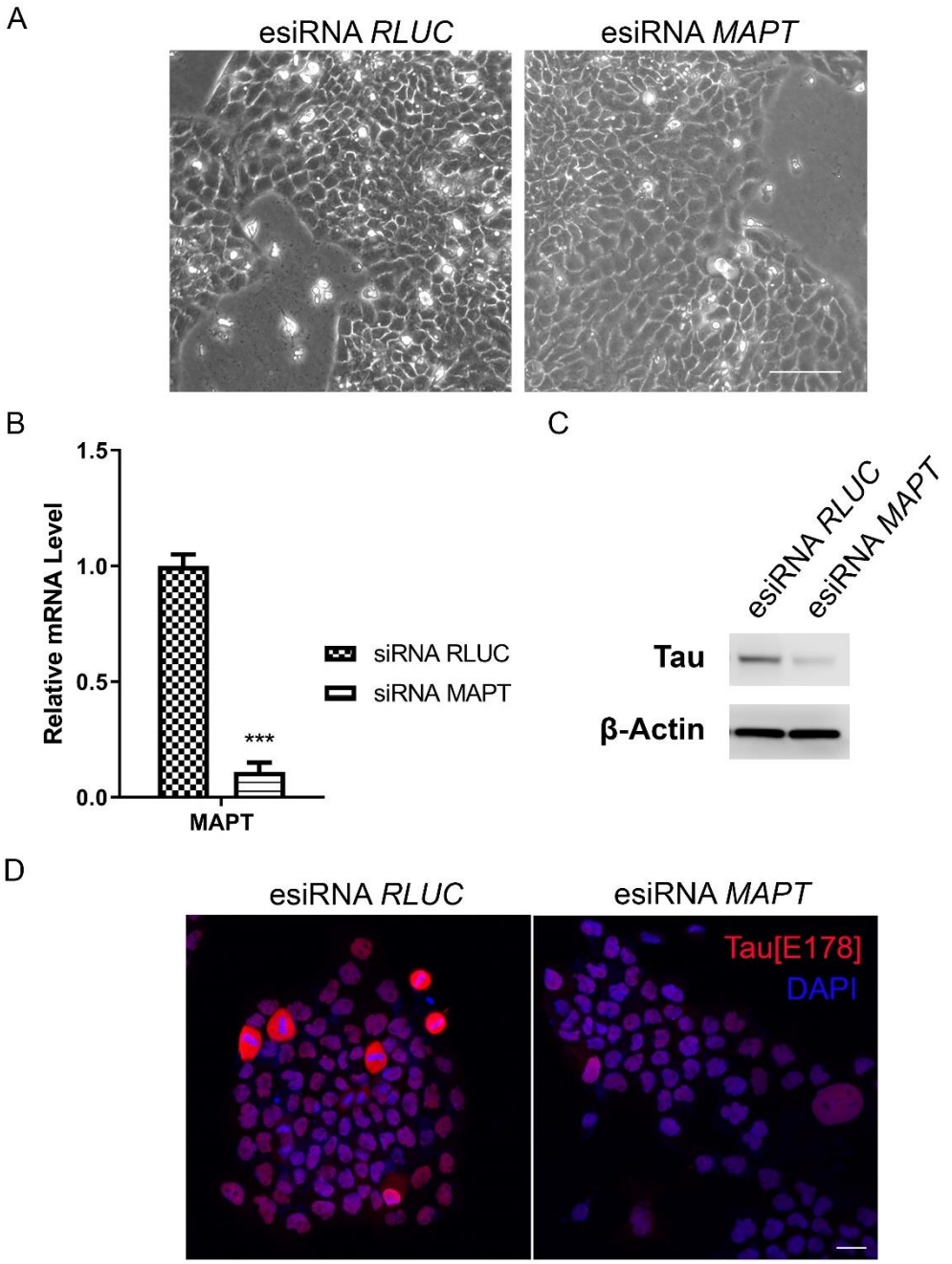

Figure 6.31. Analysis of tau expression following siRNA mediated tau knock down in A431 cells.
A. Representative cell culture images of non-transfected A431 cells and A431 cells 48 h after treatment with esiRNA *RLUC* and *MAPT* (n=3). Scale bar 100 µm. **B.** Representative RT q-PCR of tau expression following siRNA mediated tau KD. Ct values normalised to 36B4 and $2^{-\Delta\Delta Ct}$ method of analysis used. Relative expression levels are displayed as mean ± SD. Two-way ANOVA with Bonferroni correction was used to test significance; *** $p<0.001$. **C.** Western Blot analysis of tau expression in A431 cells following esiRNA treatment. Tau was successfully knocked down at a protein level. β-Actin was used as a house keeping gene. **D.** Representative immunofluorescence analysis of tau expression (red) in A431 cells following 48 h of siRNA treatment. Tau expression is successfully knocked down following 48 h of treatment with esiRNA *MAPT* compared to its controls. Nuclei counterstained with DAPI (blue). Scale bar 25 µm.

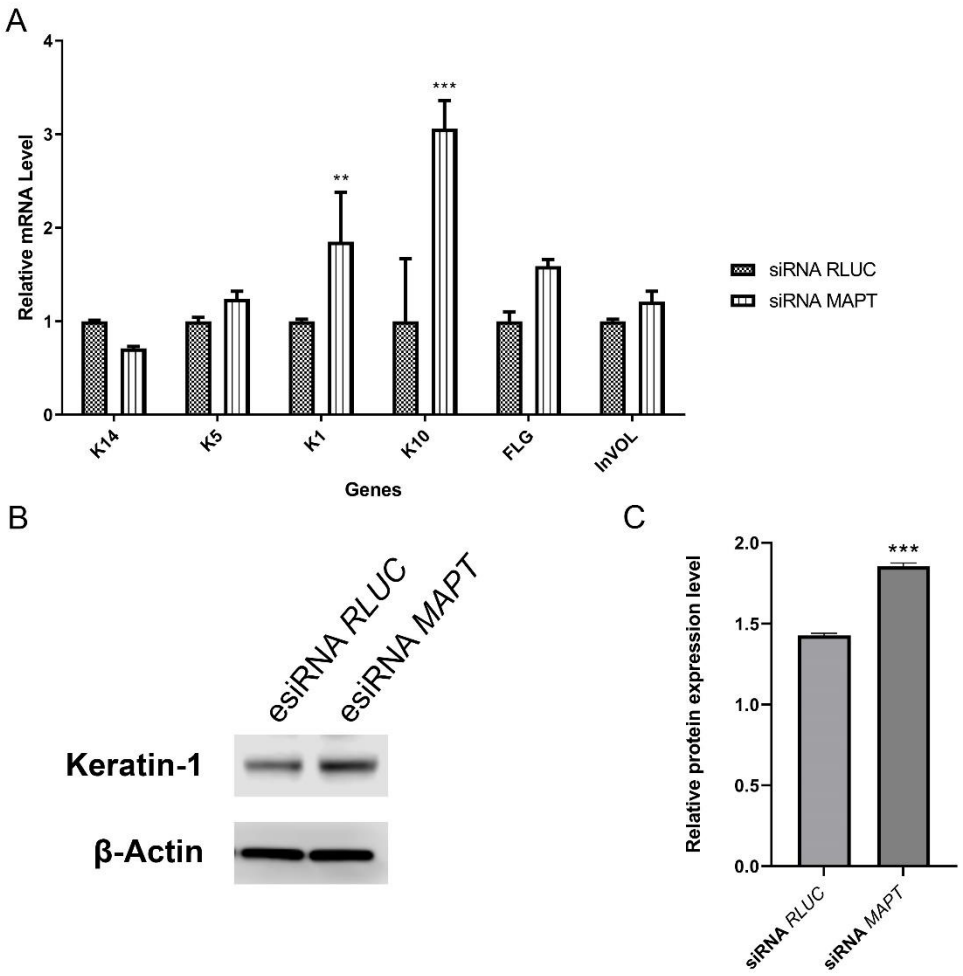

Figure 6.32. Expression of genes associated with differentiation in A431 cells following siRNA-mediated knockdown of tau.
A. Representative RT q-PCR analysis of the expression of genes associated with differentiation in SCC cells following esiRNA *MAPT* treatment with esiRNA *RLUC* as negative control (n=3). Tau knockdown resulted in a significant increase in the expression of genes associated with cell differentiation. K14 – keratin 14; K5 – keratin 5; K1 – keratin 1; K10 – keratin 10; FLG – filaggrin; Invol – involucrin. Ct values normalised to 36B4 and $2^{-\Delta\Delta Ct}$ method of analysis used. Relative expression levels are displayed as mean ± SD. Two-way ANOVA with Bonferroni correction was used to test significance; *p<0.05, ** p<0.01, *** p<0.001. **B.** Western blot analysis of keratin-1 expression following tau knockdown in A431 cells. Keratin-1 expression is significantly increased compared to both the control and negative control. β-Actin was used as a house keeping gene. **C.** Quantification of the signal intensity of keratin-1 protein expression normalised to the control. A significant increase in the relative protein expression can be observed following tau knockdown compared to both the control and negative control. Data presented as average ± SD. An unpaired *t*-test was used to test significance; *** p<0.001.

Immunofluorescence analysis of tubulin organisation following tau knockdown revealed that control cells displayed long elongated tubulin network that spanned throughout the cytoplasm to the cell periphery. However, upon tau knockdown, a number of cells reorganised their tubulin network and instead were observed at the cortical edge of the cells in a thick bundle (Figure 6.33). In Figure 6.33 cells can be seen in various stages of mitosis. Following siRNA-mediated tau knockdown the mitotic spindle looks less organised and defined compared to the control (Figure 6.33F). The tubulin and IF network are both major contributors to the cytoskeletal network. Therefore, as in epithelial cells keratin is the major constituent of the IF network, immunofluorescence analysis of keratin-14 was carried out to assess whether the disturbance to the tubulin network also reflected a disturbance to the IF network. K14 presented with a disorganised phenotype in A431 cells 48 h of tau was knocked down compared to controls (Figure 6.34). Interestingly, E-Cadherin expression was stronger in the tau KD A431 cells compared to controls, but the organisation and morphology of the E-cadherin presented with an abnormal phenotype (Figure 6.34F). E-cadherin displayed a disjointed, discontinuous morphology along the cortex of the cells when tau was KD, highlighting the change in shape following tau KD in A431 cells.

Investigation into cell cycle progression following tau knockdown revealed that there was a slightly delayed response to tau knockdown in A431 cells. However, by 72 h a significant increase in proliferation markers was observed and confirmed with immunofluorescence analysis of Ki67 (Figure 6.35). RT q-PCR of cyclin expression 72 h after siRNA-mediated tau knockdown revealed an increase in the expression of all cyclins following tau knockdown in A431 cells (Figure 6.35C).

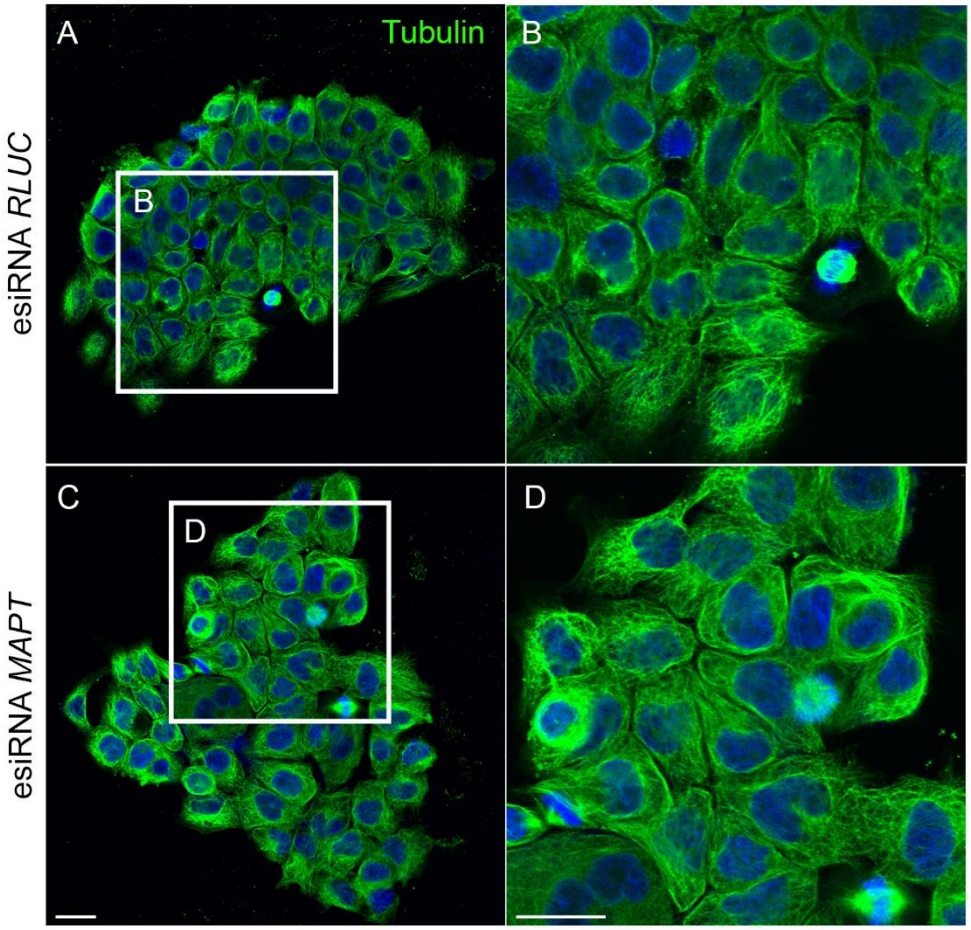

Figure 6.33. Tubulin organisation in A431 cells following esiRNA-mediated tau knockdown.
Representative immunofluorescence analysis of tubulin organisation (green) in A431 cells following *MAPT* knockdown, with esiRNA *RLUC* used as a negative control (n=3). **A&B.** esiRNA *RLUC* treated A431 cells. **C&D.** esiRNA *MAPT* treated A431 cells. Nuclei counterstained with DAPI (blue). Scale bar 25 µm.

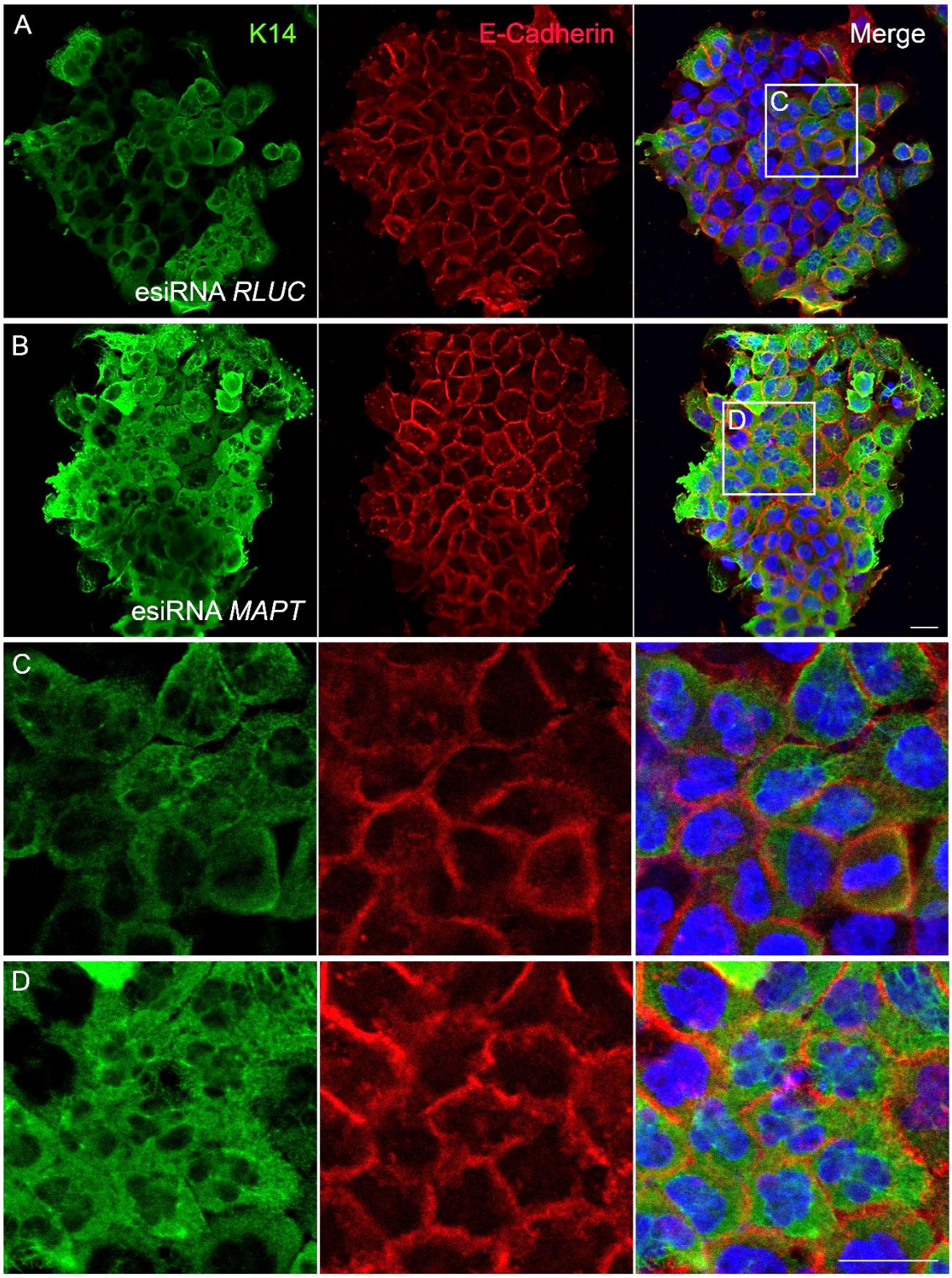

Figure 6.34. Immunofluorescence analysis of keratin and E-cadherin organisation following siRNA-mediated knockdown of tau in A431 cells. Representative immunofluorescence analysis of keratin-14 (green) and E-cadherin (red) in A431 cells 48 h after siRNA-mediated tau knockdown (n=3). **A&C.** esiRNA *RLUC* treated A431 cells. **B&C.** esiRNA *MAPT* treated A431 cells. Knockdown of tau resulted in a disorganised phenotype of keratin-14 filaments compared to controls. E-cadherin interestingly appeared to increase following tau knock down in A431 cells. Nuclei counterstained with DAPI (blue) and all channels are displayed in the right panel to allow accurate visualisation of cellular morphology. Scale bar 25 µm.

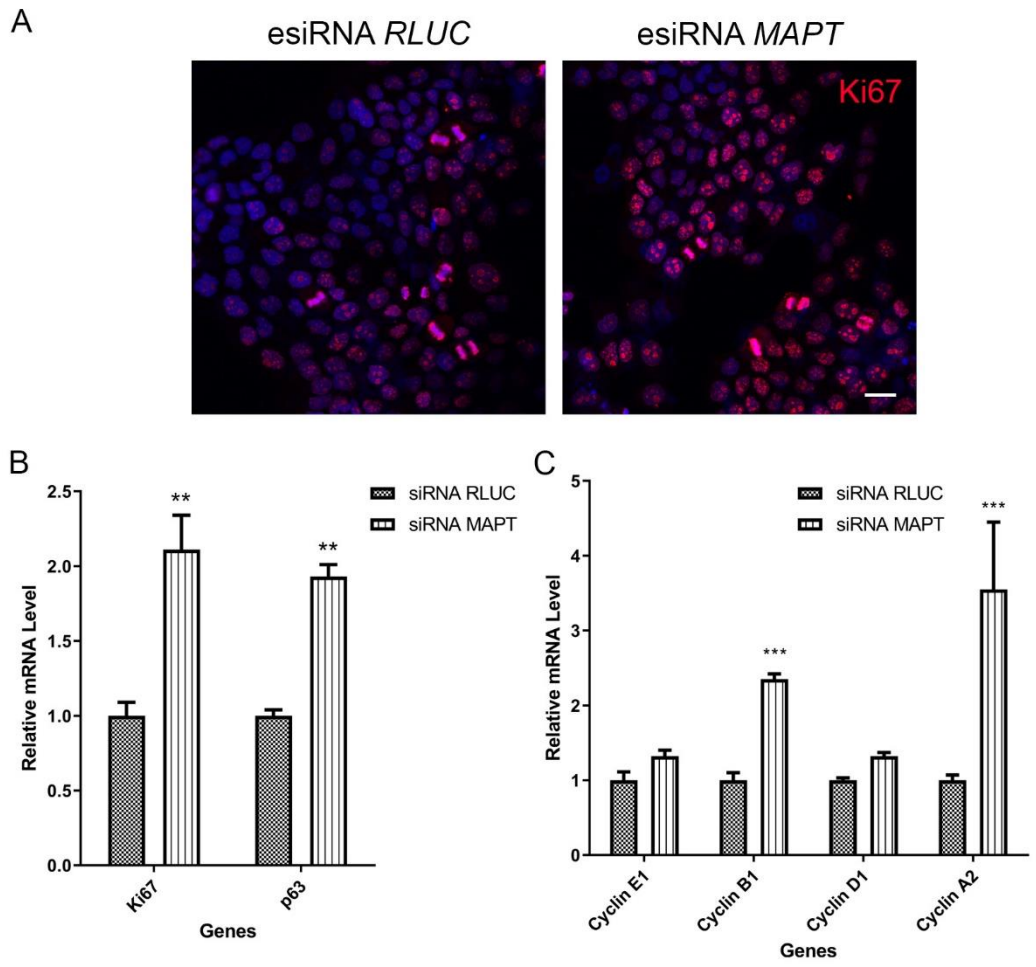

Figure 6.35. Analysis of cell proliferation following tau knockdown in SCC cells.

A. Immunofluorescence analysis of Ki67 (red) expression in A431 cells following siRNA treatment. Nuclei counterstained with DAPI (blue). Scale bar 25 µm. **B.** RT q-PCR analysis of proliferation markers showed a significant increase 72 h after tau knockdown in A431 cells compared to non-transfected and negative control cells. **C.** RT q-PCR of cyclin expression 72 h after siRNA-mediated tau knockdown. There was a significant increase in the expression of all cyclins following tau knockdown in A431 cells. Ct values normalised to 36B4 and $2^{-\Delta\Delta Ct}$ method of analysis used. Relative expression levels are displayed as mean ± SD. Two-way ANOVA with Bonferroni correction was used to test significance; *p<0.05, ** p<0.01, *** p<0.001.

6.4.2.2.2. Overexpression of 2N4R tau induces differentiation in squamous cell carcinoma cells

To continue investigating the role of tau in SCC cells, expression of tau in A431 cells was manipulated using lentiviral particles to infect cells with pINDUCER20 tau, and use the tetracycline response elements to promote the overexpression of the 2N4R tau gene. In this study, using healthy epidermal keratinocytes it was observed that the overexpression of tau resulted in an increase in keratinocyte differentiation and stratification. A common phenotype of SCC is a lack of cell differentiation, and many cancer therapies are based around inducing differentiation. Therefore, the next aim of this chapter was to investigate whether overexpression of tau in SCC cells could lead to increased differentiation and ultimately, whether this could potentially be used as a therapy to treat skin cancer. This could also help determine why patients suffering with AD (who have an overexpression of tau alongside NFT formation) may experience a lower incidence of SCC.

A431 cells were infected with the tetracycline-inducible vector, pINDUCER20 tau, for the overexpression of 2N4R (441 aa) isoform of tau (Figure 6.36), with empty vector, pINDUCER20 as control. Lentiviral infected cells, were selected using G418 to ensure only successfully infected cells which subsequently had G418 resistance were being cultured and used for experiments. 2N4R tau

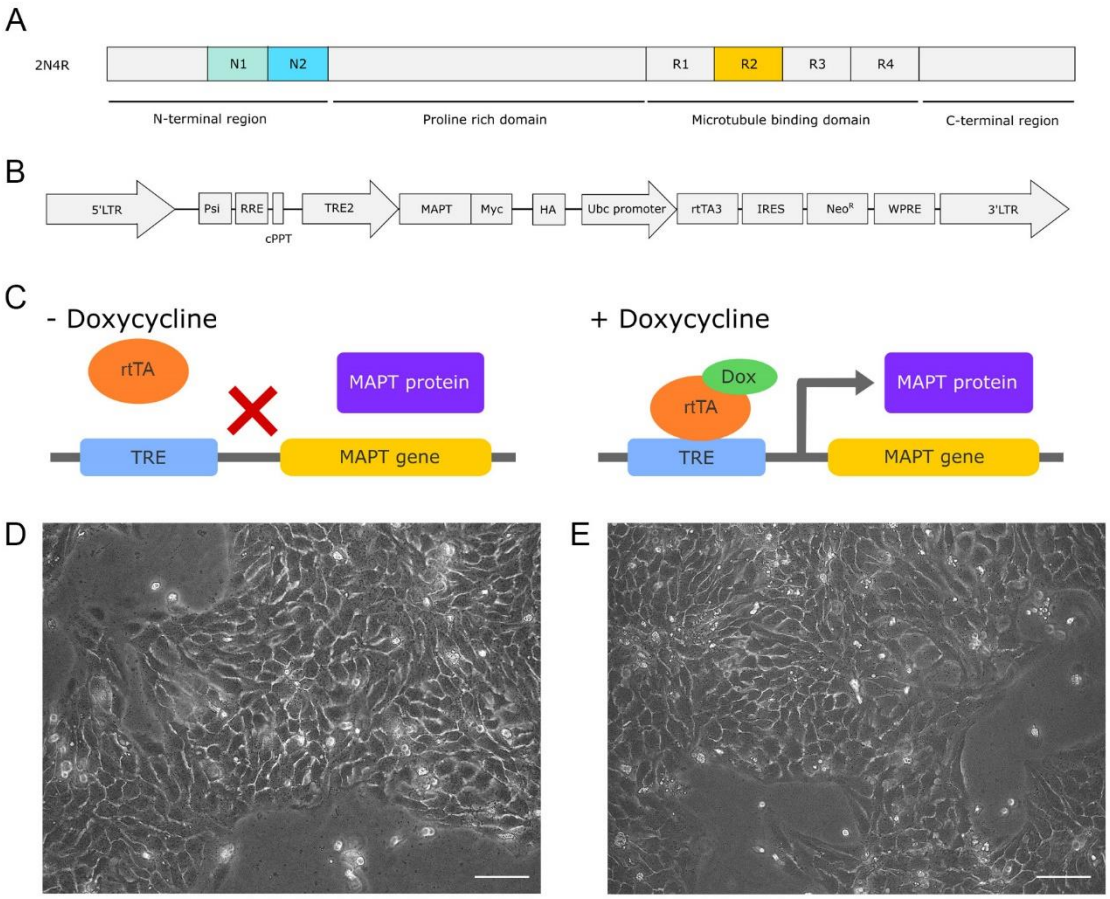

Figure 6.36. Tetracycline inducible overexpression of 2N4R (441 aa) tau in A431 cells.
A. Schematic representing the 2N4R (441 aa tau) tau isoform. **B.** pINDUCER20 tau plasmid construct used to create lentiviral particles for infection of epidermal keratinocytes. **C.** Schematic displaying how the tetracycline inducible tau overexpression system works, and how gene expression is regulated by the presence and absence of tetracycline. When no doxycycline is present, the rtTA transcription factor cannot bind to the promoter and gene expression is not induced. When doxycycline is present, doxycycline binds to the rtTA transcription factor and allows it to bind to the DNA at the Tet-op promoter, subsequently driving gene expression of 441 aa tau. rtTA – reverse tetracycline transactivator. TRE – tetracycline-responsive promoter element. tetO – Tet operator. **D.** A431 cells infected with pINDUCER20 tau without doxycycline. **E.** A431 cells infected with pINDUCER20 tau with doxycycline added to the culture medium driving 2N4R tau overexpression. Scale bar 75 µm.

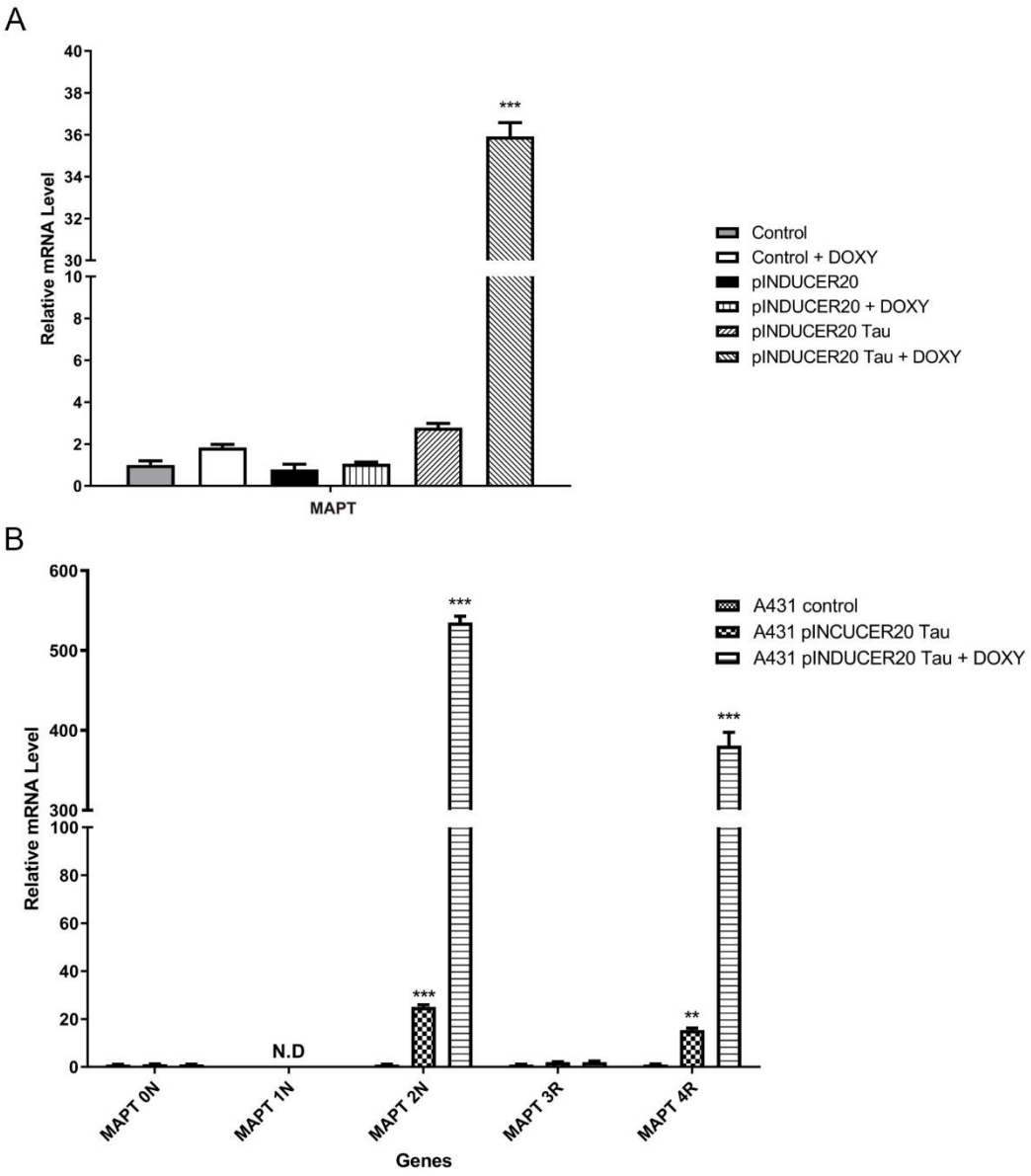

Figure 6.37. Tau gene expression following doxycycline induced 2N4R tau overexpression.

A. Representative RT q-PCR analysis of total tau expression in pINDUCER20 tau and controls following 48 h after doxycycline treatment (n=3). Tau is significantly overexpressed following doxycycline treatment compared to all of its controls. **B.** Representative RT q-PCR analysis of tau expression using isoform specific primers in pINDUCER20 tau and controls following 48 h of docycyline treatment. Ct values normalised to 36B4 and $2^{-\Delta\Delta Ct}$ method of analysis used. Relative expression levels are displayed as mean ± SD. Two-way ANOVA with Bonferroni correction was used to test significance; * $p<0.05$, **<0.01, *** $p<0.001$.

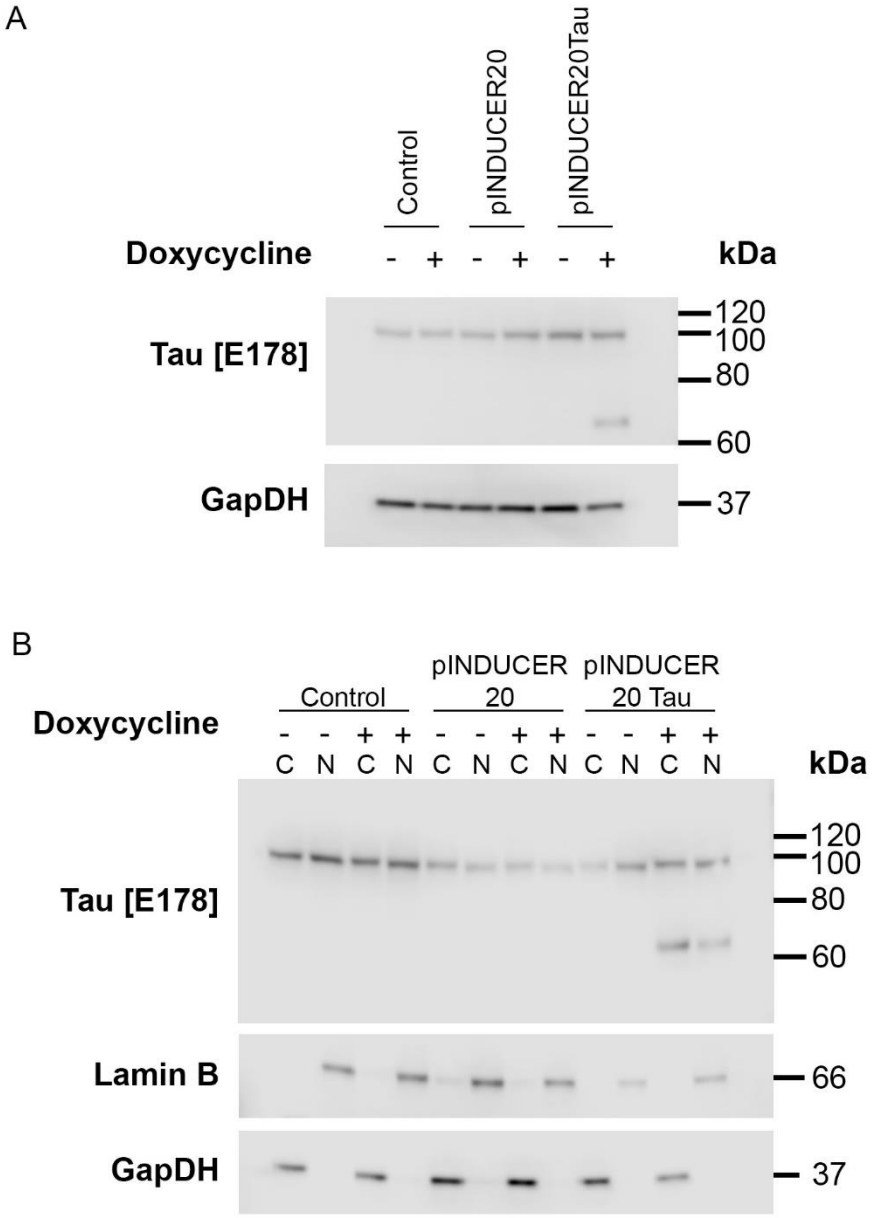

Figure 6.38. Western blot analysis of 2N4R tau overexpression in pINDUCER20 tau infected A431 cells.
A. Western Blot analysis of tau [E178] in the total protein of A431 pINDUCER20 tau mediated overexpression of 2N4R (441 aa) tau following 48 h of doxycycline treatment compared to its controls (n=3). Glyceraldehyde-3-Phosphate Dehydrogenase (GAPDH) was used as housekeeping gene. **B.** Western Blot analysis of cytoplasmic and nuclear protein fractions of pINDUCER20 tau mediated overexpression of tau [E178] compared to its controls. Lamin B1 indicates nuclear purity and GAPDH indicates cytoplasmic purity. C – cytoplasm, N - nucleus.

overexpression was induced with the addition of doxycycline to culture medium; doxycycline was used to induce gene overexpression as it has a higher binding affinity to rtTA then tetracycline, low cell toxicity and a known half-life of 24 h.

To confirm the successful infection, selection and overexpression of tau following doxycycline treatment, RNA and protein were extracted from A431 cells for analysis. RT q-PCR analysis confirmed that 48 h after doxycycline treatment tau was significantly overexpressed in A431 cells (Figure 6.37A). RT q-PCR analysis with isoform specific primers demonstrated that the 2N4R isoform of tau was exclusively overexpressed (Figure 6.37B). Although there is a slight “leakage” of 2N4R mRNA in pINDUCER20 tau compared to control, this was not translated at a protein level (Figure 6.38). Western blot analysis revealed that 441 aa tau protein overexpression was only identified in doxycycline treated pINDUCER20 tau cells (Figure 6.38A). Overexpression was identified in both the cytoplasmic and nuclear fraction of A431 cells (Figure 6.38B and Figure 6.39). Immunofluorescence analysis further confirmed tau overexpression in only pINDUCER20 tau cells treated with doxycycline. In all other A431 cells tau expression was only confined to the nucleus, expect during mitosis, but following tau overexpression, tau was also identified in the cytoplasm (Figure 6.39). Tau overexpression had very little effect on the phosphorylation status of tau in A431 cells. However, strikingly A431 cell size was noticeably larger in cells overexpressing tau, similar to observations in healthy keratinocytes (Figure 6.39).

Analysis of gene expression within differentiation associated proteins revealed that upon tau overexpression in A431 cells, a significant decrease in the expression of almost all basal cell markers occurred after 48 (Figure 6.40A). Additionally, gene expression of differentiation markers K1 and K10 were upregulated in A431 cells after tau protein overexpression (Figure 6.40B). There

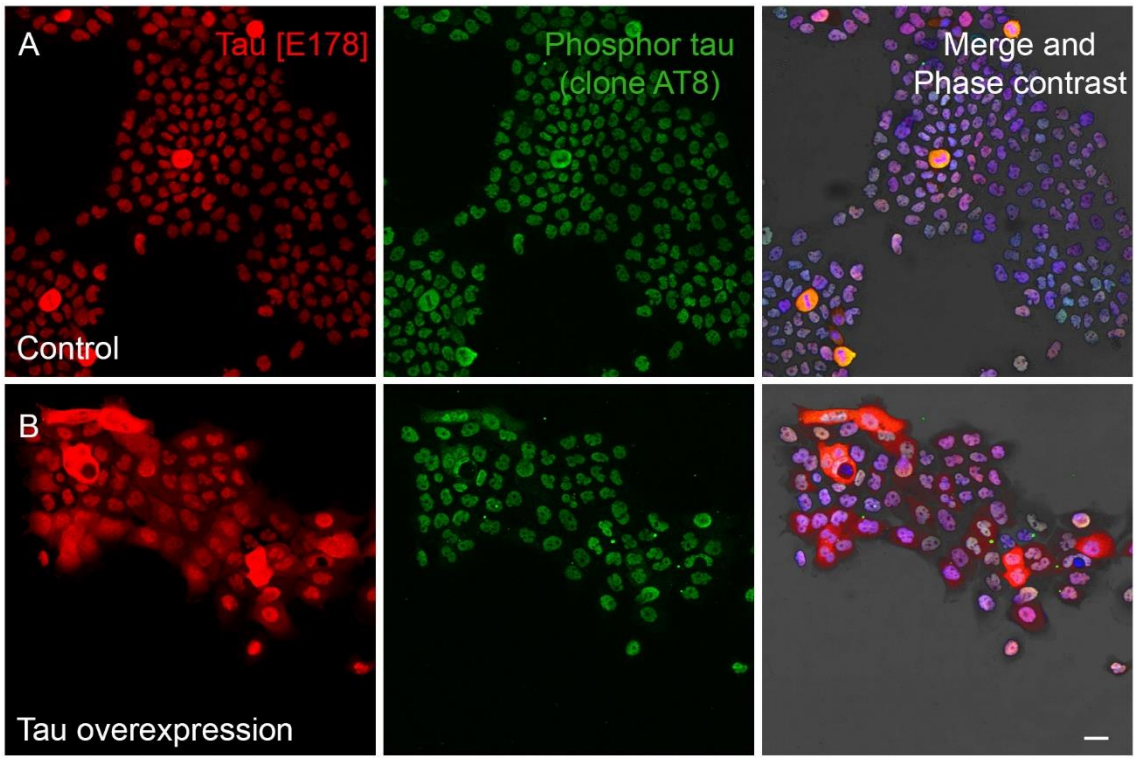

Figure 6.39. Immunofluorescence analysis of tau overexpression in A431 cells.
Representative immunofluorescence analysis of tau [E178] (red) and phosphorylated tau (AT8) (green) in A431 cells with and without tau overexpression (n=3). **A.** pINDUCER20 tau cells without doxycycline. Tau can be observed to be restricted mostly to the nucleus of the A431 cells, with little or no cytoplasmic tau protein detected, other than in mitotic cells. **B.** pINDCER20 tau A431 cells after 48 h of doxycycline treatment to induce tau overexpression. Tau can be observed in nuclear and cytoplasmic fraction of cells. Not as many cells could be observed in mitosis in this population of A431 cells. Cells are also observed to have a larger morphology than their controls. Nuclei counterstained with DAPI (blue) and all channels are displayed alongside phase contrast in the right panel to allow accurate visualisation of cellular morphology. Scale bar 25 µm.

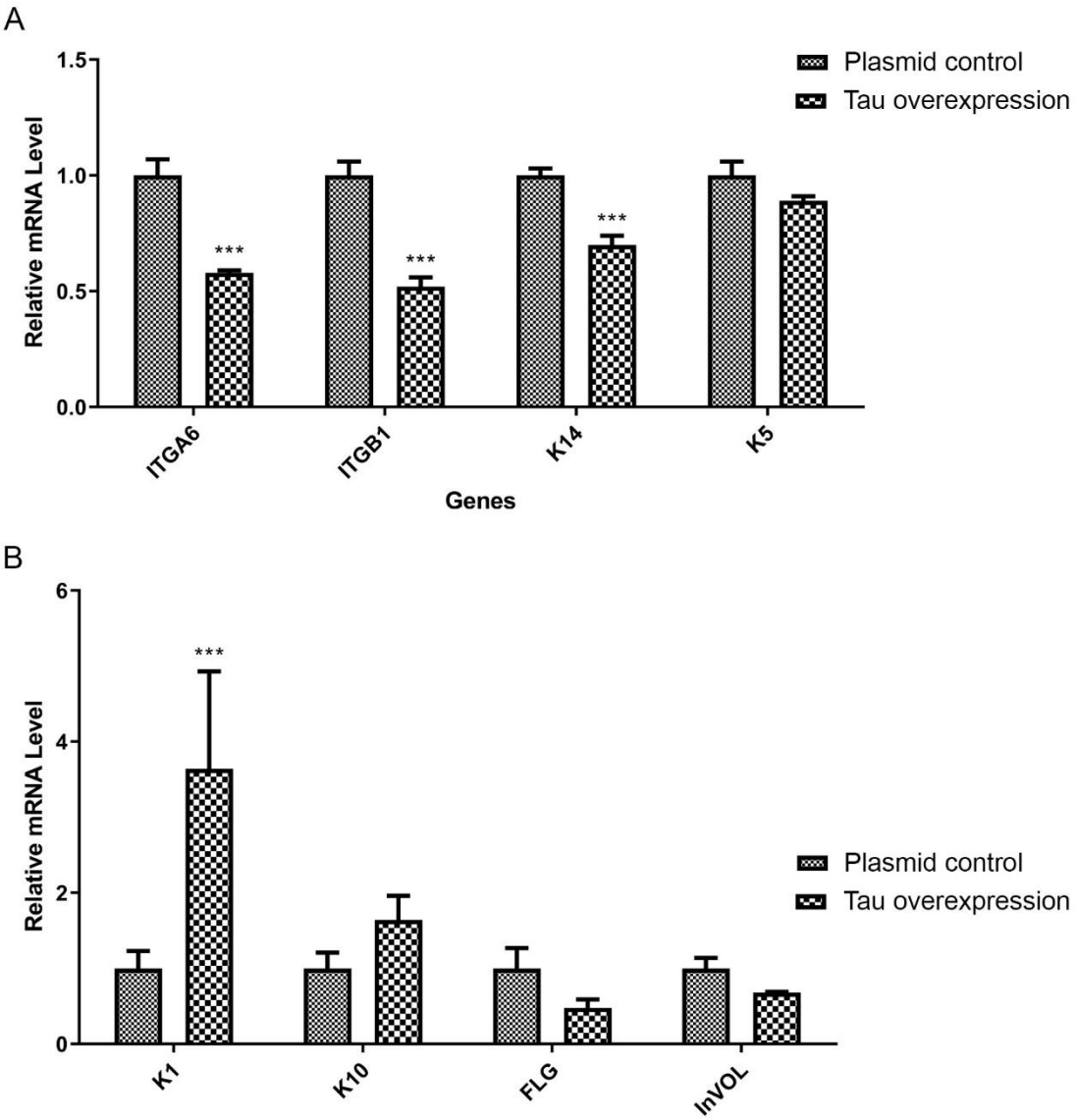

Figure 6.40. RT q-PCR analysis of gene expression in A431 cells following tau overexpression.

A. Representative RT q-PCR analysis of the relative gene expression of genes associated with an undifferentiated cell phenotype 48 hours after doxycycline induced tau overexpression in A431 cells. Gene expression was analysed by taking away the relevant control from the doxycycline treated cells, to reduce unwanted effects of doxycycline from being analysed. ITGα6 – integrin-α6; ITGβ1 – integrin-β1; K14 – keratin 14; K5 – keratin 5. **B.** Representative RT q-PCR analysis of the relative gene expression of genes associated with cell differentiation in the epidermis. K1 – keratin 1; K10 – keratin 10; FLG – filaggrin; Invol – involucrin. Ct values normalised to 36B4 and $2^{-\Delta\Delta Ct}$ method of analysis used. Relative expression levels are displayed as mean ± SD. Two-way ANOVA with Bonferroni correction was used to test significance; *** $p<0.001$.

were no significant changes in the relative gene expression of loricrin or filaggrin following tau overexpression however, a longer time may have been required to observe differences in gene expression of proteins associated with the later stages of terminal differentiation.

Immunofluorescence analysis of tubulin organisation control cells display long elongated tubulin network spanning throughout the cytoplasm to the cell periphery (Figure 6.41B and Figure 10.27). However, upon tau overexpression, tubulin appeared bundled, less organised and to have problems anchoring to the cell membrane (Figure 6.41D). Interestingly, immunofluorescence analysis consistently revealed that following tau overexpression, there were fewer A431 cells in the mitotic stage of the cell cycle compared to its controls (Figure 6.39 and Figure 6.41). To further investigate this observation, RT q-PCR analysis was performed to determine the gene expression of a panel of proteins associated with proliferation and cell cycle progression. Analysis revealed a decrease in all the assessed markers of proliferation and cell cycle progression (Figure 6.42). The relative expression of both Ki67 and p63 significantly reduced when tau was overexpressed indicating an overall decrease in cell proliferation (Figure 6.42A). Analysis of cell cycle specific progression, through the expression of cyclins and CDKs, found that both cyclin B1 and CDK1 had significantly lower expression following tau overexpression than the controls; both of which are involved in mitotic stage of the cell cycle; consistent with the observations from immunofluorescence analysis (Figure 6.42C and D). Interestingly, cyclin D1, which is involved in G_1 phase of the cell cycle, was the only cyclin not to significantly decrease in expression (Figure 6.42C). Significant decreases in cyclin E1 and cyclin A2 occurred following tau overexpression in A431 cells, both

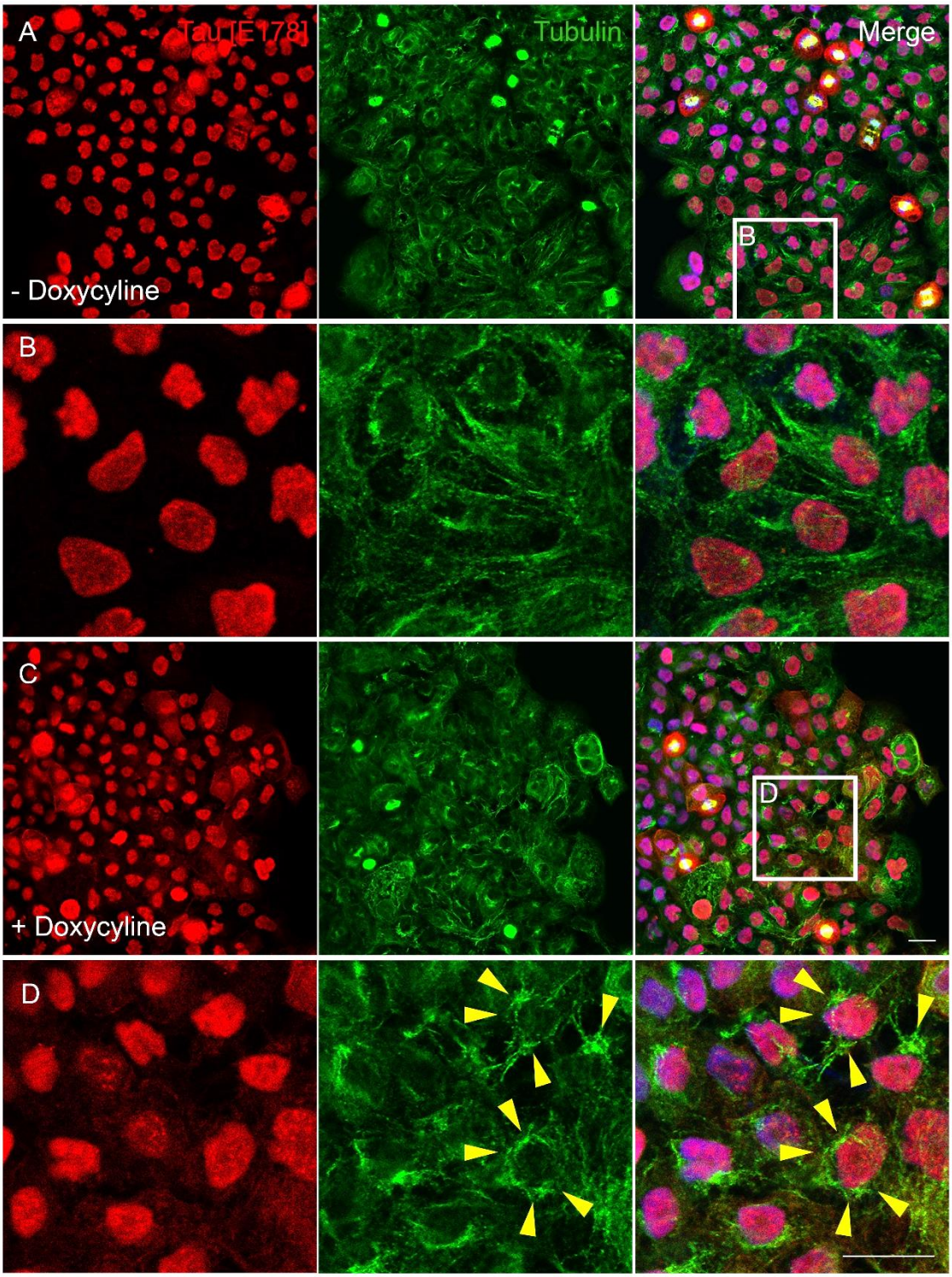

Figure 6.41. Immunofluorescence analysis of tubulin in A431 cells following tau overexpression.
Representative immunofluorescence analysis of tau (red) and tubulin (green) in A431 cells with and without the overexpression of 2N4R tau (n=3). **A&B.** pINDUCER20 tau cells without doxycycline. **C&D.** pINDUCER20 tau cells with doxycycline to drive the overexpression of 2N4R isoform of tau. Yellow arrows highlight the bundled, disorganised tubulin following tau overexpression. Nuclei counterstained with DAPI (blue) and all channels are displayed in the right panel to allow accurate visualisation of cellular morphology. Scale bar 25 µm.

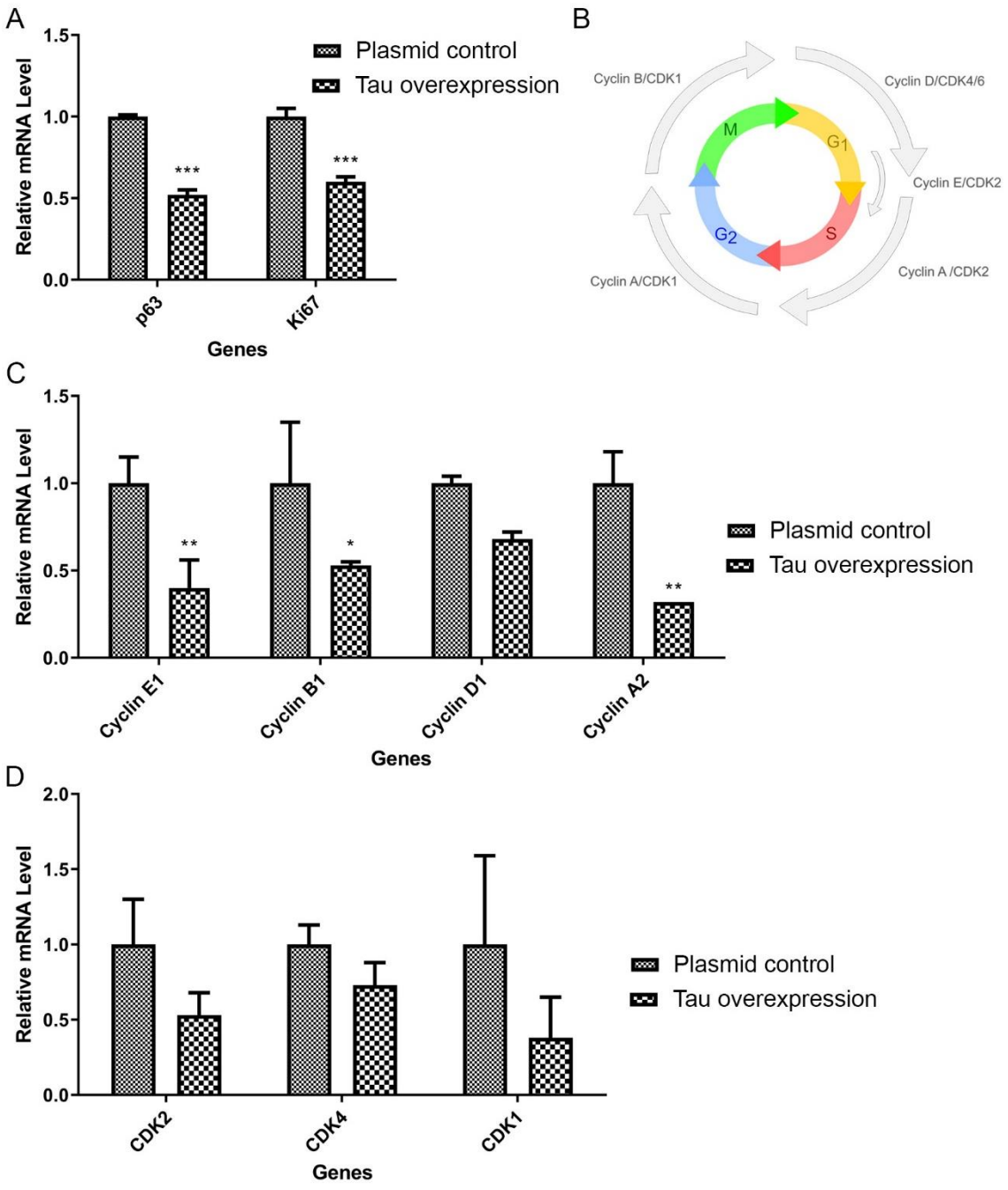

Figure 6.42. RT q-PCR analysis of genes associated with cell proliferation and cell cycle progression in A431 cells following tau overexpression.
A. Relative gene expression of p63 and Ki67 following 48 h tau overexpression in A431 cells. **B.** Schematic demonstrating the stages of the cell cycle with the associated expression of cyclin and CDKs at each phase. **C.** Relative gene expression of cyclins following 48 h tau overexpression in A431 cells. **D.** Relative gene expression of CDKs following 48 h tau overexpression in A431 cells. Ct values were normalised to 36B4 and $2^{-\Delta\Delta Ct}$ method of analysis used. Relative expression levels are displayed as mean ± SD. Two-way ANOVA with Bonferroni correction was used to test significance; *p<0.05, ** p<0.01, *** p<0.001.

of which are involved in the progression of cells into the S and G2 phases of the cell cycle (Figure 6.42C). To further investigate the effect overexpression of tau had on cell cycle dynamics of A431 cells, pINDUCER20 tau cells were co-infected with Ki67p FUCCI using G418 and blasticidin to select cells, which successfully incorporated both vectors into their genome (Figure 6.43A-C). As expected, in control A431 FUCCI cells cultured under normal culture conditions, the percentage of G_0 cells was 20%, compared to the 5% in healthy epidermal keratinocytes, reflecting the increased quiescent SC population in SCC cells (Figure 6.43). Interestingly, although most cells are usually in G_1 phase of the cell cycle, 41% of A431 cells were identified in this phase under normal culture conditions and 33% were identified in G_2/M phase. Cells co-infected with both pINDUCER20 tau and FUCCI were treated with doxycycline for 48 h before fixation, imaging and quantification. Strikingly, upon tau overexpression there was a significant decrease in the number of cells in G_0 (Figure 6.43). A significant increase in cells in G_2/M phase were also identified. Interestingly, control cells treated with FUCCI revealed an increase in G_0 cells compared to the controls, although due to the variation this did not reach the threshold for statistical significance. Although the percentage of G_1, G_2/M and S phase cells increased following tau overexpression, overall, a decreased cell numbers occurred compared to all control conditions (data not shown). This indicated decrease in cell proliferation compared to controls despite the proportionate increase in G_1-G_2/M cells and decrease in G_0 cells (Figure 6.43). Taken together, the reduction in mitotic cells, reduction in stage specific cyclins and CDKs alongside the increase in G_1 and G_2 A431 cells identified through FUCCI, suggests that A431 cells are likely to be arresting in the G_1 and G_2 phase of the cell cycle following tau overexpression.

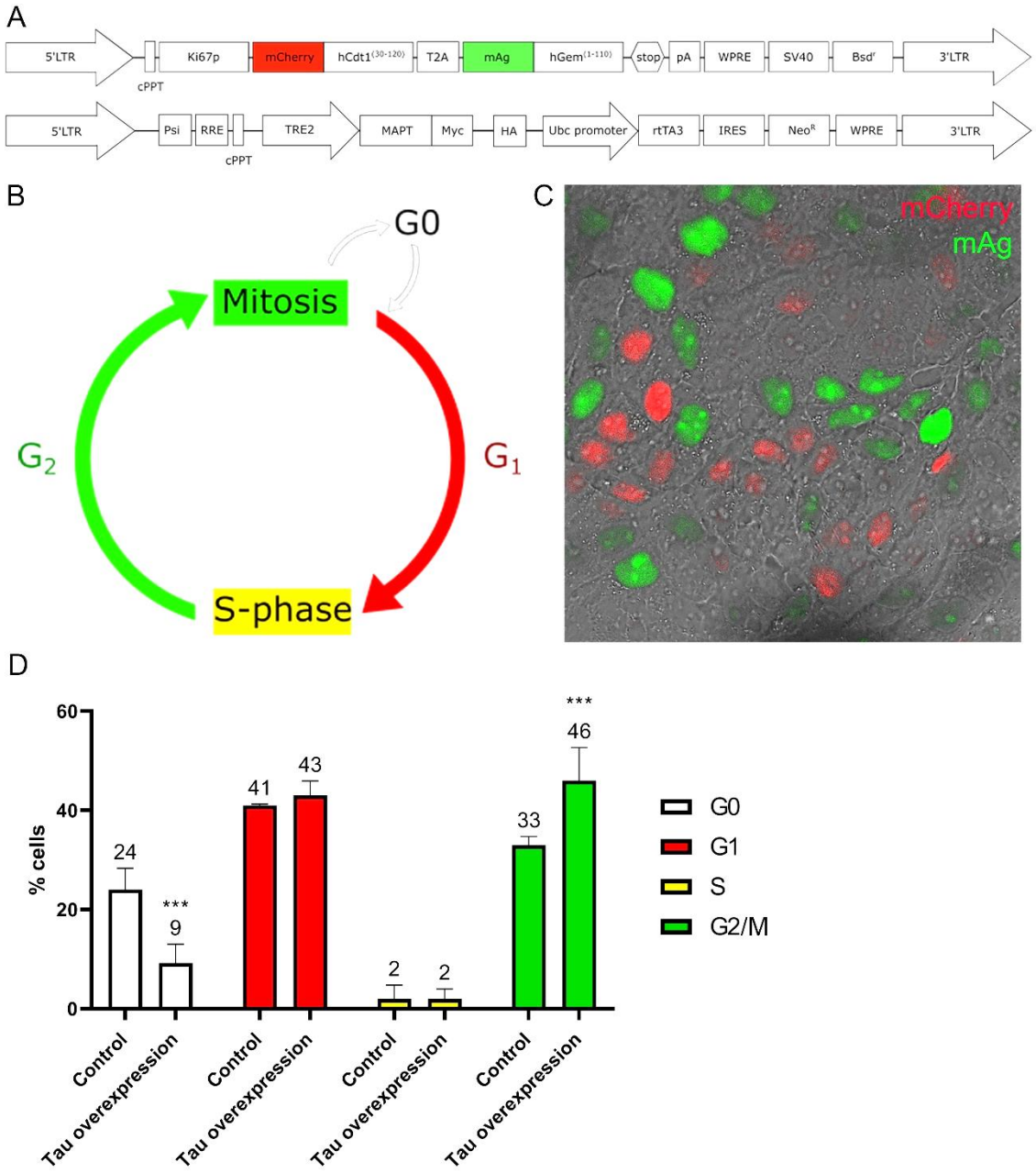

Figure 6.43. Ki67p fluorescent ubiquitination based cell cycle indicator (FUCCI) reveals a decrease in quiescent cells in squamous cell carcinoma cell line A431 following tau overexpression.

Ki67p FUCCI lentiviral reporter incorporates a Ki67 promoter that restricts the expression of the fluorophore complexes to actively cycling, allowing the identification of quiescent cells in G_0 phase of the cell cycle. **A.** Schematic demonstrating the Ki67p-FUCCI lentiviral reporter vector. **B.** Schematic demonstrating m-Cherry (red) and mAG (green) expression throughout the cell cycle. **C.** Representative cell culture image of A431 cells infected with Ki67p FUCCI under selection using blasticidin. Cells can be observed in G_1 (red), G_2 (green) and G_0 (colourless). **D.** Quantification of cell cycle status following 48 h of tau overexpression. A431 FUCCI cells were used as a control and cells were also treated with doxycycline (DOXY) in parallel to enable any unspecific effects of doxycycline treatments to be identified. Upon tau overexpression there was a significant decrease in the percentage of G_0 cells and a significant increase in G_2 cells. The percentage of cells in each stage of the cell cycle is plotted on the graph. Findings are displayed as average ± SD.

6.5. Discussion

In summary, this chapter has successfully characterised tau expression in cSCC. Using *in vivo* and *in vitro* methods to investigate tau expression in cSCC, tau displayed a district expression pattern in sub-populations of SCC cells that was dependent on their SC status. Moreover, tau influenced cell fate in SCC cells and tau manipulation *in vitro* induced cellular differentiation of SCC cell lines, suggesting that tau could be a promising target of anti-cancer drug development.

Taken together, this chapter has demonstrated that tau is functionally significant in cSCC and that its expression was linked to SCC cell fate and differentiation. However, the functional significance of tau in cSCC requires extensive research, and due to the time limitation of this project, it has not been possible to complete all functional tests in cSCC. Nevertheless, this project has highlighted tau as a promising target for novel therapies and an exciting avenue for further investigation.

SCCs are common malignant tumours in humans, and their rising incidence has become an increasing global health problem. This chapter demonstrated that in cSCC a distinct expression pattern of tau was observed, which was linked to the differentiation status of the tumours. Previous studies have shown that in other cell lines the effects of MAPs in cancer is complex, with many interacting proteins influencing the cancer cells behaviour [172,384]. This chapter presents a starting point for further research into the functional role and binding partners of tau in cSCC.

Overall tau expression was found to be higher in SCC than healthy skin. Although this was surprising initially due to their undifferentiated phenotype, elevated tau expression levels within other cancers have been widely reported by others

[285,286]. Additionally, a large proportion of SCC tumours are made up of hyper-proliferative or de-differentiated spinous cells, explaining why when compared to basal keratinocytes, SCC cells present with higher tau expression profiles.

In this study tau expression was largely found in the nucleus of SCC cells. In 80% of cSCCs p53 is mutated, allowing cells to progress through the cell cycle and contributes to their hyper proliferative status [57,118,134]. In Chapter 4 tau was linked to a possible role in the stabilisation of the mitotic spindle during mitosis, which could explain why tau is upregulated in cancer cells. Studies have demonstrated that tau can support increased proliferation [182–184] and a deficiency in tau has been linked to p53 destabilisation [242].

One of the major problems with cancer treatments is the possible relapse of a tumour. One of the reasons for this is the survival of CSC populations after treatment is due to their quiescence CSCs, which can evade some cancer therapies that target hyper-proliferative cells [383,385,386]. The development of more effective therapies is driven by a better understanding of the properties of these CSCs within specific tumours and their role in quiescence and tumour initiation. Within this study we have provided evidence tau that helps to regulate cell fate through cell adhesion, mitosis and cytoskeletal changes. Consistent with findings in healthy keratinocytes, this chapter successfully demonstrated that tau expression is lower in SCs than TACs and differentiated cells. Furthermore, we demonstrated that the alteration of tau expression *in vitro* could induce markers of cellular differentiation in SCC cell lines and reduce the CSC population.

In this study it was found that tau expression within the basal surface of cells attached to the BM was lost within large regions of SCC samples. In Chapter 5, tau was found to bind to hemidesmosome structures and involved in cell-matrix

and cell-cell networks of adhesion. The significance of the lack of tau localisation to the BM is consistent with the lack of cell adhesion in cancer cells and their invasive phenotype that is acquired in cancer cells [162,387–389]. This could be significant and indicate a change in behaviour of these basal cells, possibly to an invasive phenotype. The interaction between tumour cells and their ECM and basement are key in understanding tumorigenesis, as adhesion to the BM plays an integral role in the initial stages of tumour invasion and subsequently metastasis [387]. Cell adhesion molecules, such as E-cadherin and its associated proteins, are heavily involved in cancer pathology; loss of cell junctions enables increased cell motility, which are often associated with increased proliferation, migration and consequently invasion and metastasis [102,387]. Microtubule networks play an essential role in cell polarity and act as tracks for motor-protein-driven transport processes. Tau has been observed in this study to effect cell shape and has been linked to polarity. Thus future investigations will explore the role of tau in migration and the implications of this in cancer.

Shorter isoforms of tau were located in the basal cells of SCCs, whilst longer isoforms of tau were expressed within the suprabasal and differentiated regions of the tumour. These observations are consistent with publications linking shorter isoforms to increased plasticity [179,187,213]; possibly promoting and enhancing cancer cell migration in the tumour. Interestingly, hyper-methylation of the CpG island in the tau gene has been associated with a poor prognosis in colorectal cancer patients [288]. This hyper-methylation causes the exclusion of exon 10 from the RNA transcript of tau resulting in shorter isoforms of tau possibly enhancing cell plasticity.

Consistent with findings in healthy human skin, tau expression was highest in regions of differentiation in tumours, with tau localising within the nucleus,

cytoplasm and membrane fractions of the cells. Earlier chapters in this study indicated that the tau5 antibody appeared to be linked to the structural conformation of the tau protein. Tau5 antibody binds to the PRD of the tau protein which has been shown to be exposed upon N- and C-terminal domain binding; which is usually observed at the plasma membrane [223,224,372]. The changes in the expression pattern of tau in SCCs using the tau5 antibody could indicate changes in the sub-cellular binding of tau in SCC samples compared to healthy human skin and subsequently that the role of tau in SCC. In SCC samples tau5 localises with the plasma membrane and tubulin. Spinous cells get their name from the strong cell-cell connections with desmosomes, as sometimes during tissue processing you are able to identify the 'spines' that connect the cells, or when there is a skin condition, hence their name spinous cells. The spikes of the tau 5 staining resembled the desmosomal structures in the spinous cells. Tau is known to be associated with the C and N terminus of the protein helping to bind tubulin structures to membrane structures to enhance stability of the cytoskeletal structure [216,224,235]. Chapter 5 revealed that binding partners of tau in keratinocytes included desmosome and hemidesmosome proteins, *in vitro* analysis of the binding of the binding partners of tau in SCC requires investigation.

BCC and SCC are both common skin cancers in humans that originate from basal epidermal progenitors. However, BCCs are usually driven by activators of SHH (SmoM2), whilst SCCs are usually driven by oncogenic activators of RAS/MAPK ($HRAS^{G12V}$). SmoM2 and $HRAS^{G12V}$ undergo distinctly different patterns of differentiation. Therefore, it is not surprising that different expression profiles of tau were identified between SCC and BCC. BCCs are usually benign, they bud into their surrounding stroma but usually retain their BM and rarely spread to other

tissues. SCC on the other hand is more aggressive and invasive and initiates bidirectional tissue folds. SCCs are usually full thickness and affect the granular and corneal, whereas BCC usually have palisading basal cells that rarely ever break the BM and present instead with a thickening of the epithelium and bulging of the basal population. In this study it was expected that lower levels of tau would be detected in BCCs due to tumours arising from basal progenitors, but interestingly higher expression levels of tau were observed, particularly phosphor tau. These differences present an interesting area of future research, but unfortunately this was not possible within the scope of this project and due to time limitations this study was limited to investigate SCC.

SCC samples do not have the same morphology as healthy skin and, although CSCs are reported to reside in the epidermal-stroma border, they are not comparable to the morphology of healthy skin. In this study although basal and suprabasal ROI were captured, methods of *in situ* hybridisation would have been more accurate for determining tau isoform expression in NMSCs. Preliminary work has been conducted into *in situ* hybridisation, but unfortunately due to time limitations it has not yet been completed. In future studies BaseScope™, with isoform specific probes, will be utilised as a technique to continue the investigation into tau isoform expression in NMSCs (Figure 10.7 and Figure 10.8).

One of the other major limitations of this Chapter, occurred with the LCM analysis of SCC biopsies. In this study as only 5 of the SCC cryo frozen samples were usable and the integrity of the RNA from slow frozen biopsies was not sufficient for accurate analysis. Additionally, limitations were posed by the size of the ROI that could be captured within the tumour. RNA concentration from ROI obtained and cancer samples are known to have more extensive RNA degradation than healthy samples; due to higher levels of ROS and DNA damage within cancer

cells resulting in less stable RNA due to all of these factors. Future work will include the incorporation of more SCC samples and single cell RNAseq; enabling the analysis of individual cells within the tumour and help elucidate at a cellular level the expression profile of tau within each sub-population of cells within the tumour.

NMSC samples were taken from both male and female patients, from a range of common sites of SCC formation. The age of patients used in this study ranged between 42 - 97 years old and some of the tumour samples were from younger patients than the healthy controls. In some SCCs and BCCs the surrounding skin was used as internal (or paired) control; however, pagetoid spread needed to be considered, so although the tissue may have appeared anatomically normal, there may have been mutations to the surrounding tissue, as the skin was likely exposed to the same conditions (e.g. UV) as the tumour. For these reasons none of the data presented in this study show the surrounding tissue, but it was analysed and it was taken into account when imaging the tissue.

SCCs and BCCs display a high inner and intra-tumour heterogeneity, therefore staining and RNA expression analysed may not have been representative of the entire lesion. To help reduce any bias or limitations, representative images were taken across each region of the tumour biopsy and both technical repeats and biological repeats were conducted. In future analysis, to help overcome some of the limitations posed by tumour heterogeneity, tissue array of SCC lesions, will be used. This will allow the analysis of a larger cohort of patient samples and help to increase the significance of the data found here. Unfortunately, within this study both time and patient sample availability reduced the ability to perform further repeats to address this.

Manipulating tau gene expression *in vitro* induced cellular differentiation in A431 cells. When tau protein was KD, cell differentiation and destabilisation of the cytoskeletal network was induced. Evidence of disruption to the cell adhesion network was also identified. A recent study investigated the effect a downregulation of tau in a glioma cell line and found that it led to a decreased mobility of the cells [329]. Cytoskeletal dynamics and cell adhesion play a vital role in the phenotype of cancer cells during the EMT process. This indicates that when tau expression is disrupted cancer cell behaviour changes, as the cytoskeletal and cell adhesive network are disturbed. Additionally, this may be linked to the decreased incidence of NMSC in patients with neurodegenerative diseases; as these disorders affect the function of the tau protein therefore microtubule stability, which might inhibit the ability of cancer initiation and progression. Further research will be conducted to characterise the changes of the structural integrity of the cytoskeletal and cell adhesion system following tau KD in A431 cells.

The results of this study also demonstrated that 2N4R tau overexpression in A431 cells induces cell differentiation, consistent with observations here in healthy cell lines. This study also established that tau overexpression containing 4 MTBD depleted quiescent CSC populations in A431 cells, a significant finding with promising implications for cancer treatments. In line with studies that identified that in colorectal cancer the exclusion of exon 10, and therefore decreased tau with 4 MTBD, is associated with a poor prognosis [288].

As well as regulating microtubules, tau can increase the stability and stiffness of microtubules, reducing their flexibility [180,232]. Studies have shown that the stabilisation of microtubules are associated with the reduction of proliferation and tumour growth [169,170,172]; also limiting their ability to migrate and metastasise [155,172,285]. SCC loose cell adhesion depending on differentiation status and

invasive properties. This study found that keratins and microtubules were disturbed when tau expression was altered in A431 cells. This study proposes that tau might induce differentiation by stabilising the cytoskeleton to the membrane components, removing their ability to migrate and detach from the BM; a key phenotype of cancers. Additionally, other studies have shown that tau overexpression in can lead to changes in the location and trafficking of organelles [390]. The trafficking of organelles and cell polarisation are also essential for migration and progression of cancer.

To study and effectively prove the role intercellular events have on the initiation and progression of non-melanoma skin cancer *in vitro,* three-dimensional studies or mouse models need to be utilised to prove how these cells develop and interact at a molecular level in a native or near native micro-environment and the translational impact of the findings. The limitations of 2D work already was highlighted in the discussion of Chapter 4, which is why a 3D epidermal model was used to confirm the functional significance of the findings. However, there is currently no widely used, well characterised or commercially available 3D *in vitro* SCC model. Future work will need to continue to investigate tau function in cSCCs, with an understanding that the CSCs reside in specialised microenvironments (niches) that provide cues from cell-cell contacts and secreted factors. The CSC niche is part of the tumour microenvironment (TME), referring to the surrounding stroma and epithelium. Recent studies have started to look at how the TME contributes to tumour initiation progression and could potentially target this niche and TME for cancer therapy [383,391–393]. The findings of this chapter provide the preliminary validation for a promising area of study that deserves further investigation using animal models *in vivo.*

A high expression of tau in cancer is supported by findings in literature and high tau expression has been linked to an increased drug resistance of some cancers [285,286]. Taxanes, a group of chemotherapeutic drugs, interfere with microtubules and consequently spindle dynamics, leading to cell-cycle arrest and apoptosis. MAPs bind to the same binding site in β-tubulin as taxanes, interfering with their ability to work [287]. This study has further shown that alteration of tau levels can interfere with SCC cell fate, thus dysregulation of tau expression could be a future avenue for potential therapies. There are various drugs that have been designed to interfere with tau, many of which have been designed for AD and have reached phase 2-3 clinical trials. Following the findings of this study, preliminary work is currently being conducted to investigate if any of these drugs are able to contribute to a desirable phenotype in SCC cells and encourage their differentiation through the modulation of tau.

6.6. Conclusion

In conclusion, this chapter has demonstrated that tau expression in cSCC is linked to cell fate and the differentiation status of the tumour. Furthermore, manipulation of tau expression induced differentiation and interfered with cell proliferation. Most strikingly, overexpression of 2N4R tau reduced the quiescent SCC cell population *in vitro*, suggesting a potential application for targeted therapies. This mechanism could increase the efficacy of traditional treatments by reducing the quiescent CSC population that usually evade such treatments. Although the effects of tau on cells function in cancer is likely to be complex and influenced by many other factors, the findings of this chapter provide the preliminary indication that tau might be advantageous to cancer initiation or progression and how this could be utilised as a diagnostic marker or target to increase the efficacy of traditional cancer therapy.

7. General discussion

The overall aim of this thesis was to determine the expression and function of tau in the epidermis throughout keratinocyte stratification and differentiation, and identify any changes that take place in cSCC. Together the results have revealed that tau is differentially expressed throughout the basal, spinous and granular layers of the epidermis. Furthermore, this thesis has discovered that tau can orchestrate epidermal stratification and keratinocyte commitment to terminal differentiation, through its interaction with cell adhesion proteins and by influencing cytoskeletal changes (Figure 7.1). The thesis has also uncovered mechanisms underpinning the role of tau in keratinocyte cell fate, cytoskeletal changes during epidermal stratification and differentiation, and highlighted tau as a possible target for new therapies to tackle the rapidly increasing cSCC cases.

7.1. Tau and its association with the cytoskeleton in the epidermis

At present tau is widely associated with neurodegenerative disorders and its function in skin remained under investigated and poorly understood. This thesis has demonstrated that tau is functionally significant in the epidermis; coordinating cell adhesion networks and cytoskeletal changes to promote epidermal stratification and commitment to terminal differentiation in keratinocytes.

The cytoskeleton is a complex network essential for all stages of keratinocyte differentiation. The reorganisation and distribution of cytoskeletal components to the cell cortex is crucial for keratinocyte differentiation [22,60]. This thesis also provided evidence that tau can enhance and stabilise the cortex rearrangement of the cytoskeleton to regulate cell differentiation. Furthermore, tau KD in keratinocytes led to loss of cortex rearrangement of cytoskeletal components, loss of asymmetrical distribution of membrane proteins, loss of cell-cell adhesion

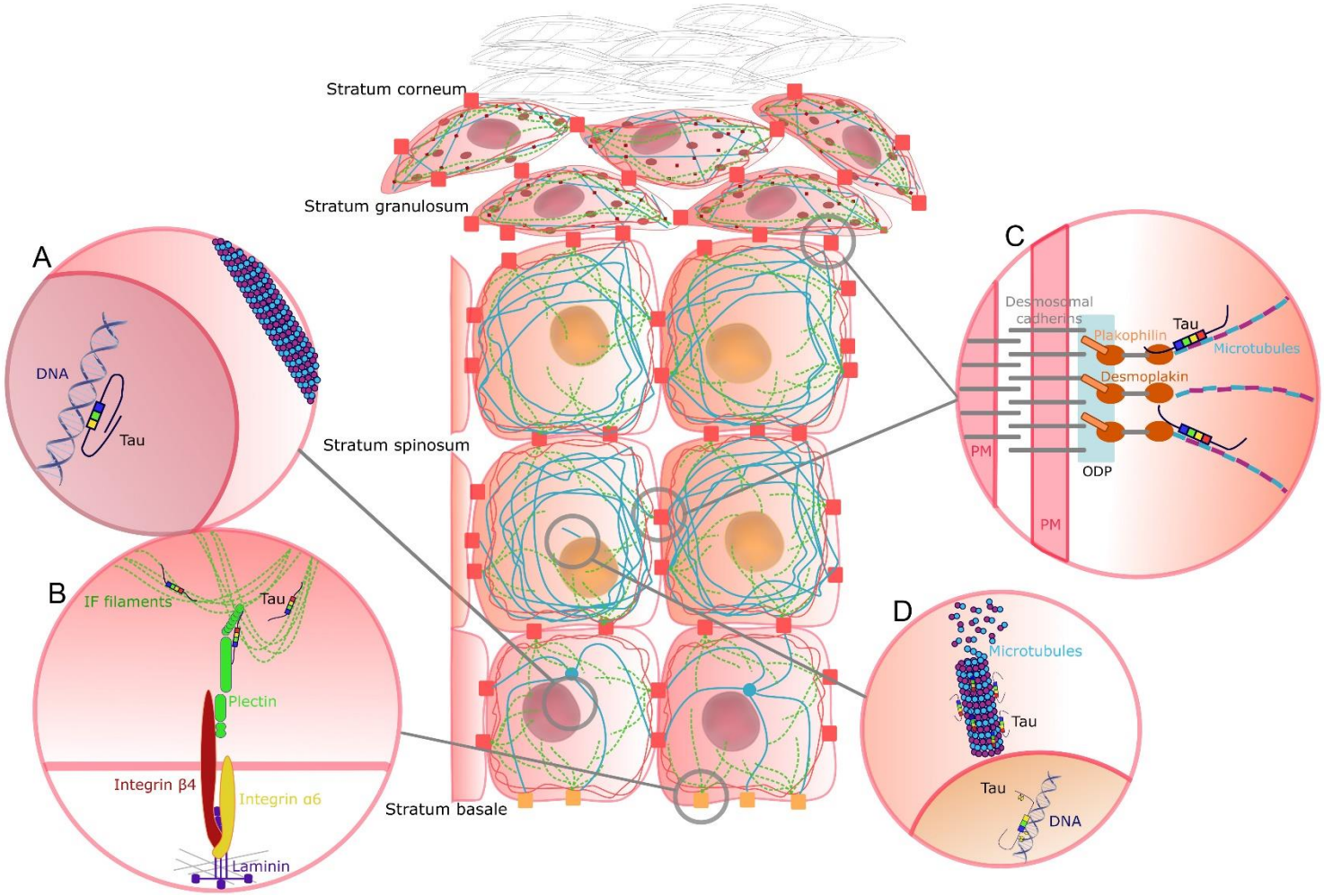

Figure 7.1. Mechanistic summary of tau function throughout the epidermis and its role in keratinocyte homeostasis and differentiation.

Tau is dynamically expressed throughout the epidermis and each layer of the epidermis displays a distinct expression pattern of tau linked to its function. **A.** In basal cells, shorter isoforms of un-phosphorylated tau are involved in the nuclear organisation and potentially in the regulation of gene expression through its interaction with histone proteins. Tau is dynamically expressed in SC and TAC populations and its expression is upregulated during mitosis to stabilise the mitotic spindle. **B.** In basal cells tau is also involved in the stabilisation of hemidesmosome structures; through interaction with plectin and the intermediate filament network tau is asymmetrically distributed to hemidesmosome structures along the BM in basal cells to stabilise the cell- ECM adhesion network. **C.** In suprabasal keratinocytes, longer isoforms of tau have been linked to cell-cell adhesion. Including the stabilisation of desmosomes through its interaction with desmoplakin, other proteins within desmosomes and interaction with components of the cytoskeleton. **D.** Tau is important for the cortex rearrangement of the cytoskeleton, interacting with actin and microtubule network of the cells. Additionally, KD of tau revealed that keratinocytes are not able to progress to the later stages of terminal differentiation. PM – plasma membrane. ODP – outer dense plaque. (Schematic is not drawn to scale).

and lack of cellular differentiation. Overexpression of 2N4R tau induced the cortex rearrangement of the cytoskeleton, increased cell differentiation, induced changes to epidermal stratification causing increased flattening of the cells and significantly thicker stratum corneum.

Hemidesmosome and desmosome structures are essential for the organisation of the cytoskeleton and the structural integrity of the epidermis [21,350]. This thesis demonstrated that tau interacts with cytoskeletal components and cytolinker proteins, to associate with hemidesmosomal and desmosomal complexes. It identified plectin as one of tau's binding partners in growing and differentiating keratinocytes and that desmoplakin was a binding partner in differentiating cells. Both plectin and desmoplakin are membrane associated, cytolinker proteins from the plakin family and share many similar structural traits [69]. Plectin deficiency in the epidermis causes aberrations to the organisation of the keratin network and disturb its anchorage to cell junctions [394]; a presentation that consistent with the findings of this thesis when tau was KD. Although the exact molecular mechanisms of interaction between tau and plectin have not been alluded within the time frame of this study, other studies have characterised interactions between plectin and MAP-1 and -2 [354]. For example, plectin has been shown to contribute to cross-bridges between the IF and MT network in fibroblasts [113]; a role to which tau has also been subscribed. Interactions of tau with plasma membrane proteins is usually through its N-terminal domain [216,223,224] and with IF through its MTBD [179,181,225]. Both of these findings are consistent with the longer tau isoform expression, and tau subcellular localisation, and reorganisation of the cytoskeletal network to the cells cortex that has been identified in differentiating keratinocytes within this study. Nevertheless, previous studies have shown that the coordination of several proteins is essential for hemidesmosome or

desmosomal complexes to trigger the reorganisation of the microtubule network from the centrosome to the cortex [18,54,66,67,69,70,72,77,96,353]. Therefore, this thesis proposes that through the interaction with other key proteins, tau is a novel regulator of epidermal homeostasis (Figure 7.1) and the implications of the dysregulation of this protein in neurological disorders and cancer deserves further research.

Interactions between the components of the cytoskeleton have been reported in numerous cell types [18,24,69,111,395], but little is understood about mechanisms behind these interactions. This thesis has elucidated that tau can interact with all components of the cytoskeleton through direct binding and indirect association through cell junctions. The role of tau as a molecular linker between cytoskeletal components in keratinocytes requires further confirmation, however, in other cell types MAPs form crosslinks and assist in the bundling between the actin and microtubule network [181,324]. The interactions between components of the cytoskeleton have also been demonstrated to influence cell shape and motility, ultimately contributing to epidermal homeostasis under physiological conditions and the migratory and invasive behaviour of cancer cells under pathological conditions [154–156,158,395].

Microtubules can also act as scaffolds and control the localisation of organelles within a cell [172]. Big tau is linked to spacing of microtubules, therefore it is likely, in line with publications in other cell lines [330], the inclusion of exon 4A in keratinocytes enables more efficient transport of cargo and organelles along microtubules. The localisation of lysosomes within a cell can be influenced by microtubule trafficking [367,396], with lysosome movement along microtubules mediated by kinesin and dynein motors [396]. This thesis further identified several proteins involved in lysosomal lumen acidification, as downstream targets of tau

overexpression in keratinocytes. This is in line with previous studies where autophagy is shown to be involved in epidermal homeostasis and upregulated in differentiating keratinocytes [366–368].

Epidermal stratification involves a carefully regulated process of symmetrical and asymmetrical cell division. Transcriptional and post-transcriptional control, extrinsic factors (influencing cell adhesion) and cell polarity all determine or contribute to spindle orientation and keratinocyte delamination [37]. Polarity is a vital characteristic of epithelial cells, yet many key regulators of this process have not yet been identified and the exact mechanisms underlying all aspects of keratinocyte polarity are not yet understood. In this thesis tau was asymmetrically distributed to the leading edge of keratinocyte cells, where the MTOC is also polarised. Additionally, tau KD lead to the loss of the asymmetrical distribution of membrane proteins and loss of cell-cell adhesion, whilst overexpression of 2N4R tau induced changes to epidermal stratification. These results build on existing evidence that in neuronal cell lines tau is involved in the remodelling of the microtubule and actin networks essential for migration [326,329,397]. Taken together, for the first time there is thus compelling evidence that tau may play a role in epithelial polarisation, migration and ultimately cell fate in the epidermis.

7.2. Tau and its role in epidermal cell fate

This thesis has provided evidence that tau is functionally significant in influencing epidermal cell fate. Epidermal cell fate entails a tightly coordinated process involving the rearrangement of intracellular junctions and cytoskeletal changes [22,27,36,321,398]. The alternative splicing of tau is widely recognised to be linked to developmental status and cellular function in neuronal cells [180,212,218,356,399]. In line with the literature, this thesis found that alternative splicing of tau was linked to

keratinocyte cell status, localisation and function; with shorter isoforms expressed in SC and TAC populations and longer isoforms expressed by differentiated keratinocyte populations. It is possible that the shorter isoforms of tau allow more dynamic alterations of keratinocyte architecture that are required for basal cell migration and plasticity. Interestingly, the overexpression of longer isoforms induced cellular differentiation in both keratinocyte and SCC cell lines. The implications of this finding could be for therapies targeting cancers, with the next stage of this project investigating how alternative splicing is regulated in keratinocytes and SCC. In other cell lines, SRSFs and ATXN3 have previously been linked to regulation of tau isoform expression [186,189,203,400,401], but nothing is currently known about the transcriptional regulation in keratinocytes. Preliminary investigation has been started and has identified several key SRSFs in the alternative splicing of tau keratinocytes.

It has previously been shown that integrin-ECM adhesion plays a role in cell fate and can control cell proliferation, delamination and consequently cell differentiation [6,8,49,321]. This thesis demonstrated that tau can also influence the asymmetrical distribution of adhesion protein plectin, and influence cell adhesion. The balance between symmetrical and asymmetrical division in the epidermis is highly regulated and linked to cell fate changes in the epidermis [9,37,398]. Similarly in this thesis, tau was dynamically expressed throughout the cell cycle; supporting the mitotic spindle during metaphase, anaphase, telophase and cytokinesis. Thus, these findings are in line with the literature whereby tau plays a role in mitotic spindle stabilisation, DNA protection and p53 regulation in other cell types [182,233,234,242]. Interestingly, it was found that one daughter cell consistently inherited higher tau levels, possibly linked to their cell status and cell fate, as TACs express higher levels of tau than SCs. Consistent with this, other studies

show that epidermal cell fate can be influenced by the inheritance of certain proteins or transcription proteins [38].

An area of particular interest for future investigation are the implications of tau localisation to the plasma membrane and the possible involvement of tau in cell signalling. The binding partners of tau identified in this thesis point to a possible role of tau in modulating intracellular communication and signalling through communication between the cytoskeleton and membrane and through interactions with integrins, filamin-B, plectin, desmoplakin and RAS related protein Rap-1b. All are all known to play a role in the regulation of development, cell adhesion, growth and differentiation [69,82,361,402]. Additionally, there are a few reports suggesting that once tau is bound to the plasma membrane, it may be secreted into the extracellular space and participate in cell signalling [224,244]. This could be significant in the suprabasal layers of the epidermis in which tau localised with desmosome structures. It could also be relevant in the basal cells, in which tau was highly expressed with hemidesmosome structures along the BM. Although there are recombinant tau proteins readily available from companies, as tau is such a large protein, studies suggest it may be hard for cells to internalise. However, Wauters *et al.* (2016) suggests that phosphorylation could allow tau to be internalised by neuron cells [244], opening an avenue for further research in keratinocyte cells.

7.3. Tau and its role in cutaneous squamous cell carcinoma

The identification of proteins or mechanisms that prevent or counteract the growth of aberrant cells during cancer development, are of high interest and are likely to have translational applications. This thesis has uncovered mechanisms underpinning epidermal homeostasis and revealed a possible target for new

therapies to tackle the rapidly increasing cSCC cases. A distinct expression pattern of tau was observed in SCC, which was linked to the differentiation status of the tumours. Future investigation will involve investigation into the use of tau as a biomarker for different stages and malignancies of cSCC biopsies. Low tau expression was identified in CSCs and within this thesis tau expression was linked to a possible role in signalling, cell adhesion and migration. Access to skin tissue was the major limitation of one of the studies, as only a small amount of tissue could be obtained. Additionally, there was a lack of patient clinical history, skin type and current medication limited our understanding of the skin samples. Future work will include sourcing more human skin samples and using a tissue array to screen a large number of skin samples, as well as seeking more detailed accompanying medical information.

Microtubules are essential for cytoskeletal assembly and function, including the regulation of the cells mitotic spindle. Therefore, previous studies have found that drugs that bind and stabilise tubulin, inhibit chromosome segregation and block cell division, leading to many of these agents being used as cancer treatments [155,156,158,173]. Data in this thesis demonstrated that the overexpression of 2N4R was sufficient to reduce cell division in SCC cells and arrest cells in G_1 and G_2 phases of the cell cycle, in line with previous studies showing that MT stabilisation is sufficient to induce cell cycle arrest [179,245,308,333].

Tau is well known as an age associated pathological protein involved in many neuropathological conditions. In AD the hyperphosphorylation and aggregation of tau has major effects on neuronal cell function, which is reflected by the neurological presentation in AD. In AD there is not only an increase of aberrant hyper-phosphorylated tau, but also total tau [274,277]. The dysregulation of proteins associated with neurodegeneration have been identified in patient skin samples

[274,277] and a negative correlation between the incidence of AD and NMSC has been identified [263–266,268,271–273]. Indeed these correlations between the tau expression in AD patient's skin, and the altered SCC prevalence in patients with AD, was the initial inspiration for exploring this mechanism within this thesis.

In the brain under physiological conditions there is a 1:1 expression of 3R:4R, however in pathological conditions such as AD there is a shift towards 4R tau expression [192,399,403,404]. Not only do 4R variants have an increased affinity for microtubules but also for protein aggregation [188,192,214,405]. Interestingly, it is reported that patients with AD quite often present with itchy dry skin, and an increased risk of AD has been identified in patients with psoriasis [348]. The findings within this thesis support this observation, as an increase in 4R tau in the epidermis led to increased cell differentiation and thickening of the stratum corneum, possibly helping to explain the phenomenon observed in patients with AD. Additionally within this thesis when the SCC cell lines were forced to overexpress 4R isoforms of tau, a reduction in CSCs and increase in cell differentiation was observed. This has potentially important implications for cSCC, and the increased differentiation of cells might be one of the reasons that there is a lower incidence of NMSC in patients with AD. Differentiation therapies have shown great success in many cancers [406], whereby the induced terminal differentiation of cancer cells leads to the successful treatment and good prognosis of a variety of cancers. Cancers usually arise from the accumulation of mutations leading to uncontrolled cell proliferation and consequently in cSCC the programme of cell differentiation is disturbed. Well differentiated cSCCs usually possess a lower metastatic potential, therefore, mechanisms that are able to induce terminal differentiation in cSCC are of interest for their translational application, highlighting the significance of the findings of this thesis.

Finally, future work will include the generation of tau KD and KO keratinocyte cell epidermal insert models to further investigate the functional significance of tau during epidermal stratification and differentiation. Collaboration is underway to investigate the control of alternative splicing of tau and reveal potential targets for the development of therapeutics. The next phase of work will also include the incorporation of more cSCC samples and performance of single cell RNAseq to allow the analysis of individual cells within the tumour and help elucidate at a cellular level the expression profile of tau within each sub-population of tumour cells. Finally, future work will also include investigating the clinical implications of this thesis by determining how the findings could be applied as a therapy in the treatment of cSCC. This thesis demonstrated that the alteration of tau expression can interfere with cSCC cell fate and that the dysregulation of tau expression could be a future avenue for potential therapies. There are a large group of drugs that have been designed for the treatment of AD and interfere with tau, many of which have reached phase 2-3 clinical trials. Preliminary work is currently being conducted to investigate if any commercially available or phase 2-3 clinical trial drugs could encourage cSCC differentiation through the modulation of tau, contributing to a desirable phenotype in cSCC. Additionally, the topical application of tau protein is also being considered, either through commercially available recombinant tau protein, or through a tau protein alternative expressed in plants. Although tau is not expressed by plants, there are other proteins in plants that replace MAPs and their application and effects will be explored [407].

In summary, the main findings of this thesis revealed that tau can orchestrate epidermal homeostasis through the regulation of epidermal differentiation and stratification (Figure 7.1). Acting through interactions with cell adhesion proteins, tau influenced cell-ECM and cell-cell interactions. Additionally, through direct

interactions with cytoskeletal components tau expression was upregulated to stabilise and orchestrate cytoskeletal dynamics during mitosis, cell differentiation and epidermal stratification. Finally, there was a distinct expression pattern of tau in cSCC, linked to the differentiation status of the tumours.

8. Conclusion

In conclusion, this thesis has uncovered mechanisms underpinning tau's role in epidermal homeostasis, keratinocyte cell fate and revealed tau as a possible new therapeutic target to help manage the rapidly increasing cSCC cases.

The clinical implications therefore, could be that tau becomes a new therapeutic target, used in combination with current therapies to increase their efficacy and help tackle the rapidly increasing cSCC cases. Prior to this thesis, the role of tau in the epidermis had not been identified. Taken together, the findings of this thesis have provided novel and exciting results, anticipated to be a starting point for more functional research into the translational applications of tau in the epidermis.

9. References

1. Fuchs, E. & Horsley, V. More than one way to skin . . . *Genes Dev.* **22**, 976–85 (2008).
2. Fuchs, E. Epithelial Skin Biology. Three Decades of Developmental Biology, a Hundred Questions Answered and a Thousand New Ones to Address. in *Current Topics in Developmental Biology* **116**, 357–374 (2016).
3. Fuchs, E. Scratching the surface of skin development. *Nature* **445**, 834–842 (2007).
4. Kolarsick, P. A. J., Kolarsick, M. A. & Goodwin, C. Anatomy and Physiology of the Skin. *J. Dermatol. Nurses. Assoc.* **3**, 203–213 (2011).
5. McGrath, J. A. & Uitto, J. Anatomy and Organization of Human Skin. in *Rook's Textbook of Dermatology: Eighth Edition* **1**, 34–86 (Wiley-Blackwell, 2010).
6. Watt, F. M. & Fujiwara, H. Cell-extracellular matrix interactions in normal and diseased skin. *Cold Spring Harb. Perspect. Biol.* **3**, 1–14 (2011).
7. Clore, J. N., Cohen, I. K. & Diegelmann, R. F. Quantitation of Collagen Types I and III during Wound Healing in Rat Skin. *Exp. Biol. Med.* **161**, 337–340 (1979).
8. Jones, P. H., Harper, S. & Watt, F. M. *Stem cell patterning and fate in human epidermis*. *Cell* **80**, (1995).
9. Watt, F. M. Epidermal stem cells: markers, patterning and the control of stem cell fate. *Philos. Trans. R. Soc. Lond. B. Biol. Sci.* **353**, 831–7 (1998).
10. Fuchs, E. & Green, H. Changes in keratin gene expression during terminal differentiation of the keratinocyte. *Cell* **19**, 1033–1042 (1980).
11. Fuchs, E. Epidermal differentiation: the bare essentials. *J. Cell Biol.* **111**, 2807–14 (1990).
12. Fuchs, E. Skin stem cells: Rising to the surface. *J. Cell Biol.* **180**, 273–284 (2008).
13. Ge, Y. & Fuchs, E. Stretching the limits: from homeostasis to stem cell plasticity in wound healing and cancer. *Nat. Rev. Genet.* **19**, 311–325 (2018).
14. Elaine Fuchs. Epidermal Differentiation: The Bare Essentials The Program of Terminal Differentiation. *J. Cell Biol.* **111**, 2807–2814 (1990).
15. Fuchs, E. & Green, H. Regulation of terminal differentiation of cultured human keratinocytes by vitamin A. *Cell* **25**, 617–25 (1981).
16. Fuchs, E. Skin Stem Cells in Silence, Action, and Cancer. *Stem Cell Reports* **10**, 1432–1438 (2018).
17. Blanpain, C. & Fuchs, E. Epidermal homeostasis: a balancing act of stem cells in the skin. *Nat. Rev. Mol. Cell Biol.* **10**, 207–217 (2009).
18. Rübsam, M. *et al.* Adherens junctions and desmosomes coordinate mechanics and signaling to orchestrate tissue morphogenesis and function: An evolutionary perspective. *Cold Spring Harb. Perspect. Biol.* **10**, a029207 (2018).
19. Breitkreutz, D., Koxholt, I., Thiemann, K. & Nischt, R. Skin basement membrane: the foundation of epidermal integrity--BM functions and diverse roles of bridging molecules nidogen and perlecan. *Biomed Res. Int.* **2013**, 179784 (2013).
20. Haines, R. L. & Lane, E. B. Keratins and disease at a glance. *J. Cell Sci.* **125**, 3923–3928 (2012).
21. Sumigray, K. D. & Lechler, T. Cell adhesion in epidermal development and barrier formation. in *Current Topics in Developmental Biology* **112**, 383–414 (Academic Press Inc., 2015).
22. Luxenburg, C. & Zaidel-Bar, R. From cell shape to cell fate via the cytoskeleton — Insights from the epidermis. *Exp. Cell Res.* **378**, 232–237 (2019).
23. Wickström, S. A. & Niessen, C. M. Cell adhesion and mechanics as drivers of tissue organization and differentiation: local cues for large scale organization. *Curr. Opin. Cell Biol.* **54**, 89–97 (2018).
24. Rizzelli, F., Malabarba, M. G., Sigismund, S. & Mapelli, M. The crosstalk between microtubules, actin and membranes shapes cell division. *Open Biol.* **10**, (2020).
25. Watt, F. M. & Hogan, B. L. M. Out of eden: Stem cells and their niches. *Science*

287, 1427–1430 (2000).
26. Kulukian, A. & Fuchs, E. Spindle orientation and epidermal morphogenesis. *Philosophical Transactions of the Royal Society B: Biological Sciences* **368**, (2013).
27. Mascré, G. *et al.* Distinct contribution of stem and progenitor cells to epidermal maintenance. *Nature* **489**, 257–262 (2012).
28. Tumbar, T. *et al.* Defining the Epithelial Stem Cell Niche in Skin. *Science (80-.).* **303**, 359–363 (2004).
29. Jones, P. H., Harper, S. & Watt, F. M. Stem cell patterning and fate in human epidermis. *Cell* **80**, 83–93 (1995).
30. Potten, C. S. the Epidermal Proliferative Unit: the Possible Role of the Central Basal Cell. *Cell Prolif.* **7**, 77–88 (1974).
31. Barrandon, Y. & Green, H. Three clonal types of keratinocyte with different capacities for multiplication. *Proc. Natl. Acad. Sci.* **84**, 2302–2306 (1987).
32. Blanpain, C. & Fuchs, E. Epidermal Stem Cells of the Skin. *Annu. Rev. Cell Dev. Biol.* **22**, 339–373 (2006).
33. Blanpain, C. & Fuchs, E. Epidermal stem cells of the skin. *Annu. Rev. Cell Dev. Biol.* **22**, 339–73 (2006).
34. Rochat, A., Kobayashi, K. & Barrandon, Y. Location of stem cells of human hair follicles by clonal analysis. *Cell* **76**, 1063–73 (1994).
35. Rompolas, P. *et al.* Spatiotemporal coordination of stem cell commitment during epidermal homeostasis. *Science (80-.).* **352**, 1471–1474 (2016).
36. Box, K., Joyce, B. W. & Devenport, D. Epithelial geometry regulates spindle orientation and progenitor fate during formation of the mammalian epidermis. *Elife* **8**, (2019).
37. Muroyama, A. & Lechler, T. Polarity and stratification of the epidermis. *Seminars in Cell and Developmental Biology* **23**, 890–896 (2012).
38. Clayton, E. *et al.* A single type of progenitor cell maintains normal epidermis. *Nature* **446**, 185–189 (2007).
39. Klein, A. M., Nakagawa, T., Ichikawa, R., Yoshida, S. & Simons, B. D. Mouse germ line stem cells undergo rapid and stochastic turnover. *Cell Stem Cell* **7**, 214–224 (2010).
40. Doupé, D. P. *et al.* A single progenitor population switches behavior to maintain and repair esophageal epithelium. *Science (80-.).* **337**, 1091–1093 (2012).
41. Lim, X. *et al.* Interfollicular epidermal stem cells self-renew via autocrine Wnt signaling. *Science (80-.).* **342**, 1226–1230 (2013).
42. Füllgrabe, A. *et al.* Dynamics of Lgr6+ progenitor cells in the hair follicle, sebaceous gland, and interfollicular epidermis. *Stem Cell Reports* **5**, 843–855 (2015).
43. Gonzalez-Celeiro, M., Zhang, B. & Hsu, Y. C. Fate by Chance, not by Choice: Epidermal Stem Cells Go Live. *Cell Stem Cell* **19**, 8–10 (2016).
44. Byrd, K. M. *et al.* Heterogeneity within Stratified Epithelial Stem Cell Populations Maintains the Oral Mucosa in Response to Physiological Stress. *Cell Stem Cell* **25**, 814-829.e6 (2019).
45. Jensen, U. B., Lowell, S. & Watt, F. M. The spatial relationship between stem cells and their progeny in the basal layer of human epidermis: A new view based on whole-mount labelling and lineage analysis. *Development* **126**, 2409–2418 (1999).
46. Lawlor, K. T. & Kaur, P. Dermal contributions to human interfollicular epidermal architecture and self-renewal. *International Journal of Molecular Sciences* **16**, 28098–28107 (2015).
47. Yamada, T. *et al.* Laminin-332 regulates differentiation of human interfollicular epidermal stem cells. *Mech. Ageing Dev.* **171**, 37–46 (2018).
48. Jones, P. H., Harper, S. & Watt, F. M. Stem cell patterning and fate in human epidermis. *Cell* **80**, 83–93 (1995).
49. Jones, P. H. & Watt, F. M. Separation of human epidermal stem cells from transit amplifying cells on the basis of differences in integrin function and expression.

Cell **73**, 713–724 (1993).
50. Lowell, S., Jones, P., Le Roux, I., Dunne, J. & Watt, F. M. Stimulation of human epidermal differentiation by Delta-Notch signalling at the boundaries of stem-cell clusters. *Curr. Biol.* **10**, 491–500 (2000).
51. Alberts, B. *et al.* Epidermis and Its Renewal by Stem Cells. *Mol. Biol. Cell* **4206**, 3–7 (2002).
52. Desai, B. V., Harmon, R. M. & Green, K. J. Desmosomes at a glance. *J. Cell Sci.* **122**, 4401–4407 (2009).
53. Saito, M., Tucker, D. K., Kohlhorst, D., Niessen, C. M. & Kowalczyk, A. P. Classical and desmosomal cadherins at a glance. *J. Cell Sci.* **125**, 2547–2552 (2012).
54. Watt, F. M., Mattey, D. L. & Garrod, D. R. Calcium-induced reorganization of desmosomal components in cultured human keratinocytes. *J. Cell Biol.* **99**, 2211–5 (1984).
55. Park, S. *et al.* Tissue-scale coordination of cellular behaviour promotes epidermal wound repair in live mice. *Nat. Cell Biol.* **19**, 155–163 (2017).
56. Sotiropoulou, P. A. & Blanpain, C. Development and homeostasis of the skin epidermis. *Cold Spring Harb. Perspect. Biol.* **4**, a008383 (2012).
57. Lapouge, G. *et al.* Identifying the cellular origin of squamous skin tumors. *Proc. Natl. Acad. Sci.* **108**, 7431–7436 (2011).
58. Hanahan, D. & Weinberg, R. A. The Hallmarks of Cancer. *Cell* **100**, 57–70 (2000).
59. Roig-Rosello, E. & Rousselle, P. The Human Epidermal Basement Membrane: A Shaped and Cell Instructive Platform That Aging Slowly Alters. *Biomolecules* **10**, 1–32 (2020).
60. Yim, E. K. & Sheetz, M. P. Force-dependent cell signaling in stem cell differentiation. *Stem Cell Res. Ther.* **3**, 41 (2012).
61. Fletcher, D. A. & Mullins, R. D. Cell mechanics and the cytoskeleton. *Nat. 2010 4637280* **463**, 485–492 (2010).
62. Morgner, J. *et al.* Integrin-linked kinase regulates the niche of quiescent epidermal stem cells. *Nat. Commun.* **6**, 8198 (2015).
63. Yap, L., Tay, H. G., Nguyen, M. T. X., Tjin, M. S. & Tryggvason, K. Laminins in Cellular Differentiation. *Trends Cell Biol.* **29**, 987–1000 (2019).
64. Leblond, C. P. & Inoue, S. Structure, composition, and assembly of basement membrane. *Am. J. Anat.* **185**, 367–390 (1989).
65. Perez-Moreno, M., Jamora, C. & Fuchs, E. Sticky business: Orchestrating cellular signals at adherens junctions. *Cell* **112**, 535–548 (2003).
66. Lechler, T. & Fuchs, E. Desmoplakin: An unexpected regulator of microtubule organization in the epidermis. *J. Cell Biol.* **176**, 147–154 (2007).
67. Walko, G., Castañón, M. J. & Wiche, G. Molecular architecture and function of the hemidesmosome. *Cell Tissue Res.* **360**, 529–544 (2015).
68. El Ghalbzouri, A., Commandeur, S., Rietveld, M. H., Mulder, A. A. & Willemze, R. Replacement of animal-derived collagen matrix by human fibroblast-derived dermal matrix for human skin equivalent products. *Biomaterials* **30**, 71–78 (2009).
69. Bouameur, J. E., Favre, B. & Borradori, L. Plakins, a versatile family of cytolinkers: Roles in skin integrity and in human diseases. *J. Invest. Dermatol.* **134**, 885–894 (2014).
70. Wiche, G. Role of plectin in cytoskeleton organization and dynamics. *J. Cell Sci.* **111**, 2477–2486 (1998).
71. Fuchs, E., Tumbar, T. & Guasch, G. Socializing with the neighbors: Stem cells and their niche. *Cell* **116**, 769–778 (2004).
72. Garrod, D. & Chidgey, M. Desmosome structure, composition and function. *Biochimica et Biophysica Acta - Biomembranes* **1778**, 572–587 (2008).
73. Lechler, T. & Fuchs, E. Asymmetric cell divisions promote stratification and differentiation of mammalian skin. *Nature* **437**, 275–280 (2005).
74. Sumigray, K. D., Chen, H. & Lechler, T. Lis1 is essential for cortical microtubule organization and desmosome stability in the epidermis. *J. Cell Biol.* **194**, 631 (2011).

75. Sumigray, K. D., Foote, H. P. & Lechler, T. Noncentrosomal microtubules and type II myosins potentiate epidermal cell adhesion and barrier formation. *J. Cell Biol.* **199**, 513–525 (2012).
76. Green, K. J. & Gaudry, C. A. Are desmosomes more than tethers for intermediate filaments? *Nat. Rev. Mol. Cell Biol.* **1**, 208–216 (2000).
77. Wacker, I. U., Rickard, J. E., De Mey, J. R. & Kreis, T. E. Accumulation of a microtubule-binding protein, pp170, at desmosomal plaques. *J. Cell Biol.* **117**, 813–824 (1992).
78. Guo, Z. *et al.* E-cadherin interactome complexity and robustness resolved by quantitative proteomics. *Sci. Signal.* **7**, (2014).
79. Tunggal, J. A. *et al.* E-cadherin is essential for in vivo epidermal barrier function by regulating tight junctions. *EMBO J.* **24**, 1146–1156 (2005).
80. Alberts, B. *et al.* Cell Junctions. (2002).
81. Bikle, D. D., Xie, Z. & Tu, C.-L. Calcium regulation of keratinocyte differentiation. *Expert Rev. Endocrinol. Metab.* **7**, 461–472 (2012).
82. Kowalczyk, A. P. & Green, K. J. Structure, function, and regulation of desmosomes. *Prog. Mol. Biol. Transl. Sci.* **116**, 95–118 (2013).
83. O'Keefe, E. J., Briggaman, R. A. & Herman, B. Calcium-induced assembly of adherens junctions in keratinocytes. *J. Cell Biol.* **105**, 807–817 (1987).
84. Elsholz, F., Harteneck, C., Muller, W. & Friedland, K. Calcium--a central regulator of keratinocyte differentiation in health and disease. *Eur. J. Dermatol.* **24**, 650–61
85. Campanale, J. P., Sun, T. Y. & Montell, D. J. Development and dynamics of cell polarity at a glance. *J. Cell Sci.* **130**, 1201–1207 (2017).
86. Kubler, M. D., Jordan, P. W., O'Neill, C. H. & Watt, F. M. Changes in the abundance and distribution of actin and associated proteins during terminal differentiation of human epidermal keratinocytes. *J. Cell Sci.* **100**, 153–165 (1991).
87. Sept, D. Microtubule Polymerization: One Step at a Time. *Current Biology* **17**, R764–R766 (2007).
88. Yang, H., Ganguly, A. & Cabral, F. Inhibition of cell migration and cell division correlates with distinct effects of microtubule inhibiting drugs. *J. Biol. Chem.* **285**, 32242–32250 (2010).
89. Mitchison, T. & Kirschner, M. Dynamic instability of microtubule growth. *Nature* **312**, 237–242 (1984).
90. Gardner, M. K., Zanic, M. & Howard, J. Microtubule catastrophe and rescue. *Current Opinion in Cell Biology* **25**, 14–22 (2013).
91. Holy, T. E. & Leibler, S. Dynamic instability of microtubules as an efficient way to search in space. *Proc. Natl. Acad. Sci. U. S. A.* **91**, 5682–5685 (1994).
92. Muroyama, A. & Lechler, T. A transgenic toolkit for visualizing and perturbing microtubules reveals unexpected functions in the epidermis. *Elife* **6**, (2017).
93. Asare, A., Levorse, J. & Fuchs, E. Coupling organelle inheritance with mitosis to balance growth and differentiation. *Science (80-.).* **355**, (2017).
94. Cetera, M., Leybova, L., Joyce, B. & Devenport, D. Counter-rotational cell flows drive morphological and cell fate asymmetries in mammalian hair follicles. *Nat. Cell Biol.* **20**, 541–552 (2018).
95. Muroyama, A. & Lechler, T. Microtubule organization, dynamics and functions in differentiated cells. *Dev.* **144**, 3012–3021 (2017).
96. Lecland, N., Hsu, C.-Y., Ecile Chemin, C. ´, Merdes, A. & Bierkamp, C. Epidermal development requires ninein for spindle orientation and cortical microtubule organization. (2019). doi:10.26508/lsa.201900373
97. Brodu, V., Baffet, A. D., Le Droguen, P. M., Casanova, J. & Guichet, A. A developmentally regulated two-step process generates a noncentrosomal microtubule network in Drosophila tracheal cells. *Dev. Cell* **18**, 790–801 (2010).
98. Sluder, G. Centrosomes and the cell cycle. in *Journal of Cell Science* **94**, 253–275 (1989).
99. Rice, R. H. & Green, H. Presence in human epidermal cells of a soluble protein precursor of the cross-linked envelope: Activation of the cross-linking by calcium ions. *Cell* **18**, 681–694 (1979).

100. Koria, P. & Andreadis, S. T. Epidermal morphogenesis: The transcriptional program of human keratinocytes during stratification. *J. Invest. Dermatol.* **126**, 1834–1841 (2006).
101. Luxenburg, C., Amalia Pasolli, H., Williams, S. E. & Fuchs, E. Developmental roles for Srf, cortical cytoskeleton and cell shape in epidermal spindle orientation. *Nat. Cell Biol.* **13**, 203–214 (2011).
102. Kee, S. H. & Steinert, P. M. Microtubule disruption in keratinocytes induces cell-cell adhesion through activation of endogenous E-cadherin. *Mol. Biol. Cell* **12**, 1983–1993 (2001).
103. McMullan, R. *et al.* Keratinocyte Differentiation Is Regulated by the Rho and ROCK Signaling Pathway. *Curr. Biol.* **13**, 2185–2189 (2003).
104. Sumigray, K. D., Foote, H. P. & Lechler, T. Noncentrosomal microtubules and type II myosins potentiate epidermal cell adhesion and barrier formation. *J. Cell Biol.* **199**, 513–525 (2012).
105. Lee, W. H. *et al.* Upregulation of class II β-tubulin expression in differentiating keratinocytes. *J. Invest. Dermatol.* **124**, 291–297 (2005).
106. Ramaekers, F. C. S. & Bosman, F. T. The cytoskeleton and disease. *J. Pathol.* **204**, 351–354 (2004).
107. BSCB. Cytoskeleton – the movers and shapers in the cell | British Society for Cell Biology. *Bscb.Org* (2019). Available at: https://bscb.org/learning-resources/softcell-e-learning/cytoskeleton-the-movers-and-shapers-in-the-cell/. (Accessed: 13th September 2021)
108. Lengsfeld, A. M., Löw, I., Wieland, T., Dancker, P. & Hasselbach, W. Interaction of Phalloidin with Actin. *Proc. Natl. Acad. Sci. U. S. A.* **71**, 2803 (1974).
109. Feng, Y. & Walsh, C. A. The many faces of filamin: A versatile molecular scaffold for cell motility and signalling. *Nat. Cell Biol.* **6**, 1034–1038 (2004).
110. Fuchs, E. A Structural Scaffolding of Intermediate Filaments in Health and Disease. *Science (80-.).* **279**, 514–519 (1998).
111. Hohmann & Dehghani. The Cytoskeleton—A Complex Interacting Meshwork. *Cells* **8**, 362 (2019).
112. Ganguly, A., Yang, H., Sharma, R., Patel, K. D. & Cabral, F. The role of microtubules and their dynamics in cell migration. *J. Biol. Chem.* **287**, 43359–43369 (2012).
113. Svitkina, T. M., Verkhovsky, A. B. & Borisy, G. G. Plectin sidearms mediate interaction of intermediate filaments with microtubules and other components of the cytoskeleton. *J. Cell Biol.* **135**, 991–1007 (1996).
114. Van Citters, K. M., Hoffman, B. D., Massiera, G. & Crocker, J. C. The role of F-actin and myosin in epithelial cell rheology. *Biophys. J.* **91**, 3946–3956 (2006).
115. Stratigos, A. J. *et al.* European interdisciplinary guideline on invasive squamous cell carcinoma of the skin: Part 2. Treatment. *Eur. J. Cancer* **128**, 83–102 (2020).
116. UK, C. R. Non-melanoma skin cancer incidence statistics | Cancer Research UK. *Non Melanoma Skin Cancer Incidence Statistics* (2015). Available at: https://www.cancerresearchuk.org/health-professional/cancer-statistics/statistics-by-cancer-type/non-melanoma-skin-cancer/incidence#heading-Two. (Accessed: 21st February 2022)
117. Alam, M. & Ratner, D. Cutaneous squamous-cell carcinoma. *New England Journal of Medicine* **344**, 975–983 (2001).
118. Que, S. K. T., Zwald, F. O. & Schmults, C. D. Cutaneous squamous cell carcinoma: Incidence, risk factors, diagnosis, and staging. *J. Am. Acad. Dermatol.* **78**, 237–247 (2018).
119. Kallini, J. R., Hamed, N. & Khachemoune, A. Squamous cell carcinoma of the skin: epidemiology, classification, management, and novel trends. *Int. J. Dermatol.* **54**, 130–140 (2015).
120. Tokez, S. *et al.* Assessment of Cutaneous Squamous Cell Carcinoma (cSCC) in situ Incidence and the Risk of Developing Invasive cSCC in Patients with Prior cSCC in situ vs the General Population in the Netherlands, 1989-2017. *JAMA Dermatology* **156**, 973–981 (2020).

121. Lomas, A., Leonardi-Bee, J. & Bath-Hextall, F. A systematic review of worldwide incidence of nonmelanoma skin cancer. *Br. J. Dermatol.* **166**, 1069–1080 (2012).
122. Wheeler, B. W., Kothencz, G. & Pollard, A. S. Geography of non-melanoma skin cancer and ecological associations with environmental risk factors in England. *Br. J. Cancer* **109**, 235–241 (2013).
123. Xiang, F., Lucas, R., Hales, S. & Neale, R. Incidence of nonmelanoma skin cancer in relation to ambient UV radiation in white populations, 1978-2012 empirical relationships. *JAMA Dermatology* **150**, 1063–1071 (2014).
124. Cassarino, D. S., DeRienzo, D. P. & Barr, R. J. Cutaneous squamous cell carcinoma: a comprehensive clinicopathologic classification. Part One. *J. Cutan. Pathol.* **33**, 191–206 (2006).
125. Natarajan, V. T., Ganju, P., Ramkumar, A., Grover, R. & Gokhale, R. S. Multifaceted pathways protect human skin from UV radiation. *Nat. Chem. Biol.* **10**, 542–551 (2014).
126. Martincorena, I. & Campbell, P. J. Somatic mutation in cancer and normal cells. *Science* **349**, 1483–1489 (2015).
127. Martincorena, I. *et al.* High burden and pervasive positive selection of somatic mutations in normal human skin. *Science (80-.).* **348**, 880–886 (2015).
128. Hanahan, D. & Weinberg, R. A. The hallmarks of cancer. *Cell* **100**, 57–70 (2000).
129. Hanahan, D. & Weinberg, R. A. Hallmarks of Cancer: The Next Generation. *Cell* **144**, 646–674 (2011).
130. Kuri, P. & Rompolas, P. Differentiation keeps skin cancer at bay. *Nature Cell Biology* **20**, 1237–1239 (2018).
131. Das Mahapatra, K. *et al.* A comprehensive analysis of coding and non-coding transcriptomic changes in cutaneous squamous cell carcinoma. *Sci. Rep.* **10**, 1–12 (2020).
132. Jian, Z., Strait, A., Jimeno, A. & Wang, X. J. Cancer Stem Cells in Squamous Cell Carcinoma. *Journal of Investigative Dermatology* **137**, 31–37 (2017).
133. Reeves, M. Q., Kandyba, E., Harris, S., Del Rosario, R. & Balmain, A. Multicolour lineage tracing reveals clonal dynamics of squamous carcinoma evolution from initiation to metastasis. *Nat. Cell Biol.* **20**, 699–709 (2018).
134. Li, Y. Y. *et al.* Genomic analysis of metastatic cutaneous squamous cell carcinoma. *Clin. Cancer Res.* **21**, 1447–1456 (2015).
135. Chitsazzadeh, V. *et al.* Cross-species identification of genomic drivers of squamous cell carcinoma development across preneoplastic intermediates. *Nat. Commun.* **7**, (2016).
136. Hameetman, L. *et al.* Molecular profiling of cutaneous squamous cell carcinomas and actinic keratoses from organ transplant recipients. *BMC Cancer* **13**, 58 (2013).
137. Pickering, C. R. *et al.* Mutational landscape of aggressive cutaneous squamous cell carcinoma. *Clin. Cancer Res.* **20**, 6582–6592 (2014).
138. Hammerman, P. S. *et al.* Comprehensive genomic characterization of squamous cell lung cancers. *Nature* **489**, 519–525 (2012).
139. Hu, B. *et al.* Multifocal epithelial tumors and field cancerization from loss of mesenchymal CSL signaling. *Cell* **149**, 1207–1220 (2012).
140. Rivlin, N., Brosh, R., Oren, M. & Rotter, V. Mutations in the p53 tumor suppressor gene: Important milestones at the various steps of tumorigenesis. *Genes and Cancer* **2**, 466–474 (2011).
141. Boukamp, P. Non-melanoma skin cancer: What drives tumor development and progression? *Carcinogenesis* **26**, 1657–1667 (2005).
142. White, A. C. *et al.* Defining the origins of Ras/p53-mediated squamous cell carcinoma. *Proc. Natl. Acad. Sci. U. S. A.* **108**, 7425–7430 (2011).
143. Broders, A. C. Squamous-Cell Epithelioma of the Skin a Study of 256 Cases. *Ann. Surg.* **73**, 141–160 (1921).
144. Cassarino, D. S., DeRienzo, D. P. & Barr, R. J. Cutaneous squamous cell carcinoma: a comprehensive clinicopathologic classification. *J. Cutan. Pathol.* **33**, 261–279 (2006).

145. Stratigos, A. J. *et al.* European interdisciplinary guideline on invasive squamous cell carcinoma of the skin: Part 1. epidemiology, diagnostics and prevention. *Eur. J. Cancer* **128**, 60–82 (2020).
146. Hashim, P. W., Chen, T., Rigel, D., Bhatia, N. & Kircik, L. H. Actinic Keratosis: Current Therapies and Insights Into New Treatments. *J. Drugs Dermatol.* **18**, s161-166. (2019).
147. Siegel, J. A., Korgavkar, K. & Weinstock, M. A. Current perspective on actinic keratosis: a review. *Br. J. Dermatol.* **177**, 350–358 (2017).
148. Combalia, A. & Carrera, C. Squamous Cell Carcinoma: An Update on Diagnosis and Treatment. *Dermatol. Pract. Concept.* **10**, e2020066 (2020).
149. Lapouge, G. *et al.* Skin squamous cell carcinoma propagating cells increase with tumour progression and invasiveness. *EMBO J.* **31**, 4563–4575 (2012).
150. Anand, S. *et al.* Fluorouracil Enhances Photodynamic Therapy of Squamous Cell Carcinoma via a p53-Independent Mechanism that Increases Protoporphyrin IX levels and Tumor Cell Death. *Mol. Cancer Ther.* **16**, 1092–1101 (2017).
151. Spira, A. I. & Carducci, M. A. Differentiation therapy. *Curr. Opin. Pharmacol.* **3**, 338–343 (2003).
152. Li, Y. Y. *et al.* Genomic analysis of metastatic cutaneous squamous cell carcinoma. *Clin. Cancer Res.* **21**, 1447–1456 (2015).
153. Corchado-Cobos, R., García-Sancha, N., González-Sarmiento, R., Pérez-Losada, J. & Cañueto, J. Cutaneous squamous cell carcinoma: From biology to therapy. *Int. J. Mol. Sci.* **21**, (2020).
154. Fife, C. M., McCarroll, J. A. & Kavallaris, M. Movers and shakers: Cell cytoskeleton in cancer metastasis. *British Journal of Pharmacology* **171**, 5507–5523 (2014).
155. Aseervatham, J. Cytoskeletal remodeling in cancer. *Biology (Basel).* **9**, 1–40 (2020).
156. Ong, M. S. *et al.* Cytoskeletal proteins in cancer and intracellular stress: A therapeutic perspective. *Cancers* **12**, (2020).
157. Amin, E. *et al.* Rho-kinase: Regulation, (dys)function, and inhibition. *Biological Chemistry* **394**, 1399–1410 (2013).
158. Zhang, X. *et al.* Novel Insights into the Role of the Cytoskeleton in Cancer. *Cytoskelet. - Struct. Dyn. Funct. Dis.* (2017).
159. Borovski, T., De Sousa E Melo, F., Vermeulen, L. & Medema, J. P. Cancer Stem Cell Niche: The Place to Be. *Cancer Res.* **71**, 634–639 (2011).
160. Puram, S. V. *et al.* Single-Cell Transcriptomic Analysis of Primary and Metastatic Tumor Ecosystems in Head and Neck Cancer. *Cell* **171**, 1611-1624.e24 (2017).
161. Zhou, P. *et al.* The epithelial to mesenchymal transition (EMT) and cancer stem cells: implication for treatment resistance in pancreatic cancer. *Mol. Cancer* **16**, 52 (2017).
162. Kalluri, R. & Weinberg, R. A. The basics of epithelial-mesenchymal transition. *J. Clin. Invest.* **119**, 1420–8 (2009).
163. Zeisberg, M. & Neilson, E. G. Biomarkers for epithelial-mesenchymal transitions. *J. Clin. Invest.* **119**, 1429–1437 (2009).
164. Thiery, J. P. Epithelial–mesenchymal transitions in tumour progression. *Nat. Rev. Cancer* **2**, 442–454 (2002).
165. Larue, L. & Bellacosa, A. Epithelial–mesenchymal transition in development and cancer: role of phosphatidylinositol 3′ kinase/AKT pathways. *Oncogene* **24**, 7443–7454 (2005).
166. Lamouille, S., Xu, J. & Derynck, R. Molecular mechanisms of epithelial–mesenchymal transition. *Nat. Rev. Mol. Cell Biol.* **15**, 178–196 (2014).
167. Debaugnies, M. *et al.* YAP and TAZ are essential for basal and squamous cell carcinoma initiation . *EMBO Rep.* **19**, (2018).
168. Heerboth, S. *et al.* EMT and tumor metastasis. *Clin. Transl. Med.* **4**, 6 (2015).
169. Francis, S. & Antonipillai, J. Cytoskeletal molecules play a major role in cancer progression. *Insights Biomed.* **2**, 9 (2017).
170. Jordan, M. A. & Wilson, L. Microtubules as a target for anticancer drugs. *Nature Reviews Cancer* **4**, 253–265 (2004).

171. Bhat, K. M. R. & Setaluri, V. Microtubule-associated proteins as targets in cancer chemotherapy. *Clin. Cancer Res.* **13**, 2849–2854 (2007).
172. Parker, A. L., Kavallaris, M. & McCarroll, J. A. Microtubules and their role in cellular stress in cancer. *Front. Oncol.* **4 JUN**, 153 (2014).
173. Person, F. *et al.* Prevalence of βIII-tubulin (TUBB3) expression in human normal tissues and cancers. *Tumor Biol.* **39**, 1–11 (2017).
174. Koegel, H. *et al.* Loss of serum response factor in keratinocytes results in hyperproliferative skin disease in mice. *J. Clin. Invest.* **119**, 899–910 (2009).
175. Cassimeris, L. & Spittle, C. Regulation of microtubule-associated proteins. *Int. Rev. Cytol.* **210**, 163–226 (2001).
176. Weingarten, M. D., Lockwood, A. H., Hwo, S. Y. & Kirschner, M. W. A protein factor essential for microtubule assembly. *Proc. Natl. Acad. Sci. U. S. A.* **72**, 1858–1862 (1975).
177. Iqbal, K., Liu, F., Gong, C.-X. & Grundke-Iqbal, I. Tau in Alzheimer disease and related tauopathies. *Curr. Alzheimer Res.* **7**, 656–64 (2010).
178. Mandelkow, E.-M. & Mandelkow, E. Biochemistry and cell biology of tau protein in neurofibrillary degeneration. *Cold Spring Harb. Perspect. Med.* **2**, a006247 (2012).
179. Samsonov, A., Yu, J. Z., Rasenick, M. & Popov, S. V. Tau interaction with microtubules in vivo. *J. Cell Sci.* **117**, 6129–6141 (2004).
180. Bunker, J. M., Wilson, L., Jordan, M. A. & Feinstein, S. C. Modulation of microtubule dynamics by tau in living cells: Implications for development and neurodegeneration. *Mol. Biol. Cell* **15**, 2720–2728 (2004).
181. Elie, A. *et al.* Tau co-organizes dynamic microtubule and actin networks. *Sci. Rep.* **5**, 1–10 (2015).
182. Cross, D., Tapia, L., Garrido, J. & Maccioni, R. B. Tau-like proteins associated with centrosomes in cultured cells. *Exp. Cell Res.* **229**, 378–387 (1996).
183. Sjöberg, M. K., Shestakova, E., Mansuroglu, Z., Maccioni, R. B. & Bonnefoy, E. Tau protein binds to pericentromeric DNA: A putative role for nuclear tau in nucleolar organization. *J. Cell Sci.* **119**, 2025–2034 (2006).
184. Rossi, G. *et al.* A new function of microtubule-associated protein tau: involvement in chromosome stability. *Cell Cycle* **7**, 1788–94 (2008).
185. Drubin, D. G. & Kirschner, M. W. Tau protein function in living cells. *J. Cell Biol.* **103**, 2739–2746 (1986).
186. D'Souza, I. & Schellenberg, G. D. Determinants of 4-repeat tau expression. Coordination between enhancing and inhibitory splicing sequences for exon 10 inclusion. *J. Biol. Chem.* **275**, 17700–17709 (2000).
187. Guo, T., Noble, W. & Hanger, D. P. Roles of tau protein in health and disease. *Acta Neuropathol.* **133**, 665–704 (2017).
188. Caillet-Boudin, M. L., Buée, L., Sergeant, N. & Lefebvre, B. Regulation of human MAPT gene expression. *Molecular Neurodegeneration* **10**, (2015).
189. Park, S. A., Ahn, S. Il & Gallo, J. M. Tau mis-splicing in the pathogenesis of neurodegenerative disorders. *BMB Reports* **49**, 405–413 (2016).
190. Goedert, M., Spillantini, M. G., Jakes, R., Rutherford, D. & Crowther, R. A. Multiple isoforms of human microtubule-associated protein tau: sequences and localization in neurofibrillary tangles of Alzheimer's disease. *Neuron* **3**, 519–26 (1989).
191. Goedert, M., Spillantini, M. G., Potier, M. C., Ulrich, J. & Crowther, R. A. Cloning and sequencing of the cDNA encoding an isoform of microtubule-associated protein tau containing four tandem repeats: differential expression of tau protein mRNAs in human brain. *EMBO J.* **8**, 393–9 (1989).
192. Liu, F. & Gong, C. X. Tau exon 10 alternative splicing and tauopathies. *Mol. Neurodegener.* **3**, 8 (2008).
193. Andreadis, A. Tau gene alternative splicing: Expression patterns, regulation and modulation of function in normal brain and neurodegenerative diseases. *Biochimica et Biophysica Acta - Molecular Basis of Disease* **1739**, 91–103 (2005).
194. Boyne, L. J., Tessler, A., Murray, M. & Fischer, I. Distribution of big tau in the

central nervous system of the adult and developing rat. *J. Comp. Neurol.* **358**, 279–293 (1995).
195. Goedert, M., Spillantini, M. G. & Crowther, R. A. Cloning of a big tau microtubule-associated protein characteristic of the peripheral nervous system. *Proc. Natl. Acad. Sci. U. S. A.* **89**, 1983–1987 (1992).
196. Dugger, B. N. *et al.* The Presence of Select Tau Species in Human Peripheral Tissues and Their Relation to Alzheimer's Disease. *J. Alzheimer's Dis.* **51**, 345–356 (2016).
197. Akerman, S. C. *et al.* Neurodegenerative Disease-Related Proteins within the Epidermal Layer of the Human Skin. *J. Alzheimer's Dis.* **69**, 463–478 (2019).
198. Kim, J. Y., Illigens, B. M., McCormick, M. P., Wang, N. & Gibbons, C. H. Alpha-Synuclein in Skin Nerve Fibers as a Biomarker for Alpha-Synucleinopathies. *J. Clin. Neurol.* **15**, 135 (2019).
199. Fischer, I. & Baas, P. W. Resurrecting the Mysteries of Big Tau. *Trends in Neurosciences* **43**, 493–504 (2020).
200. Berget, S. M., Moore, C. & Sharp, P. A. Spliced segments at the 5' terminus of adenovirus 2 late mRNA. *Proc. Natl. Acad. Sci. U. S. A.* **74**, 3171–3175 (1977).
201. Krämer, A. The structure and function of proteins involved in mammalian pre-mRNA splicing. *Annual Review of Biochemistry* **65**, 367–409 (1996).
202. Jurica, M. S. & Moore, M. J. Pre-mRNA splicing: Awash in a sea of proteins. *Molecular Cell* **12**, 5–14 (2003).
203. Will, C. L. & Lührmann, R. Spliceosome structure and function. *Cold Spring Harb. Perspect. Biol.* **3**, 1–2 (2011).
204. Nilsen, T. W. The spliceosome: The most complex macromolecular machine in the cell? *BioEssays* **25**, 1147–1149 (2003).
205. WANG, Y. *et al.* Mechanism of alternative splicing and its regulation. *Biomed. Reports* **3**, 152 (2015).
206. Matlin, A. J., Clark, F. & Smith, C. W. J. Understanding alternative splicing: towards a cellular code. *Nat. Rev. Mol. Cell Biol. 2005 65* **6**, 386–398 (2005).
207. Verta, J. P. & Jacobs, A. The role of alternative splicing in adaptation and evolution. *Trends Ecol. Evol.* **37**, 299–308 (2022).
208. Bush, S. J., Chen, L., Tovar-Corona, J. M. & Urrutia, A. O. Alternative splicing and the evolution of phenotypic novelty. *Philos. Trans. R. Soc. B Biol. Sci.* **372**, (2017).
209. Baralle, F. E. & Giudice, J. Alternative splicing as a regulator of development and tissue identity. *Nature Reviews Molecular Cell Biology* **18**, 437–451 (2017).
210. Yeo, G., Holste, D., Kreiman, G. & Burge, C. B. Variation in alternative splicing across human tissues. *Genome Biol.* **5**, 1–15 (2004).
211. Avila, J. The tau code. *Front. Aging Neurosci.* **1**, 1–5 (2009).
212. Hefti, M. M. *et al.* High-resolution temporal and regional mapping of MAPT expression and splicing in human brain development. *PLoS One* **13**, e0195771 (2018).
213. Takuma, H., Arawaka, S. & Mori, H. Isoforms changes of tau protein during development in various species. *Dev. Brain Res.* **142**, 121–127 (2003).
214. Malmanche, N. *et al.* Developmental Expression of 4-Repeat-Tau Induces Neuronal Aneuploidy in Drosophila Tauopathy Models. *Sci. Rep.* **7**, 1–14 (2017).
215. Maina, M. B., Al-Hilaly, Y. K. & Serpell, L. C. Nuclear tau and its potential role in alzheimer's disease. *Biomolecules* **6**, 2–20 (2016).
216. Brandt, R., Léger, J. & Lee, G. Interaction of tau with the neural plasma membrane mediated by tau's amino-terminal projection domain. *J. Cell Biol.* **131**, 1327–1340 (1995).
217. Sotiropoulos, I. *et al.* Atypical, non-standard functions of the microtubule associated Tau protein. *Acta neuropathologica communications* **5**, 91 (2017).
218. Uberti, D., Rizzini, C., Spano, P. & Memo, M. Characterization of tau proteins in human neuroblastoma SH-SY5Y cell line. *Neurosci. Lett.* **235**, 149–153 (1997).
219. Smith, C. J., Anderton, B. H., Davis, D. R. & Gallo, J. M. Tau isoform expression and phosphorylation state during differentiation of cultured neuronal cells. *FEBS Lett.* **375**, 243–248 (1995).

220. Andreadis, A. Tau gene alternative splicing: Expression patterns, regulation and modulation of function in normal brain and neurodegenerative diseases. *Biochim. Biophys. Acta - Mol. Basis Dis.* **1739**, 91–103 (2005).
221. Zabik, N. L., Imhof, M. M. & Martic-Milne, S. Structural evaluations of tau protein conformation: Methodologies and approaches. *Biochem. Cell Biol.* **95**, 338–349 (2017).
222. Goode, B. L., Chau, M., Denis, P. E. & Feinstein, S. C. Structural and functional differences between 3-repeat and 4-repeat tau isoforms: Implications for normal tau function and the onset of neurodegenerative disease. *J. Biol. Chem.* **275**, 38182–38189 (2000).
223. Sallaberry, C. A. *et al.* Tau and Membranes: Interactions That Promote Folding and Condensation. *Front. Cell Dev. Biol.* **9**, 2632 (2021).
224. Pooler, A. M. & Hanger, D. P. Functional implications of the association of tau with the plasma membrane. *Biochemical Society Transactions* **38**, 1012–1015 (2010).
225. Kellogg, E. H. *et al.* Near-atomic model of microtubule-tau interactions.
226. Jeganathan, S., Von Bergen, M., Brutlach, H., Steinhoff, H. J. & Mandelkow, E. Global hairpin folding of tau in solution. *Biochemistry* **45**, 2283–2293 (2006).
227. Barbier, P. *et al.* Role of tau as a microtubule-associated protein: Structural and functional aspects. *Front. Aging Neurosci.* **10**, 204 (2019).
228. Harada, A. *et al.* Altered microtubule organization in small-calibre axons of mice lacking tau protein. *Nature* **369**, 488–491 (1994).
229. Méphon-Gaspard, A. *et al.* Role of tau in the spatial organization of axonal microtubules: keeping parallel microtubules evenly distributed despite macromolecular crowding. *Cell. Mol. Life Sci.* **73**, 3745–3760 (2016).
230. Dehmelt, L. & Halpain, S. The MAP2/Tau family of microtubule-associated proteins. *Genome Biol.* **6**, 1–10 (2005).
231. He, H. J. *et al.* The proline-rich domain of tau plays a role in interactions with actin. *BMC Cell Biol.* **10**, (2009).
232. Prezel, E. *et al.* Tau can switch microtubule network organizations: from random networks to dynamic and stable bundles. *Mol. Biol. Cell* **29**, 154–165 (2018).
233. Sultan, A. *et al.* Nuclear Tau, a key player in neuronal DNA protection. *J. Biol. Chem.* **286**, 4566–4575 (2011).
234. Violet, M. *et al.* A major role for Tau in neuronal DNA and RNA protection in vivo under physiological and hyperthermic conditions. *Front. Cell. Neurosci.* **8**, (2014).
235. Kempf, M., Clement, A., Faissner, A., Lee, G. & Brandt, R. Tau binds to the distal axon early in development of polarity in a microtubule- and microfilament-dependent manner. *J. Neurosci.* **16**, 5583–5592 (1996).
236. Drubin, D. G., Feinstein, S. C., Shooter, E. M. & Kirschner, M. W. Nerve growth factor-induced neurite outgrowth in PC12 cells involves the coordinate induction of microtubule assembly and assembly-promoting factors. *J. Cell Biol.* **101**, 1799–1807 (1985).
237. GORCES, V. G. *et al.* Effects of DNA on Microtubule Assembly. *Eur. J. Biochem.* **105**, 7–16 (1980).
238. Federico, C. *et al.* Phosphorylated nucleolar Tau protein is related to the neuronal in vitro differentiation. *Gene* **664**, 1–11 (2018).
239. Baquero, J. *et al.* Nuclear Tau, p53 and Pin1 Regulate PARN-Mediated Deadenylation and Gene Expression. *Front. Mol. Neurosci.* **12**, 242 (2019).
240. Lu, J., Li, T., He, R. Q., Bartlett, P. F. & Götz, J. Visualizing the microtubule-associated protein tau in the nucleus. *Sci. China Life Sci.* **57**, 422–431 (2014).
241. Sultan, A. *et al.* Nuclear Tau, a key player in neuronal DNA protection. *J. Biol. Chem.* **286**, 4566–4575 (2011).
242. Sola, M. *et al.* Tau affects P53 function and cell fate during the DNA damage response. *Commun. Biol.* **3**, 1–15 (2020).
243. Rousseaux, M. W. *et al.* TRIM28 regulates the nuclear accumulation and toxicity of both alpha-synuclein and tau. *Elife* **5**, (2016).
244. Wauters, M., Wattiez, R. & Ris, L. Internalization of the extracellular full-length tau inside Neuro2A and cortical cells is enhanced by phosphorylation. *Biomolecules*

6, (2016).
245. Mietelska-Porowska, A., Wasik, U., Goras, M., Filipek, A. & Niewiadomska, G. Tau protein modifications and interactions: Their role in function and dysfunction. *Int. J. Mol. Sci.* **15**, 4671–4713 (2014).
246. Pîrşcoveanu, D. F. V. *et al.* Tau protein in neurodegenerative diseases - a review. *Rom. J. Morphol. Embryol.* **58**, 1141–1150 (2017).
247. W Nichols, T. Hyperphosphorylation of Tau Protein in Down 's Dementia and Alzheimer's Disease: Methylation and Implications in Prevention and Therapy. *J. Alzheimer's Dis. Park.* **04**, 1–8 (2014).
248. Iqbal, K., Liu, F., Gong, C.-X. & Grundke-Iqbal, I. Tau in Alzheimer disease and related tauopathies. *Curr. Alzheimer Res.* **7**, 656–64 (2010).
249. Hoover, B. R. *et al.* Tau Mislocalization to Dendritic Spines Mediates Synaptic Dysfunction Independently of Neurodegeneration. *Neuron* **68**, 1067–1081 (2010).
250. Bossy-Wetzel, E., Schwarzenbacher, R. & Lipton, S. A. Molecular pathways to neurodegeneration. *Nat. Med.* **10**, S2–S9 (2004).
251. Uronen, R. L. & Huttunen, H. J. *Genetic risk factors of Alzheimer's disease and cell-to-cell transmission of Tau*. *J Neurol Neuromedicine* **1**, (2016).
252. Alonso, A. D. *et al.* Hyperphosphorylation of Tau Associates with changes in its function beyond microtubule stability. *Frontiers in Cellular Neuroscience* **12**, (2018).
253. Sergeant, N., Delacourte, A. & Buée, L. Tau protein as a differential biomarker of tauopathies. *Biochimica et Biophysica Acta - Molecular Basis of Disease* **1739**, 179–197 (2005).
254. Caillet-Boudin, M. L. *et al.* Brain pathology in myotonic dystrophy: When tauopathy meets spliceopathy and RNAopathy. *Frontiers in Molecular Neuroscience* **6**, (2014).
255. D'Souza, I. *et al.* Missense and silent tau gene mutations cause frontotemporal dementia with parkinsonism-chromosome 17 type, by affecting multiple alternative RNA splicing regulatory elements. *Proc. Natl. Acad. Sci. U. S. A.* **96**, 5598–5603 (1999).
256. Hasegawa, M., Smith, M. J., Iijima, M., Tabira, T. & Goedert, M. FTDP-17 mutations N279K and S305N in tau produce increased splicing of exon 10. *FEBS Lett.* **443**, 93–96 (1999).
257. Hutton, M. *et al.* Association of missense and 5'-splice-site mutations in tau with the inherited dementia FTDP-17. *Nature* **393**, 702–704 (1998).
258. Alzheimer's Disease International. World Alzheimer Report 2018 | Alzheimer's Disease International. (2018). Available at: https://www.alz.co.uk/research/world-report-2018. (Accessed: 20th July 2019)
259. Mueed, Z. *et al.* Tau and mTOR: The hotspots for multifarious diseases in Alzheimer's development. *Front. Neurosci.* **13**, 1017 (2019).
260. Rose, M. R. *et al.* What is aging? *Front. Genet.* **3**, 134 (2012).
261. Wang, C., Lisanti, M. P. & Liao, D. J. Reviewing once more the c-myc and Ras collaboration: Converging at the cyclin D1-CDK4 complex and challenging basic concepts of cancer biology. *Cell Cycle* **10**, 57–67 (2011).
262. Finkel, T., Serrano, M. & Blasco, M. A. The common biology of cancer and ageing. *Nature* **448**, 767–774 (2007).
263. Ma, L.-L. *et al.* Association between Cancer and Alzheimer's Disease: Systematic Review and Meta-Analysis. *J. Alzheimer's Dis.* **42**, 565–573 (2014).
264. Roe, C., Behrens, M., Xiong, C., Miller, J. & Morris, J. Alzheimer disease and cancer. *Neurology* **64**, 895–898 (2013).
265. Catalá-López, F. *et al.* Alzheimer's disease and cancer: Current epidemiological evidence for a mutual protection. *Neuroepidemiology* **42**, 121–122 (2014).
266. Ou, S. M. *et al.* Does Alzheimer's disease protect against cancers? A nationwide population-based study. *Neuroepidemiology* **40**, 42–49 (2012).
267. Gargini, R., Segura-Collar, B. & Sánchez-Gómez, P. Novel functions of the neurodegenerative-related gene tau in cancer. *Front. Aging Neurosci.* **11**, 231 (2019).

268. Musicco, M. *et al.* Inverse occurrence of cancer and Alzheimer disease: A population-based incidence study. *Neurology* **81**, 322–328 (2013).
269. Roe, C. M., Behrens, M. I., Xiong, C., Miller, J. P. & Morris, J. C. Alzheimer disease and cancer. *Neurology* **64**, 895–898 (2005).
270. Behrens, M. I., Lendon, C. & Roe, C. M. A common biological mechanism in cancer and Alzheimer's disease? *Curr. Alzheimer Res.* **6**, 196–204 (2009).
271. Driver, J. A. *et al.* Inverse association between cancer and Alzheimer's disease: Results from the Framingham Heart Study. *BMJ* **344**, 19 (2012).
272. Roe, C. M. *et al.* Alzheimer disease identification using amyloid imaging and reserve variables: Proof of concept. *Neurology* **75**, 42–48 (2010).
273. White, R. S., Lipton, R. B., Hall, C. B. & Steinerman, J. R. Nonmelanoma skin cancer is associated with reduced Alzheimer disease risk. *Neurology* **80**, 1966–1972 (2013).
274. Schmidt, S. A. J., Ording, A. G., Horváth-Puhó, E., Sørensen, H. T. & Henderson, V. W. Non-melanoma skin cancer and risk of Alzheimer's disease and all-cause dementia. *PLoS One* **12**, e0171527 (2017).
275. Dugger, B. N. *et al.* Tau immunoreactivity in peripheral tissues of human aging and select tauopathies. *Neurosci. Lett.* **696**, 132–139 (2019).
276. Auburger, G. *et al.* Primary Skin Fibroblasts as a Model of Parkinson's Disease. (2012). doi:10.1007/s12035-012-8245-1
277. Ildefonso, R.-L. *et al.* Presence of Phosphorylated Tau Protein in the Skin of Alzheimer´s Disease Patients. (2015). doi:10.4172/2155-9929.S6-005
278. Mattiuzzo, N. R., Toulza, E., Jonca, N., Serre, G. & Guerrin, M. A large-scale multi-technique approach identifies forty-nine new players of keratinocyte terminal differentiation in human epidermis. *Exp. Dermatol.* **20**, 113–118 (2011).
279. Fabre-Jonca, N., Viard, I., French, L. E. & Masson, D. Upregulation and redistribution of E-MAP-115 (epithelial microtubule- associated protein of 115 kDa) in terminally differentiating keratinocytes is coincident with the formation of intercellular contacts. *J. Invest. Dermatol.* **112**, 216–225 (1999).
280. Rodríguez-Leyva, I. *et al.* α-Synuclein inclusions in the skin of Parkinson's disease and parkinsonism. *Ann. Clin. Transl. Neurol.* **1**, 471–8 (2014).
281. Rodriguez-Leyva, I. *et al.* The Presence of Alpha-Synuclein in Skin from Melanoma and Patients with Parkinson's Disease. *Mov. Disord. Clin. Pract.* **4**, 724–732 (2017).
282. Botchkarev, V. A. *et al.* Neurotrophins in Skin Biology and Pathology. *J. Invest. Dermatol.* **126**, 1719–1727 (2006).
283. Rodriguez-Leyva, I. *et al.* The Presence of Alpha-Synuclein in Skin from Melanoma and Patients with Parkinson's Disease. *Mov. Disord. Clin. Pract.* **4**, 724–732 (2017).
284. Rodríguez-Leyva, I. *et al.* Parkinson disease and progressive supranuclear palsy: Protein expression in skin. *Ann. Clin. Transl. Neurol.* **3**, 191–199 (2016).
285. Smoter, M. *et al.* The role of Tau protein in resistance to paclitaxel. *Cancer Chemother. Pharmacol.* **68**, 553–557 (2011).
286. Yang, J. *et al.* Microtubule-associated protein tau is associated with the resistance to docetaxel in prostate cancer cell lines. *Res. Reports Urol.* **9**, 71–77 (2017).
287. Dye, R. B., Fink, S. P. & Williams, R. C. *Taxol-induced flexibility of microtubules and its reversal by MAP-2 and Tau*. *Journal of Biological Chemistry* **268**, (1993).
288. Wang, C. *et al.* MAPT promoter CpG island hypermethylation is associated with poor prognosis in patients with stage II colorectal cancer. *Cancer Manag. Res.* **11**, 7337–7343 (2019).
289. Bartels, F. *et al.* Neuronal autoantibodies associated with cognitive impairment in melanoma patients. *Ann. Oncol.* **30**, 823–829 (2019).
290. Kleffman, K. *et al.* Melanoma-secreted Amyloid Beta Suppresses Neuroinflammation and Promotes Brain Metastasis. *Cancer Discov.* **4**, 10016 (2022).
291. Meerbrey, K. L. *et al.* The pINDUCER lentiviral toolkit for inducible RNA interference in vitro and in vivo. *Proc. Natl. Acad. Sci. U. S. A.* **108**, 3665–3670

(2011).
292. Singer, D. *et al.* Prominin-1 controls stem cell activation by orchestrating ciliary dynamics. *EMBO J.* **38**, e99845 (2019).
293. Zielke, N. & Edgar, B. A. FUCCI sensors: Powerful new tools for analysis of cell proliferation. *Wiley Interdiscip. Rev. Dev. Biol.* **4**, 469–487 (2015).
294. Gossen, M. & Bujard, H. Tight control of gene expression in mammalian cells by tetracycline-responsive promoters. *Proc. Natl. Acad. Sci. U. S. A.* **89**, 5547–5551 (1992).
295. de Fougerolles, A., Vornlocher, H. P., Maraganore, J. & Lieberman, J. Interfering with disease: A progress report on siRNA-based therapeutics. *Nat. Rev. Drug Discov.* **6**, 443–453 (2007).
296. Yang, D. *et al.* Short RNA duplexes produced by hydrolysis with Escherichia coli RNase III mediate effective RNA interference in mammalian cells. *Proc. Natl. Acad. Sci. U. S. A.* **99**, 9942–9947 (2002).
297. Moore, C. B., Guthrie, E. H., Huang, M. T. H. & Taxman, D. J. Short hairpin RNA (shRNA): design, delivery, and assessment of gene knockdown. *Methods Mol. Biol.* **629**, 141–158 (2010).
298. Meyerholz, D. K. & Beck, A. P. Principles and approaches for reproducible scoring of tissue stains in research. *Laboratory Investigation* **98**, 844–855 (2018).
299. Chomczynski, P. & Sacchi, N. Single-step method of RNA isolation by acid guanidinium thiocyanate-phenol-chloroform extrac1. Chomczynski P, Sacchi N (1987) Single-step method of RNA isolation by acid guanidinium thiocyanate-phenol-chloroform extraction. Anal Biochem 162:156–9. doi: 10. *Anal. Biochem.* **162**, 156–9 (1987).
300. Chukwu, J. E., Congdon, E. E., Sigurdsson, E. M. & Kong, X. P. Structural characterization of monoclonal antibodies targeting C-terminal Ser 404 region of phosphorylated tau protein. *MAbs* **11**, 477–488 (2019).
301. Carmel, G., Mager, E. M., Binder, L. I. & Kuret, J. The structural basis of monoclonal antibody Alz50's selectivity for Alzheimer's disease pathology. *J. Biol. Chem.* **271**, 32789–95 (1996).
302. Malia, T. J. *et al.* Epitope mapping and structural basis for the recognition of phosphorylated tau by the anti-tau antibody AT8. *Proteins Struct. Funct. Bioinforma.* **84**, 427–434 (2016).
303. Chukwu, J. E., Congdon, E. E., Sigurdsson, E. M. & Kong, X.-P. Structural characterization of monoclonal antibodies targeting C-terminal Ser 404 region of phosphorylated tau protein. *MAbs* **11**, (2019).
304. Maina, M. B., Al-Hilaly, Y. K., Serpell, L. C., Wischik, C. M. & Harrington, C. biomolecules Nuclear Tau and Its Potential Role in Alzheimer's Disease. doi:10.3390/biom6010009
305. Ibáñez-Salazar, A. *et al.* Oxidative Stress Modifies the Levels and Phosphorylation State of Tau Protein in Human Fibroblasts. *Front. Neurosci.* **11**, 495 (2017).
306. Muroyama, A., Seldin, L. & Lechler, T. Divergent regulation of functionally distinct γ-tubulin complexes during differentiation. *J. Cell Biol.* **213**, 679–692 (2016).
307. Breuzard, G. *et al.* Molecular mechanisms of Tau binding to microtubules and its role in microtubule dynamics in live cells. *J. Cell Sci.* **126**, 2810–2819 (2013).
308. Holmfeldt, P., Brattsand, G. & Gullberg, M. MAP4 counteracts microtubule catastrophe promotion but not tubulin-sequestering activity in intact cells. *Curr. Biol.* **12**, 1034–1039 (2002).
309. Haque, N., Gong, C. X., Sengupta, A., Iqbal, K. & Grundke-Iqbal, I. Regulation of microtubule-associated proteins, protein kinases and protein phosphatases during differentiation of SY5Y cells. *Mol. Brain Res.* **129**, 163–170 (2004).
310. Lacroix, B. *et al.* In situ imaging in C. elegans reveals developmental regulation of microtubule dynamics. *Dev. Cell* **29**, 203–216 (2014).
311. Tabassum, D. P. & Polyak, K. Tumorigenesis: it takes a village. *Nat. Rev. Cancer 2015 158* **15**, 473–483 (2015).
312. Bordeaux, J. *et al.* Antibody validation. *BioTechniques* **48**, 197–209 (2010).

313. Ossola, B. *et al.* Neuronal expression of pathological tau accelerates oligodendrocyte progenitor cell differentiation. *Glia* **64**, 457–471 (2016).
314. Liu, Y., Beyer, A. & Aebersold, R. On the Dependency of Cellular Protein Levels on mRNA Abundance. *Cell* **165**, 535–550 (2016).
315. Akan, P. *et al.* Comprehensive analysis of the genome transcriptome and proteome landscapes of three tumor cell lines. *Genome Med.* **4**, 86 (2012).
316. Ghadially, R. 25 years of epidermal stem cell research. *Journal of Investigative Dermatology* **132**, 797–810 (2012).
317. TILL, J. E. & McCULLOCH, E. A. A direct measurement of the radiation sensitivity of normal mouse bone marrow cells. *Radiat. Res.* **14**, 213–222 (1961).
318. Sakaue-Sawano, A. *et al.* Visualizing Spatiotemporal Dynamics of Multicellular Cell-Cycle Progression. *Cell* **132**, 487–498 (2008).
319. Henderson, L., Lim, C. & Zambon, A. A live-cell reporter that differentiates between quiescent and cycling cells. *The FASEB Journal* **28**, 1148.14 (2014).
320. Bryant, J. & Francis, D. The eukaryotic cell cycle. Preface. *SEB Exp. Biol. Ser.* **59**, (2008).
321. Watt, F. M. Epidermal stem cells: markers, patterning and the control of stem cell fate. *Philos. Trans. R. Soc. Lond. B. Biol. Sci.* **353**, 831–7 (1998).
322. Bikle, D. D., Xie, Z. & Tu, C.-L. Calcium regulation of keratinocyte differentiation. *Expert Rev. Endocrinol. Metab.* **7**, 461–472 (2012).
323. Elsholz, F., Harteneck, C., Muller, W. & Friedland, K. Calcium--a central regulator of keratinocyte differentiation in health and disease. *Eur. J. Dermatol.* **24**, 650–61
324. Cabrales Fontela, Y. *et al.* Multivalent cross-linking of actin filaments and microtubules through the microtubule-associated protein Tau. *Nat. Commun.* **8**, 1–12 (2017).
325. de Garcini, E. M. *et al.* Differentiation of neuroblastoma cells correlates with an altered splicing pattern of tau RNA. *FEBS Lett.* **299**, 10–14 (1992).
326. Yi, S. *et al.* Tau modulates Schwann cell proliferation, migration and differentiation following peripheral nerve injury. *J. Cell Sci.* **132**, jcs222059 (2019).
327. Pontvianne, F. *et al.* Identification of Nucleolus-Associated Chromatin Domains Reveals a Role for the Nucleolus in 3D Organization of the A. thaliana Genome. *Cell Rep.* **16**, 1574–1587 (2016).
328. Hale, C. M. *et al.* SMRT analysis of MTOC and nuclear positioning reveals the role of EB1 and LIC1 in single-cell polarization. *J. Cell Sci.* **124**, 4267–4285 (2011).
329. Breuzard, G. *et al.* Tau regulates the microtubule-dependent migration of glioblastoma cells via the Rho-ROCK signaling pathway. *J. Cell Sci.* **132**, (2019).
330. Fischer, I. & Baas, P. W. Resurrecting the Mysteries of Big Tau. *Trends Neurosci.* **43**, 493–504 (2020).
331. Nunez, J. & Fischer, I. Microtubule-associated proteins (MAPs) in the peripheral nervous system during development and regeneration. *J. Mol. Neurosci.* **8**, 207–22 (1997).
332. Mahanty, S. *et al.* Keratinocyte differentiation promotes ER stress-dependent lysosome biogenesis. *Cell Death Dis.* **10**, 1–17 (2019).
333. Hsu, C. Y. *et al.* Stabilization of microtubules restores barrier function after cytokine-induced defects in reconstructed human epidermis. *J. Dermatol. Sci.* **91**, 87–96 (2018).
334. Patel, S., Xi, Z. F., Seo, E. Y., McGaughey, D. & Segre, J. A. Klf4 and corticosteroids activate an overlapping set of transcriptional targets to accelerate in utero epidermal barrier acquisition. *Proc. Natl. Acad. Sci. U. S. A.* **103**, 18668–18673 (2006).
335. Raymond, A. A. *et al.* Lamellar bodies of human epidermis: Proteomics characterization by high throughput mass spectrometry and possible involvement of clip-170 in their trafficking/sectretion. *Mol. Cell. Proteomics* **7**, 2151–2175 (2008).
336. Holmes, N. E. & Charles, P. G. P. Safety and Efficacy Review of Doxycycline. *Clin. Med. Ther.* **1**, CMT.S2035 (2009).

337. Delobel, P. *et al.* Stable-Tau Overexpression in Human Neuroblastoma Cells: An Open Door for Explaining Neuronal Death in Tauopathies. *Ann. N. Y. Acad. Sci.* **1010**, 623–634 (2003).
338. Lutolf, M. P., Gilbert, P. M. & Blau, H. M. Designing materials to direct stem-cell fate. *Nature* **462**, 433–441 (2009).
339. Langer, R. & Vacanti, J. P. *Tissue Engineering*. (1993).
340. Urciuolo, F., Imparato, G., Guaccio, A., Mele, B. & Netti, P. A. Novel Strategies to Engineering Biological Tissue In Vitro. in *Methods in molecular biology (Clifton, N.J.)* **811**, 223–244 (2012).
341. Yang, J. *et al.* Reconstruction of functional tissues with cell sheet engineering. *Biomaterials* **28**, 5033–5043 (2007).
342. Yamada, K. M. & Cukierman, E. Modeling Tissue Morphogenesis and Cancer in 3D. *Cell* **130**, 601–610 (2007).
343. Brown, R. A., Wiseman, M., Chuo, C. B., Cheema, U. & Nazhat, S. N. Ultrarapid engineering of biomimetic materials and tissues: Fabrication of nano- and microstructures by plastic compression. *Adv. Funct. Mater.* **15**, 1762–1770 (2005).
344. Todorović, V. *et al.* Small Molecule IL-36γ Antagonist as a Novel Therapeutic Approach for Plaque Psoriasis. *Sci. Rep.* **9**, 1–15 (2019).
345. De Jong, W. H. *et al.* Round robin study to evaluate the reconstructed human epidermis (RhE) model as an in vitro skin irritation test for detection of irritant activity in medical device extracts. *Toxicol. Vitr.* **50**, 439–449 (2018).
346. Pedrosa, T. do N. *et al.* A new reconstructed human epidermis for in vitro skin irritation testing. *Toxicol. Vitr.* **42**, 31–37 (2017).
347. Lechler, T. & Fuchs, E. Asymmetric cell divisions promote stratification and differentiation of mammalian skin. *Nature* **437**, 275–280 (2005).
348. Kim, M., Park, H. E., Lee, S. H., Han, K. & Lee, J. H. Increased risk of Alzheimer's disease in patients with psoriasis: a nationwide population-based cohort study. *Sci. Rep.* **10**, 1–7 (2020).
349. Brohée, S. & van Helden, J. Evaluation of clustering algorithms for protein-protein interaction networks. *BMC Bioinformatics* **7**, (2006).
350. Litjens, S. H. M., de Pereda, J. M. & Sonnenberg, A. Current insights into the formation and breakdown of hemidesmosomes. *Trends Cell Biol.* **16**, 376–383 (2006).
351. Wiche, G. Plectin-mediated intermediate filament functions: Why isoforms matter. *Cells* **10**, 2154 (2021).
352. Fuchs, P. *et al.* Unusual 5' transcript complexity of plectin isoforms: Novel tissue-specific exons modulate actin binding activity. *Hum. Mol. Genet.* **8**, 2461–2472 (1999).
353. Andrä, K., Nikolic, B., Stöcher, M., Drenckhahn, D. & Wiche, G. Not just scaffolding: Plectin regulates actin dynamics in cultured cells. *Genes Dev.* **12**, 3442–3451 (1998).
354. Herrmann, H. & Wiche, G. Plectin and IFAP-300K are homologous proteins binding to microtubule-associated proteins 1 and 2 and to the 240-kilodalton subunit of spectrin. *J. Biol. Chem.* **262**, 1320–1325 (1987).
355. Adair-Kirk, T. L. *et al.* Keratinocyte-Targeted Expression of Human Laminin γ2 Rescues Skin Blistering and Early Lethality of Laminin γ2 Deficient Mice. *PLoS One* **7**, e45546 (2012).
356. Rico, T. *et al.* Tau Stabilizes Chromatin Compaction. *Front. Cell Dev. Biol.* **9**, 2818 (2021).
357. Freilich, R. *et al.* Competing protein-protein interactions regulate binding of Hsp27 to its client protein tau. *Nat. Commun.* **9**, 1–11 (2018).
358. Kundel, F. *et al.* Hsp70 Inhibits the Nucleation and Elongation of Tau and Sequesters Tau Aggregates with High Affinity. *ACS Chem. Biol.* **13**, 636–646 (2018).
359. Chen, Y. H., He, R. Q., Liu, Y., Liu, Y. & Xue, Z. G. Effect of human neuronal tau on denaturation and reactivation of rabbit muscle D-glyceraldehyde-3-phosphate dehydrogenase. *Biochem. J.* **351**, 233–240 (2000).

360. Wang, Q. *et al.* Proteomic analysis of neurofibrillary tangles in Alzheimer disease identifies GAPDH as a detergent-insoluble paired helical filament tau binding protein. *FASEB J.* **19**, 1–12 (2005).
361. Lu, J. *et al.* Filamin B mutations cause chondrocyte defects in skeletal development. *Hum. Mol. Genet.* **16**, 1661–1675 (2007).
362. Zhu, L. *et al.* Structure of Rap1b bound to talin reveals a pathway for triggering integrin activation. *Nat. Commun.* **8**, 1–12 (2017).
363. Olson, O. C. & Joyce, J. A. Cysteine cathepsin proteases: Regulators of cancer progression and therapeutic response. *Nat. Rev. Cancer* **15**, 712–729 (2015).
364. Levine, B. & Kroemer, G. Biological Functions of Autophagy Genes: A Disease Perspective. *Cell* **176**, 11–42 (2019).
365. Mindell, J. A. Lysosomal acidification mechanisms. *Annu. Rev. Physiol.* **74**, 69–86 (2012).
366. Li, L., Chen, X. & Gu, H. The signaling involved in autophagy machinery in keratinocytes and therapeutic approaches for skin diseases. *Oncotarget* **7**, 50682–50697 (2016).
367. Koenig, U. *et al.* Cell death induced autophagy contributes to terminal differentiation of skin and skin appendages. *Autophagy* **16**, 932–945 (2020).
368. Akinduro, O. *et al.* Constitutive Autophagy and Nucleophagy during Epidermal Differentiation. *J. Invest. Dermatol.* **136**, 1460–1470 (2016).
369. Baker, M. *et al.* Mutations in progranulin cause tau-negative frontotemporal dementia linked to chromosome 17. *Nature* **442**, 916–919 (2006).
370. He, Z. & Bateman, A. Progranulin (granulin-epithelin precursor, PC-cell-derived growth factor, acrogranin) mediates tissue repair and tumorigenesis. *J. Mol. Med.* **81**, 600–612 (2003).
371. Festa, B. P., Barbosa, A. D., Rob, M. & Rubinsztein, D. C. The pleiotropic roles of autophagy in Alzheimer's disease: From pathophysiology to therapy. *Curr. Opin. Pharmacol.* **60**, 149–157 (2021).
372. Jebarupa, B., Muralidharan, M., Arun, A., Mandal, A. K. & Mitra, G. Conformational heterogeneity of tau: Implication on intrinsic disorder, acid stability and fibrillation in Alzheimer's disease. *Biophys. Chem.* **241**, 27–37 (2018).
373. Giard, D. J. *et al.* In vitro cultivation of human tumors: establishment of cell lines derived from a series of solid tumors. *J. Natl. Cancer Inst.* **51**, 1417–23 (1973).
374. Yee, C., Krishnan-Hewlett, I., Baker, C. C., Schlegel, R. & Howley, P. M. Presence and expression of human papillomavirus sequences in human cervical carcinoma cell lines. *Am. J. Pathol.* **119**, 361–366 (1985).
375. Rosdy, M., Bernard, B. A., Schmidt, R. & Darmon, M. Incomplete epidermal differentiation of A431 epidermoid carcinoma cells. *In Vitro Cell. Dev. Biol.* **22**, 295–300 (1986).
376. St. John, L. S., Sauter, E. R., Herlyn, M., Litwin, S. & Adler-Storthz, K. *Endogenous p53 gene status predicts the response of human squamous cell carcinomas to wild-type p53*. *Cancer Gene Therapy* **7**, (2000).
377. Kalluri, R. & Zeisberg, M. Fibroblasts in cancer. *Nat. Rev. Cancer* **6**, 392–401 (2006).
378. Boumahdi, S. *et al.* SOX2 controls tumour initiation and cancer stem-cell functions in squamous-cell carcinoma. *Nature* **511**, 246–250 (2014).
379. Visvader, J. E. Cells of origin in cancer. *Nature* **469**, 314–322 (2011).
380. Plaks, V., Kong, N. & Werb, Z. The cancer stem cell niche: How essential is the niche in regulating stemness of tumor cells? *Cell Stem Cell* **16**, 225–238 (2015).
381. Schofield, R. The relationship between the spleen colony-forming cell and the haemopoietic stem cell. *Blood Cells* **4**, 7–25 (1978).
382. Batlle, E. & Clevers, H. Cancer stem cells revisited. *Nat. Med.* **23**, 1124–1134 (2017).
383. Miao, Y. *et al.* Adaptive Immune Resistance Emerges from Tumor-Initiating Stem Cells. *Cell* **177**, 1172-1186.e14 (2019).
384. Bhat, K. M. R. & Setaluri, V. Microtubule-associated proteins as targets in cancer chemotherapy. *Clin. Cancer Res.* **13**, 2849–2854 (2007).

385. Ge, Y. *et al.* Stem Cell Lineage Infidelity Drives Wound Repair and Cancer. *Cell* **169**, 636-650.e14 (2017).
386. Chen, D. *et al.* Targeting BMI1+Cancer Stem Cells Overcomes Chemoresistance and Inhibits Metastases in Squamous Cell Carcinoma. *Cell Stem Cell* **20**, 621-634.e6 (2017).
387. Stewart, R. L. & O'Connor, K. L. Clinical significance of the integrin α6β4 in human malignancies. *Lab. Investig.* **95**, 976–986 (2015).
388. Canel, M., Serrels, A., Frame, M. C. & Brunton, V. G. E-cadherin-integrin crosstalk in cancer invasion and metastasis. *J. Cell Sci.* **126**, 393–401 (2013).
389. Fiore, V. F. *et al.* Mechanics of a multilayer epithelium instruct tumour architecture and function. *Nature* **585**, 433–439 (2020).
390. Ebneth, A. *et al.* Overexpression of tau protein inhibits kinesin-dependent trafficking of vesicles, mitochondria, and endoplasmic reticulum: Implications for Alzheimer's disease. *J. Cell Biol.* **143**, 777–794 (1998).
391. Maman, S. & Witz, I. P. A history of exploring cancer in context. *Nat. Rev. Cancer* **407**, 359–376 (2018).
392. Lim, B., Woodward, W. A., Wang, X., Reuben, J. M. & Ueno, N. T. Inflammatory breast cancer biology: the tumour microenvironment is key. *Nat. Rev. Cancer* **18**, 485–499 (2018).
393. Lowy, C. M. & Oskarsson, T. Tenascin C in metastasis: A view from the invasive front. *Cell Adh. Migr.* **9**, 112–24 (2015).
394. Osmanagic-Myers, S. *et al.* Plectin-controlled keratin cytoarchitecture affects MAP kinases involved in cellular stress response and migration. *J. Cell Biol.* **174**, 557–568 (2006).
395. Seltmann, K., Fritsch, A. W., Käs, J. A. & Magin, T. M. Keratins significantly contribute to cell stiffness and impact invasive behavior. *Proc. Natl. Acad. Sci. U. S. A.* **110**, 18507–18512 (2013).
396. Pu, J., Guardia, C. M., Keren-Kaplan, T. & Bonifacino, J. S. Mechanisms and functions of lysosome positioning. *J. Cell Sci.* **129**, 4329–4339 (2016).
397. Valencia, R. G. *et al.* Plectin dysfunction in neurons leads to tau accumulation on microtubules affecting neuritogenesis, organelle trafficking, pain sensitivity and memory. *Neuropathol. Appl. Neurobiol.* **47**, 73–95 (2021).
398. Kulukian, A. & Fuchs, E. Spindle orientation and epidermal morphogenesis. *Philosophical Transactions of the Royal Society B: Biological Sciences* **368**, 20130016 (2013).
399. Qian, W. & Liu, F. Regulation of alternative splicing of tau exon 10. *Neuroscience Bulletin* **30**, 367–377 (2014).
400. Konermann, S. *et al.* Transcriptome Engineering with RNA-Targeting Type VI-D CRISPR Effectors. *Cell* **173**, 665-676.e14 (2018).
401. Yan, W. X. *et al.* Cas13d Is a Compact RNA-Targeting Type VI CRISPR Effector Positively Modulated by a WYL-Domain-Containing Accessory Protein. *Mol. Cell* **70**, 327-339.e5 (2018).
402. Watt, F. M. Epidermal stem cells: Markers, patterning and the control of stem cell fate. *Philos. Trans. R. Soc. B Biol. Sci.* **353**, 831–837 (1998).
403. Spicakova, T., O'Brien, M. M., Duran, G. E., Sweet-Cordero, A. & Sikic, B. I. Expression and silencing of the microtubule-associated protein Tau in breast cancer cells. *Mol. Cancer Ther.* **9**, 2970–2981 (2010).
404. Muralidar, S., Ambi, S. V., Sekaran, S., Thirumalai, D. & Palaniappan, B. Role of tau protein in Alzheimer's disease: The prime pathological player. *Int. J. Biol. Macromol.* **163**, 1599–1617 (2020).
405. Sato, C. *et al.* Tau Kinetics in Neurons and the Human Central Nervous System. *Neuron* **97**, 1284-1298.e7 (2018).
406. de Thé, H. Differentiation therapy revisited. *Nat. Rev. Cancer* **18**, 117–127 (2017).
407. Kesten, C. *et al.* The companion of cellulose synthase 1 confers salt tolerance through a Tau-like mechanism in plants. *Nat. Commun.* **10**, (2019).
408. Hsieh, Y. C. *et al.* Tau-Mediated Disruption of the Spliceosome Triggers Cryptic RNA Splicing and Neurodegeneration in Alzheimer's Disease. *Cell Rep.* **29**, 301-

316.e10 (2019).
409. Chang, J. K. *et al.* Tolfenamic Acid: A Modifier of the Tau Protein and its Role in Cognition and Tauopathy. *Curr. Alzheimer Res.* **15**, 655–663 (2018).
410. Manczak, M. & Reddy, P. H. Abnormal interaction between the mitochondrial fission protein Drp1 and hyperphosphorylated tau in Alzheimer's disease neurons: Implications for mitochondrial dysfunction and neuronal damage. *Hum. Mol. Genet.* **21**, 2538–2547 (2012).
411. Wang, F. *et al.* RNAscope: A novel in situ RNA analysis platform for formalin-fixed, paraffin-embedded tissues. *J. Mol. Diagnostics* **14**, 22–29 (2012).

10. Appendix

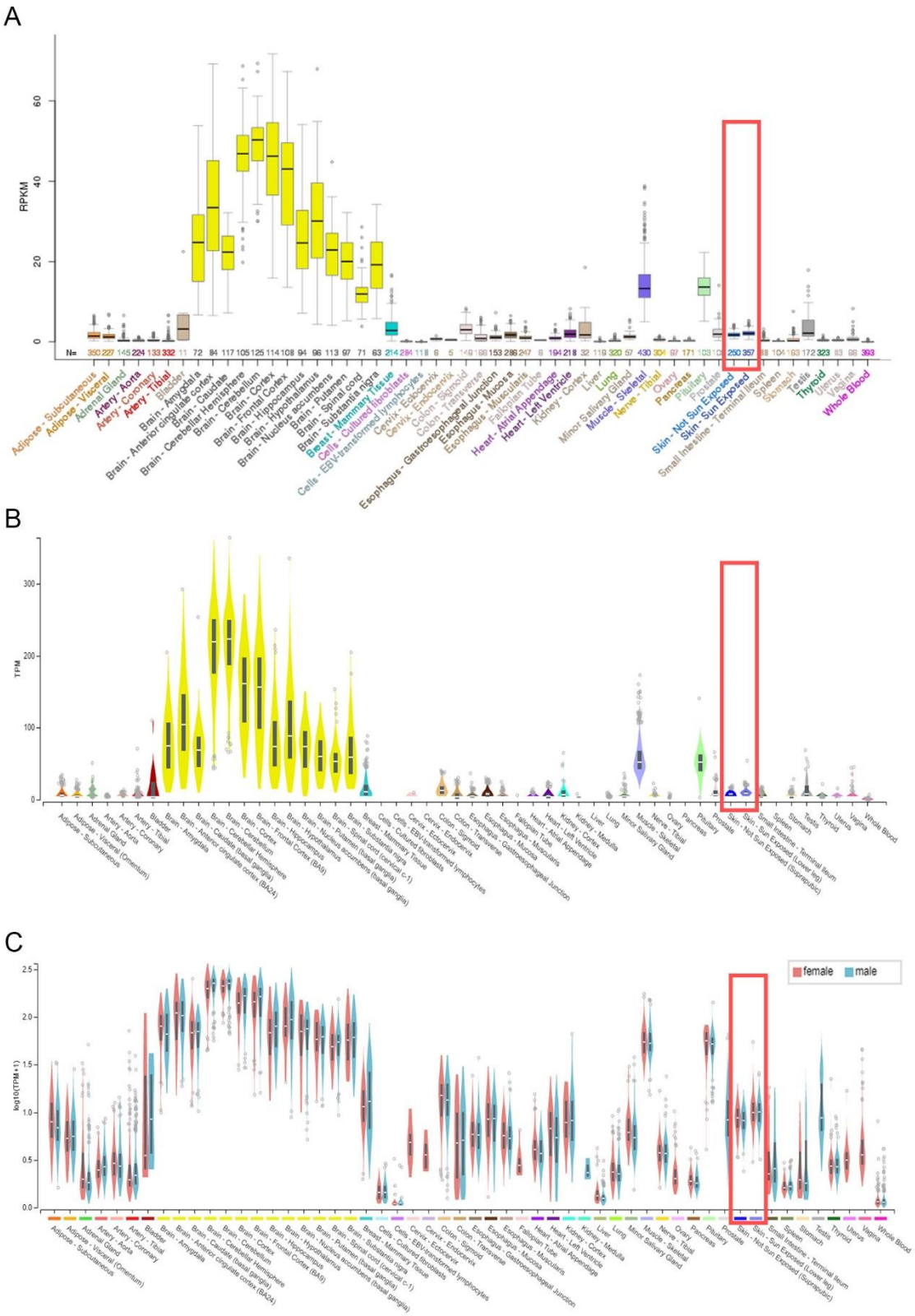

Figure 10.1. GTEx analysis of gene expression of tau in 53 tissues.
Tau expression throughout 53 tissues in the human body from GTEx Analysis Release V8 (dbGaP Accession phs000424.v8.p2). **A.** Highlighted box shows tau expression in non-sun-exposed and sun-exposed skin; 1.7 RPKM 2.0 RPKM respectively. **B.** Not sun-exposed (suprapublic) n=604 median TPM=7.394. Sun-

exposed (lower leg) n=701, median TPM=9.013. **C.** Male and female expression of *MAPT* in different tissues throughout the body shows no significant difference in the expression of tau between males and females. Data taken from https://www.gtexportal.org/home/gene/ENSG00000186868.

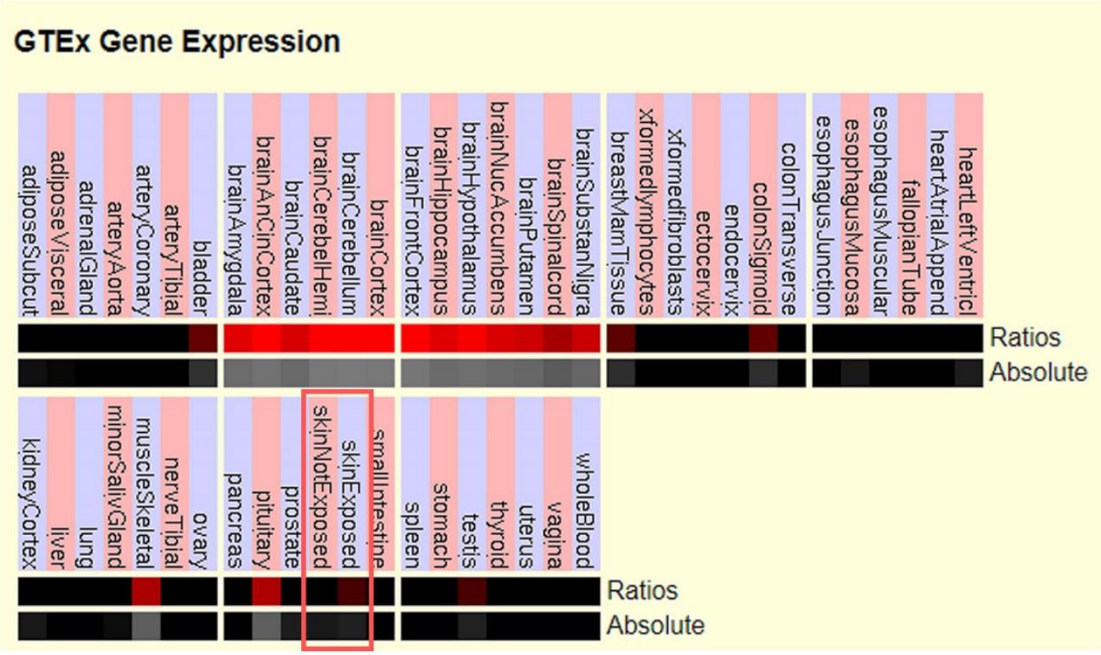

Figure 10.2. GTEx gene expression of tau across different tissues in the body.
Microarray expression data from UCSC GTEx Analysis Release V8 (dbGaP Accession phs000424.v8.p2) reveals that tau expression is higher in sun exposed skin samples than non-exposed skin samples.

Table 10.1. Human microtubule associated protein tau (*MAPT*) transcript variants.

	NCBI transcript variant	Accession number	Number of exons	Ensemble	Number of base pairs (bp)	Exons transcribed														Inserts/ repeats	Number of amino acids (aa)	MW (kDa)	Apparent MW (kDa)
						0	1	2	3	4	4A	5	6	7	8	9	10	11	12	13				
BigTau	6	NM_001123066	15	*MAPT*-205	6644	x	x	x	x	x	x	x	x	x	x	x	x	x	x	x	2N4R	776	79	120
PNS-tau	1	NM_016835	14	*MAPT*-212	6590	x	x	x	x	x	x	x	x	x		x	x	x	x	x	2N4R	758	76	110
htau40	2	NM_005910	12	*MAPT*-204	5639	x	x	x	x	x		x		x		x	x	x	x	x	2N4R	441	45.9	67
htau39	8	NM_001203252	11	*MAPT*-207	5546	x	x	x	x	x		x		x		x		x	x	x	2N3R	410	42.6	62
htau34	5	NM_001123067	11	*MAPT*-206	5552	x	x	x		x		x		x		x	x	x	x	x	1N4R	412	42.9	59
-	9	NM_001377265	13	*MAPT*-201	6815	x	x	x		x	x	x	x	x		x	x	x	x	x	1N4R	833	84	-
htau37	7	NM_001203251	10	*MAPT*-209	5459	x	x	x		x		x		x		x		x	x	x	1N3R	381	39.7	54
-	10	NM_001377266	11	*MAPT*-203	6524	x	x	x		x	x	x		x		x		x	x	x	1N3R	736	74	-
-	11	NM_001377267	9	-	4139	x	x	x		x		x		x		x		x		x	1N3R	280	28	-
htau24	3	NM_016834	10	*MAPT*-208	5465	x	x			x		x		x		x	x	x	x	x	0N4R	383	40.0	52
htau23	12	NM_001377268	10	-	5525	x	x			x		x		x		x		x	x	x	0N3R	352	36.7	48
-	4	NM_016841	9	*MAPT*-202	5372	x	x			x		x		x		x		x	x	x	0N3R	325	33	-

Transcript variants 2, 8, 5, 7, 3 and 12 are the six widely reported isoforms found in the CNS [178,190,191].

Table 10.2. List of primary antibodies used in this study for Immunofluorescence

Antibody	Reactivity	Host	Cat no.	Lot no.	Company	Dilution
Bmi1	H, M, R	Rb	HPA030472	C89795	Sigma	1:200
CD80	H	G	AF140	AAE0217121	R&D systems	1:50
E-cadherin	H, M	G	BAF748	CXW0315091	R&D systems	1:200
Granulin	H	R	HPA008763	000017373	Sigma	1:200
Integrin-α6 (CD49f)	H	R	14-0495-82	E03784-1633	eBioscience	1:200
Keratin-1	H, R	Rb	905204	B220351	Biolegend	1:5000
Keratin-14	H, M, R, P	Rb	PRB-155p-100	B278818	Covance	1:10,000
Ki67	H	M	M7240	20003301	Dako	1:200
Ki67	H, M, R	Rb	Ab15580	GR3198221-1	Abcam	1:200
Loricrin	H, M	Rb	905101	B244909	Biolegend	1:1000
P53 (pab240)	H	M	Scc-99	J0217	SantaCruz	1:200
Periostin	H	G	Af3548	YIG0114101	R&D systems	1:300
DyLight™ Phalloidin-554		-	13054	Lot:3	Cell signalling	1:200
PhosphorTau (AT8)	H	M	MN1020	UD2732842	Invitrogen	1:200
Plectin	H	Rb	AB32528	GR3377025-3	Abcam	1:250
SNAPIN	H, M	M	MAB7795	CHJQ012111A	R&D systems	1:200
Tau [E178]	H, M, R	Rb	Ab320579	GR3254929-4	Abcam	1:200
Tau5	H, M, R, S, C	M	AB80579	GR3220174-6	Abcam	1:200
Tenascin C	H, M	R	MAB2138	-	R&D systems	1:300
Tubulin	H, M	R	Ab6161	GR229236-2	Abcam	1:200
Vimentin	H, M, R	R	MAB2105	UUQ021041	R&D systems	1:500

H – human, M – mouse, Rb – rabbit, R – rat, G – goat, S – sheep, C – cow, P – pig.

Table 10.3. List of secondary antibodies used in this study for Immunofluorescence.

Antibody	Reactivity	Host	Cat no	Batch	Company	Dilution
Alexa Fluor-488	Rabbit	Donkey	A21206	1387792	Invitrogen	1:300
Alexa Fluor-568	Rabbit	Donkey	A10042	1964370	Invitrogen	1:500
Alexa Fluor-647	Rabbit	Donkey	A31573	1903516	Invitrogen	1:500
Alexa Fluor-488	Mouse	Donkey	A21202	1796361	Invitrogen	1:300
Alexa Fluor-568	Mouse	Donkey	A10037	1303018	Invitrogen	1:500
Alexa Fluor-568	Goat	Donkey	A11057	1711491	Invitrogen	1:500
Alexa Fluor-633	Goat	Donkey	A21082	1301826	Invitrogen	1:500
Alexa Fluor-488	Rat	Donkey	A21208	1932496	Invitrogen	1:300
Alexa Fluor-597	Rat	Donkey	A21209	1398009	Invitrogen	1:500

Table 10.4. Reverse transcription programme details.

	Step 1	Step 2	Step 3	Step 4
Temperature (°C)	25	37	85	4
Time (Min)	10	120	5	∞

Table 10.5. RT-PCR programme details.

Step	Description	Temperature	Duration (mm:ss)	Cycle (nº)
1	Initial denaturation	95	05:00	1
2	Denaturation	95	00:10	45
	Annealing	60	00:20	
	Elongation	72	00:10	
3	Final denaturation	95	00:05	1
	Start melting curve	65	01:00	
	End melting curve	Up to 96	Continuous	

Table 10.6. List of primers used in this study for RT q-PCR.

Gene name	Gene ID	Forward primer (5'-3')	Reverse primer (5'-3')	Size
36B4	6175	GCAATGTTGCCAGTGTCTGT	GCCTTGACCTTTTCAGCAAG	142
ATP6AP2	10159	AGCTGGCAGGTTTGGATGAA	ACTTGCTGGGTTCTTCGCTT	230
CDK1	983	ACAGGTCAAGTGGTAGCCATG	CCATGTACTGACCAGGAGGG	225
CDK2	1017	CGGATCTTTCGGACTCTGGG	ACTGGCTTGGTCACATCCTG	239
CDK4	1019	GGATGACTGGCCTCGAGATG	AGCCACTCCATTGCTCACTC	222
CLN5	1203	ACATTTCCCCATCTCCGACC	TTTGGTTGAACATGTTTCTAAGCTG	194
Cyclin A2	890	AACTTCAGCTTGTGGGCACT	CAGTTTGCAGGCTGCTGATG	226
Cyclin B1	891	CCCCTGCAGAAGAAGACCTG	AGTGACTTCCCGACCCAGTA	188
Cyclin D1	595	GGCGGAGGAGAACAAACAGA	TGTGAGGCGGTAGTAGGACA	181
Cyclin E1	898	TGGCGTTTAAGTCCCCTGAC	AAGGCCGAAGCAGCAAGTAT	197
DLL1	28514	GCACGGACCTCAAGTACTCC	ATGCTGCTCATCACATCCAG	200
DSG	1829	AGGTATGGCCAAGGAAGCCACGA	ATAGCGCCTGTGGCCCCTGTAA	153
FLG	2312	AAACCATCGTGGATCTGCTC	TGGGATCCATGTCTCTCTCC	204
GRN	2896	GATGGTCAGTTCTGCCCTGT	CCCTGAGACGGTAAAGATGC	174
GAPDH	2597	ATCACTGCCACCCAGAAGAC	CAGTGAGCTTCCCGTTCAG	148
IVL	3713	GGCCCTCAGATCGTCTCATA	CACCCTCACCCCATTAAAGA	131
ITGA2	3673	AAGCCGAAGTACCAACAGGA	TTCCCACTGCAGGTAGGTCT	193
ITGA3	3678	CTATTTTGGCAGCGCCATT	ATGCTGGCCACAGATAAACC	213
ITGA6	3655	ACCCAGATATTGCAGTTGGA	TTCGATCAAGGTCCATGTTT	158
ITGAV	3685	TCACCAACTCCACATTGGTT	AGGTTGAAGCTGCTCCCTTT	203
ITGB1	3688	AACTGCACCAGCCCATTTAG	TCTGTGGAAAACACCAGCAG	203
ITGB4	3691	GCTACACCATGGAAGGTGAC	CTTAAAGCCCACCATGTGAC	227
Ki67	4288	GAATTGAACCTGCGGAAGAG	TTTGCTGTTCTGCCTCAGTC	141
KRT5	3852	GCCCAGTATGAGGAGATTGC	AGATTGGCGCACTGTTTCTT	200
KRT1	3848	ATCAATCTCGGTTGGATTCG	TCCTGCTGCAAGTTGTCAAG	190
KRT10	3858	ATGCTGAAGCCTGGTTCAAT	TGCACACAGTAGCGACCTTC	205
KRT14	3861	CTCCTCCTCCCAGTTCTCCT	GGGATCTTCCAGTGGGATCT	208
LAMA5	3911	CAATGCCTCGGCTCCATCAG	CGGGCCAGCAATCTCTGT	130
LOR	4014	GCAGGTCACTCAGACCTCGT	CCTCCAGAGGAACCACCTC	203
Lrig1	26018	CGCTCTACCCCAGTAACCAC	GCCATTGGAAACAAGCAAGT	200
MAPT	4137	TTGGGTCCCTGGACAATATC	GTGGTCTGTCTTGGCTTTGG	104
MAPT	4137	AAGATCGGCTCCACTGAGAA	ATGAGCCACACTTGGAGGTC	199
MAPT 0N	4137	GCTGGCCTGAAAGCTGAAG	ATCGCTTCCAGTCCCGTCT	120
MAPT 1N	4137	CAACAGCGGAAGCTGAAGAA	GTGACCAGCAGCTTCGTCTT	68
MAPT 2N	4137	ACTCCAACAGCGGAAGATGT	GTGACCAGCAGCTTCGTCTT	159
MAPT 3R	4137	AGGCGGGAAGGTGCAAATA	GCCACCTCCTGGTTTATGATG	100
MAPT 4R	4137	CGGGAAGGTGCAGATAATTAA	TATTTGCACACTGCCGCCT	109
NCBP1	4686	AGAAGGCTTGGCTGGTGTTT	GGTAATAGGCGTGCAACTGT	90
NCBP2	22916	AAAGCTATGCGGAAAACGCC	ATACTCATCCCGAACCTGGC	143
Notch1	18128	CTGAAGAACGGGGCTAACAA	CAGGTTGTACTCGTCCAGCA	213
PPT1	5538	GAGATTGGGAAGACCCTGATGG	AGGGAGTCCAAAAACACCTTGAT	240
SNAPIN	23557	GTACACGCCGTCAGAGAGAG	GCAACACTGTGGTTTAGCCG	212
Tp63	8626	CTCCACCTTCGATGCTCTCT	TGGGGTCATCACCTTGATCT	196

Table 10.7. List of antibodies used in this study for Western Blotting.

Antibody	Reactivity	Host	Cat no	Batch	Company	Dilution
β-actin	H, M, R	Rabbit	NED8457p	Lot 5	Cell signalling	1:500
GAPDH	H, M, R	Mouse	Sc-32233	H2114	SantaCruz	1:500
Granulin	H	Rabbit	HPA008763	000017373	Sigma	
Keratin-1	H, R	Rabbit	905204	B220351	Biolegend	1:500
Lamin B1	H, M	Rabbit	AB16048	GR302354-1	Abcam	1:500
PhosphoTau (AT8)	H	Mouse	MN1020	UD2732842	Invitrogen	1:200
SNAPIN	H, M	Mouse	MAB7795	CHJQ012111A	R&D systems	1:250
Tau [E178]	H, M, R	Rabbit	Ab320579	GR3254929-4	Abcam	1:200
Tau5	H, M, R	Mouse	AB80579	GR3220174-6	Abcam	1:200
HRP-linked antibody	M	Horse	7076	Lot 28	Cell signalling	1:500
HRP-linked antibody	Rb	Goat	7074	Lot 26	Cell signalling	1:500

H – Human, M – mouse, Rb – rabbit, R – rat.

Table 10.8. esiRNA sequences used in this study.

esiRNA (sigma)	Sequence
RLUC EHURLUC	GATAACTGGTCCGCAGTGGTGGGCCAGATGTA AACAAATGAATGTTCTTGATTCATTTATTAATTAT TATGATTCAGAAAAACATGCAGAAAATGCTGTTA TTTTTTTACATGGTAACGCGGCCTCTTCTTATTT ATGGCGACATGTTGTGCCACATATTGAGCCAGT AGCGCGGTGTATTATACCAGACCTTATTGGTAT GGGCAAATCAGGCAAATCTGGTAATGGTTCTTA TAGGTTACTTGATCATTACAAATATCTTACTGCA TGGTTTGAACTTCTTAATTTACCAAAGAAGATCA TTTTTGTCGGCCATGATTGGGGTGCTTGTTTGG CATTTCATTATAGCTATGAGCATCAAGATAAGAT CAAAGCAATAGTTCACGCTGAAAGTGTAGTAGA TGTGATTGAATCATGGGATGAATGG
Human *MAPT* (esiRNA1)	AAGGTGACCTCCAAGTGTGGCTCATTAGGCAAC ATCCATCATAAACCAGGAGGTGGCCAGGTGGAA GTAAAATCTGAGAAGCTTGACTTCAAGGACAGA GTCCAGTCGAAGATTGGGTCCCTGGACAATATC ACCCACGTCCCTGGCGGAGGAAATAAAAAGATT GAAACCCACAAGCTGACCTTCCGCGAGAACGC CAAAGCCAAGACAGACCACGGGGCGGAGATCG TGTACAAGTCGCCAGTGGTGTCTGGGGACACG TCTCCACGGCATCTCAGCAATGTCTCCTCCACC GGCAGCATCGACATGGTAGACTCGCC

Table 10.9. shRNA sequences used in this study.

shRNA		Target sequence
Luciferase control	Sense	5’GATCCGTGCGTTGTTAGTACTAATCCTATTTGT GAAGCAGATGAAATAGGGTTGGTACTAGCAACG CACTTTTTG 3’
	Antisense	3'GCACGCAACAATCATGATTAGGATAAACACTT CGTCTACTTTATCCCAACCATGATCGTTGCGTG AAAAACTTAA 5'
1881 Tau	Sense	5′GATCCTGGTGAACCTCCAAAATCACTTCCTGT CAGATGATTTTGGAGGTTCACCATTTTTG 3′
	Antisense	3′CTGGTGAACCTCCAAAATCACTTCCTGTCAGA TGATTTTGGAGGTTCACCATTTTTGAATT 5′
2112 Tau	Sense	5′GATCCAACTGAGAACCTGAAGCACCAGCTTCC TGTCAGACTGGTGCTTCAGGTTCTCAGTGTTTTT G 3′
	Antisense	3′CAACTGAGAACCTGAAGCACCAGCTTCCTGTC AGACTGGTGCTTCAGGTTCTCAGTGTTTTTGAAT T 5′

Table 10.10. Human skin samples used in this study.

Patient number	Sample	DOB	Gender	Sample fixation	Sample location
Patient 1	Healthy	-	-	Cryo	-
Patient 2	Healthy	-	-	Cryo	-
Patient 3	Healthy	-	-	Cryo	-
Patient 4	Healthy	-	-	Cryo	-
Patient 5	Healthy	-	-	Cryo	-
Patient 6	Healthy	10.12.1936	Male	Cryo	-
Patient 7	Healthy	19.02.1935	Male	Cryo	-
Patient 8	Healthy	-	-	FFPE	-
Patient 9	Healthy	-	-	FFPE	-
Patient 10	Healthy	-	-	FFPE	-
Patient 11	Healthy	-	-	FFPE	-
Patient 12	Healthy	-	-	FFPE	-
Patient 13	SCC	-	-	cryo	-
Patient 14	SCC	-	-	Cryo	-
Patient 15	SCC	08/12/1937	Male	Cryo	Sternal
Patient 16	SCC	15/11/1918	Female	Cryo	Centroparietookzipital
Patient 17	SCC	10/11/1957	Female	Cryo	Lower leg
Patient 18	SCC	14/02/1923	Female	Cryo	Head
Patient 19	SCC	07/09/1935	Male	cryo	Forehead
Patient 20	SCC	07/01/1936	Female	slow frozen biopsy	Nose
Patient 21	SCC	30/04/1944	Male	slow frozen biopsy	Cheek
Patient 22	SCC	25/07/1935	Male	slow frozen biopsy	Cheek
Patient 23	SCC	08/11/1929	Male	slow frozen biopsy	Forehead
Patient 24	SCC	03/11/1980	Male	slow frozen biopsy	Parotis
Patient 25	SCC	03/11/1980	Male	slow frozen biopsy	-

Patient 26	SCC	31/05/1941	Male	slow frozen biopsy	-
Patient 27	SCC	31/05/1941	Male	slow frozen biopsy	Ear
Patient 28	SCC lesional	26/06/1929	Male	FFPE	Temple
Patient 29	SCC lesional	23/01/1935	Male	FFPE	Preauricular
Patient 30	SCC lesional	06/10/1929	Male	FFPE	Forehead
Patient 31	SCC lesional	19/09/1931	Female	FFPE	Temporal
Patient 32	SCC lesional	13/06/1973	Female	FFPE	-
Patient 33	SCC lesional	05/03/1940	Male	FFPE	Scull
Patient 34	SCC perilesional	23/01/1935	Male	FFPE	Preauricular
Patient 35	SCC perilesional	06/10/1929	Male	FFPE	Neck
Patient 36	SCC perilesional	19/09/1931	Female	FFPE	Temporal
Patient 37	SCC perilesional	13/06/1973	Female	FFPE	Groin
Patient 38	-	-	-	FFPE	-
Patient 39	BCC lesional	29/05/1929	Male	FFPE	Shoulder
Patient 40	BCC lesional	29/05/1929	Male	FFPE	Temple
Patient 41	BCC lesional	13/04/1949	Male	FFPE	Shoulder
Patient 42	BCC perilesional	06/10/1929	Male	FFPE	Chest
Patient 43	BCC lesional	06/10/1929	Male	FFPE	Chest
Patient 44	BCC lesional	29/05/1929	Male	FFPE	Neck
Patient 45	BCC lesional	07/02/1938	Male	FFPE	Shoulder
Patient 46	BCC perilesional	29/05/1929	Male	FFPE	Shoulder
Patient 47	BCC perilesional	29/05/1929	Male	FFPE	Temple
Patient 48	BCC perilesional	13/04/1949	Male	FFPE	Shoulder
Patient 49	BCC perilesional	29/05/1929	Male	FFPE	Neck
Patient 50	BCC perilesional	07/02/1938	Male	FFPE	Shoulder

Summary of patient information of samples used in this study. Gender, date of birth (DOB) and sample location were unknown for most of the healthy human skin samples, but more information was supplied with the SCC and BCC biopsies. Samples were prepared either cryo-frozen, slow frozen or FFPE.

Table 10.11. Commercial tau antibodies used in this study.

Antibody	Clone	Class	Light chain type	Host	Specificity	Refs
Tau	E178	Monoclonal	IgG	Rabbit	Immunised short peptide sequence. 15 amino acids. The immunogen corresponds to a fragment within the C-terminal region of the protein that is present in all isoforms with or without post-translational modifications.	277,300,408–410
Tau	Tau-5	Monoclonal	IgG1	Mouse	Ser210-Arg230. Full length native protein. Binds to the unmodified PRD.	301
Phosphor Tau	AT8	Monoclonal	IgG1	Mouse	The antibody recognised a phosphatase-sensitive epitope on PHF-Tau. No cross reactivity with normal Tau has been observed. The epitope contains the phosphorylated Ser202 residue (numbering according to human Tau40). Ser202/Thr205 primary phosphor epitope of AT8, S199/s202 and T205/s208.	302,303

It has been reported that different fixation protocols can affect the observed cellular localisation of tau in immunofluorescence studies [183,184,234,240]. Formaldehyde and triton protocols have been reported to detach the tau protein from microtubules so that a cytoplasmic localisation is observed [184], but with this fixation method it has been reported that mitotic spindle and cytoskeleton localisation are not always observed with antibodies against tau. Whereas methanol fixation allows the tau protein to be correctly localised with microtubules [184], but can be found to extract a portion of the cytoplasmic protein. The detection of nuclear tau is traditionally performed with formaldehyde and triton protocols as in some cases methanol fixation does not adequately preserve the integrity of the nucleus and DNA [184]. Therefore, to reduce the possibility of inaccurate protein staining from being analysed, different fixation protocols were tested with the antibodies used for this study (Figure 10.3). Immunofluorescence was performed in parallel with frozen samples fixed with 4% PFA or acetone and in formalin fixed paraffin embedded (FFPE) samples to establish if any changes in the physiological localisation of tau were observed with these different tissue preparation techniques. Immunofluorescence staining with tau [E178] and phosphorylated tau (clone AT8) revealed that all fixation techniques displayed similar expression patterns, but 4% PFA fixation resulted in a decrease cytoplasmic expression in the suprabasal cells. Although it has been reported that formaldehyde and triton protocols detach the protein from microtubules so that a cytoplasmic localisation is observed this was not observed in this study. Using a 4% PFA fixation method did not result in an increased staining profile of tau in the cytoplasm of epidermal cells, but in fact caused a reduction of observed tau expression in the cytoplasm of keratinocytes throughout the epidermal tissue. Acetone and methanol fixation methods have been reported to allow for the

cytoplasmic detection of tau but insufficient nuclear staining. However, it was found that acetone allowed for the detection of both cytoplasmic and nuclear staining. FFPE samples also showed strong tau staining comparable to acetone fixation methods in frozen tissue samples, with tau expression observed in the cytoplasm and nuclear fraction of the cells (Figure 10.3). Therefore, frozen samples were fixed in ice cold acetone for tau staining throughout this study, unless stated otherwise.

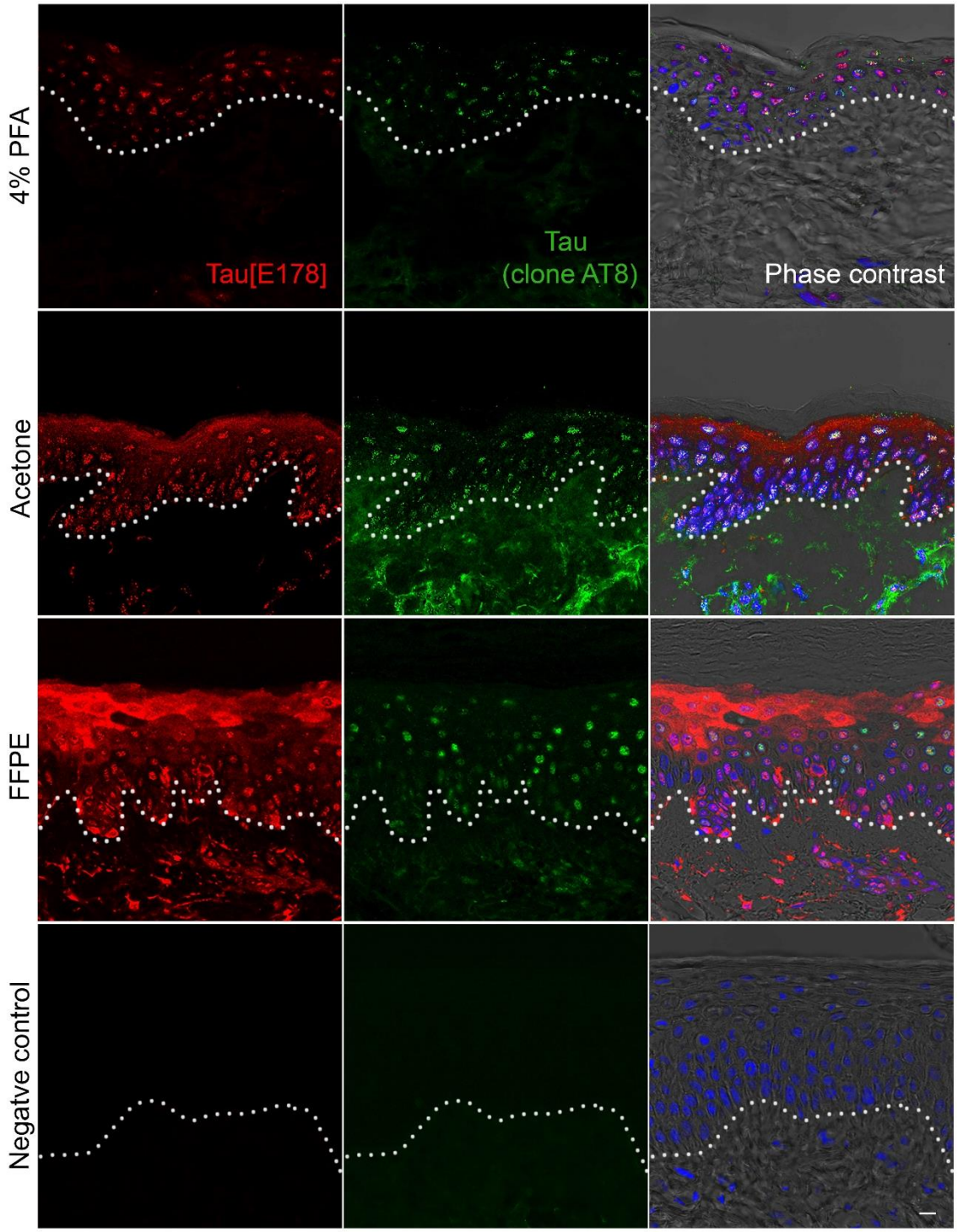

Figure 10.3. Optimisation of sample preparation techniques to visualise the expression profile of tau in the epidermis.
Comparison of fixation techniques to evaluate any changes in tau expression or localisation through immunofluorescence analysis in healthy human skin samples (n=12). Frozen samples were fixed with 4% PFA or ice cold acetone and compared to the FFPE samples and stained in parallel with tau [E178] (red) and phosphorylated tau (clone AT8) (green). Although publications have indicated that different fixation techniques can alter the observed tau localisation, this was not observed in this study. Staining revealed that acetone and FFPE both resulted in nuclear, cytoplasmic and membrane staining. Although 4% PFA showed a

similar expression pattern, cytoplasmic staining was much weaker than and not as effective as acetone and FFPE fixed samples. White dotted line represents the basement membrane. Scale bar 10 µm.

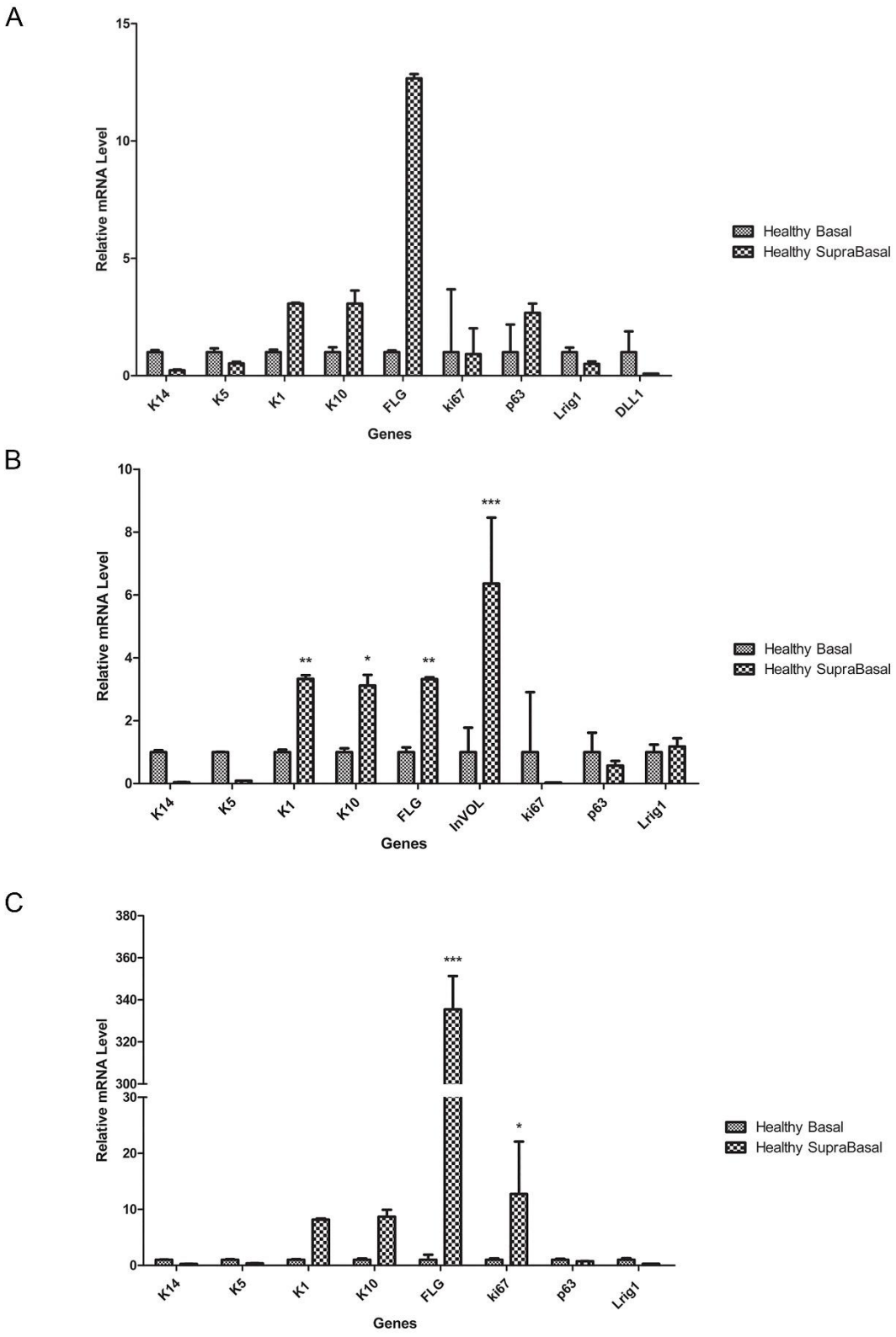

Figure 10.4. Successful isolation of epidermal populations from healthy human skin using Laser Capture Microdissection.

Representative RT q-PCR analysis using differentiation markers allowed the confirmation of the correct capture of basal and suprabasal regions of interests using LCM. Representative expression patterns from patient 3 captured ROI are displayed showing the two distinct populations were successfully isolated, with GAPDH as a reference gene. **A.** Patient 2. **B.** Patient 6. **C.** Patient 7. Ct values normalised to GAPDH and $2^{-\Delta\Delta Ct}$ method of analysis used. Relative expression

levels are displayed as mean ± SD. Two-way ANOVA with Bonferroni correction was used to test significance; *** p<0.001. (n=6).

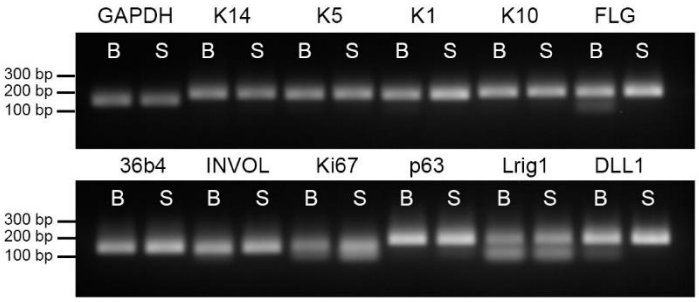

Figure 10.5. Representative image of a semi-quantitative PCR agarose gel showing the validation of primers from q-PCR products in the two captured epidermal populations from LCM of healthy human skin samples.
White bars indicate the successful amplification of cDNA region of interest and have been detected by the D-Digit® scanner. B – Basal, S – Suprabasal.

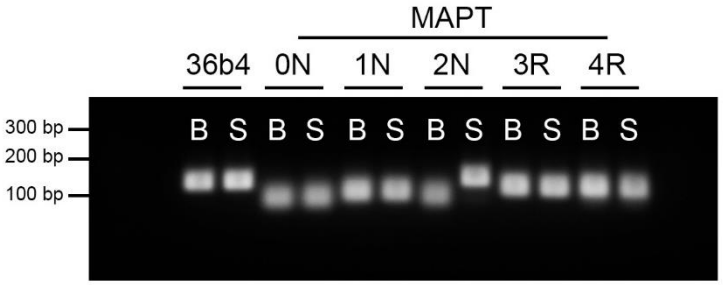

Figure 10.6. Representative image of semi-quantitative PCR agarose gels validating the *MAPT* isoform primers from q-PCR products from the two captured epidermal populations of healthy human skin using LCM.
RT q-PCR products were run on a 1.5% agarose gel to allow for visualisation of the amplified product. White bars indicate amplification of the cDNA sequence of interest while blank spaces indicate that the primer was not effective at amplifying the gene of interest as it cannot be detected by the D-Digit® scanner. All isoform specific primers products display a single band.

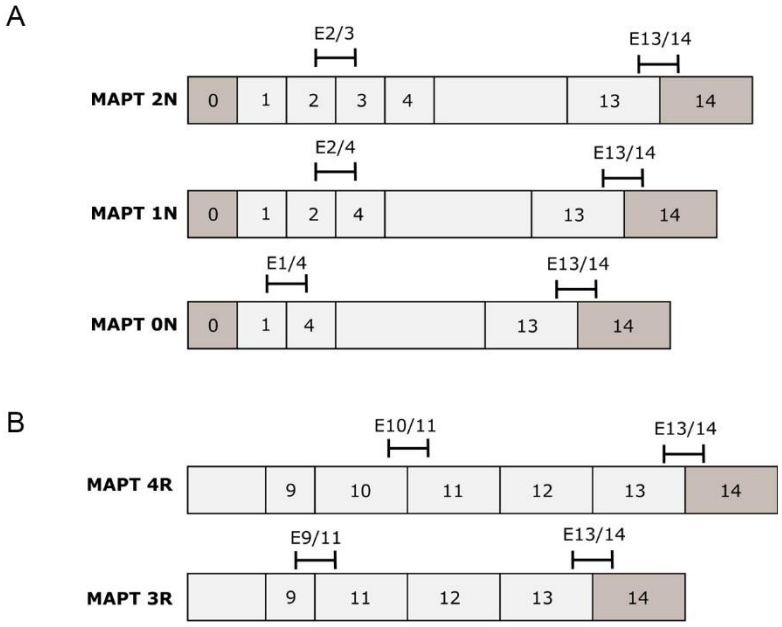

Figure 10.7. Schematic illustrating where BaseScope™ probes bind on the tau RNA transcript on all 5 transcript variants of tau.
1ZZ BaseScope™ probes were designed to detect transcript variants of tau. Probes were designed to cross exon boundaries of transcript variants as demonstrated in the schematic. Exon 0 and 14 are transcribed but not translated. **A.** BaseScope™ probes designed to the N terminal region of the tau mRNA transcript. Alternative splicing of exon 2 and 3 yielding isoforms 2N, 1N and 0N. **B.** C terminal region of tau mRNA transcript encoding for the microtubule binding region. Alternative splicing of exon 10 yielding variants 3R and 4R. A 1ZZ probe was designed to cross exon 13/14 to detect all transcript variants of tau. Diagram drawn using Inkscape by CI.

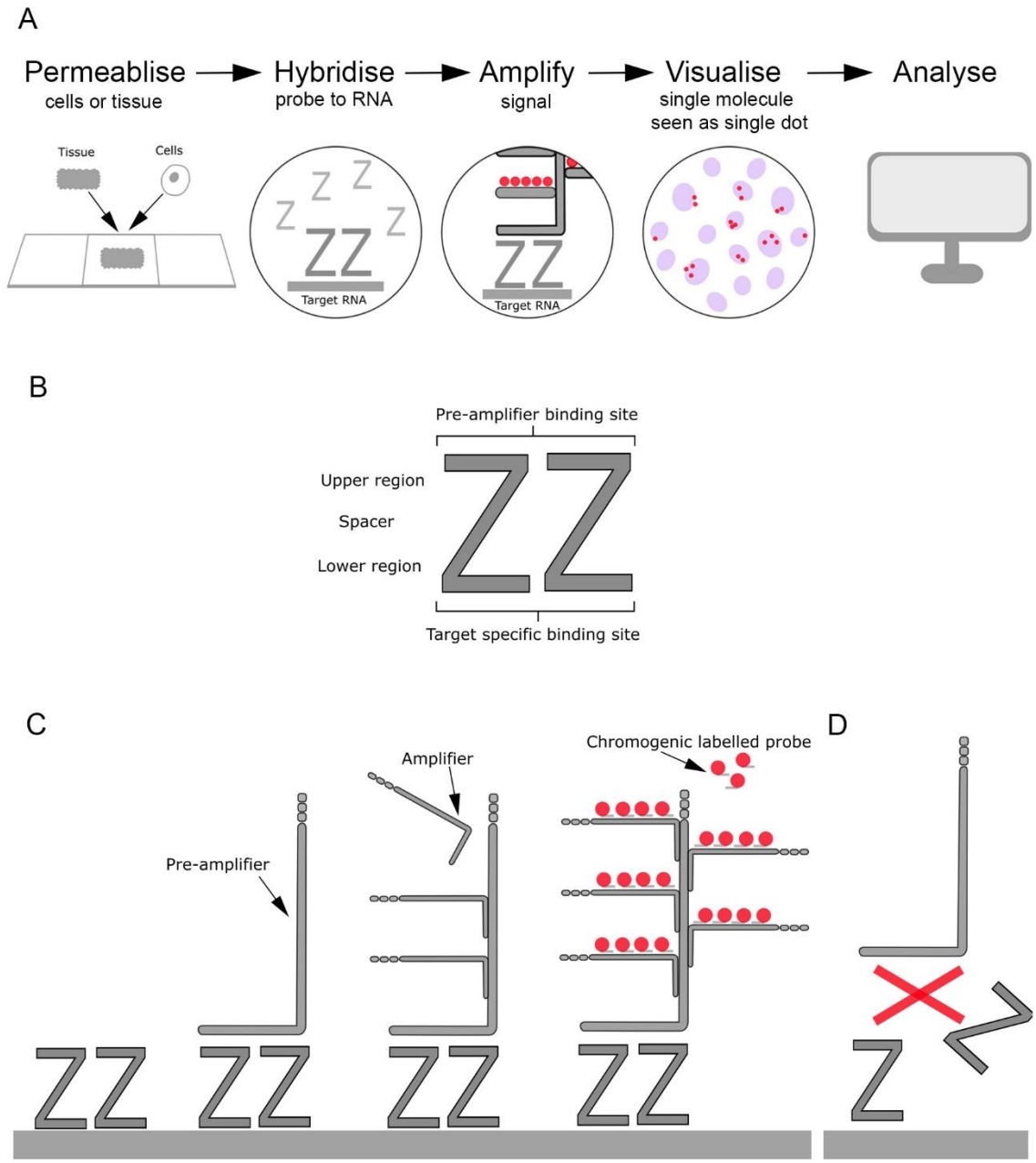

Figure 10.8. Schematic of BaseScope™ technology and work flow.
A. A schematic demonstrating the BaseScope™ assay work flow. Samples are sectioned onto SuperFrost™ slides at 20 µm and dried at -20°C for 1 h. Samples are subsequently fixed in ice cold 4% PFA, and permeablised with hydrogen peroxide and protease IV. Probes are hybridised to sample for 2 h at 40°C in a humidified oven. Amplification steps are subsequently carried out to amplify the binding sites for the fast red chromogenic probes. The samples are briefly incubated with the fast red chromogen, then counterstained with haematoxylin and ammonia water before mounting and samples are visualised. Each distinct dot of chromogen precipitate is a single RNA transcript. Staining is analysed by quantifying dots per cell and allocating a score. **B.** Schematic of the BaseScope™ 1 ZZ probe design. **C.** BaseScope™ signal amplification workflow, whereby the probes are hybridized to a cascade of amplifiers and labelled with chromogenic probes for visualisation. **D.** The specificity of the BaseScope™ probes means that only when both ZZs are bound that the preamplifier will bind [411].

In this study, experiments *in vitro* were performed using two primary healthy keratinocyte cell types; neonatal human epidermal keratinocytes (HEKn) and pooled adult primary human epidermal keratinocytes (HPEKp). Tau isoform expression has been reported to vary between developmental stages of some cells and tissues. However, changes in isoform expression in the skin are unreported, and therefore it was not known if a developmental dependent expression of tau isoforms was also found in skin tissue. Before using neonatal and adult cell lines to investigate tau isoform expression, it was first investigated whether the developmental stage of the cell lines had any effect on tau isoform expression under normal culture conditions. RT q-PCR analysis revealed there was no significant difference in total tau expression between HEKn and HPEKp cells (Figure 10.9). Additionally, there was no significant difference between any of the tau isoform expression levels in neonatal and adult keratinocytes (Figure 10.9). 0N and 4R expression was consistent between the two cell lines, unlike the expression changes reported in brain tissue. 1N isoforms were not detected in HEKn or HPEKp cells in culture. 2N and 3R relative expression varied slightly between the two cell lines, but not significantly; 2N isoform is slightly increased in HPEKp cells, while 3R isoform were found to be slightly downregulated in HPEKp cells (Figure 10.9).

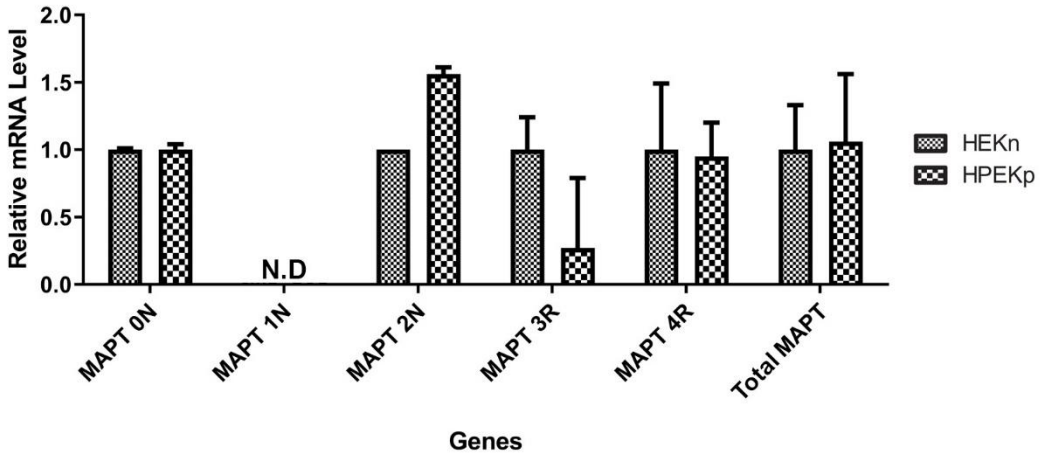

Figure 10.9. Relative expression of tau isoforms in neonatal and adult epidermal keratinocytes.
Un-fractioned human neonatal (HEKn) and adult (HPEKp) epidermal keratinocyte cells cultured under basal culture conditions showed no significant difference between the relative expression levels of total, or isoform specific variants of tau. RT q-PCR analysis of total and isoform variants of tau, displayed as relative expression, normalised to HEKn cells, with 36B4 as a reference gene. Relative expression levels are displayed as mean ± SD. Two-way ANOVA with Bonferroni correction was used to test significance. N.D. – not detected.

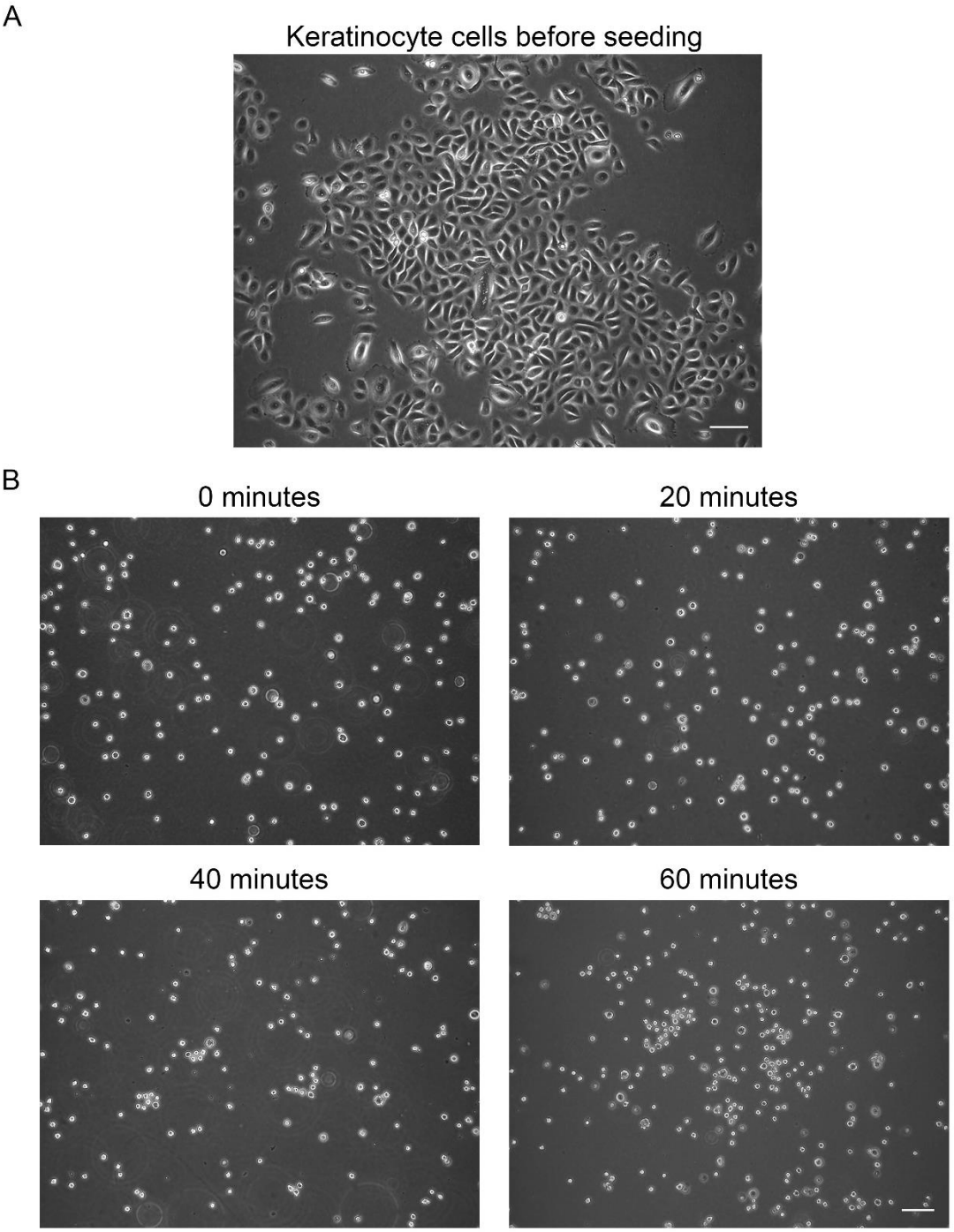

Figure 10.10. Cell culture images of attached and floating cells at 20, 40 and 60 min after seeding onto basement membrane protein coating.
Low passage epidermal keratinocyte cells were detached as normal and seeded into cell culture dishes coated with basement membrane proteins laminin, collagen IV and fibronectin. RNA was collected from the attached and floating population at 20, 40 and 60 min after cell seeding. **A.** Representative cell culture image of keratinocytes before detachment. **B.** Representative cell culture images of keratinocytes after seeding onto basement membrane coated dishes at 20, 40 and 60 min of incubation. Straight after cell seeding all HEKn cells could be observed floating in the media, but by 20 min a small fraction of cells had attached to the coating. The proportion of HEKn cells that attached to the coating increased 40 min after seeding and again by 60 min. Scale bar 100 µm.

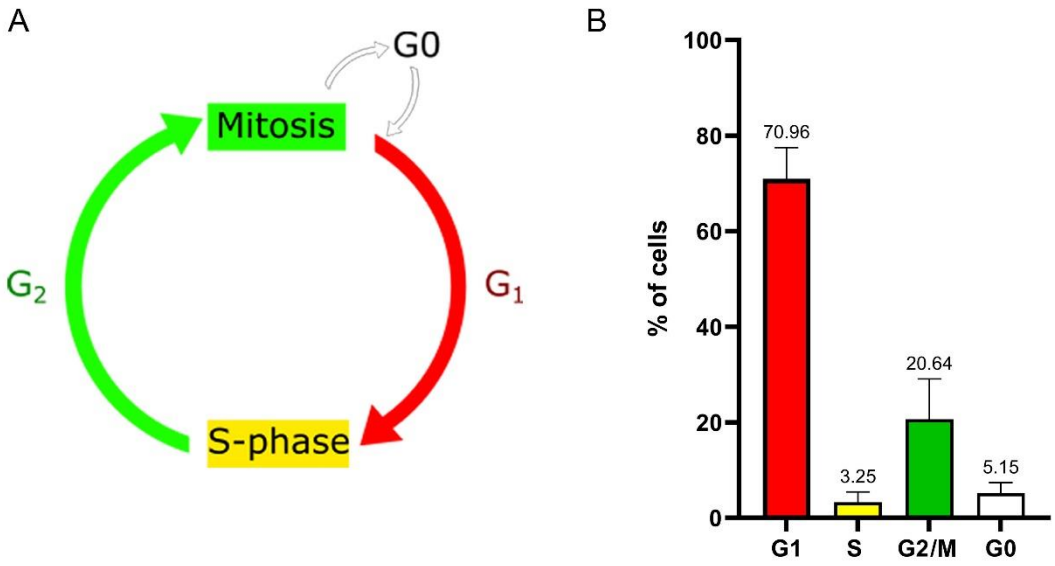

Figure 10.11. Distribution of growing keratinocytes in phases of the cell cycle using Ki67p FUCCI lentiviral reporter system.
A. Schematic demonstrating m-Cherry (red) and mAG (green) expression throughout the cell cycle in FUCCI infected cells. **B.** Quantification of HPEKp cell cycle status under normal cell culture conditions. HPEKp cells infected with Ki67p FUCCI fixed and cells in each phase of the cell cycle were counted from confocal images through their expression of mCherry (red) or mAg (green). The percentage of cells in each stage of the cell cycle is plotted on the graph. Results are displayed as average ± SD.

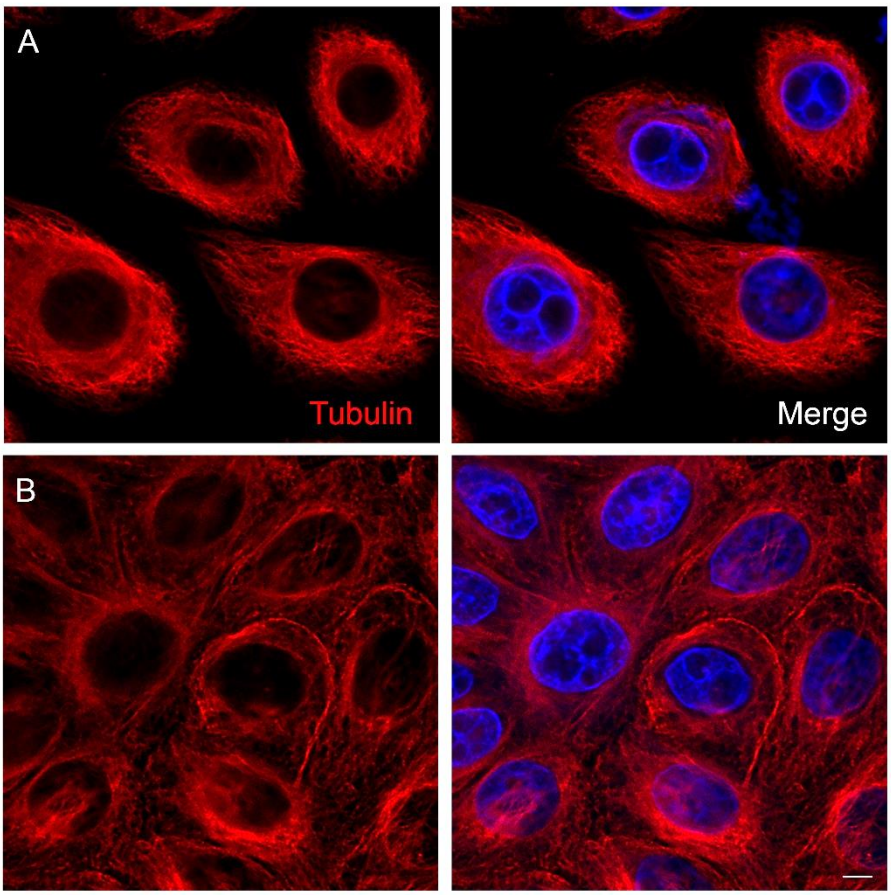

Figure 10.12. Tubulin cytoskeletal network locates to the cortical edge of keratinocytes after differentiation.
Representative immunofluorescence analysis of tubulin (red) in control and differentiated keratinocytes. **A.** Microtubules in growing HEKn cells can be observed growing from the centre of the cell to the cells periphery. **B.** In calcium differentiated HEKn cells the organisation of the tubulin cytoskeletal system is lost and instead a cortical array of microtubules was observed. Scale bar 5 µm.

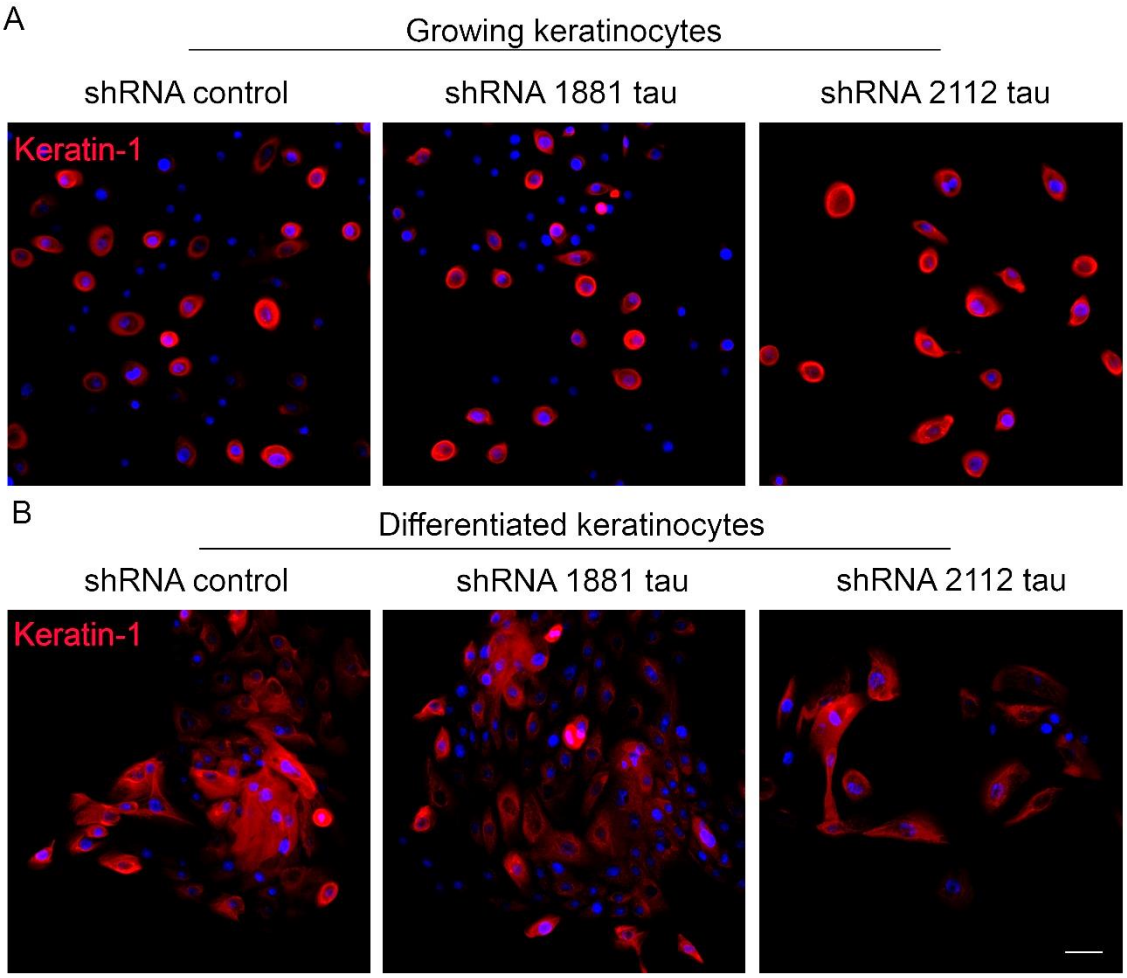

Figure 10.13. Keratin-1 expression is increased following shRNA-mediated tau knockdown in keratinocytes.
Representative immunofluorescence analysis of keratin-1 (red) following shRNA-mediated tau KD in epidermal keratinocytes. Stable HPEKp cell lines were generated with 1881, 2112 tau shRNA with luciferase shRNA used as a control. **A.** Growing keratinocyte conditions. **B.** Differentiating keratinocytes. Nuclei counterstained with DAPI (blue). Scale bar 50 µm.

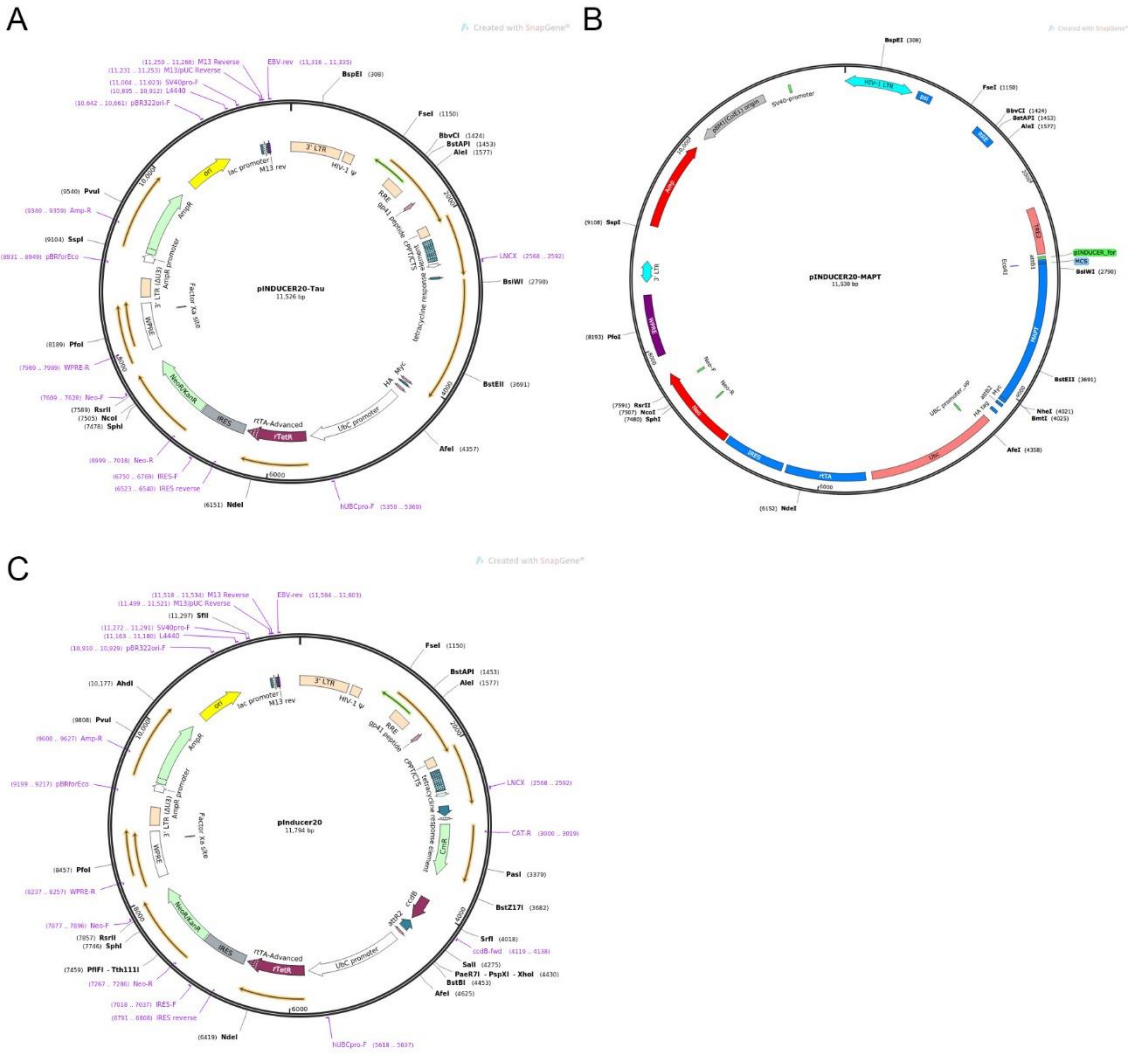

Figure 10.14. pINDUCER20 tau and pINDUCER20 plasmid maps.
A. AddGene Full Sequence map for pINDUCER20 tau. pINDUCER20 Tau was a gift from Huda Zoghbi (AddGene plasmid # 92201). **B.** Map Image for pINDUCER20-Tau. **C.** AddGene Full Sequence Map for pInducer20. pINDUCER20 was a gift from Stephen Elledge (AddGene plasmid #44012). Plasmid maps taken from AddGene website.

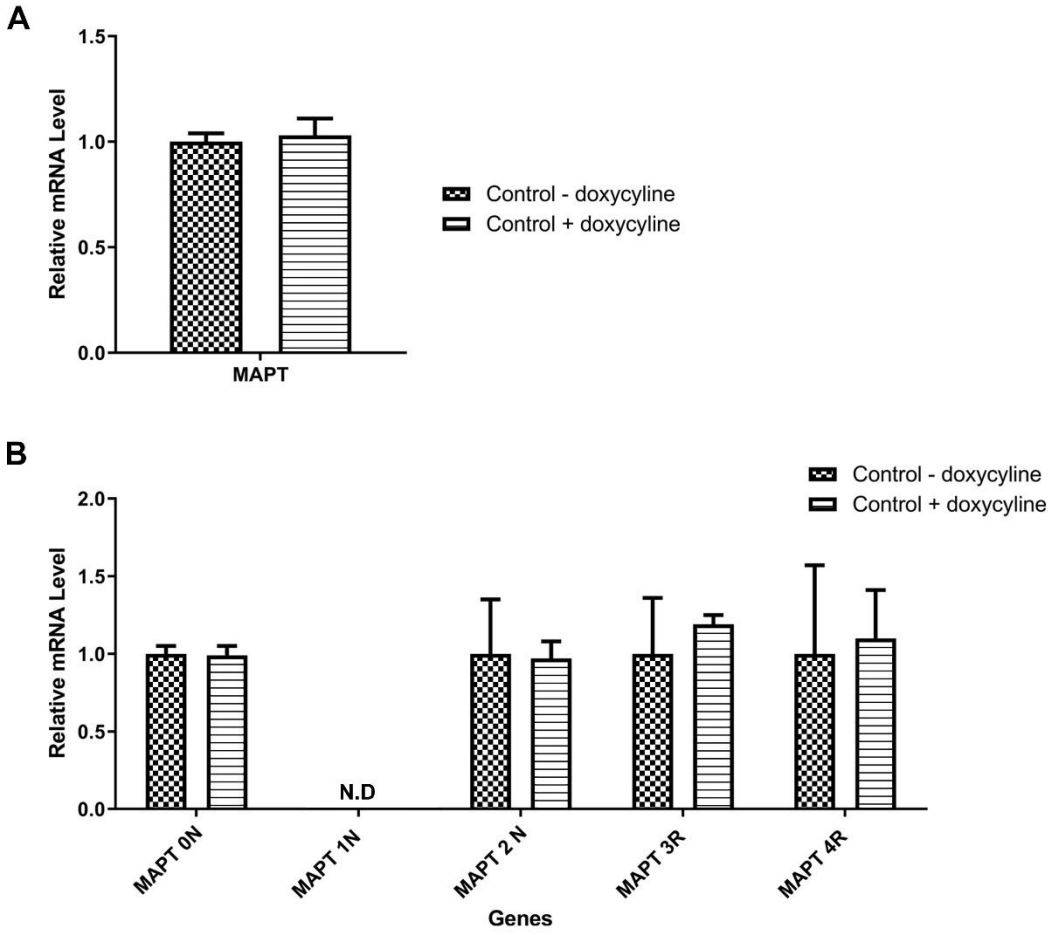

Figure 10.15. Total and isoform expression following doxycycline treatment in keratinocyte cells.

Keratinocyte cells were treated with doxycycline for 72 h as a control for the tetracycline dependent tau overexpression in pINDUCER20 tau HPEKp cells. RNA was collected from HPEKp cells cultured under normal culture conditions with and without the addition of doxycycline. **A.** RT q-PCR analysis revealed no difference between total tau expression 72 h after treatment with doxycycline. Ct values normalised to GAPDH and $2^{-\Delta\Delta Ct}$ method of analysis used. Relative expression levels are displayed as mean ± SD. Two-way ANOVA with Bonferroni correction was used to test significance; *p<0.05, ** p<0.01, *** p<0.001.

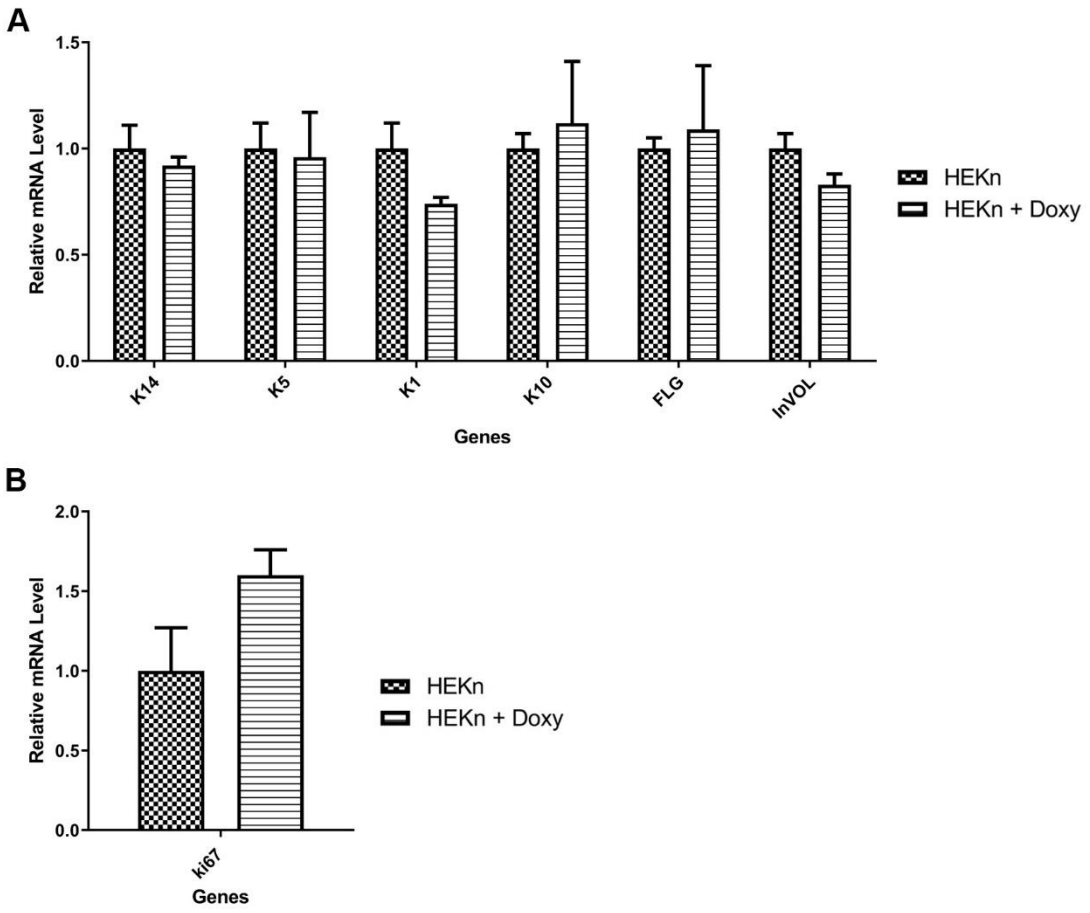

Figure 10.16. Doxycycline treatment has little to no effect in the expression of differentiation associated genes in epidermal keratinocytes.
HEKn cells were treated with doxycycline for 48 h as a control for the tetracycline dependent tau overexpression in pINDUCER20 tau HEKn cells. RNA was collected from HEKn cells cultured under normal culture conditions with and without the addition of doxycycline. **A.** RT q-PCR analysis from total RNA collected 48 h after doxycycline treatment showed no significant difference in the relative gene expression following 48 h of treatment with doxycycline. **B.** RT q-PCR analysis showed a slight increase in Ki67 expression after doxycycline treatment, however this did not reach the threshold for statistical significance. Ct values normalised to GAPDH and $2^{-\Delta\Delta Ct}$ method of analysis used. Relative expression levels are displayed as mean ± SD. Two-way ANOVA with Bonferroni correction was used to test significance; *p<0.05, ** p<0.01, *** p<0.001.

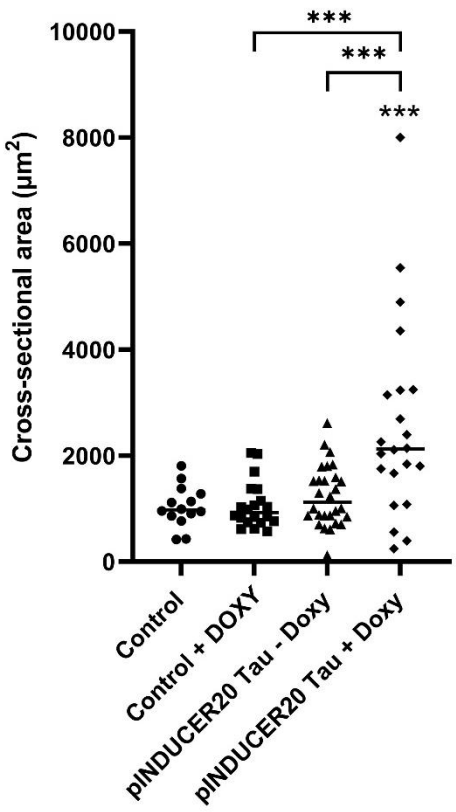

Figure 10.17. Increased keratinocyte cell size following tau overexpression. Analysis of the cross-sectional area of keratinocytes revealed that when tau is overexpressed the average basal cell size is significantly increased compared to all control conditions. HEKn cells 72 h after doxycycline treatment were measured using immunofluorescence analysis for tubulin and actin. 3-5 images were measured for each condition. Every basal cell within the boarder of each image was measured using phalloidin staining to outline the cell. One-way ANOVA with Bonferroni correction was used to test significance; *** $p<0.001$.

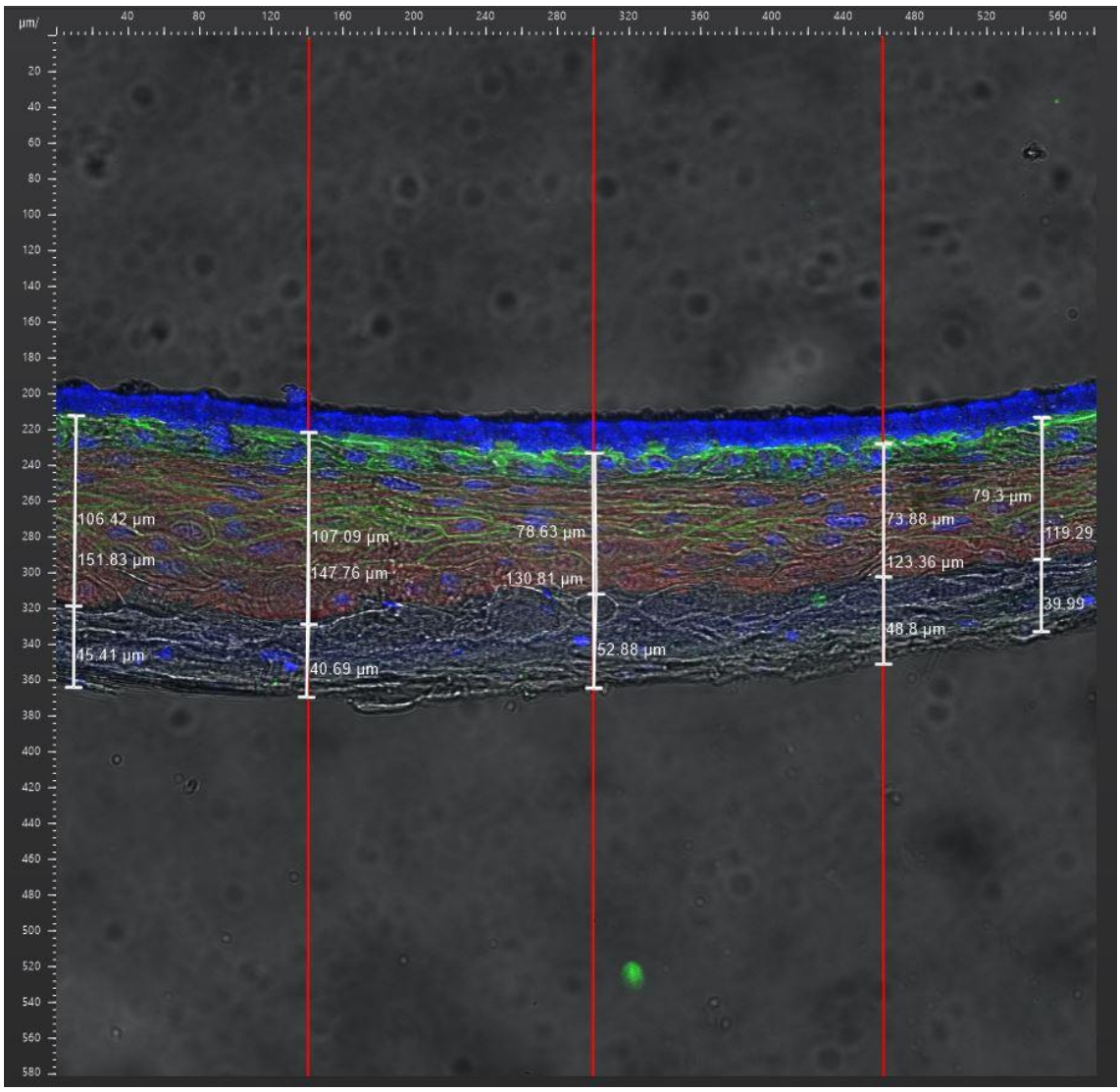

Figure 10.18. Quantification of EpiDerm™ thickness.
Epidermal thickness was measured in LASX software. Measurements were taken at five defined points on every image to ensure no bias could take place; lines were drawn as layer over image denoting where the 5 measurements would be taken. Total thickness was measured from the surface of the insert to the top of the corneum, while the cellular thickness (basal to granular) was measured from the surface of the insert to the top of the granular layer and the acellular thickness (corneal) was measured from the top of the granular layer to the surface of the corneal layer.

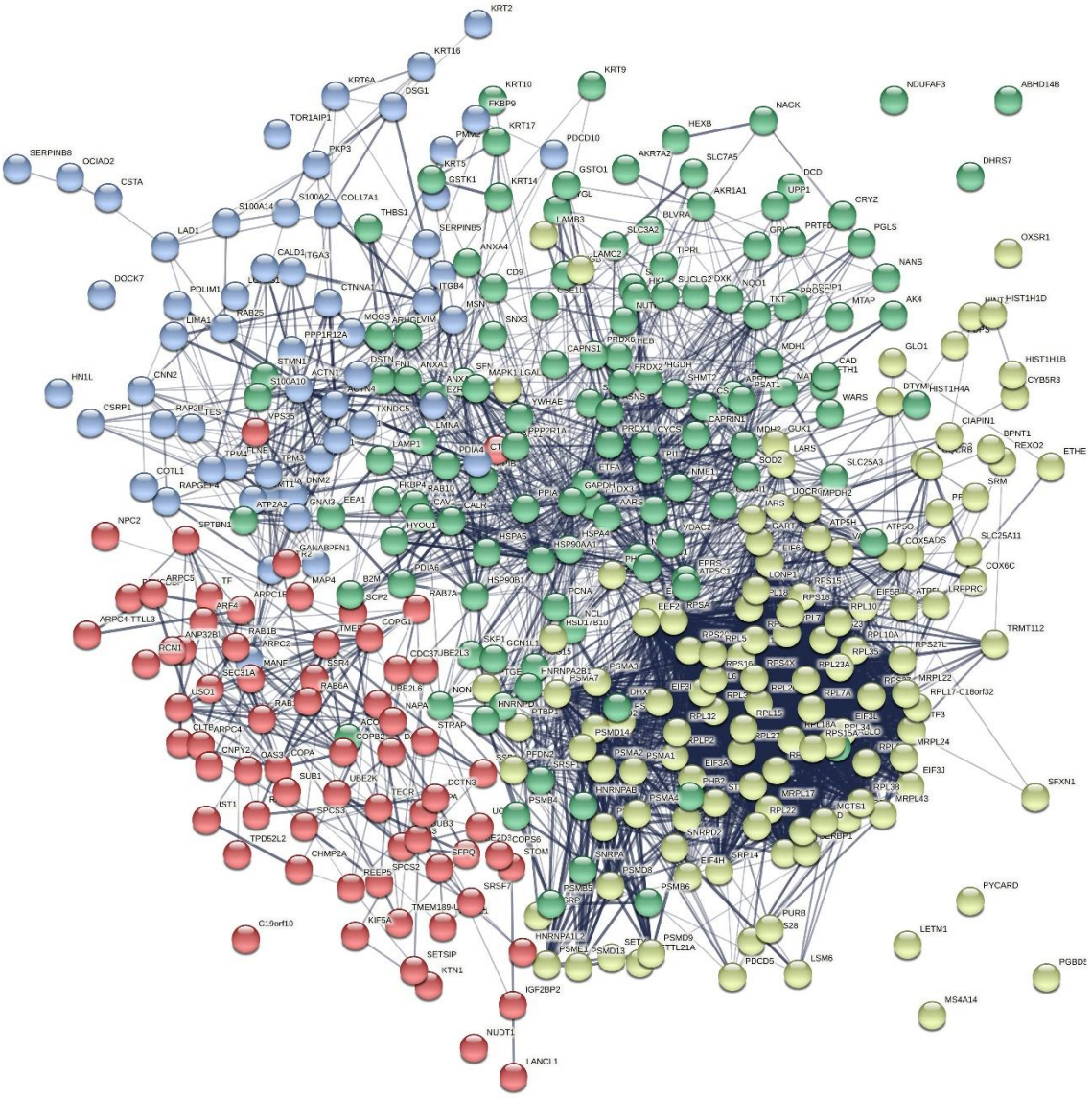

Figure 10.19. STRING analysis of proteins downregulated following calcium treatment in epidermal keratinocytes.
Schematic representation of the protein interactions between 375 proteins downregulated in HPEKp cells 72 h after calcium induced differentiation. The colour of the nodes represent the 4 clusters and the dotted lines between nodes represent the edges between clusters. The thickness of the lines between nodes represents the strength of the supporting data. STRING analysis revealed the protein network has 4810 interactions, significantly more interactions than the 1999 expected.

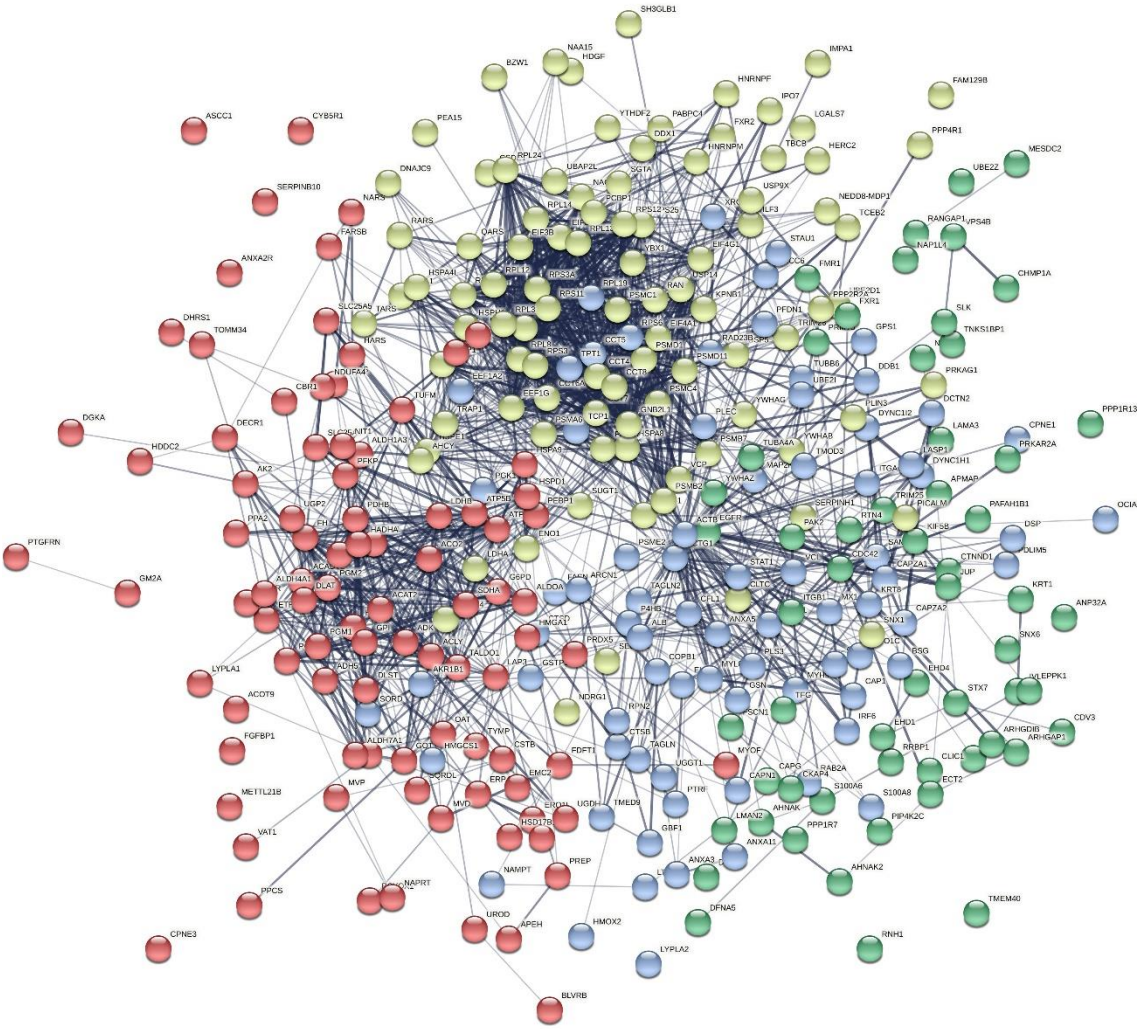

Figure 10.20. STRING analysis of proteins upregulated following calcium differentiation in epidermal keratinocytes.
Schematic representation of the protein interactions between 321 proteins upregulated in HPEKp cells 72 h after calcium induced differentiation. The colour of the nodes represent the 4 clusters and the dotted lines between nodes represent the edges between clusters. The thickness of the lines between nodes represents the strength of the supporting data. STRING analysis revealed the protein network has 3201 interactions, significantly more interactions than the 1329 expected.

A

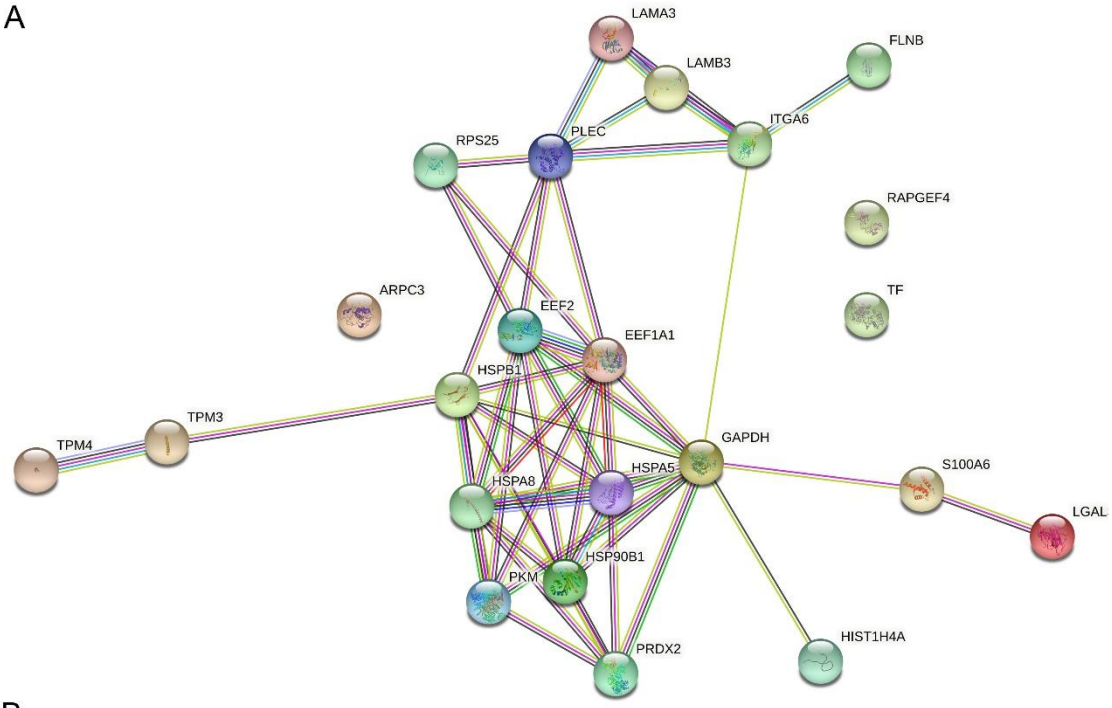

B

Network Stats

number of nodes: 23
number of edges: 50
average node degree: 4.35
avg. local clustering coefficient: 0.607

expected number of edges: 17
PPI enrichment p-value: 3.99e-11
your network has significantly more interactions than expected (what does that mean?)

Functional enrichments in your network

Biological Process (Gene Ontology)

GO-term	description	count in network	strength	false discovery rate
GO:0031581	Hemidesmosome assembly	4 of 12	2.45	4.56e-05
GO:0007015	Actin filament organization	5 of 254	1.22	0.0269
GO:0030036	Actin cytoskeleton organization	6 of 516	1.0	0.0464
GO:0007010	Cytoskeleton organization	8 of 1126	0.78	0.0483
GO:0071310	Cellular response to organic substance	12 of 2369	0.63	0.0131
GO:0070887	Cellular response to chemical stimulus	14 of 2919	0.61	0.0026
GO:0010033	Response to organic substance	13 of 3011	0.57	0.0199
GO:0051716	Cellular response to stimulus	18 of 6489	0.37	0.0269

Molecular Function (Gene Ontology)

GO-term	description	count in network	strength	false discovery rate
GO:0044183	Protein folding chaperone	3 of 26	1.99	0.0053
GO:0045296	Cadherin binding	7 of 334	1.25	0.00015
GO:0050839	Cell adhesion molecule binding	9 of 538	1.15	2.91e-05
GO:0003779	Actin binding	6 of 438	1.07	0.0071
GO:0005198	Structural molecule activity	6 of 635	0.91	0.0437
GO:0008092	Cytoskeletal protein binding	8 of 973	0.84	0.0071
GO:0044877	Protein-containing complex binding	9 of 1216	0.8	0.0053
GO:0003723	RNA binding	11 of 1649	0.75	0.0011
GO:0005515	Protein binding	21 of 7026	0.41	0.00013

Figure 10.21. STRING analysis of tau binding partners under growing culture conditions.

A. Schematic representation of the 23 proteins identified to bind to tau in keratinocytes under growing cell culture conditions. STRING analysis revealed 50 edges compared to the expected number of 17 edges, meaning that the network had significantly more interactions than expected for a random set of proteins of a similar size. Edges represent protein-protein associations and each edge also represents the known, predicted or other features about each protein-protein association. Cyan and purple lines represent known interactions from curated databases and experimentally determined interactions respectively. Predicted interactions are in green, red and dark blue to represent gene neighbourhood, gene fusions and gene co-occurrence respectively. Other associations are in yellow, black and light blue to represent textmining, co-expression and protein homology respectively. **B.** Hemidesmosome assembly,

cytoskeleton organisation and cell adhesion were some of the biological processes and molecular functions that were highlighted from STRING analysis.

A

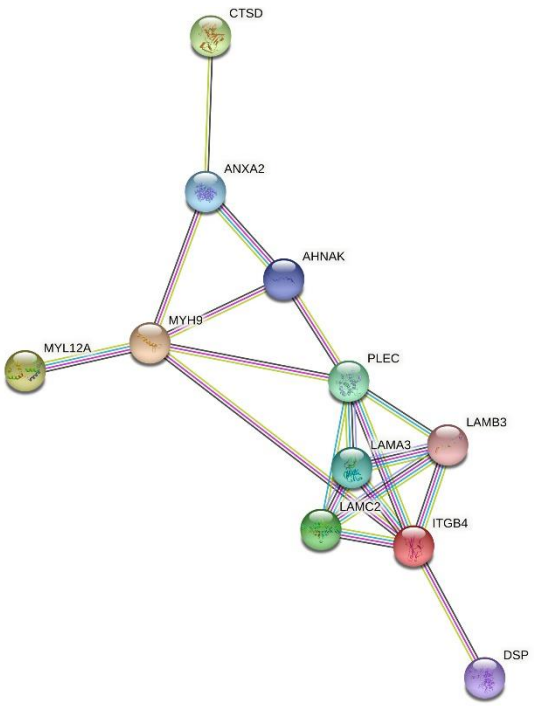

B

Network Stats

number of nodes:	11	expected number of edges:	1
number of edges:	19	PPI enrichment p-value:	< 1.0e-16
average node degree:	3.45	*your network has significantly more interactions than expected (what does that mean?)*	
avg. local clustering coefficient:	0.755		

Functional enrichments in your network

Biological Process (Gene Ontology)

GO-term	description	count in network	strength	false discovery rate
GO:0031581	Hemidesmosome assembly	5 of 12	2.87	2.08e-09
GO:0034109	Homotypic cell-cell adhesion	3 of 57	1.97	0.0078
GO:0007229	Integrin-mediated signaling pathway	3 of 94	1.75	0.0255
GO:0001704	Formation of primary germ layer	3 of 116	1.66	0.0436
GO:0030198	Extracellular matrix organization	5 of 338	1.42	0.0015
GO:0034330	Cell junction organization	6 of 493	1.34	0.00032
GO:0098609	Cell-cell adhesion	5 of 505	1.25	0.0078
GO:0009611	Response to wounding	5 of 532	1.22	0.0090
GO:0007155	Cell adhesion	8 of 925	1.19	1.64e-05

Molecular Function (Gene Ontology)

GO-term	description	count in network	strength	false discovery rate
GO:0044548	S100 protein binding	2 of 14	2.41	0.0358
GO:0005178	Integrin binding	4 of 147	1.68	0.0028
GO:0050839	Cell adhesion molecule binding	8 of 538	1.42	2.79e-07
GO:0045296	Cadherin binding	4 of 334	1.33	0.0342
GO:0005198	Structural molecule activity	5 of 635	1.15	0.0251

Cellular Component (Gene Ontology)

GO-term	description	count in network	strength	false discovery rate
GO:0005610	laminin-5 complex	2 of 3	3.07	0.00070
GO:0030056	Hemidesmosome	2 of 7	2.71	0.0021
GO:0043256	Laminin complex	3 of 11	2.69	0.00010
GO:0043034	Costamere	2 of 19	2.27	0.0091
GO:0005604	Basement membrane	4 of 96	1.87	0.00010
GO:0042383	Sarcolemma	3 of 132	1.61	0.0089
GO:0062023	Collagen-containing extracellular matrix	5 of 396	1.35	0.00045
GO:0005925	Focal adhesion	4 of 405	1.24	0.0090
GO:0005911	Cell-cell junction	4 of 490	1.16	0.0157
GO:0070161	Anchoring junction	6 of 820	1.11	0.00058
GO:0070062	Extracellular exosome	9 of 2099	0.88	0.00010
GO:0005615	Extracellular space	10 of 3195	0.75	0.00010
GO:0005576	Extracellular region	11 of 4166	0.67	0.00010

Figure 10.22. STRING analysis of tau binding partners under keratinocyte differentiation cell culture conditions.

A. Schematic representation of the 11 proteins identified to bind to tau in keratinocytes under differentiated cell culture conditions. STRING analysis revealed 19 edges compared to the expected 1 edge, meaning that the network had significantly more interactions than expected for a random set of proteins of a similar size. Edges represent protein-protein associations and each edge also

represents the known, predicted or other features about each protein-protein association. Cyan and purple lines represent known interactions from curated databases and experimentally determined interactions respectively. Predicted interactions are in green, red and dark blue to represent gene neighbourhood, gene fusions and gene co-occurrence respectively. Other associations are in yellow, black and light blue to represent textmining, co-expression and protein homology respectively. **B.** Hemidesmosome assembly, cytoskeleton organisation and cell adhesion were some of the biological processes and molecular functions that were highlighted from STRING analysis.

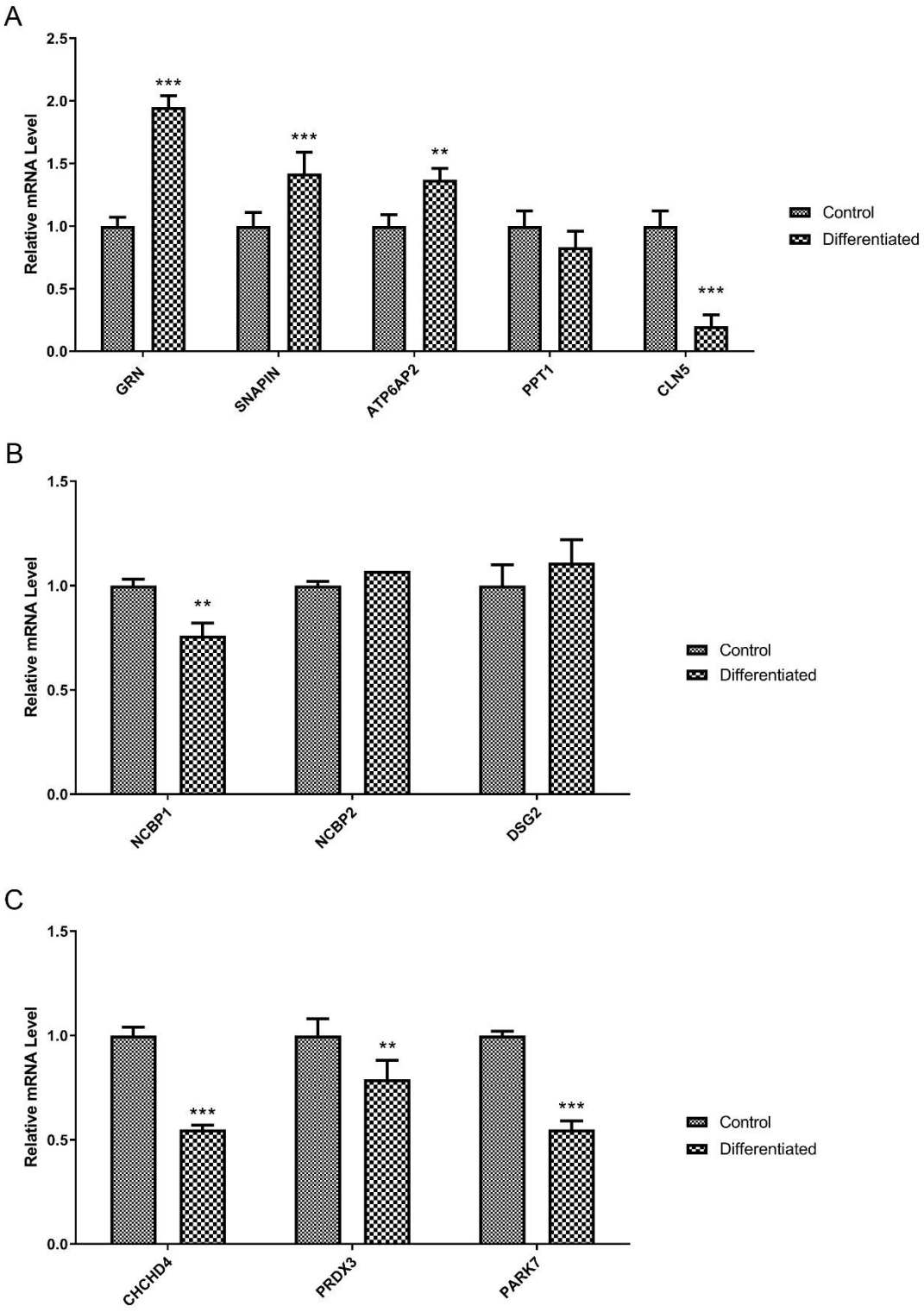

Figure 10.23. Gene expression of proteins identified in proteomics in growing and differentiated keratinocytes

Representative RT q-PCR analysis of the relative gene expression of growing and differentiated keratinocytes. The gene expression of proteins that were highlighted by proteomics to be significantly upregulated following tau overexpression were investigated in growing and differentiated keratinocyte cells. Ct values normalised to 36B4 and $2^{-\Delta\Delta Ct}$ method of analysis used. Relative expression levels are displayed as mean ± SD. Two-way ANOVA with Bonferroni correction was used to test significance; ** $p<0.01$, *** $p<0.001$.

BCC is a common form of NMSC that usually arises in lighter skin individuals from intermittent high intensity exposure to UV radiation. Indeed most BCCs are detected early and with treatment have a good prognosis. However, if left undetected, can grow into nerves and other structures and especially in locations such as the face, can cause significant damage. BCCs dramatically vary from SCCs in their molecular phenotype, driver mutations, clinical presentation, treatment and prognosis. BCCs are rarely invasive and usually result from the expansion of basal cells in nests, budding down into the dermis, but rarely do these cells detach and rupture the basement membrane. Rather, BCCS grow in nodules. BCCs are often not full thickness and the granular and corneal layers usually remain intact. Some classical features of BCC are nests of small cells with a large nucleus and little cytoplasm, resulting in a blueish appearance, these are called basaloid cells. A classical feature of basaloid cells in BCCs are the palisading that occurs around the periphery of the nests, whereby cells obtain a tall phenotype lining the basal later of the nests in a crowded parallel row (Figure 10.24). Another classical feature of BCCs in dermatopathology is the blueish areas that surround the nests of tumour cells; this is called mucin in dematopathology, but in other areas of pathology this can be referred to as myxoid change. This mucin is made of ground substances such as hyaluronic acid from the surrounding fibroblasts surrounding the tumour nests and causes a pool around the cells. Often when biopsied tissue is processed, it forms a cleft artefact, in which the tumour separates from the stroma. This artefact is unique in BCCs enabling it to be used as a diagnostic indicator. The growth patterns of BCCs can also vary, but the most common nodular pattern of growth is where atypical cells grow with one main nodule with multiple smaller nodules protruding around the edges (Figure 10.24A and B). Conversely, the growth pattern of BCCs

can be more subtle with nests budding down and pushing into the epidermis, but not detaching and growing in distinct nodules, rather displaying a superficial pattern of BCC (Figure 10.24C).

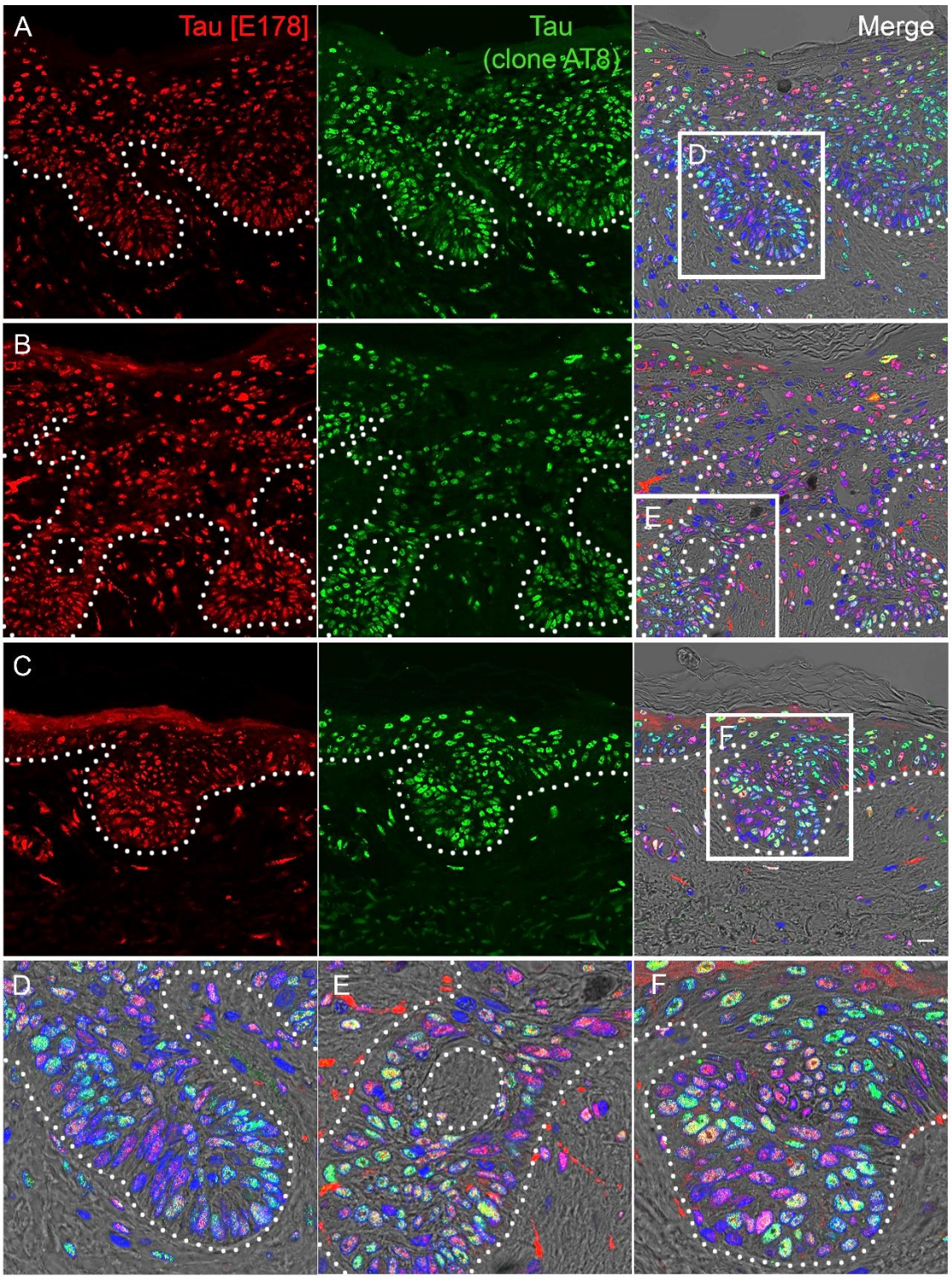

Figure 10.24. Tau expression in basal cell carcinoma.
Representative immunofluorescence analysis of tau expression in basal cell carcinoma samples (n=5). **A,B&C.** Tau [E178] (red) was observed restricted to the nucleus in most cells throughout each nest of tumour cells. Interestingly, there was a significant increase in both the number of cells, and expression density of phosphorylated tau (green) throughout BCC samples compared to SCC and healthy human skin. **D,E&F.** High magnification images of tau expression in nests of basaloid cells in BCC samples. Nuclei counterstained with DAPI (blue) and displayed with phase contrast images for visualisation of sample morphology. White dotted lines represent the epidermal-stromal boundary. Scale bar 10 µm.

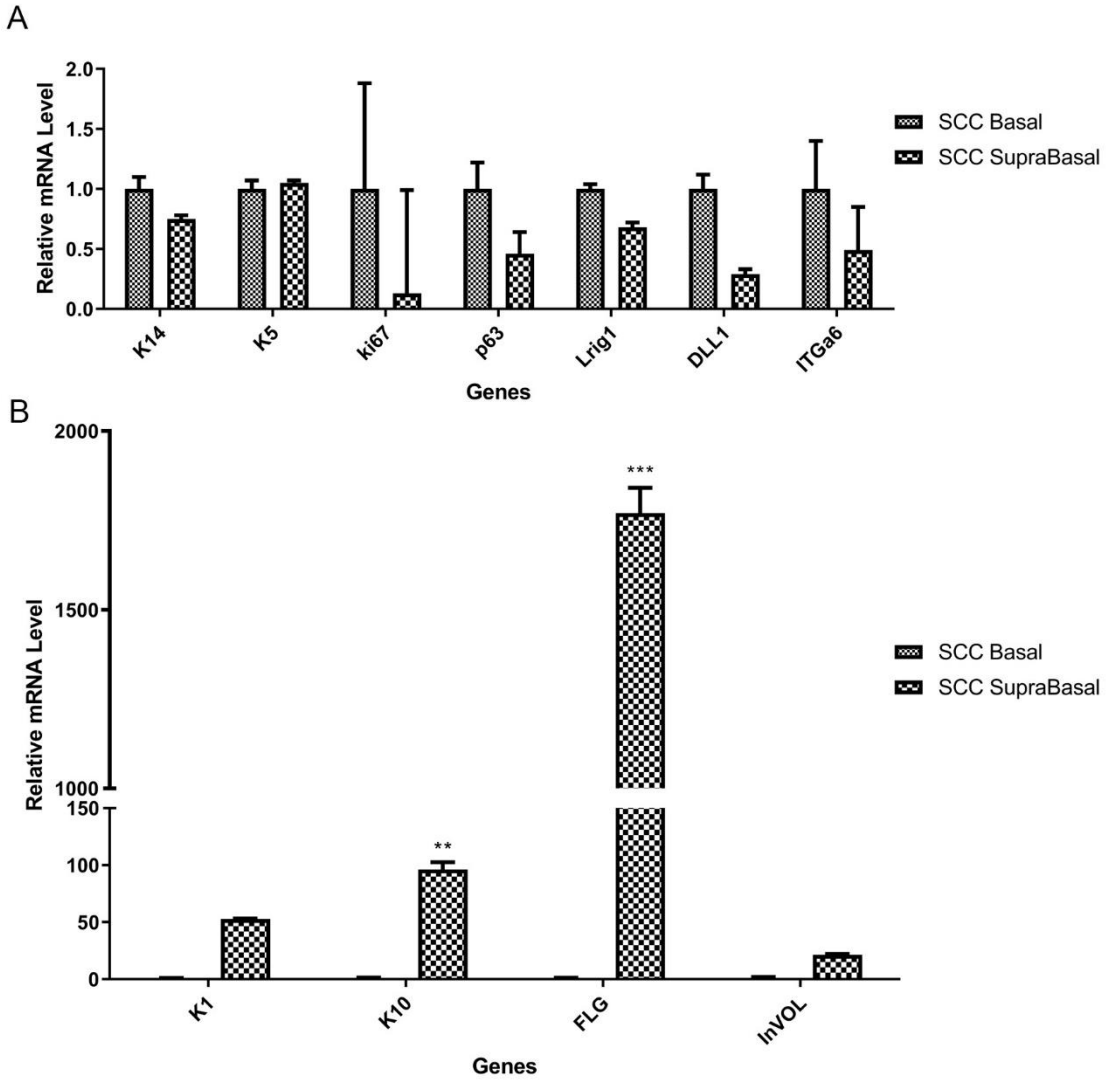

Figure 10.25. Successful isolation of regions of interest in squamous cell carcinoma samples using Laser Capture Microdissection.
Representative RT q-PCR analysis of gene expression in basal and suprabasal ROI in SCC sample from patient 18 captured with LCM. **A.** Relative gene expression of genes associated with a basal phenotype were downregulated in the captured suprabasal tissue. **B.** Relative gene expression of genes associated with differentiation were upregulated in suprabasal ROI compared to basal populations. Ct values normalised to GAPDH and $2^{-\Delta\Delta Ct}$ method of analysis used. Relative expression levels are displayed as mean ± SD. Two-way ANOVA with Bonferroni correction was used to test significance; *p<0.05, ** p<0.01, *** p<0.001.

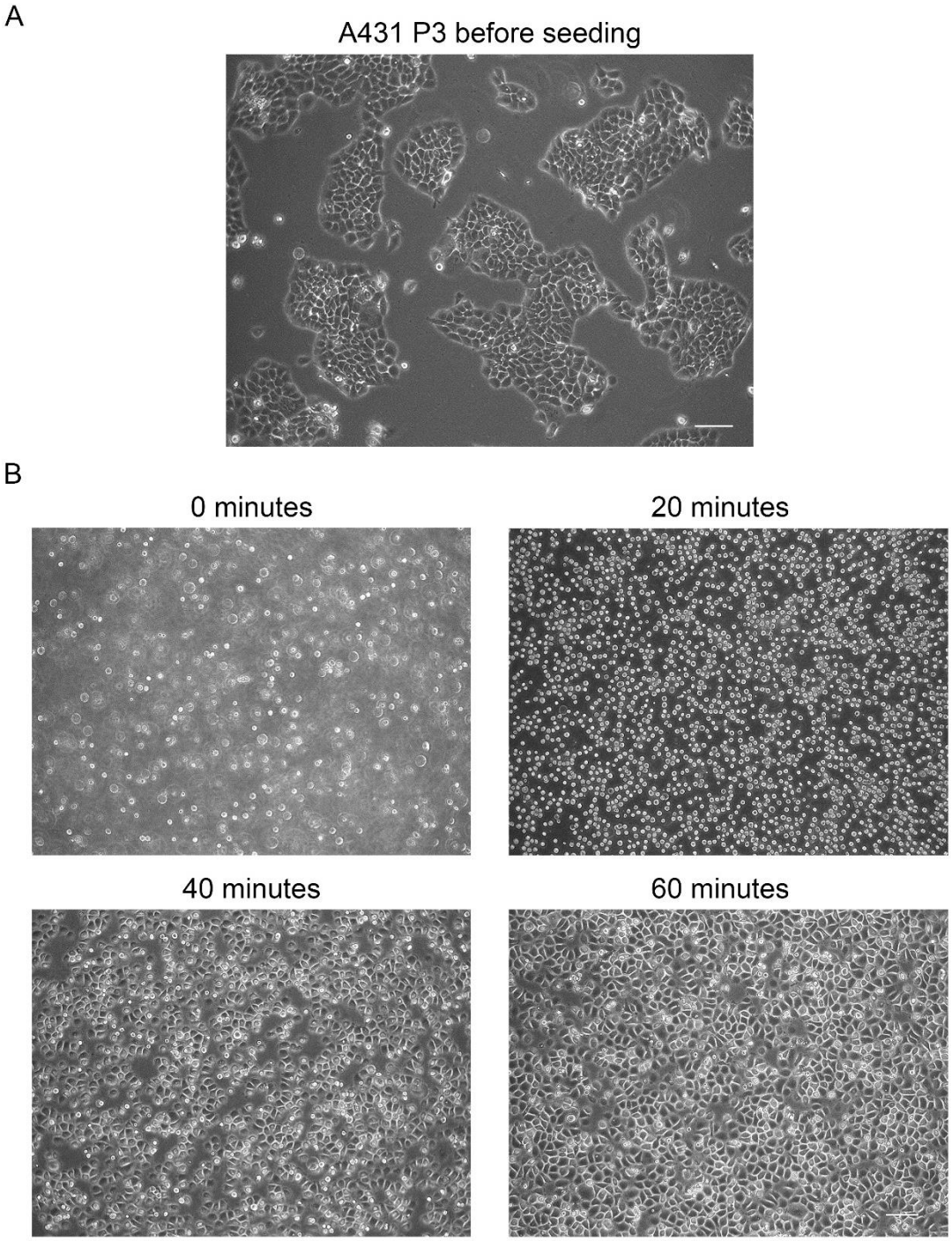

Figure 10.26. Cell culture images of attached and floating A431 cells 20, 40 and 60 min after seeding onto basement membrane protein coating.
Squamous cell carcinoma cells, A431, readily attach to basement membrane coated dishes. RNA was collected from the attached and floating population at 20, 40 and 60 min after cell seeding. **A.** Representative cell culture images of A431 cells before detachment and cell seeding. **B.** Representative cell culture images of A431 cells after seeding into basement membrane coated dishes 0, 20, 40 and 60 min after cell seeding. Immediately after cell seeding all A431 cells could be observed floating in the media, but by 20 min a large fraction of cells had attached to the coating. The proportion of HEKn cells that attached to the coating increased 40 min after seeding and again by 60 min. By 40 and 60 min after cell seeding, A431 cells could be observed growing on the surface of the dishes. Scale bar 100 µm.

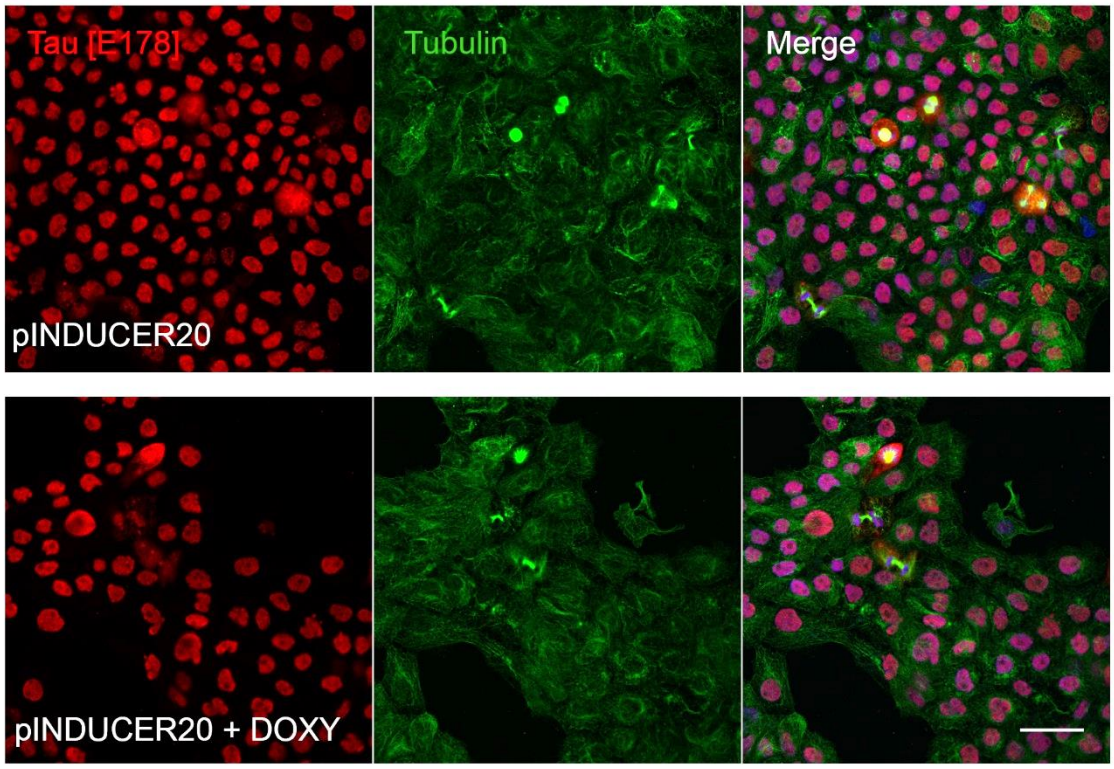

Figure 10.27. Tubulin dynamics do not significantly change following doxycycline treatment in A431 cells.
Representative immunofluorescence analysis of tau (red) and tubulin (green) in empty vector control, pINDUCER20 infected A431 cells with and without the doxycycline treatment. Nuclei counterstained with DAPI (blue). Scale bar 25 µm.

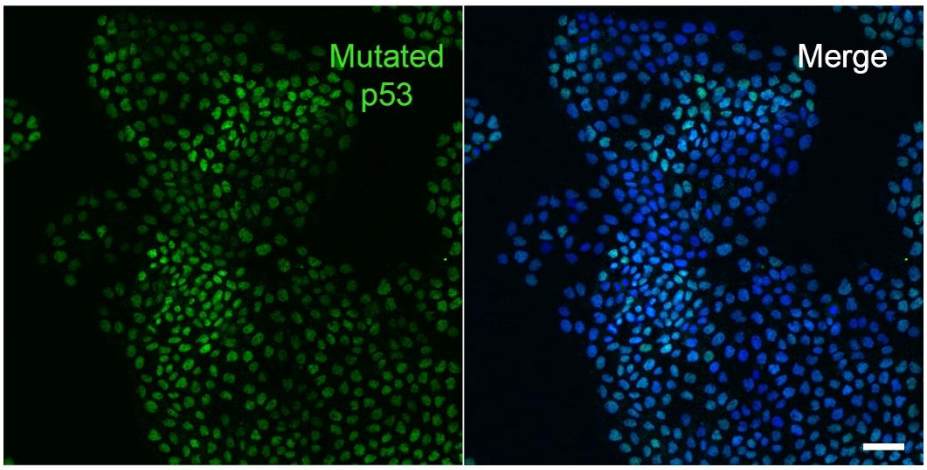

Figure 10.28. P53 mutation in A431 cells.
Representative immunofluorescence analysis of mutated p53 (pab240) (green) in A431 cells. Nuclei counterstained with DAPI (blue). Scale bar 50 µm.

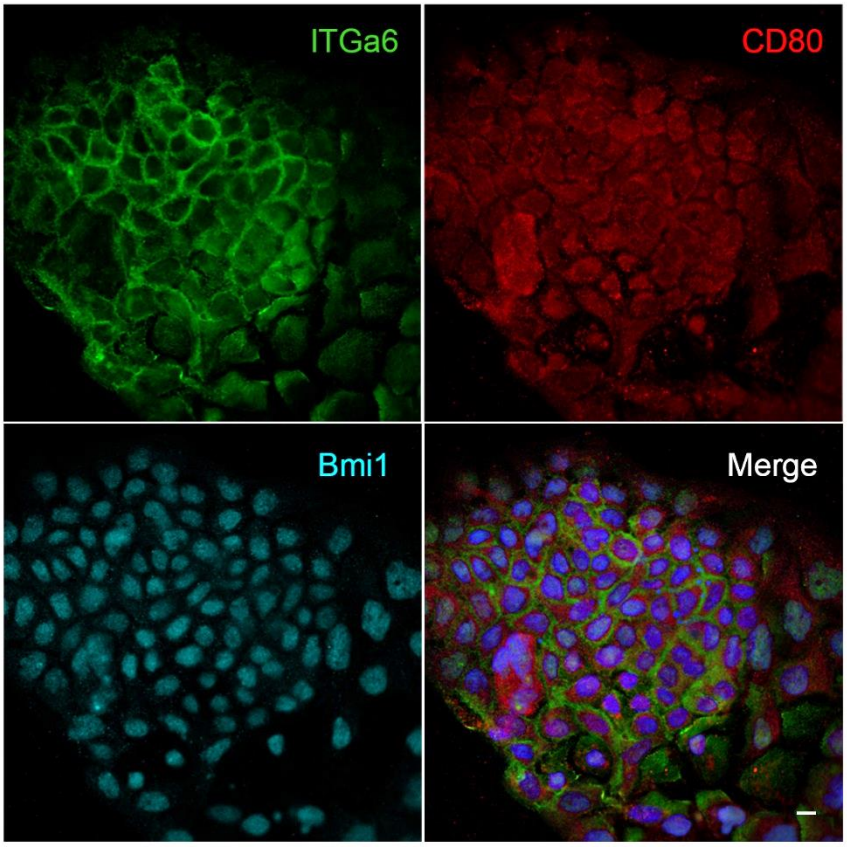

Figure 10.29. Integrin-α6, CD80 and bmi1 expression in A431 cells.
Representative immunofluorescence analysis of integrin-α6 (green), CD80 (red) and bmi1 (cyan) in A431 cells. Nuclei counterstained with DAPI (blue). Scale bar 10 µm.